TDR 2001: The Second International Symposium and Workshop on Time Domain Reflectometry for Innovative Geotechnical Applications

TDR 2001 Proceedings

Introduction

Ordering Information

Copyright Information

BIBLIOGRAPHIC INFORMATION

Second International Symposium and Workshop on Time Domain Reflectometry for Innovative Geotechnical Applications, Infrastructure Technology Institute at Northwestern University, Evanston, IL, 2001.

Second International Symposium and Workshop on Time Domain Reflectometry for Innovative Geotechnical Applications

Editor: Charles H. Dowding
Production editors: Shanna M. McGarry and Sarah Eadie
Copy editor: Shanna M. McGarry

This publication contains papers presented at the Second International Time Domain Reflectometry (TDR) Symposium and Workshop for Innovative Geotechnical Applications held at Northwestern University, September 5-7, 2001, in Evanston, Illinois. The objective of the Conference was to provide a forum for the exchange of information about the current state of TDR innovation between practitioners and researchers in all levels of the public and private sector.

Printed in the United States of America
Printed, August 2001

ISBN 0-9712631-0-8

Back to Beginning

OBTAINING PROCEEDINGS

TDR Proceedings Online

Electronic copies of the proceedings are available for free online at:
http://www.iti.northwestern.edu/tdr/tdr2001/proceedings/

TDR Proceedings on CD-ROM

The CD-ROM version of the Proceedings is available for $25.00 (this includes shipping and handling costs.)

TDR Proceedings - Hard Copy

An 8.5"x 11" laser printed hard copy of the TDR Proceedings is available for $100.00 (this includes shipping and handling costs.)

Both hard copies and CD-ROMs are available by contacting the following:

Infrastructure Technology Institute Knowledge Services
Seeley G. Mudd Library for Science & Engineering
Northwestern University
2233 North Campus Drive
Evanston, Illinois
60208-3530
iti@northwestern.edu

Please make check or purchase order payable to: Northwestern University
Prices are subject to change without notice

Back to Beginning

PROCEEDINGS OF THE SECOND INTERNATIONAL SYMPOSIUM AND WORKSHOP ON TIME DOMAIN REFLECTOMETRY FOR INNOVATIVE GEOTECHNICAL APPLICATIONS

Compiled and Edited by Charles H. Dowding [1], Shanna M. McGarry [2] and Sarah Eadie [3]

Introduction by Charles H. Dowding[1]

[1] Professor, Department of Civil Engineering, Northwestern University, Evanston, IL
[2] Student, Medill School of Journalism, Northwestern University, Evanston, IL
[3] Cyberian, Infrastructure Technology Institute, Northwestern University, Evanston, IL

ABSTRACT

This publication contains papers prepared for the Second International Symposium and Workshop on Innovatgive Geo-Appliacations of Time Domain Reflectometry (TDR) held at Northwestern University on September 5-7, 2001. The symposium was underwritten by the Infrastructure Technology Institute at Northwestern University , which is funded by the U.S. Department of Transportation to deploy advanced instrumentation in transportation infrastructure matters. The proceedings is organized according to technical topics. **Hardware** concentrates on differing considerations of instrumentation such as calibration and newly developed sensors. **Soil Moisture** focuses on the widest use of TDR instrumentaion and is divided into two sections: general and monitoring. **Rock and Soil Deformation** presents applications of TDR to monitor deforamtions anywhere along a cable. **Environmental Monitoring** concentrates on the measurement of solutes in pore fluids. **Subgrade Monitoring** focuses on appliactions of TDR for construction of roadways. The session on **Optical TDR and Structural Monitoring** concentrates use of TDR to monitor cracking in structures.

INTRODUCTION

This second international symposium and workshop is organized to assemble researchers and practitioners that have adapted metallic cable Time Domain Reflectometry (MTDR) and optical fiber TDR (OTDR) for a wide variety of geotechnical applications. It is underwritten by the Infrastructure Technology Insitiute (ITI) at Northwestern University, which is funded by the U.S. Department of Transportaion. It continues the tradition of periodic gathering of researchers and instrument manufacturers from around the world to cross-fertilize their efforts. Repetition of this symposium demonstrates the breadth and depth of the potential of metallic and optical TDR for survellance and monitoring in the geo-environment. While the basic physics of TDR technology is not

new, the transducers and applications are, and TDR is rapidly developing as an important tool for environmental, infrastructure and mining surveillance.

Comparisons of OTDR and MTDR applications in the geo-environment reveal striking similarities. A metallic cable or optical fiber is both the transmission and sensing medium. Systems can be configured to allow the possibility of measurement continuously along great lengths. Whereas other measurement technologies restrict measurement to a predetermined location. Still others restrict measurement to sensors at the end of the cable or fiber. Both utilize portable electronics that can be detached to allow monitoring at several locations with a singular pulser-recorder. Alternatively, one tester can be connected to several cables or fibers via multiplexers.

Simultaneous transmission and measurement qualities are relatively rare. Properties of metallic cables and optical fibers can be preferentially optimized to enhance their performance as a transmission medium and/or as a transducer. For example, a coaxial cable can be embedded in a structure or unstable slope to monitor deformation and fracture development anywhere along the cable, or connected to a coaxial probe to monitor changes in soil moisture and contaminant transport. Optical fibers can be manufactured with variable refractive indices and embedded in a structure to monitor dynamic strains at desired locations along the fiber or manufactured with a sheath of spiral-wound fiber and polymers to monitor changes in water content and chemistry along the fiber.

While this symposium has concentrated upon the scientific and engineering aspects of these technologies, commercialization of the technology is essential for its incorporation in monitoring activities. Intense use of MTDR in the power industry and OTDR in telecommunications, and now MTDR for moisture monitoring in agriculture provide a sufficiently large market to drive commercial development of the technology. For instance, MTDR pulser-recorders are declining in price while increasing in functionality. The same is true for coaxial cable utilized in MTDR applications. It is available in a large variety of configurations at inexpensive prices. If TDR technology had been dependent solely on the resource/infrastructure/environmental market, prices would be much higher.

Commercialization requires a knowledgeable cadre of companies that are capable of installing and maintaining MTDR and OTDR transducers, cables, and fibers as well as interpreting their output. Development of these companies since the first symposium points to the commercial viability of this technology. It is hoped that this symposium and these proceedings will further demonstrate this vitality.

TDR technology has matured to the stage where standardization of technique and terminology will be helpful in its commercialization. The beginnings of standardization are evidenced by the meeting at the symposium of representatives of the American Society of Testing and Materials to investigate the development of guidelines. The short courses offered in conjunction with the symposium also underscore the growing acceptance and maturation of TDR technology. Publication of the book, Geo-Measurement by Pulsing TDR Cables and Probes (Dowding and O'Connor, 1999) provides another support for the orderly development of the field.

Development of digital publishing and the Internet since the first symposium has lead to a revolutionary change in the publication of these proceedings. Individual papers were all submitted, reviewed, edited and combined electronically. No hard copies were sent by mail. The review process was facilitated by the symposium home

pages that displayed the program and author instructions and allowed reviewers password-protected access to the first drafts of the papers. This process demonstrates the leverage of digital technology, which in turn underscores the inherent advantage of digital monitoring technologies such as TDR.

This radical departure from past practices reduced the printing and distribution costs by an order of magnitude. It is no longer necessary to charge high prices to recover these costs. Electronic publication eliminates printing, storing, accounting, shipping, etc. of hard copy version of the proceedings.

The proceedings are published in PDF format on a Compact Disc (CD) and are available for downloading from the ITI server at **http://www.iti.northwestern.edu/tdr/tdr2001/proceedings/.** The CD has been assigned an ISBN number and will registered with the United States Library of Congress, which will receive archival copies. As such the CD will be listed in the Books in Print database just as any other symposium proceedings published in hard copy. The CD is offered in a reproducible format to ensure the widest possible dissemination. To ensure identification of the authors and the symposium after downstream reproduction, the title page of each article contains the postal and electronic address as well as organization logo of at least the corresponding author and the URL address of the ITI server from which the CD can be accessed.

ACKNOWLEDGEMENT

All manuscripts were reviewed for technical content and editorial consistency by the organizing committee and technically competent peers. The contributions of Joel Greene of Campbell Scientific Inc., William Herkelrath of the United States Geological Survey, Dryver Houston of the University of New Hampshire, Kevin O'Connor of TDR Inc., and Everett Springer of Los Alamos National Laboratory, are gratefully appreciated. The major contributions of Michael Babik (Northwestern University Civil Engineering Student) in the early stages of organizing are also acknowledged.

REFERENCES

O'Connor, K.M., Dowding, C.H. (1999) Geo-Measurement by Pulsing TDR Cables and Probes, CRC Press, Boca Raton, FL, 402 pp

.

Table of Contents

Author Index

Environmental Monitoring

Hardware

Optical TDR and Structural Monitoring

Rock and Soil Deformation Monitoring

Soil Moisture

Soil Moisture Monitoring

The State of the Practice (Keynote Presentations)

Subgrade Monitoring

Back to Beginning

Keynote Paper Presentations: The State of the Practice

Frequency Domain Modeling of TDR Waveforms in Order to Obtain Frequency Dependent Dielectric Properties of Soil Samples: A Theoretical Approach
T. Heimovaara, *IWACO Consultants, The Netherlands*

Innovations in Optical Reflectometry Including TDR
Keith Wanser, R. Belansky and T. Pongetti, *California State University – Fullerton*

Detection of Shearing in Soft Soils with Compliantly Grouted TDR Cables
C. H. Dowding, *Northwestern University*; R.G. Cole, *Geosyntec*; C.E. Pierce, *University of South Carolina*

Back to Table of Contents

FREQUENCY DOMAIN MODELING OF TDR WAVEFORMS IN ORDER TO OBTAIN FREQUENCY DEPENDENT DIELECTRIC PROPERTIES OF SOIL SAMPLES: A THEORETICAL APPROACH

Timo J. Heimovaara

IWACO Consultants for Water and Environment, PO Box 8520, 3009 AM Rotterdam,
The Netherlands, T.Heimovaara@rtd.iwaco.nl

ABSTRACT

Frequency domain modeling of TDR waveforms is a robust and physically sound way of interpreting TDR waveforms. This paper presents a theoretical approach in which features of TDR waveforms are related to frequency dependent dielectric properties. The dielectric properties of samples are described with the extended Debeye relaxation equation. The transmission line is modeled with a multi-section scatter function. The results clearly show that dielectric relaxation causes a decrease in rise time due to a dispersion of the TDR signal. The dispersion is caused by the fact that the frequencies in the TDR signal move at different velocities through the transmission line. Inverse modeling of TDR waveforms is feasible, assuming a single layer sample and Debeye relaxation results in averaged dielectric properties. The modeled waveforms can deviate significantly from waveforms measured on layered samples.

INTRODUCTION

Time Domain Reflectometry is a very versatile measurement technique with which it is possible to measure a number of soil properties such as volumetric soil water content and bulk soil electrical conductivity. The presentations at this conference clearly illustrate the diversity of different applications of TDR in geo-sciences.

Knowledge about the frequency dependent dielectric permittivity is essential when applying remote sensing techniques in order to obtain information on for instance the distribution of the water content over wide areas. Examples of such techniques are passive radar remote sensing and Ground Penetrating Radar etc. Heimovaara (1994) suggested that it should be possible to measure the frequency dependent dielectric permittivity in a frequency range between 7 MHz and about 1.5 GHz. In order to do this, he followed the approach used earlier by Clarkson *et al.* (1977) in which the S_{11} –scatter function of a single section transmission line (TL) was used to describe the TDR waveforms. Heimovaara (1994) directly solved the complex dielectric permittivity from the S_{11}-scatter function for each frequency. Due to the nature of the scatter function and the non-ideal properties of the measurement system, this

approach only worked for frequencies up to 250 MHz. Later Heimovaara *et al*. (1996) proposed to use the frequency domain approach to fit the measured waveforms in the time domain. To do this the dielectric behavior of the TL was described by optimizing parameters in the extended Debeye relaxation curve (Hasted, 1973). Huisman *et al*. (2000) showed that the parameters obtained by fitting the Debeye model to measured waveforms are related to the apparent dielectric permittivity obtained from travel time measurements. In addition, the reproducibility of this inverse method is potentially higher than the reproducibility of the traditional travel time analysis because no expert judgment is required in the wave form analysis. Another advantage of the inverse approach is that the analysis is based on a physical model of the TL that is being measured.

Feng *et al*. (1999) and Nguyen (1999) presented a similar approach based on the application of the S_{11}-scatter function of a multi-section transmission line. This approach makes it possible to explicitly account for the properties of cables, connectors etc. in the TL being measured which should improve the results. Feng *et al*. (1999) claim that this approach should also allow for extracting the dielectric properties of layered samples.

Knowing the dielectric properties of soils allow us to develop models which explain these properties from the soil composition. Weerts (2000) presented an approach in which the similarity between models describing the dielectric properties, the electrical conductivity, gas diffusion and hydraulic conductivity was investigated. Robinson and Friedman (2001) present mixing models showing the effect of particle size distribution on the dielectric properties and as a consequence on water content measurements with dielectric methods. This type of studies on soil properties can only be carried out if good measurements can be made. TDR can be useful method if we understand the theoretical basis so that we can correctly interpret TDR measurements.

This paper focuses on the multi-section scatter function presented by Feng *et al*. (1999) in order to show how we can put this model to use in order to obtain information about soil properties. A sensitivity analysis is carried out to test certain aspects of the model. Finally, an inverse modeling approach is presented in order to obtain the parameters describing the frequency dependent properties of soil samples.

THEORY

Modeling TDR waveforms in the frequency domain is based on the convolution theorem in which the time domain waveform, *r(t)* is related the incident or input signal, $v_0(t)$, and a system function, *s(t)* describing how the system under test influences the input signal (refs….). The convolution in the time domain is a multiplication in the frequency domain:

$$R(f) = V_0(f)S(f) \qquad [1]$$

in which R is the Fourier transform of the (measured) Time Domain waveform, V_0 is the Fourier transform of the incident signal generated by the cable tester and S is the Fourier transform of the system function, all a function of frequency f.

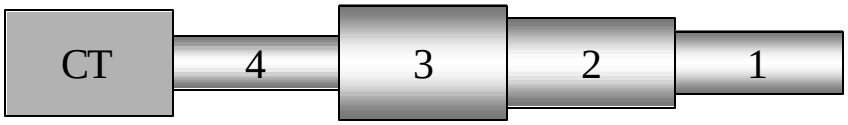

Fig. 1. *Overview of the multi-section transmission line connected to the cable tester (CT). The numbers indicate the TL-section numbering convention adopted for this paper following the approach by Feng* et al*. (1999).*

Knowing $V_0(f)$ and $S(f)$ allows us to calculate $R(f)$ and applying an inverse Fourier transform results in the corresponding Time Domain Waveform (Heimovaara, 1994). The input function, $V_0(f)$, is often measured with the cable tester. $S(f)$ can be described with a so-called scatter function which gives a complete description of all multiple reflections in the transmission line in the frequency domain. Feng *et al*. (1999) presented an approach that makes it relatively easy to determine the scatter function for a wide range of different transmission line configurations. Figure 1 gives an example of a multi-section TL connected to a cable tester (CT) together with the TL section numbering convention adopted for this paper. TL section number 1 is the section that lies at the end of the multi-section TL. The corresponding multi-section S_{11} (reflection) scatter function measured by the CT is given as:

$$S_{11}^{k} = \frac{r_s^k(f) + S_{11}^{k-1}(f)\exp(-2\gamma L)}{1 + r_s^k(f) S_{11}^{k-1}(f)\exp(-2\gamma L)} \qquad [2]$$

with

$$r_s^k(f) = \frac{Z_{k-1}(f) - Z_k(f)}{Z_{k-1}(f) + Z_k(f)} \qquad [3]$$

being the reflection coefficient between the different sections k of the TL indicated in figure 1, $Z_k(f)$ is the frequency dependent impedance of TL section k and is calculated with:

$$Z_k(f) = \frac{Z_{0,k}}{[\varepsilon^*(f)]^{1/2}} \qquad [4]$$

in which $Z_{0,k}$ is the characteristic impedance of TL section k and $\varepsilon^*(f)$ is the complex frequency dependent dielectric permittivity. The characteristic impedance of the CT is assumed to be 50 Ω. The losses due to dielectric relaxation and direct current (DC) conductivity assuming TEM mode propagation are given by:

$$\gamma L = \frac{i 2\pi f L [\varepsilon^*(f)]^{1/2}}{c} \qquad [5]$$

in which γ is the complex frequency dependent propagation parameter, L is the length of the probe, c is electromagnetic wave velocity in vacuum (3×10^8 ms^{-1}), and i is $(-1)^{1/2}$. In order to calculate the scatter function of a multi section TL one must make an assumption concerning the final reflection. For an open ended TL, S_{11}^0 is equal to 1, for a shorted TL, S_{11}^0 equals –1 and for a matched TL S_{11}^0 equals 0. The

algorithm for calculating the total scatter function of the multi section TL is then to loop through all sections starting at section 1 and calculate the appropriate scatter function.

Several approaches can be used to obtain the input signal $V_0(f)$. Heimovaara (1994) proposed to measure the input function of a multi-wire probe connected to a TL by removing the inner wire of the probe. This allowed the TDR waveforms to be modeled with a single section scatter function. Feng *et al*. (1999) obtained the input function by taking a measurement with the cable tester connected to a 50 Ω test device and then they accounted for all separate sections in their TL. Another approach is to adopt a model for an ideal input signal. In this paper, the input signal in the time domain is described with the following function:

$$v_{0,m}(t) = \frac{1 + \mathrm{erf}[a(t - t_0)]}{2} \qquad [6]$$

in which erf is the error function, a is a parameter signifying the inverse of the rise time, t is the time in the time domain signal, t_0 is the position where the input signal starts to jump to 1.

Normally, the sample is contained in section 1 of the TL. Several models can be used to describe the frequency dependent complex dielectric permittivity of a sample. In this paper the dielectric permittivity is described with the extended Debeye relaxation function (Hasted, 1973):

$$e^*(f) = e_\infty + \frac{e_s - e_\infty}{1 + i\frac{f}{f_{rel}}} - i\frac{s_{DC}}{2pfe_0} \qquad [7]$$

in which s_{DC} is the DC conductivity of the total TL, e_0 is the dielectric permittivity of free space (8.854×10^{-12} Fm^{-1}), e_s is the relative static permittivity, $e_¥$ is the relative high frequency permittivity and f_{rel} is the relaxation frequency, defined as the frequency at which the permittivity equals $(e_s+e_¥)/2$.

METHODS

Measurements

Three TDR measurements were taken with a Tektronix 1502B metallic TDR cable tester. The measurements were carried out with the same system as was used by Heimovaara (1994). The only modification to the software was that the waveforms were sampled with 4096 instead of 1024 points.

The first measurement was a waveform of the CT without a connected device. This resembles a short at the connector because the front of the CT is shorted when no TL is connected. The second measurement was a measurement of a BNC connected to a SMA adapter in order to estimate an open end. The third measurement was a measurement of the 50 Ω test device supplied with the Tektronix 1502B.

MODELING

Input signal

The parameters for the input signal (Eq. 6) were obtained by inverse modeling in the frequency domain. Equation 6 was fit to the measurement of the 50 Ω test-device that can be considered to be a representation of the input function generated by the CT.

Sensitivity analysis of waveforms to the Debeye parameters

Equation 7 contains four parameters, e_s, $e_¥$, f_{rel} and s_{DC}. We can understand what the effect is of these four parameters on the waveforms by carrying out a sensitivity analysis in which the parameters are varied one by one while leaving the other parameters at their default values. Table 1 shows the default parameter values together with the ranges in which these parameters varied.

Parameter	Default value	Range
ε_s	25	5 – 25
ε_∞	5	1 – 25
f_{rel}	$5x10^8$	$10 - 10^{10}$
σ_{DC}	0	$10^{-6} – 1$

Table 1. *Parameter values used for understanding the sensitivity of the waveform to variations in the parameters from Eq. 7*

Forward modeling of the interface of the CT and a multi-section waveform

Taking a close look at all three measured waveforms (figure 2) shows that the signal for negative times is identical. The small reflections in this part are caused by impedance transitions within the CT that are only passed once by the signals. In order to remove these reflections from the signal, the measured signal for the 50 Ω testing device was subtracted from all other measurements. The input function is generated within the CT and in order to apply this input function we must at least account for the TL section within the CT. This can be done with the multi-section scatter function. This was carried out on a trial and error basis in which the Z_0, L, e_s, $e_¥$, f_{rel} were optimized. The DC conductivity, s_{DC} was assumed to be zero.

Inverse modeling of the dielectric properties of the sample in TL section 1

TDR is mostly applied in soil science to obtain the dielectric properties of a soil. These dielectric properties are then used to estimate the volumetric water content and the bulk electrical conductivity. Heimovaara (1994) have used an inverse procedure to estimate the dielectric properties. One approach is to solve the complex dielectric permittivity for each frequency in the frequency domain (Heimovaara,1994; Friel and Or, 1999). The problem with this approach that any errors in the model are then directly mapped in the calculated dielectric permittivity values. The errors in the model are primarily due to the fact that description of the characteristic impedance $Z_{0,k}$ *(f)* of the TL sections is not adequate for most TDR probe configurations. The errors become very large for the higher frequencies and the algorithms used to solve the permittivity from the measurements become very unstable.

Another approach is to assume that the complex dielectric permittivity can be modeled with a function describing the frequency dependent properties. In this approach the dielectric relaxation model serves to average the errors. Many such functions are available, such as the Debeye relaxation function used in this study (equation 7), but others are the Cole-Cole relaxation curve, multiple relaxation curves, dielectric mixing models etc. In order to test the inverse modeling approach a series of numerical

experiments was carried out. The first experiment was to calculate a waveform from known parameters and then use this calculated waveform in order to optimize the parameters from Eq. 7 with the simplex algorithm implemented in MATLAB. The parameters for this homogeneous sample experiment are presented in table 2.

The second experiment was to calculate a waveform for a sample that consisted of two layers with different dielectric properties. This experiment can be thought to represent a sample that consists of a dry and a wet layer. Two scenarios were tested, wet on top of dry and dry on top of wet. In both situations the layer had the same length. The parameters are shown in table 2. Again the parameters in Eq. 7 were optimized adopting the assumption that a single relaxation model can describe the waveforms and assuming a single layer sample.

	Z_0	L	e_s	e_∞	f_{rel}	s_{DC}
experiment 1 homogeneous sample						
section 1	180	0.20	25	3	$5x10^8$	0.0073
section 2	180	0.02	5	5	1	0
section 3	75.8	3.00	2.3	2.3	1	0
experiment 2						
scenario1 (Wet-Dry)						
section 1	180	0.10	5	3	$5x10^8$	0.0073
section 2	180	0.10	25	3	$5x10^8$	0.073
section 3	180	0.02	5	5	1	0
section 4	75.8	3.00	2.3	2.3	1	0
scenario2 (Dry–Wet)						
section 1	180	0.10	25	3	$5x10^8$	0.073
section 2	180	0.10	5	3	$5x10^8$	0.0073

Table 2: *Parameters describing the transmission line sections used for generating waveforms used in for the inverse modeling of the Debeye parameters in equation 7.*

RESULTS

Measurements

Fig. 2 shows the three measured waveforms. At approximately –2 ns we see the rise of the applied incident signal. The reflected signals are superimposed on the incident signal, therefore the measured reflection coefficient in this figure is from 0 to 2. The connector at the front end of the CT lies at 0 ns.

The three signals are nearly identical (except for small jitters due to noise in the electronics of the CT) before 0 ns, after that they deviate in an expected manner. The ripples in the signals are caused by multiple reflections in the connector at the front end of the CT and the TL inside the CT between the voltage measurement device and the connector. The three signals are as expected, the open end gives a reflection coefficient of nearly 1, the 50 Ω match a reflection coefficient of approximately 0 and the short a reflection coefficient of approximately –1. The measurements are clearly not ideal because in addition to the small reflections there are significant deviations from the expected theoretical values.

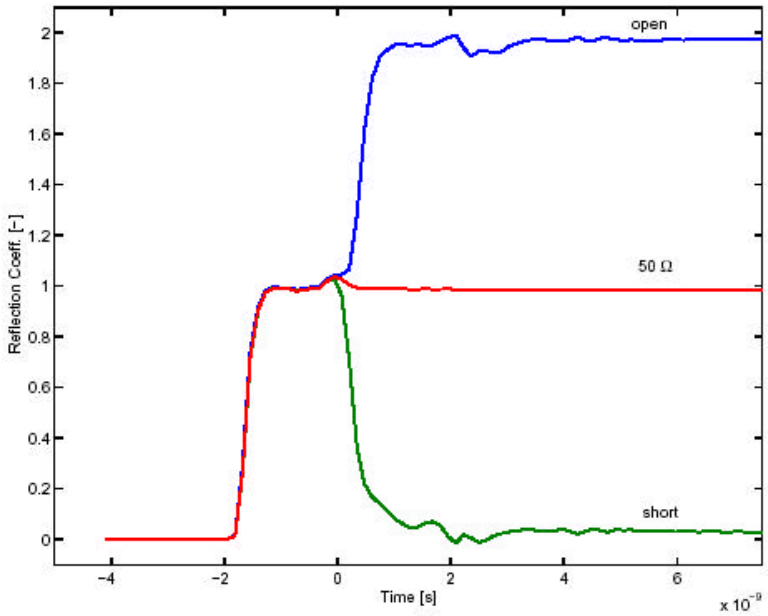

Fig. 2. *Waveforms of the CT without a connecting TL (short) of the CT with the 50 W test device as TL (50 W) and of the CT with a BNC tot SMA connector as TL (open).*

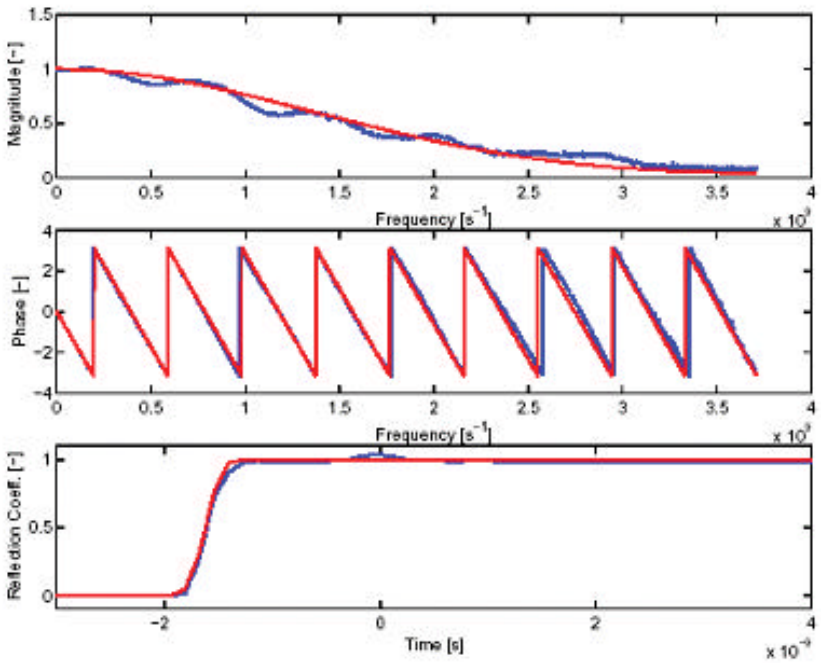

Fig. 3. *Measured (50 W test-device) and modeled input signal (Eq. 6). The top figure gives the magnitude of the frequency domain signal, the middle figure the phase and the figure at the bottom the time domain signals.*

MODELING AND SENSITIVITY ANALYSIS

Input function

Fig. 3 gives an overview of the measured and modeled input function, $v_0(t)$ and $V_0(f)$. The input function is modeled with equation 6. As can be seen in the bottom figure the modeled function gives a close fit in the time domain with only small deviations. The effects of these deviations in the frequency domain are shown in the figure at the top and in the middle. On the whole, the model fits the frequency domain characteristics rather well. Using the modeled input function in order to generate waveforms in the time domain will result in slightly smoother waveforms. The optimized parameters were –1.62 ns for t_0 and 6.42 ns^{-1} for α corresponding to a rise time of 156 ps.

Relaxation frequency (f_{rel})

The shape of the TDR waveforms depends on the value of the four Debeye parameters. Understanding this behavior is important when using TDR to obtain soil properties.

Relaxation is the drop in magnitude of the dielectric permittivity at the relaxation frequency. This phenomenon is caused by the fact that (polar) molecules want to rotate in a rotating electrical field. When the frequency rises, the molecules cannot completely follow anymore and tend to lag behind. At the relaxation frequency the phase difference between the signal and the rotation of the molecules is 90° and the energy loss is maximal.

Fig. 4A shows waveforms generated by varying only the relaxation frequency in the Debeye relaxation curve. This figure clearly illustrates the effect frequency dominated properties can have on TDR measurements. The relaxation frequency is a very dominant parameter when it falls within the measurement range of the TDR system. Relaxation softens the curves and as a result the travel time to the dominant reflection, commonly used to determine the apparent dielectric permittivity ($e_{apparent}$), decreases. The value of the relaxation frequency determines how dominant e_s or $e_¥$ are.

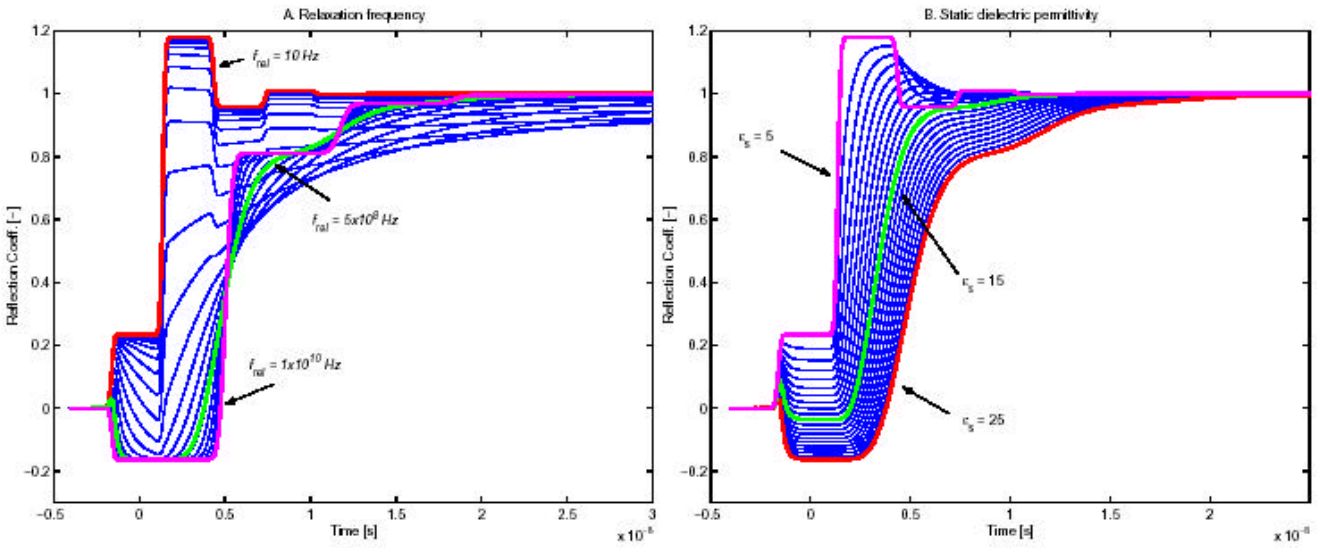

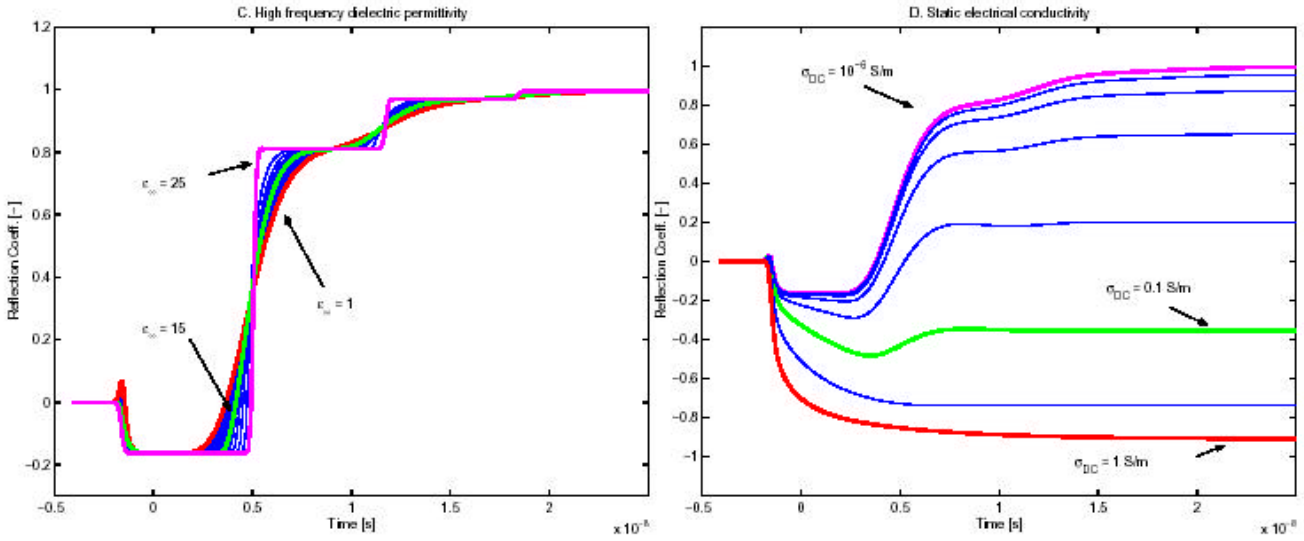

Fig. 4. *Effect of the four Debeye parameters (f_{rel},e_s, $e_¥$ and s_{DC}) on TDR waveforms*

High values of f_{rel} cause the waveform to be dominated by e_s (the thick line in Fig. 4A marked by $f_{rel} = 1x10^{10}$ *Hz*). Low values of f_{rel} result in waveforms dominated by $e_¥$ (the thick line marked by $f_{rel} = 10$ *Hz*) and finally intermediate values are the result of relaxation frequencies falling in the measurement range of TDR (the thick line marked by $f_{rel} = 5x10^8$ *Hz*). When f_{rel} falls within the measurement range, the results from the travel time analysis give apparent dielectric permittivity values which have an intermediate value between e_s or $e_¥$. Because the different frequencies in the signal feel different dielectric permittivity values they will move through the TL at different velocities. Therefore, the result of the dielectric relaxation process shows up as an increased rise time of the reflection. The final level of the waveform is not influenced. The increase in rise time at the end of the reflection softens the curve and makes a determination with the travel analysis procedure less certain.

Heimovaara *et al*. (1996) showed that the measurement bandwidth of the cable tester lies between the 7 MHz and 1.5 GHz. Relaxation frequencies that fall outside this bandwidth result in curves with 'sharp' reflections. The rise time of the signal is not influenced by the sample as all frequencies in the signal move at the same velocity.

Fig. 4A also illustrates the point that long times are associated with low frequencies and short times with the high frequencies. The lines representing the intermediate frequencies show at the first reflection (at –0.2 ns) an increase due to the low permittivity 'felt' by the high frequencies in the signal ($e_¥ = 5$). As a result these frequencies move through the TL $\sqrt{5}$ times faster than the low frequencies in the signal, resulting in a higher reflection coefficient at shorter times. Another feature clearly shown in this figure is that the levels of the multiple reflections are dominated by e_s (or $e_¥$ if f_{rel} is smaller than 7 MHz).

Static and high frequency dielectric permittivity (e_s and e_∞)

Fig. 4B and C show the effects of varying e_s and e_∞ at an intermediate value of f_{rel}. The influence of e_s and e_∞ on the waveforms depends on the value of f_{rel}. If f_{rel} is small, e_s will not have any effect and the waveform will totally be determined by e_∞. For high values of f_{rel} it will be the other way around. Values of f_{rel} that fall within the measurement range of the CT cause the effective permittivity to be some average of e_s and e_∞. Changes in the value of this 'apparent' dielectric permittivity result in changes in the impedance in the TL section and the travel time of the EM waves through the TL section. Therefore changes in the apparent dielectric permittivity result in changes in the reflection coefficient and in the position of the reflection of the end of the probe.

Fig. 4 also clearly show that a smaller difference between e_s and e_∞ result in steeper rise times due to a smaller relaxation.

Bulk electrical conductivity (σ_{DC})

Fig. 4D shows that the effect of varying the bulk electrical conductivity is a general lowering of the waveform. As is well known, σ_{DC} dominates the final level of the waveform and this is the reason why this level allows us to accurately measure the bulk electrical conductivity with TDR. Also clearly shown is that a high value of σ_{DC} results in a signal in which no reflections can be seen at all. All energy in the signal is then dissipated by conductive losses in the sample and as a result nothing is left to reflect. This example seems to show that σ_{DC} does not result in an increase in the rise time of the reflections, on the contrary, the rise time seems to decrease. The reason for this requires a closer investigation.

Forward modeling of the interface of the CT and a multi-section TL

The TL section within the CT was described with the multi-section scatter function and the theoretical input function fit to the 50 Ω signal. Two models gave reasonable results. The parameters obtained on the basis of trial and error method are shown in table 3. The plots are shown in . The 50 Ω signal was subtracted from the open ended signal in order to remove the effects of the small impedance mismatches within the CT.

Parameter	WF1	WF2
Z_0	80	80
L	0.21	0.195
e_s	2.4	2.5
e_∞	2.1	1.9
f_{rel}	1.35e8	3e9
σ_{DC}	3.8×10^{-5}	3.8×10^{-5}

Table 3. *Parameters for the multi-section scatter function model that describe the open ended CT signal.*

It is clear that the single relaxation dielectric permittivity model in combination with a single section scatter function is not the exact model. However, the general features of the model are well described by the combination of the two. The waveform clearly indicates that a relaxation occurs in this TL section (WF1). However the levels of the permittivity in WF1 are too small. Modeling the connector with a single TL section is too simple. The problem is that a compromise has to be made between a lower relaxation frequency in order to fit the measured waveform after the reflection and a higher relaxation frequency to fit the model before the reflection.

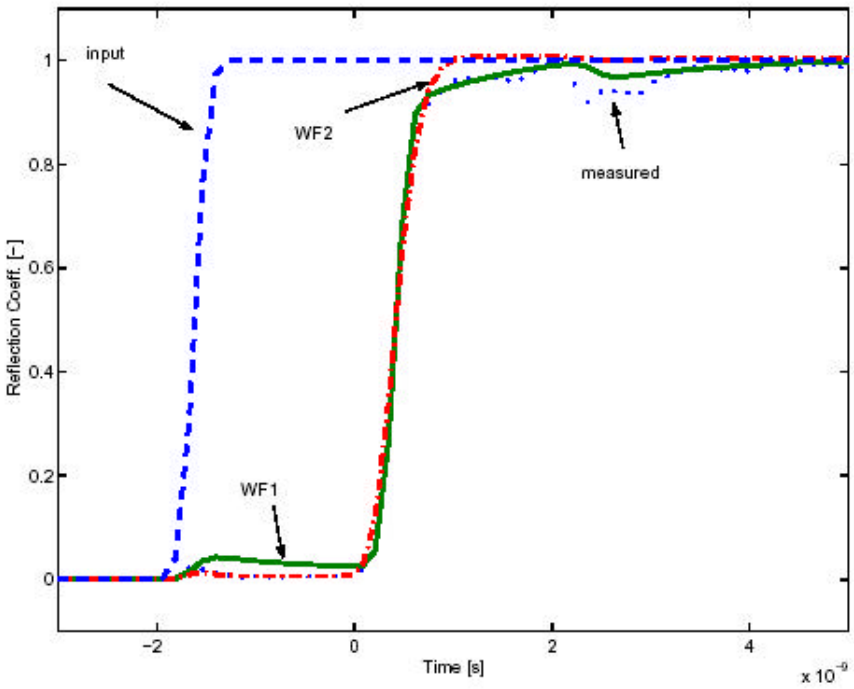

Fig. 5. *Plot of the measured open signal (dots), the theoretical input function and two modeled estimations of the measured signal. The measured signal is obtained by subtracting the measured signal of the 50 W test device.*

Inverse modeling of the dielectric properties of the sample in TL section 1

If the multi-section scatter function in combination with the Debeye relaxation function can give such a good description of TDR waveforms, is it possible to obtain the model parameters from measured waveforms by inverse modeling? In order to get an impression of the possibilities three scenarios were tested, inverse modeling of a calculated waveform assuming a sample consisting of a single layer and inverse modeling of a calculated waveform assuming layered samples (Dry-Wet and Wet-Dry). The calculated waveforms are assumed to represent measured waveforms. As can be seen in Fig. 5A, inverse modeling of the single relaxation parameters for a homogenous sample (that follows the Debeye relaxation) works very well.

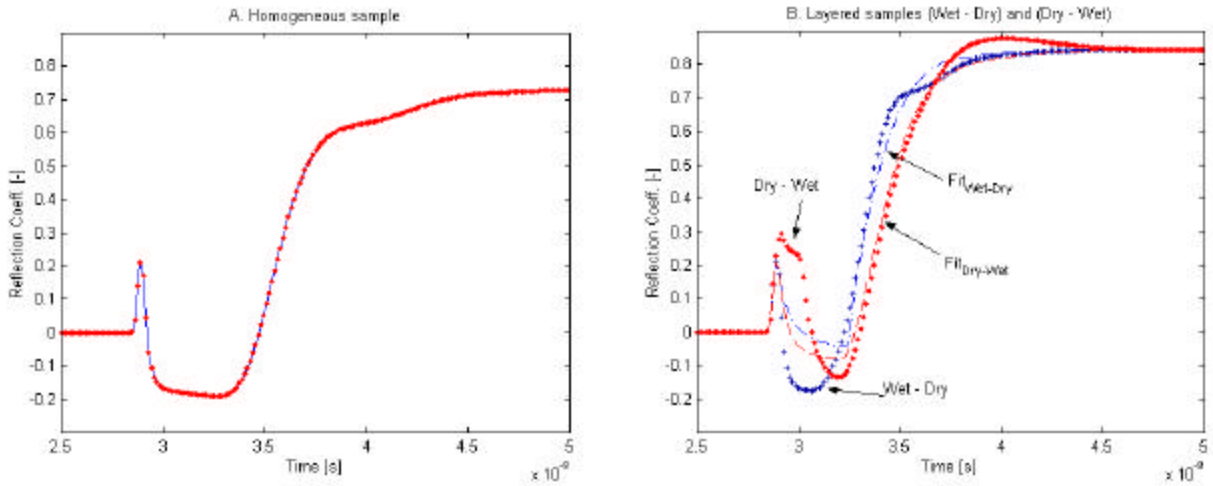

Fig. 5. *Calculated waveforms (symbols) and waveforms calculated from inversely modeled parameters (lines) for three scenarios: homogenous sample (A) and layered samples (B).*

Clearly, the inverse modeling of the layered sample with a single section TL is not able to give a good fit of the 'measured' waveforms. The single section TL model for the probe does not have enough

complexity to account for the complex signal. However, the total DC conductivity of the sample is correctly estimated. Attempting to apply a multi-layer sample model would be difficult because we are confronted with a large number of parameters, which can have wide ranges.

The more interesting question from a practical approach is how to interpret the result. Does the single layer result represent the averaged case and can we use the results for water content estimations etc. It is clear that the results from the two cases differ. The parameters for the layered samples are shown in table 4. A first graphical interpretation of the waveforms indicates that the travel times of the first reflection of the inversely modeled waveforms lie close to the 'measured' waveforms. The general rise time is more or less the same, however the reflection of the probe does not drop as low as the measured waveforms. The low impedance values in the 'measured' signals are due to the high value of σ_{DC} of the wet section that cannot be matched by the average value for σ_{DC} obtained in the inverse modeling.

parameter	initial estimate	Wet-Dry	Dry-Wet
ε_s	25	13.86	16.42
ε_∞	3	7.15	5.97
f_{rel}	5 x 10^8	1.81 x 10^8	2.53 x 10^8
σ_{DC}	0.0073	0.004	0.004

Table 4. *Parameters obtained by inverse modeling of the waveforms calculated with the parameters shown inTtable 2.*

This example also shows that the suggestion by Heimovaara (1996) to use ε_∞ as an approximation for $\varepsilon_{apparent}$ is not always feasible. The apparent permittivity in this case will lie much closer to ε_s than ε_∞. However, we may question if a relaxation frequency of 500 MHz is a realistic choice for soils. Weerts *et al*. (2001) showed that the Debeye relaxation model is a very flexible model for describing TDR waveforms. This flexibility results in identification problems in inverse modeling procedures.

DISCUSSION

This paper has demonstrated that the multi-section scatter function is a very flexible model that can be used to describe many details we find in measured TDR waveforms. This modeling approach can teach us how to recognize specific dielectric relaxation phenomena in TDR waveforms, especially if we incorporate more advanced and complex models for describing the dielectric properties of our samples. For example, does the relaxation process remove frequencies from the TDR signal? The results presented in this paper show that dielectric relaxation causes the different frequencies to move at different velocities, which disperses the wave front. DC conductivity decreases the amplitude of the different frequencies, which eventually causes the frequencies to be removed from the waveform.

A major potential problem of the multi-section models is that the number of parameters can become very large. As a result inverse modeling of these parameters becomes less feasible. It is therefore necessary to come up with methods with which the parameters in multi-section TL can be estimated on a routine basis. Another approach, although not completely correct, is to assume that the input signal is generated at the interface between the cable and the probe as was proposed by Heimovaara (1994, 1996). This approach cannot accurately account for the multiple reflections of connectors and other small mismatches occurring in the TL. This approach has the advantage of not requiring an excessive amount of parameters.

It is very important to realize that the approach used depends very much on the model used to describe the dielectric properties of the different TL-sections. The Debeye model is one of the most easy ones to apply, however as shown in the last example it often is not complex enough to describe the true dielectric behavior of soils. In the approach used in this paper, we assume that the dielectric properties of a soil sample can be described with a single relaxation Debeye curve. Other models of the dielectric properties of soils do exist and can be used as well. TDR waveforms can be an excellent way to test the capability of models to describe the dielectric properties. Close inspection of waveforms can indicate heterogeneity in the sample and it can give an impression of how well the model averages these properties.

The most important advantage of the inverse modeling approach is that it is based on a physical description of the measurement system. The results have been shown to be more reproducible than results obtained from the travel time analysis. However if this inverse modeling approach is to gain wide acceptance in field type applications on the routinely applied TDR probes, the challenge of using inverse modeling to estimate all the parameters in a multi-section TL has to be met.

ACKNOWLEDGMENTS

The author thanks Sander Huisman for his comments on an earlier version of this manuscript.

REFERENCES

Clarkson, T.S., Glasser, L., Tuxworth, R.W. and Williams, G., 1997, An appreciation of experimental factors in time-domain spectroscopy, Adv. Mol. Rel. Proces., **10**, 173-202.

Friel, R. and Or, D., 1999, Frequency analysis of time-domain reflectometry (TDR) with application to dielectric spectroscopy of soil constituents, Geophysics, **64**, No. 3, 707-718.

Hasted, J.B., 1973, Aqeous dielectrics, Chapman and Hall, London

Heimovaara, T.J., 1994, Frequency domain analysis of time domain reflectometry waveforms 1. Measurement of the complex dielecrtric permittivity of soils, Water Resour. Res., **30**, No. 2,189-199

Heimovaara, T.J., de Winter E.J.G., van Loon, W.K.P., and Esveld, D.C., 1996, Frequency-dependent dielectric permittivity from 0 to 1 GHz: Time domain reflectometry measurements compared with frequency domain network analyzer measurements, Water Resour. Res., **32**, No. 12, 3603-3610.

Nguyen, B.L. 1999, Dielectric measurements for saturation determination, PhD-Thesis, Technical University Delft.

Robinson, D.A., and Friedman, S.P., 2001, Effect of particle size distribution on the effective dielectric permittivity of saturated granular meida, Water Resour. Res., **37**, 1, 33-40.

Weerts, A.H., Huisman, J.A., and Bouten, W., 2001, Information content of time domain reflectometry waveforms, Water Resour. Res., in press.

INNOVATIONS IN OPTICAL REFLECTOMETRY INCLUDING OTDR

Keith H. Wanser[1], Richard Belansky[2], and Thomas Pongetti[3]

[1]Department of Physics, California State University Fullerton, Fullerton, CA 92834; kwanser@fullerton.edu,
[2]Department of Physics, California State University Fullerton, Fullerton, CA 92834; rhbelansky@west.raytheon.com
[3]Department of Physics, California State University Fullerton, Fullerton, CA 92834; tpradmon@aol.com

ABSTRACT

In the present work we present some recent innovations in optical reflectometry, both continuous wave and pulsed. In particular, we discuss several properties and applications of *Elastica*[1] fiber optic strain/displacement transducers. The transmission and reflection properties of multimode and single mode fiber *Elastica* are presented. The results of variable mode excitation and the whispering gallery effect on the response properties are discussed. A novel SMF/MMF/SMF *Elastica* structure is introduced which is able to control and stabilize sensor mode excitation. OTDR data on enhanced reflection of *Elastica* fiber sensors and preliminary results of a novel theory explaining the effect in terms of rapid changes in waveguide curvature are presented.

INTRODUCTION

In recent years many different types of fiber optic sensors have been employed in a variety of measurement contexts [Culshaw 1998]. Optical reflectometry has been widely used to interrogate the sensors, both continuous wave and pulsed. In all cases, one of the most important areas is to develop strain/displacement transducers that have high sensitivity, large dynamic range, good linearity, low hysteresis, low force constants, convenient mounting methods, capability of operation in harsh environments, ease of multiplexing, and of utmost importance for widespread use, low cost.

In the last several years the optical fiber Bragg grating (FBG) has been successfully employed in numerous sensing applications [Ansari 1998, Culshaw 1998]. The primary sensing applications have involved short period FBG's operated in a reflection mode to sense strain or displacement. Long period FBG's are operated in a transmission mode and are usually used for other types of sensing applications, such as chemical sensing, due to their sensitivity to the properties of the material surrounding the

[1] *Elastica*^{TM} is a trademark of South Coast Spectrum, Laguna Hills, CA 92654.

cladding. The methods of interrogation of FBG sensors are also numerous. While there are many advantages of using fiber Bragg gratings, there are also several disadvantages of using them. Among the problems associated with the use of FBG sensors are; (1) Extremely high thermal sensitivity (about 7 ppm/°C thermal apparent strain), (2) very limited maximum strain (about 1-2%), (3) complicated and expensive optical interrogation and signal processing techniques required to overcome a number of technical difficulties, (4) large force constant (~89.6 N/mm = 9.14 x 10^3 g Force/mm), which limits the use of such sensors in applications involving soft materials such as soils, (5) thermal erasure of desirable types of gratings at high temperatures (greater than 300°C), limiting their use in high temperature environments. Although these difficulties can be largely overcome, doing so adds considerable expense and complexity to the measurement system.

In the present work, we will focus on a much simpler strain/displacement transducer with many properties that overcome these disadvantages of the fiber Bragg grating, and that are much easier and less expensive to fabricate than FBG's. This transducer, called the *Elastica* because of its shape, is based on the curvature loss of an optical fiber in a buckled configuration. Surprisingly, this simple and versatile transducer configuration has many desirable properties for infrastructure monitoring, including the use of OTDR to interrogate it. Although this transducer is simple in its fabrication and operation, a quantitative theoretical description of its operation is actually much more complicated than that of the fiber Bragg grating.

OPERATIONAL CHARACTERISTICS OF *ELASTICA* FIBER OPTIC SENSORS

Recently we have introduced a new class of fiber optic strain-displacement sensors which are based on precisely controlled nonlinear buckling of optical fibers and the resulting optical bending loss (not microbending) [Voss and Wanser, 1997]. These sensors, named *Elastica*, offer many advantages over other fiber optic sensors due to their simplicity, low-cost, large strain range, linearity, high fatigue cycle endurance [Wanser *et al*., 1998], high temperature capability [Wanser and Voss, 1997a], extremely low force constant (~0.02 N/mm = 35.2 g Force + 2.0 g Force/mm), great flexibility in mounting method, and low thermal apparent strain. The all-fiber sensors of this type are capable of detecting displacements ranging from a few nanometers to several millimeters. In addition, both unidirectional and omnidirectional responses have been demonstrated, the latter being particularly useful in the detection of cracks [Wanser and Voss, 1994a, Voss and Wanser 1994]. *Elastica* fiber sensors can be interrogated in both reflection and transmission modes, with either continuous or pulsed light, depending on the desired application.

An additional advantage of the *Elastica* fiber sensor is that the sensor gauge length can be readily adjusted from a few millimeters to a meter or more (with the addition of an actuator or pushrod [Wanser and Voss, 1997a]). Larger gauge lengths are desirable in applications involving inhomogeneous materials, where an average strain over a given length scale is often desired or in situations where a large area must be covered with the fewest possible gauges. Sensor gauge factor and sensing range can also be adjusted by using different straight lengths of fiber *L*o. The large sensing range of the *Elastica* fiber sensor allows its application in measurement of fatigue crack and creep monitoring of structures, situations that would destroy conventional and other fiber optic strain gauges such as the fiber Bragg grating (FBG) or the extrinsic Fabry Perot interferometer (EFPI).

Optical Transmission Response

The uniaxial *Elastica* fiber sensor configuration and buckled fiber shape is shown in figure 1. As the distance between points A and E in figure 1a is varied, the optical transmission of the fiber changes due to changing waveguide curvature loss. The optical transmission T vs. the displacement Δx curves of four similar *Elastica* multimode fiber sensors of lengths Lo = 5, 10, 15, 20 mm, are shown in figure 2. The light source, fiber type, and experimental testing conditions were the same as for the 10 mm length sensor, which has been reported on previously [Voss and Wanser 1997].

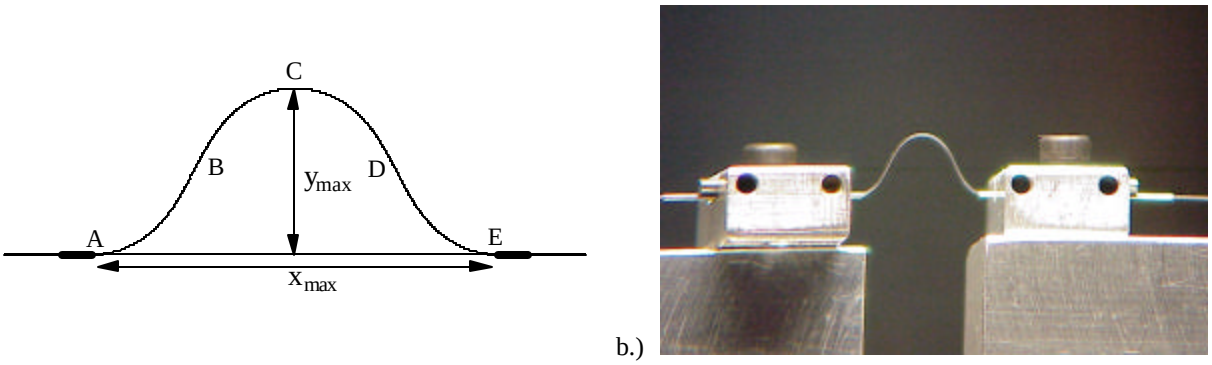

Fig. 1. *a.) Schematic of uniaxial type of Elastica fiber sensor. The distance between the two fiber clamping points A and E is varied. b.) Photograph of an Elastica fiber sensor attached with aluminum mounting brackets to aluminum fingers on micropositioners. Straight length Lo = 14.93 mm, Dx = 5.0 mm, corresponding to 33.3% compression.*

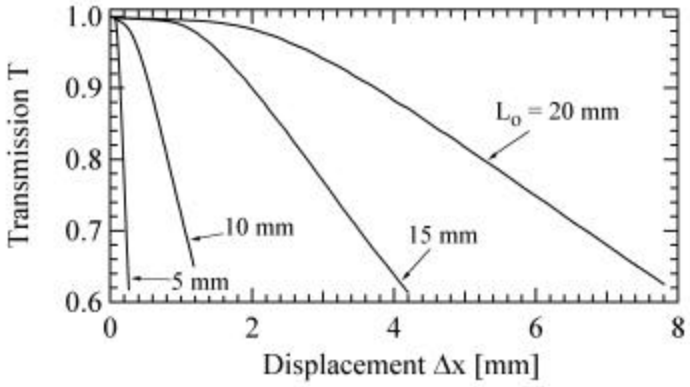

Fig. 2. *Transmission response of four different length Elastica multimode fiber sensors at a wavelength of 840 nm. Note the good linearity, large sensing range, and adjustable slope sensitivity.*

As can be seen from figure 2, the linear sensing range for the different length sensors varies from about 150 µm to 6 mm. As an example, the linearity of the 10 mm length sensor has been reported to be within 0.2% over a 1 mm sensing range [Voss and Wanser, 1997]. Similarly, the slope of the *Elastica* transmission response is a strong function of the sensor straight length Lo. The Lo = 10 mm sensor has a slope of dT/dx = -3.325 x 10^{-4}/µm, a gauge factor $G = (LG/T)\,|dT/dx|$ = 3.93 and a linear sensing range of 6% strain in either direction about a bias point of 1.5 mm displacement (assuming a sensor gauge length LG = 8.5 mm). The 16 bit resolution-limited displacement sensitivity of the Lo = 10 mm *Elastica*

fiber sensor is 46 nm in the linear region, which corresponds to a strain resolution of 5.4 μstrain for an 8.5 mm sensor gauge length.

The considerably higher sensitivity of the *L*o = 5 mm *Elastica* is shown in figure 3. Although this sensor is limited to displacements of about 0.8 mm, corresponding to a maximum strain of 16%, the sensitivity of dT/dx = - 2.4 x 10^{-3}/μm is a factor of 7.2 higher than a 10 mm length *Elastica*. The 16 bit resolution-limited displacement sensitivity is 6.4 nanometers, corresponding to a strain resolution of 1.3 μstrain, and the gauge factor is G = 14.5 for a gauge length of 4.8 mm. This large gauge factor combined with small size makes such short length *Elastica* suitable for a variety of high sensitivity applications, including harsh environments. For comparison, conventional resistance strain gauges and fiber Bragg grating strain sensors have nominal gauge factors of 2 and 0.784 respectively, and considerably smaller strain sensing ranges.

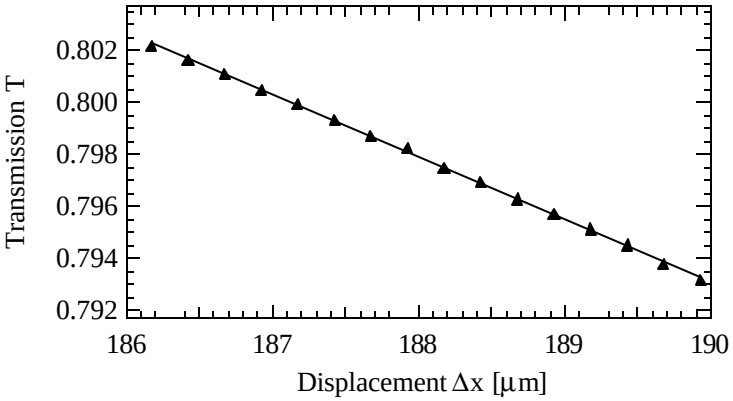

Fig. 3. *Expanded view of data for Lo = 5 mm Elastica multimode fiber sensor showing linear fit. Data points spaced apart by 0.25 mm are easily resolved with low noise. Sampling rate was 4 Hz.*

Theory and Experiments for the Transmission Response of Single Mode Fiber *Elastica*

Although the multimode fiber *Elastica* sensors are quite useful and promising, currently the quantitative understanding of their operation is empirical. It is desirable to have quantitative theoretical device models in order to optimize the design of such sensors and to better understand them. In order to model the operation of the highly multimode fiber *Elastica*, one must know the fraction of the total power carried by each of the several hundred propagating bound modes as well as calculate the radiation loss of each one over the shape function of the *Elastica*. The loss from each mode, weighted by the fractional power carried by the mode must then be summed over all the modes in order to obtain the total optical transmission through the device. This must be computed for each displacement value in order to calculate the transmission vs. displacement curves, a formidable computational task at best. What makes this problem more difficult is that in spite of a large body of literature on bending loss in optical fibers, it turns out that existing expressions for the bending loss of higher order waveguide modes are highly inaccurate by orders of magnitude [Belansky, 2001, Marcuse, 1993]. As an example of this we point out that it was found that the bend attenuation coefficient of the LP_{11e} (even) and LP_{11o} (odd) modes differ by more than two orders of magnitude [Marcuse, 1993, Poole and Wang, 1993], even though the only difference in the mode patterns is in their orientation with respect to the plane of the bend. In contrast, the "standard" bend loss formula [Marcuse, 1976] predicts no difference in attenuation between these modes.

Given this state of affairs, since it is known that the Marcuse bending loss coefficient expression for the lowest order LP_{01} fiber mode is reasonably accurate when corrected for the photoelastic effect [Sharma, 1984], we decided to try to see if a quantitative understanding of the transmission response of a single mode fiber *Elastica* could be obtained, before embarking on our more ambitious plans to calculate the transmission response of multimode fiber in various curved configurations.

In the adiabatic loss model, which neglects the transition loss effects due to the abrupt change in the radius of curvature from a straight fiber segment to a curved fiber segment, the power transmission coefficient *T* through the curved fiber section of length *L*o is given by

$$T = \exp\left(-\int_0^L ds\, a(s) \right) \qquad [1]$$

where *s* is the arc length along the fiber, and a is the power attenuation coefficient for the fundamental mode of step index fiber given by

$$a(s) = \frac{C}{\sqrt{h\,|R(s)|}} \exp\left(-h\,|R(s)| / R_c\right) \qquad [2]$$

where h is the photoelastic correction factor, given by

$$h = \frac{1}{\left\{1 - \frac{n^2}{2}\left[(1-s)p_{12} - s\,p_{11}\right]\right\}} = 1.277 \quad , \qquad [3]$$

p_{11} and p_{12} are the material photoelastic constants, s is the Poisson ratio, and the numerical value is appropriate to the parameters for fused silica. For bending loss corrections, one should use the cladding index of refraction *n* in the formula for h, since the outer turning point or radiation caustic is in the cladding.

The constants *C* and R_C are given for step index fibers by

$$C = \frac{\sqrt{p}\,U^2}{2\sqrt{a}\,V^2\,W^{3/2}\,K_1^2(W)} \qquad [4]$$

$$R_c = \frac{3b^2a^3}{2W^3} \qquad [5]$$

where $K_1(W)$ is the modified Bessel function of order one, b is the (straight) fiber propagation constant, a is the fiber core radius, and *U* and *W* are the dimensionless waveguide parameters determined by the lowest order solution to the eigenvalue equation [Snyder and Love, 1983].

Experimental data of the transmission as a function of displacement for four different length (*L*o = 5.30, 10.21, 14.82, and 20.14 mm) *Elastica* employing Corning SMF 28 (single mode fiber) and an ELED

operating at a wavelength of 1310 nm were obtained. Standard Corning SMF 28 was used, since the fiber parameters are well characterized and known from the manufacturer, thus allowing a good comparison of theory and experiment. A computer program was written to compute and integrate the power attenuation coefficient over the shape function of the *Elastica*, for each value of the displacement *Dx* of the *Elastica*. The results of the calculation are shown below in figure 4 for one of the sensors. As can be seen from the figure, the theoretical results fit the overall data very well, with the exception of the small oscillations, which are characteristic of coupling to cladding/whispering gallery modes [Belansky, 2001], thus validating this approach. Excellent agreement of theory and experiment is also obtained for each of four different sensor lengths using the same bending loss parameters. A full description of these experiments and theory will be presented elsewhere.

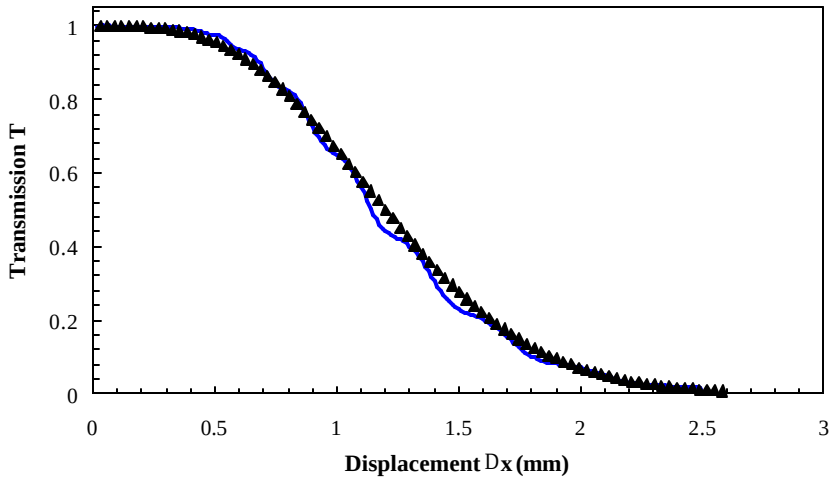

Fig. 4. *Transmission loss of a 14.82 mm Elastica employing SMF28 fiber at 1310 nm. Data curve shows small oscillations due to cladding mode "whispering gallery" effects. Triangular points are theoretical calculation, solid line is experimental data. Note the excellent overall agreement of theory and experiment*

Reflection Properties of *Elastica* Fiber Sensors

The transmission mode *Elastica* fiber sensor is very low cost and extremely simple to use due to the fact that no fiber beamsplitters or other optical components are required (at least for a single sensor), and the effects of backreflections from connector interfaces and fiber intrinsic Rayleigh scattering are insignificant, thus minimizing sources of error. In fact, due to the extremely low cost of silicon photodetector chips with on-board signal processing electronics, an extremely low cost method of sensor "multiplexing" is simply to run one fiber and photodetector for each sensing channel. Surprisingly, this approach is lower in cost and easier to implement than more sophisticated optical and electronic multiplexing techniques and. yields the greatest number of surviving sensor channels in the case of fiber cable damage arising from various hazards.

In some situations however, it is desirable to have only a single fiber going out to and returning from each sensor. The reasons for this are varied, such as to minimize the sensor size, or to reduce unwanted additional fibers, which sometimes get in the way. In continuous wave (CW) reflection mode operation, a 2 x 2 fiber beamsplitter is utilized in order to both send and receive light to and from the sensor. This causes some complications, as care must be exercised to reduce sources of backreflections from connectors and fiber ends, which can cause offsets due to light reaching the detector which has not passed through the sensor.

In figures 5 and 6 we show the single pass transmission, T_1, double pass reflection, T_2, and the square of the single pass transmission responses, of single mode and multimode fiber *Elastica* operating at 1310 nm. Each sensor remained in exactly the same mounting for both reflection and transmission measurements. The only difference between the reflection and transmission optical setups was whether

or not the output lead of the *Elastica* was connected directly to the detector (through a long length of fiber to insure cladding light removal), or a mirror placed on the end of the fiber and the unused return leg of the 2 x 2 coupler connected to the detector instead. In both cases, the 2 x 2 beamsplitter was used to input light to the sensor, and all other optical connections were the same. If the sensor is strictly reciprocal, one naively expects that the double pass transmission response T_2 is simply the square of the single pass response T_1. In fact this is the case if there is no differential mode attenuation. As can be seen from the figure, this is very accurately true for the single mode *Elastica* and hence its reflection response is highly reciprocal. The fact that the multimode *Elastica* exhibits an apparent (as opposed to true) nonreciprocity is evidence for some mode depopulation taking place in the sensor, as is to be expected on theoretical grounds due to differential mode attenuation [Wanser *et al*. 1994c, 1994d, Belansky, 2001].

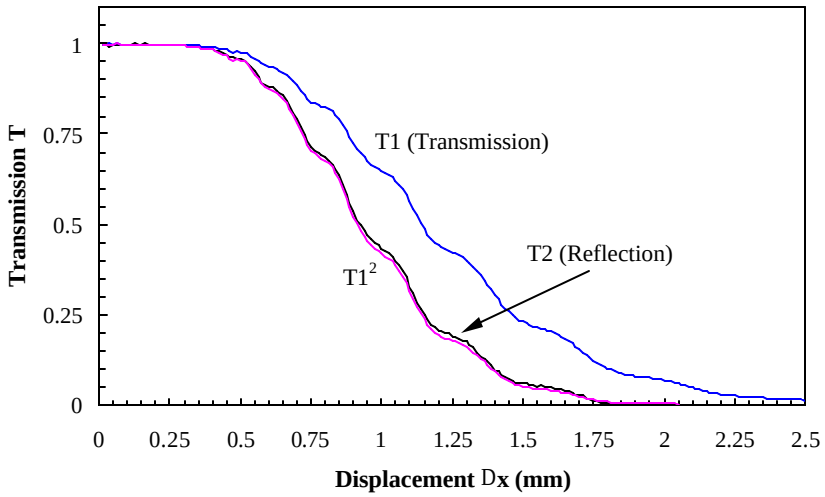

Fig. 5. *Comparison of transmission and reflection response of an Lo* =14.82 mm *single mode fiber Elastica. T_1, single pass transmission, T_2, double pass reflection, T_1^2 is the square of the single pass transmission data.*

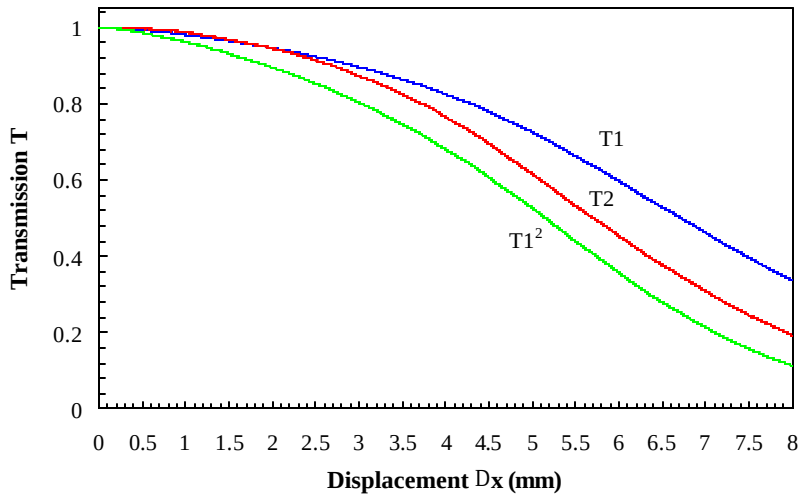

Fig. 6. *Transmission and reflection response for the 14.93 mm multimode Elastica at an ELED drive current of 36 mA. The double pass transmission is higher than the square of the single pass transmission, indicating differential mode attenuation and apparent nonreciprocity.*

Mode Excitation Effects in Multimode *Elastica* Fiber Sensors

The previous section hints at an effect that occurs with multimode fiber *Elastica*. In all cases described so far, great care has been taken to insure that the multimode fiber *Elastica* mode power distribution (MPD) is nearly uniform, or at least the equilibrium MPD. This was done by using sufficiently long input and output fiber leads to insure the removal of cladding light and also by using appropriate light sources, such as LED's, which insure excitation of all fiber modes (i.e overfill launch conditions). In order to understand the effects of varying mode power distribution on the response properties of fiber *Elastica*, we used a single mode fiber (Corning SMF 28) to launch light into a 50 µm core diameter graded index fiber. By mounting both fibers on micropositioners, we varied the longitudinal and lateral spacing between the two cleaved fiber ends, thus producing variable mode excitation of the multimode fiber which contained an *Elastica* fiber sensor downstream from it, after a 1

km spool of fiber on the input to insure the removal of cladding light. A novel method to insure accurate lateral fiber alignment was developed [Belansky, 2001]. In this method, the fiber *Elastica* is compressed to about 33% strain and the photodetector voltage peaked while scanning the lateral micropositioners. This alignment technique insured that primarily the fundamental mode of the multimode fiber is excited by the single mode fiber. In fact, calculations show that when the endfaces of the SMF 28 and 50 micron graded index fibers are in contact, 82.7% of the single mode fiber power is launched into the fundamental LP_{01} mode of the multimode fiber. Since there is a significant bend attenuation difference between the fundamental and higher order modes, this differential mode attenuation effect allows one to accurately laterally align the core of the single mode fiber with the core of the multimode fiber [Belansky, 2001].

In figure 7 we show the transmission response of an *L*o = 14.93 mm *Elastica* for various longitudinal spacings between the SMF 28 single mode fiber used to excite it and the end of the multimode fiber. As the fiber longitudinal spacing increases, the SMF 28 output beam diameter on the MMF endface increases, thus appreciably and efficiently exciting higher order fiber modes and increasing the fraction of power carrried by higher order modes in the MMF. These higher order modes are considerably more lossy than the fundamental LP_{01} mode, and as the fraction of power carried by them increases, the slope of the fiber transmission curve dramatically increases. As a side benefit, the curves also become more linear.

These measurements clearly demonstrate the importance of using a controlled or at least constant MPD when employing multimode fiber *Elastica*. There are several different ways to control the MPD, primary among them is to launch light into the MMF *Elastica* with a single mode fiber and a controlled gap between the ends of the two fibers. This can be accomplished with a capillary tube for example. The advantages of using Multimode fiber *Elastica* as opposed to single mode fiber *Elastica* is that the whispering gallery effect oscillations of the SMF *Elastica* result in variable slope sensitivity.

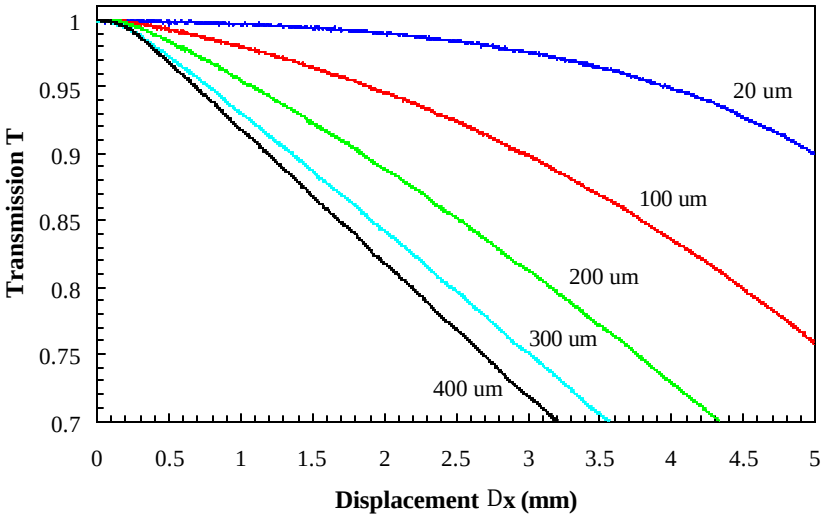

Fig. 7. *Transmission response measurements for the 14.93 mm MMF Elastica for different longitudinal spacings between the SMF28 and MMF fibers.*

Transmission Response of SMF/MMF/SMF *Elastica*

In the previous 2 sections, we have seen that the transmission or reflection response of a multimode fiber *Elastica* depends on the mode excitation conditions. In general, these conditions can change in a multimode fiber, especially if the fiber cable is subject to changing bends upstream from the sensor. It is usually desirable to use an overfill launch condition combined with a significant length of fiber to insure that a reproducible mode power distribution is achieved.

Unfortunately, one can not always count on having nearly equal MPD or equilibrium MPD [Wanser *et al*., 1994c, 1994d].

In order to control the mode distribution coming into the multimode fiber *Elastica*, and thus eliminate a major source of input lead sensitivity, one can use a single mode fiber to excite primarily the fundamental mode of the multimode fiber *Elastica*, and then use a single mode fiber on the output in order to gather only the light remaining in the fundamental mode after passing thru the sensor. This SMF/MMF/SMF type of structure operates somewhat differently than the simple MMF *Elastica*, in that the loss out of the fundamental mode is mostly due to mode coupling to other bound modes. This is in contrast to the situation that occurs in the case of a pure MMF *Elastica* with all bound modes excited, where the loss is due to the higher order bound modes coupling to the cladding or radiation modes. In the case of primarily fundamental mode excitation, the higher order bound modes of the MMF are strongly rejected by the SMF output mode filter, and thus the device should be more sensitive than a MMF *Elastica* with only the fundamental mode excited, and no output mode rejection.

In figure 8 we show the transmission response of such a structure. Note that the transmission response with the output SMF is much more sensitive to displacement than for the case of the MMF excited by the single mode fiber, but with no output mode filter. A notable feature with the SMF/MMF/SMF structure is that in the absence of bending, one can theoretically get about 67% (1.7 dB loss) of the light thru the structure (the loss is incurred in the square of the excitation efficiency from the mismatch of the fundamental mode of the SMF and the MMF). Coupling back into the SMF from the MMF incurs a loss penalty. Another interesting feature is the absence of whispering gallery oscillations in the SMF/MMF/SMF structure response, unlike the pure SMF *Elastica* of figure 5. Such oscillations are undesirable from a sensor point of view, since it is preferable that the device response be as smooth as possible.

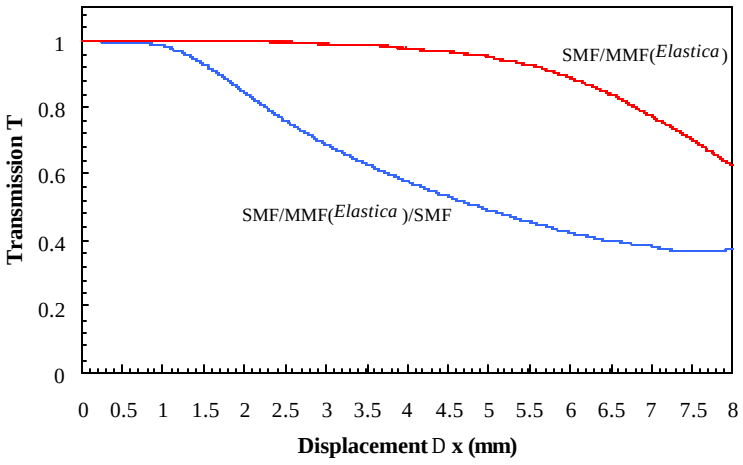

Fig. 8. *Transmission response comparing the SMF/MMF Elastica structure with primarily fundamental mode excitation and the SMF/MMF/SMF Elastica structure, Lo =14.93 mm. Note increased sensitivity due to output SMF mode filter, as evidenced by the large shift in threshold displacment and significantly increased loss at high displacements.*

Theoretical modeling of the SMF/MMF/SMF structure and the effects of variable mode excitation is currently in progress. It is an understatement to say that it is somewhat involved. The first and most time consuming task was to develop a unified and quantitatively accurate picture of the MMF core and cladding modes, so that one can study the coupled mode theory of the curved MMF. We have developed such a unified approach to graded index fiber core and cladding modes which is easily implemented on a PC. Once the modes of the staight fiber are computed, they form a convenient basis set in which to expand the field of the curved fiber.

OTDR Interrogation of Multimode *Elastica* and Enhanced Reflection Effects

When using Optical Time Domain Reflectometry to interrogate *Elastica* fiber optic sensors, it has been noticed that the traces often have a reflection preceding the loss across the sensor [Wanser and Voss, 1994a, Wanser *et al*., 1994b]. This is not the case for ordinary type of intensity loss transducers, such as those based on microbending or smooth macrobending [Wanser *et al*., 1993]. This enhanced reflection effect is very useful when using OTDR, since it gives a reflection signal that is considerably larger than the weak Rayleigh background signal, thus improving the signal to noise ratio rather than reducing it, as in ordinary intensity based sensors interrogated by OTDR. The effect of this improved signal to noise ratio is to allow much more rapid and accurate acquisition of data by requiring fewer signal averages for a given level of accuracy [Wanser et al., 1994c, 1994d].

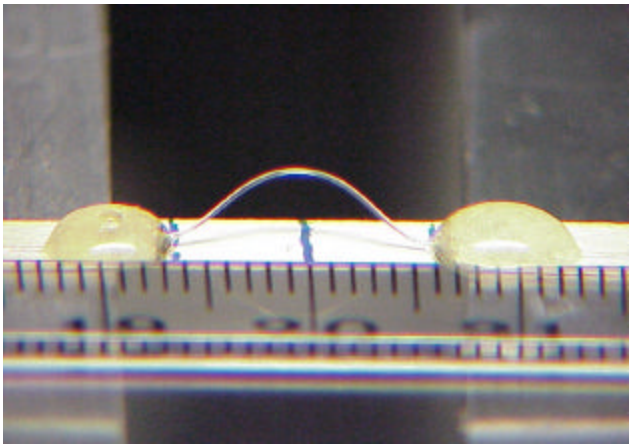

Fig. 9. *Elastica fiber sensor mounted on an elastomeric substrate.*

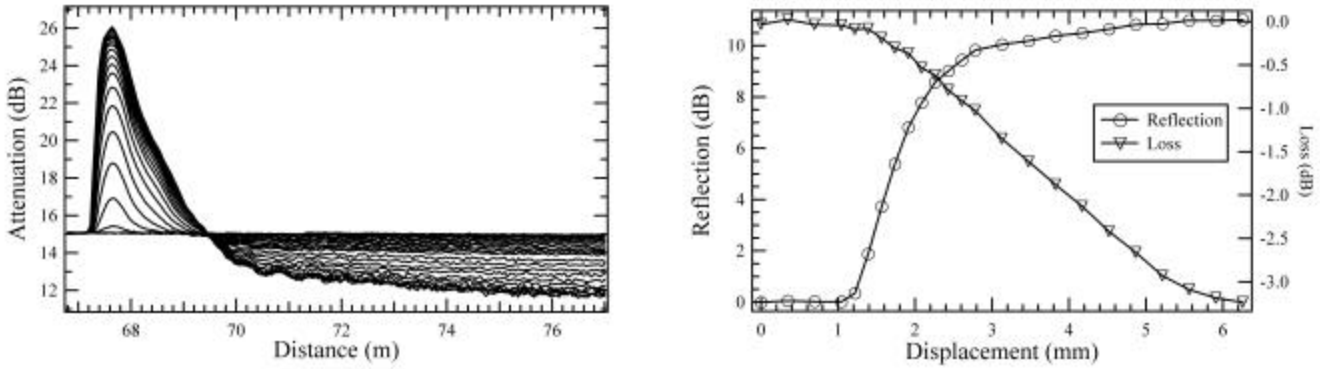

Fig. 10. *a.) OTDR traces for successive displacements of a 15.4 mm Elastica. Note the magnitude of the reflections compared to the loss. b.) Plot of reflection and loss data vs. displacement.*

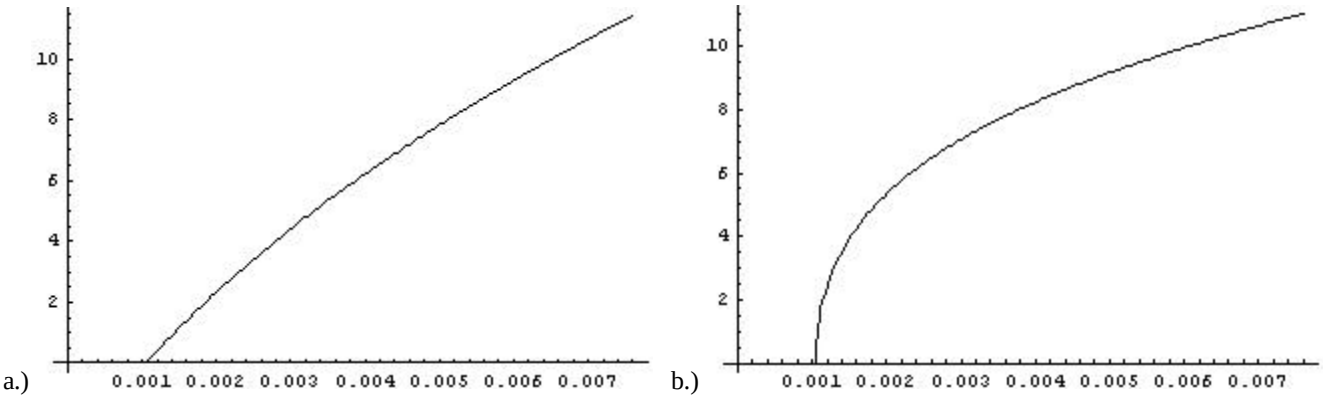

Fig. 11. *a.) Attenuation in dB vs. displacement (mm) for $1/R^2(0)$ reflection. b.) Attenuation in dB vs. displacement (mm) for 1/R(0) reflection, note the general agreement with the shape of the reflection curve of figure 9b.*

It was decided to investigate this effect in more detail, since its origin is not known and there was no theory describing it. A 15.4 mm *Elastica* was fabricated and mounted to an elastomeric substrate, as shown in figure 9. The purpose of this is to increase the sensing range of the transducer [Voss and Wanser, 1994, Wanser and Voss, 1997b] and allow mounting in cases where a large area is to be covered. OTDR data taken with 3 ns pulses at a wavelength 850 nm is shown in figure 10a. Note the increasingly large reflections from the sensor as a function of displacement as opposed to the much smaller change in loss. In figure 10b is plotted both the reflection data (as a dB gain) and the loss data. For this transducer, the reflection increases about 11 dB, while the corresponding loss for the same displacement is only about 3 dB. In addition, the reflection has a much larger slope and thus a higher sensitivity than the loss and also reaches saturation more quickly.

As part of an ambitious curved waveguide device modeling effort, we are currently investigating the theoretical explanation of these enhanced reflection results, a brief sketch of which will be given here. Details will be presented elsewhere. When the wave equation describing the curved fiber is transformed to the local coordinate system of an equivalent straight fiber, several additional terms involving the fiber radius of curvature appear. We have found an additional term in the wave equation which has to do with the rate of change of the inverse radius of curvature, that has been neglected in all prior work on optical fibers. This change in curvature term leads to significant back reflections in cases where the radius of curvature changes rapidly, or suddenly, such as in the case of a straight section of waveguide to one with a radius of curvature.

The back reflected modal amplitude is given by an expression which involves the Fourier transform of the derivative of the inverse curvature distribution of the fiber (all prior expressions have involved only the Fourier transform of the inverse curvature itself, not its derivative). The power reflection coefficient is proportional to the square of this Fourier transform.

As a very simple example of this formalism, for the special case of a sudden change in waveguide curvature, such as occurs in the transitions near points A and E in figure 1a., for the case of equal mode power distribution, the power reflection coefficient $\Re$ is given by

$$\Re = \frac{a^2 f}{R^2(0)}$$

with the dimensionless factor

$$f = \sum_{a,m}^{BM} \frac{b_m^2}{4 b_a^2 a^2 N_{bm}} \left| \int_A d^2x f_a \, r\cos\theta \, f_m \right|^2 \qquad [6]$$

In the above expression, $R(0)$ is the fiber radius of curvature at point A in figure 1a, N_{bm} is the number of bound modes of the fiber, b_a is the propagation constant for the ath mode of the fiber whose mode function is f_a, the integral involves overlaps between the fiber mode functions and the sums are over all the bound modes of the fiber. Note that this expression predicts that the shape of the reflection vs. displacement curve should scale as the inverse square of the initial fiber radius of curvature as a function

of *Elastica* displacement, as the other factors *a* and *f* are independent of the fiber displacement. Evaluation of the factor *f* is a formidable task, involving summing over several thousand terms for a multimode fiber, but since it is a proportionality constant, it is not necessary to do so in order to determine the shape of the reflection vs. displacement curve predicted by equation 6.

Figure 11 shows 2 graphs involving the initial radius of curvature of the fiber at points A and E as functions of displacement. Figure 11 a plots the inverse second power of the initial radius of curvature as a function of *Elastica* displacement, and figure 11 b plots the inverse first power of the initial radius of curvature as a function of displacement. As can be seen from the figures, the inverse first power is much closer to the shape of the experimental curve than the inverse second power, thus showing that the simple model of two isolated reflections due to sudden curvature at points A and E is inadequate. Currently we are investigating various curvature distributions as a function of displacement and modifications of these results due to fiber attenuation in the intervening space between points A and E in figure 1a. We are also developing methods to calculate the overlap integrals and perform the sum over all the modes that is required to calculate the absolute magnitude of the reflection, in order to validate that it arises from rapid changes in waveguide curvature.

Fiber Optic Strain Monitoring Inside a Power Plant Boiler

An important application for strain monitoring is in high temperature and harsh environments. As shown in figure 12, *Elastica* fiber sensors employing gold coated fiber and put in protective enclosures have been used to measure strain on a 48 foot long, 24 in. diameter steam pipe operating at ~1000°F inside the flue gas stream of a fossil fuel power plant [Wanser and Voss, 1997a]. Such large cold reheat headers commonly exhibited large permanent lateral deformations of several inches for unknown reasons, so a structural monitoring program was undertaken to diagnose the problem, since replacement of these headers is extremely costly.

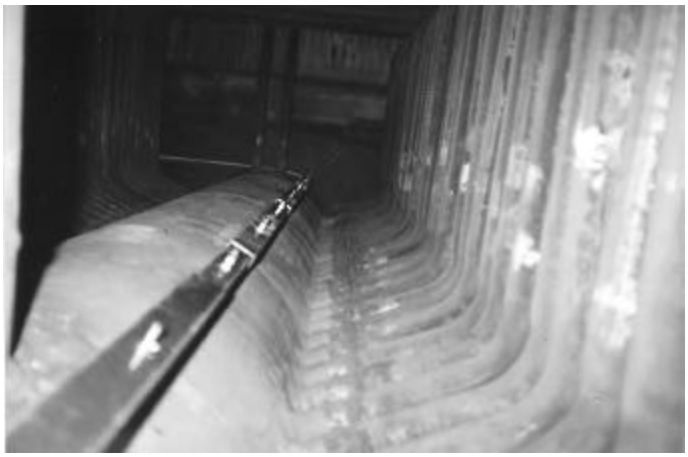

Fig. 12. *Photo of cold reheat header inside power plant boiler. Note numerous reheat tubes, and line of assembled sensors with enclosures, offset to avoid vertical reheat tubes.*

Several *Elastica* fiber sensors were mounted on the steam pipe and its strain was monitored for 6 months using a computer controlled OTDR system. Examination of station operating logs showed a correlation between the electrical load of the plant and the strain, indicating that the deflection the header experiences is related to the amount and pressure of the steam it carries. Consequently, we expect definite 24 hour periods in the strain of the header, as figure 13 demonstrates. Note the excellent strain resolution of the OTDR based sensor system. It is interesting that this large cyclic lateral bowing is near the room temperature yield point of the pipe material of 0.25% strain, thus explaining the permanent deformation which the pipe exhibits at room temperature, since the yield

point decreases with temperature. This 6 month high temperature structural monitoring program showed the stability and robustness of *Elastica* strain sensors for demanding measurements in harsh environments.

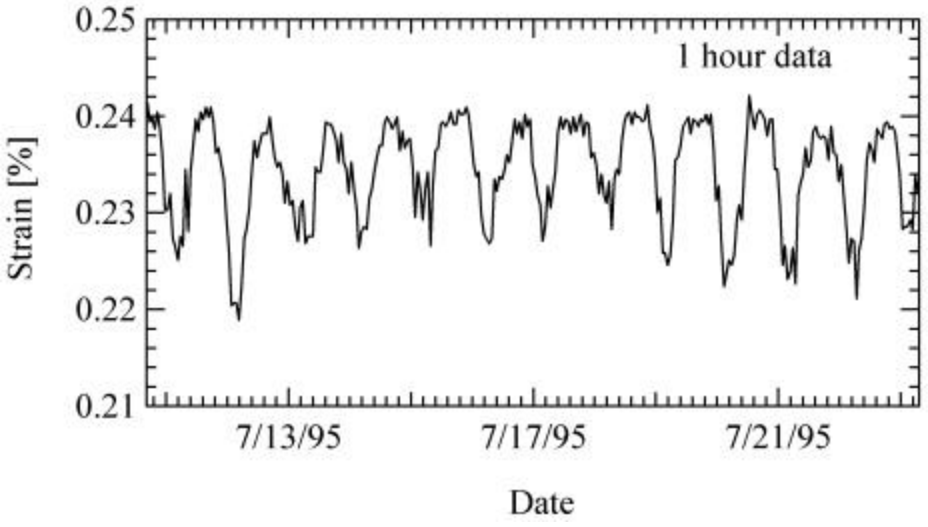

Fig. 13. *Cyclic header bowing at ~1000°F as measured with an Elastica fiber optic sensor and OTDR. Strain follows 24 hour power loading periods. Note sensor resolution of about 10 micro strain. Data sampling time was one hour.*

Inertial Balance with *Elastica* Fiber Optic Sensor

Elastica fiber sensors are well suited to a wide variety of demanding structural monitoring and engineering mechanics as well as geotechnical measurement situations. In order to demonstrate their utility in a simple situation on a vibrating "structure", we decided to upgrade a classic experiment in the introductory physics lab, the inertial balance. The inertial balance apparatus consists of two spring arms attached to a fixed mounting at one end and a platform which oscillates laterally at the other end. Students determine the period as a function of mass added to the platform by manually counting oscillations and unknown masses are measured once the period-added mass relationship is determined. This is a tedious and dizzying experience, especially if one counts 100 oscillations for several of the shorter periods (required for 1% accuracy), which are less than one second. Furthermore, the students have no experimental evidence that the balance acts like a damped simple harmonic oscillator.

A 10 mm length reflection mode *Elastica* fiber sensor was magnetically attached near the fixed end of one spring arm of the inertial balance, as shown in figure 14. This was possible due to the extremely low force constant of *Elastica* fiber sensors, (in the range of 0.02 N/mm) which produces negligible loading to the structure when it is attached to it. This important property of *Elastica* fiber sensors ensures excellent strain transfer, even for very soft, low-modulus and flexible materials, and allows numerous methods of attachment to the structure of interest. The sensor was prebiased to 1.17 mm and calibrated by displacing the balance platform laterally and measuring the sensor response. The sensor response was extremely linear for platform lateral displacements as large as ± 4 cm (which is much larger than is usually used in student experiments).

Figure 15 shows the damping of the oscillations of the balance with 3 kg mass added to the platform, when released with an initial 4 cm lateral displacement. Figure 16 shows the harmonic nature of the oscillations and analysis of the data reveals an oscillation frequency of 0.51 Hz. Clearly students can learn much more about damped harmonic motion from such detailed data, and have a much more enjoyable learning experience in the process. This application is just one simple example of how the novel properties of *Elastica* fiber sensors can be easily and cost effectively employed in numerous structural monitoring and engineering mechanics measurement situations.

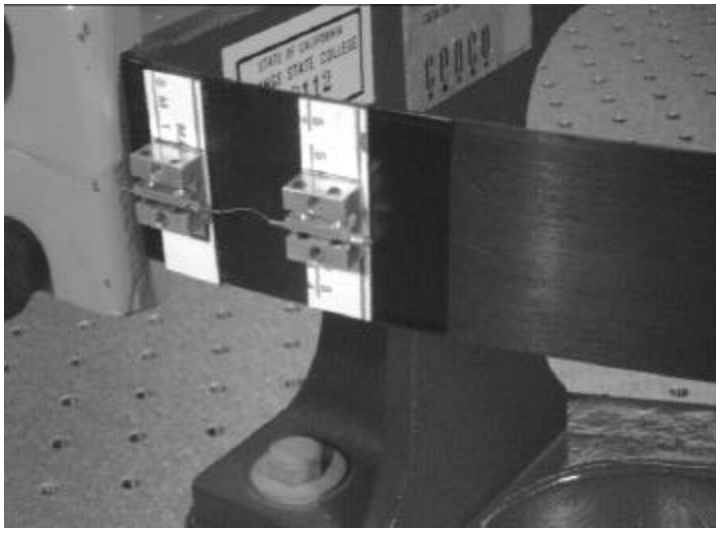

Fig. 14. *Close up of reflection mode Elastica fiber sensor magnetically mounted on inertial balance. Sensor brackets are attached to balance arm springs with two thin flat magnets (white rectangles).*

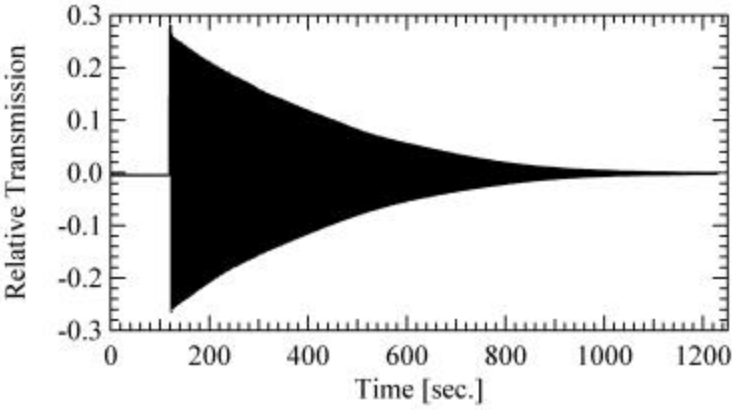

Fig. 15. *Ring down of inertial balance with 3 kg mass added to 0.883 kg platform, as measured with a 10 mm Elastica fiber optic sensor.*

SUMMARY

We have presented several unique properties of *Elastica* fiber sensors which allow their use in many demanding sensing applications. While much progress on the use of *Elastica* fiber optic sensors has been made, there are many additional aspects of these sensors that need further investigation so that they can be designed for even better performance in the future. The enhanced reflection aspects of the sensors need to be quantitatively understood for applications involving OTDR and a promising theory for this effect has been formulated. The use of combined SMF/MMF/SMF structures operated in reflection mode is very promising to eliminate input lead mode sensitivity and whispering gallery nonlinear effects associated with single mode fiber *Elastica*. We invite those of you who are involved in geotechnical and infrastructure work to consider the advantages of using *Elastica* fiber sensors in your novel applications in order to prove their usefulness in a variety of situations. We believe that these sensors will eventually find wide use due to their many unique operating characteristics, ease of fabrication and attachment, and potential for low cost. Please feel free to contact us if you are interested in using *Elastica* fiber sensors in your research and development projects or other applications.

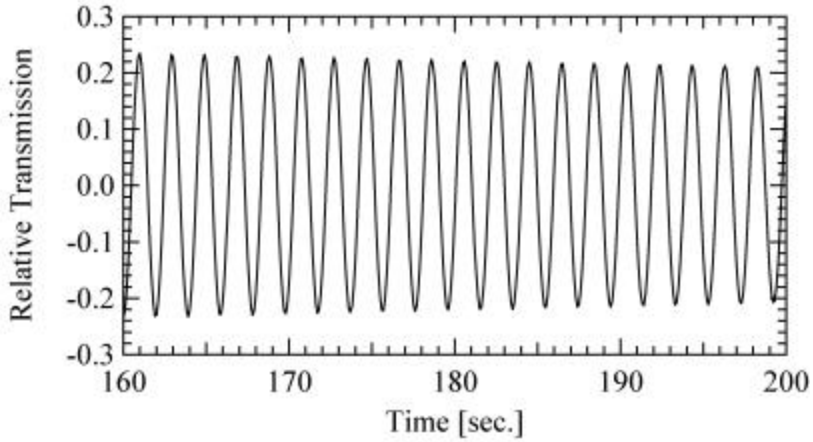

Fig. 16. *Expanded view of 3 kg added mass data showing 0.51 Hz oscillations of the balance sampled at 10 Hz.*

ACKNOWLEDGEMENTS

We especially wish to thank Karl Peters for encouragement, fabrication of fiber mirrors, and support of the infrastructure of the laboratory. This work was partially supported by NSF grant ECS 98-00030.

REFERENCES

Belansky, R. H., 2001, Curvature Effects in Single Mode and Multimode Optical fibers and Fiber Bragg Gratings, M.S. Thesis, California State University Fullerton, Fullerton, CA.

---------- 1998, *Elastica* Fiber Optic Sensors for Structural Monitoring; Fiber Optic Sensors for Construction Materials & Bridges: F. Ansari, ed., Technomic Publishing, Lancaster, PA, 231-242.

Culshaw, B., 1998, Collected Papers of the International Conferences on Optical Fiber Sensors (OFS) 1983-1997, Compiled and published by SPIE, OSA, and IEEE/LEOS.Marcuse, D., 1976, Curvature Loss Formula for Optical Fibers, J. Opt. Soc. Am., **66**, 216-220.

Marcuse, D., 1993, Bend Loss of Slab and Fiber Modes Computed with Diffraction Theory, IEEE J. Quantum Electronics, **29**, 2957-2961.

Poole, C. D., and Wang, S. C., 1993, Bend-induced loss for the higher-order spatial mode in a dual-mode fiber, Opt. Lett., **18**, 20-23.

Sharma, A.B., Al-Ani, A.-H., and Halme, S.J., 1984, Constant-curvature loss in monomode fibers: an experimental investigation, Appl. Opt. **23**, 3297-3301.

Snyder, A. W. and Love, J. D., 1983, Optical Waveguide Theory, Chapman and Hall, London, 481.

Voss K. F. and Wanser K. H., 1994, Fiber Sensors for Monitoring Structural Strain and Cracks; Proc. 2nd European Conference on Smart Structures and Materials (ECSSM 2), Glasgow, Scotland: SPIE, 144-147.

----------, 1997, Fiber-Optic Strain-Displacement Sensor Employing Nonlinear Buckling; Applied Optics, **36**, 2944-2946.

Wanser, K. H., Haselhuhn, M., Lafond, M., and Williams, J., 1993. Distributed Fiber Optic Sensors for Civil Structures using OTDR, Applications of Fiber Optic Sensors in Engineering Mechanics, F. Ansari, ed., American Society of Civil Engineers, New York, 303-327.

Wanser, K. H. and Voss, K. F., 1994a, Crack Detection using Multimode Fiber Optical Time Domain Reflectometry; Distributed and Multiplexed Fiber Optic Sensors IV, Proc. SPIE 2294, 43-52.

---------, 1997a, Fiber Optic Strain Monitoring Inside a Power Plant Boiler, *Intelligent Civil Engineering Materials and Structures*, F. Ansari, A. Maji, and C. Leung, eds., American Society of Civil Engineers, New York, 213-228.

----------, 1997b, Strain Sensors Having Ultra-High Dynamic Range, U. S. Patent #5,668,324.

Wanser, K. H., Voss, K. F., and Francis, K. R., 1998, *Elastica* Fiber Optic Sensors for Structural Monitoring; Fiber Optic Sensors for Construction Materials & Bridges: F. Ansari, ed., Technomic Publishing, Lancaster, PA, 231-242.

Wanser K. H., Voss, K. F., and Griffiths R. W., 1994b. Distributed Fiber Optic Sensors for Structural Health and Vibration Monitoring using Optical Time Domain Reflectometry, Proc. First World Conference on Structural Control (1WCSC), Pasadena, CA, WA3-3-WA3-12.

Wanser, K. H. , Voss, K. F., and Kersey, A. D., 1994c. Novel Fiber Devices and Sensors based on Multimode Fiber Bragg Gratings, Proc. 10th International Conference on Optical Fiber Sensors, Glasgow, Scotland, 265-268.

----------, 1994d, Multimode Fiber Bragg Gratings for Real Time Structural Monitoring using Optical Time Domain Reflectometry; Time Domain Reflectometry in Environmental, Infrastructure, and Mining Applications, U. S. Bureau of Mines Special Publication SP 19-94, 472-483.

DETECTION OF SHEARING IN SOFT SOILS WITH COMPLIANTLY GROUTED TDR CABLES

C.H. Dowding[1], R.G. Cole[2], C.E. Pierce[3]

[1] Professor, Department of Civil Engineering, Northwestern University, Evanston, IL; c-dowding@northwestern.edu
[2] Engineer, Geosyntec, Huntington Beach, CA; colerichard@hotmail.com
[3] Asst. Professor, Department of Civil Engineering, University of South Carolina; piercec@engr.sc.edu

ABSTRACT

This article presents field and laboratory data that support the use of TDR cable deformity to monitor deformation in soil. While TDR has been employed successfully in rock with 100's of installations world wide, it has yet to be shown convincingly to be operable in soft soils. This article is a first step to over come that deficiency. Two case histories are presented herein to illustrate proper installation procedures in soft soils. Force equilibrium and force-deformation analyses of the installed cable-grout composites are employed to quantitatively describe observed behavior as well as provide methods to configure cable-grout composites in other geologies. Optimal combinations of flexible cables and compliant grouts are described to assist in future installations.

Key Words: soil, slope stability, monitoring, remote operation, TDR, coaxial cables, shear zone, localized shearing, slope inclinometer

INTRODUCTION

Surveillance of deformation with TDR (time domain reflectometry) cables is similar to radar probing in a cable. A voltage pulse is launched along a cable grouted into the surrounding rock or soil by an up-hole pulser as shown in Figure 1 a&b). The signal propagates down the cable until it intersects a change in the cable geometry caused by a deformity of the surrounding medium. This deformity reflects a portion of the signal shown by the spike in c). Just as with radar, the time of flight to the reflection is proportional to the distance between pulser and deformity. The intensity of the reflection spike is proportional to the change in cable geometry, which in turn is proportional to the amount of shearing in the rock or soil. TDR's completely digital nature renders it a natural candidate for remote monitoring. Furthermore its ability to detect thin shear zones make it an ideal tool to measure strain localization and compliments the slope inclinometer.

This article presents field and laboratory data that support the use of TDR technology to monitor deformation in soil. While TDR has been employed successfully in rock with 100's of installations world wide (O'Connor & Dowding, 1999), it has yet to be shown convincingly to be operable in soft soils. This article is a first step to over come that deficiency. Two case histories are presented herein to illustrate proper installation procedures in soft soils. Force equilibrium and force-deformation analyses of the installed cable-grout composites are employed to quantitatively describe observed behavior as well as provide methods to configure cable-grout composites in other geologies. Optimal combinations of flexible cables and compliant grouts are described to assist in future installations.

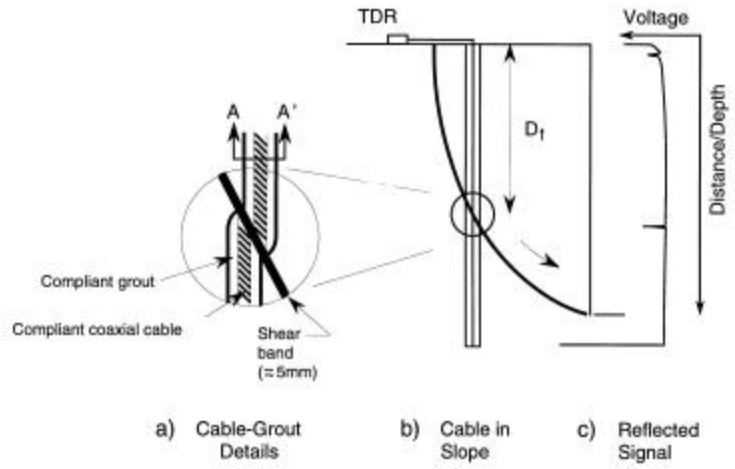

Fig. 1. *Geometry of coaxial cable grouted in failing slope and the TDR voltage spike reflected by the cable distortion produced by the intersecting shear zone.*

EXAMPLE TDR PERFORMANCE

Until recently, TDR measurements have been successful mainly in rock as shown in Figure 2a. The cable in this example is being sheared during collapse of overburden above a longwall mine as the 300m wide face advances by underneath. Spike amplitudes grow at a) b) & c) as the face advances and causes shear displacement along discontinuities in the collapsing rock mass above the mine. Eventually the cable was severed at c) and then b) as shear stresses propagated upward. Use of this technology is well-documented (Dowding and Huang, 1994, and O'Connor and Dowding, 1999).

If properly installed, recent experience shown in Figure 2b illustrates that TDR technology can detect shear deformation in soft soil, just as in rock. In this example a standard 22 mm diameter, aluminum outer conductor cable was grouted in a 98 mm hole that passed through the bottom of the shear zone within the soft clay layer underlying a deforming fill. A low strength, cement-bentonite grout was employed in an attempt to approach the soil strength without being so soft as not to be able to kink or deform the cable. As shown, two spikes appeared in the shear zone, e), after some 2 mm of incremental displacement as measured by an adjacent slope inclinometer. The grout's unconfined compressive strength of 0.5 Mpa (70 psi) was only some 10 to 20 times greater than the unconfined compressive strength of the clay, 0.025-0.05 Mpa (3.5 to 7 psi) (Cole, 1999). Others (Anderson and Welch, 2000, and Kane, 2000) are beginning to report successful installations of TDR cables in soils to monitor shearing deformations.

COMPARISON OF TWO CASE HISTORIES OF CABLE RESPONSES IN DEFORMING SOIL

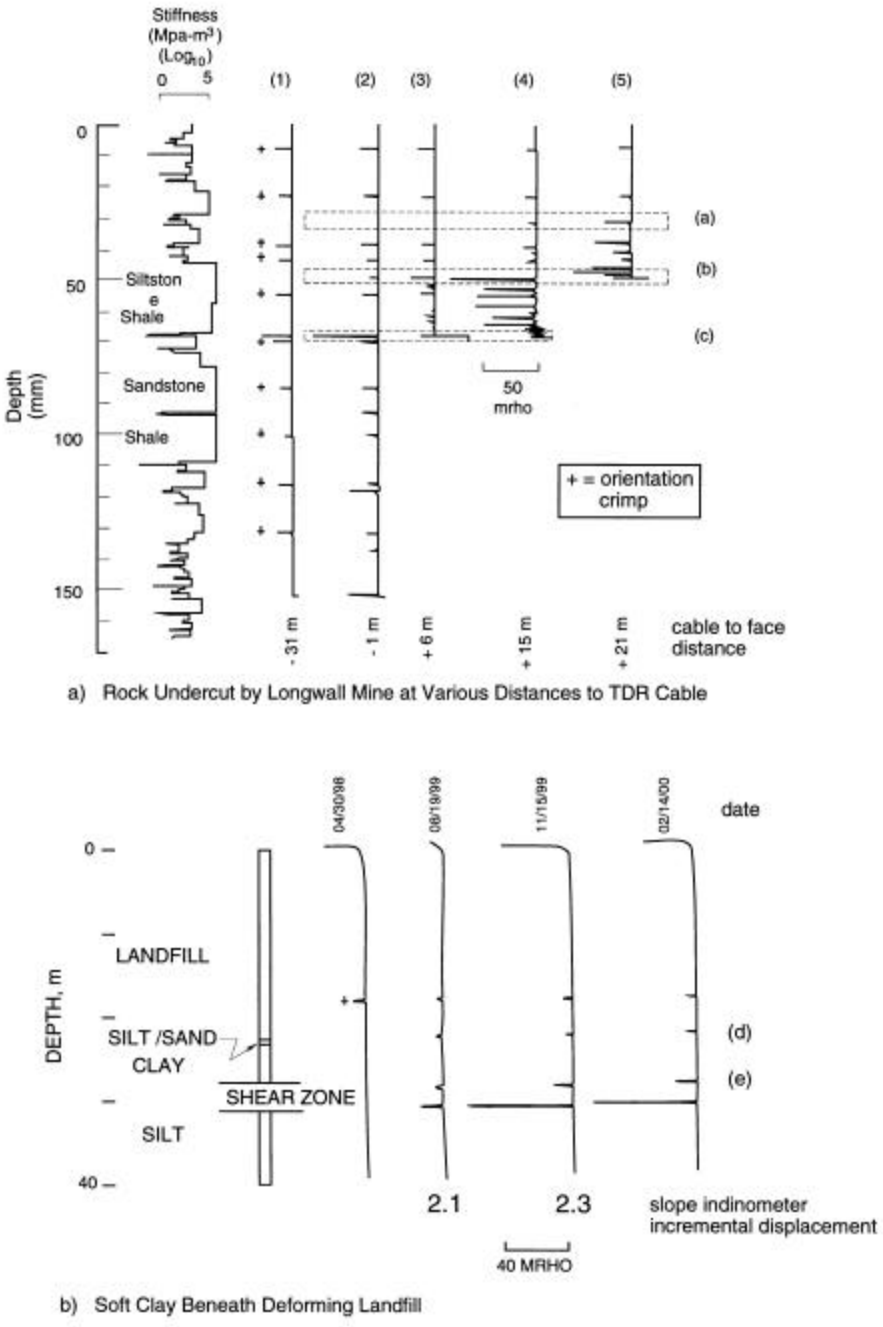

Fig. 2. *Comparison of the TDR voltage reflection signatures from distortions of coaxial cables grouted in rock a) and soft soil b) undergoing large deformations*

Two case studies, summarized in Table 1, have been chosen for description for their uniformity of observation, as well as to set the stage for later analysis. At both sites, slope inclinometers were installed adjacent to the cables for comparison of deformation. Among the three different cables installed, a standard, solid aluminum outer conductor cable was installed at each site. Each case involves cables installed in soft glacial lake clay in or near Chicago with similar diameter holes. However, there are differences in the grout strength and bending stiffness of the cable-grout composites. As elaborated below, the response varied significantly between cables and sites. The landfill case involved greater and more localized movement then the braced cut and produced the greatest deformation of the solid aluminum coaxial cable in combination with the weakest grout. This combination had the least composite bending stiffness.

Field sensitivity of the weakly grouted, aluminum outer conductor cable can be estimated by comparing the slope inclinometer incremental displacement with the cable reflection response at the fill in Figure 3. Incremental displacement is the change in displacement over the 60-cm wheel-base of the slope inclinometer. The combination of incremental displacement along the casing produces, the more common cumulative displacement profile. Consider the TDR response within the shear zone, e) in Figure 2b. In August 1999 the inclinometer incremental displacement reached 2mm at

the elevation of the TDR spike, and the TDR cable reflection was 2% (or 20 milli rhos, mD) of the input voltage signal. The actual reflection magnitude was most likely greater since the reflection exceeded the range at that reading and was truncated. Three months later the reflection had reached 9% and the incremental displacement had increased to 2.3 mm. There was a cumulative displacement of 20 mm across the 3 m thick shear zone.

The importance of soil stiffness can be seen by the early response of the spike d). Early in August of 1998, 4 months after installation, the TDR cable responded with a 0.5% reflection at the silt layer between the stiffer overlying fill and the underlying soft clay. The stiffer fill probably provided sufficient adjacent soil stiffness so that small shears kinked the cable with no measurable inclinometer incremental displacement. The amplitude of this spike has not changed since August 1998.

A measure of the sensitivity of the slope inclinometer to displacement along thin or narrow shear bands can be gleaned from these data. Reflection sensitivity of bare cable subjected to direct shear in the laboratory (in a metal shear box that holds only the cable) is also plotted in Figure 3. Laboratory sensitivity is the ratio of TDR reflected voltage to direct shearing deformation by the box. Field sensitivity is the ratio of TDR reflected voltage to inclinometer incremental displacement at the elevation of the reflection spike. The laboratory sensitivity is far less than that in the field, which may indicate that the inclinometer is under reporting incremental displacement along thin zones within the shear band. While this is an almost heretical observation with respect to the slope inclinometer, it seems probable given its inherent difficulty in detecting movement along thin shear bands (Bromhead, 1986). This difference between laboratory and field sensitivity cannot be explained by insensitivity of the TDR cable. In this case it is much more sensitive in the field than the laboratory when field sensitivity is based on rudimentary inclinometer incremental displacement.

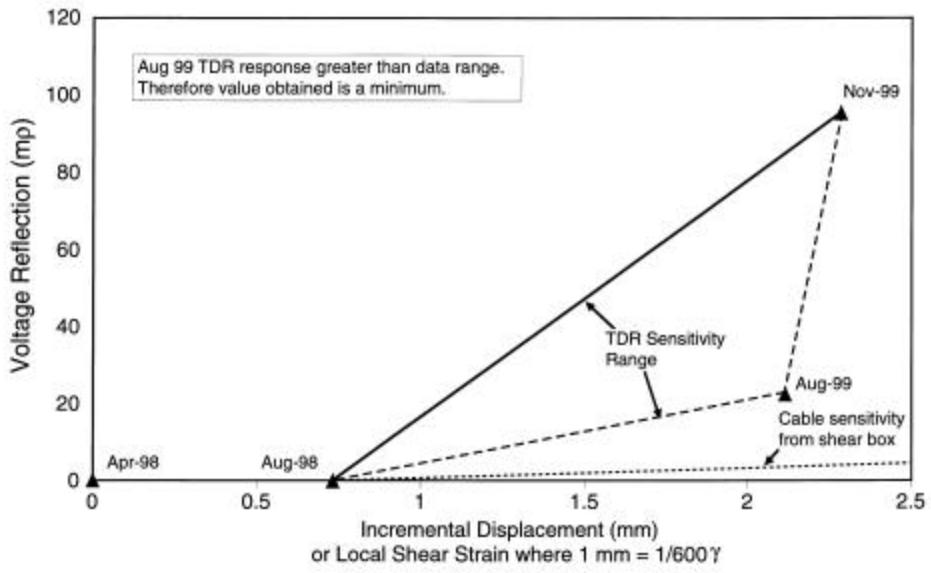

Fig. 3. *Comparison of voltage reflections and inclinometer incremental displacements in the shear zone of the deforming soft soil described in Figure 2b).*

At the braced cut the much smaller cumulative displacements (and thus strains), only 5 mm over the 12 m height of the excavation, produced no TDR response. There are two possible reasons for this non-response. First, there was far less movement of the soil mass beside the excavation. The comparative cumulative displacement at the fill shear zone was 20 mm across a shear zone thickness of only 3 m. Second, the grout

around the braced cut cables was a great deal stronger than at the fill site. Thus greater displacements of the soil would be required to develop the soil reaction necessary to shear through the grout and kink the cable, as will be shown below in the deformation analysis of soil-inclusion interaction.

	Cable					Grout						Cable-Grout	Soil			Response	
Case History	Type	Diam (mm)	Imp (Ohm)	Length (m)		Hole Diam (mm)	q_u (MPa)	E (MPa)	Grout Mix (%)			Bending Stiffness, EI (GN.m^2)	Type	q_u (Mpa)	E (MPa)	Cable Reflection % of Initial Voltage	Cumulative (incremental displacements (mm) *
				Train	Lead				W	C	B						
Deforming Fill	Solid Aluminum	22.2	75.0	39.6	0.0	98.0	0.5	100.0	65.0	33.0	2.0	7.6	Soft Glacial Clay	0.025 to 0.050	6 to 25	10.0	20 (2.3)
	Braided outer conductor	12.7	75.0	29.9	0.0	74.0	3.9	800.0	48.0	50.0	2.0	2.0	Soft Glacial Clay	0.025 to 0.050	6 to 25	0.0	11 (1.5)
Braced Excavation	Solid Aluminum	22.2	75.0	18.2	8.2	98.0	1.2	285.0	65.0	38.0	2.0	8.6	Soft Glacial Clay	0.034	5.2	0.0	5 (0?)
	Braided outer conductor	21.0		12.6	9.4	98.0	1.2	285.0	65.0	38.0	2.0	8.4	Soft Glacial Clay	0.034	5.2	0.0	5 (0?)

Table 1 * as of November '99

Neither of the other non-standard braided cables, described in Table 1, responded at either site. At the braced cut, the more compliant cable has not responded since there has not been sufficient deformation to fail the grout. At the fill site, the small, braided cable-grout composite is stiffer because of the stronger grout. Furthermore, at this location in the slope, the maximum incremental displacement in the shear zone is only 1.5 mm and the cumulative displacement across the shear zone is only 11 mm. Therefore, it is logical that for these three reasons -- cable size, grout strength, & compliance -- there would be less TDR response.

FORCE BALANCE ESTIMATE OF MAXIMUM GROUT STRENGTH FOR SOFT SOIL

Interaction between a cable/grout composite and a shearing soil mass is analogous to the resistance and behavior of soil nails as shown in Figure 4a. As the shear zone applies a shear force and moment to the intersecting cable/grout composite, its deformation first elicits an elastic response along length L_o in 4b, which upon further deformation becomes plastic, with a maximum bearing resistance, p_{max}. Soil nails are designed (currently based upon beam on an elastic foundation analysis) to prevent shear zones while simultaneously maintaining an elastic soil response. On the other hand the TDR cable-grout configuration (or design) must shear easily while maintaining an elastic soil response above and below the shear zone to localize kinking as much as possible.

Cable/grout-soil interaction can be crudely approximated by equating the force necessary to shear through a grout filled hole to the passive reaction offered by soft clay to that deformation. As shown in Figure 4b, if the shear deformation is imposed upon the grout filled hole, it will be resisted by the soil adjacent to the shear band on the upstream side of the deformation direction. It is important that there be little plastic deformation of this adjacent soil so that the shear band in the grout is as sharply defined as possible. The more abrupt the boundary between the upstream and downstream passive resistance zones in the soil, the narrower the fracture zone within the grout, the sharper the kink within the cable, and

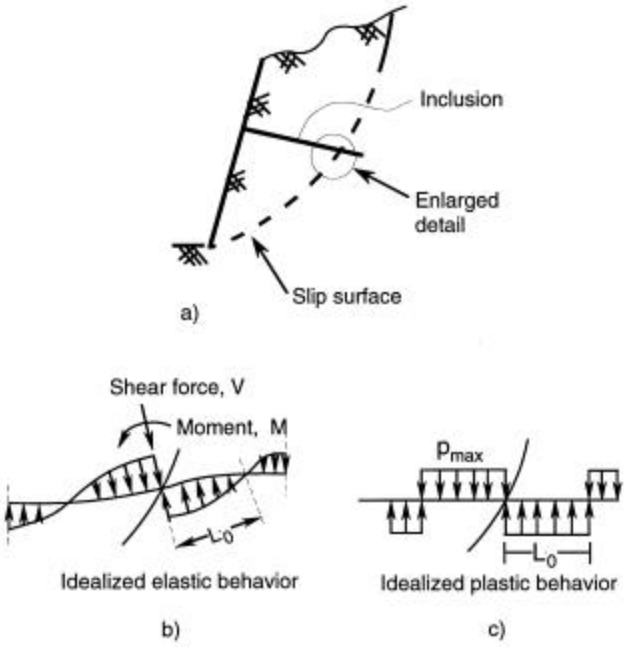

Fig. 4. *Force-balance model for interaction of cable-grout inclusion in soil showing development of localized elastic and plastic soil reaction to increasing displacement along localized slip (shear) surface .(zone).*

thus the larger will be the reflected TDR voltage signal per unit shear deformation. These tendencies have been observed in laboratory measurements as will be discussed below.

Balancing shear forces within the grout with soil bearing forces requires that soil resistance be estimated. Bearing capacity factors for deep foundations as well as those for anchors deeply buried in soft clay provide guidance in the matter. If the soil resisting force is normalized by the cross sectional area, resistance can be calculated as a function of the soil shear strength, S_{us}. Based on two-dimensional plastic analysis, soil resistance is 9 times the shear strength. Three-dimensional studies of the extraction of isolated circular and square anchors (McKenzie, 1955) revealed that soil resistance may be as high as 14 times the un-drained shear strength. If it is assumed that this resistance is distributed equally along a grouted cable for a length of one diameter, D, then it will act over an area of D^2 (i.e., assume L_o in Figure 4b is D). Thus, the maximum soil bearing resistance or capacity is

$$(9 - 14)\, S_{us}\, D^2 \qquad [1]$$

The shear force within of the grout can be estimated as the bore hole area times the shear strength of the grout, S_{ug},

$$S_{ug}\, \pi\, D^2/4 \qquad [2]$$

Equating (1) and (2) then allows an estimate of the maximum strength of the grout that can be employed relative to that of the soil to preserve the narrowest or "true" width of an intersecting shear zone

$$(9 - 14)\, S_{us}\, D^2 = S_{ug}\, \pi\, D^2/4,$$

thus

$$S_{ug} / S_{us} = (4/\pi)\,(9\text{-}14) = 11 \text{ to } 18 \qquad [3]$$

This estimate can be checked for reasonableness by comparing the properties of the soil and grout for the landfill case history. As shown in Table 1, soil shear strength was 0.0125 to 0.025 MPa and the grout shear strength was 0.25 Mpa for the responding cable. Thus the ratio of grout to soil shear strength was 10 to 20, which is similar to that estimated from force-balance considerations.

A further check on the reasonableness of the force balance approach can be obtained from laboratory behavior of the cable-grout composite, Cole (1999). His results showed that a force of 2.8 kN (640 lbs) was necessary to shear a 22 mm diameter aluminum outer conductor cable sealed into a slotted 200 mm (4 in) diameter PVC pipe by a grout with an unconfined compressive strength of 0.6 Mpa (i.e., shear strength of 0.3 Mpa (43 psi)). Shearing by this weak grout was sufficient to produce a significant voltage reflection at the end of a 15m cable. Can a soft clay produce sufficient reaction (without failing) over a sufficiently narrow zone to produce the 2.8 kN force necessary to shear the grout and thus kink the cable? The maximum soil force calculated with equation (1) is:

$$(9 \text{ to } 14)\ (0.0125 \text{ to } 0.025 \text{ MPa})\ D^2 = 1.2 \text{ to } 3.6 \text{ kN}$$

These estimated soil resistances bracket the force necessary to sufficiently deform the cable-grout composite and produce a significant TDR reflection.

FORCE-DEFORMATION INTERACTION OF CABLE-GROUT INCLUSION WITH SOFT CLAY

The next level of analytical sophistication beyond force balance would be a force – deformation analysis. Since soil and inclusion stiffness effects are included in "p-δ" approaches for the analysis of laterally loaded piles, these seemed ideal candidates. Consequently, LPILE (Reese & Wang, 1989) was adapted for use with grouted cables by Pierce (1998), and was validated by analyzing indentation depths of cables sheared with "compliant" grouts. LPILE extends the linearly elastic, Winkler spring theory to include a nonlinear response of the soil surrounding the inclusion. This nonlinear response for soft soils, shown in Figure 5, consists of three regions. First with region (1) the soil (spring) responds linearly (elastically) up to a deformation, δ, of 5% of the inclusion diameter, D, at a maximum resistance per unit length, p, ½ the ultimate resistance, p_{max}. Next, in region (2), the response is deformation hardening for δ up to 16 (0.05D) according to the relationship in Figure 5. Finally, in region (3) the response is fully plastic, with $p = p_{max}$. This approach is slightly more sophisticated than previous two dimensional, bilinear approaches employed to analyze soil nails shown in Figure 4 (Schlosser, 1982).

Instead of a pile, the inclusion is a cable-grout composite with the aluminum coaxial cable. Its bending stiffness is calculated (Equation 4 in the next section) with a standard composite approach that includes the cable and grout column. The ultimate strength of the soil is taken to be $9\ S_{u,}$ in order to be consistent with previous use of LPILE to match field results. Thus the ultimate resistance per length is $9\ S_{us}\ D$. Figure 5 presents the resulting p-δ relationship for cables grouted in soft glacial lake clays at the fill site and the braced cut. Properties of the composites and soils employed in the analysis for these two sites were presented in Table 1.

Pierce's adaptation of LPILE for grouted cables is based on calculation of the soil deformation necessary to fracture the grout in the (grout-cable)-soil composite. Calculated deformation necessary for grout fracture should correlate with the lateral deformation associated with the first significant TDR reflection. This approach was confirmed in the laboratory by shearing a cable-grout (no soil) composite and comparing the measured and LPILE calculated indentation of the cable into the grout. To simulate field response, the force necessary to fracture the grout is applied to the cable-grout inclusion and the resulting deformation of the surrounding soil is calculated via LPILE. The lateral load necessary to fracture the 500 kPa grout-cable composite was assumed to be the same as that for the 600 kPa grout or

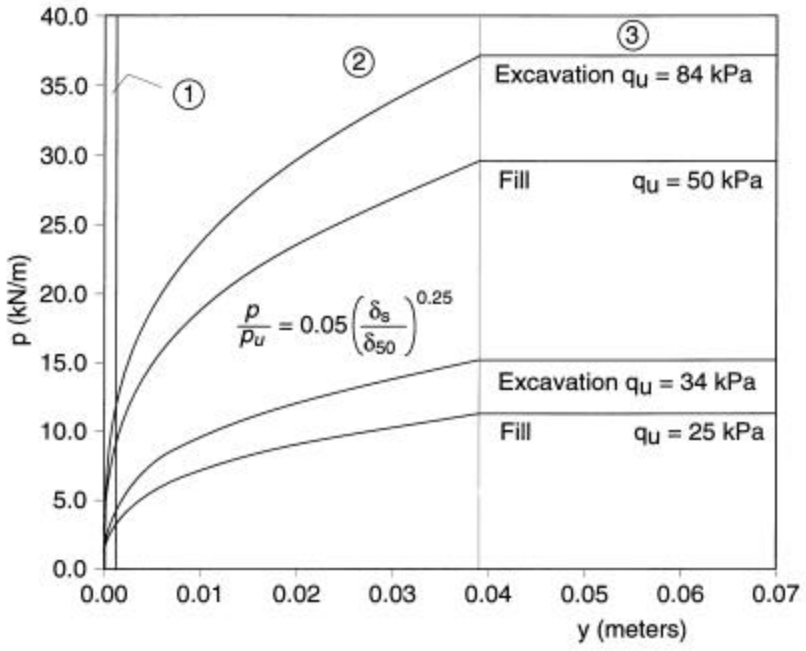

Fig. 5. *Nonlinear lateral force (p) - displacement (*) relationships for interaction of soft clays with 100 mm diameter cable-weak grout composites at the fill and excavation sites.*

2.9 kN (Cole, 2000). The force necessary to fracture higher strength grouts with the same size hole and cable was simply scaled proportionally to the grout strength.

Figure 6 compares the deformed shape of the cable-grout composite calculated with the cable-grout-soil properties from the two sites. The analysis in Figure 6 shows that applying the grout fracture force to the cable-grout composite beneath the fill will deform the surrounding soil by 5 to 21 mm. Or in other words, some 5 to 21 mm of local shearing is required at the shear zone beneath the fill to mobilize the force necessary to fracture the cable-grout composite, depending upon the soil strength. (qu = 25 to 50Kpa) Local shearing means that which occurs across a thin (thickness measured in mm's) localized shear zone. For comparison with the measured deformation, as discussed in the case history section, Figure 3 compares TDR waveforms and inclinometer incremental displacement. Between April of 1998 and August of 1998 there was only 1.5 mm of incremental displacement (across the vertical distance of 60 cm between inclinometer wheels). There was no cable deformation detected using TDR. By August of 1999, additional incremental displacement of 0.06 mm had occurred in the shear zone for a total of 2.1 mm. There had also been some 20 mm of cumulative displacement across the 3 m thick shear zone since cable installation. This incremental and cumulative displacement field, as measured by the inclinometer, produced two significant reflections in the shear zone as seen at e) in Figure 2.

The same analysis of the cable-grout composite for the soil at the braced cut, reveals that some 12 to 43 mm of local shearing would be required because of the much stronger grout. With only 5mm of cumulative displacement, over a 12 m depth, no cable deformation has been detected using TDR. During installation, a field change resulted in repositioning of a lower tier anchor, which penetrated both the TDR cable and the adjacent inclinometer, rendering them both inoperable below this depth. As a result, cumulative displacements were estimated from an inclinometer located on the opposite side of the excavation.

The LPILE model has limitations but provides a rational basis for estimating the amount of movement required to fracture the grout at the landfill. There are several reasons why the calculated displacements exceed the field measurements. First, the inclinometer is not sensitive to the incremental displacement across thin shear zones as discussed in the case history section. Thus the localized field displacement is probably larger than measured with the inclinometer. Secondly, the bearing capacity factor, (N, = 9)

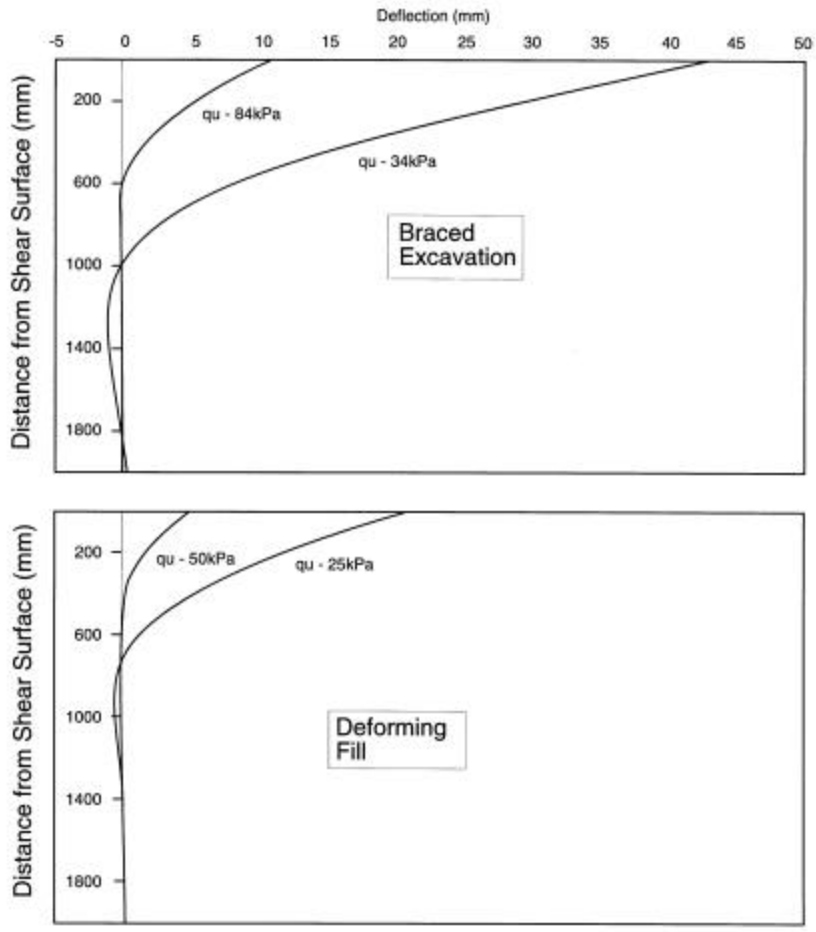

Fig. 6. *Calculated transverse cable deflections at the excavation and fill sites produced by application of interface shear forces equal to the appropriate failure loads for the weak grout filled holes*

employed to estimate the bearing resistance of the clay is less than the 14, which might have been more appropriate as described in the force balance analysis. The lower N was employed for consistency with LPILE experience. Since LPILE analyses have been validated at smaller depth–to-diameter ratios for piles, use of a larger N may be more appropriate. Use of N = 12 would have reduced the calculated deformation necessary to fracture the grout by 33 %. These reduced deformations would have been more consistent with field measurements.

LPILE has additional limitations because it is fundamentally not a three dimensional model and the behavior of a grouted cable intersected by a shear zone is a three-dimensional interaction problem. This deficiency is partly compensated with the p-y curves, which are based on three dimensional load tests; however, a three-dimensional finite element model to simulate the soil-grout-cable interaction would improve on the two dimensional approach. A finite element approach would also allow the cable-and grout to be modeled as two separate materials, rather than a composite as was the case in this analysis.

PRACTICAL CONSIDERATIONS

Compliant Coaxial Cable Properties

Five cable attributes contribute to their sensitivity when grouted into soft soil. They will be only briefly summarized here; more complete discussion can be found in previous publications (Cole, 1999; Pierce, 1998; Will, 1997). Most importantly, the cable should have both a low axial bending stiffness as well as a low transverse shear stiffness to match that of the surrounding low strength grout and soil. Second, the diameter should be large to track shear displacements as long as possible. Third, its characteristic impedance should be between 50 and 75 ohms to match commercially available pulser impedances and reduce reflections at the cable-pulser interface. Low characteristic impedance also reduces attenuation

of the launched and reflected voltage pulses, which is the forth consideration. Finally, the cable must have a high laboratory reflection sensitivity to produce as large a reflection as possible per unit shear deformation.

Coaxial cables consist of three principal components: inner conductor, dielectric separator, and concentric outer conductor. Electrical details of the variations of cable construction and the implications for geotechnical use is extensively discussed in O'Connor and Dowding (1999), and will not be covered herein. However, there are a few fundamental constraints on cable design (Pierce, 1998). For impedances between 50 and 75 ohms, the diameter ratio of inner to outer conductors must be 2.3 to 3.5 if the separator material has a dielectric constant of one. Thus large diameter cables tend to have large inner conductors to preserve low impedance. Fortunately larger inner conductors also reduce attenuation.

The six cables listed in Table 2 were evaluated with the above five attributes in mind. The lower three in the table were purchased commercially and the upper three were built at Northwestern University. Of the commercially available cables, the 22 mm, solid aluminum outer conductor, foam polyethylene dielectric cable (5th entry in the table) was the least expensive with a cost of under $3 (US) per m when purchased in 600 m spools. This is the standard cable employed for the cable TV industry and most TDR installations in rock.

The two foam polyethylene cables built in-house (2nd and 3rd entries in the table) were produced by replacing the aluminum outer conductor of the standard cable with silver paint or braid. These cables required an additional outer jacket to protect the modified outer conductor and prevent water penetration. The braided model has the greater potential for mass production. The most unusual in-house cable (1st entry in table) was produced with highly compressible insulating foam, but was so compressible that it could not be employed more than 10 m below the water table (Cole, 1999). However, its properties facilitate direct measurement of displacement above the water table.

Cable Description	Cable Model Number	Inner Conductor		Dielectric		Outer Conductor		Jacket		Calculated Bending Stiffness, EI (kN.m^2)	Measured Shear Stiffness (kN/m)*
		Material	Dia (mm)	Material	Dia (mm)	Material	Dia (mm)	Material	Dia (mm)		
Braided Foam	N/a	Copper refrigeration tubing	15.88	Cellular foam	27.4	Tin/copper braid	28.2	PVC Shrink-wrap	29.0	47	n/a
Painted Foam Polyethylene	N/a	Solid copper	4.93	Micro cellular polyethylene foam	20.24	Colloidal Silver Paint	20.24	Vinyl Electrical Tape	21.5	5.4	400
Braided Foam Polyethylene	N/a	Solid copper	4.93	Micro cellular polyethylene foam	20.24	Tin/copper braid	21.02	PVC Shrink-wrap	21.85	6.2	480
Braided Polyethylene	Pasternack Enterprises RG218/U	Bare copper	4.95	Solid polyethylene	17.27	Bare copper braid	18.48	PVC	22.10	13	650
Solid Aluminum Foam Polyethylene	Commscope Parameter III 875 Cable	Copper clad aluminum	4.93	Micro cellular polyethylene foam	20.24	Aluminum	22.23	n/a	n/a	275	1760
Solid Aluminum Foam Polyethylene	Cablewave FXA 12-50	Copper clad aluminum	2.77	Micro cellular polyethylene foam	11.43	Aluminum	12.70	n/a	n/a	38	980

* Cable Stiffness - Measured using shear box at 1 mm deformation.

Table 2. *Compliant TDR cables. Properties of commercially available and specially manufactured cables.*

The last two columns in Table 2 present alternative methods of describing stiffness. Axial bending stiffness was calculated with the standard moment of inertia equation to determine a composite axial bending stiffness

$$E_C = \frac{\sum E_i I_i}{I_C} = \frac{E_{ic} I_{ic} + E_d I_d + E_{oc} I_{oc} + E_j I_j}{I_C} \qquad [4]$$

Where the subscripts C, ic, d, oc and j refer to the entire cable, inner conductor, dielectric, outer conductor, and jacket respectively.

The last column in Table 2 presents a shearing stiffness which was measured by shearing cable between two aluminum blocks with a 2mm aperture (Pierce, 1998) . The resulting force–displacement relations are shown in Figure 7. Tabulated stiffness is at 1mm displacement between the opposing shear blocks. It correlates with that calculated from bending considerations, although the relationship is not precise. There is no value for the braided foam as it was so compliant that its response differed completely from the other cable.

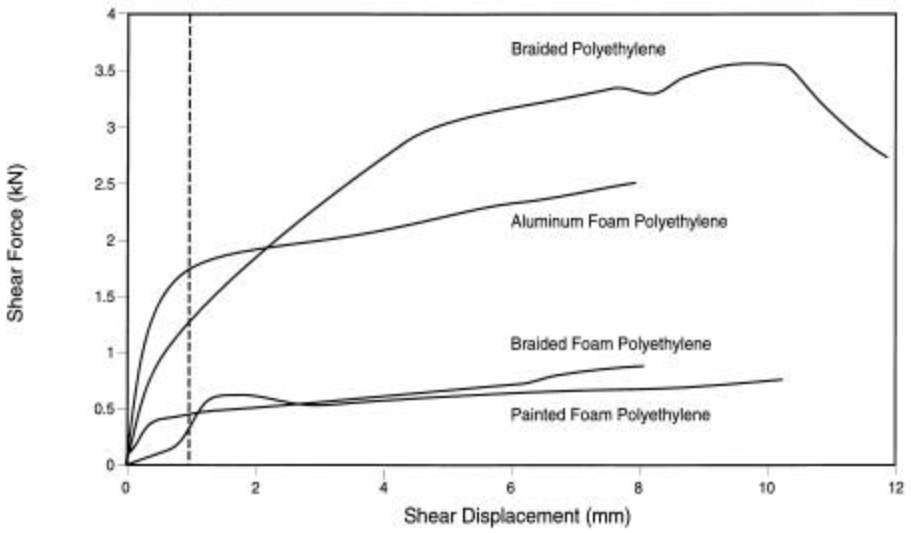

Fig. 7. *Comparative resistances to transverse shearing of commercial and specially constructed cables.*

The signal sensitivity for cables 2,3 & 5 in the table were all equal. At 15 m from the pulser, they all produced a 0.2 % reflection per mm of displacement in the single shear device used to measure shearing stiffness.

Cables 3, 4 & 5 are the preferred cables with 5 the optimum. They are large in diameter, and have similar sensitivities. While the braided outer conductor, foam polyethylene dielectric (cable # 3) is the most compliant, it must be specially manufactured, which renders its use impractical at this time. However, for experimental verification of localization, it would be the best cable. That leaves the braided and solid outer conductor cables. The commercial, braided outer conductor cable (cable #4) has a solid polyethylene dielectric, which requires roughly 40 % greater force to sever. This greater strength will ultimately require greater soil resistance and local soil failure will render it less sensitive than the aluminum outer conductor. Thus, at this time, the standard commercially available cable (cable #5) remains the optimal choice for soil, as long as it's placed with low strength grouts in small diameter holes.

Production of Compliant Grouts

The need to control the strength and compliance of grouts led to an intensive study of their fluid and hardened state properties. Results of this widely ranging study (Pierce, 1998, Aymard, 1996, and Will, 1997) can only be summarized here. As discussed in the force-balance section, it is necessary for the grout strength to be high enough to deform cable but low enough to fail without penetrating the soil. These two requirements can be met by employing a family of weak cement-bentonite grouts that can be pumped through the standard water pump on a drilling rig.

Strength and deformation properties of grouts employed in the two case studies presented herein are shown in Table 1 and fall between the two stars in Figure 8, a tripartitie plot of water, cement, bentonite content. Strengths were determined from samples extracted from the drill rig circulation reservoir (normally a 55 gal drum). These samples were collected in standard molds and unconfined compression tests were performed at 28 days (Table 1).

There are a number of important steps to follow in grout placement; however, the three most important are hydration of the bentonite, addition of a minor amount of expansive agent, and tremie placement from the bottom of the hole upward. To meet expected design strengths, the bentonite must be hydrated and well mixed for at least several hours. Approximately 1 kg (2.2 lbs.) of expansive agent are added (for each 94 lb bag of Portland cement) during mixing of the three components to counteract shrinkage. The expansion agent also dramatically increases fluidity, which is an important attribute for inexpensive field installation with drilling rig water pumps or other highly portable devices. Finally, the grout should be introduced from the bottom by pumping through a +/- 25 mm flush-coupled PVC pipe to ensure expulsion of water and any errant drill cuttings.

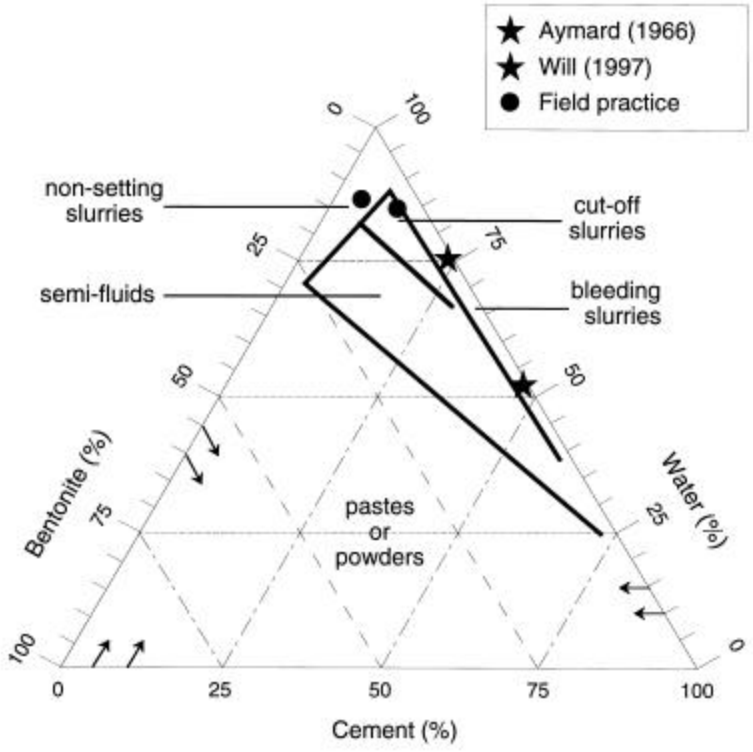

Fig. 8. *Comparison of the water, cement & bentonite mixture percentages for the pumpable, weak grout mixes employed in this study and those employed for other purposes*

Integration with Slope Inclinometer Measurements

Monitoring of shear deformation within soil by TDR cable technology offers an opportunity to detect thin localized shear zones and to remotely monitor site response. Current understanding of soil deformation is based upon response of slope inclinometers. The 60 cm wheel base of inclinometers limits their resolution of thin or localized shear bands even when readings are taken at a fraction of the wheel base. This observation is not meant to demote slope inclinometers as they have been the mainstay of geotechnical

engineering for decades and have served their purpose well. However installation of specially designed coaxial cables in soil now presents an opportunity to search for thin, localized zones. The all-digital operation and up-hole electronics of TDR technology is an advantage when configuring remotely operable systems.

CONCLUSIONS AND RECOMMENDATIONS

This article presents field and laboratory data that support the use of TDR technology to monitor deformation in soil. While TDR has been employed successfully in rock with hundreds of installations world wide, there has been doubt about its usefulness for soft soils. Two case histories were presented herein to illustrate proper installation procedures in soft soils. Force equilibrium and force-deformation analyses of the installed cable-grout composites were employed to provide quantitative of observed behavior as well as guidance for the configuration of cable-grout composites in soil. As a result of this study the following conclusions are tentatively advanced:

1) Analytical techniques confirm field observations that it is possible to shear compliant cable-grout composites in soft soils. However stiffness of the cable-grout composite must be sufficiently low.
2) Grout strength and hole size are major factors in the compliance and deformation of the cable-grout composites. Grout strength should be no greater than 10 to 20 times the soil strength and the hole diameter should be as small as possible.
3) Stiff coaxial cable can respond to large shear zone deformations in soft soil if installed with weak grouts. Grout strength must still be great enough to kink the cable.
4) More compliant cable, which can be specially manufactured, would allow use of yet lower strength grouts.
5) Three-dimensional models of the soil-grouts-shear zone interaction are needed. The geometry of this highly interactive region cannot be rigorously analyzed with two-dimensional models.
6) Installation standards are needed to ensure proper installation. While cable installation is seductively simple, the proper relative compliance described herein cannot be over looked and requires thoughtful installation.

ACKNOWLEDGEMENTS

The authors gratefully acknowledge the support of the National Science Foundation (Civil Mechanical Systems Grant 23236) and the US Department of Transportation sponsored Infrastructure Technology Institute at Northwestern University. We are also deeply indebted to STS and GAI geotechnical firms for their facilitation of the installation of cables and acquisition of inclinometer data respectively. Finally we would like to thank Dr Kevin O'Connor of GeoTDR without whose assistance these field installations would not have been possible.

REFERENCES

Anderson, N and Welch, D., 2000, "Practical Applications of Time Domain Reflectometery (TDR) to Monitor and Analyze Soil and Rock Slopes" ASCE STP Measurement of Soil and Rock Properties and Performance,

Aymard, N., 1996, "Low Strength Grouts for Embedding TDR Cables in Soils," Master of Science Thesis, Department of Civil Engineering, Northwestern University, Evanston, Illinois.

Bromhead, E.N., 1985, The Stability of Slopes, Chapman and Hall, New York.

Cole, R.G., 1999, Compliant TDR Cable/Grouts Composites to Measure Localized Soil Deformation, Master of Science Thesis, Department of Civil Engineering, Northwestern University, Evanston, IL.

Dowding, C.H. and Huang, F.C., 1994, Telemetric Monitoring for Early Detection of Rock Movement with Time Domain Reflectometry, Journal of the Geotechnical and Geoenvironmental Engineering of the American Society of Civil Engineers, V. **120**, No. 8.

Kane, W. F., 2000, "Monitoring of Slope Movement with Time Domain Reflectometry", Geotechnical Field Instrumentation: Applications for Engineers and Gelologists, ASCE Seattle Section Geotechnical Group

MacKenzie, T.R., 1955, Strength of Deadman Anchors in Clay, Master of Science , Princeton University, Princeton, New Jersey.

O'Connor, K.M. & Dowding, C.H., 1999, GeoMeasurements by Pulsing TDR Cables and Probes, CRC Press, Boca Raton, FL 402 pp.

Pierce, C.E., 1998, "Time Domain Reflectometry Measurements of Localized Soil Deformation," Ph.D Dissertation, Department of Civil Engineering, Northwestern University, Evanston, Illinois.

Reese, L.C. and Wang, S.-T., 1989, Documentation of Computer Program LPILE, LPILE1, Version 3.0 Ensoft, Inc., Austin, Texas.

Will D.M., 1997, Cement-Bentonite Grouts Compatible with Compliant TDR Cables, Master of Science Thesis, Department of Civil Engineering, Northwestern University, Evanston, Illinois.

Hardware

In-line TDR Moisture Sensors for Agro-Industrial Processing
M. Stacheder, P. Blume, R. Fundinger, K. Koehler and R. Ruf, *IMKO Micromodultechnik GmbH, Germany*

Evaluation of Shaft-Mounted TDT Readings in Disturbed and Undisturbed Media
G. C. Topp, D. R. Lapen, and M. Edwards, *Agriculture & Agri-Food Canada*; G. D. Young, *E.S.I. Environmental Sensors, Inc., Canada*

Determination of the Wetting Front in Drip Irrigation Using TDR Multi-Wire Probe
E. E. Matsura, C. F. Souza and R. Testelaf, *UNICAMP/Feagri - Departamento de Água e Solo, Brazil*

On the Use of the TDR TRIME-tube System for Profiling Water Content in Soils
J. P. Laurent, *Laboratoire d'étude des Transferts en Hydrologie et Environnement, France*; P. Ruelle and L. Delage, *CEMAGRAF, France*; N. Bréda, A. Chanzy and C. Chevallier, *INRA, France*

Calibration of CS615 and TDR instruments for Marhurangi, Tarrawarra and Point Nepean Soils
M. Duncan, *National Institute Of Water and Atmospheric Research, New Zealand*; A. Western, C. Olszak, J. Thompson, T. Anderson, R. B. Grayson, D. Wilson and R. Young, *University of Melbourne, Australia*

A Cost Effective Soil Moisture Instrument Based on Time-Domain Transmission Measurement
Z. J. Sun and G. D. Young, *E.S.I. Environmental Sensors Inc., Canada*

Back to Table of Contents

IN-LINE TDR MOISTURE SENSORS FOR AGRO-INDUSTRIAL PROCESSING

Markus Stacheder[1], Peter Blume[2], Robin Fundinger[3], Kurt Koehler[4], and Ruediger Ruf[5]

[1]IMKO Micromodultechnik GmbH, Im Stoeck 2, D-76275 Ettlingen, Germany; m.stacheder@imko.de
[2]IMKO Micromodultechnik GmbH, Im Stoeck 2, D-76275 Ettlingen, Germany; p.blume@imko.de
[3]IMKO Micromodultechnik GmbH, Im Stoeck 2, D-76275 Ettlingen, Germany; r.fundinger@imko.de
[4]IMKO Micromodultechnik GmbH, Im Stoeck 2, D-76275 Ettlingen, Germany; k.koehler@imko.de
[5]IMKO Micromodultechnik GmbH, Im Stoeck 2, D-76275 Ettlingen, Germany; r.ruf@imko.de

ABSTRACT

TDR is applicable for a broad variety of capillary porous materials. Especially the moisture determination in the drying process of agricultural products is of great importance. Based on the TRIME-TDR-technique – already presented on the TDR-Symposium in 1994 – a new application focuses on in-line sensor designs for monitoring and controlling agricultural process cycles in order to optimize produce quality and energy consumption.

The TRIME-GW sensors for in-line measurements are either rod probes with two metallic wave guides or non-invasive surface probes, individually adaptable to plant and process requirements. A read out unit with selection switch allows selection of different product densities as well as an on-site calibration of the system for accurate gravimetric moisture determinations. The system is connectable to any stored program control (SPC) via analog output.

Successful performance of the system is demonstrated by two major applications:

1. Automatic control of corn drier by direct corn moisture measurements inside the drying chamber at temperatures of up to 130°C.

2. Optimized processing of pilled sugar beat seeds in rotational pilling plants with moisture exceeding 40 % by weight.

The new system received the 1999 innovation award of the German Agricultural Society.

INTRODUCTION

Drying agricultural products is necessary all over the world in order to make them non-perishable and to achieve the optimum water content for the purposes of processing and trade.

Throughout the world, enormous amounts of energy are being wasted due to inadequate drier control, losses in goods' values and dry-produce damage are being accepted, and valuable manpower is squandered in manual process-monitoring. Exceptional rationalisation potential has become visible in the drying of basic foodstuffs that can be exploited to the advantage of foods producers, processing-plant operators and the foods consumer. The incentives for improved moisture control are considerable according to a study of Conrad (1997). Savings in energy of 0.5 .. 1 $/ton and additional sale margins of 1 .. 3 $/ton, depending on product, passing amounts and specific process, are realisable by using on-line or in-line measuring sensors. Existing automatic control systems based on measuring temperature or the moisture of extracted air are inherently imprecise, subject to the influence of interfering factors (air moisture, temperature fluctuations) and partly require intensive maintenance. Consequently drier are normally controlled based on results of hourly manual samples analysed for moisture in the lab. A manually supervised and controlled drying process is labour-intensive and full of potential errors because the technology utilised for measuring the grain moisture is antiquated or simply has not been fully developed.

We have been developing an in-line whole-grain moisture measurement system TRIME-GW for a higher degree of process transparency and drying precision. The in-line measuring system allows continuous measurement of grain moisture and improved process-monitoring in grain drying. The optimisation and rationalisation of working procedures, the reduction of losses in the value of goods and the energy savings are the benefits of the new technique.

METHOD AND MATERIALS

TRIME-technology was derived from the Time Domain Reflectometry principle, a meanwhile well established electromagnetic measurement technique for determination of soil moisture (Topp *et al.* 1980) and other porous materials. The transit time of a voltage pulse that propagates along metallic wave guides yields the dielectric constant of the porous material, which is a function of the water content. Originally developed especially for soil moisture determination and already presented at the 1994-TDR-Symposium in Evanston (Stacheder *et al*. 1994), we found out that the TRIME-technique yields potential for far more materials than soil, from which the moisture measurement in cereal grains is one of the most challenging and both ecologically and economically interesting.

Although cereal grains such as corn, wheat, rye, etc. are typical porous materials, there are some differences to soil that had to be considered in the sensor design. The porosity of the bulk grain is higher, the bulk densities and absolute maximum moistures are lower compared to normal soils, therefore, no PVC-coating of the metallic wave guides in order to raise the reflected pulse is necessary as it is normally the case for the TRIME soil moisture probes due to the special pulse evaluation method (Stacheder *et al*. 1994).

The desire to measure the moisture directly inside the drier within the process flow requires some specific features. Whether continuous-flow/roof drier, rotary drier, shovel/flip drier or belt drier, TRIME-GW with rod probe, or non-invasive surface or wedge-shaped probes can be adapted to numerous applications (Figure 1).

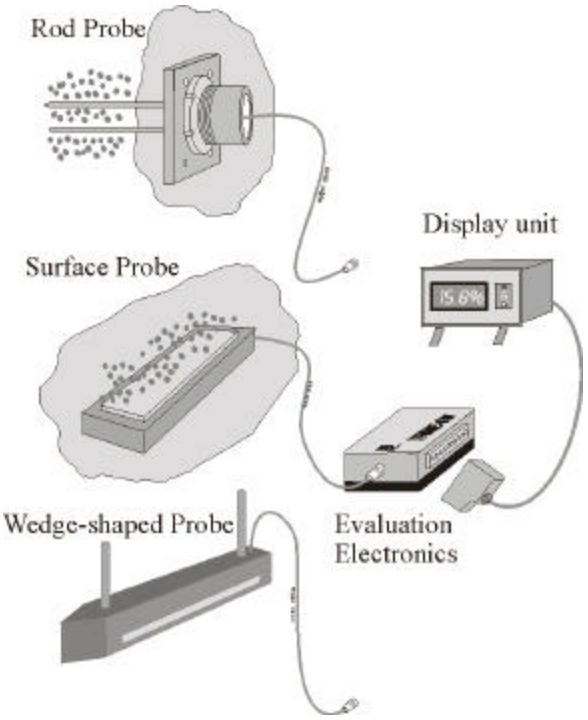

Fig. 1. *TRIME-GW probe types with electronic housing and display unit.*

Due to the high temperatures that can occur during the drying process, there is a need for high-temperature resistant probe heads and plugs. The evaluation electronics are housed in a small and robust aluminium die-cast box that is combined with a display unit.

For trading purpose, the gravimetric water content of cereals on a wet mass basis is needed, and absolute accuracy of around ± 1 % by weight are indispensable. Since TDR basically determines the volumetric moisture, we added a material selection switch that allows selection of 15 different calibration steps dependent on grain product or density. A good and sufficient probe-material contact is indispensable. The probes must be installed at a spot, where they are covered with sufficient material and where the flow of the material is either constant or comes to a rest, so that a rather constant bulk density is achieved and gravimetric moisture can be deduced from volumetric moisture measurement.

Depending on probe type the penetration depth of the measurement field can reach up to 15 cm. Since the geometry of the drier differ significantly and the metallic surrounding can interfere with the probes measurement field, the system offers the possibility of fine-tuning and on-site calibration to compensate for this effect.

TRIME-GW results can be displayed on LED for manual control, incorporated into a monitoring system via an analogue output of (0)4 - 20 mA, or documented with a linear plotter or PC. The modular concept of the system allows any enhancements. Automatic operation can be set up due to connection to Stored-Program-Control (SPC) or limit switch (Artmann *et al*. 1999).

RESULTS

Material calibration and accuracy

The system was calibrated for a broad variety of cereals such as for example corn, wheat, rye, barley, oats or oil seed rape. Reference method was the oven-drying technique at 105 °C or 130 °C until constant weight. Figure 2 shows the relationship between the TRIME pseudo transit time, a dimensionless number between 0 and 800, and the gravimetric moisture of wheat samples determined

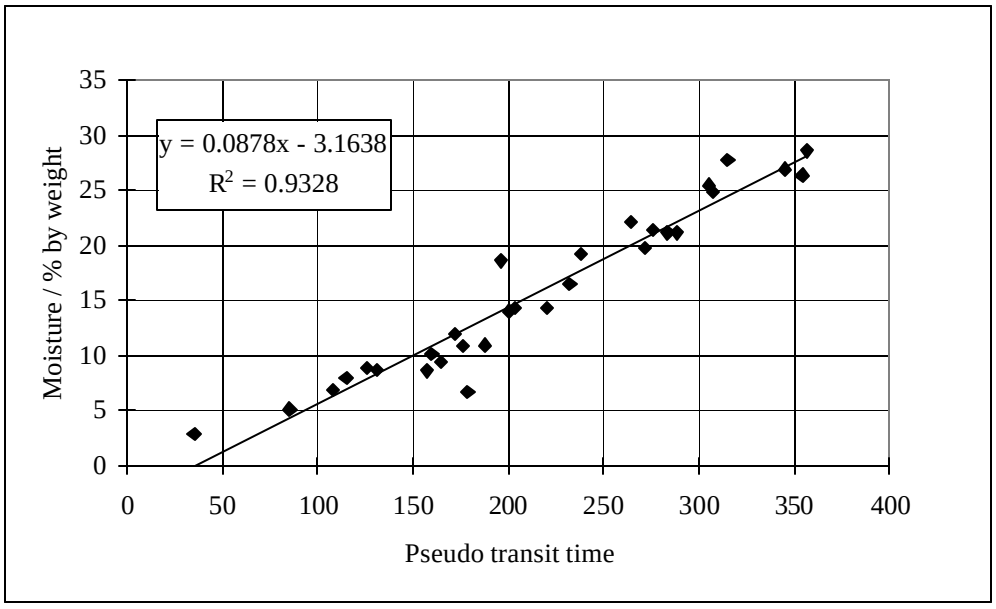

Fig. 2. *Relationship between TRIME-GW pseudo transit time and wet mass moisture of wheat determined with the oven drying method.*

with oven drying technique at 130 °C. The regression is very good and a linear calibration function could be established.

The achievable accuracy for the whole-grain in-line sensor was tested by the German Agricultural Society (DLG 2000). Table 1 shows the random mean square error (rmse) of the measured TRIME moisture from the reference gravimetric moisture for different cereals and moisture ranges.

Cereal	**Moisture Range [% by weight]**	**RMSE [% by weight]**
Barley	12 – 18	0.82
Wheat	6 – 16	1.07
Rye	10 – 19	0.60
Corn	12 – 18	1.35
Corn	26 – 37	0.89
Oil Seed Rape	6 – 18	0.31
Sun Flowers	6 – 10	0.72
Sun Flowers	10 – 18	1.40

Table 1. *Random mean square error (rmse) of TRIME-GW moisture from reference gravimetric moisture*

Influence of material temperature

During the first pilot tests in drying plants in co-operation with the German Agricultural Society, we found an influence of temperature on the TDR moisture measurement. A similar effect was already found for soils with compounds that show high specific surfaces and thus a high amount of bound water

such as clays (Stacheder 1996). In contrast to the decrease of the dielectric constant of free water with increasing temperature, this effect leads to an increase of dielectric constant with temperature and thus measured water content. The effect can be explained by the Brown Molecular Movement which increases with temperature so that the bound water dipoles are successively cut loose and are free to rotate and finally contribute to a higher dielectric constant. Figure 3 shows the relationship between temperature, measured TRIME moisture and reference moisture for different corn samples. It becomes obvious that this effect also depends on absolute corn moisture.

In the range of the target moisture of dried corn at around 13 – 14 % by weight, this effect is the most significant and we found an influence of about 1.2 % by weight per10°C. The influence of temperature decreases with increasing moisture and above 25 % by weight this effect can be nearly neglected.

To compensate for this effect we integrated a temperature sensor in the tip of one rod of the TRIME-GW rod probe for temperature measurements. The equation for temperature compensation depending on absolute moisture is:

$$q_{comp} = q_{meas} + (T - a_0) \cdot a_2 \cdot q_{meas} + (T - a_0) \cdot a_1 \qquad [1]$$

with θ_{comp} as compensated moisture, θ_{meas} as measured TRIME moisture, T as measured temperature, and α_0 (= 20), α_1 (= -0.0021786) and α_2 (= 0,00714286) as experimentally determined coefficients. The equation is integrated in the TRIME software for automatic compensation.

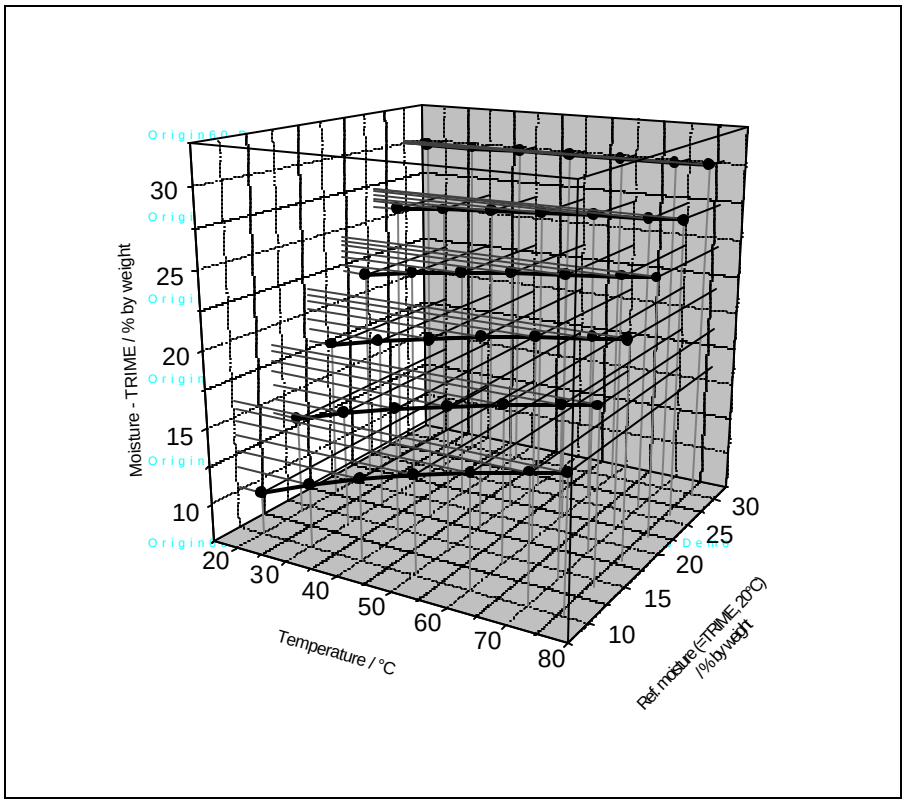

Fig. 3. *Influence of corn temperature and absolute corn moisture on TRIME-GW moisture measurements.*

Measurement results in rotary drier

Figure 4 shows the drying cycle of a load of corn in a rotary drier. A TRIME-GW rod probe was installed at the drier wall and adapted to the driers geometry. Then moisture and temperature were measured continuously. From time to time corn samples were taken from near the probe for moisture reference measurements with the oven drying method and a portable moisture meter based on resistance measurements. Also the temperature in the vitiated air was measured.

The correlation between TRIME-GW moisture and oven drying method is very good. Only at higher moistures TRIME-GW shows a little overestimation. The portable moisture meter underestimates moisture significantly, which is probably due to a missing temperature compensation. The correlation between temperature in vitiated air, which is mainly identical with temperature in the grains, and the temperature determined with the TRIME-GW sensor is excellent, so that the values can be used for correct temperature compensation.

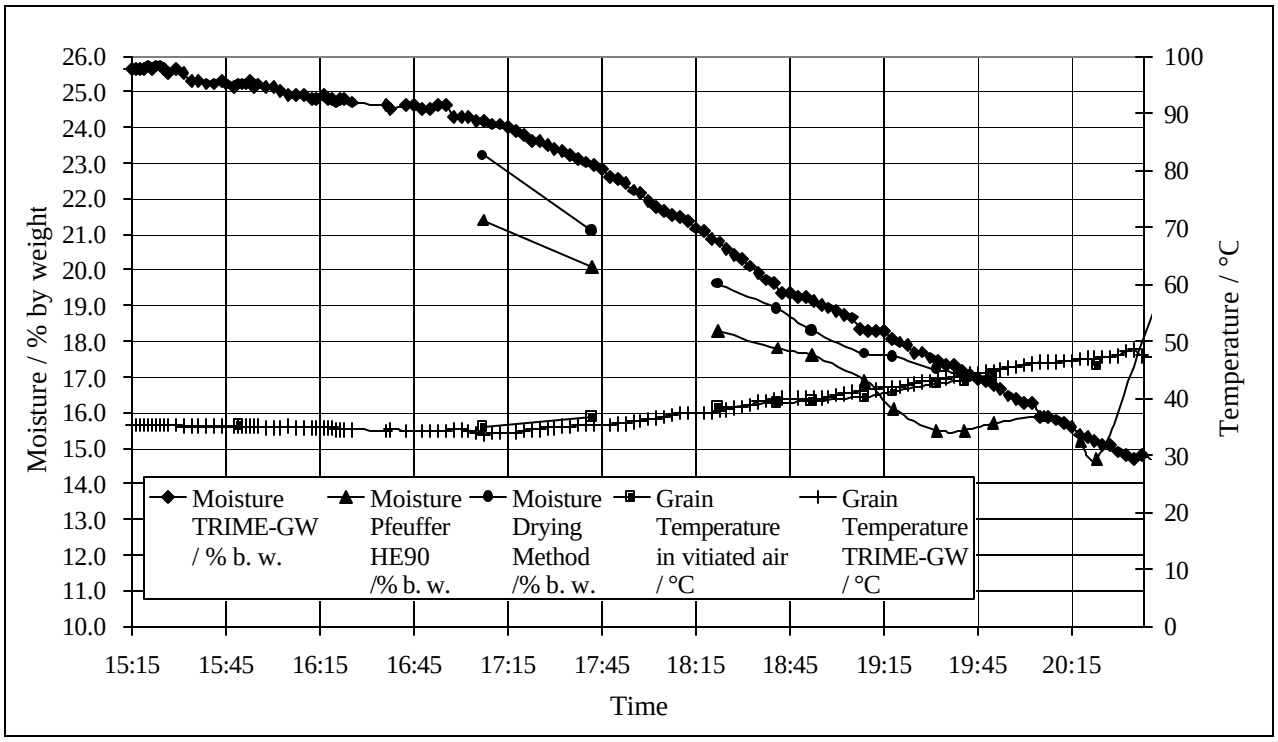

Fig. 4. *Temperature in vitiated air, TRIME-GW measurements of moisture and temperature compared to oven drying method and resistance meter (Pfeuffer) for corn in a rotary drier.*

Measurement results in fluidised bed drier

One of the most important problems is the contact between the probes wave guides and the material. Especially when the material moves very fast or is even whirled as for example in fluidised bed drier, this must be paid attention for.

In the following application a surface probe was used to determine the moisture of sugar bead seeds during a refinement process. In this process the seeds are filled in a rotational pilling machine, where they are mixed with a nutrient pulp based on wood fibres with a moisture of around 40 % by weight. Due to the rotational process the seeds are embedded in the nutrient mass, and finally pills with 0.5 cm in diameter are formed. After pilling, the seeds are dried in a fluidised bed process until a final moisture of around 15 % by weight.

Inside the pilling machines there are fixed metallic wings, which act as mixing tools that permanently turn the pills while rotating. Due to the rotating forces, the pills are pressed to the wings so that there is sufficient material for the moisture determination. Yet the first installation spot was not placed properly, so that the probe was not covered with sufficient material. This is obvious from the measurement results shown in Figure 5. The first few minutes from the beginning of the rotational process, the measured moisture is too low compared to gravimetric moisture.

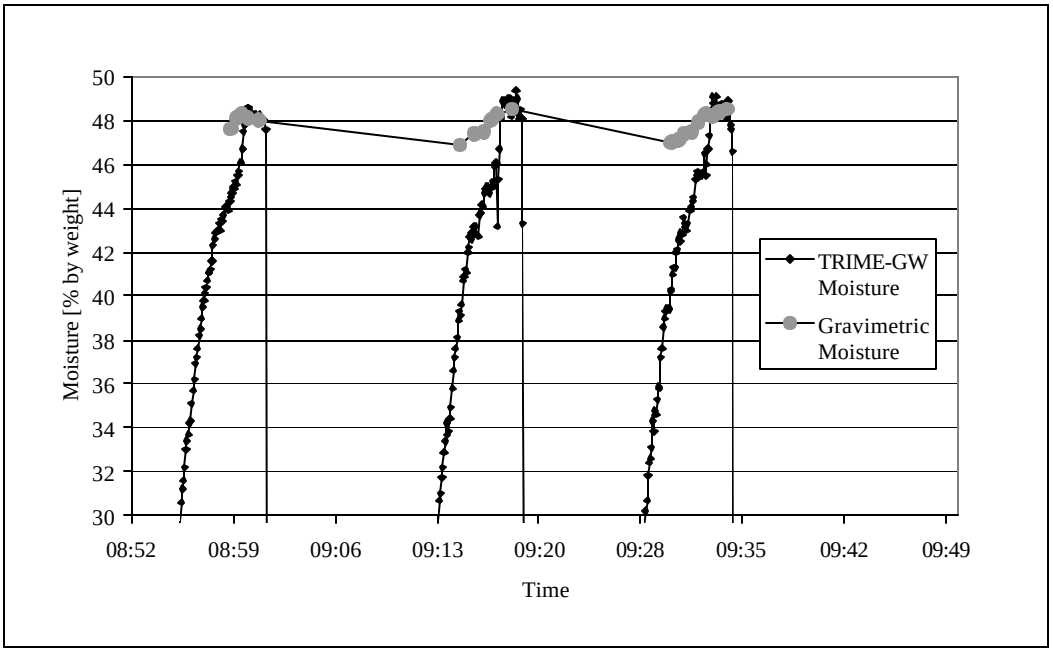

Fig. 5. *Moisture measurement in rotational pilling machines. TRIME-GW sensor not sufficiently covered with material.*

After the position was changed, the problem was solved and excellent measurement results were achieved during the whole processing and drying cycle. Comparison of TRIME-GW moisture and gravimetric moisture determined with oven drying can be seen in Figure 6.

SUMMARY

TRIME-TDR technology could successfully be adapted for wet mass water content determination in various agricultural products. Special in-line sensors with rod or non-invasive surface probes offer the possibility of continuous measurements for in-line monitoring of product moisture in different drier and delivery areas. Advantages and accuracy of the new sensors are considerable. Spatial and temporal resolution is excellent and representative measuring volumes and whole grain measurements minimise errors due to sampling and milling and enhance the ease of operation.

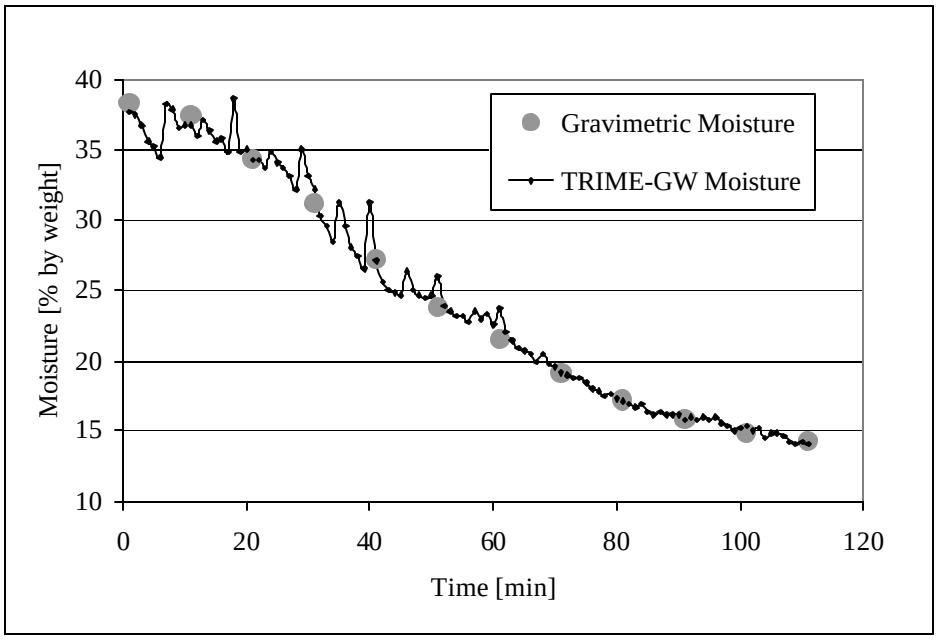

Fig. 6. *Moisture measurements in pilled sugar bead seeds. Comparison of TRIME-GW and gravimetric moisture in a fluidised bed drier.*

An integration in processing and controlling programs is possible for reliable automatic operation of drier with reduced risks in over- and underdrying and higher economical benefits due to energy savings and higher yields.

An influence of temperature on TDR moisture measurements in cereals was found. The effect is compensated by suitable software.

REFERENCES

Artmann, L., Blume, P., Fundinger, R., Koehler, K., Pfeiffer, B.-M., and Stacheder, M., 1999, Automation of grain drying plants: New sensors for modern controlling (*in german*): Schüttgut, **5**, No. 4, 574-576.

Conrad, T., 1997, Possible savings in the grain drying process using precise and fast on-line measurement technologies. Steinbeis Transfer Center for Agronomy, Environmental Technics and Power Economies: Internal Report, University of Hohenheim,Germany, 8 p.

DLG (German Agricultural Society), 2000, In-line moisture measurement system TRIME-GW: Test protocol 4866 (*in german*), 7 p.

Stacheder, M., Fundinger, R., and Koehler, K., 1994, A new time domain reflectometry system (TRIME) to measure soil moisture and electrical conductivity: Proc. Symp. on TDR in environmental, infrastructure, and mining applications, 1994, U.S. Bureau of Mines Spec. Publ. SP 19-94: 56-65

Stacheder, M.,1996, TDR in geotechnical applications - Measurement of water content, electrical conductivity and solute transport (*in german*): Schr. Angew. Geol. Karlsruhe, 40: 170 p.

Topp, G.C.; Davis, J.L. and Annan, A.P., 1980, Electromagnetic determination of soil water content: Measurements in coaxial transmission lines: Water Resour. Res., 16: 574-582.

EVALUATION OF SHAFT-MOUNTED TDT READINGS IN DISTURBED AND UNDISTURBED MEDIA

G.C. Topp[1], D.R. Lapen[2], G.D. Young[3], and M. Edwards[4]

[1]Eastern Cereal and Oilseed Research Centre, Agriculture and Agri-Food Canada
Ottawa, Ontario, Canada, K1A 0C6; toppc@em.agr.ca
[2]Eastern Cereal and Oilseed Research Centre, Agriculture and Agri-Food Canada
Ottawa, Ontario, Canada, K1A 0C6; lapend@em.agr.ca
[3] E.S.I. Environmental Sensors Inc., Suite 100, 4243 Glanford Ave.
Victoria, British Columbia, Canada, V8Z 4B9; jyoung@esica.com
[4]Eastern Cereal and Oilseed Research Centre, Agriculture and Agri-Food Canada
Ottawa, Ontario, Canada, K1A 0C6; edwardsm@em.agr.ca

ASTRACT

TDR/TDT (time domain reflectometry/transmissometry) measurements using insertable probes are made in soil modified by insertion of the probe. The major factors affecting the interpretation of the TDR/TDT signal are water and solid redistribution in the soil during probe insertion and how far the electromagnetic field reaches into the soil. Nevertheless, the consequence of local soil disturbance on the TDR/TDT reading is not precisely known. Field and laboratory measurements were made with a helical wrapped parallel pair transmission line configured as a single probe (15 mm diam.) and operated in TDT mode on the Terra.Point® penetrometer shaft. Ambient water contents were measured using the Terra.Point® TDT instrument and with independent multi-pronged (3 and 6 mm diam.) TDR probes. TDT readings were calibrated against liquids of known permittivity. In soil columns of silty clay loam and sandy loam textures both TDR and TDT estimates of water content were compared at a range of uniform water contents. Similar measurements comparing the two instruments were made in the field. The TDT instrument was shown to provide a reliable measure of relative permittivity and thus of soil water content with a resolution of " 0.02 m^3 m^{-3} The apparent water content increase arising from insertion of the TDT probe was estimated at about 0.01 m^3 m^{-3} in the field but somewhat larger in the sandy loam soil in the laboratory. Liquid and air referencing periodically of the TDT estimates was useful in substantiating the performance of the TDT instrument.

INTRODUCTION

TDR is widely used for soil water measurement both for water content and bulk soil conductivity (Topp and Ferré, 2000). The broad applicability of TDR has been enhanced by the flexibility of probe configurations that allow the TEM (transverse electromagnetic) wave propagation of the signal. Ferré and Topp (2000) have reviewed some of the findings from a variety of probes. In all of these, the goal behind probe design was to obtain an improved measure of water content for samples of specific size and shape. The same flexibility of probe design for TDR increases the possibility of combining TDR

with other techniques to provide measurement of water content with other soil parameters. A number of soil parameters and processes are highly dependent on water content. This thinking led to the combined soil penetrometer and water content sensor (Young *et al.*, 2000; Vaz and Hopmans, 2001). The cone, used to sense the cone resistance or soil strength, was followed into the soil by a water content sensor, so that both soil parameters were measured in the same soil in an *in situ* manner. Soil water content must be accounted for in evaluating resistance measures. Although mounting TDR sensors on a single probe has advantages for accessing soil the sensitivity to water content is more confined than with multiple probes. In addition, the transmission line for signal propagation in soil results in a more complex reflected wave form to interpret. Young *et al.* (2000) used successfully time domain transmissiometry (TDT) on a single probe arrangement, where travel time is determined by comparing transmit time delay of a similar sharp rise time pulse. The shape of transmitted pulses, not complicated by a returning reflection, is often an easier signal to interpret. TDT and TDR are based on the same principle of measuring travel time or propagation velocity as a measure of relative dielectric permittivity.

The evaluation of combination probes adds complexity, in that, interactions between parameter measurements must be removed or taken into account. One interaction is the effect of friction imposed by the water content sensor on cone resistance values. Vaz and Hopmans (2001) used a water content sensor of equal diameter as the cone on a cone penetrometer while Young *et al* (2000) used a water content sensor of slightly larger diameter than the cone to help insure good water content sensor-soil contact as the probe moved vertically through the soil. Irrespective of either approach, both techniques measure soil dielectric properties that have been "disturbed", as water content measurements are made after the passage of the cone. The precise physical nature of such a disturbance is unclear, but appears strongly related to the soil physical condition and the manner of probe insertion into the soil.

Roth *et al.*(1997) evaluated the impact on TDR measurements of the disturbance caused by insertion of varying diameter rods. They concluded that soil should be removed before insertion of rods > 10 mm in diameter to alleviate the effect of soil disturbance around the rods on the water content measurement. With diameter > 12.7 mm, the combination water content/penetrometer probe (Young *et al*, 2000; Vaz and Hopmans, 2001) were expected to show effects of disturbance that have not been detected and quantified. Topp *et al.* (2001) showed possible disturbance effects which implied greater concentration of soil and water adjacent to the probe. Vaz and Hopmans (2001) detected effects of disturbance for only one soil type, a sand, and disturbance was toward less dense soil and water adjacent to the probe. Vaz and Hopmans (2001) indicated how difficult it was to confirm and quantify independently the soil disturbance because of the limited extent of the disturbed soil around the probe.

In this paper, comparisons were made between probe calibrations in liquids (non-deformable medium) of known relative permittivity with those derived from soils with known relative permittivity and physical properties. Differences between liquid and soil calibration results provides a means for quantifying, in a relative manner, the effect of soil disturbance imposed by the single penetrometer probe on water content readings. The sensor on the penetrometer was operated in TDT mode and compared with TDR using conventional triple pronged probes

MATERIAL AND METHODS

Description of the Terra.Point® Penetrometer Combination Instrument

The general operation of the Terra.Point® penetrometer with both water content and cone resistance measurement capability was described by Young *et al.* (2000) and Topp *et al.* (2001) (Fig. 1). The Terra.Point® system uses a lightweight, twelve-volt electric motor driven, screw jack assembly to provide a steady velocity for probe insertion of approximately 28 mm/sec. The length of travel is 400 mm. The drive mechanism is mounted on a supporting frame made of lightweight materials which also houses the sensor signal conditioning electronics and a datalogger/controller. The frame is supported vertically by three horizontal legs on which the operator(s) stands to hold the mechanism down during operation. The power for the whole system, including the drive motor, is supplied by a 12V, gel-cell battery carried in a backpack.

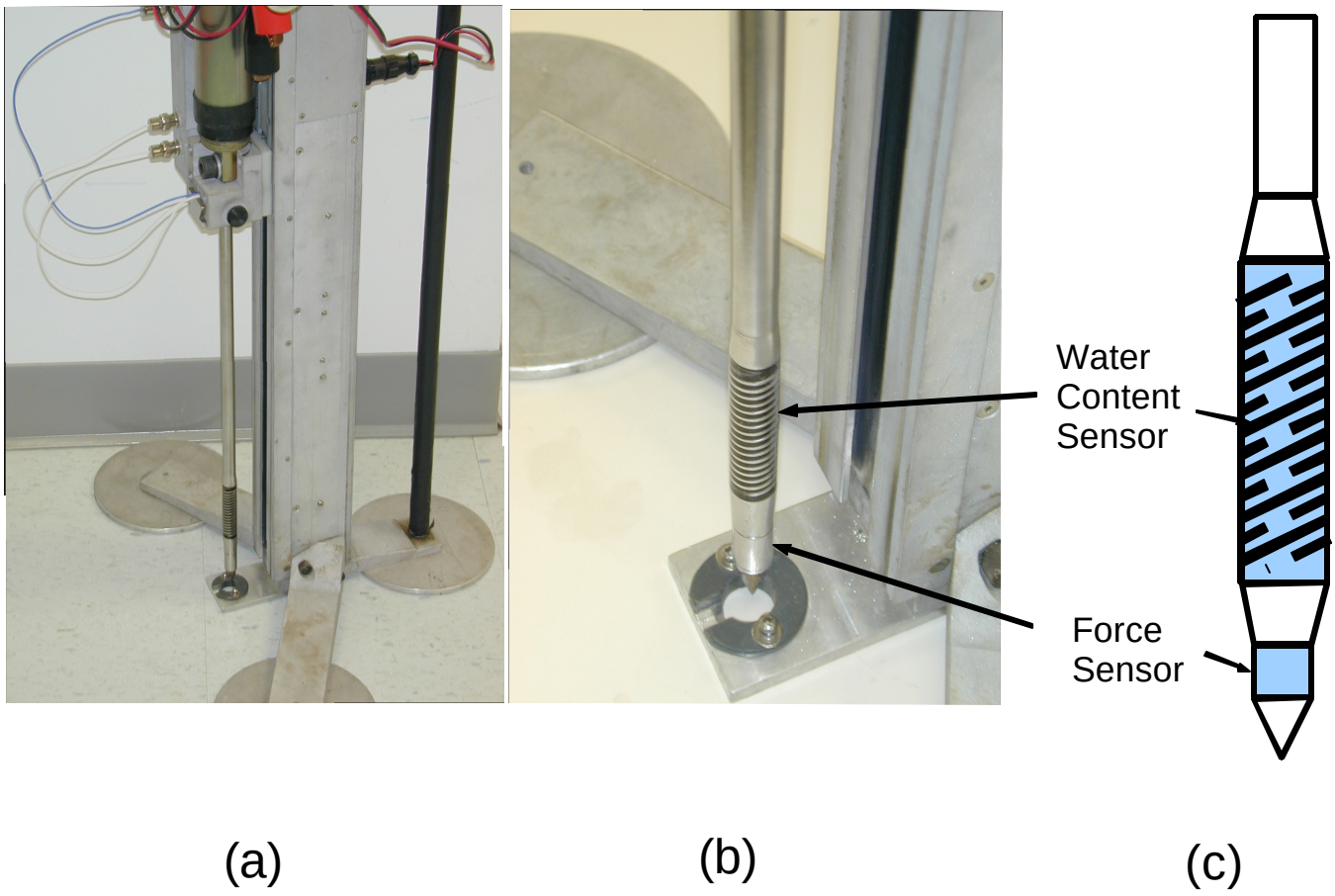

Fig. 1. (a) *Terra.Point® penetrometer probe with part of the insertion frame,* **(b)** *the probe with sensors components identified, and* **(c)** *schematic details of the TDT helical parallel pair transmission line, not to scale. The length of the sensing region was 6 cm.*

The Helical-Wrapped TDT Probe

Topp *et al.* (2001) desribed briefly the helical parallel pair water content sensor, which is similar to that of Vaz and Hopmans (2001) which they called coiled. Our sensor used an additional 50 S coaxial cable connected to the lower end of the parallel pair helix, to convey the transmitted signal after it passed along the helix to the TDT circuit for analysis. The time delay in the return of the transmitted signal caused by soil or other media surrounding the helical probe was converted to a relative voltage. This voltage relates directly to propagation velocity and thus to water content. The water content sensor consists of a stainless steel tubular core in which cables pass from the water content sensor and cone force sensor (Fig 1). The tubular core is surrounded by epoxy resin in which the helical pair is embedded. The fabrication sequence was to machine the stainless steel tube (i.d.=4.5 mm) exterior from 15.8 mm to 9 mm diameter for a length of 65 mm for the water content sensor. The portion removed by machining was replaced by an epoxy casting resin (Sealtronic 21AC-7V from Industrial Formulators, Burnaby, BC). Two parallel helical grooves (square in x-section) were cut to a depth of 1.5 mm and separated by 3 mm. This was accomplished by machining a double-start thread of 4 threads per inch (25.4 mm). Stainless steel rod circular in cross-section, of 1.5 mm diameter, was formed into two helical springs with 12.5 mm i.d. and 6 mm separation along the axis. Each spring was "threaded" into each helical groove in the epoxy cast and retained in place with additional epoxy in the groove and around the rod. After hardening, the assembly was machined to 15 mm diameter to provide a smooth exterior surface and exposing the stainless steel helical pair for direct contact with soil.

At each end of the helical pair, a hole was drilled through to the central cavity, allowing insertion of 50 S coaxial cables into and along the central core of the probe to the TDT circuit. At the ends of the helical sensor, the shield and centre conductor of the 50 S cables were separated. The shields were connected (soldered) to each end of one helical rod. The centre conductors were soldered to the ends of the other helix. These connections were carefully embedded in epoxy so they were not exposed to abrasion during insertion of the probe into the soil.

Calibration of the TDT Sensor

Reference calibration in liquids of known relative permittivity

A series of organic liquids of known relative permittivity, that spanned the range of relative permittivity values encountered in soils (Table 1), were used to calibrate the sensor. The gain and zero of the TDT circuit were set so that voltage output was well within its operating range (0-5V) when in air (minimum relative permitivity) or immersed in water (maximum permittivity). Voltage readings were recorded when the probe was in air and when immersed in each of the chosen liquids (Table 1). The voltage difference associated with each medium was a direct result of the increase in propagation velocity along the helical probe caused by the interaction of the EM wave with the liquid.

Laboratory and field calibration in soils of known relative permittivity

A series of soil columns were prepared at a sequence of water contents starting from air-dry. Two soils of differing texture, North Gower SiCL and Matilda SL, were used. Soil samples, whether air-dried or wetted, were sieved (2 mm) and packed by hand into a cylindrical plastic container, 25 cm long by 15 cm diam. The sieved soil was added to the container in pre-weighed increments to fill 5 cm. Each

increment was hand-packed by tapping as needed to force a 15 cm diam. plunger to the top of the 5 cm incremental height. The intended bulk density for the soils was 1.20 Mg m^{-3} for the SiCL soil and 1.55 Mg m^{-3} for the SL. The wetting sequence used was from initial air-dry to fully wetted with a series of incremental additions of tap water. Wetting of the soil was carried out by adding approximately 150 mL of tap water to the required soil. About 1/3 of the soil was spread evenly on a tray to about 20 mm deep. A portion of the water was sprinkled over the surface of the spread soil; another 1/3 of the soil was added and water sprinkled on it and so on until all soil and water had been added. Soil and liquid were mixed thoroughly in the tray and passed through a series of sieves to break into about 2 mm sized particles and packed uniformly as described above. The upper limit on volumetric water content was determined by the limit on manipulation and mixing of the wetted soil to allow uniform packing. A 1502C cable tester (Tektronix Inc., Beaverton, OR) and 20 cm wave guides (three-pronged type) were used to estimate the bulk relative permittivity of the soil in the column (20 cm depth) and at 6, 12, and 18 cm depths to evaluate the potential for water content gradients in the columns. The Terra.Point® penetrometer was positioned above the soil column so that the penetrometer would insert the probe directly into the soil as in field operation. The Terra.Point® data were collected over the 25 cm depth of the soil column.

Medium	Reference ε_r	$\sqrt{\varepsilon_r}$
Cyclohexane	2.02	1.42
Benzene	2.27	1.51
Amyl acetate	4.75	2.18
Ethyl acetate	6.02	2.45
1-octanol	10.34	3.22
2-butanol	16.56	4.07
1-butanol	17.51	4.18
2-propanol	19.92	4.46
Ethanol	24.6	4.96
Ethanol:water (2:1)	43.2	6.57
Ethanol:water (1:1)	52.5	7.25
Ethanol:water (1:3)	66.45	8.15
Water	80.4	8.97

Table 1. *Relative dielectric permittivity of liquids*

An in-field calibration of the Terra.Point® water content sensor was carried out by comparing TDR measured water contents (TRASE model 6050, Soilmoisture Equipment Corporation, Santa Barbara, CA) over the top 15 cm to the average of the outputs of the Terra.Point® sensor for the same depth interval. The TDR determinations were made within 10 cm of the location of insertion of the Terra.Point® probe, using a 3-pronged probe of 6 mm prongs separated 35 mm. Reference determinations with the Terra.Point® probe were made in air, tap water and 2-propanol after approximately every 30 readings in the soil to check for zero and calibration drift. The Terra.Point® outputs were used to develop a calibration from field soil to compare with that obtained in laboratory.

RESULTS AND DISCUSSION

Reference Liquid Calibration of TDT Probe

The use of reference liquids achieved two purposes, firstly, to assess the TDT method for the measurement of relative permittivity where the liquid has ideal physical properties to assure good contact with the sensor and secondly, to provide data against which to compare equivalent readings from soil. The reference liquids (Table 1) showed a highly linear response between square root of relative permittivity ($\sqrt{e_r}$) and TDT voltage output, Fig. 2, with an r = 0.998. The liquids provided a complete seal around the probe and therefore the liquids were considered effectively "undisturbed" or "ideal-deformable" media with the desired contact and uniformity exterior to the probe surface. A linear regression $\sqrt{e_r} = 1.26 + 2.39V$ provides a very convenient calibration relationship by which to convert V from TDT to $,_r$. These voltages readings in Fig. 2 are all relative to readings taken in air. Thus the intercept ($\sqrt{e_r} = 1.26$) gives relative permittivity higher than that of air because the epoxy material in the helical transmission line forms part of the measured dielectric, resulting in an over-estimate for which corrections could be made. These corrections would use mixing laws and follow the procedure given by Vaz and Hopmans (2001). The high linearity of the relationship in Fig. 2 and the lack of any consistent deviation or bias from linearity indicates this correction would have a minor impact on the relationship.

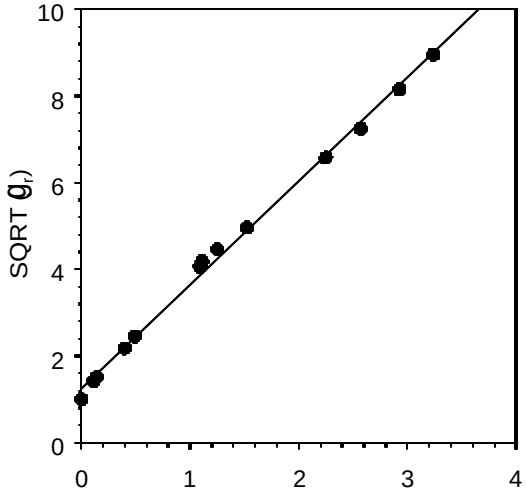

Fig. 2. *The square root of relative permittivity of selected liquids, $\sqrt{e_r}$, (Table 1) as a function of the output voltage, V, recorded from the TDT sensor. The line is the regression reported in the text.*

TDT Probe Measurements in Soil Columns

The uniformity of soil packing in the columns was assessed using TDR. Variable length wave guides inserted into the column soil immediately after TDT measurements showed uniform vertical soil water content profiles. Similarly, lateral uniformity was ascertained from randomly located replicate measurements between the central TDT location and the column wall. Therefore, the apparent relative permittivity, $\sqrt{e_{ra}}$, for the bulk column, as determined via TDR using the 20 cm wave guides (usually average of three readings around the TDT probe insertion locale), was related to TDT (V) measures at the three depth positions for each soil column. The chosen depth increments were the length of the sensor, 6 cm, starting immediately after complete immersion of the sensor at the soil surface.

For all depth positions (0-6, 6-12 and 12-18 cm), the North Gower SiCL columns (Fig.3) showed linear relationships between $\sqrt{e_{ra}}$ by TDR and V by TDT. In addition, the linear relationships were consistent with that for the liquid reference materials, having slopes of 2.23, 2.31 and 2.42 V^{-1} for the depths 0-6,

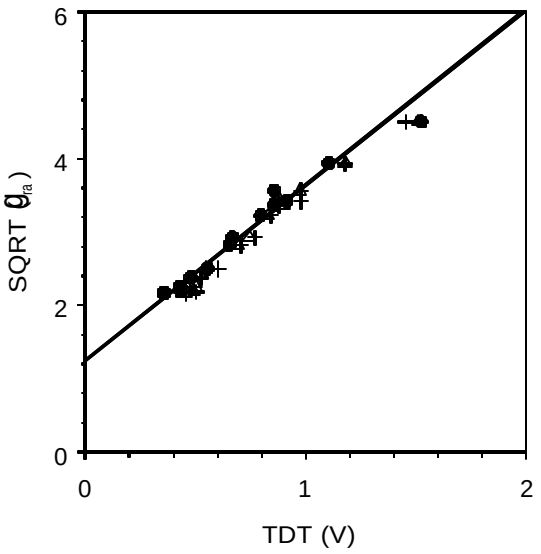

Fig. 3. *North Gower silty clay loam soil column data, $\sqrt{e_{ra}}$ from TDR versus TDT voltage, for 0-6 cm depth (solid circle), 6-12 cm depth (hollow triangle), and bottom reading (12-18 cm depth) (crosshair). The solid line is the liquid reference line from Fig. 2.*

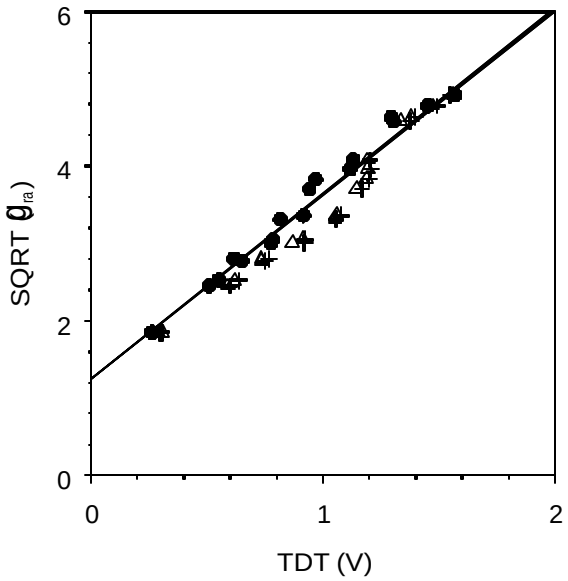

Fig. 4. *Matilda sandy loam soil column data, $\sqrt{e_{ra}}$ from TDR versus TDT voltage, for 0-6 cm depth (solid circle), 6-12 cm depth (hollow triangle), and bottom reading (12-18 cm depth) (crosshair). The line is the liquid reference line from Fig. 2.*

6- 12 and 12-18 cm, respectively. Although these slopes are similar to the value 2.39 V^{-1} for the reference liquids, there is an indication from Fig. 3 that 0-6 cm depth measurements were closer to the reference line, while at the other depths the recorded TDT voltages were slightly larger. This leads to the suggestion that with progressive movement of the probe through the column, there was greater potential for the TDT to overestimate true soil water content within the probe's area of influence. In soil water content terms, the maximum deviation from the liquid reference line, as derived from the bottom (12-18 cm) depth measurements, was . 0.02 m^3 m^{-3}. Overestimation was not entirely unexpected since insertion of the probe displaces water and soil toward the probe perimeter. The pressure gradients imposed by the probe would likely retain more water in the soil next to the probe, rather than vice versa.

A similar but more exaggerated pattern was shown by the Matilda SL columns (Fig.4). Again, the 0-6 cm depth relationship was linear, having a slope of 2.52, and for the most part similar in form to those for the liquids and the silty clay loam soil. There is a tendency for a slightly lower TDT voltage in the range of $\sqrt{e_{ra}}$ = 3.5 to 4.5, indicating TDT gave an under-estimate in the mid-water content range. For the deeper depths, however, the TDT gave an over-estimate of $\sqrt{e_{ra}}$ in the range from 2 to 4 for the sandy loam soil. The relationship between $\sqrt{e_{ra}}$ and *V* for the 6-12 and 12-18 cm depths is also non-linear. The degree of overestimation, expressed in terms of soil water content, did not exceed 0.05 m^3 m^{-3}. The soil column data converge with the liquid line at around $\sqrt{e_{ra}}$ = 4 which suggests that the factors that augmented water next the probe were effectively eliminated at soil water contents approaching saturation.

Field Calibration of the TDT Sensor

The field calibration of the TDT probe provided unexpectedly good fit to the reference line for the liquids (Fig.5). On a whole, there was the expected slight overestimation in the TDT field results, however, in this case it was quite small at < 0.01 m^3 m^{-3}. The soil water content range from about 0.14 to about 0.36 m^3 m^{-3}, covers the most dynamic and usual range encountered in most field soils. The field soils were similar to the soils used in the soil columns. The linear correlation coefficient was 0.95 and there was a high degree of linearity. The linear regression equation $\sqrt{e_{ra}} = 1.18 + 2.32V$ was similar to that given for the reference liquids. As expected, the scatter or variability about the line was greater for the field results as the data include spatial variability. The TDR probe was inserted near but not coincident with the TDT probe. Even with the variability given in Fig. 5 a SEE of 0.182 was obtained, which corresponds to a water content resolution of " 0.02 m^3 m^{-3} for the TDT based estimates.

Hence a calibration relationship which could be used functionally by an operator has the form,

$$q_v = 0.267V - 0.040 \qquad [1]$$

where 2_v is the volumetric water content and V is the TDT voltage output relative to that obtained with the probe suspended in air. Eqn (1) makes use of the linear equation given by Topp and Reynolds (1998) between 2_v and $\sqrt{e_{ra}}$ to convert the field-based relationship (dashed line, Fig. 5) between TDT and TDR to water content.

As with any instrument, the TDT has shown two kinds of drift over time. A change of "zero", i.e. the reading in air, may occur with no change in sensitivity, which is "zero" drift. This occurred, particularly, during warm-up or during-the-day temperature changes. In addition, some changes in "gain" or sensitivity were also observed but not related to any specific causal factor. Although we have not characterised or quantified these drifts we have followed a referencing procedure where periodic measurements were made in reference liquids, water and 2-propanol. From these measurements, and those in air, we were able to compensate the TDT voltage output fully for the drifts which occurred to our instrument during field measurements. The drift corrections were generally < " 0.02 m^3 m^{-3}, expressed on a water content basis. The wide scope of measurements using the Terra.Point® penetrometer in the field have been carried out at ambient temperatures from 0 to +30EC. The use of this referencing procedure was necessary to assure the excellent resolution capability we obtained and is similar to the rigour of measurement that we used in the early development of TDR for field applications.

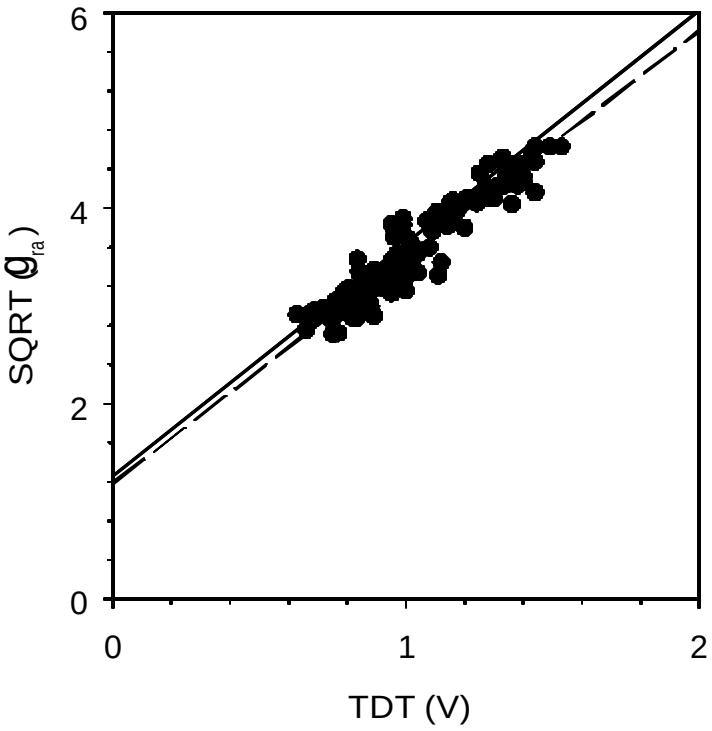

Fig. 5. *Field soil data, $\sqrt{e_{ra}}$ by TDR versus TDT voltage, for 112 locations taken 0-15 cm depth (solid circle). The solid line is the liquid reference line from Fig. 2. The dashed line is the linear regression through the field data as given in the text.*

CONCLUSIONS

We used liquids of different reference relative permittivity to confirm the TDT system as a reliable approach for measurement of relative permittivity, giving values equivalent to TDR. The use of TDT depends on signal travelling through the sensor transmission line using separate send and retrieve cables, making single probe format more usual. The likelihood of soil disturbance within the measured zone was high for a 15 mm diameter probe. We were able to identify probable soil disturbance effects on the TDT measurements of < 0.05 m^3 m^{-3} in a sandy loam soil column and < 0.03 m^3 m^{-3} for a silty clay loam column. In the field calibrations, the increased concentration of water around the probe that was attributed to disturbance from probe insertion was < 0.01 m^3 m^{-3}. The water content resolution of " 0.02 m^3 m^{-3} is equivalent to TDR which was used as the reference method in this study. The periodic referencing procedure, using air, water and 2-propanol, was very beneficial for monitoring the consistency of instrument performance and highly recommended, particularly, when calibrating or evaluating instrument performance. The TDT single probe has been shown to be straight-forward to use and to provide estimates of soil water content that are equivalent to those obtained from TDR. More detailed studies are needed to elucidate the thickness of the measurement region around the TDT probe.

REFERENCES

Ferré, P.A. and Topp, G.C., 2000, Time-domain reflectometry sensor techniques for soil water content measurements and electrical conductivity measurements. In Sensors Update vol. 7, H. Baltes, W. Gopel and J. Hesse Ed.s, Wiley-VCH, Weinheim. 277-300.

Roth, A., Weis, W.,Matthies, D. , Hess, U., and Ansorge, B., 1997, Changes in soil structure caused by insertion of time domain reflectometry probes and their influence on the measurement of soil moisture. Water Resour. Res. **33**, 1585-1593.

Topp, G.C. and Reynolds, W.D., 1998, Time domain reflectometry: a seminal technique for measuring mass and energy in soil. Soil and Tillage Res., **47**, 125-132.

Topp, G.C. and Ferré, P.A., 2000, Measuring Water Content in Soil using TDR: A State-of-the-Art in 1998. In Comparison of soil water measurement using the neutron scattering, time domain reflectometry and capacitance methods. International Atomic Energy Agency, Vienna, Austria. IAEA-TECDOC-1137, 111-124.

Topp, G.C., Adams, B.A., Young, G.D., and Lapen, D.R., 2001, Practical considerations for the use of a combination penetrometer and water content sensor. *In* W.D. Reynolds, C.F. Drury and C.S. Tan, eds., Proc. Soil Structure/ Carbon Workshop, Leamington, ON, Aug. 23-25, 1999, 403-414.

Vaz, C.M.P. and Hopmans, J.W., 2001, Simultaneous measurement of soil penetration resistance and water content with a combined penetrometer-TDR moisture probe. Soil Sci. Soc Amer. J. **65**, 4-12.

Young, G.D., Adams, B.A. and Topp,G.C., 2000, A portable data collection system for simultaneous cone penetrometer force and volumetric soil water content measurements. Can. J. Soil Sci., **80**, 23-31.

DETERMINATION OF THE WETTING FRONT IN DRIP IRRIGATION USING TDR MULTI-WIRE PROBE

C. F. Souza[1], E. E. Matsura[2], and R. Testezlaf[3]

[1]UNICAMP/FEAGRI – Departamento de Água e Solo
Cx. Postal 6011, 13081-970, Campinas-SP-Brazil; cfsouza@agr.unicamp.br
[2]UNICAMP/FEAGRI – Departamento de Água e Solo
Cx. Postal 6011, 13081-970, Campinas-SP-Brazil; matsura@agr.unicamp.br
[3]UNICAMP/FEAGRI – Departamento de Água e Solo
Cx. Postal 6011, 13081-970, Campinas-SP-Brazil; bob@agr.unicamp.br

ABSTRACT

The adequate estimation of wetting front is fundamental to determine the number of drippers per plant and its location below the plant canopy in drip irrigation. Measurements of wetting front dimensions are usually made by opening trenches, which is a time consuming method and sometimes imprecise. Recent scientific developments have created the possibility to monitor the soil moisture content using electronic sensors. The objective of this research is to study the possibility of using TDR Multi-wire probes (Time Domain Reflectometry) with electrical impedance discontinuities in the determination of the wetting front dimensions in drip irrigation application. The experiment was divided in two parts. In the first one, the laboratory performance of two Multi-wire probe configurations was studied and the probes reliability to monitor the water content variation in a porous media profile was evaluated. The second part was conducted in a 250 L bucket and the water dynamic process was monitored during 48 h, after a 5 mm of water application using a drip system. The results showed the viability of estimating the wetting front using TDR equipment coupled the Multi-wire probes with electrical impedance discontinuities.

INTRODUCTION

The knowledge of the wetted front design in the soil profile is important to optimize the drip irrigation management in agriculture. The drip irrigation is characterized by application of small amounts of water at high frequency and directly in the root zone. This type of application keeps the water content near to field capacity in a partly soil volume, commonly known as wetting front. The knowledge of the wetting front location is important, because besides the water, its concentrate the applied products through the irrigation water, such as fertilizers, fungicides, nematicides, etc. The adequate estimation of the wetting front dimensions is fundamental to determine the number of drippers per plant and its location under the plant canopy. Measures of wetted front dimensions are usually made by opening trenches where the

water is applied. Another method to monitor the soil moisture content is by electronic means, such as specific sensors.

The TDR technique for measuring water content and electrical conductivity of the soil solution is becoming increasingly popular. Its outstanding advantages are accuracy, speed, reproducibility, good theoretical basis, a well-defined and selected sampled volume, and the fact that water content and salinity are measured in exactly the same volume. The method is based on the fact that the speed of propagation of microwave pulses in conducting cables inserted in the soil very sensitive to its water content. This is the result of a large difference in the relative dielectric permittivities of water (81), air (1), and soil particles (3-5). Basically, a cable test and a sensor with metallic rods tied by coaxial cable are needed.

In TDR, the propagation velocity of a high-frequency electromagnetic signal is determined by:

$$v = c/\sqrt{e_b}$$

Where v is the propagation velocity, c is the propagation velocity of electrical signals in vacuum or free space ($3x10^8$ m/s), and e_b is the apparent dielectric constant of the soil. In the application of TDR to soil water measurement, a fast rise-time voltage pulse travels in the soil guided by a transmission line or wave guide of length, L, and the pulse reflects back from the end. By determining the travel time, t, of the pulse sent through the transmission line, it is possible to obtain the velocity during the two-way travel as $v = 2L/t$. Combining the two mathematical expressions, the apparent dielectric constant of the measured soil can be calculated by:

$$e_b = (ct/2L)$$

The most recent research on the TDR technology show a tendency in the direction of understanding the technique better and improving the probes configuration.

There is considerable flexibility in the probes design, which allows the measurement of water content. A wide variety of TDR probes or transmission lines have been developed and evaluated, both experimentally and theoretically. The initial TDR laboratory measurements were made in coaxial transmission lines (Topp et al., 1980). For field application, it was necessary to use a configuration that would allow us to monitor the exchange of the soil water content near of the probe, which was not possible using coaxial probe. The parallel-wire transmission line was adopted and used successfully in field (Topp & Davis, 1985). Multi-wire soil probes, which emulate coaxial transmission lines (Zegelin et al., 1989), were designed. They observed that signals from the new probes allowed more reliable and accurate volumetric water content and dielectric constant measurements.

The continuous-rod probes are comprised of two or three parallel metal rods completely surrounded by the medium to be measured, which when horizontally installed, are ideal to monitor the water content in a soil profile in laboratory. However, the installation of horizontal continuous-rod probes in the field requires either excavation outside the domain of interest and long rods to avoid disturbing the medium of interest, or repacking of the soil around buried probes. These requirements make horizontal continuous-rod probes unsuitable for many field applications.

The tendency to use the technique of TDR to measure the soil water content is relatively new in Brazil. Helping the diffusion of the technique, the objective of this research is to study the possibility of using TDR Multi-wire probes with electrical impedance discontinuities in the determination of the wetting front dimensions in drip irrigation application.

MATERIALS AND METHODS

Experiments were conducted in the Hydraulic, Irrigation and Drainage Laboratory of the Agricultural Engineering College (State University of Campinas/Unicamp). The experiment was divided in two parts. In the first one, the laboratory performance of two Multi-wire probe configurations was studied and the probes reliability to monitor the water content variation in a porous media profile was evaluated. The second part was conducted in a 250 L bucket and the water dynamic process was monitored during 48 h, after 5 mm of water application using a drip system. All measurements were made with a Trase System I[1] (Soilmoisture Equipment Corp., Santa Barbara, CA) equipped with a multiplexer (Trase Multiplexer model 6020B5). The TDR signal analysis was done manually by equipment display. ε_b readings were monitored in the tests.

Part 1

Performance of the Multi-wire probes with electrical impedance discontinuities

The objective of this test was to evaluate in the laboratory the performance of two Multi-wire probes with 0.10 and 0.20 m segmentations, denominated Probe 1 and 2, respectively. The probes used were designed to monitor the soil water content profile using a series of rod diameter changes. Each change in the rod diameter causes a change in the impedance of the probe, resulting in a characteristic reflection on the waveform. The travel time between these reflections defines the water contents in the regions between each discontinuity.

The probes have 4 stems of 0.675 m in length. The Probes 1 and 2 were divided in 7 and 4 segments, respectively. In both probes, the reading of the last segment was not considered because probes with high impedances without a balun installed result in end reflections with small amplitudes, thus making it difficult to analyze the waveforms. The ends of the stems were made with a sharp segment (0.075 m) to facilitate the penetration in the soil. The probes have an expected reading depth of 0.60 m. The design probes are shown in Figure 1 (Topp et al. 1982; Souza et al., 1999). The probes were manufactured in brass, except the intermediary spaces of smaller diameter, which are made of stainless steel.

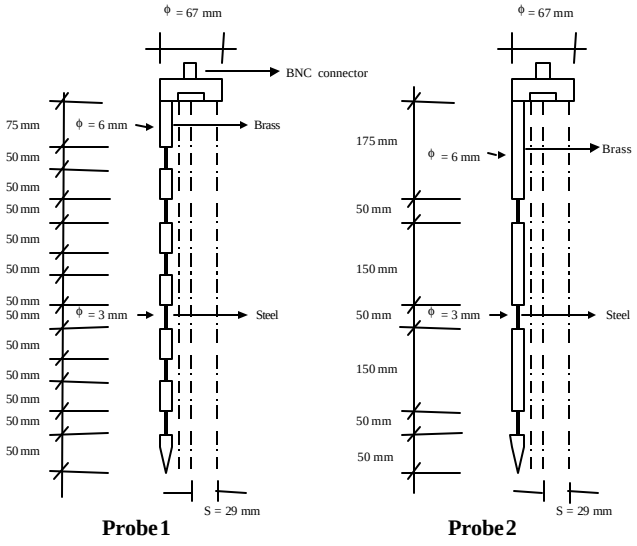

Fig. 1. *Schematic diagram of the Multi-wire Probe 1 and 2*

[1] Reference to registered mark does not constitute endorsement for the authors.

The probes were placed separately in a plastic cylinder box of 0.25 m in diameter and 0.90 m in length filled with distilled water to determine the probes characteristic impedance.

The characteristic impedance (Z_0, Ω) value is used to evaluate the performance of the TDR probe. The impedance of a transmission line (i.e., a probe) is a function of its geometry (spacing and diameter of rods) in addition to the dielectric constant of the medium in which the probe is installed. The difference in probe impedance is due to different diameters or rods spacing. So, different reflections in TDR waveforms can detect from the interfaces which different diameters or spacing of the rods are combined. Some combinations could result in probes with high impedance that, in turn give rise to final reflections with small amplitudes, thus making it difficult to analyze the waveforms. The impedance for a coaxial probe type transmission line can be approximated using (1) (Zegelin et al., 1989):

$$Z_0 = 60 / \sqrt{e_b}\ Ln(b/a) \qquad [1]$$

Where ε_b is the dielectric constant of a material surrounding the transmission line, *a* and *b* are the diameter of the inner and outer conductors, respectively. Alternatively, Z_0 can be measured by determining the line's reflection coefficient ρ_{ref} when the line is filled with a uniform and dielectric material with dielectric constant ε_b (Zegelin et al., 1989).

$$Z_0 = Z_u \sqrt{e_{b_{ref}}} \left(1 + r_{ref} / 1 - r_{ref}\right) \qquad [2]$$

$$r_{ref} = \left(V_1 / V_2\right) - 1 \qquad [3]$$

Where:

Z_u = TDR Load Impedance ≈ 50 Ω.
V_1 = local minimum voltage. (Obtained from the waveform)
V_0 = initial voltage. (Obtained from the waveform)
The Z_0 values were estimated from equations (1) and (2) for the developed Multi-wire probes with electrical impedance discontinuities.

Evaluation of the probes reliability to monitor the water content variation in a porous media profile

The evaluation was accomplished in thick sand; thereby the constructive effect of the probes was evaluated isolating the possible effects of the soil. The air-dried sand was packed in two plastic cylinder boxes of 0.25 m of diameter and 0.90 m of length, with bulk density of 1,650 kg/m^3. After the installation of the probes (Probe 1 and 2), 1 L of water was applied on the surface of the sand by a dripper with 4 emission points (8 L/h). The Topp calibration equation was used to calculate volumetric water content, θ (Topp et al., 1980). The water dynamics process in the sand was monitored during 8 h.

Part 2

Evaluation of the Multi-wire probe in the determination of the wetting front in drip irrigation

In this study, we consider the possibility of using Multi-wire TDR probes with electrical impedance discontinuities to determine the wetting front development under drip irrigation. The evaluation was accomplished in Dusky Red Latosol soil type. The air-dried soil was packed in two plastic cylinder boxes of 0.60 m in diameter and 0.90 m in length, with soil having the following physical properties: initial water content (m^3/m^3), total porosity (%) e bulk density equal 0,10, 53 and 1,200, respectively. In these recipients 10 Multi-wire probes (similar Probe 2) were placed for wetted front determination. The probe choice was based on the laboratory results that indicated the reliability of the probe configuration to describe the profile soil at a greater depth than 0.40 m. The 10 probes were distributed symmetrically in 4 directions with spacing of 0.08 m (Figure 2), starting from the emitter, which is placed in the center of the cylinder. The wetting front evolution for an application depth of 15 mm was evaluated, by monitoring during 6 days under the discharge rate of 2 and 4 L/h.

The applied depth was divided in 3 irrigations with 2 days of intervals, in order to analyze the necessity of estimating the wetting front using 2 or more consecutive irrigations. The evaporation effect was reduced using a plastic film on the recipient during the evolution of the wetting front. The used calibration equation was estimated in field condition and is equal to

$$q = 3x10^{-5} * e_b^{\,3} - 0.0017 * e_b^{\,2} + 0.0415 * e_b - 0.0603.$$

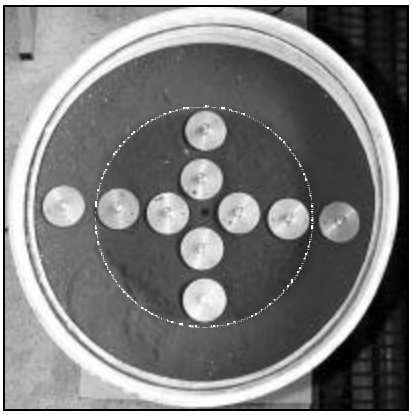

Fig. 2. *Symmetrical disposition of the TDR probes and soil water content.*

RESULTS AND DISCUSSION

Part 1

Performance of the Multi-wire probes with electrical impedance discontinuities

The estimated characteristic impedances are shown in Table 1. Analyzing the results obtained by the equation (1), it can be observed that the values calculated for the Multi-wire probes are close to the values of the common probes (3-wire). According to Zegelin et al. (1989), the Multi-wire probes present lower values of measured impedance, but did not exceed 173 Ω. The probe impedance values showed that the designed dimensions were appropriate to be used in soil water monitoring.

Figure 3 shows the difference between the graph readings obtained for the two probes, and how difficult is to interpret peaks impedance for the Probe 1 due to the reflection phenomenon. This phenomenon was caused by the interface between different electric property materials. Using (1), impedances of 136 and 177 Ω were found for the brass segments and stainless steel, respectively. Summarizing, the signal loss was caused by the rod design that has different material and geometry along its length.

Probes	Dimension (2*s)/d, mm/mm	Z_0, W	
		Geometric (1)	Measured (2)
Probe 1 (segment number)			
1	58/6	136	171
2	58/6	136	170
3	58/6	136	169
4	58/6	136	168
5	58/6	136	167
6	58/6	136	166
Probe 2 (segment number)			
1	58/6	136	168
2	58/6	136	167
3	58/6	136	166
Probe 3-wire – 0.10 m	20/2.1	135	198
Probe 3-wire – 0.20 m	28/3.1	132	196

The length for each segment of the Probe 1 and 2 is, respectively, 0.10 and 0.20 m

Table 1. *Characteristic impedance*

Evaluation of the Multi-wire probe in monitoring the water content variation in a porous media profile

Table 2 shows the results of the water dynamics process in tested porous media. To obtain values of water content in the same depths for Probes 1 and 2, the average of each depth was estimated by taking the average of the measured water content of the segments 1 and 2, 3 and 4, and 5 and 6 for Probe 1. It was verified that there are no differences of water content readings between the different probes, showing that both have similar characteristics in the electromagnetic waves propagation along the guide. However, Probe 1 showed more difficulty in interpreting the impedance peaks in its extremities (Table 2 and Figure 4) than Probe 2. This behavior confirmed the previous observations, showing that the high number of segmentations considerably increased the reflections of the pulse. In agreement with these observations, Topp & Davis (1985) presented results showing the difficulty of waveforms interpretation in probes with more than five segments.

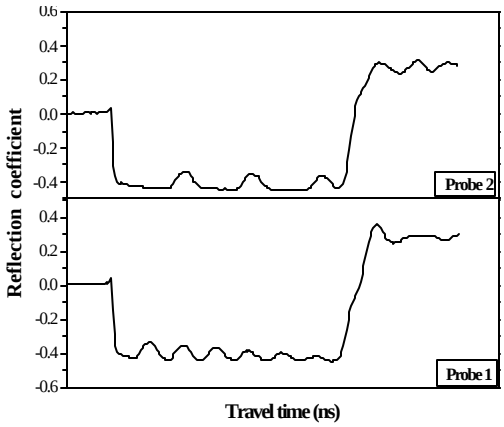

Fig. 3. *Comparison of travel time signal readings*

Time (h)	Volumetric water content, m^3/m^3					
	Depth (0 - 0.20 m)		Depth (0.20 - 0.40 m)		Depth (0.40 - 0.60 m)	
	Probe 1	Probe 2	Probe 1	Probe 2	Probe 1	Probe 2
0:00	0.04	0.04	0.04	0.04	NE	0.04
0:10	0.14	0.13	0.04	0.04	NE	0.04
0:20	0.26	0.26	0.09	0.08	NE	0.04
0:30	0.21	0.21	0.17	0.17	NE	0.04
1:15	0.17	0.17	0.23	0.23	NE	0.04
3:10	0.14	0.14	0.20	0.20	NE	0.08
4:00	0.13	0.12	0.20	0.20	NE	0.10
5:00	0.13	0.12	0.18	0.18	NE	0.11
6:10	0.11	0.11	0.18	0.18	NE	0.12
8:00	0.11	0.11	0.18	0.18	NE	0.12

NE = Not estimated due to difficulty to interpret of the impedance peaks.

Table 2. *Comparison among volumetric water content results in function of the time for probe 1 and 2*

In Figure 4, it was possible to identify water content variations of the porous media water dynamics. Although Probe 1 exhibited limitations, it offers a better detail of the water content of the porous media profile, showing the variation in each 0.10 m.

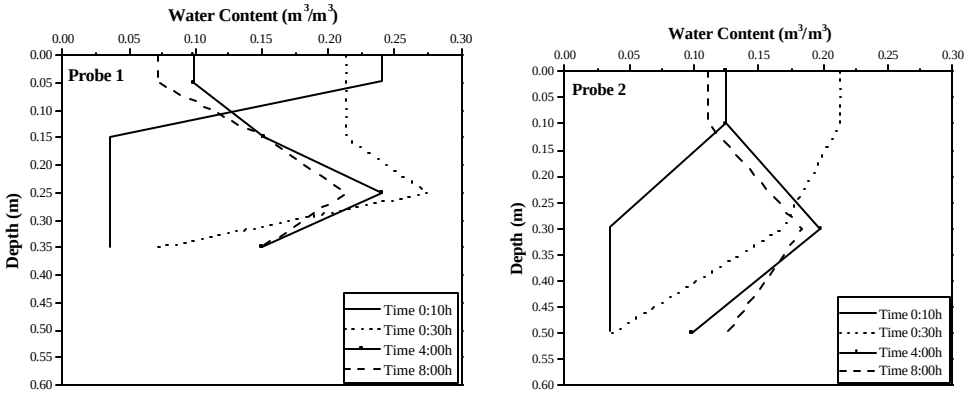

Fig. 4. Comparison between the probes 1 and 2 in the estimate of the porous media profile water content

Part 2

Evaluation of the Multi-wire probe in the determination of the wetting front in drip irrigation

The use of Multi-wire probes in the TDR equipment showed a speedy determination of the soil water content in dynamic processes. This evaluation is based in acquisitions of the water content variations in the wetting front, which was below a 2 minutes of intervals. This characteristic was possible due the use of a multiplexer, which automates the acquisition of the water content readings.

For all treatments in our experimental conditions, a symmetry of the water movement was found between the x and y-axes. This symmetry permits the use of just two probes in the last observation circle. The wetting front did not reach the probes disposed 0.24 m of the emitter, making faster readings and producing a smaller amount of graphs for the interpretation. The advantage of producing a small amount of graphs became interesting due to equipment memory limitation, which is approximately 180 graphs. It was also observed that it is possible to use one quadrant to monitor the wetting front in laboratory conditions, due to the soil homogeneity.

The wetted front evolution was monitored at 2 hourly intervals, but in Figure 5 the soil water content profiles 48 h after each irrigation are presented. It was possible to verify that doubling the rate (2 for 4 L/h), a larger water horizontal movement evolution took place in the soil and, consequently, there was decrease of the vertical movement. These results agree with the observations done by Bresler et al. (1971) and Keller & Bliesner (1990).

We observe that the higher values of the water content are concentrated in the central area of wetted front, confirming the results obtained by Botrel (1988) and Zanini (1991).

An expansion of the different axes (x, y) for successive irrigations was also verified. These results coincide with the tendency observed by Nogueira et al. (1999). The authors found an expansion of the wetted volume due to second and third irrigation in field conditions. The requirement to accomplish 2 or more successive irrigations to estimate the wetted front was confirmed, evidencing that initial conditions of the water content is essential for wetted front determination. The knowledge of these initial soil conditions is also important when a mathematical model is used to simulate water movement in the soil profile. Bad simulations can promote crop stress risks, salinity problems and bad distribution of the root system.

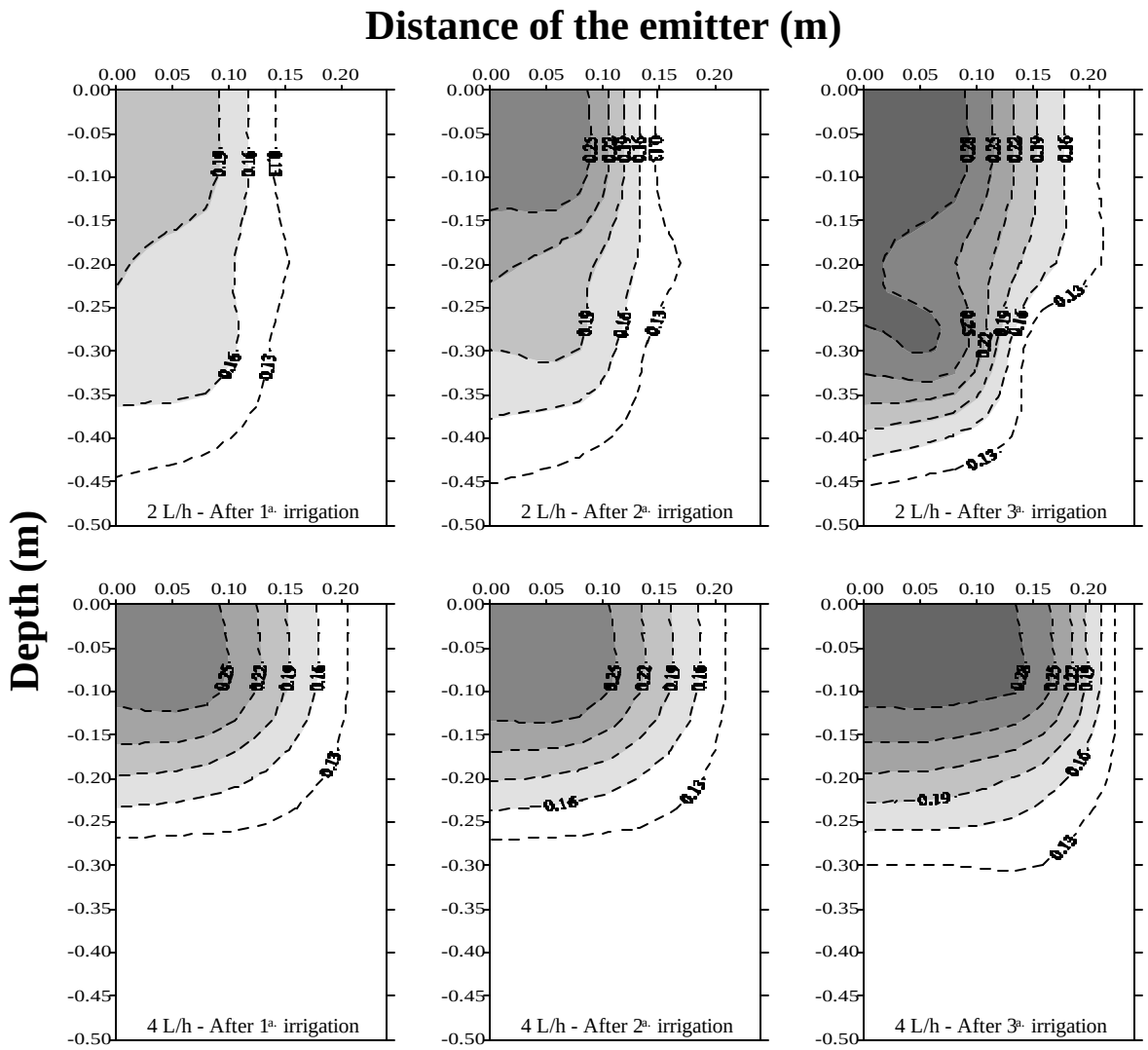

Fig. 5. *Evaluation of the wetting front in drip irrigation for 2 and 4 L/h rate*

CONCLUSION

By using different Multi-wire probe configurations, it was possible to obtain the water content measurements in water dynamic processes in the laboratory, which is very desirable in studies to optimize irrigation management. However, the configuration of Probe 1 showed limitations for interpreting the impedance peaks in its extremities.

The results demonstrated the viability of using the Multi-wire probes with electrical impedance discontinuities to determine the wetting front in drip irrigation.

We suggest future research on the evaluations of other probe configurations with smaller segments, which will help to detail the water content in the profile in order to decrease the soil space variability.

REFERENCES

Botrel, T. A., 1988, *Simulação da distribuição espacial da água em solo irrigado com gotejador*, Piracicaba, Tese de Doutorado - ESALQ-USP, 61 p.

Bresler, E., Heller, J., Diner, N., Bem Asher, J., Brandt, A., Goldberg, D., 1971, Infiltration from a trickle source: II. Experimental data and theoretical predictions: Soil Science Soc. Am. Proc., **35**, 683-689.

Dasberg, S., Bresler, E., 1985, *Drip irrigation manual*. Bet Dagan/Israel: International Irrigation Information Center, (Puplications 9

Keller, J.; Bliesler, R. D., 1990, *Sprinkle and trickle irrigation*. New York: Van Nostrand Reinhold, 652 p.

Nogueira, C. C. P.; Coelho, E. C.; Leão, M. C. S., 1999, Efeito da irrigação subsequente nas dimensões do bulbo molhado por gotejamento superficial e subsuperficial. In: CONGRESSO CHILENO DE INGENIERIA AGRICOLA, 3, Chillán. *Anais*...Chillán: Universidad de Concepcion, 92-97.

Souza, C. F.; Matsura, E. E.; Testezlaf, R., 1999, Desempenho de sondas multihaste segmentada para o monitoramento da umidade do solo por meio da técnica de TDR. In: CONGRESSO BRASILEIRO DE ENGENHARIA AGRÍCOLA, **28**, Pelotas. *Anais*... Pelotas: SBEA/UFPel,. [CD ROM]

Topp, G. C., Davis, J. L., and Annan, A. P., 1980, Electromagnetic determination of soil water content: measurements in coaxial transmission lines, Water Resources Res., **16**, 574-582.

Topp, G. C., Davis, J. L., and Annan, A. P., 1982, Electromagnetic determination of soil water content using TDR: I. Applications to wetting fronts and steep gradients, Soil Sci. Soc. Am. J., **46**, 672-84.

Topp, G. C., and Davis, J. L., 1985, Measurement of soil water content using time domain reflectometry (TDR): a field evaluation, Soil Sci. Soc. Am. J., **49**, 19-24.

Zanini, J. R., 1991, Distribuição de água e de ion K^+ no solo, aplicados por fertirrigação em gotejamento. Irrigação e Tecnologia Moderna, **45**, 13-24.

Zegelin, S. J., White, I., and Jenkins, D. R., 1989, Improved fields probes for soil water content and electrical conductivity measurements using TDR, Water Resources Res., **25**, 2367-2376.

ON THE USE OF THE TDR TRIME-TUBE SYSTEM FOR PROFILING WATER CONTENT IN SOILS

Jean-Paul Laurent[1], Pierre Ruelle[2], Laurent Delage[2], Nathalie Bréda[3], André Chanzy[4], Claude Chevallier[5]

[1]Laboratoire d'étude des Transferts en Hydrologie et Environnement, Grenoble-France, jean-paul.laurent@hmg.inpg.fr
[2]CEMAGREF, Unité de recherche "Irrigation", Montpellier-France, pierre.ruelle@cemagref.fr
[3]INRA, Ecophysiologie Forestière, Champenoux-France, breda@nancy.inra.fr
[4]INRA, Unité "Climat Sol et Environnement", Avignon-France, achanzy@avignon.inra.fr
[5]INRA, Domaine INRA SAD, Saint Laurent de la Prée-France, chevalli@stlaurent.lusignan.inra.fr

ABSTRACT

The TRIME-tube system manufactured by the German company Imko has been designed for profiling water-content in soils. A specific cylindrical 18 cm long probe "T3" is successively positioned at different depths into a 42 mm inner diameter, 1 mm thick plastic access tube where TDR measurements are taken using the associated "TRIME-FM" instrument which directly converts measured transit-times in terms of soil water-contents displayed on its front-panel. The use of this system is particularly straightforward because all the TDR measurement parameters are automatically recognized by the electronics when the probe is plugged. As it can appears like a possible and interesting alternative to the classical neutron probe technique, the purpose of our group was to evaluate the TRIME performances compared to other independent soil moisture measurement methods. Five experimental sites, exhibiting various real field conditions, have been equipped with plastic access tubes (fiberglass, polycarbonate or PVC) and water-content profiles monitored over long periods. This paper summarizes the main results of these tests. The problem of TRIME-tube calibration is particularly highlighted and two possible approaches are proposed. Finally, propositions are made to optimize its use and improve the system itself.

INTRODUCTION

In most countries, the use of nuclear techniques in agronomy is now drastically limited or, even, forbidden. For this reason, as an alternative to the "Soil Moisture Neutron Probe" (SMNP) many dielectric sensors and instruments have been developed during the last twenty years for measuring soil water content. Most of them give only local or average water-contents and only a few systems have direct profiling capabilities. The Imko TRIME-tube system is one of these and, in the frame of the French national research program in hydrology (PNRH), we wanted to test its performances under real field conditions. We will first present briefly this system. Then, we will describe the experiments that we

have realized to compare it to, either, SNMP or classical gravimetric technique. Finally, the problem of TRIME-Tube calibration will be discussed.

THE TRIME-TUBE SYSTEM

Description

The TRIME system has been developed for various applications and, talking only about soil water content, several instruments and probes are available (Imko, 2000). The TRIME-tube system considered here (Fig. 1) consists in two parts: the "TRIME-FM3" and a specific probe: the "T3" probe. The TRIME-FM3 is a battery powered TDR instrument with an internal impedance of 75 Ω. The T3-probe is a cylindrical TDR probe designed to be easily positioned inside a plastic access tube. With an overall length of 20 cm, it has to opposites rows of 4 metallic plates that forms a two-rods 18 cm long wave-guide mounted on springs to ensure a good and regular contact with the inner face of the access tube.

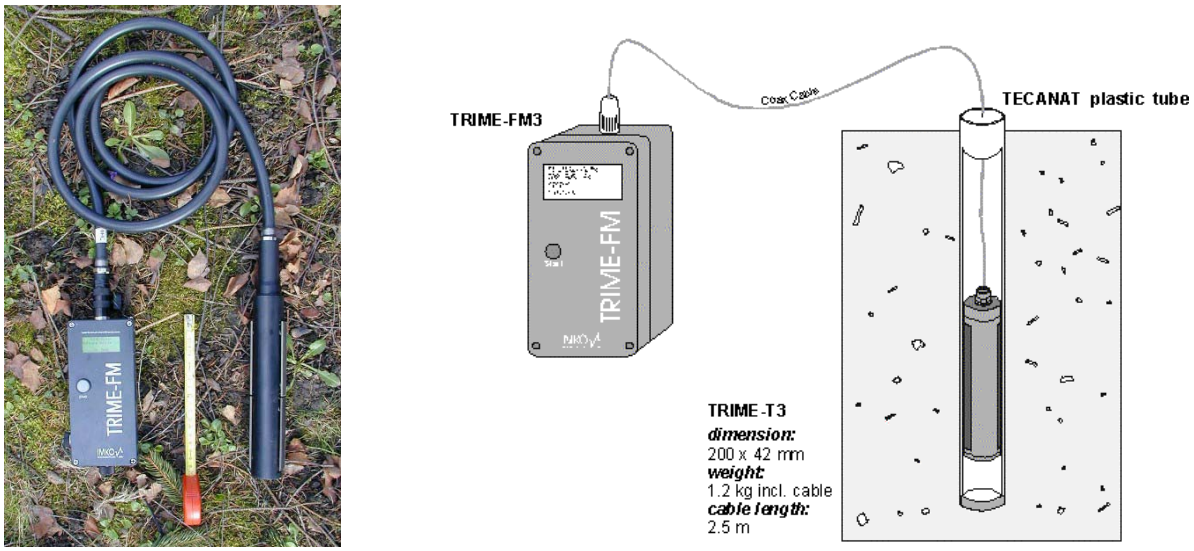

Fig. 1. *The TRIME-Tube system*

Access tube installation

Correct installation of the access tube is a crucial point when using the TRIME-tube system. The objective is to keep the contact with the surrounding soil as good as possible. To allow wave propagation into the outer medium, TRIME access tubes must be made out of plastic materials. Initially, Imko sold fiberglass tubes which have been replaced, now, by polycarbonate Tecanat® tubes and we have also successfully tested PVC. The overall length of the T3-probe cable permits to work with access tubes up to 2.5 m but, in most cases, length of 1, 1.5 or 2 m are retained. TRIME access tubes have an inner diameter of 42 mm with a 1 mm wall-thickness. One can easily guess that introducing such relatively brittle tubes into a natural soil implies particular precautions and, actually, it's highly recommended to use a specific access tube installation kit. Two types are available from Imko (Fig. 2 from Imko TRIME-FM Operating Manual) but we consider that the "tripod" model in the one that offers the best guarantee of a good final result.

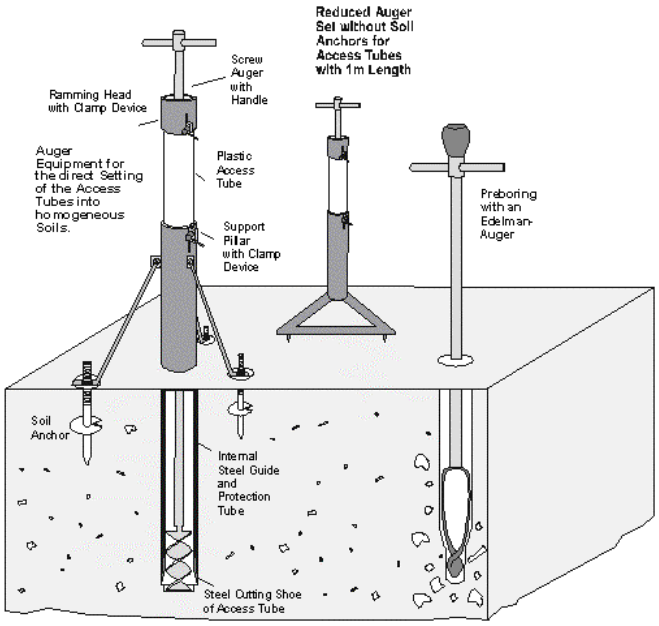

Fig. 2. *TRIME tube installation kits.*

During the installation of the access tube with this tripod installation guide, a protection steel tube of the same length is placed inside the plastic tube to avoid to press directly on the top of it and to prevent abrasion when removing the soil with an auger. One has to proceed by successive steps – forcing down the whole set access tube + internal protection steel tube for approximately 10 cm striking with a sledge hammer on the ramming head, removing the corresponding excavated soil with the auger – again and again until the top of the tripod is reached that is to say about 45 cm above the soil surface. Then, the guide is removed and the installation is completed with the same procedure as described above without any mechanical guide. Three kind of problems may alter, or, even, compromise, this installation procedure: i) it's very hard to install tubes in dry soils. If it's compatible with further intended measurements, a solution may be to wet first the spots where the tubes have to been put in; ii) on the contrary, high water contents can also create some problems: highly deformable soil consistency resulting in air gaps, difficulties to maintain the tube in place when extracting the auger; iii) rocky soils present the worst situation: risks to break the tubes, locking at a given depth with the impossibility to go any deeper. If such conditions have to be faced, the only solution is to dig a hole with a diameter much larger, put the access tube in and refill with a material "similar" to the original soil which is not really easy to define clearly.

Signal processing and calibration

The TRIME-FM is a "push-button" TDR instrument. This means that it has, programmed in its internal electronics, all the signal processing and conversion functions necessary for displaying directly a water-content at the end of a measurement. It proceeds in four steps:

1. A transit-time t_p is measured by an original technique which can be schematized as follows (see "TRIME theory" section in Imko, 2000): the starting of the TDR-generator rising step switches on a counter. Then a voltage comparator is active until the first reflection at the end of the probe is detected and the counter is stopped. The resulting count is finally corrected to take into

account the real shape of this reflection. This simple patented technique explains the relatively low cost of the TRIME-FM and its miniaturization degree. But, on the other hand, with this system, it is not possible to visualize full TDR-waveforms as other more sophisticated TDR instruments currently do. This is clearly a limitation when a physical interpretation of problematic results has to be searched for.

2. This measured transit-time (an integer) is then transformed into a "pseudo-transit-time" t'_p applying a linear relationship :

$$t'_p = \frac{t_p - Offset}{Divisor} \qquad [1]$$

where *Offset* and *Divisor* are two parameters adjusted normally once for all by operating a "basic calibration" of the TRIME-FM with its associated T3-probe. This operation is enabled by plugging a special "calibration-connector" on the left side of the device. At first approximation, this pseudo-transit-time can be seen as the part of the transit-time that is due to the propagation into the active part of the probe, only.

3. A "standard-moisture" θ_1 is then calculated using a polynomial adjusted on measurements taken on several soils at various water-contents (Stacheder, 1996):

$$\begin{aligned}\theta_1 = {} & -1.8161\ 10^{-1} + 1.9522\ 10^{-3}\ t'_p - 3.9357\ 10^{-6}\ t'^2_p \\ & + 2.4477\ 10^{-9} t'^3_p + 4.1356\ 10^{-12} t'^4_p - 3.0264\ 10^{-15} t'^5_p\end{aligned} \qquad [2]$$

4. Finally, a second "material-moisture" θ_2 is evaluated again with a 5th degree polynomial:

$$\theta_2 = C_0 + C_1.\theta_1 + C_2.\theta_1^2 + C_3.\theta_1^3 + C_4.\theta_1^4 + C_5.\theta_1^5 \qquad [3]$$

where C_0, $C_1 \ldots C_5$ are the coefficients of a material calibration curve. This is this value witch is displayed on the LCD four lines screen of the TRIME device. Initially, $C_1 = 1$ and the other coefficients are set to zero. This means that, without any special calibration, $\theta_2 = \theta_1$ and the material moisture is taken as the standard moisture.

All the parameters appearing in (1), (2) and (3) are accessible trough the SM-TOOLS utility freely distributed by Imko (www.imko.de/download). It is extremely useful to store this configuration in a safe place when receiving a new system. Doing so will offer the valuable possibilities: i) of restoring the standard configuration in case of problem ; ii) of back-calculating pseudo-transit times if needed to re-calibrate afterwards existing TRIME measurements : see next section. The basic calibration already mentioned above is systematically done in the Imko factory. If an association TRIME-M/T3-probe uniquely characterized by its serial number is modified in any way, it has to be done again. For that purpose, the manufacturer recommends the use of two references media – dry and water-saturated fine glass-beads – conditioned in cylindrical containers of at least 20 cm diameter. The built-in basic-calibration procedure will adjust the display to 0 and 44 %, respectively, when taking measurements on

the T3-probe placed successively in tube sections on the same type as the used access tube positioned vertically in the center of these two containers.

EXPERIMENTAL COMPARISON WITH THE SOIL MOISTURE NEUTRON PROBE

Experimental sites and measurement procedures

Two sites have been especially equipped for this experimental comparison: one in Grenoble in a urban environment and the other at the Lavalette experimental station of the Cemagref-Montpellier in a cultivated field. The installation in Grenoble took place in 1999 with three 1.5 m access tubes: Aluminum, Tecanat and PVC. During the whole summer and autumn 2000, measurements have been taken with a Troxler 4300 neutron probe and the TRIME S/N 7646. SMNP measurements were done on the three tube types. The installation in Montpellier has been realized in September 2000 with a single 1 m Tecanat tube in which systematic measurements with a SOLO 25 SNMP and the TRIME S/N 9112 have be done weekly until December 2000. In addition to these two main experiments dedicated only to the TRIME evaluation, three other sites of our French PNRH network (www.lthe.hmg.inpg.fr/medite) were also considered because of the particular problems they exhibit towards utilization of the TRIME-Tube technique. Table 1 summarizes the main characteristics of all these sites.

Place	Coordinates	Environment	Soil
Grenoble, University Campus	45°7' N 5°53' E	Urban area, Grass	Sandy Loam, negligible clay, low electrical conductivity pore-water
Montpellier Lavalette Station, Cemagref	43°40'N 3°50' E	Cultivated Soil	Silty-sandy-clayed texture, calcite
Avignon, St. Paul Station, INRA	43°57 N 4°48’ E	Cultivated Soil , Calcite	Silt-loam (27% clay, 11% sand), calcite
Champenoux, INRA-Nancy	48°44’ N 6°20’ E	Forest	Silty Clay Loam, enriched clay horizon (45% Clay), hydromorphic
St Laurent de la Prée, INRA	45°59’ N 1°1’ O	Humid zone, Wheat, Corn, Grass	Nearly 100% clay : “Bri” (Chlorite)

Table 1. *Main characteristics of the experimental sites considered here for evaluating TRIME performances*

Main results and discussion

When comparing straightforwardly SNMP data and TRIME measurements gathering all depths and dates for one tube (see examples of Fig. 3), it appears very clearly that the TRIME with its standard calibration over-estimates soil water-contents. This is particularly obvious at high water-contents. This results is somewhat surprising because earlier works (Laurent, 2000) have shown a fairly good

agreement between SNMP and TRIME-tube measurements without any particular calibration. Of course, we have tried to explain this behavior by verifying the validity of the standard calibration relation (2). For that purpose, since our TRIME-FM devices were initially factory-calibrated, we have inverted our water-contents readings θ_1 in terms of pseudo-transit times t'_p using the following inverse form of (2):

$$t'_p = 127.81 + 111\,\theta_1 + 14956\,\theta_1^2 - 65014\,\theta_1^3 + 129340\,\theta_1^4 - 1.35\,10^5\,\theta_1^5 + 7.07\,10^4\,\theta_1^6 - 1.45\,10^4\,\theta_1^7 \qquad [4]$$

Plotting now SNMP water-contents vs. pseudo-transit times (Fig. 4), back-calculated by (4), illustrates that, at least for the cases of Grenoble and Montpellier, the corresponding points significantly deviate from the standard calibration (2). Two kinds of explanation can be proposed to justify this difference: i) the considered soils have "non-standard" dielectric behaviors or ii) "something" has changed since the standard calibration (2) has been established by Imko following the works of Stacheder (Stacheder, 1996). The former hypothesis is not likely to be predominant: we know the physical and dielectric properties of these soils and TDR measurements taken in it with other TDR systems have shown that offsets from the "standard" well-known Topp polynomial they could exhibit were interpretable in terms of fluctuations in measurable factors like density or mineralogical composition. On the hand, some elements in the TRIME-tube design might have altered the validity of the original standard calibration: replacement of the initial fiberglass tubes by polycarbonate, some changes in the electronics, in the signal processing algorithms? … At the moment we write this paper, the question remains opened.

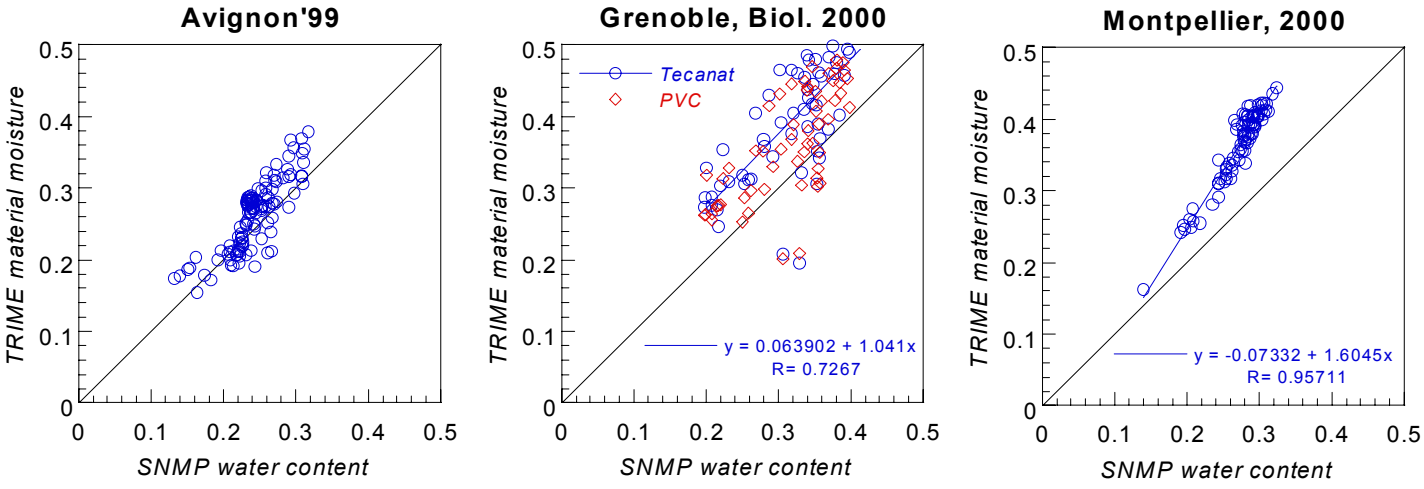

Fig. 3. *Direct comparison of measured water-contents for all dates and depths for three experimental sites.*

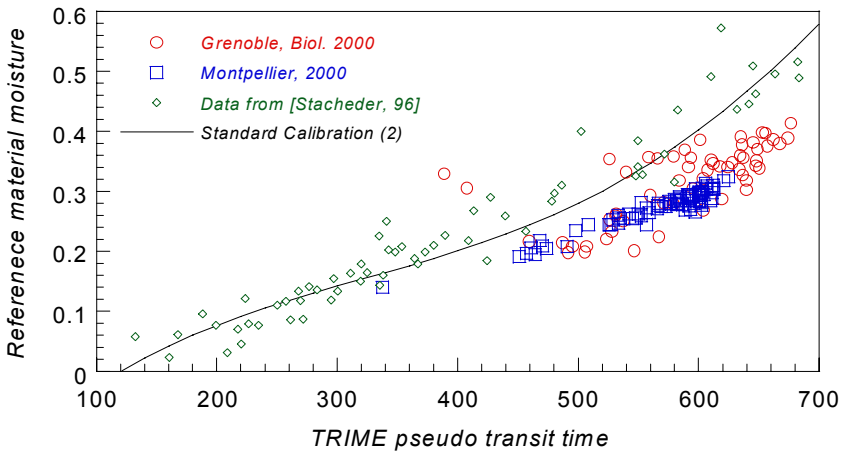

Fig. 4. *Deviation of our results on two sites from the TRIME standard calibration curve (2)*

Nevertheless, even with this observed discrepancy, the TRIME-tube method can be set operational taking the opportunity of introducing a specific material calibration (3). As first approximation not taking into account the influence of different soil horizons, correlations like those of Fig. 3 can be used to build a linear correction $\theta_2 = a + b \times \theta_1$ between the standard moisture θ_1 and the corresponding "true" material moisture θ_2. On our data, this simple approach yields a = 0.6243, b = 0.045 for the soil of Montpellier and a = 0.9605, b = -0.0614 for Grenoble. This correction has proved to be satisfactory both in terms of water-content profiles (Fig. 5) or water storages: Fig. 6. Doing this empirical calibration is more or less equivalent to calibrating a neutron probe. Here, SMNP measurements were taken as reference but, of course, the neutron probes we used were calibrated against gravimetric water-content measurements. Thus, these sampled gravimetric moistures could have been used directly to calibrate the TRIME measurements exactly like the common procedure for neutron probes.

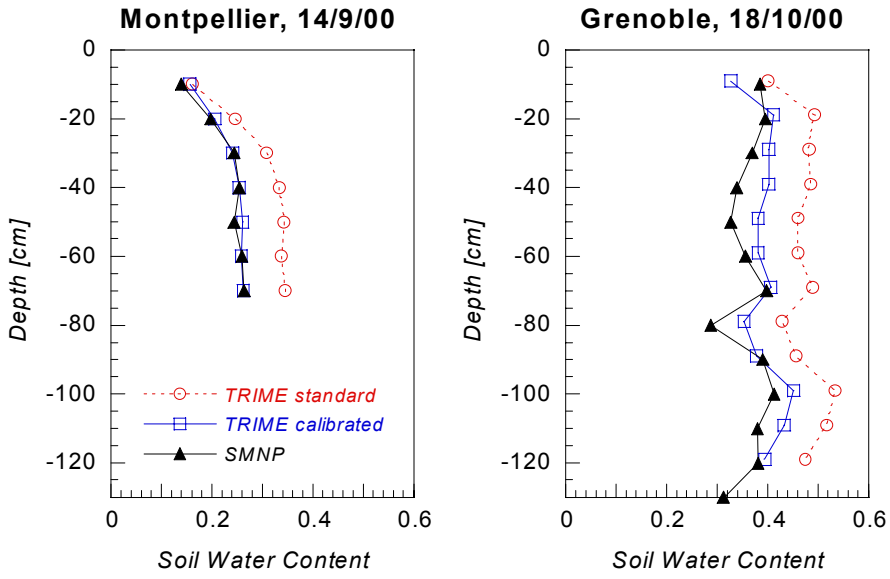

Fig. 5. *Examples of comparison of soil moisture profiles before and after TRIME calibration.*

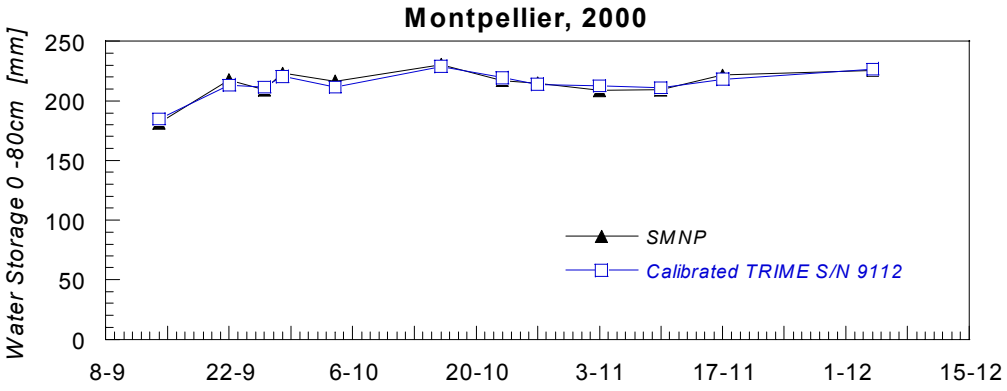

Fig. 6. *Example of water storage monitored by a calibrated TRIME compared to its equivalent estimated from SMNP data.*

Moreover, we found out that TRIME-tube measurements on long periods have a good and realistic dynamic response: see example on Fig. 7. Water-content variations were always visible even near the surface and their hydrological interpretation in relation with external stresses (rain intake, evaporation) or internal processes (root uptake, infiltration, drainage) in agreement with what we knew and measured on the observed systems. Particular soil profile organizations were also detectable (for example, the soil profile on Fig. 7 has clearly three-layers central part acting as "capillary barrier") and the above described calibration technique can be applied independently to each layer to refine water-profile monitoring. For all these reasons, we consider that the TRIME-tube system offers real profiling capabilities even if a specific calibration is still needed.

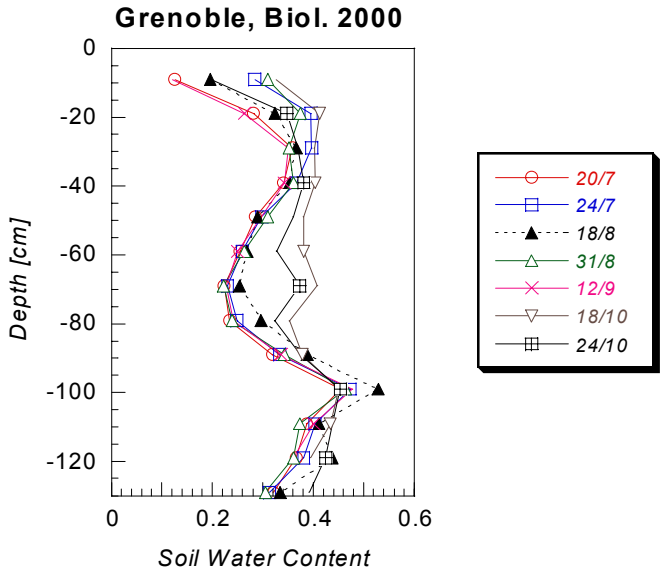

Fig. 7. *Example of water profile monitoring with a TRIME-tube system.*

TENTATIVE DEVELOPMENT OF A "PHYSICAL" TRIME CALIBRATION TECHNIQUE

The empirical – or "field" – calibration method proposed in the previous section may be sufficient for many applications but it has some disadvantages: i) a field campaign will have necessarily two phases: a first in which measurements are gathered to build a calibration curve and a second when it can be used or re-applied to previously acquired data; ii) in a given field situation, the whole range of water-content, texture, density… is rarely accessible. Therefore, it would be very useful to develop a more general calibration approach for the TRIME-tube technique. Of course, the built-in standard calibration curve (2) could probably be improved but we think that it would better to try to develop a more physically based approach. To go in this direction, we suggest to split the problem in two parts: instead of converting directly measured pseudo-transit times into water-contents, let us first consider the relation between the quantity measured by the instrument (pseudo transit time, for instance) and a parameter characterizing the dielectric properties of the surrounding soil (propagation time, dielectric constant) and then, only, the relation between this parameter and the water-content. Presented like this, it's easy to see that this latter calibration is not different of what is required for other types of TDR measurements and we can hope to solve the former – than we can call "instrument calibration" – once for all.

To investigate this instrument calibration problem, experiments have been made both in the field and in our laboratories. Immediately, a difficulty has to be faced: although pseudo-transit times measured by the TRIME-FM instrument are directly accessible when it is controlled under the SM-TOOLS utility from a PC through its serial interface, we have already mentioned that it is not possible to visualize its TDR-waveforms and, consequently, no classical TDR analysis can be made. To overcome this problem, a special DIN-BNC adaptor have been wired that allows TDR waveforms to be acquired connecting a Tektronix 1502B/C or a Trase system at the extremity of the T3-tube probe cable. Fig. 8 shows how such TDR waveforms look like. With this "trick", we are able to determine which propagation time is really "seen" by the probe inside its access tube and to quantify the permittivity K_{mes} the TRIME should measure in these conditions. Fig. 9 illustrates measurements acquired with this procedure on reference media listed in Table 2. This kind of tests clearly shows that – at least for the investigated experimental conditions: negligible electrical conductivity, good contact between a liquid and the tube – the pseudo-transit time t'_p measured by the TRIME-FM device is actually a realistic image of the "true" TDR waveform propagation time along the active part of the T3-probe. Moreover, it provides empirical models of the soil permittivity K vs. measured permittivity K_{mes} or K vs. t'_p relationships.

At Avignon during summer 1999, we tried to verify these relations under real field conditions comparing K_{mes} data with corresponding K measurements taken directly on three-rods TDR probes placed in the surrounding soil. The results were somewhat disappointing. Two main reasons could explain that: i) water-content spatial variability on short distances; ii) dependence of the above mentioned relations on soil/tube contact nature and quality. Of course, if the latter is the principal explanation, it would reduce the interest of the suggested instrument calibration which should be then re-done or adapted for each new installation. To clarify this point, we are now in the process of designing laboratory experiments on undisturbed core-sample of soils of all our sites. Numerical simulation of the TRIME measurement could also help.

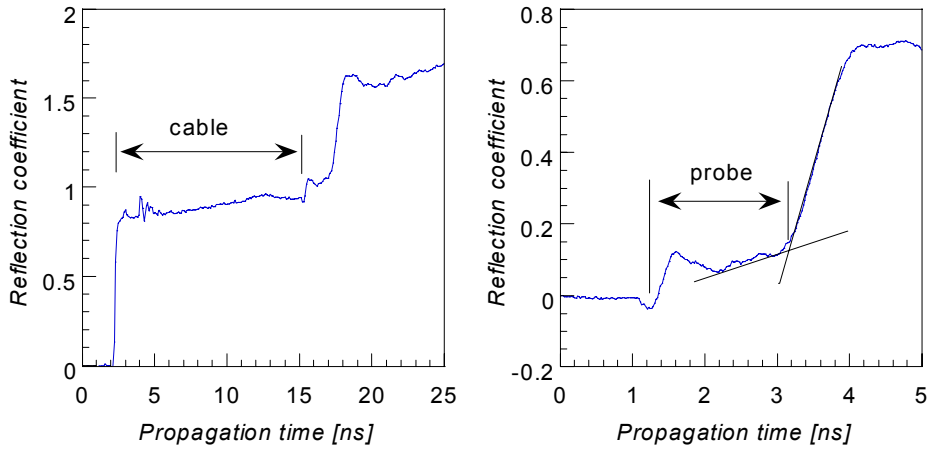

Fig. 8. *Example of TDR signals acquired with a Tektronix on a T3-Probe. Water-saturated glass beads. Left : complete signal, right : detail of the useful part corresponding to the propagation in the probe itself.*

	t'_p	t_p [ns]	K_{mes}	K
Air	-1.7	1.73	2.08	1.12
∅ 4 mm dry glass beads	123.8	1.85	2.38	2.90
∅ 450µm dry glass bead	129.1	1.91	2.53	3.69
Ethanol-saturated ∅ 4 mm glass beads	400.8	2.66	4.91	13.12
Ethanol	590.1	2.94	6.00	22.75
Water-saturated ∅ 4 mm glass beads	608	3.18	7.02	31.56
Distilled water	803	3.71	9.56	76.61

Table 2. *TRIME and TDR measurements on the T3-Probe in reference media. Tecanat tubes. t'_p : pseudo transit-time measured by the TRIME-FM, t_p : real propagation time determined on the acquired TDR waveforms, K_{mes} : corresponding measured permittivity inside the tube, K : material dielectric constant measured with a three-rod 20 cm long probe*

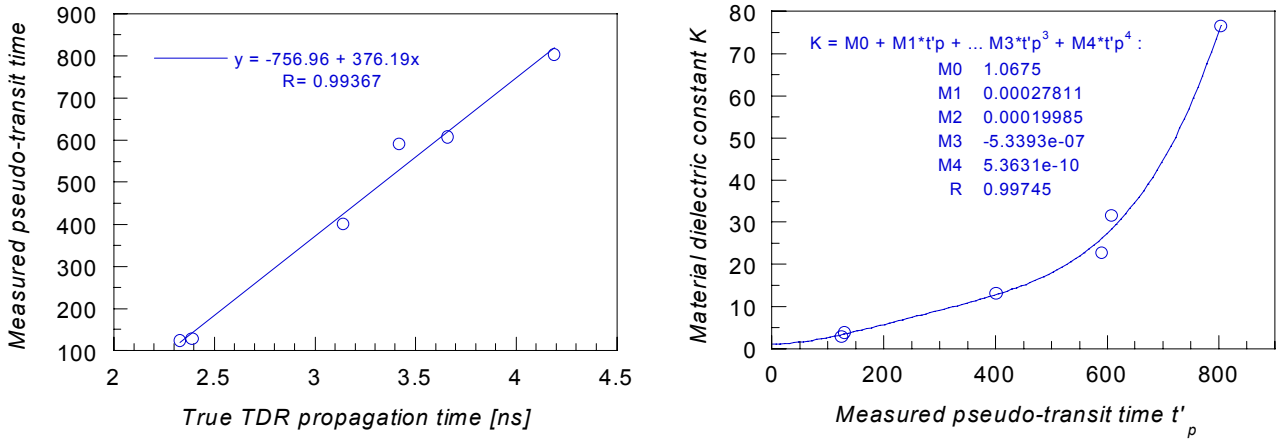

Fig. 9. *TRIME and classical TDR measurements taken in reference media of Table 2.*

Nevertheless, unless we consider that TRIME instrument calibration is still an ongoing research topic for us, we have applied the above conceptual frame to two unsolved problems concerning the application of this system: i) at St. Laurent de la Prée, in the western part of France near the sea, TRIME measurements taken in long 2.5 m tubes installed in a humid zone led to erroneous very high water content readings : Fig. 10 left ; ii) at Champenoux, in the eastern part of France, the same kind of measurements in a forest environment gave fairly erratic results : either the instrument displayed more or less realistic water-contents or the measurement were impossible because of an internal error "Salinity too high".

We have been able to solve the first one in the following manner: TDR waveforms have been systematically acquired with a Trase on the T3-probe positioned at every depths and the corresponding permittivity K_{mes} determined on it. A $K(K_{mes})$ relation has been assumed and the soil permittivity K vs. water-content was supposed to follow the Topp polynomial. So, it has been possible to build a set of reference material moistures which plotted versus TRIME readings allow to adjust a material moisture calibration: Fig. 10, right. This calibration introduces clearly a very strong "correction" which can be justified by the particular nature of the considered soil (Table 1).

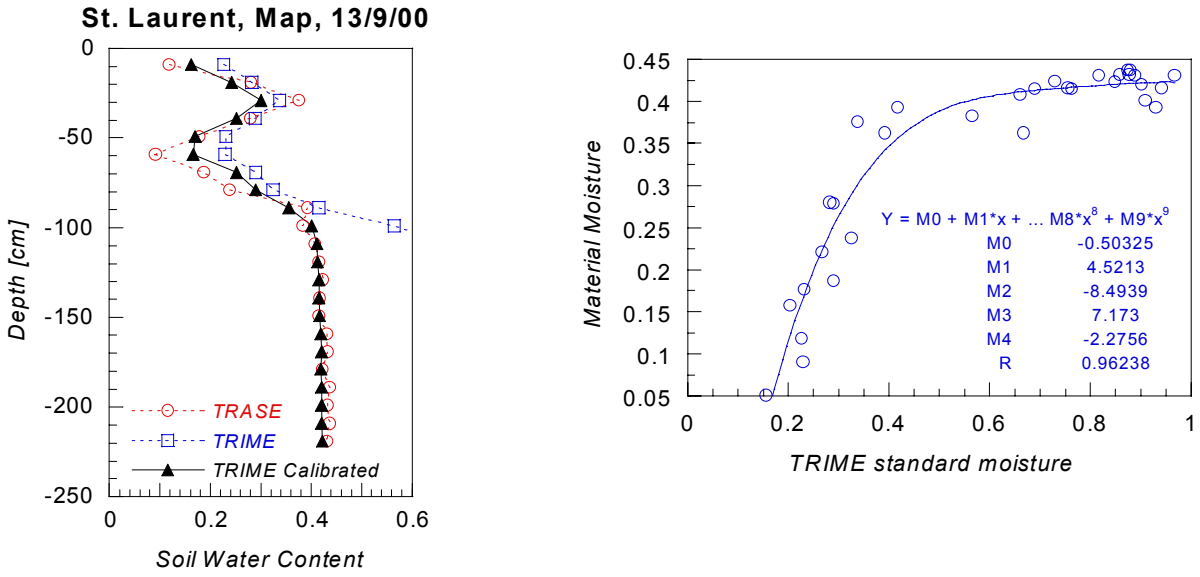

Fig. 10. *Calibration of the TRIME-tube measurements at St. Laurent de la Prée (see text).*

We try to reproduce this procedure at Champenoux but we failed although SMNP et gravimetric data were also available for this site. The reason for this is illustrated on Fig. 11: reflections at the end of the probe exhibit heavy scattering. The deeper the measurement is acquired, the smoother the reflected pulse. This drives the TDR-level on the propagation step to fall under the level on the incident step and the internal algorithm of the TRIME-FM is not designed to treat correctly such a situation.

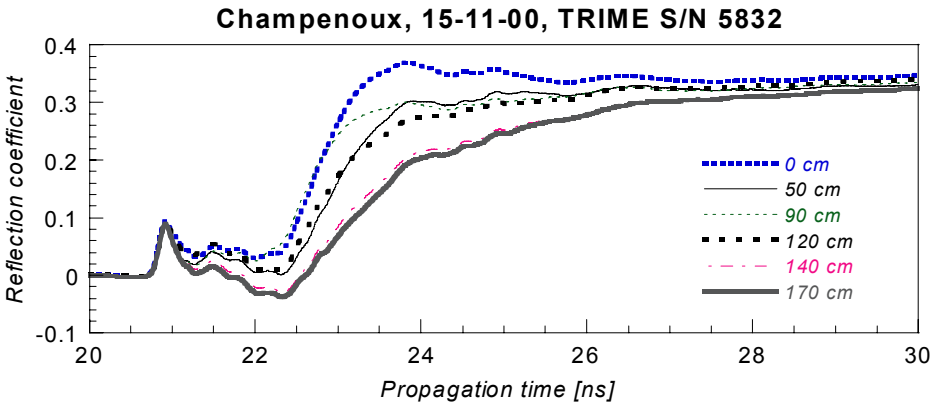

Fig. 11. *Examples of TDR-waveforms acquired on the T3-probe in a tube in the Champenoux forest.*

Among our sites, Champenoux is not the one with the highest clay content. The electrical conductivity is not particularly high, either. Complementary works have then to be undertaken to understand why such relaxing behavior has been observed and to evaluate the probability of finding again such a situation.

CONCLUSION

The TRIME-tube method for profiling soil water content have been extensively tested in various real field conditions. The results have been compared with independent water-content measurements. Complementary laboratory tests have been undertaken to clarify some points about the TRIME internal calibration and signal processing. An adaptor have been developed to be able to connect directly a T3-probe on a classical TDR-system in order to analyze more closely the physics of such a TDR measurement inside an access tube.

At the end of this work, we consider that: i) in most cases, the TRIME-tube system is really operational for profiling soil water-content; ii) it has to be calibrated. For that purpose, a simple field calibration similar to that of a neutron probe can be applied; iii) when calibrated, it leads to fairly accurate and sensitive readings that can be used for monitoring a profile on long periods.

Some points can be improved: a parameter directly linked to the internal measurement (pseudo-transit time, for instance) should be always displayed, the standard calibration may be updated, the ergonomics of the installation guide could be enhanced… Nevertheless, the Trime-tube is already one of the very few dielectric soil water-content profiling systems designed especially for soil physics. From a theoretical point of view, the relation between the permittivity measured inside the tube and the soil permittivity outside has to be investigated both experimentally and by numerical simulation. This is a condition for developing a more general, physically based, calibration approach.

ACKNOWLEDGEMENTS

This work has been funded both by the French *"Programme National de Recherche en Hydrologie"* from the INSU-CNRS and under a contract with the FAO/IAEA joint section *"Soil and Water Management & Crop Nutrition"*, Vienna. Thanks also to Dr. M. Stacheder and R. Fundinger from Imko GmbH for their open-minded and efficient collaboration.

REFERENCES

Imko GmbH, 2000, Soil and Material Moisture brochure, 55p, www.imko.de/download.

Imko GmbH, Operating Manual TRIME-FM, 28p.

Laurent, J.P., 2000, Profiling water content in soils by TDR: experimental comparison with the neutron probe technique, IAEA-TECDOC-1137, AIEA-Vienna, 81-104.

Stacheder, M., Fundinger, R., Koehler, K., 1994, A new Time Domain Reflectometry (TRIME) to measure soil moisture and electrical conductivity; Symposium and Workshop on Time Domain Reflectometry in environmental infrastructure and mining applications, Evanston, 56-65.

Stacheder, M., 1996, Die Time Domain Reflectometry in der Geotechnik, Messung von Wassergehalt, elektrischer Leitfähigkeit und Stofftransport, PhD Thesis, Schriftenreihe angewandte Geologie, Karlsruhe, 179p.

CALIBRATION OF CS615 AND TDR INSTRUMENTS FOR MAHURANGI, TARRAWARRA AND POINT NEPEAN SOILS

Andrew W Western[1], Maurice J Duncan[2] , Chris Olszak[3], Julian Thompson[4], Tom Anderson[5], Rodger B Grayson[6], David Wilson[7] and Rodger Young[8]

[1,3,4,5,6,7,8] Centre for Environmental Applied Hydrology and Cooperative Research Centre for Catchment Hydrology, Department of Civil and Environmental Engineering, The University of Melbourne, Victoria 3010, Australia; a.western@civag.unimelb.edu.au; r.Grayson@civag.unimelb.edu.au; d.Wilson@civag.unimelb.edu.au; r.young@civag.unimelb.edu.au
[2]National Institute of Water and Atmospheric Research,
P O Box 8602, Christchurch, New Zealand; m.duncan@niwa.cri.nz

ABSTRACT

Campbell Scientific CS615 instruments for soil moisture measurement have been installed in surface and sub-soils at 18 locations at one field site in New Zealand and at 7 locations at two field sites in Australia. Spatial patterns of soil moisture have also been collected at each of these sites on several occasions, using a Time Domain Reflectometer (TDR). Each type of instrument was calibrated after field sampling and after a review of the literature indicated that it might be necessary. Calibration for temperature and soil moisture effects was carried out in the laboratory using repacked soils. Satisfactory temperature calibrations were achieved for both instruments, but for the TDR it made little material change to the soil moisture estimates. Satisfactory soil moisture calibrations were also achieved for the TDR for each soil. There was a good relationship between soil moisture contents of the repacked soils measured by both instruments. However, the relationship between field CS615 measurements and those taken close-by using TDR showed a consistent departure that was greatest at high soil moisture levels. The TDR measurements were consistent with soil samples from the field assessed using the gravimetric method. Possible reasons for the departure are advanced.

INTRODUCTION

Campbell Scientific CS615 instruments have been installed at 18 locations in the Mahurangi River catchment, New Zealand, at four locations in the Tarrawarra Catchment, Australia and at three locations at Point Nepean, Australia. At each of these locations probes have been installed at two depths. The upper probe always sampled the 0-30cm depth range. The lower probe was installed to sample the bottom of the B-horizon. In many cases the lower probe was installed over the 30-55cm depth range but in some cases it was installed deeper. In the Mahurangi catchment instruments are located in four clusters, one at each of Satellite Station, Carran's, Claydon's and Marine Road. There is only one soil type at each of these study areas, with the exception of Satellite Station, where there are two different

soil types – one on the valleys and the other on the hills. The Tarrawarra and Point Nepean sites have relatively uniform soil conditions at the CS615 installations.
Spatial patterns of soil moisture have also been collected at each of these sites on several occasions. These have been measured using a Soilmoisture Equipment Corporation TRASE Time Domain Reflectometer (TDR) mounted on the University of Melbourne's TDAS system (Tyndale-Biscoe *et al*., 1998). These patterns consist of a grid of point measurements of soil moisture in the 0-30cm depth range.

Calibration of each instrument type was undertaken after initial field sampling and a review of the literature (e.g., Hook and Livingston, 1996; Seyfried and Murdock, 2001) indicated that there were likely to be significant soil type effects on the calibration relationships for these instruments, given the high clay contents of many of the soils of interest (Table 1). This paper describes a laboratory calibration of the above instruments for a variety of soil types found at the field sites.

METHODS

Soil sampling

Four soil samples from each sample location were obtained from the field for use in the laboratory calibrations. Two samples were from the 0-30cm layer. The first was approximately 10 litres in volume to provide soil material for the laboratory calibration. The second sample of approximately 0.5 litres, was used to establish the bulk density of the soil under field conditions using standard gravimetric methods. The third and fourth samples were taken from the installation depth of the deeper CS615s in each soil type. Again a large sample and a smaller bulk density sample were taken. Soil electrical conductivity (1:5 dilution) was also determined in the laboratory following Tucker and Beatty, (1974). Soils were packed in a 335mm long, 153.5mm diameter, polyvinyl chloride cylinder. A 20 cm long 3 wire TDR probe (Soilmoisture Equipment Corporation buriable probe), a Campbell Scientific CS615 probe (30 cm long) and a K-type thermocouple were inserted into the sample from the end of the cylinder. Tests were conducted in air and water to ensure that the soil moisture probes were not affected by the edges of the cylinder.

A TRASE TDR with version 2100 firmware was used to measure the dielectric constant. A Datataker DT500 datalogger was used to measure the period of the signal from the CS615 and the soil temperature. The desired soil temperatures were obtained by placing the cylinders in an Envirotherm environmental chamber or the laboratory cool room. All weighing was performed using a ±0.1g electronic balance.

Laboratory Procedures

The aims of the calibration were to:

1) Determine temperature correction relationships for the CS615 sensor.
2) Determine a calibration relationship between period, P, and volumetric soil moisture for the CS615 sensor.
3) Determine temperature correction relationships for the TDR sensor.
4) Determine a calibration relationship between dielectric constant, k, and volumetric soil moisture for the TDR.

The measurement approach was to use soil samples repacked to the bulk density measured in the field. For the Mahurangi and Tarrawarra soils the nominal test moisture contents were 20, 30, 40 and 50%m^3/m^3 and temperatures were 7, 20, 25, and 35 °C. For the Point Nepean soils the nominal moisture contents were 0, 5, 10, and 15%m^3/m^3. These values were selected to cover the range of conditions expected in the field.

The following steps were followed to obtain measurements at each nominal moisture content for each soil sample. First soils were oven dried and an appropriate mass of soil and volume of water were mixed to obtain the correct moisture content and bulk density. The sample was thoroughly mixed and then allowed to sit for at least 24 hours to allow the moisture to redistribute evenly through the sample. The moist soil was then packed into the testing cylinder so that the cylinder was just full. The TDR, CS615 and temperature sensors were then inserted into the soil sample and the sample canister was sealed. The canister was then placed in a constant temperature chamber and a series of measurements of *P*, *k* and *T* were made at the desired temperatures. The soil temperature was allowed to equilibrate for 24 hours before each measurement. Finally the volumetric soil moisture was determined by standard gravimetric methods.

RESULTS

Field sample bulk density and salinity

Bulk density ranged from 1.26 to 1.35 t/m^3 at Carran's, from 1.18 to 1.25 t/m^3 at Claydon's, from 1.15 to 1.55 t/m^3 on the satellite Station hills, from 0.98 to1.08 t/m^3 on the Satellite Station flats, from 1.07 to 1.2 t/m^3 at Marine Road, and was 1.47 t/m^3 at Point Nepean. No bulk density results are available from Tarrawarra. There was no trend in the bulk density between surface and deep samples. All the soil salinities were quite low (Table 1).

CS615 - Temperature Correction

The temperature response of the CS615 instrument is linear but dependent on the soil moisture content. Figure 1 shows a typical graph of the sensor signal *P* as a function of soil temperature. The slope of the lines in Figure 1 can be interpreted as a temperature correction coefficient for correcting the raw measurements of *P*.

$$P_{25} = P - C_{cs615}(T - 25) \qquad [1]$$

In 1 P_{25} is the corrected period, *P* is the measured period at temperature *T* and C_{cs615} is the temperature correction coefficient (i.e., the slope of a line in Figure 1).

Given that C_{cs615} varies with the wetness of the soil, some means of predicting C_{cs615} is required. Figure 2 shows the relationship between C_{cs615} and P_{25} for all soil samples from all sites. The best-fit linear relationship between the two variables is also shown. This relationship has an R^2 of 0.86 and a standard error of 0.00174 ms/ºC, which is sufficiently accurate for field applications. The relationship developed for predicting C_{cs615} is given in Equation 2.

$$C_{cs615} = 0.0128P_{25} - 0.0112 \quad [2]$$

Equation 2 can be substituted into 1 to obtain a temperature correction equation that can be applied directly to the raw measurements of *P* and *T*.

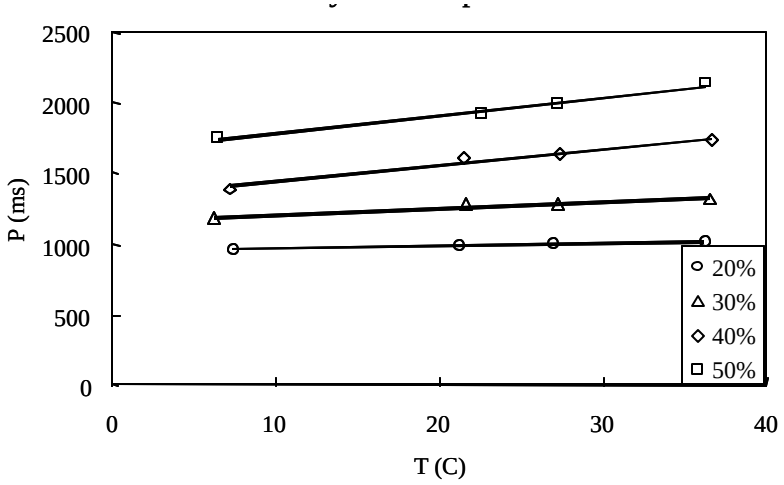

Fig. 1. *Variations in P with temperature (example for Clayden's deep soil).*

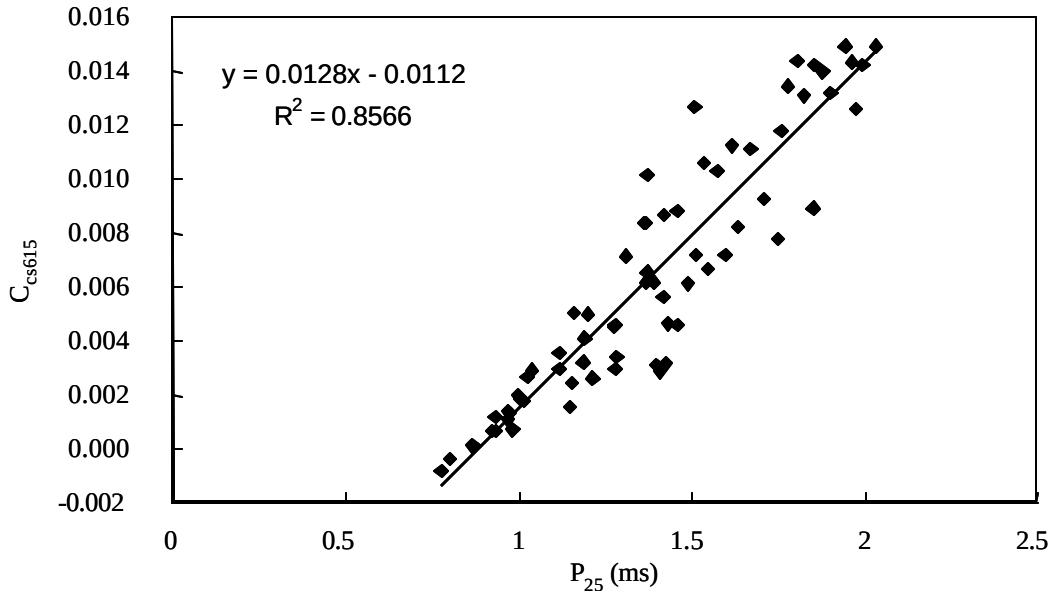

Fig. 2. *Variations in C_{CS615} with P_{25} for all soil samples.*

$$P_{25} = \frac{P + 0.0112(T - 25)}{1 + 0.0128(T - 25)} \quad [3]$$

Campbell Scientific Inc. (1996) provide a correction procedure that adjusts the estimated soil moisture; however, as shown below, there is a large amount of variability in the soil moisture calibration relationship. This means that finding a general correction based on soil moisture is likely to be difficult. Also as it is temperature effects on the sensor/soil response that are being corrected for, it is likely that the temperature effects are more strongly related to the raw signal than to the measured soil moisture. Therefore the above procedure was adopted in preference to the Campbell Scientific recommendations.

CS615 - Soil Moisture

Plots of volumetric soil moisture, q, against P_{25} were drawn for each soil sample and inspected for erroneous data points. Where data appeared suspect measurements were repeated. Then data for like soils were grouped together (e.g., the data for two shallow soil samples at Clayden's were combined). Figure 3 shows all the data together with the calibration relationship recommended by Campbell Scientific Inc. (1996). Clearly there are substantial differences between the recommended and laboratory derived calibration relationship for some of the soils. There is also a significant amount of scatter in the data; however, a close inspection indicates that most of this scatter is between soil types rather than scatter within each soil type. Therefore individual calibration relationships were developed for each soil type. Where the shallow and deep soils at a particular location had similar calibration relationships, these data were also combined. The number of data points, R^2 values, and standard errors for each calibration relationship are given in Table 1. Where the number of data points is small some care should be taken in interpreting the error statistics. The average standard error for our calibration of the CS615 is 2.3%m^3/m^3, which is similar to the standard error claimed in the instrument manual for typical soil specific calibrations. Note that the systematic error increases the measurement error if the factory calibration is used.

Soil	Clay content (%)	Salinity (1:5 dilution) (dS/m)	CS615 Calibration			TDR Calibration		
			n	R^2	Standard error %m^3/m^3	n	R^2	Standard error %m^3/m^3
Carran's Shallow	35	0.5	9	0.98	1.45	5	0.99	1.00
Carran's Deep	54	0.4				4	0.96	2.59
Clayden's Shallow	43	0.6	7	0.91	3.37	7	0.94	2.63
Clayden's Deep	49	0.4	4	1.00	0.19	4	0.97	2.15
Satellite Stn. Hills Shallow	27	0.3	6	0.96	2.08	6	0.96	2.12
Satellite Station Hills Deep	30	0.2	6	0.83	3.69	6	0.95	2.10
Satellite Station Flats Shallow	59	0.5	5	0.76	4.84	4	0.77	3.56
Marine Road Shallow	53	0.5	5	0.94	2.20	5	0.89	3.10
Marine Road Deep	59	0.3	6	0.96	2.14	6	0.98	1.32
Tarrawarra Shallow	28	0.2	7	0.98	1.22	7	0.96	1.22
Tarrawarra Deep	58	0.2	8	0.93	2.70	8	0.91	3.18
Point Nepean	0	0.2	4	0.99	1.10	4	0.98	1.42

Table 1. *Clay content and salinity combined with error statistics for laboratory derived CS615 and TDR calibration relationships for each soil. The instrument manuals specify an accuracy of +-2% for the factory TDRcalibration and +- 2% with soil specific calibration for the CS615.*

In general, quadratic relationships were used for the fitted calibration curves, given the non-linear nature of the data. Quadratic curves appear to provide adequate fits while recognizing the limitations imposed by the small number of data points. At Marine Road, the use of quadratic curves led to very little improvement over linear curves. This combined with the need for some extrapolation at these sites suggests that the linear model is most appropriate for Marine Road soils. At Point Nepean where the soils are sandy, there is very little difference between the manufacturer's recommended calibration relationship and the laboratory data.

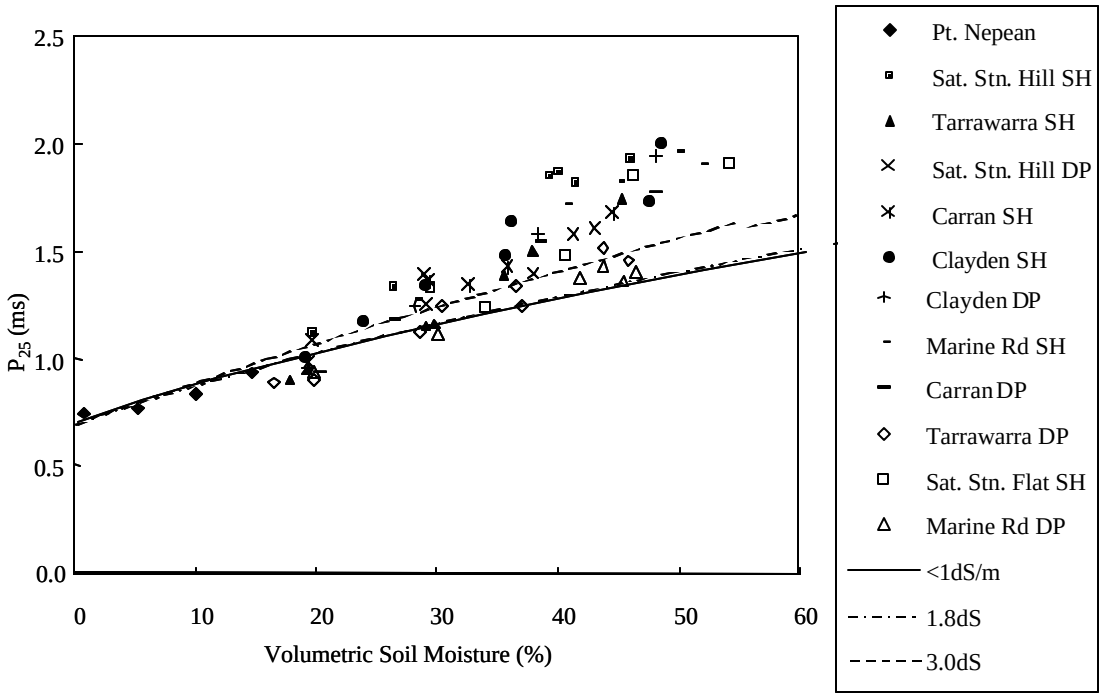

Fig. 3. *The relationship between q and P_{25} for all the soils. The calibration relationships for soils of different salinities recommended by Campbell Scientific are also shown (Campbell Scientific Inc, 1996).*

TDR - Temperature Correction

A similar approach to that used for the CS615s is used for temperature correction of the TDR data. This resulted in the following temperature correction equation.

$$k_{25} = \frac{k - 0.022(T - 25)}{1 - 0.003(T - 25)} \qquad [4]$$

The temperature effects on the TDR are much less marked than on the CS615. For example a winter volumetric soil moisture condition of 50%m^3/m^3 and temperature of 10ºC corresponds to a value of *k* of about 40. The temperature adjustment to *k* for these conditions is –1.4 or a reduction in volumetric moisture content of 0.8%, which is significantly less than the random measurement error standard deviation (about 1.5%) for a single point. Thus temperature correction of the TDR data has little practical impact for most field applications.

TDR - Soil Moisture

Plots of volumetric soil moisture, *q*, against *k* were drawn for each soil sample and inspected for erroneous data points. Where data appeared suspect measurements were repeated. Then data for like soils were grouped together (e.g., the data for two shallow soil samples at Clayden's were combined). Figure 4 shows all the data together with the calibration relationships recommended by Topp *et al*. (1980) and Soilmoisture Equipment Corporation (1996). Clearly there are substantial differences between the recommended calibration relationships and some of the soils. There is also a significant amount of scatter in the data; however, a close inspection indicates that most of this scatter is again between soil types rather than scatter within each soil type. Therefore individual calibration relationships were developed for each soil type. The number of data points, R^2 values, standard errors for these calibration relationships are given in Table 1. Where the number of data points is small some care should be taken in interpreting the error statistics. The average standard error for our calibration of the TDR is 2.2%m^3/m^3, which is similar to the standard error claimed in the instrument manual, although the systematic difference between the soil specific and factory calibration increases the measurement error if the factory calibration is used.

In general quadratic relationships have been used for the fitted calibration curves, given the non-linear nature of the data. Quadratic curves appear to provide adequate fits while recognizing the limitations imposed by the small number of data points. In general the Topp curve provides an upper envelope to the *q*-*k* relationship. A common reason cited in the literature (e.g., Dasberg and Hopmans, 1992; Dirksen and Dasberg, 1993; Hook and Livingston, 1996) for deviation from Topp's relationship is the influence of water that is bound to clay particles by hydrogen bonding effects. These water molecules are restrained against rotation in an externally applied electric field to some degree and thus contribute less than expected to the dielectric constant. Hence the value of *k* is expected to be less than the Topp curve indicates for a given moisture content where this effect is present, as is common in high clay content soils. The deviation between the Topp curve and Soil Moisture Equipment Corporation's calibration may possibly also be due to this effect since Soilmoisture Equipment Corporation used sandy, sandy loam and clay soils for moisture contents below 40% but clay soils above 40% (Soilmoisture Equipment Corporation, 1996). For the sandy soils at Point Nepean, there is very

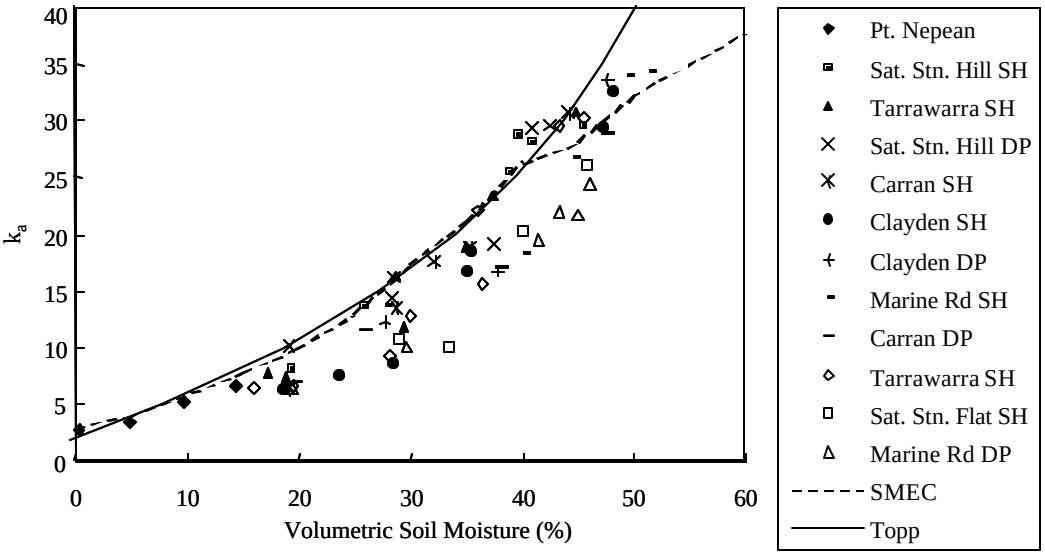

Fig. 4. The relationship between k and *q. The calibration relationships recommended by Topp* et al. *(1980) and Soilmoisture Equipment Corporation (1996) are also shown.*

little difference between the manufacturers recommended calibration relationship and the laboratory data.

Comparisons

Laboratory comparison of TDR and CS615

Figure 5 shows a comparison of volumetric soil moisture measured in the laboratory for soils for which comparative field data exist. It should be noted that the data shown in Figure 5 are the same as those used to develop the calibration relationships. Thus the data provides a check on the internal consistency of the calibration relationships but not really an independent check of the calibration relationships. It can be seen that there is a good relationship between the CS615 and TDR measurements.

Field comparison of TDR and CS615

During each TDR field campaign, each CS615 soil moisture station was visited and several, generally four, TDR measurements were performed in close proximity (about 0.5-1m) to the CS615 sensor installed at the surface. The measurements were performed in a ring around the installed CS615. The typical separation between the TDR measurement points was about 1m, which is similar to the proximity to the CS615. Both the CS615 and TDR sensors were inserted over the 0-30cm depth range for these measurements so the measurements should be comparable providing the small scale soil moisture variability is small. A single factor ANOVA conducted on the TDR data grouped by a combination of site and date (i.e. each group contains data from only one site and time) results in a within group variance of 2.4(%m^3/m^3)^2. This can be interpreted as a combination of the small-scale soil moisture variability and the random measurement error for the TDR. If the CS615 and TDR have the same measurement error, it would be expected that the differences between the TDR and CS615 would have a variance twice this value, that is about 5(%m^3/m^3)^2, if there were no other source of error. The overall variation in soil moisture conditions between the various campaigns for the TDR data collected at the CS615 sites is 64(%m^3/m^3)^2. The implication of the relative magnitude of

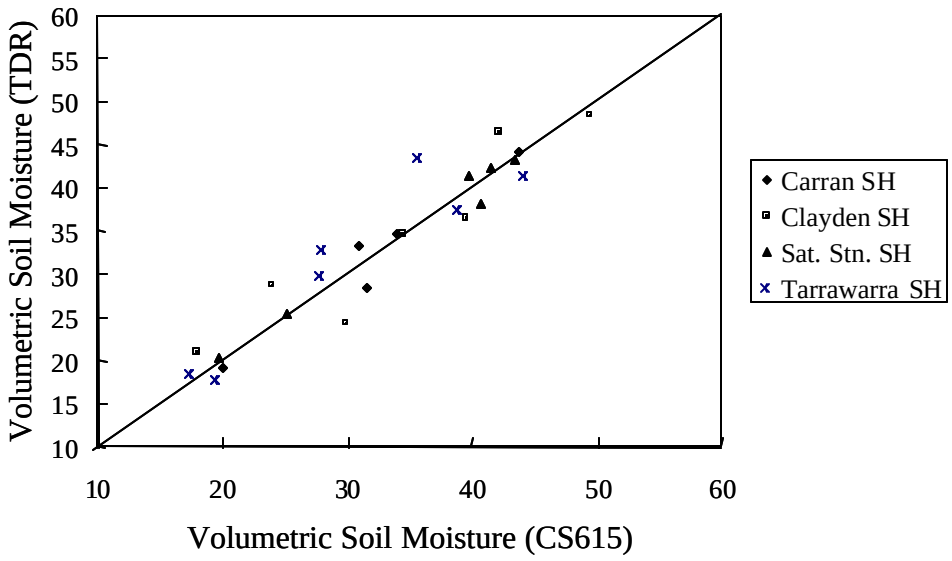

Fig. 5. *A comparison of TDR and CS615 measurements of soil moisture in the laboratory for soils with comparative field data. The soil moisture values are calculated using the calibration relationships developed above for each soil. Note that this data is derived from the same data used to develop the calibration relationships for each soil.*

these variances is that it should be possible to assess the comparative performance of the two instruments in the field.

Figure 6 shows a comparison of field measured soil moisture for three CS615 sites at each of Clayden's and Carran's, six CS615 sites at Satellite Station and four CS615 sites at Tarrawarra. For the New Zealand sites data were collected on six occasions and for the Tarrawarra site data were collected on seven occasions. However on the first New Zealand sampling occasion these data were collected only a short time after the CS615 stations were installed. As these data appeared to be quite different from later occasions they were excluded from the comparison.

The data show good relationships between CS615 and TDR measurements at individual study areas and the three New Zealand study areas appear reasonable consistent with each other. However there is a substantial difference between the CS615 and TDR measurements, particularly for the New Zealand research sites. The reason for this difference is unclear at this time and the problem will be discussed further below.

The factory calibrations were also applied to each instrument and the results of the comparison between CS615 and TDR with the factory calibrations is shown in Figure 7. There is more agreement between the study areas but also more scatter when the factory calibration relationships are applied. When the factory calibrations for temperature and soil moisture are used the CS615 soil moisture measurements are higher than those from the TDR.

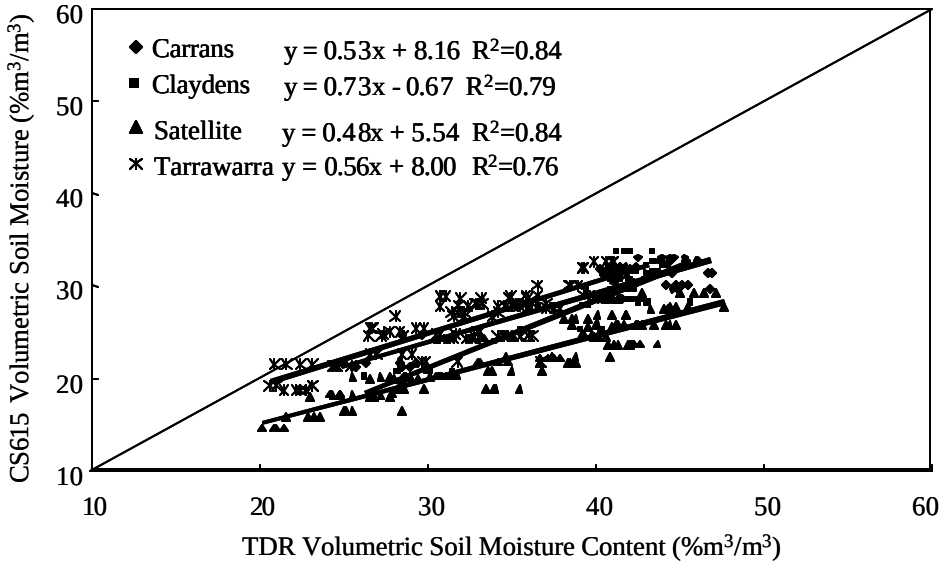

Fig. 6. *Comparison of CS615 and TDR measurements in the field with laboratory calibrations applied. Data from the first New Zealand campaign has been excluded to exclude the effects of recent installation on the CS615 data.*

Table 2 provides a comparison of variances of the differences between the TDR and CS615, *Dq*, where *Dq* is defined by Equation 5 and q_{TDR} and q_{CS615} are the moisture contents measured using the TDR and CS615 respectively.

$$\Delta q = q_{TDR} - q_{CS615} \qquad [5]$$

Three different variances are provided in Table 2. The first is the within site variance or the variance remaining after mean differences in Dq between individual CS615 sites have been removed. This provides a measure of any random errors affecting both the CS615 and TDR measurements, as well as any trend in Dq with soil moisture. If there were only random errors and the measurement precision of both the CS615 and TDR were identical, then, as explained above, this variance would be expected to be about $5(\%m^3/m^3)^2$ based on the differences between TDR measurements conducted at each site and for each field campaign. The second variance is the within study area variance or the variance in Dq remaining after mean differences in Dq between study areas are removed. This within study area variance incorporates the errors contributing to within site variance plus any differences between either the CS615 sensors or calibrations (both CS615 and TDR) within each study area. The third variance is the total variance in Dq for a given pair of calibration relationships.

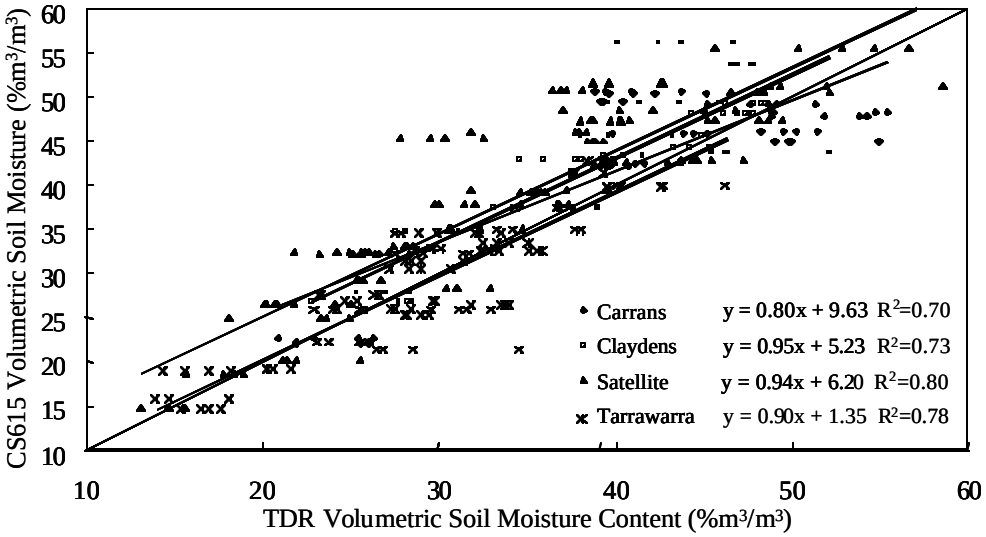

Fig. 7. *Comparison of CS615 and TDR measurements in the field with factory calibrations applied. Data from the first New Zealand campaign has been excluded to exclude the effects of recent installation on the CS615 data.*

There are two rows in Table 2 corresponding to the two calibration relationships underlying Figures 6 and 7. Comparing the total variances in Dq for the three cases indicates that the laboratory calibration provides a more precise comparison between the instruments than using the factory calibration. However there is a substantial amount of correlation between Dq and q that is evident in Figure 6 i.e. slope of data not equal to one. This correlation increases the variance of Dq slightly. Variances shown in brackets in Table 2 have had this effect removed and it is clear that it does not materially affect the comparisons. For all the calibration relationships there is a small increase in variance due to moving from grouping by site to grouping by study area. This indicates some difference between CS615 sensors and/or calibration relationships (both CS615 and TDR) at each study area but the difference is fairly small. This analysis indicates that the laboratory calibrations are superior to the factory calibrations, provided the reason for the systematic differences between sites and the correlations between Dq and q can be explained (and thus eliminated).

Field Comparison of Gravimetric and TDR

Gravimetric soil moisture samples were collected from the field at the same time as TDR measurements were made on one occasion for each field site in New Zealand and on several occasions at Tarrawarra. Figure 8 shows bulk density plotted against these gravimetrically determined volumetric moisture content. Clearly there are trends in bulk density as a function of moisture content. This indicates that there are some problems with the gravimetric data. Nevertheless a comparison between the TDR moisture content measurements (calculated using the laboratory calibration) and the gravimetric moisture content measurements is made in Figure 9. The comparison is good given the quality of the gravimetric data. The same comparison was made using the factory calibration for the TDR with similar results.

Calibration relationship	Within site variance	Within study area variance	Total variance
Laboratory (Fig. 6)	9.3 (6.0)	10.1 (7.6)	16.7
Factory (Fig.7)	17.1 (15.9)	19.9 (17.5)	23.4

Table 2. *Variances for the difference between TDR and CS615 moisture content measurements, Dq, in the field with different calibration relationships. Total variance as well as variance that is not explained by differences in the mean at each CS615 station and at each of the four study areas are shown.*

Given the quality of the gravimetric data, it is not possible to distinguish between the two different calibrations. These comparisons do however give confidence that the TDR is approximately correct and that the systematic differences between the TDR and CS615 are primarily due to the CS615 data.

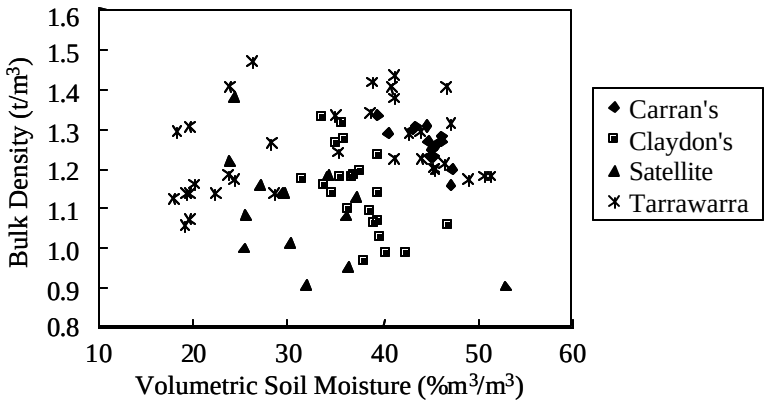

Fig. 8. *Bulk density as a function of gravimetrically determined volumetric soil moisture for field samples used to compare with TDR in Figures 9.*

DISCUSSION

The reason(s) for the difference between field measurements of soil moisture by the CS615 and the TDR have been explored. From the section above it appears that the errors most likely lie with the CS615 or its environment. A number of checks have been carried out in an attempt to explain the differences. These have concentrated on potential problems in the laboratory and field including:

1. Errors in the logging programs used in both the field and laboratory.

2. Errors in the bulk density of the repacked cores. Overall repacked bulk densities were about 10% less than the field values. There were slight trends in the repacked bulk density, generally toward reduced bulk density for higher

moisture contents but these errors were less than 5% for most soils and are unlikely to cause the observed errors.

3. Changes in salinity due to rewetting. The soils were rewet using tap water in the laboratory and this may have increased the salinity of the soil. Figure 3 shows Campbell Scientific's calibrations for three different salinities. All the soils tested have fairly low salinities, certainly less than 3dS/m. Thus the effect of salinity indicated by the factory calibrations is relatively small compared with the difference between our laboratory and the factory calibrations. This probably counts against a salinity effect as big as the observed differences.

4. There are differences between the soil conditions, and thus possibly the moisture, for the TDR and CS615 measurements in the field since the CS615 stations have stock excluded but the effect seems much too big for this to be a possible explanation. However, TDR measurements were often taken just inside the exclusion area by deflecting the fence and at Tarrawarra TDR measurements for site 1 (of 4 sites) were taken well within a larger exclusion area containing a variety of meteorological instruments and similar differences between the TDR and CS615 were observed at this site as at the other three Tarrawarra sites.

5. Effects of soil sterilization by Gamma irradiation for the New Zealand soils (required for quarantine purposes) are possible but seem unlikely as there should be no physical or chemical change.

6. There could be an effect of soil structure or gaps between the soil and sensor. The structure is certainly different between the field and laboratory due to the destructuring of the laboratory samples during the calibration process. This may affect the electrical contact between the CS615 and the soil and thus reduce the electrical conductivity effects for highly structured soil. Highly structured soil may also have a greater proportion of voids in close proximity to the sensor electrodes where the sensitivity to k is greatest. Both of these effects would tend to reduce the measured P in the more highly structured field soils and could explain our results. Similar effects would also occur if gaps developed between the sensor and the soil in the field due to shrinking and swelling of the soil. Both the Mahurangi and Tarrawarra soils crack extensively during dry periods.

The first three potential sources of error have been explored and eliminated as not being large enough to explain the differences, although some move the data in the correct direction. Potential errors 4 and 5 would appear to be small. The bulk densities of the soils (Figure 8) are not particularly high and are thus not indicative of compaction due to stock trampling. In relation to potential error 6 the soils would be expected to expand upon being wetted and thus reduce any error caused by this mechanism at high soil moisture contents,

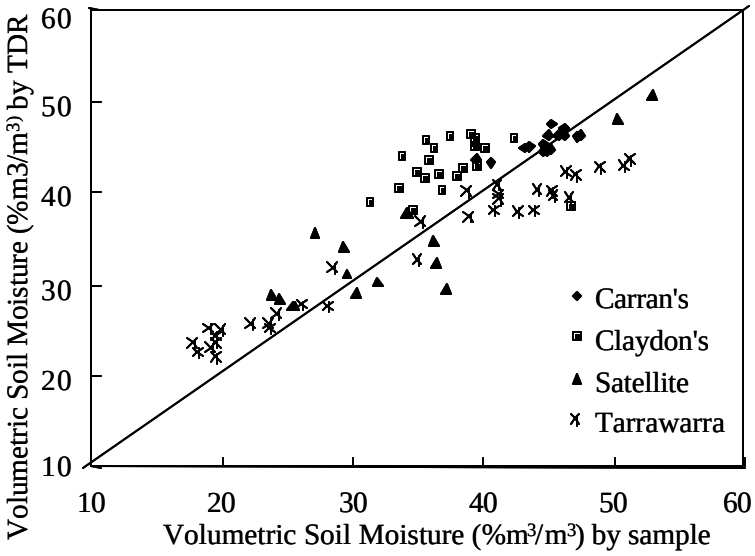

Fig. 9. *Comparison of gravimetrically determined volumetric soil moisture with TDR using laboratory calibrations.*

but the differences get larger at high soil moisture contents. Nevertheless the soils do crack at low soil moisture levels and this remains a potential source of error. The evidence at hand suggests that there was a behavioural difference between the CS615s in the laboratory and in the field.

CONCLUSIONS AND RECOMMENDATIONS

The following conclusions can be drawn.

1. A new temperature correction procedure for the CS615s has been proposed.

2. The temperature effects on the TDR are minor, being greatest for wet conditions and cold soils. Temperature correction of winter TDR measurements close to saturation would generally result in a correction of less than 1%m^3/m^3.

3. The soil moisture calibrations derived in the laboratory and the standard errors for those calibrations are generally very good for both the TDR and CS615. The CS615 soil moisture calibration curves deviate markedly from the manufacturer's and nearly always result in a lower soil moisture estimate for a given sensor response, compared to the manufacturers curve.

4. The TDR volumetric soil moisture to soil dielectric constant calibration curves deviate from the manufacturer's and the Topp relationships in the manner expected for clayey soils where there is an effect of bound water.

5. The random errors for the comparison between the CS615 and TDR in the field indicate that the laboratory calibrations are the most precise (smallest random error).

6. A major concern is the systematic error between the CS615 and TDR field measurements that exists when the laboratory calibrations are applied. This error results in an underestimation by the CS615 compared with the TDR and this increases as moisture content increases. A less pronounced systematic error in the opposite direction occurs when the factory calibrations are applied. This error tends to be constant.

7. Comparison of TDR and gravimetric samples in the field give good confidence in the TDR calibration relationships.

ACKNOWLEDGEMENTS

The authors wish to acknowledge the financial support of the Australian Research Council (grants C39813076, A39801842, C39804872) and the New Zealand Public Good Science Fund (contracts CO1635, CO1817). We also wish to express our gratitude to Graeme Mackay, Pete Pattinson, and Kathy Walter (all of NIWA), who have contributed considerable technical expertise, to the Mahurangi residents who have generously given us access to their land, and to Mark Seyfried for sharing his experiences of calibrating soil moisture instruments with us.

REFERENCES

Campbell Scientific Inc. 1996, CS615 Water content reflectometer: Instruction manual. Version 8221-07. Revision 10.96: Campbell Scientific Inc., Logan Utah, 11pp.

Dasberg, S., and Hopmans, J.W., 1992, Time domain reflectometry calibration for uniformly and nonuniformly wetted sandy and clayey loam soil: Soil Science Society of America Journal, **56**, 1341-1345.

Dirksen, C., and Dasberg, S., 1993, Improved calibration of Time Domain Reflectometry soil water content measurements: Soil Science Society of America Journal, **57**, 660-667.

Hook, W.R. and Livingston, N.J., 1996, Errors in converting time domain reflectometry measurements of propagation velocity to estimates of soil water content: Soil Science Society of America Journal, **60**, 35-41.

Seyfried, M.S., and Murdock, M.D., 2001, Response of a new soil water sensor to variable soil, water content, and temperature: Soil Science Society of America Journal, **65**, 28-34.

Soilmoisture Equipment Corporation, 1996, Trase Operating Instructions, version 2000: Soilmoisture Equipment Corporation, Santa Barbara.

Topp, G.C., Davis, J.L., and Annan, A.P., 1980, Electromagnetic determination of soil water content: Measurements in coaxial transmission lines: Water Resources Research, **16**, 574-582.

Tucker, B.M., and Beatty, H.J., 1974, pH, Conductivity and Chlorides. In: J. Loveday (Editor), Methods for Analysis of Irrigated Soils: Commonwealth Agricultural Bureau, Farnham Royal, England, pp. 100-107.

Tyndale-Biscoe, J.P., Moore, G.A. and Western, A.W., 1998, A system for collecting spatially variable terrain data: Computers and Electronics in Agriculture, **19**, 113-128.

A COST EFFECTIVE SOIL MOISTURE INSTRUMENT BASED ON TIME-DOMAIN TRANSMISSION MEASUREMENT

Z.J. Sun[1] and G.D. Young[2]

[1]E.S.I. Environmental Sensors Inc., 100-4243 Glanford Avenue, Victoria, British Columbia, Canada. V8Z 4B9; jason@esica.com
[2]E.S.I. Environmental Sensors Inc., 100-4243 Glanford Avenue, Victoria, British Columbia, Canada. V8Z 4B9; jyoung@esica.com

ABSTRACT

A cost effective soil moisture instrument based on time-domain transmission (TDT) measurement has been developed. A fast-rising pulse is applied to one end of the probe and the time of the pulse arriving at the other end of the probe is measured. The relationship between the one-way transmission time and volumetric soil water content has been established. This TDT technique doesn't require acquisition of a graphic reflection waveform nor automatic interpretation of the waveform, therefore the circuit is simple compared to typical Time-Domain Reflectometry (TDR) instruments. A series of tests have been conducted in sandy, loamy, and clayey soils with different levels of salinity. Results show that for soil consisting of less than 40% of clay and with electrical conductivity (saturated extract) less than 2 dS/m, the accuracy, resolution and repeatability of a TDT instrument is very comparable to those of TDR instrument.

IINTRODUCTION

During the last decades time domain reflectometry (TDR) has attracted attention from soil scientists and irrigation managers for its capability of providing an accurate and nondestructive soil water content measurement. However a TDR instrument is expensive due to (1) requiring acquisition of a graphic reflection waveform and automatic interpretation of the waveform. (2) requiring generation of a step function with very fast rise time (in the order of tens to hundreds of pico-seconds or at GHz bandwidths in terms of frequency) in order to overcome measurement uncertainty caused by variations in soil texture and salinity. The high price of the TDR instrument is barrier to wide acceptance by farmers and irrigation managers. For many arable soils when the clay content is less than 40% and soil electrical conductivity is less than 2 dS/m (saturated extract), the fast rise time may be an unnecessary luxury. Soil moisture instruments based on time domain transmission technology (TDT) requires a much lower operational frequency and do not require a graphic waveform acquisition and interpretation. The performance of a TDT moisture instrument is almost as good as TDR under normal arable soil

conditions, with only a fraction of the price of the latter. TDT soil moisture instruments are attracting more and more attention from farmers and irrigation managers. It may become a major type of soil moisture instrument in irrigation management in the near future.

PRINCIPLE OF TIME-DOMAIN TRANSMISSIOMETRY

An electromagnetic wave propagating in a material medium moves with a velocity that is modified by the material dielectric characteristics. Consequently, measurement of the propagation time over a known distance of the wave can be used to calculate the dielectric characteristics. To apply the measurement technique to determination of water content in a porous dielectric medium, an electromagnetic pulse is guided through the medium by a transmission line. A porous medium is assumed to be composed of a uniform solid material, air spaces, and liquid water. Because the dielectric constant of liquid water is approximately 20 times larger than that of most materials and 80 times larger than that of air, the dielectric constant of the moist, porous medium is determined primarily by the volume fraction of water present. When the propagation time is determined using direct time measurements, the techniques are called time-domain techniques. There are two families of time domain techniques called time domain reflectometry (TDR) and time domain transmissometry (TDT). These techniques are distinguished by where the receiver is located with respect to the transmission line (probe) in the medium of interest. In the transmission technique, the receiver is located at the far end of the probe and determines the time of arrival of the pulse at the far end of the probe. The one-way propagation time is the measurement. In the reflection technique, the receiver is co-located with the pulse transmitter, the probe end is left open (or is shorted), and the propagating pulse is reflected from this discontinuity and travels back along the probe toward the transmitter and receiver. The round-trip propagation time is the measurement. There are advantages and disadvantages for each of these techniques:

TDR

(1) The signal is emitted and received at the same end. The mechanical configuration is simple. (2) Shorting diodes can be applied for precise detection of the time mark of the end reflection (Hook *et al*. 1992). (3) Shorting diodes can also be used to segment the probe, providing the ability for soil moisture profile measurement using a single probe. (4) Multiple reflections sometime make the reflected signal ambiguous and a waveform display and interpretation is required, which in turn requires sophisticated circuitry to sort out various reflections. (5) The instrument is expensive.

TDT

(1) Need to access to both ends of the probe for signal emitting and receiving. In some applications, this required probe geometry make the installation of TDT probes more difficult than TDR probes. (2) Less sensitive to waveform corruption by connections, and multiple reflections, and so no graphic display and interpretation of waveform is required, leading to simple circuitry. (3) It may operate at relatively low frequency, and instrument is again simpler and inexpensive. (4) More susceptible to soil texture (especially clay content) and soil salinity if operating at low frequency. (5) Limited moisture range for output linearity.

PROBE GEOMETRY OF TDT MOISTURE SENSORS

As TDT uses signal transmitted through the probe, the signal emitting and receiving are separated at different ends of a transmission line (probe). This means that the whole measurement arrangement (terminal for signal emitting, probe and terminal for signal receiving) must form a loop. The transmission line (probe) should be as smooth as possible to avoid signal loss by emission at the sharp turns and corners. These restrictions and requirements limit the probe geometry configuration. In general operation, the TDT probe and associated signal electronics packages are buried in soil, therefore it is less mobile than the TDR probe. However, It is still possible to simplify the probe configuration without sacrificing the accuracy of TDT moisture instrument. Figure 1 shows how a simpler probe geometry is evolved from a loop of transmission line. Testing results (data not shown) indicated that in homogenous medium, the performance of geometry 1(b) is as good as that of 1 (a). However, if the medium is heterogeneous in texture and/or moisture, the geometry 1(a) gives better results.

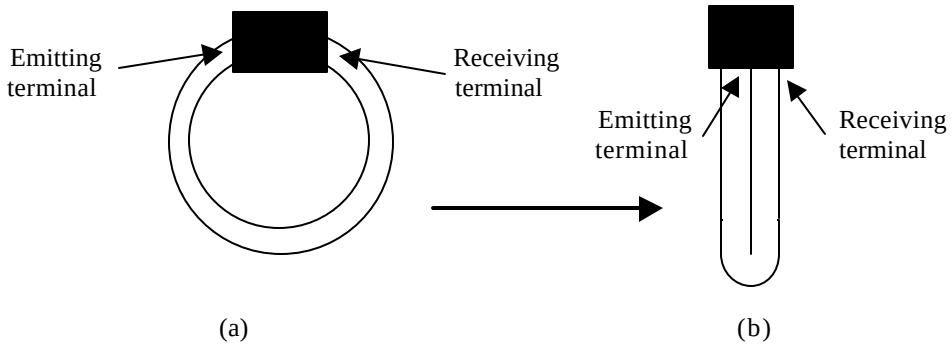

Fig. 1. *The probe geometry of TDT moisture sensor (a) Original geometry (b) The simplified geometry, the inner circle in (a) is shrunk to a bar in (b).*

PERFORMANCE OF TDT MOISTURE SENSOR IN SALINE SOLUTION

Figure 2. shows the performance of a TDT soil moisture instrument (Gro.Point, ESI Environmental Sensors Inc. Victoria, BC, Canada) in saline solution. The different electrical conductivity (EC) of the solution was generated by adding different amounts of sea salt to distilled water at room temperature. The probe was totally or partially immersed in solution. There are no significant changes in displayed moisture from TDT moisture instrument when electrical conductivity of solution increasing up to 3.5 dS/m for probe being either totally or partially immersed in solution. The no significant change in displayed moisture when the probe was totally immersed in solution could possibly be explained by signal saturation. However in partially immersed condition, TDT soil moisture instrument only suffered minor influence for EC up to 3.8 dS/m. The moisture correction for EC of 0.0124 m^3m^{-3} per dS/m may be employed. If the tolerance of accuracy for moisture is 0.02 m^3m^{-3}, then the TDT moisture instrument doesn't require a special calibration for salinity up to EC = 1.6 dS/m (0.02 m^3m^{-3}/0.0124 m^3m^{-3}). This may satisfy many agricultural applications.

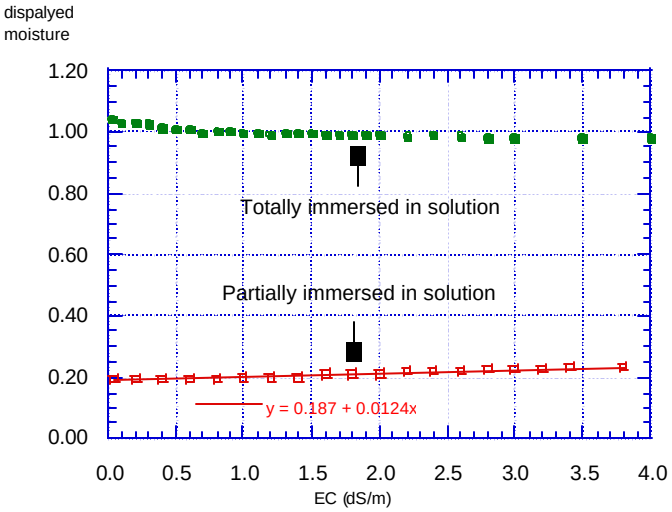

Fig. 2. *The performance of TDT moisture instrument (Gro.Point) in salt solution.*

PERFORMANCE OF TDR MOISTURE INSTRUMENT IN SANDY AND LOAMY SOILS

The TDT moisture instrument under testing (Gro.Point) has a current output (4-20 mA). Figure 3. shows that there is a linear relationship between the current output and volumetric water content of the testing medium in a defined moisture range. In sandy soil, the linearity holds from 0.08 m^3m^{-3} up to saturation (0.25 m^3m^{-3}). The upper limit for linearity can be observed when placing the sensor in a clayey soil (50% of clay content), the linearity holds up to water content of 0.40 m^3m^{-3}. This moisture range will meet most of the agricultural application demands. The deviation from linearity at high moisture range in clayey soil may be attributed to soil electrical conductivity that includes both soil solution conductivity and soil particle surface conductivity. For a detailed discussion of this issue, please refer to our paper in the same issue.

We cannot explain why the linearity doesn't hold at very low moisture even in sandy soil. White *et al*. (1994) found a significant deviation from linearity to occur for regression between the square root of the apparent dielectric constant and volumetric water content at moisture levels less than 0.05 m^3m^{-3} for a soil-graphite mixture. They attributed this to the formation of a bound water phase with apparent dielectric constant less than that of the solid phase.

Figure 4. shows that in non-saline sandy soil (90 % of sand) and loamy soil (34 % clay content), the measured water content using a TDT moisture instrument (Gro.Point) is very close to that of the references measurement (oven-dry method determined). The largest standard deviation is less than 0.02 m^3m^{-3}. The sensor was pre-calibrated in this loamy soil at two moisture levels (0.07 m^3m^{-3} and 0.40 m^3m^{-3}) and measurements were conducted at several moisture levels between these levels. We believe that this was the maximum accuracy the instrument can achieve with soil specific calibration. The data was a little more spread along the 1:1 line in sandy soil testing because all the sensors were pre-calibrated in loamy soils not in sandy soil. For these conditions, the performance of TDT moisture instruments is as good as that of TDR moisture instruments, and the stability of TDT instrument is even better than that of TDR (data not shown).

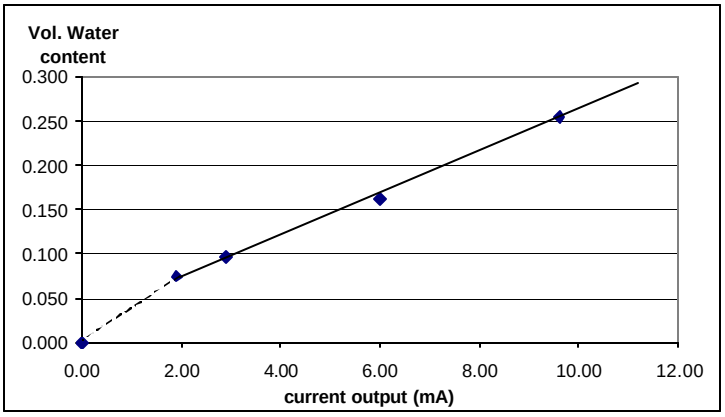

Fig. 3a. *The linearity of the relationship between current output and volumetric water in a sandy soil.*

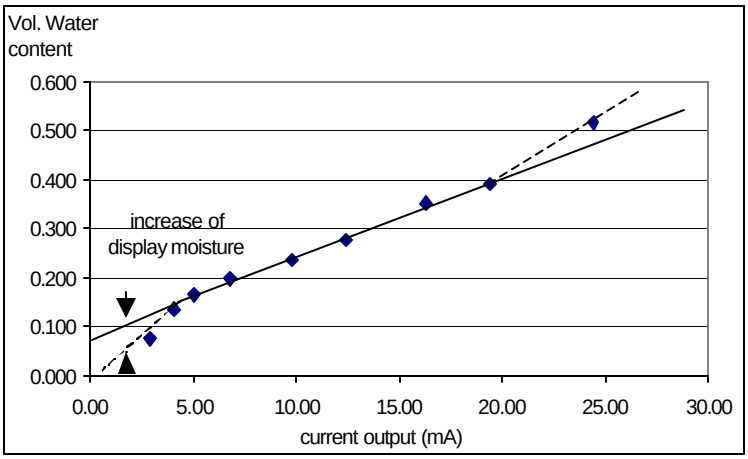

Fig. 3b. *The linearity of the relationship between current output and volumetric water in a clayey soil.*

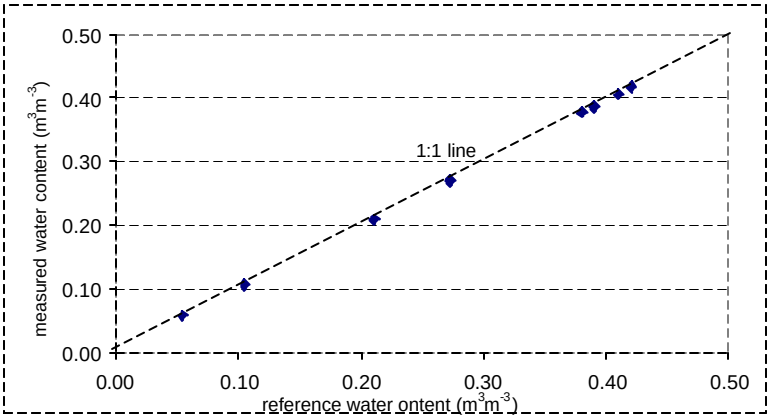

Fig. 4a. *The performance of TDT moisture sensors in loamy soil with soil specific calibration*

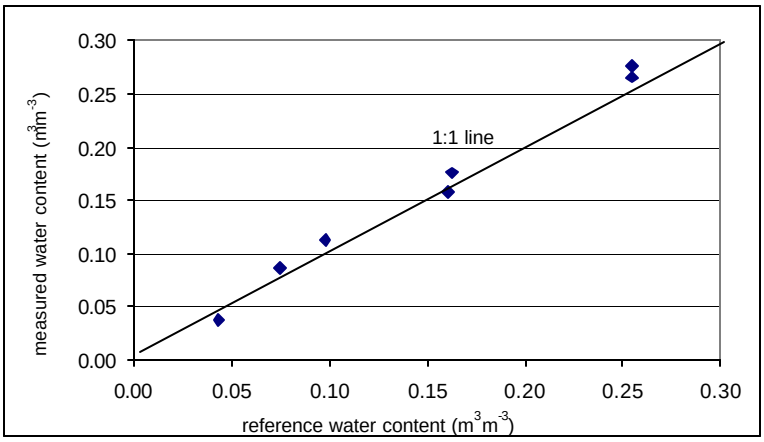

Fig. 4b. *The performance of TDT moisture sensors in sandy soil, which was pre-calibrated in a loamy soil*

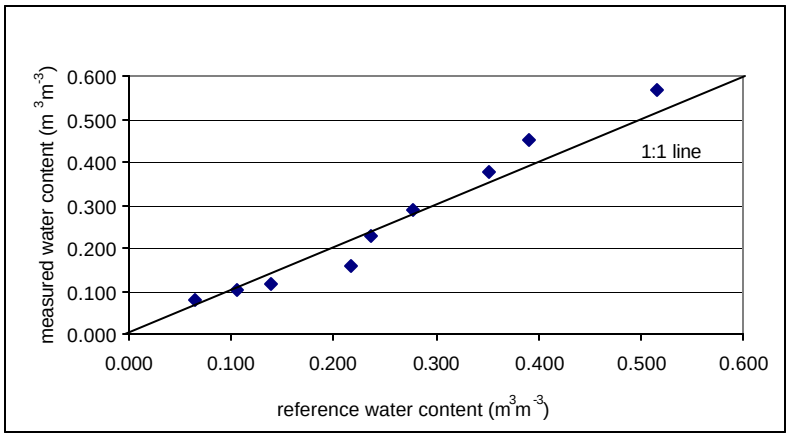

Fig. 5. *The performance of TDT moisture sensors in clayey soil, which was pre-calibrated in a loamy soil.*

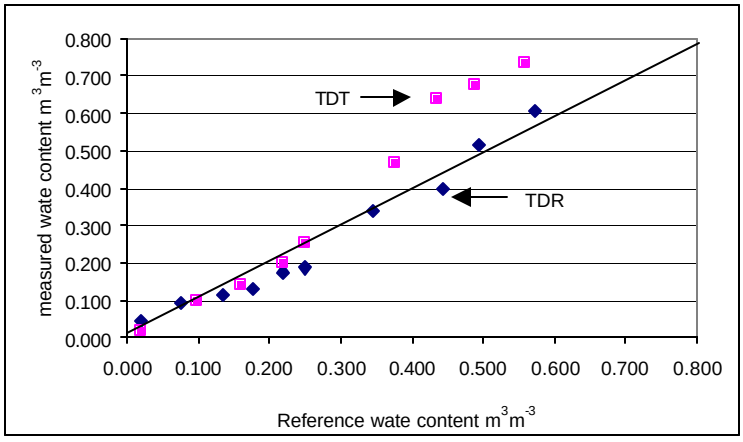

Fig. 6. *The performance of TDR moisture instrument (Moisture.Point) and TDT moisture instrument (Gro.Point) in saline clay soil.*

PERFORMANCE OF TDR MOISTURE INSTRUMENT IN CLAY SOIL AND SALINE SOIL

TDT moisture instrument (Gro.Point) works well in a non saline clay soil - Rideau Clay that consists of 50% of clay, 35% of silt and 15% of sand for water content up to 0.40 m^3m^{-3}. The instrument starts overestimating water content beyond this moisture. The maximum overestimation is 0.06 m^3m^{-3}. This overestimation may be attributed to: (a) The electrolytes are attached to the clay particle surface by static electrical force, creating extra polarization, which would further interact with the electromagnetic wave that is travelling in the soil, impeding its propagation. The longer signal travel time leads to a high current output, or higher moisture reading. (b) The current flow through the migration of the electrolytes in soil solution dissipates the signal energy and increases the rise time of the received signal. The increased rise time delays triggering a time recording circuit, resulting in a higher moisture reading.

It is interesting to find there is no severe underestimation of soil water in low moisture range (less than 0.10 m^3m^{-3}) caused by bound water that characterized by its much lower dielectric constant (Shang, 1994). In Figure 3 (b), one may find that there is a dip for the linear relationship between current output and reference water content. The displayed moisture will be higher than the reference when the linear relationship is applied in low moisture range. This compensates, to some extent, the underestimation. The underestimation is much severer in the moisture range from 0.10 to 0.20 m^3m^{-3}. In the case of the TDR moisture

instrument, we found a similar situation where the maximum bound water effect doesn't happen at very low moisture range. There is also a dip at low moisture range in the linear relationship between time delay and soil water contents (data not shown) if delay is expressed as T/T_{air}. Where T is the signal travel time along a probe in the medium, and T_{air} is the travel time in free air over the same distance. The increased displayed moisture will compensate the effect of bound water when the linear relationship between T/T_{air} and water content is applied.

In saline clay soil conditions, the TDT soil moisture instrument shows a significant overestimation in soil water content when the moisture goes above 0.30 m^3m^{-3}. Meanwhile, a TDR soil moisture instrument (Moisture.Point MP-917) only shows a little overestimation (Figure 6). The soil used is Rideau clay with 50% of clay, 35% of silt and 15% of sand. The salinity was generated by adding KCl solution. The electrical conductivity of saturated extract (EC_e) was 3.5 dS/m. The smaller effect of the TDR moisture instrument is attributed to its higher operational frequency. Theoretically, the term which affects the propagating of an electromagnetic wave in a material medium is $\sigma/2\pi f$, where σ is the electrical conductivity and f is the frequency (Rao, 1987). The higher the frequency, the less the effect. In clay soils with high percentage of montmorillonite, the overestimation by TDT moisture instrument starts at EC_e = 2 dS/m. The high surface electrical conductivity caused by its large specific surface area and high affinity to cations is the major cause for the overestimation. Therefore, in saline soil or clay soil with high percentage of montmorillonite mineral, the TDR instrument is a better choice than the TDT instrument unless the later has been soil specific pre-calibrated.

SUMMARY

Time-domain transmissiometry based soil moisture instrument can work satisfactorily in normal agricultural soils with some limitations. The main limitations are (a) linearity holds in a moisture range from 0.08 to 0.40 m^3m^{-3}. (b) the threshold for soil salinity and clay content under which the TDT instrument will work properly is lower than those of TDR. The TDT moisture instrument can still work well if a soil specific calibration has been done. The simple circuit, ease of operating and low price make it very attractive.

REFERENCES

Hook, W.R., Livingston, N.J., Sun, Z.J. and Hook, P.B., 1992, Remote Diode Shorting Improves Measurement Soil Water by Time domain Reflectometry. Soil Sci. Soc. Am. J. **56**, 1383-1391

Rao, N.N., 1987, Wave equation and solution for material medium. in Elements of engineering electromagenetics. 2nd ed. Prentice-Hall, New Jersey, 286-293.

Shang, J. Q., 1994, Quantitative Determination of Potential Distribution in Stern-Gouy Double-layer Model. Can. Geotech. J. **31**, 624-636

White, I., Zegelin, S.J., Topp, G.C. and Fish, A., 1994, Effect of Bulk Electrical Conductivity on TDR Measurement of Water Content in Porous Media. Pages 294-308. in Symposium and Workshop on Time Domain Reflectometry in Environmental, Infrastructure, and Mining Applications. United States Department of Interior Bureau of Mines.

Soil Moisture

Full Waveform Analysis of a Non-uniform and Dispersive TDR Measurement System
C. P. Lin, *National Chiao Tung University, Taiwan*

Improved Calibrations of TDR Measurements Using Artificial Neural Networks
M. Persson, *Lund University, Sweden*

Frequency-Domain Methods for Extending TDR Measurement Range in Saline Soils
S. Jones and D. Or, *Utah State University*

Dielectric Properties of Bound Water: Application to Porous Media Surface Area and Grain Moisture Determination
J. Wraith, *Montana State University*; D. Or and S. Jones, *Utah State University*

TDR Signal Modeling Using the Electric Line Approach: Model Validation and Signal Inversion to Retrieve Soil Moisture Profile
A. Chambarel and E. Ferry, *Université d'Avignon, France*; J. P. Laurent, *LTHE/CNRS, France*; A. Chanzy, *INRA, France*; P. Todoroff, *CIRAD, France*; P. Ferrari, *Université de Chambéry, France*

TDR Signal Simulation Using a Wave Guide 2D Model
A. Chambarel, H. Bolvin and E. Ferry, *Laboratory of Complex Hydrodynamics, Avignon, France*

A Time Domain Reflectometry Borehole Packer for Use in Rock
S. W. Truss, L. J. West and P. Winship, *University of Leeds, Great Britain*; M. Nakhkash and Y. Huang, *University of Liverpool, Great Britain*

The Sample Area of Time Domain Reflectometry Probes in Proximity to Sharp Dielectric Permittivity Boundaries
P.Ferré, *University of Arizona*; H.Nissen and P. Moldrup, *Aalborg University, Denmark*; J. H. Knight, *CSIRO Land and Water, Australia*

The Sensitivity of Time Domain Reflectometry Probes to Spatially Heterogeneous Electrical Conductivities
P.Ferré, *University of Arizona*; H.Nissen and P. Moldrup, *Aalborg University, Denmark*; J. H. Knight, *CSIRO Land and Water, Australia*

Saline Clayey Soil Moisture Measurement Using Time Domain Reflectometry
Z.J. Sun and G. D. Young, *E.S.I. Environmental Sensors Inc., Canada*

Development and Applications of TDR Inversion Algorithms with High Spatial Resolution for Moisture Profile Determination
S. Schlaeger, C. Huebner, A. Scheurmann and J. Gottlieb, *University of Karlsruhe, Germany*

Back to Table of Contents

FULL WAVEFORM ANALYSIS OF A NON-UNIFORM AND DISPERSIVE TDR MEASUREMENT SYSTEM

Chih-Ping Lin

Department of Civil Engineering, National Chiao Tung University,
1001 Ta-Hsueh Road, Hisnchu, Taiwan; cplin@cc.nctu.edu.tw

ABSTRACT

The spectral analysis and the concept of input impedance are used to develop a wave propagation model for a TDR measurement system that can account for dielectric dispersion of the material and non-uniform nature of the transmission line. The numerical procedure of the wave propagation model is relatively simple and becomes a powerful tool for parametric studies, data interpretations, and inverse analyses. The dielectric permittivity, the reference characteristic impedance, and the length of each uniform section characterize a non-uniform transmission line. Results indicate that inversion of these three parameters will result in definite non-uniqueness, but uniqueness can be achieved when one of the three parameters is known. The inversion of impedance profile from TDR waveforms with known dielectric properties can be used for data interpretation of rock and soil deformation; while the inversion of dielectric spectrum from TDR waveforms with known impedance can be used to study soil dielectric properties.

INTRODUCTION

Time domain reflectometry (TDR) has experienced dramatic developments over the past 20 years. It has become a valuable tool for the measurement of soil water content and monitoring of relative displacement in rocks and soils. The two major features of TDR waveforms used for data interpretation are the travel time of the TDR waveform in the probe for water content measurement and the voltage amplitude of the reflected waveform from relative displacement. However, much more information on the dielectric properties of the soil is contained in the measured TDR waveforms. In addition, the amplitude of the reflected waveform from shear displacement is affected by the cable loss and multiple reflections. To extract extra information when measuring dielectric properties of materials and to interpret the data more reasonably when monitoring relative displacement require a more fundamental understanding of the wave propagation in the TDR probe.

In a TDR system, there can be more than one type of transmission line. A 50-Ω cable connecting the cable tester and the TDR probes is a coaxial transmission line. The measurement probe could be either a coaxial line or multiple rod line. We also need a transitional device (or probe head) to connect the cable and measurement probe. Therefore, most likely, the TDR system consists of cable tester (e.g., Tektronix 1502B) and non-uniform transmission line as shown in Figure 1. Furthermore, the surrounding medium may vary along the measurement probe in the case where the soil column is not homogeneous along the line axis (z). And the cross-sectional dimension may vary along the coaxial cable when it is subject to relative deformation. If the cross-sectional dimensions of the line or the properties of the surrounding medium vary along the line axis, then the per-unit-length parameters in the transmission-line equation will be functions of the position variable, z. This makes the resulting partial differential equations very difficult to solve. Such transmission lines are said to be non-uniform lines.

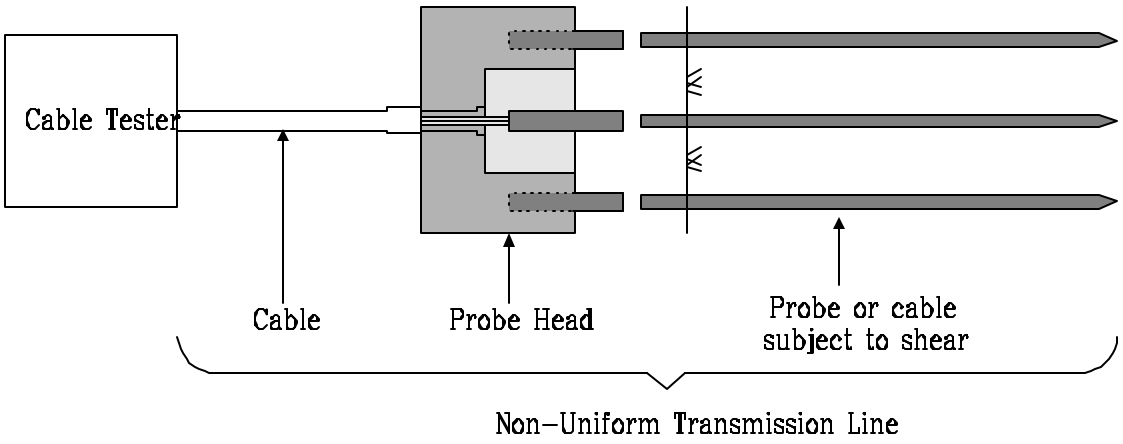

Fig. 1. *Components of a transmission line in the TDR system.*

To realistically model TDR waveforms, it is necessary to account for dielectric dispersion of material under test and non-uniform nature of a transmission line measurement system. Yanuka *et al*. (1988) presented a model that consider multiple reflections in a non-uniform transmission line but does not consider the frequency dependency of the material dielectric permittivity. Heimovaara (1994) used spectral analysis to account for dielectric dispersion but his method is only applicable to a uniform transmission line (i.e. a matched system and a homogeneous material). This paper presents an approach that formulates multiple reflections of multi-section TDR measurement system in frequency domain to take into account of dielectric dispersion of material under test and non-uniform nature of the transmission line. A numerical spectral algorithm is used to simulate wave propagation in a non-uniform and dispersive transmission line. This wave propagation model serves as a forward model in a model-based inversion to back-calculate impedance profile of a cable or to determine dielectric properties of insulating materials. Results of the simulation are compared to the actual TDR waveforms of some calibration materials.

DIELECTRIC DISPERSION MODEL

The dielectric permittivity is in general a complex number and a function of frequency:

$$e(f) = e'(f) - je''(f) \qquad [1]$$

in which f is the frequency; e' and e'' are the real and imaginary part of permittivity, e. The real part of permittivity is often what we call the dielectric constant. It is a measure of how much energy from an external electric field is stored in a material. The imaginary part of permittivity is called the loss factor and is a measure of how dissipative or lossy a material is to an external electric field. It is convenient to define the equivalent permittivity $e^* = e' - j(e'' + s / 2pf)$ to represent the total effect of permittivity, e, and conductivity, s. In terms of relative permittivity ($e_r = e/e_0$), e_r^* can be written as

$$e_r^* = e_r' - j\left(e_r'' + \frac{s}{2pfe_0}\right) \qquad [2]$$

in which e_0 is the dielectric permittivity of free space (equal to 8.854×10^{12} F/m in MKS system). For a homogeneous material, the dielectric dispersion within TDR bandwidth may be described by Debye equation (Hasted, 1973).

$$e_r^*(f) = [e_\infty + \frac{e_s - e_\infty}{1 + jf / f_{rel}}] - \frac{js}{2pfe_0} \qquad [3]$$

where e_s is the real value of dielectric permittivity at $f = 0$, $e_¥$ is the real value of dielectric permittivity at $f \rightarrow \infty$; and f_{rel} is a modified average relaxation frequency related to the molecular polarization. For wet soils, the interaction between liquid phase and solid phase becomes significant when the particle size gets small. The resulting dielectric spectrum may be described more realistically by a sum of two or more different Debye's parameters having closely spaced relaxations (e.g. one for bound water and one for free water). In this study, some liquids whose dielectric permittivity can be described very well by Debye equation will be used to verify the wave propagation model.

SOLUTION OF TRANSMISSION LINE WAVE EQUATION

The interaction between electric and magnetic energy gives rise to the propagation of electromagnetic waves. Due to the special field structure (i.e. Transverse Electromagnetic Model) inside the transmission line, line current and voltage between conductors can be uniquely defined and used to describe the electromagnetic wave propagation in a transmission line. The general solution to a uniform transmission line in phasor form is

$$\hat{V}(z) = \hat{V}^+ e^{-gz} + \hat{V}^- e^{gz} \qquad [4a]$$

$$\hat{I}(z) = \frac{\hat{V}^+}{Z_c} e^{-gz} - \frac{\hat{V}^-}{Z_c} e^{gz} \qquad [4b]$$

where $\hat{V}$ is the voltage between two conductors and $\hat{I}$ is the line current. g is the propagation constant (wave number), which is a function of dielectric permittivity. It can be written as

$$g = \frac{j2pf}{c}\sqrt{e_r^*} \qquad [5]$$

in which c is the speed of light. Z_c is the characteristic impedance, which is a function of dielectric permittivity and cross-sectional geometry of the transmission line. It can be written as

$$Z_c = Z_p / \sqrt{e_r^*} \qquad [6]$$

where the reference characteristic impedance, Z_p, is the characteristic impedance of the transmission line filled with air, which is only a function of the cross-sectional geometry of the transmission line. $\hat{V}^+$ and $\hat{V}^-$ in (4) are two unknown constants in the general solution. Equation (4) can be interpreted as the sum of forward- and backward-traveling waves with 2 unknown coefficients.

In the case of a uniform transmission line, an equivalent circuit shown in Figure 2 can represent a TDR system. The line is terminated at the load end, $z = l$, with a load impedance, $\hat{Z}_L$. At the source end, $z = 0$, an independent voltage source V_S and a source impedance, Z_S, terminate the line. Thus, the boundary conditions are

$$\hat{V}(0) = \hat{V}_S - Z_S\hat{I}(0) \qquad [7a]$$

$$\hat{V}(l) = Z_L\hat{I}(l) \qquad [7b]$$

At this point, we could apply the boundary conditions to solve for unknown coefficients $\hat{V}^+$ and $\hat{V}^-$ (two unknowns, two equations). Substituting the solution of $\hat{V}^+$ and $\hat{V}^-$ back to (4), we can then solve for the voltage or current along the transmission line. The solution of special interest is the voltage at $z = 0$, which is the sampling voltage display on the TDR oscilloscope. However, in order to extend the usefulness of the solution, input impedance approach will be taken.

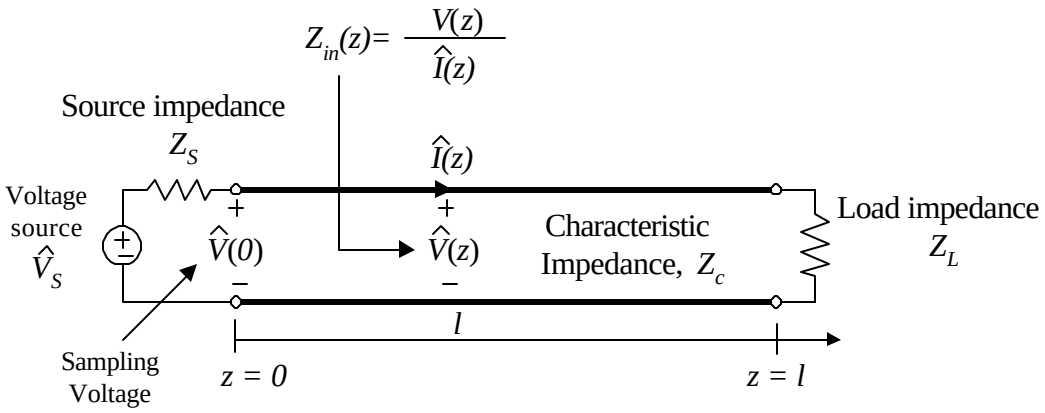

Fig. 2. *Equivalent circuit of a TDR system and definition of input impedance Z_{in}.*

The concept of input impedance is similar to the equivalent stiffness in mechanical dynamics in which force and displacement are analogous to the voltage and current. As shown in Figure 2, the input impedance $Z_{in}(z)$ is the equivalent impedance when looking into the circuit (i.e. the uniform transmission line) at position z (Magnusson *et al*., 1992). It is defined as

$$Z_{in}(z) = \frac{\hat{V}(z)}{\hat{I}(z)} = Z_c \frac{\hat{V}^+ e^{-gz} + \hat{V}^- e^{gz}}{\hat{V}^+ e^{-gz} - \hat{V}^- e^{gz}} \qquad [8]$$

If the input impedance at the source end (i.e. the impedance at the source end looking into the transmission line) can be determined, the sampling voltage $\hat{V}(0)$ can be calculated by the boundary condition at the source end (7a).

First, the boundary condition at the load end (7b) can be written as

$$Z_{in}(l) = \frac{\hat{V}(l)}{\hat{I}(l)} = Z_L \qquad [9]$$

Then, the impedance at $z = 0$ can be derived as a function of the input impedance at z = l as (Lin *et al*. 2001)

$$Z_{in}(0) = Z_c \frac{Z_{in}(l) + Z_c \tanh(gl)}{Z_c + Z_{in}(l) \tanh(gl)} \qquad [10]$$

where

$$\tanh(gl) = \frac{e^{gl} - e^{-gl}}{e^{gl} + e^{gl}} = \frac{1 - e^{-2gl}}{1 + e^{-2gl}} \qquad [11]$$

Using the terminal condition at $z = 0$ and $\hat{I}(0) = \hat{V}(0) / Z_{in}(0)$, $\hat{V}(0)$ is determined as

$$\hat{V}(0) = \frac{Z_{in}(0)}{Z_{in}(0) + Z_S} \hat{V}_S \qquad [12]$$

TDR SYSTEM WITH A NON-UNIFORM TRANSMISSION LINE

In a general non-uniform transmission line, the per-unit-length line parameter will be functions of z. In this case the transmission line differential equations become non-constant-coefficient differential equations. Although the differential equations remain linear (if the surrounding medium is linear), they are difficult to solve. However, if we can approximate the non-uniform line as a discretely uniform line as shown in Figure 3, (4) still represents the general solution for each uniform section.

For each of the n uniform sections, the general solution consists of the sum of forward and backward traveling waves with two unknown coefficients. Therefore, there are a total of $2n$ unknown coefficients ($\hat{V}_i^+$, $\hat{V}_i^-$). The terminal conditions are the same as in (7). This leaves $2n$ unknown coefficients with only two boundary conditions. The continuity constraints at the discontinuities between the terminations provide $2(n-1)$ more equations; and we could apply the $2n$ boundary conditions to solve for $2n$ unknown coefficients. However, the concept of input impedance enables a more systematic explicit procedure. Instead of solving the simultaneous equation, the simplified procedure involves calculating the input impedance from the end termination to the source termination. The analysis starts with the point farthest from the signal source, transforming the impedance back successively to the next discontinuity until the input is reached. This is done using (10) in a bottom-up fashion, which relates the impedance at the two ends of the uniform section of transmission line (Lin *et al*. 2001).

$$\begin{aligned}
Z_{in}(z_n) &= Z_L \\
Z_{in}(z_{n-1}) &= Z_{c,n} \frac{Z_L + Z_{c,n} \tanh(g_n l_n)}{Z_{c,n} + Z_L \tanh(g_n l_n)} \\
Z_{in}(z_{n-2}) &= Z_{c,n-1} \frac{Z_{in}(z_{n-1}) + Z_{c,n-1} \tanh(g_{n-1} l_{n-1})}{Z_{c,n-1} + Z_{in}(z_{n-1}) \tanh(g_{n-1} l_{n-1})} \\
&\vdots \\
Z_{in}(0) &= Z_{c,1} \frac{Z_{in}(z_1) + Z_{c,1} \tanh(g_1 l_1)}{Z_{c,1} + Z_{in}(z_1) \tanh(g_1 l_1)}
\end{aligned} \qquad [13]$$

where $Z_{c,i}$, g_i, and l_i, are the characteristic impedance, propagation constant, and length of each section. Once the input impedance looking into the entire line is obtained by use of (13), the sampling voltage $\hat{V}(0)$ can then be solved using (12).

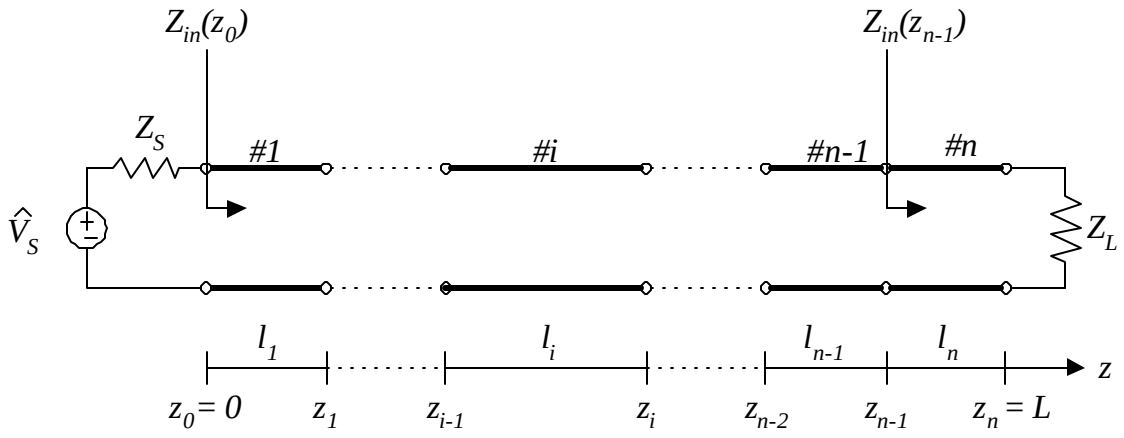

Fig. 3. *Representation of a non-uniform line as a cascade of uniform sections.*

Equations (13) and (12) provide the system function to simulate TDR waveforms of any TDR measurement system which may consist of different types of transmission lines and insulating materials. For a given TDR measurement system, we need to know the length l_i, the reference impedance Z_{pi}, the equivalent dielectric permittivity e_i* of each uniform section of the non-uniform transmission line, and the terminal impedances, Z_S and Z_L to predict the TDR waveform. Let the voltage source of the TDR be denoted by $V_S(t)$, the sampling voltage be denoted by $V_{TDR}(t)$, and the FFT algorithm by function $FFT(\ )$. The simulation of a TDR waveform takes the following steps:

1. Determine appropriate window size for frequency and time to avoid aliasing in discrete Fourier Transform.
2. $\hat{V}_S = FFT(V_S)$.
3. Determine $\hat{V}(0)$ from (13) and (12).
4. $V_{TDR}(t) = IFFT(\hat{V}(0))$.

CALIBRATION OF TDR MEASUREMENT SYSTEM

The calibration of transmission line parameters can be carried out by the model-based backward analysis. It can be seen from above that the properties of a non-uniform transmission line are the dielectric permittivity, the reference characteristic impedance, and the length of each uniform section. Two characteristics of a wave propagating in a non-uniform transmission line are the reflection/transmission at the interfaces of the mismatches and the propagation delay through each section. The reflection/transmission of waves depends on the impedance of the two sections adjacent to the interface, which are in turn functions of the reference characteristic impedance and dielectric permittivity of the insulating medium. The propagation delay is a function of the length of the section and the propagation constant, which is in turn a function of dielectric permittivity of the insulating medium. Different combinations of reference impedance and dielectric permittivity can result in the same impedance, while different combinations of section length and dielectric constant can result in the same propagation delay. Therefore, there are only two degrees of freedom in these three parameters. Considering the three characteristics of the non-uniform line together in the calibration will result in non-uniqueness.

The coaxial cable commonly used has nominal impedance of 50 Ω. However, The TDR pulses traveling on the coaxial cable are actually dispersive (i.e. the characteristic impedance is a function of frequency) and the rise time increases in duration substantially as the voltage pulse propagate along a cable. Long cables tend to filter out the higher frequencies of the TDR signal, thus reducing the bandwidth in the measurement (Heimovaara, 1993). When monitoring soil/rock deformation, the reference characteristic impedance and frequency-dependent dielectric property of the cable can be calibrated by inversion from the measured waveform of a cable with known length. The frequency-dependent dielectric permittivity may be modeled by the Debye equation. As an example, the waveform of a 1m coaxial cable with open end is use to back-calculate the reference impedance and the dielectric property of the cable. The results shown that the cable has a reference impedance Z_p = 71.24 ohm and Debye's parameters (e_s, $e_¥$, f_{rel}, s) = (2.56, 2.04, 2.34 MHz, 0 S/m). The comparison of the predicted and measured waveforms is shown in Figure 4. The slight difference between predicted waveform and the measured waveform are due to the BNC connector at the open end.

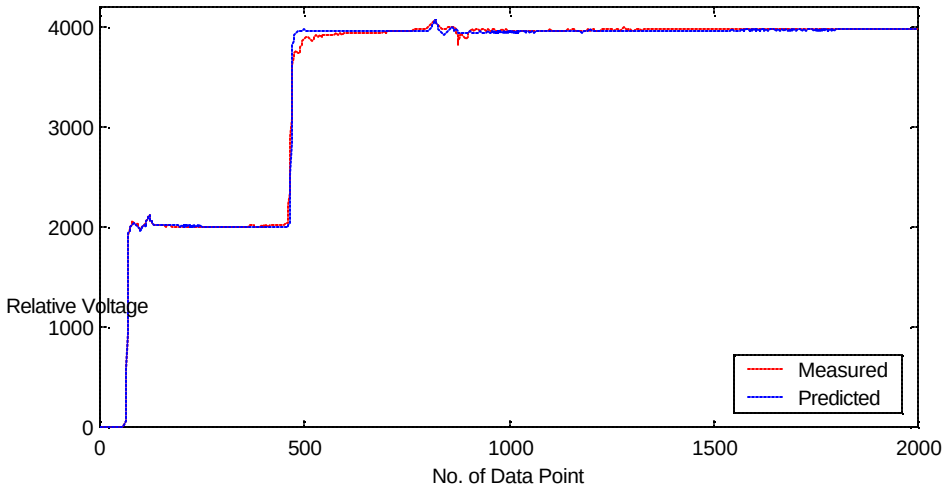

Fig. 4. *Measured and predicted TDR waveforms of the coaxial cable connected to the cable tester.*

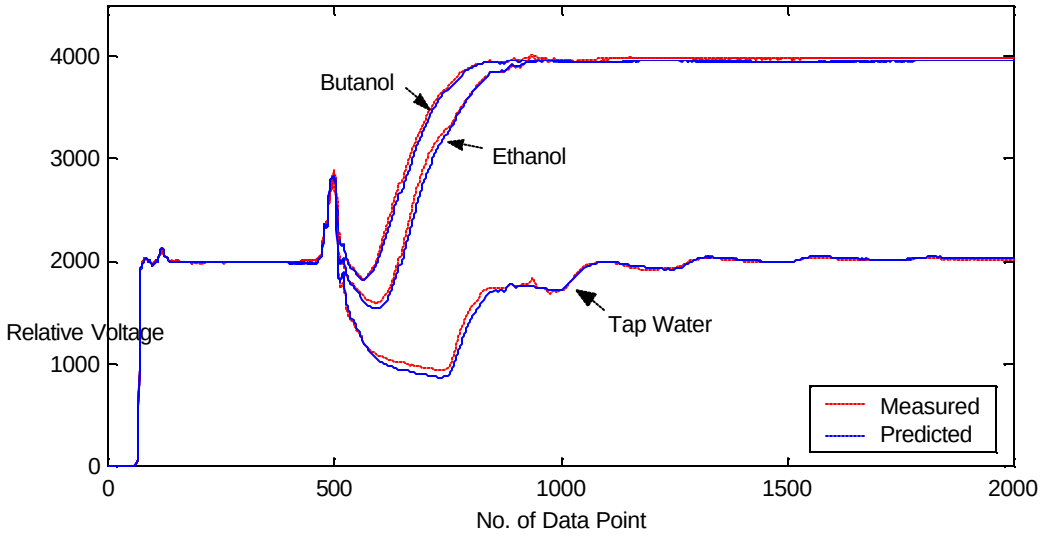

Figure 5. *Comparison of the measured and predicted TDR waveforms measured in various liquids.*

When measuring soil dielectric properties, a material with known dielectric properties is used for calibrating probe impedance and probe length. In this study, de-ionized water is used. The results of the system calibration were checked with measurements in materials with known dielectric properties listed in Table 1. The comparisons of the simulated and measured TDR waveforms for tap water, butanol alcohol, and ethanol alcohol are shown in Figure 5. It is observed that the simulated waveforms match the measured ones very well. This further validates the wave propagation model and results of the system calibration. The slight difference in the early part of the TDR waveforms (i.e. short-time response) reflects errors in high frequencies. This indicates that the higher order mode may have developed in addition to the TEM assumptions at high frequencies (Lin, 2001).

Dielectric parameters		ε_s	ε_∞	f_{rel}, *GHz*	σ_{dc}, *S/m*
Butanol	Expected	17.70	3.30	0.274	0
	Estimated	17.33	3.45	0.260	0.000015
Ethanol	Expected	25.20	4.52	0.782	0
	Estimated	24.75	7.05	0.759	0.000038
De-ionized water	Expected	79.90	4.22	17.000	0
	Estimated	80.92	3.80	16.470	0.00067
Tap water	Expected	80.20	4.22	17.400	0.0666
	Estimated	78.64	3.54	15.500	0.0676

Table 1. *Estimation of the dielectric parameters for the aqueous samples*

DIELECTRIC SPECTRUM BY WAVEFORM MATCHING

One can obtain the dielectric spectrum directly by solving the system function at each frequency. However, the accuracy and precision decreases as the frequency increases. It was observed that although the error in the system function at individual frequencies may be significant, the overall matches between the measured value and theoretical value in the system function and time-domain waveform are very good [Lin, 2001]. Therefore, it is possible to measure the dielectric spectrum by waveform matching based on a dielectric model such as Debye equation.

The estimation of the dielectric parameters for the aqueous samples is listed in Table 1. The associated dielectric spectrum is compared to the expected spectra for butanol in Figure 6. For materials with relaxation frequency well within the TDR bandwidth, the inverse solution gives a very good estimate. When the relaxation frequency of the material such as water gets close to or beyond the TDR bandwidth, the uncertainty of estimation for ε_∞ and f_{rel} becomes significant. The inverse solution cannot resolve the dielectric spectra beyond the TDR bandwidth for a material with relaxation frequency higher than the TDR bandwidth. There are many different values of ε_∞ and f_{rel} that can give similar dielectric spectra within the TDR bandwidth. However, the inverse solution still provides a very good estimation of dielectric spectra within the TDR bandwidth.

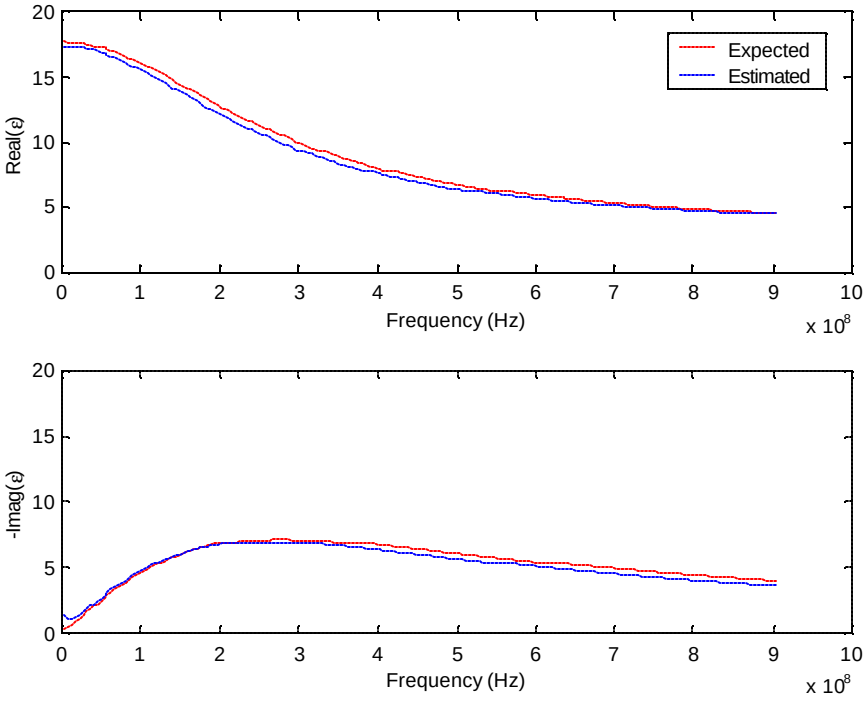

Fig. 6. *Measured dielectric spectrum of butanol alcohol from the estimation of Debye 's parameters through waveform matching.*

SUMMARY

In general, the transmission line in a TDR measurement system is a non-uniform line and the dielectric permittivity of the insulating material may be frequency dependent. The spectral analysis and the concept of input impedance are used to develop a wave propagation model for a TDR measurement system that can account for dielectric dispersion of the material and non-uniform nature of the transmission line. The numerical procedure of the wave propagation model is relatively simple and becomes a powerful tool for parametric studies, data interpretation, and inverse analysis.

The dielectric permittivity, the reference characteristic impedance, and the length of each uniform section characterize a non-uniform transmission line. Results indicate that inversion of these three parameters will result in definite non-uniqueness, but uniqueness can be achieved when one of the three parameters is known. The reference impedance and the dielectric property of a cable with known length are calibrated with measured waveform of the coaxial cable with open end. The impedance and the length of a TDR probe are calibrated with measured TDR waveform in de-ionized water. The excellent match between the simulated and the measured waveforms verifies the wave propagation model. The inversion of impedance profile from TDR waveforms with known dielectric properties can be used for data interpretation of rock and soil deformation; while the inversion of dielectric spectrum from TDR waveforms with known reference characteristic impedance can be used to study soil dielectric properties.

ACKNOWLEDGEMENTS

The author gratefully acknowledges the National Science Council in Taiwan for the financial support through projects NSC 89-2218-E-009-100 and NSC 89-2218-E-009-104. The author extends his thanks to Dr. Vincent Drnevich, Dr. Robert Nowack, Dr. Richard Deschamps, and Dr. Wei Feng for their valuable advice and discussions.

REFERENCES

Hasted, J.B., 1973, Aqueous Dielectric, Chapman and Hall, London.

Heimovaara, T. J., 1993, Design of Triple-Wire Time Domain Reflectometry Probes in Practice and Theory, Soil Sci. Soc. Am. J., **57**, 1410-1417.

Heimovaara, T.J., 1994, Frequency domain analysis of time domain reflectometry waveforms 1. Measurement of the complex dielectric permittivity of soils, Water Resour. Res., **30**, 189-199.

Lin, C.P., Drnevich, V.P., and Deschamps, R.J., 2001, Analysis of a Non-uniform and Dispersive TDR Measurement System, Submitted to Water Resour. Res.

Lin, C.P., 2001, Measurement of Dielectric Spectrum with a Non-uniform TDR System, Submitted to Water Resour. Res.

Magnusson, P. G., Alexander, G. C., Tripathi, V. K, 1992, Transmission Lines and Wave Propagation, 3rd ed., CRC, Boca Raton.

Yanuka, M., Topp, G.C., Zegelin, S., and Zebchuk, W.D., 1988, Multiple reflection and attenuation of time domain reflectometry pulses: Theoretical considerations for applications to soil and water, Water Resour. Res., **24**, 939-944.

IMPROVED CALIBRATIONS OF TDR MEASUREMENTS USING ARTIFICIAL NEURAL NETWORKS

Magnus Persson

Department of Water Resources Engineering, Lund University,
Box 118, 221 00 Lund, Sweden: magnus.persson@tvrl.lth.se.

ABSTRACT

Time domain reflectometry (TDR) has been proven to take accurate readings of the apparent dielectric constant K_a and bulk electrical conductivity σ_a. These measurements have been used for estimations of water content (θ) and concentration of different chemicals. The concentration of an ionic pollutant or tracer can be estimated from the soil solution electrical conductivity σ_w. Several different calibration equations have been used to describe the K_a-θ and σ_a-σ_w-θ relationships. In the present study, artificial neural networks (ANNs) were used for calculations of θ and σ_w from TDR measurements in pure sand. The results showed that the ANN performed consistently better than several other models, suggesting the suitability of ANNs for accurate TDR calibrations. The ANN was also used for predicting the K_a-θ relationship using soil physical parameters for ten different soil types. The K_a-θ relationship for each soil type was predicted using the other nine for calibration. It was shown that the ANN predictions were comparable to a soil specific calibration. Thus, by using ANN, highly accurate data can be obtained without the need for elaborate soil specific calibration experiments.

INTRODUCTION

Transport of pollutants in the unsaturated zone is a serious threat to the environment and human health. Accurate solute transport models are keys for successfully assessing the environmental risk of pollutant spreading. Detailed measurements of water content, θ, and pollutant concentrations are important when constructing and calibrating such models. A recently developed electromagnetic measuring technique capable of accurate measurements is time domain reflectometry (TDR). The TDR technique utilizes the dielectric constant, K_a, and bulk electrical conductivity, σ_a, for calculation of θ and solute concentration (Topp *et al.*, 1980; Dalton *et al.*, 1984).

The K_a measurement has been related to θ using purely empirical models (Topp *et al.*, 1980; Ledieu *et al.*, 1986), empirical-conceptual models (Birchak *et al.*, 1974), and physical-conceptual models (de Loor, 1964). Several studies have shown that the K_a-θ relationship is dependent also on soil type (e.g. Roth *et al.*, 1990), percentage of organic matter and bulk density (e.g. Jacobsen and Schjønning, 1993; Hook and Livingston, 1996), electrical conductivity (e.g. Dalton, 1992), and temperature (e.g. Pepin *et al.*, 1995; Persson and Berndtsson, 1998). In many cases, the actual physical process that induces the effects on the K_a-θ relationship is not fully understood, although studies have shown that the effects are small in most cases (e.g. Topp *et al.*, 1980). The model still most widely used is the 'universal' Topp equation, particularly in situations when no soil-specific calibration is available. It is important to note, however, that using the Topp equation for a mineral soil with a moderate clay content might lead to errors of about 0.02 m^3 m^{-3} or more. Thus, in studies where high accuracy is needed, a soil-specific calibration is normally required. This is generally an elaborate procedure, even if some recent studies have provided more efficient calibration methods (e.g., Young *et al*., 1997). The data obtained from a soil specific calibration experiment can be used for obtaining the best fit parameters of a third-order polynomial equation or a linear relationship between $K_a^{0.5}$ and θ. To avoid such an elaborate procedure, the soil physical parameters can be used to obtain the K_a-θ relationship, without the need for soil-specific calibration.

The relationship between the σ_a measurement and the soil solution electrical conductivity, σ_w, which, in turn, can be related to the concentration of an ionic solvent, is more difficult to describe since it is highly dependent also on θ and soil texture. As for the K_a-θ relationship, several types of σ_a-σ_w-θ models have been proposed, e.g. purely empirical models (Persson, 1997), empirical-conceptual models (Mualem and Friedman, 1991), and physical-conceptual models (Rhoades *et al.*, 1976). However, it is important to note that all these models have serious drawbacks in that, for example, they need to be calibrated for each soil type and are only applicable for a specific range in θ and σ_w. Thus, as of now, there is no unifying theory for the σ_a-σ_w-θ relationship, making novel approaches appealing.

Given that the underlying dynamics or the 'exact' equations involved in the dielectric response of unsaturated soil are not well known, one possible way to understand the process seems to be through an approach that is capable of representing arbitrarily the (complex nonlinear) process that relates the inputs and outputs of the system. In this regard, Artificial Neural Networks (ANNs), developed based on the network of the human brain, may be a potential alternative. The advantage of the ANN is that with no *a priori* knowledge of the actual physical process and, hence, the 'exact' relationship between sets of input and output data, the network can be 'trained' to 'learn' such a relationship and, therefore, seems to be particularly suitable for physically complicated processes. Since the beginning of the nineties, ANNs have been successfully applied to hydrology-related problems, such as rainfall forecasting (e.g. French *et al.*, 1992), rainfall-runoff modeling (e.g. Hsu *et al.*, 1995), and water quality modeling (e.g. Maier and Dandy, 1996). With respect to soil-related problems, ANNs have been used for prediction of water retention characteristics from other, more easily measured, soil variables like particle size distributions and bulk density (Schaap and Bouten, 1996; Koekkoek and Booltink, 1999). The results obtained are very encouraging.

With the encouraging results thus obtained using ANNs for hydrology and soil related problems, an attempt is made in the present study to examine the possibility of using ANNs for calibration of TDR measurements. Two different data sets are used. In the first set, collected in pure sand, the measured K_a is used for calculation of θ, and σ_a and θ for the calculation of σ_w. The second data set was collected in

ten different soil types. For this data set, the K_a-θ relationship is estimated using physical parameters of the soils. An attempt was also made to study the influence of the different soil physical parameters. The performance of the ANNs is compared with several existing models for the K_a-θ and σ_a-σ_w-θ relationships, both empirical and physically based.

THEORY

Models for the K_a-q relationship

The K_a of air, soil particles and water is 1, 2-5, and 80 respectively, which makes the measured bulk K_a highly dependent on θ. Topp *et al*. (1980) used a third order polynomial equation to describe the K_a-θ relationship. Ledieu *et al*. (1986) proposed a linear relationship between θ and the square root of K_a. Some dielectric mixing models have also been used for determination of θ from K_a. In these models the bulk soil K_a is calculated from K_a and volumetric content of each phase in the soil, normally soil particles, water and air. Birchak *et al*. (1974) presented a semi-empirical dielectric α model. The de Loor model (de Loor, 1964), is a physical model based on the concept that water and air represent disc shaped inclusion in a host medium (solid soil). The de Loor model has been proven to make reliable predictions of θ. Even though the model does not contain any fitting parameters, several studies have shown that it gives more accurate data than the Birchack model (Jacobsen and Schjønning, 1995). The porosity, which is needed for the dielectric mixing models can be estimated from the bulk density by measuring (or assuming) the particle density.

Models for the σ_a-σ_w-q relationship

The σ_a of the soil depends mainly on three variables; (*i*) the volumetric water content, (*ii*) the electrical conductivity of the soil solution, and (*iii*) a geometry factor, which accounts for the complex geometry of the soil matrix (Mualem and Friedman, 1991). The σ_a is also affected by the surface conductivity of the soil matrix σ_s. For unsaturated soils, Rhoades *et al.* (1976) described the σ_a as

$$\sigma_a = \sigma_w \theta T(\theta) + \sigma_s \qquad [1]$$

where $T(\theta)$ is the transmission coefficient. Rhoades *et al.* (1976) proposed a linear relationship between $T(\theta)$ and θ, i.e. $T(\theta)=c\theta+d$, where c and d are soil specific parameters. Mualem and Friedman (1991) had a slightly different approach using the tortuosity factor $F_g(\theta)$ instead of the transmission coefficient to account for the complex geometry of the soil matrix. They proposed that F_g should be equal to the ratio of the hydraulic conductivity of the soil $K_{soil}(\theta)$ to that of a bundle of straight capillaries $K_{cap}(\theta)$. Furthermore, Mualem and Friedman (1991) showed that if a simple power expression is used to describe the water retention function, the σ_a can be described as (neglecting σ_s)

$$\sigma_a = \sigma_w \theta^b / \theta_{sat} \qquad [2]$$

where θ_{sat} is the water content at saturation and b is a calibration coefficient. A value of 2.5 was found to fit most soils. Heimovaara *et al.* (1995) used a similar approach, but instead of the power function suggested by Mualem and Friedman (1991), they used a general equation by van Genuchten (1980) to model the water retention curve, leading to

$$s_a = s_w q^{b+1} \frac{\left[1-(1-\Theta^{1/m})^m\right]^2}{1-(1-\Theta^{1/q})^q} \qquad [3]$$

where β is a calibration coefficient, Θ is the relative saturation $[(\theta_w - \theta)/(\theta_{sat} - \theta)]$, m and q are empirical parameters obtained by fitting water retention data to two forms of the empirical water retention function, one with m=1-1/n and the other with q=1-2/p (van Genuchten, 1980; Heimovaara *et al.*, 1995). A comparison of the performance of some of the models presented can be found in Persson (1997).

Neural networks

An ANN is a massively parallel-distributed information-processing system that has certain performance characteristics resembling biological neural networks of the human brain (Haykin, 1994). The particular advantage of the ANN is that, even if the 'exact' relationship between sets of input and output data is unknown but is acknowledged to exist, the network can be 'trained' to 'learn' that relationship, requiring no *a priori* knowledge of the actual physical processes.

Fig. 1 shows a schematic diagram of a three-layer feed forward back propagation ANN, consisting of input, hidden, and output layers. The number of nodes, or neurons, in the input and output layers corresponds to the number of input and output variables, respectively. The number of nodes in the hidden layer can be chosen arbitrarily, and the optimum number of nodes has to be found by trial and error.

All input nodes ***J*** containing input data ***X*** are connected via certain weights $\boldsymbol{W_{jk}}$ to all hidden nodes ***K***. At each node the input from all connections are summarized and the sum is used in a nonlinear transformation function to produce an output. This procedure is repeated for the output nodes ***L***, weights $\boldsymbol{W_{kl}}$ are multiplied with the hidden nodes output, and a nonlinear transformation function is used to produce output data ***Y***. Different types of transfer functions can be used, but in most applications a sigmoid function is used as is done in the present study.

Initially, the weights are chosen randomly. For subsequent iterations the values of the weights are optimized in an iterative calibration procedure, called training, using the back propagation algorithm (Rumelhart *et al.*, 1986). After the training procedure, the ANN model is used for producing output for an independent data set input using the weights obtained during training. The performance of the ANN is determined using the root mean square error, RMSE, and the coefficient of determination, r^2.

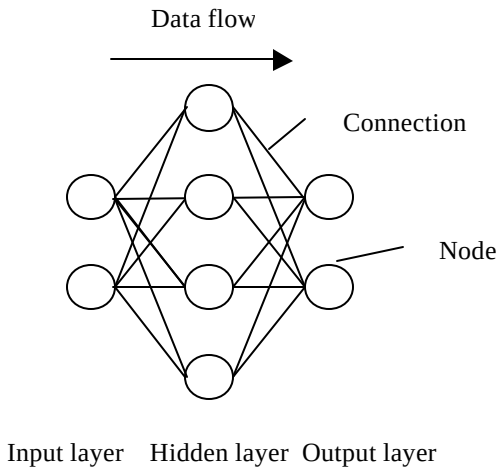

Fig. 1. *A schematic description of a 2-4-2 ANN.*

MATERIALS AND METHODS

TDR measurements in sand

All TDR measurements were made using a Tektronix 1502C metallic TDR cable tester (Beaverton, OR). Three-rod probes were used, which were 0.2 m long and had a wire spacing of 0.05 m (Soilmoisture Equipment Corp., Santa Barbara, CA). The data sets for calculations of θ and σ_w were obtained during a detailed calibration in a cylinder with homogeneous sand with a particle diameter of 0.3-0.5 mm. Water content and σ_w ranged from 0.05-0.35 $m^3\ m^{-3}$ and 0.43-4.82 dS m^{-1} respectively. In total, 378 measurements were made for the K_a-θ calibration and 287 for the σ_a-σ_w-θ calibration. Further details can be found in Persson (1997).

The data for the K_a-θ and σ_a-σ_w-θ relationships were used in the different models described above to get the best fit parameters. In both data sets, about 10% of the measurements were selected for validation. The validation data for the K_a-θ relationship were selected in the following way. First, the data set was sorted by the input data column, then every tenth value was selected for the validation series. For the σ_a-σ_w-θ relationship, the data was first sorted by θ and every fifth value was selected as validation data. Then, the data was sorted by σ_a and the procedure was repeated. This ensured that the data were selected randomly and that both the calibration and validation data sets covered the entire range of the data sets.

TDR measurements in soil

A detailed calibration of the K_a-θ relationship was carried out in soils collected at five different locations in Denmark. From each location, soil was sampled from both the plough layer and the subsoil, resulting in ten different soil textures (see Table 1). The soil was air dried, sieved, and mixed with water. The soil was then packed into PVC cylinders (1.18 m long and 0.19 m in diameter) and TDR measurements were taken using two rod probes connected to a Trace system I, model 6050X1 (Soilmoisture Equipment Corp., Santa Barbara, CA).

Location	Clay	Silt	Sand	Organic matter	Soil type
	%				
Jyndevad					Orthic Haplohumod
Topsoil	3.6	6.4	86.9	3	
Subsoil	2.5	1.9	95	0.5	
Foulum					Typic Hapludult
Topsoil	6.7	30.8	58.8	3.7	
Subsoil	11.4	21.9	66.4	0.3	
Askov					Typic Hapludalf
Topsoil	10.7	22.2	64.5	2.5	
Subsoil	23.5	20	56.2	0.4	
Ødum					Not classified
Topsoil	12.4	28.6	56.9	2	
Subsoil	17.5	26.4	55.8	0.3	
Rønhave					Typic Agrudalf
Topsoil	13.8	30.5	53.5	2.2	
Subsoil	17.4	28.9	53.2	0.5	

Table 1. *Physical parameters for the ten soil types.*

The bulk density varied between 1.24 to 1.80 Mg m^{-3} and was measured for each sample. Gravimetrical determination of the water content was carried out by drying the soil at 110°C for 48 h. More information concerning the measurements can be found in Jacobsen and Schjønning (1993).

Neural networks

In the present study, a three-layer feed forward back propagation ANN was used. The simulations were made using the Winnn32 (version 1.2) program. Before simulation, all data sets were standardized. Several ANNs were constructed with different numbers of nodes in the hidden layer (k). For the K_a-θ relationship in the sand a 1-k-1 ANN was used with K_a and θ as input and output respectively. The σ_a-σ_w-θ relationship in the sand had σ_a and θ as input and σ_w as output, thus a 2-k-1 ANN was used. The number of nodes in the hidden layer was varied between 2 and 10 in order to find the optimum number. First, 100,000 iterations were made for each value of k. The model that gave the lowest RMSE was then chosen and tested against the validation data set. More iterations will generally lead to lower RMSE for the calibration data, but it will also increase the risk of overtraining. An overtrained ANN 'learns' the noise as well as the signal, leading to a low RMSE for the calibration data, but a significantly higher RMSE for the validation data.

For the measurements in the soils, a three-layer feed forward back propagation ANN was also used. First, the number of nodes in the hidden layer was optimized. This was done by constructing a 6-k-1 ANN and let k vary from 2-15. Then, 100,000 iterations were made for each ANN using the entire data series. For each k value, two simulations were made to minimize the effects of the initial weight values. The k value that gave the lowest RMSE is chosen for the subsequent ANN simulations (i.e., k=9). The dependency of each of the six inputs (K_a, bulk density, organic matter, clay, silt, and sand content) is investigated using the ANN. This has previously been done for this data set using traditional regression analysis (Jacobsen and Schjønning, 1993). First, a 1-9-1 ANN using only K_a as input is constructed and the RMSE is determined. Then, each of the other five inputs is added and, thus, five 2-9-1 ANN were run and the RMSEs can be compared. In this analysis, the simulation ends after 100,000 iterations. Two simulations using different initial weights were conducted for each ANN. Finally, the ANN model is used for predicting the K_a-θ relationship for each of the ten soil types using the other nine for calibration. As input, K_a and the three soil physical parameters that give the most significant improvement were chosen. Thus, ten 4-9-1 ANN were run.

RESULTS AND DISCUSSION

Calculations of θ and s_w in sand

In general, the RMSE is decreasing with increasing k, but at high values of k, the RMSE increased slightly again. In the present study, I chose to use k=8 and k=9 for the K_a-θ and σ_a-σ_w-θ relationships respectively, since these k values provided the lowest RMSE. The RMSE decreased rapidly for the first iterations, after which it decreased slowly. During the entire simulation, the RMSE for the calibration and validation data sets were similar, indicating that the model was not overtrained. In the following comparison between ANN and other models, the RMSE and r^2 values are calculated for the entire data series, including both calibration and validation data.

The r^2 and RMSE of the calculated θ using the models presented above are presented in Table 2. The result from the 1-8-1 ANN is also included in the table. The model by Topp *et al.* (1980) consistently overestimated θ by around 0.02 m^3 m^{-3} while the θ prediction using the Birchak and de Loor models underestimated θ. This underestimation increased as θ increased. For the other models, there was no trend in the residuals (data not shown). The sand studied has a very well defined relationship between K_a and θ. Consequently, all models gave low RMSE and high r^2. It is interesting to note that (i) the dielectric mixing model presented by de Loor (1964) gave good results even if the model did not contain any calibration parameter; and (ii) the ANN gave better results than the polynomial regression. Since the ANN is capable of capturing non-linearities in the data, I believe that the improvement in using ANN instead of traditional calibration equations can be more significant for soils with high clay or organic matter content. These soil types typically exhibit more complicated K_a-θ relationships (see, e.g. Hook and Livingston, 1996).

Model	Best fit parameters	RMSE [m^3 m^{-3}]	r^2
Topp *et al.* (1980)*	N/A	0.0237	0.9930
Three-order polynomial**	p_1=-0.092, p_2=0.036, p_3=-0.0012, p_4=2.47E-5	0.0078	0.9941
Linear***	e=-0.210, f=0.119	0.0081	0.9935
Birchack *et al.* (1974)	α=0.62	0.0248	0.9940
deLoor (1964)	N/A	0.0147	0.9934
1-8-1 ANN	N/A	0.0064	0.9960

* $\theta_w=-0.053+0.0292K_a-0.00055K_a^2+4.3E\text{-}6K_a^3$
** $\theta_w=p_1+p_2K_a+p_3K_a^2+p_4K_a^3$
*** $\theta_w=e+fK_a^{0.5}$

Table 2. *Comparison of different models for q calculations.*

The results for the σ_w prediction using equation (1), (2), and (3) together with the 2-9-1 ANN are presented in Table 3. Again, the ANN had the lowest RMSE and highest r^2 compared to the other models including the empirical four-order polynomial regression. For all models except the ANN model, the error in the σ_w estimation increased with σ_w. The improvement in using the ANN for the σ_w calculation is much larger compared to the calculation of θ. In fact, the ANN model showed both larger r^2 and lower RMSE using standardized values for the σ_w measurement compared to the θ measurement. This result is a bit surprising since the σ_w measurement is normally considered more uncertain than the θ measurement due to the more complicated σ_a-σ_w-θ relationship. The results presented here suggest that the uncertainty of the σ_w estimation is mainly due to the fact that the models not being sophisticated enough, not in the scatter of the data.

Model	Best fit parameters	RMSE [dS m^{-1}]	r^2
Mualem and Friedman (1991)	b=2.25	0.1965	0.9768
Heimovaara *et al.* (1995)	β=1.22	0.1900	0.9767
Rhoades *et al.* (1976)*	c=2.15, d=-0.06	0.2074	0.9727
Persson (1997)**		0.0927	0.9899
2-9-1 ANN	N/A	0.0441	0.9989

* Neglecting σ_s
** $\sigma_a=\sigma_w(0.10-2.45\theta_w+22.34\theta_w^2-70.29\theta_w^3+86.81\theta_w^4)$

Table 3. *Comparison of different models for s_w calculations.*

TDR measurements in soil

For *k* values between 2 and 6, the RMSE decreases and thereafter is more or less constant. This result is in agreement with previous studies (e.g., Shaap and Bouten, 1996). A *k* value of 9 is chosen for the final model. The results for the 1-9-1 using only K_a as input and the five 2-9-1 ANNs using K_a and one other soil physical parameter as inputs are presented in Table 4 (for the standardized data). From the table it can be seen that inclusion of any soil physical parameter improved the K_a-θ calibration significantly. The most important parameters are bulk density, clay content, and organic matter content. Assuming that these parameters are not highly correlated (which is valid for the actual data), this result is in agreement with the regression analysis for this data set presented in an earlier study (Jacobsen and Schjønning, 1993). These parameters have also been shown to affect the K_a-θ relationship in other studies (e.g., Malicki *et al*., 1994; Hook and Livingston, 1996).

Input	RMSE
	[m^3 m^{-3}]
K_a	0.0326
K_a, clay content	0.0264
K_a, silt content	0.0277
K_a, sand content	0.0283
K_a, organic matter content	0.0262
K_a, bulk density	0.0225

Table 4. *The RMSE of the predicted data using different inputs.*

The r^2 and the RMSE values for each soil type using the Topp equation, a third order polynomial equation with optimized parameters for all ten soil types (system-specific) and with optimized parameters for each soil type (soil-specific), the de Loor model, and the ANN output are presented in Tables 5 and 6. The highest r^2 and the lowest RMSE for each soil type are marked in bold face. From the tables it can be seen that the ANN always performs much better than the Topp equation and the system-specific equation. Especially, the Topp equation gives poor results with RMSE from 0.019 to 0.101 m^3 m^{-3}. This is not surprising since Jacobsen and Schjønning (1993) showed that the Topp equation gave poor predictions for high θ. The system-specific calibration gives good results comparable to other system-specific results presented in previous studies (e.g., Topp *et al*., 1980; Roth *et al*., 1992). The de Loor model gives results comparable to the system-specific equation. The RMSE and r^2 for the de Loor model presented in Tables 3 and 4 are calculated using an assumed value of the particle density, the values were only slightly improved by using the measured values.

Soil	Topp *et al*. (1980)	System specific	de Loor	Soil specific	4-9-1 ANN
Jyndevad, topsoil	0.9812	0.9870	0.9872	0.9883	**0.9902**
Jyndevad, subsoil	0.9964	0.9912	0.9971	0.**9974**	0.9946
Foulum, topsoil	0.9885	0.9915	0.9889	0.9917	**0.9924**
Foulum, subsoil	0.9827	0.9905	0.9805	0.9926	**0.9928**
Askov, topsoil	0.9863	0.9904	0.9883	0.9915	**0.9944**
Askov, subsoil	0.9737	0.9828	0.9728	**0.9962**	0.9945
Ødum, topsoil	0.9788	0.9849	0.9817	0.9857	**0.9898**
Ødum, subsoil	0.9790	0.9840	0.9783	0.9870	**0.9884**
Rønhave, topsoil	0.9806	0.9854	0.9677	0.9880	**0.9894**
Rønhave, subsoil	0.9571	0.9641	0.9618	0.9699	**0.9719**

Table 5. *The r^2 value for the ten soil types using different models.*

Soil	Topp *et al*. (1980)	System specific	de Loor	Soil specific	4-9-1 ANN
	[m^3 m^{-3}]				
Jyndevad, topsoil	0.050	0.010	0.012	0.008	**0.007**
Jyndevad, subsoil	0.101	0.035	0.010	0.008	**0.007**
Foulum, topsoil	0.060	0.009	0.026	**0.008**	**0.008**
Foulum, subsoil	0.045	0.012	0.010	**0.003**	0.005
Askov, topsoil	0.046	0.008	0.016	0.006	**0.005**
Askov, subsoil	0.019	0.005	0.013	**0.001**	0.003
Ødum, topsoil	0.039	0.013	0.019	0.011	**0.008**
Ødum, subsoil	0.056	0.023	0.010	**0.006**	0.009
Rønhave, topsoil	0.077	0.019	0.057	**0.012**	0.014
Rønhave, subsoil	0.074	0.031	0.019	**0.011**	0.015

Table 6. *The RMSE for the ten soil types using different models*

It is interesting to note that the soil-specific calibration gives very low RMSE (0.001-0.012 m^3 m^{-3}), lower than that obtained in many other studies, e.g., Nadler *et al*. (1991) (RMSE=0.015 m^3 m^{-3}) and Ledieu *et al*. (1986) (RMSE=0.019 m^3 m^{-3}). In the detailed calibration by Young *et al*. (1997), however, similar RMSE was obtained (0.005-0.007 m^3 m^{-3}). The ANN prediction consistently gives r^2 and RMSE in the same range as the soil-specific calibration, and in about half of the soil types the ANN actually performed better than the soil-specific calibration. This clearly shows the applicability of the ANN for prediction of the K_a-θ relationship.

I believe that the ANN prediction can be improved if a data set with a wider range of soil textures is used for the calibration set. Other parameters, e.g., electrical conductivity, specific surface, and temperature can also be incorporated in the model. It is important, however, that the soil for which the prediction is made would not be too different from those used in the calibration data set since the ANN is a purely data-learning method. The ANN method presented in this study should, therefore, be regarded as a system-specific model since errors associated with different TDR systems and calibration procedures might be larger than the ones obtained using the ANN.

SUMMARY

Artificial neural networks (ANNs) have found many applications recently and seem to be a very good alternative to ordinary regression analysis. I used an ANN model for calibration of TDR measured K_a and σ_a to θ and σ_w in sand. The performance of the ANNs was compared with several models made available in the literature, empirical, conceptual, and physically based. In all cases, the ANN performed better than any other model, which was reflected in the low RMSE and high r^2. The present study shows that ANNs can be used successfully for calibration of any measurement, especially where the (nonlinear) relationship between the measured values and the parameter of interest is difficult to describe physically. It should be noted that constructing and calibration an ANN model takes longer time than applying a conventional model. However, when high accuracy is desired, it is worth the extra effort.

The universal calibration equation for θ is presented by Topp *et al*. (1980) has been successfully applied to many different mineral soil types with relatively small errors (normally around 0.02 m^3 m^{-3}). Few

attempts have been made to improve the K_a-θ calibration by including soil physical parameters. Thus, when accurate results are needed for a specific soil type, a special calibration experiment has to be carried out.

In the present study, ANNs were used to predict the K_a-θ relationship using soil physical parameters. The data set analyzed have previously been presented by Jacobsen and Schjønning (1993), and contains a detailed calibration of the K_a-θ relationship for 10 different soils including sand, loamy sand, sandy loam, sandy clay loam and loam. Besides K_a, five different soil physical parameters were used, bulk density, clay, silt, sand, and organic matter content. By inclusion of one parameter at the time in a 2-9-1 ANN it was found that the parameters that improved the calibration most were bulk density, followed by clay and organic matter content. These results are in agreement to the analysis originally made by Jacobsen and Schjønning (1993) for the data set.

In order to show the applicability of using ANNs to predict the K_a-θ relationship for an independent data set, the measurements from one soil type was used for validation and the other nine soil types as calibration. In this analysis, K_a was used together with bulk density, clay and organic matter content as input data in a 4-9-1 ANN. It was shown that the ANN provided significantly better prediction of θ than the Topp equation and Eq. [1] with optimized parameters for all ten soils (system specific calibration). Furthermore, the ANN prediction gave r^2 and RMSE in the same range, and in about half of the soil types better results, compared to a soil-specific calibration. Thus, by using ANN it is possible to obtain very accurate results without the need for soil specific calibration experiments.

ACKNOWLEDGEMENTS

This study was funded by the Swedish Research Council for Engineering Sciences and the Swedish Natural Science Research Council. I would also like to thank Ole H. Jacobsen and Per Schjønning, Department of Crop Physiology and Soil Science, Tjele, Denmark for supplying the TDR measurements in soil.

REFERENCES

Birchak, J. R., Gardner, C. G., Hipp, J. E., and Victor, J. M., 1974, High dielectric constant microwave probes for sensing soil moisture: Proc. IEEE, **62**, 93-98.

Dalton, F. N., 1992, Development of time-domain reflectometry for measuring soil water content and bulk soil electrical conductivity: *In* G. C. Topp and W. D. Reynolds (ed.) Advances in measurement of soil physical properties: Bringing theory into practice. SSSA Special Publication no. 30 pp 143-167. SSSA, Inc. Madison, WI.

Dalton, F. N., Herkelrath, W. N., Rawlins, D. S., and Rhoades, J. D., 1984, Time-domain reflectometry: Simultaneous measurements of soil water content and electrical conductivity with a single probe: Science, **224**, 989-990.

De Loor, G. P., 1964, Dielectric properties of heterogeneous mixtures: Appl. Sci. Res. B3, 479-482.

French, M. N., Krajewski, W. F., and Cuykendal, R. R., 1992, Rainfall forecasting in space and time using a neural network: J. Hydrol., **137**, 1-37.

Haykin, S., 1994, Neural networks: a comprehensive foundation: Mac-Millan, New York, USA.

Heimovaara, T. J., Focke, A. G., Bouten, W., and Verstraten, J. M., 1995, Assessing temporal variations in soil water composition with time domain reflectometry: Soil Sci. Soc. Am. J., **59**, 689-698.

Hook, W. R., and Livingston, N. J., 1996, Errors in converting time domain reflectometry measurements of propagation velocity to estimates of soil water content: Soil Sci. Soc. Am. J., **60**, 35-41.

Hsu, K., Gupta, H. V., and Sorooshian, S., 1995, Artificial neural network modeling of the rainfall-runoff process: Water Resour. Res., **31**, 2517-2530.

Jacobsen, O. H., and Schjønning, P., 1993, A laboratory calibration of time domain reflectometry for soil water measurement including effects of bulk density and texture: J. Hydrol., **151**, 147-157.

---------- 1995, Comparison of TDR calibration functions for soil water determination: *In* L. W. Petersen and O. H. Jacobsen (ed.) Proceedings of the symposium: Time-domain reflectometry applications in soil science. Research Centre Foulum, Denmark, Sep. 16. 1994. SP report, **3**, No. 11, 25-33. Danish Institute of Plant and Soil Sci., Lyngby, Denmark.

Koekkoek, E. J. W., and Booltink, H., 1999, Neural network models to predict soil water retention: European J. Soil Sci., **50**, 489-495.

Ledieu, J., de Ridder, P., de Clerck, P., and Dautrebande, S., 1986, A method of measuring soil moisture by time-domain reflectometry: J. Hydrol., **88**, 319-328.

Maier, H. R., and Dandy, G. C., 1996, The use of artificial neural networks for the prediction of water quality parameters. Water Resour. Res., **32**, 1013-1022.

Malicki, M. A., Plagge, R., and Roth, C. H., 1994, Influence of matrix on TDR soil moisture readings and its elimination: In Proceedings of Symposium and Workshop on Time Domain Reflectometry in Environmental, Infrastructure, and Mining Applications. Evanston, Illinois, Sep. 7-9, 1994. Special Publication SP19-94, pp. 294-308. US Department of the Interior, Bureau of Mines, Washington, DC.

Mualem, Y., and Friedman, S. P., 1991, Theoretical prediction of electrical conductivity in saturated and unsaturated soil: Water Resour. Res., **27**, 2771-2777.

Nadler, A., Dasberg, S., and Lapid, I., 1991, Time domain reflectometry measurements of water content and electrical conductivity of layered soil columns: Soil Sci. Soc. Am. J., **55**, 938-943.

Pepin, S., Livingston, N. J., and Hook, W. R., 1995, Temperature-dependent errors in time domain reflectometry determinations of soil water: Soil Sci. Soc. Am. J., **59**, 38-43.

Persson, M., 1997, Soil solution electrical conductivity measurements under transient conditions using time domain reflectometry: Soil Sci. Soc. Am. J., **61**, 997-1003.

Persson, M., and Berndtsson, R., 1998, Texture and electrical conductivity effects on temperature dependency in time domain reflectometry: Soil Sci. Soc. Am. J., **62**, 887-893.

Rhoades, J. D., Ratts, P. A., and Prather, R. J., 1976, Effects of liquid-phase electrical conductivity, water content, and surface conductivity on bulk soil electrical conductivity: Soil Sci. Soc. Am. J., **40**, 651-655.

Roth, C. H., Malicki, M.A., and Plagge, R., 1992, Empirical evaluation of the relationship between soil dielectric constant and volumetric water content as the basis for calibrating soil moisture measurements by TDR: J. Soil Sci., **43**, 1-13.

Roth, K., Schulin, R., Flühler, H., and Attinger, W., 1990, Calibration of time domain reflectometry for water content measurement using a composite dielectric approach: Water Resour. Res., **26**, 2267-2273.

Rumelhart, D. E., Hinton, G. E., and Williams, R. J., 1986, Learning internal representations by error propagation. Parallel distributed processing: MIT Press, Cambridge, **1**, 318-362.

Schaap, M. G., and Bouten, W., 1996, Modelling water retention curves of sandy soils using neural networks: Water Resour. Res., **32**, 3033-3040.

Topp, G. C., Davis, J. L., and Annan, A. P., 1980, Electromagnetic determination of soil water content: Measurements in coaxial transmission lines: Water Resour. Res., **16**, 574-582.

van Genuchten, M. T., 1980, A closed-form equation for predicting the hydraulic conductivity of unsaturated soils: Soil Sci. Soc. Am. J., **44**, 892-898.

Young, M. H., Fleming, J. B. Wierenga, P. J., and Warrick, A. W., 1997, Rapid laboratory calibration of time domain reflectometry using upward infiltration: Soil Sci. Soc. Am. J., **61**, 707-712.

FREQUENCY-DOMAIN METHODS FOR EXTENDING TDR MEASUREMENT RANGE IN SALINE SOILS

Scott B. Jones[1] and Dani Or[2]

[1]Dept. Plants, Soils, and Biometeorology, Utah State University, Logan, UT 84322-4820; sjones@mendel.usu.edu
[2]Dept. Plants, Soils, and Biometeorology, Utah State University, Logan, UT 84322-4820;dani@mendel.usu.edu

ABSTRACT

Water content and electrical conductivity of soils are routinely determined using time-domain reflectometry (TDR) based on analysis of signal travel time along buried waveguides. In soils with appreciable electrical conductivity, travel time analysis becomes progressively inaccurate due to signal attenuation to the point of failure (typically at $EC_b > 2$ dS m^{-1}). We demonstrate that information on bulk dielectric permittivity, lost in travel time analysis in saline soils, can be recovered in the frequency domain by using shorter waveguides to reduce signal attenuation. We implement a robust algorithm for the time-to-frequency domain transformation (Nicolson, 1973) that does not rely on waveform differentiation. This algorithm uses signal de-ramping to eliminate noise induced by standard differentiation and to reduce truncation errors arising from finite sample size. The methodology was tested using coaxial cells and three-wire TDR probes under a wide range of solution electrical conductivities (0 to 24 dS m^{-1}). Reliable estimates of bulk dielectric permittivity for EC's up to 24 dS m^{-1} in a silt loam soil were obtained using 2 and 3 cm TDR probes. In addition to bulk dielectric permittivity, this method provides additional frequency-dependent and electrical conductivity information derived in the estimation of the Cole-Cole parameters.

INTRODUCTION

Time Domain Reflectometry (TDR) offers simultaneous and accurate method for water content and electrical conductivity determination in soils and other porous media. Waveform reflections necessary for permittivity measurements can be totally attenuated in lossy (highly saline) materials. Soil texture, salinity, probe geometry and water content all influence permittivity measurements. Nadler et al. (1999) found that under field capacity in sandy and loamy soils, TDR could be safely used up to an apparent electrical conductivity, EC_a, of approximately 2 dS m^{-1}. TDR applications are therefore limited to soils with relatively low salinity unless measures to preserve waveform reflection from the end of a waveguide are taken. Rod coating methods have been successfully used to reduce signal attenuation and

preserve permittivity information in highly saline soils. Since these coatings significantly influence the resulting permittivity, rod-coating calibration is required (Mojid et al., 1998) making this a less appealing method.

Time-domain methods employ a step voltage which propagates down a low-loss coaxial line and whose voltage remains relatively constant until a change in material is encountered. At the interface of two materials with different permitivities, a portion of the signal is reflected and the remainder is transmitted through the new material. In lossy materials, the presence of free ions give rise to attenuation of the transmitted signal along the travel path due to ion migration between rods of different polarity. For material samples of finite length, a reflection occurs at the sample-air interface, resulting in a chain of signal reflections as the new reflected signal again reflects and transmits at the sample-cable interface resulting in multiple reflections shown in Fig 1.

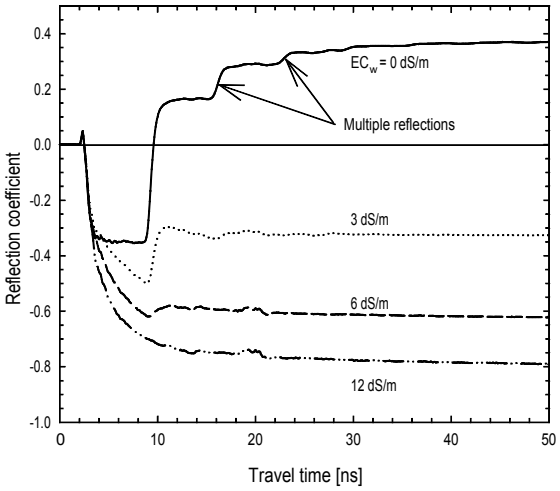

Fig. 1. *TDR waveforms showing attenuation of the second reflection point and subsequent loss of permittivity (water content) measurement capability.*

Conversion of TDR waveforms into the frequency domain provides additional frequency-dependent dielectric information (Heimovaara, 1994; Friel and Or, 1999). Information on electrical conductivity, relaxation frequency, static and apparent permittivity may be extracted using this procedure. The disadvantages of this approach are that the process including fast Fourier transformation (FFT) of the waveform and fitting of an appropriate model to the transformed scatter function can be laborious. The procedure, however, has the potential to be automated to make it more amenable to realtime measurements.

The objectives of this work address both technical and theoretical aspects, the former objectives were to determine the extent to which dielectric and electrical information in saline porous media can be extracted by a) transforming TDR waveforms to the frequency domain via Fourier analysis, and b) using shorter probes to reduce attenuation. The latter objectives were to improve time to frequency transformation by a) introducing and testing the Nicolson (1973) ramping algorithm as a substitute for waveform differentiation and b) implementing a more robust system input function for deriving the scatter function.

THEORETICAL

Transformation of the measured and input signal waveforms from the time to the frequency domain yields the system response or the so-called scatter function that represents interactions between the material (dielectric permittivity) and the electric field in a given waveguide geometry. Hence, for a given geometry (coaxial in this study), The transformed scatter function may be used to infer the material dielectric properties using the Debye (1929) or Cole-Cole (1941) models for dielectric permittivity.

As a TDR input signal, v(t), traverses the waveguide, the response function, r(t), reflects interactions between the applied EM field and the sample. These interactions are summarized in the waveform, r(t), described by the following convolution integral (van Gemert, 1973)

$$r(t) = \int_{-\infty}^{t} v_0(t-\tau)s(\tau)d\tau \qquad [1]$$

where τ is the time lag variable of integration and s(τ) is dependent upon the probe geometry and the material properties. Application of the convolution theorem reduces this integral to a simple product in the frequency domain. The Fourier transforms of the frequency-dependent response, R(f), system, $S_{11}(f)$, and input, $V_0(f)$ functions described by (Lathi, 1992)

$$R(f) = V_0(f)S_{11}(f) \qquad [2]$$

where f [Hz] is the frequency. In general the Fourier transform is written as

$$X(f) = \int_{-\infty}^{\infty} x(t)e^{(-i2\pi ft)}dt \qquad [3]$$

where $i = (-1)^{1/2}$ and r(t) and $v_o(t)$ are substituted for x(t).

The measurement of reflections along a transmission line is a common method used in both time and frequency domain spectroscopy. In each case the signal is analyzed similarly with only the dependent variable differing (i.e., time or frequency). The multiple reflections in a coaxial transmission line can be modeled according to the scatter function given by Clarkson et al. (1977) as

$$S_{11}(f) = \frac{\rho + e^{-2\gamma L}}{1 + \rho \cdot e^{-2\gamma L}} \qquad [4]$$

where ρ is the reflection coefficient described as

$$\rho = \frac{1 - z[\varepsilon^*(f)]^{0.5}}{1 + z[\varepsilon^*(f)]^{0.5}} \qquad [5]$$

in which z is the impedance ratio of the cable, z_c, and probe, z_p, (i.e., $z = z_c/z_p$), $\varepsilon^*(f)$ is the complex dielectric permittivity and γL is the TEM mode propagation constant written as

$$\gamma L = \frac{i2\pi fL\,[\varepsilon^*(f)]^{0.5}}{c} \qquad [6]$$

in which L [m] is the probe length and c is the speed of light constant (3 x 10^8 m s^{-1}).

The frequency-dependent complex dielectric constant, $\varepsilon^*(f)$, may be described by the following parametric model of Debye (1929) as modified by Cole and Cole (1941), written as

$$\varepsilon^*(f) = \left[\varepsilon_\infty + \frac{\varepsilon_s - \varepsilon_\infty}{1 + \left(i \frac{f}{f_{rel}} \right)^{(1-\beta)}} \right] - i \frac{\sigma_{dc}}{2\pi f \varepsilon_0} \qquad [7]$$

where ε_s is the static dielectric permittivity, ε_4 is the permittivity at infinite frequency, f_{rel} is the dielectric relaxation frequency of the material, σ_{DC} is the low frequency electrical conductivity [S m^{-1}], ε_0 is the permittivity of free space (8.854 x 10^{-12} F m^{-1}) and β is a parameter added by Cole and Cole (1941) to describe the spread in relaxation frequency which tends to increase as the complexity of the mixture increases (e.g., minerals, biological materials). For pure liquids with a single relaxation frequency such as water or ethanol, β is zero resulting in the original debye model.

EXPERIMENTAL

A Tektronix 1502B cable tester was used to obtain time domain reflectometry (TDR) waveforms. Waveforms were collected and analyzed using WINTDR99, an analysis software package (Or et al., 1999) available at http://psb.usu.edu/wintdr99/index.html. The maximum sampling frequency was 14.9 GHz (distance/division = 0.25 m) and waveforms consisted of 2510 data points. Both coaxial (length = 19, 6, and 2 cm) and 3-wire (Length = 2, 3, 6, 10, and 15 cm) TDR probes (Fig. 2) were used for measurements in solutions and a saturated sand and in saturated Millville Silt Loam soil. Distilled water, Ethanol and Octanol-1 were used as solutions in the coaxial cell maintained at 25EC. Potassium chloride solutions of 0, 3, 6, 12, 18, 24 dS m^{-1} in saturated sand and solutions of 36 and 48 dS m^{-1} were also used in a saturated Millville silt loam soil.

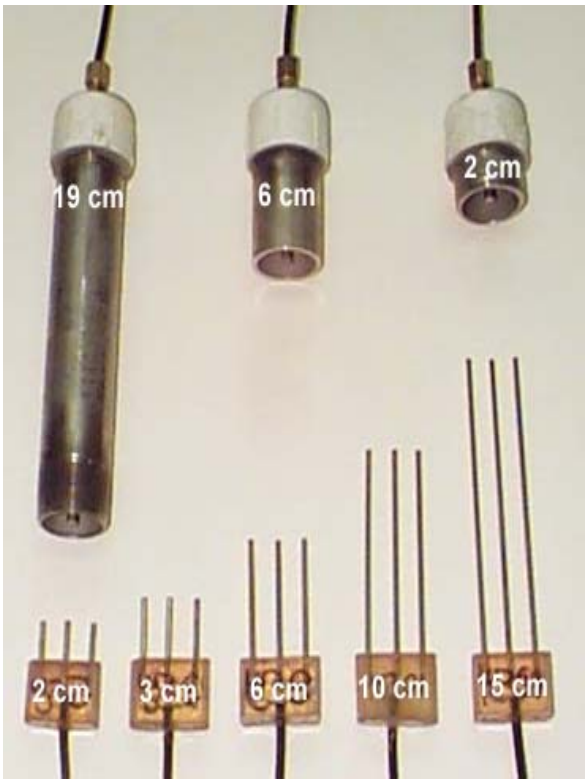

Fig. 4. *Coaxial and three-wire TDR probes, of varying length, used for permittivity and electrical conductivity measurements in different media.*

AUTOMATION CONSIDERATIONS

Waveform collection

The size of the waveform used for frequency domain analysis is a function of the sampling frequency (distance per division per screen) and the total number of consecutive screens which are collected, each screen or window from the Tektronix contains 251 data points. The combination of

sampling frequency and number of screens or windows collected will determine the frequency content obtained in the frequency domain. The available frequency content in time domain analysis was found by Heimovarra (1994) to lie in the range 20 kHz to 1.5 GHz. Automated waveform collection may be performed using TDR analysis software such as WINTDR99 whose output from each measurement may then be combined to form a waveform of desired length. For example, we collected 10 consecutive screens yielding a waveform of 2510 data points. The time (t) or distance (x) between two consecutive points in the waveform are computed to find the maximum sampling frequency. With a distance per division (dd) setting of 0.25 m, and assuming a velocity of propagation, V_p, equal to 0.99, we calculate the maximum sampling frequency
(f_{max}) from

$$f_{\max} = \frac{1}{\Delta t} = \frac{c \cdot V_p}{2 \cdot \Delta x} = \frac{251 \cdot c \cdot V_p}{2 \cdot dd \cdot ds} \qquad [8]$$

where c is the speed of light, the number of divisions per screen (ds) was 10 for the Tektronix device and the division by 2 accounts for the doubling of the travel distance in the reflection measurement. For the conditions described above, f_{max} = 15 GHz based on V_p of 0.99. The lowest frequency content, including all points in the waveform, can be calculated using eq. (8), as f_{min} = c Vp / (2) x N), where N = 2510 data points, giving f_{min} = 6 MHz.

Input function derivation

The input function provides a way of removing the unwanted noise caused by the cable and impedance transition to the probe. The input function can be obtained by removing one of the conductors from the probe and obtaining the waveform shown in Fig. 3. Removal of one of the conductors may not be possible, especially for pre-manufactured TDR probes. An alternate approach is to generate an artificial input function, which requires only the measurement of the waveform with the probe in air and an algorithm to determine the initial slope of the waveform and the reflection coefficient at the distal point shown in Fig 3. The resulting artificially generated waveform has another advantage, which is to avoid the secondary reflections of the waveform where the central conductor was removed from the probe.

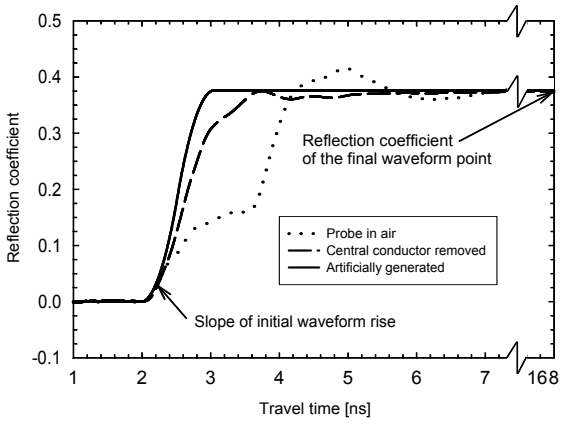

Fig. 3. *Waveforms derived from TDR measurements using a 3-wire probe in air, with the central conductor removed and an artificially generated waveform. The input function may be represented by the waveform with the central conductor removed or, as an alternative ,it may be generated based on the initial slope and final value of a waveform measured in air.*

Waveform preparation and transformation

Transformation of a discrete waveform, derived in the time domain, to the frequency domain is accomplished using a discrete Fourier transformation (DFT) technique. The fast Fourier transform (FFT) is commonly employed for this purpose and is generally included as a function in modern mathematical software programs. Simply

taking the FFT of the waveform from TDR is problematic in that the last point of the waveform is generally non-zero and introduces frequency errors. Heimovaara (1994) used the backward difference of the waveform with the assumption that zeroes result at the beginning and end of the data. Noise enhancement introduced when taking the derivative of two similar quantities in digital systems can be significant and therefore Nicolson (1973) suggested simply subtracting a ramp from the step response as illustrated in Fig. 4. The linear ramp is subtracted from the original waveform W(n) at each point, n (0<n<N), and is scaled according to the final point N. The modified waveform, $W^*(n)$, ensures a final value of zero, written as

$$W^*(n) = W(n) - W(N)\frac{n}{N} \qquad [9]$$

A key feature of this algorithm is that the DFT of W*(n) produces the same response as an infinite train of samples truncated out, so for discrete frequencies, τ, where $\tau = (2Bf_s)n/N$, there is no error, which is not the case for $\tau \neq (2Bf_s)n/N$ (Nicolson, 1973).

After applying the Nicolson ramping algorithm or differentiating each waveform (both input and response functions), they require further preparation prior to applying the discrete fast Fourier transform (FFT). The total number of data points in the final waveform, prior to Fourier transformation should be greater than or equal to the number of points in the original measured waveform, N, and equal to 2^k where k is an integer. For the case of 2510 data points, which lies between $2^{11} = 2048$ and $2^{12} = 4096$, we ultimately require 4096 data points and therefore pad the final waveform between 2510 and 4096 data points using zeros.

After zero padding, the waveform is transformed using FFT, a function in most mathematical or spreadsheet software. The scatter function, $S_{11}(f)$, is obtained by dividing the transformed response function, R(f), by the transformed input function, $V_o(f)$, from eq. (2).

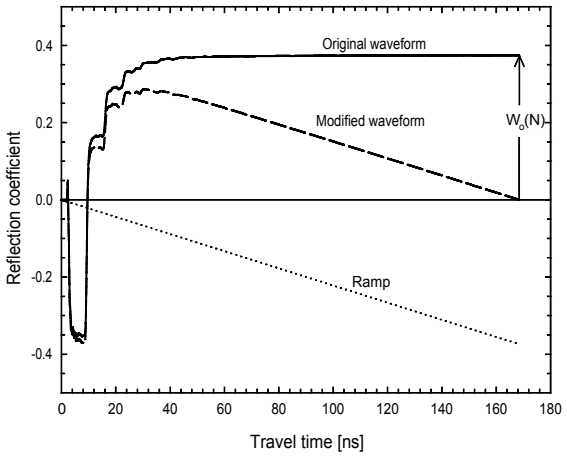

Fig. 4. *Original waveform (response function) with the Nicolson (1973) ramping algorithm applied to yield the modified waveform.*

Transformed scatter functions plotted in Fig. 5, derived from TDR measurements in three liquids of known permittivities, illustrate the dependence of the scatter function's characteristic period on dielectric permittivity. Note a distinct change in the S_{11} periodicity for the alcohols due to the onset of dielectric relaxation in the 600-900 MHz region shown in Fig. 5.

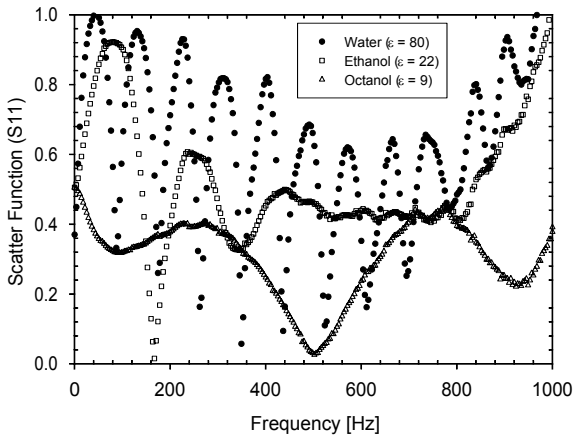

Fig. 5. *The periodic nature of the S_{11} is proportional to the dielectric permittivity of the material (e.g., water, ethanol, octanol).*

Dielectric permittivity determination

The shape and periodic pattern of the S_{11} provides definition for fitting the modeled scatter function using eqs. (5) - (8). Probe parameters in eqs. (5) - (7) are known or measured. The 5 coefficients of the Cole-Cole model (eq. (8)) were either assumed constant ($\$ = 0$, $F_{DC} = EC_b$) or used as fitting parameters (g_s, g_4, f_{rel}) for modeling the discrete S_{11} data. An optimization routine was established with an objective function which minimized the sum of squared differences between the transformed S_{11} and the modeled S_{11}. Key fitting features in the optimization include the first and second peaks and the valley in between, which, for Octanol, comprises the entire frequency range shown in Fig 5. The static permittivity parameter was found to be most sensitive to matching these features. Further work is needed for understanding the interaction between theses fitting parameters and their influence on the resulting permittivity. For example, we expect g_s to be greater than g_4 so it may be that g_4 can be expressed as a function of g_s for initial guesses of these parameters. Also, if we know the measurement frequency range of the TDR (e.g., 20 kHz to 1.5 GHz), it may be possible to estimate the average frequency content of the TDR measurement and calculate the dielectric permittivity as a function of this frequency using eq. (7). An additional benefit of the optimized parameters comes in the information on real and imaginary permittivities and relaxation effects described by the Cole-Cole parameters.

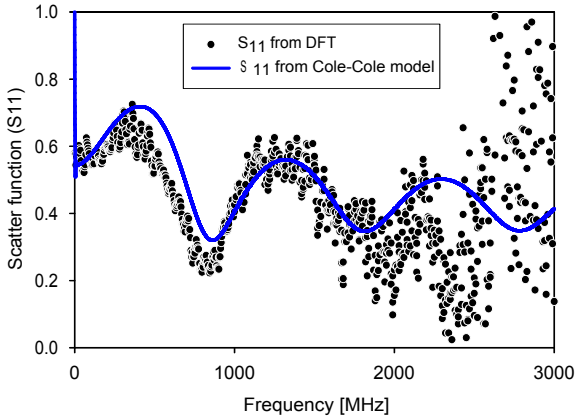

Fig. 6. *Scatter functions derived from DFT of the measured waveform and from the Cole-Cole (1941) model. The measured waveform was obtained using a 3-wire TDR probe in saturated sand for $EC_w = 18$ dS m^{-1}.*

RESULTS

Both coaxial and 3-wire TDR probes were used to obtain permittivity measurements in saturated sand having variations in solution electrical conductivity. Fig. 6 shows the S_{11} derived from the DFT of the TDR measured waveform using a 3 cm probe ($EC_w = 18$ dS m^{-1}). The optimized Cole-Cole parameters

were $g_s = 27$, $g_4 = 24$, $f_{rel} = 1.1$ GHz, $F_{DC} = 0.42$ S m^{-1}, and $ was set to zero. Despite the increased dispersion of the data beyond about 1.5 GHz (upper frequency range for TDR), there is sufficient structure in the scatter function within the TDR frequency range for fitting the Cole-Cole model to the data. A critical feature for fitting is the first harmonic ("valley") in the S_{11}, to which additional weight can be applied for more efficient optimization. Longer probe length increases signal attenuation, which reduces the S_{11} amplitude to the point where parameter optimization ultimately fails.

The comparison of bulk permittivity determinations using time domain analysis and frequency domain analysis are illustrated in Fig. 7 where both are given as a function of solution electrical conductivity. The dielectric permittivity of the saturated Millville silt loam soil is indicated as shaded grey in the figure at a permittivity of around 27. Shorter TDR probes (e.g., < 10 cm) are unreliable in time domain analysis and results for 10 and 15 cm probes diverge for solution electrical conductivities much greater then 6 dS m^{-1}. In the frequency domain analysis, permittivity determinations using longer probes fail and diverge as a function of probe length. Results using a 3 cm probe length, provide reliable permittivity values approaching 30 dS m^{-1}. Results from the 2 cm probe are similar, but diverge at lower EC levels than the 3 cm probe. The benefit of extending the permittivity measurement range under saline conditions comes at the sacrifice of time domain analysis capability, where shorter probes are incompatible.

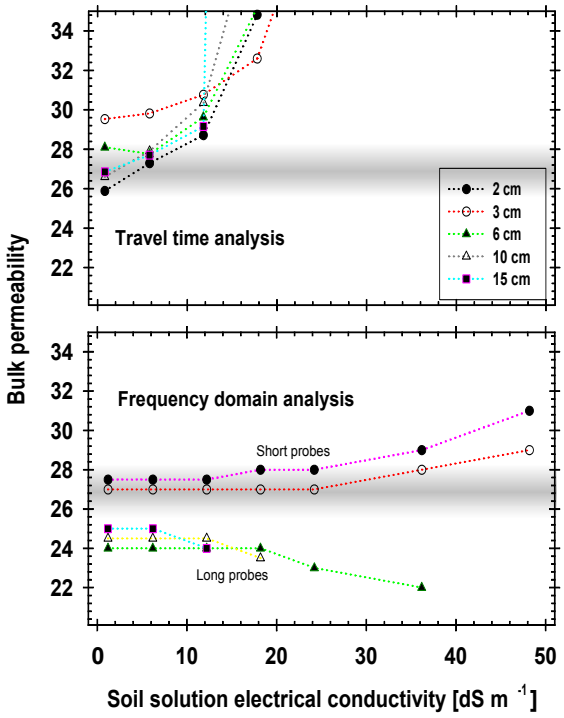

Fig. 7. *Bulk permittivity determined using time domain analysis and frequency domain analysis as a function of soil solution electrical conductivity. The shaded region indicates the bulk permittivity of saturated Millville silt loam soil where probes of specified length were inserted for measurements.*

CONCLUSIONS

Automation of time- to frequency-domain transformation of TDR waveforms facilitates measurement of bulk permittivity for water content determination in saline soils where time domain analysis fails. Enhancement of recoverable permittivity information was attainable using shorter TDR probes. Automation of this process, should provide reliable and near real-time measurement of water content under saline conditions. The Nicloson ramping algorithm provides a robust method for preparing waveforms for discrete Fourier transform. Use of an artificially generated input function in the time domain provides a convenient and rapid means of obtaining the input function and which avoids the need to remove a conductor from the TDR probe. Information on sample dielectric permittivity is preserved in the frequency domain for lossy media with electrical conductivities 4 times greater than the practical upper limit in travel time analysis of TDR waveforms.

REFERENCES

Clarkson, T.S., L. Glasser, R.W. Tuxworth, and G. Williams, 1977, An appreciation of experimental factors in time-domain spectroscopy, Adv. Molecular Relaxation Interaction processes, **10**, 173-202.

Cole, K.S., and R.H. Cole, 1941, Dispersion and adsorption in dielectrics: I--Alternating current characteristics, J. Chem. Phys., **9**, 341-351.

Friel, R., and D. Or, 1999, Frequency analysis of time-domain reflectometry (TDR) with application to dielectric spectroscopy of soil constituents, Geophysics, **64** No. 3, 1-12.

Heimovaara, T.J., 1994, Frequency domain analysis of time domain reflectometry waveforms: 1, Measurement of the complex dielectric Permittivity of soils, Water Resour. Res., **30**, 189-199.

Lathi, B.P., Linear Signal and Systems Analysis, Cambridge Press, Berkeley, 1992.

Mojid, M.A., G.C.L. Wyseure, and D.A. Rose,1998, The use of insulated time-domain reflectometry sensors to measure water content in highly saline soils, Irrig. Sci., **18**, 55-61.

Nadler, A., A. Gamliel, and I. Peretz, 1999, Practical aspects of salinity effect on TDR-measured water content: A field study, Soil Sci. Soc. Am. J., **63**, 1070-1076.

Nicolson, A.M., 1973, Forming the fast fourier transform of a step response in time-domain metrology, Electronics Lett., **9**, 317-318.

Or, D., B. Fisher, R.A. Hubscher, and J.M. Wraith, 1998, WinTDR98 v4.0 - Users Guide (Windows-based time domain reflectometry program for measurement of soil water content and electrical conductivity), 1432, Utah Agric. Exp. Sta. Res. Rpt., Logan, UT.

vanGemert, M.J.C., 1973, High-frequency time-domain methods in dielectric spectroscopy, Philips Res. Repts., **28**, 530-572.

Debye, P., Polar Molecules, Dover, Mineola, New York, 1929.

DIELECTRIC PROPERTIES OF BOUND WATER: APPLICATION TO POROUS MEDIA SURFACE AREA AND GRAIN MOISTURE DETERMINATION

Jon M. Wraith[1], Dani Or[2], and Scott B. Jones[3]

[1]Land Resources and Environmental Sciences Dept., Montana State University, Bozeman, MT 59717-3120; jwraith@montana.edu
[2]Department of Plants, Soils, and Biometeorology, Utah State University, Logan, UT 84322-4820; dani@mendel.usu.edu
[3]Department of Plants, Soils, and Biometeorology, Utah State University, Logan, UT 84322-4820; sjones@mendel.usu.edu

ABSTRACT

The dielectric properties of molecular layers of water bound to solid surfaces or to macromolecules are substantially different than those of free water. Consequently, determination of moisture content from dielectric properties of porous mixtures, such as soils and rocks having moderate to substantial surface area and cereal grains, is affected by the amount and energy state of bound water. We use earth materials and seed or grain products as specific examples having high economic and environmental relevance. A physical model that considers modified properties of water near solid surfaces is presented. The thermo-dielectric sensitivity of TDR-measured bulk dielectric permittivity (ε_b) to bound water reflects interactions with the porous medium surface area, and permits model inversion to infer specific surface area (A_s) from measured response to thermal perturbation. Measured $\varepsilon_b(T)$ using TDR along with independently measured mass water contents and bulk densities are used in the model to calculate A_s for soils and sand-clay mixtures having a range in A_s and wetness. Results are in agreement with A_s of the mixtures measured using ethylene glycol monoethyl ether (EGME) monolayer adsorption. Estimation of bound water within grains or legumes is a critical component towards predicting water content from dielectric permittivity measurements. Application of the physical model to this problem is also discussed and compared to permittivity measurements in starch and grain samples.

INTRODUCTION

Time domain reflectometry (TDR) is commonly used to infer liquid water content and bulk electrical conductivity of soils and other porous media. Estimation of soil water content (2) from measured ε_b using TDR travel time analysis is based on the dominance of the high dielectric permittivity of liquid water relative to that of other common soil constituents. Bound water, water that is closely adjacent to solid surfaces, is subject to a number of forces that hinder its response to an imposed electromagnetic field resulting in lower ε_b than free liquid water. Water closest to solid surfaces is held most tightly, and

has lowest measured ε_b. Successive molecular layers of water have increasingly higher ε_b until that of free water is reached at about 3 molecular layers from the solid (Bockris *et al*., 1966, Sposito and Prost, 1982). Water incorporated into starches may also be considered as bound in the sense that it is rotationally constrained in response to an alternating electromagnetic field imposed by TDR. In this paper we discuss development and preliminary applications of a physical model to describe the relationships between bound and free water contents of porous media and food grains, the measured responses in ε_b using TDR under ambient or imposed temperature (T) changes, and specific surface areas and grain moisture contents.

Physical Model of Thermodielectric Behavior of Bulk and Bound Soil Water

Experimental results (Wraith and Or, 1999) showed that ε_b of soils measured using TDR exhibits temperature dependence proportional to soil specific surface area and wetness. Or and Wraith (1999) developed a physical model to explain the temperature influence on measured ε_b using TDR as the result of an interplay between two competing processes.
The dielectric permittivity of liquid water decreases with increasing temperature (Weast, 1986), while bound water surrounding solid surfaces becomes more rotational with increasing temperature, thereby increasing its effective dielectric permittivity as measured using TDR. Hence the relative proportion of bulk and bound water governs the measured response to changes in temperature. The authors termed this phenomenon the 'thermodielectric effect'.

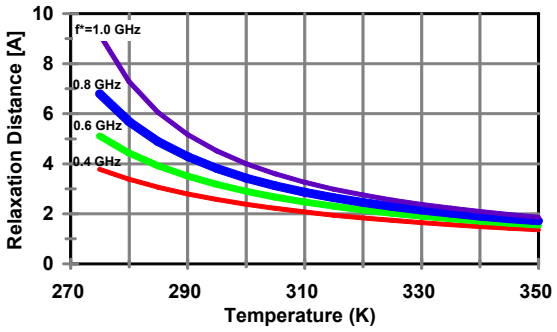

Fig. 1. *Dielectric relaxation distance from solid surfaces as function of temperature.*

Water molecules near solid surfaces are subjected to various forces which modify their properties relative to bulk water (Bockris *et al*., 1963; Low, 1976). The impact of these modified properties on dielectric response was investigated by considering the effects of temperature and distance-dependent viscosity profiles (Low, 1976) on the polar orientation of water molecules using the Debye (1929) model for relaxation time of rigid spheres:

$$\tau(x,T) \;=\; \frac{4\,\pi\, r^3\, \eta_0(T) \exp^{\frac{a}{x\,T}}}{k\,T} \qquad [s] \qquad [1]$$

where k is the Boltzmann constant, T is temperature, r is the radius of a water molecule (r . 1.8-2.5 Å), x is distance from solid surface, $\eta_0(T)$ is the known temperature dependent viscosity of bulk water, and *a* is a coefficient derived by Low (1976). The dielectric relaxation time, τ, is related to relaxation frequency by: $f_{rel}=1/(2\pi\tau)$. It has been observed that soil constituents undergoing dielectric relaxation at frequencies within the TDR-bandwidth become 'partially invisible' to travel-time analysis of reflection waveforms used to determine the bulk dielectric permittivity of the medium. An important example is

soil water in the form of ice which exhibits dielectric relaxation at low frequencies (in the kHz range; Hasted, 1973) and hence has dielectric permittivity about 1/20th that of liquid water. We postulate that rotationally-hindered (bound) water near solid surfaces which exhibits dielectric relaxation at frequencies lower than bulk water is 'partially invisible' to TDR. That is, a given amount of bound water has much lower effect on measured travel time and hence ε_b than does the same amount of bulk water. Molecular water layers having dielectric relaxation at frequencies below a certain cutoff frequency (f^*) are considered as bound in the model, with lower ε than for free water. We are in the process of incorporating differential ε for specific vicinal molecular water layers into the thermodielectric model, but the version used here assumed a single value of ε for all bound water. For a given TDR cutoff frequency (f^*) and temperature (T), the thickness (x) of the rotationally-hindered water layer that is less 'visible' to TDR measurement at that temperature (Fig. 1) is calculated as:

$$x(T) = \frac{a}{\&d\,\%\,T\,\ln(m[f^*]\,T)} \qquad [\text{Å}] \qquad [2]$$

with the constant $m[f^*] = k/(8\pi^2 r^3 c f^*)$. Evidence suggests that ε_b determined by travel-time analyses of TDR waveforms is influenced mostly by the high frequency components near 1 GHz (Heimovaara, 1994) which was chosen as a cutoff frequency for our preliminary analyses.

This model can be used to provide predictions for the temperature-dependent volume fraction of bound water $\theta_{bw}(T)$ as the product of the thickness of the 'relaxed' water layer surrounding solids, which is a function of temperature only (Fig. 1; Or and Wraith, 1999), and the specific surface area, A_s. The volume fraction of bound water for a soil having specific surface area per unit mass A_s ($m^2\ kg^{-1}$) at temperature T is:

$$\theta_{bw}(T) = x(T)\,A_s\,\rho_b \qquad [3]$$

where ρ_b ($kg\ m^{-3}$) is the soil bulk density, and x(T) is expressed in meters. For soils with a known mass water content subjected to thermal perturbation, the specific surface area may be estimated directly from Eq. (3) because (within the model framework) bound water thickness is a function of temperature only. This provides the basis for model inversion to estimate A_s.

Bound Water in Cereal Grains, Oilseeds and Legumes

Moisture content is a critical factor in harvesting, processing, storing and marketing cereal grains, oilseeds, and legumes. Efficient and accurate determination of moisture content using EM measurement techniques is difficult due to the intricate makeup of these biologically complex grains combined with a lack of economical, reliable and non-destructive measurement devices. Advancements to measurement capability may result from improved modeling of the water phase within the grains. Unlike soils, which are generally assumed to have a fixed surface area exposed to the water phase, constituents of cereal grains exhibit dynamic surface areas. The major constituent is starch (~70%), with lesser amounts of proteins (10%), lipids (5%) and fiber (2%). Relaxation times in corn starch were shown to increase with

increasing moisture content (Leung *et al*., 1976). Botlan *et al*. (1998) found that the quantity of bound water (mono-layered) increased regularly over the full range of water contents studied (0.14 to 0.94 kg/kg) even when a large amount of 'weakly bound' water was present. This suggests that the mono-layered bound water fraction may increase with increasing moisture content. This may arise from swelling and increased solubilization of the amorphous regions of the starch grain comprised of amylose and amylopectin polymers. During the 'whole kernel' drying process, the quantity of bound water may be diminished initially by the reduction in turgor pressure, which leads to water being squeezed out of crevices. Subsequently, shrinkage, folding and rearrangement of tissues may result in a continued reduction in kernel volume and in reduced accessible internal surface area. The source of this 'dynamic surface area' may occur within the highly branched amylopectin clusters of starch or within the amorphous regions of the kernel containing proteins and is likely a function of polymer type as well as moisture level (Leung *et al*. 1976). This phenomenon may partially explain the irregular nature of the dielectric permittivity-water content relationship of starch which exhibits a reduced rate of permittivity rise with increasing moisture content near mid-range moisture levels (Fig. 2). Other temperature related phenomena have also been noted. Leopold (1983) showed a shift in slope of the otherwise linear seed volume - temperature relationship of soybeans just below 20 EC, suggesting a phase change, which may be due to lipid or protein constituents within the seed.

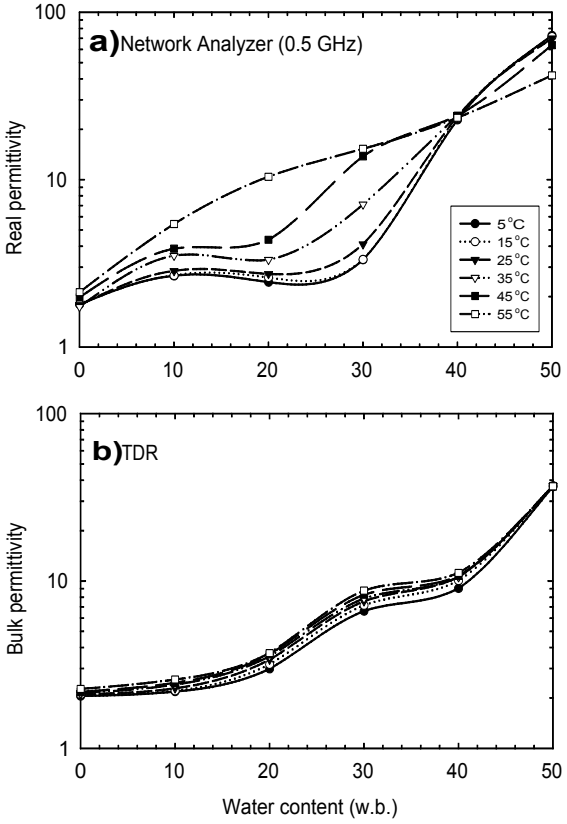

Fig. 2. *Measured permittivity of corn starch as a function of water content (wet basis) using a) a network analyzer at 0.5 GHz and b) a time domain reflectometer with temperature variations shown.*

Role of the Maxwell-Wagner Effect on Measured Bulk Dielectric Permittivity

The Maxwell-Wagner (MW) effect is a different mechanism that could potentially contribute to the effect of temperature on ε_b measured by TDR. The MW effect results from the distribution of conducting and non-conducting elements in the soil mixture and is dominant at the 1-500 MHz frequency range. In soils, the MW effect is manifested by a transition from high measured dielectric permittivity at low frequencies to lower values at higher frequencies (Heimovaara, 1994; Campbell, 1990), with the largest transition occurring at the MW relaxation frequency. To illustrate the effect, we consider a soil saturated with a solution having electrical conductivity σ_{dc}, and where the solid particles are nonconducting. It can be shown (Hilhorst, 1998) that the MW relaxation frequency is a function of the dielectric permittivities of water and solids, the electrical conductivity, and a geometrical linkage function (N) that is dependent on porosity and surface area:

$$f_{MW} = \frac{\sigma_{dc}}{2\pi\varepsilon_0\left[\varepsilon_{MW_w} - (\varphi - 1)\varepsilon_{MW_s}\right]} \quad [Hz] \qquad [4]$$

Equation (4) suggests that increasing the electrical conductivity due to higher temperature would result in MW relaxation at higher frequencies, potentially within the TDR measurement range. We conducted preliminary tests to evaluate the role of this effect on ε_b measurements using TDR. In these tests we varied only the solution electrical conductivity (EC), keeping all other variables constant. The results for saturated glass spheres showed no effect on measured bulk dielectric permittivity for different solution EC values.

Topp *et al*. (2000) recently investigated the influences of the real (ε') and imaginary (ε'') components of ε_b using TDR. By assuming a single (unspecified) characteristic frequency for TDR, they experimentally found modest deviations between measured ε_b (TDR) and calculated ε', as soil wetness and/or electrical conductivity increased. They concluded that specific calibrations may be needed for highest accuracy under conditions of dielectric or ohmic (dc) signal loss. However, the magnitudes of deviation measured in their study were substantially less than for our work concerning measured ε_b responses to variable temperature. Importantly, the loss effects identified by Topp *et al*. (2000) predict a uni-directional influence of temperature, i.e. that increasing temperature and hence electrical conductivity would always result in increased measured ε_b. However, our research showed increasing, decreasing, or nearly constant ε_b depending on the relative magnitudes of competing bulk and bound water dielectric responses. Hence we consider it highly unlikely that the Maxwell-Wagner effect or related imaginary components of ε_b (Or and Wraith 1999) are responsible for the observed ε_b responses to changing temperature.

METHODS

Because of the dependence of the measured thermodielectric response using TDR on the bound water content, which is in turn dependent on the specific surface area, the measured thermodielectric response of wetted porous media may be used to estimate their specific surface areas. This is accomplished by inversion of the physical model, such that the measured dielectric permittivity responses of a porous medium having known bulk density and 2 are used along with the model to infer the A_s that must be present in order to produce the measured thermodielectric response. This serves both as a verification for the physical model itself, and as an evaluation of a potential new method to determine A_s for porous media. The specific surface area of soils and other porous media has critical importance to a number of physical and chemical processes, yet is seldom measured.

Replicate mixtures of fine sand with standard clays (montmorillonite, kaolinite), and six soils from Montana and Utah, were uniformly packed into coaxial TDR cells. The media encompassed a range in surface areas and water contents. After filling with the sand-clay mixtures, the ends were sealed using threaded PVC caps with silicone sealant. These were immersed in circulating water baths to impose multiple discrete levels of constant temperature over the range 5 to 50 ^{o}C. A coaxial cell filled with distilled and deionized (DI) water was included in each replicate batch to serve as a control. Cells were maintained at each temperature for about 3 d. Bulk dielectric permittivity was measured at 0.5-h increments, and measured replicate cell mean $\varepsilon_b(T)$ were used in the model to infer specific surface area

of the coaxial cell contents. The mixture specific surface areas were independently measured using EGME adsorption (Carter *et al*., 1986).

Temperature response of corn starch permittivity was measured in a similar manner in coaxial cells of varying water content in a controlled temperature circulating water bath. Permittivity measurements were made by Tektronix 1502B cable tester interfaced to a computer using WINTDR99 analysis software. In addition, independent measurements of permittivity were conducted at the same water contents using a network analyzer (HP8753C with 85070A dielectric probe) for comparison. Corn starch samples were packed into a 60 ml container which was sealed against the dielectric probe and contained in a temperature controlled cell. Samples were packed to a bulk density of 0.5 g cm^{-3} at each moisture level. Leung *et al*. (1976) gave mono-layer coverage estimates in relatively dry corn starch using NMR, from which was estimated a surface area of approximately 400 m^2/g (Jones and Or, 1999).

RESULTS AND DISCUSSION

Soils and Clay-Sand Mixtures: Measured $\varepsilon_b(T)$ for the soils and sand-clay mixtures were consistent with previous findings (Wraith and Or, 1999), and further documented the phenomenon of increased ε_b with increased T as a result of the bound water response (e.g., Fig 3). Greater signal attenuation at high T for some high ε or high A_s media led to uncertainty in TDR waveform travel time analysis, due to 'flattening' of the second reflection signifying the end of the probe. Porous media having high total ε and/or low A_s demonstrated dominance of the temperature dependent dielectric permittivity of free water, while those having low ε and/or high A_s followed the bound water response of increasing measured ε_b with increasing T (Fig. 3).

Optimization of measured A_s to measured $\varepsilon_b(T)$ using the physical model revealed an apparent lag in the T response. The model was modified to reflect an 'effective' (smaller than measured) temperature, which produced better agreement between measured and estimated ε_b (Fig. 4). Although the estimated surface areas for both modeling approaches (actual T, 'effective' T) were identical, these consistent findings observed for all soils and mixtures suggest that modifications are required to account for the observed lag in thermal response. The most likely areas of improvement involve the separation of the first few molecular layers of water (currently treated as a continuum) to discrete layers whose activation energy for rotation will be calculated rigorously using Morse functions (Bockris *et al*.,

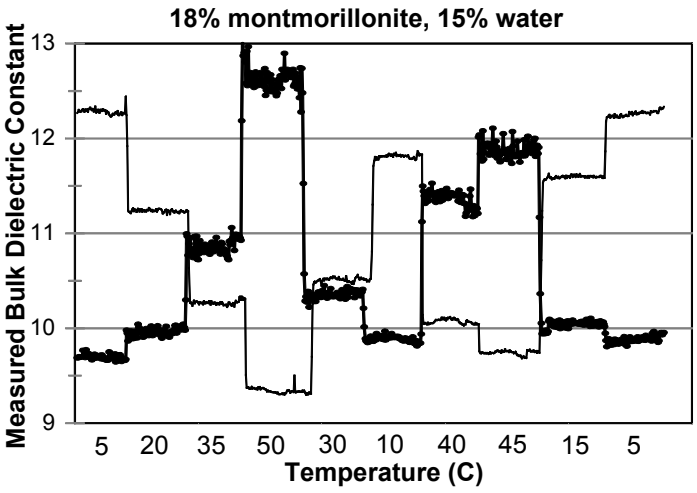

Fig. 3. *Measured time series of ε_b in response to step changes in T. Thick line with symbols is sand-clay mixture response, thin line is DI water.*

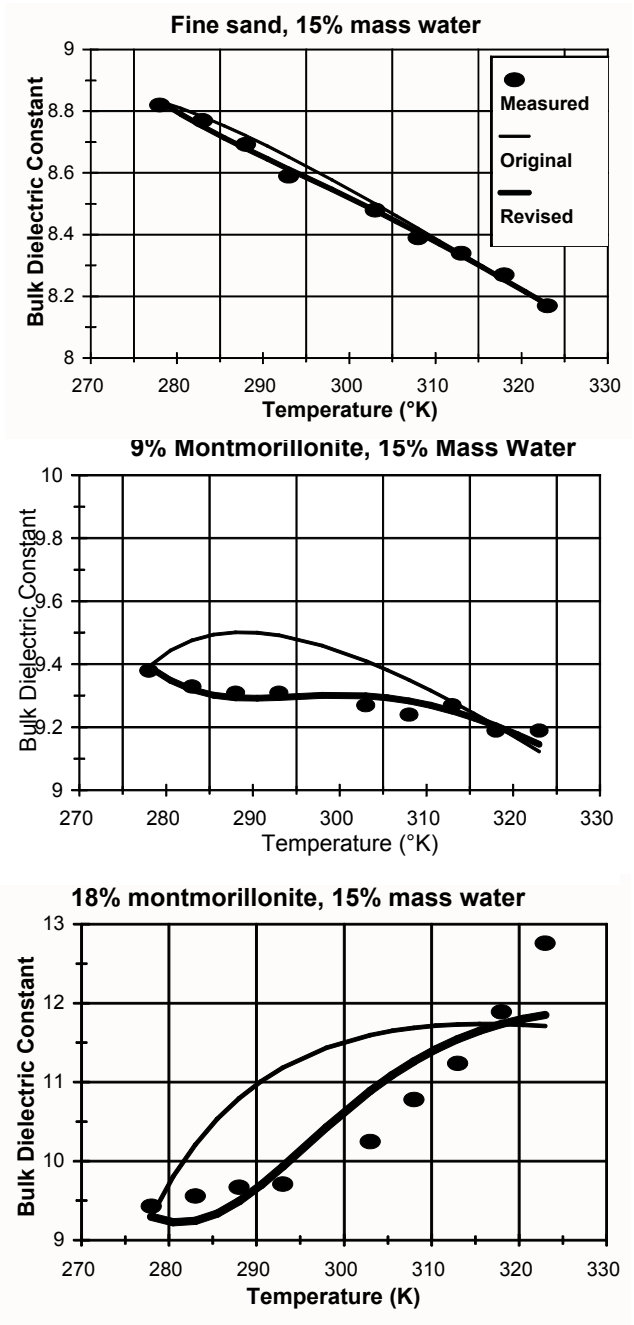

Fig. 4. *Mean measured $\varepsilon_b(T)$ (symbols) for three sand-clay mixtures. Dominance of bulk water (top) for low surface areas, and bound water (bottom) for high surface areas are illustrated. Also shown is effective neutralization of the competing responses (middle) for moderate surface areas. Additional influences of total water content are not shown in this example. Model predictions use actual T (thin lines) and 'effective' T (thick lines) illustrate the requirement to explicitly consider the measured lag in temperature response that we interpret as resulting from activation energy barriers for rotation of individual bound water layers .*

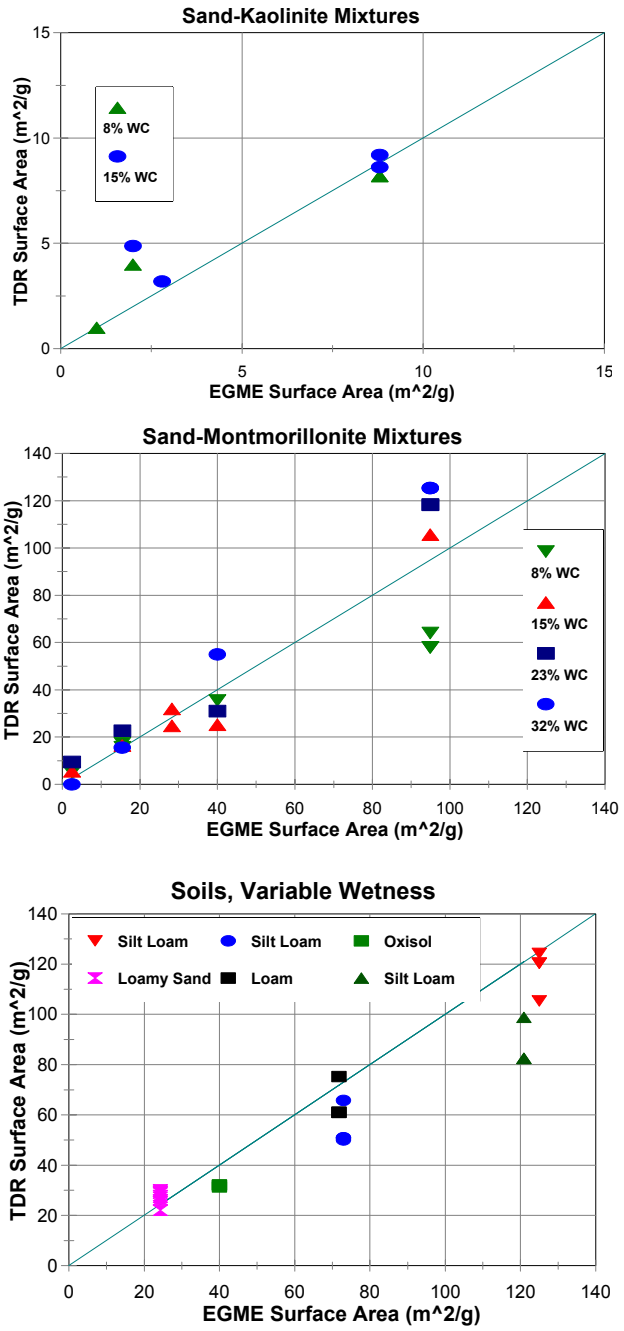

Fig. 5. *Specific surface areas of sand-clay mixtures and soils measured using EGME and from TDR by inversion of the thermodielectric model. Subsequent calculations indicate that apparent TDR under-estimate for highest sand-clay surface area at 8% water content (2 down triangles in middle fig.) is a result of insufficient water to cover all surface areas with 3 molecular water layers as assumed in the model.*

1966) or a similar approach. Such modeling approach will specify the thermal energy required to raise the energy level of each discrete layer of water molecules above the 'rotational threshold'. In addition, other aspects of water-clay surface interactions such as those resulting from counter-ions in the diffuse double layer will be considered. Estimated A_s based on model optimization to measured $\varepsilon_b(T)$ were in agreement with those independently measured using the standard laboratory EGME method (Fig. 5). This constitutes effective 'proof of concept' for the thermodielectric model, and provides for optimism in developing an alternative method to routinely measure A_s of porous media.

Corn Starch and Grain Measurements: Measured dielectric permittivity in moistened corn starch increased with increasing temperature and water contents up to 40 percent (Fig. 2), where a transition occurred and the temperature dependent relationship were inverted. The reversal in the temperature-permittivity trend occurred at higher water contents where the starch granule was approaching water saturation, leading to a buildup of "free" water within and eventually between granules. At low water contents, the increase in permittivity with increased temperature (for a fixed water content) followed the prediction given by Eq. (1-3). At high water content, temperature increase leads to reduced permittivity of the moist starch, similar to the reduction in free water permittivity with increasing temperature. The large permittivity differences at mid range moisture contents suggest an abundance of bound water which is liberated upon heating and the non-linear nature of the permittivity increase with added water also suggests an evolution of the surface area with wetting or drying.

Configuration of the water associated with solids combined with surface area evolution leading to changes in bound water fraction were suggested by Jones and Or (1999) to cause the distinct plateau in the permittivity-water content curve shown in Fig. 2 for corn starch and also noted in whole corn kernel measurements. TDR measured permittivities in corn starch illustrated the same temperature-dependent permittivity relationship shown by network analyzer measurements, but with reduced permittivity differences between temperature changes.We computed the differences between permittivities at 55 and 5 EC scaled by the permittivity at 25 EC for both TDR and network analyzer measurements at 0.5 and 5 GHz frequencies (Fig. 6). The results show marked differences between TDR and network analyzer measurements within the TDR frequency band (0.5-1.0 GHz). As seen earlier (Fig. 2) the transition of the water phase from primarily bound to an apparent dominance of free water seems to occur at about 40 percent water content, where the network analyzer results become negative. Results from the TDR show a much smaller increase in scaled permittivity difference with water content, followed by a reduction near granule saturation, where the data tend towards zero. Differences between network analyzer and TDR results may be attributed in part to the smaller sampling volume (~1 cm^3) of the network

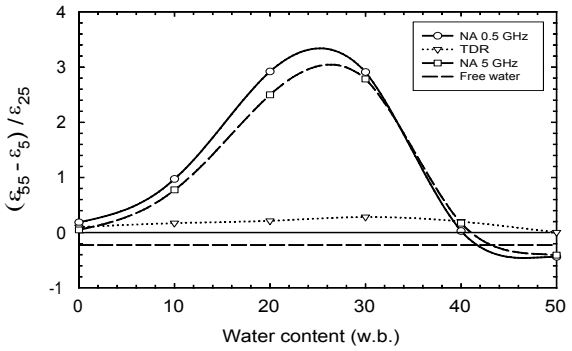

Fig. 6. *Relative permittivity difference between measurements (TDR and network analyzer, NA) at 55 and 5 EC in corn starch of varying water contents (wet basis). The dashed horizontal line indicates the relative difference for free water.*

analyzer which is prone to errors due to localized compaction (i.e., higher bulk density at the probe-starch interface) and perhaps to redistribution of water due to thermal gradients induced by the metallic probe-cable apparatus.

SUMMARY

Bound water in porous media including soils and food grains influences the measured dielectric permittivity using TDR and other electromagnetic measurements. We discussed recent work concerning two practical applications of the measured bound water response: estimating specific surface area of porous media based on dielectric permittivity changes with temperature perturbation, and estimating the moisture content of cereal grains. Each of these requires fundamental knowledge concerning the physical and electrical responses of water associated with solid surfaces.

The method described here uses the behavior of water to estimate wettable A_s of porous media based on the measured thermodielectric response using TDR. Good agreement of TDR thermodielectric A_s estimates with standard EGME A_s determination are highly encouraging. Increasing T degrades the 'quality' of TDR waveforms for travel time analysis, due to increased attenuation. This may limit the ability to make inferences for high A_s materials at high T. We found an apparent threshold temperature effect in measured $_b$. The physical model was revised to account for this temperature lag by using an 'effective temperature', and the underlying mechanism is under consideration. We anticipate incorporating the 'discrete energy well' concepts (Bockris *et al*., 1966) to describe this phenomenon. However, the model provided similar A_s estimates using either T or 'effective' T. Further investigations are underway, and we anticipate that the thermodielectric measurement approach may provide an effective alternative approach for A_s estimation of soils and other wetted (or wettable) porous media. Finally, these results combined with others not included in this paper strongly indicate that the thermodielectric phenomenon is important to remotely-sensed land surface wetness measurements. In addition to providing required thermal corrections to remotely sensed data, this may lead to an ability to map surface soil textures (strongly related to A_s) from existing or new satellite platforms.

Improved grain and starch moisture content measurements is of significant economic value. Evidence suggests that these measurement are also affected by the presence of appreciable amounts of bound water. We anticipate that incorporation of the thermodielectic phenomenon into dielectric mixing models used for measurement interpretation could offer an improvement in measurement accuracy under field conditions and other environments encountered in the food processing industry where large temperature fluctuations are expected.

ACKNOWLEDGMENTS

Partial funding was provided by NRI Competitive Grants Program/USDA (Agreement no. 95-37102-2175), and the Israel-US Binational Agricultural Research and Development (BARD) Fund (Project IS-2839-97). We gratefully acknowledge research grants from Campbell Scientific Inc. and HarvestMaster (Logan, Utah) and Pioneer Hi-Bred (Johnston, IA).

REFERENCES

Bockris, J.O'M., Devanathan, M.A.V., and Muller, K., 1963, On the structure of charged interfaces: Proceedings Royal Society London, Series A, **274**, 55-79.

Bockris J. O'M., Gileadi, E., and Muller, K., 1966, Dielectric relaxation in the electric double layer: Journal of Chemical Physics, **44**, 1445-1456.

Botlan, D.L., Rugraff, Y., Martin, C., and Colonna, P., 1998, Quantative determination of bound water in wheat starch by time domain NMR spectroscopy: Carbohydrate Research, **308**, 29-36.

Campbell, J.E., 1990, Dielectric properties and influence of conductivity in soils at one to fifty megahertz: Soil Science Society of America Journal, **54**, 332-341.

Carter, D.L., Mortland, M.M., and Kemper, W.D., 1986, Specific surface, in Klute, A. (ed.), Methods of soil analysis, Part 1, Physical and mineralogical methods, 2nd Ed.: ASA, Madison, WI, 413-423.

Debye, P., 1929, Polar Molecules, Dover Publications, Mineola, New York.

Hasted, J.B., 1973, Aqueous Dielectrics, Chapman and Hall, London.

Heimovaara, T.J., 1994, Frequency domain analysis of time domain reflectometry waveforms: 1. Measurements of complex dielectric permittivity of soils: Water Resources Research, **30**, 189-199.

Hilhorst, M.A., 1998, Dielectric characterisation of soil: PhD Dissertation, The DLO, Institute of Agricultural and Environmental Engineering, Wageningen, The Netherlands.

Jones, S.B., and Or, D., 1999, Thermal and geometrical effects on bulk permittivity of mixtures containing bound water, in Proceedings Third Workshop on Electromagnetic Wave Interaction with Water and Moist Substances, Athens, GA, 222.

Leopold, A.C., 1983, Volumetric components of seed imbibition: Plant Physiology, **73**, 677.

Leung, H.K., Steinberg, M.P., Wei, L.S., and Nelson, A.I., 1976, Water binding of macromolecules determined by pulsed NMR: Journal of Food Science, **41**, 297-300.

Low, P.F., 1976, Viscosity of interlayer water in montmorillonite: Soil Science Society of America Journal, **40**, 500-505.

----------, 1979, Nature and properties of water in montmorillonite-water systems: Soil Science Society of America Journal, **43**, 651-658.

Or, D., and Wraith, J.M., 1999, Temperature effects on soil bulk dielectric permittivity measured by time domain reflectometry: A physical model: Water Resources Research, **35**, 371-383.

Sposito, G., and Prost, R., 1982, Structure of water adsorbed on smectites: Chemical Review, **82**, 553-572.

Topp, G.C., Zegelin, S., and White, I., 2000, Impacts of the real and imaginary components of relative permittivity on time domain reflectometry measurements in soils: Soil Science Society of America Journal, **64**, 1244-1252.

Weast, R.C., 1986, Handbook of Chemistry and Physics, 67th ed., CRC Press, Boca Raton, FL.

Wraith, J.M., and Or, D., 1999, Temperature effects on soil bulk dielectric permittivity measured by time domain reflectometry: Experimental evidence and hypothesis development: Water Resources Research, **35**, 361-369.

TDR SIGNAL MODELLING USING THE ELECTRIC LINE APPROACH: MODEL VALIDATION AND SIGNAL INVERSION TO RETRIEVE SOIL MOISTURE PROFILE

André Chambarel[1], Evelyne Ferry [2], André Chanzy [3],
Jean-Paul Laurent [4], Pierre Todoroff [5], Philippe Ferrari [6].

[1]LHC, Université d'Avignon, 33 rue Pasteur, F-84000 Avignon, France;
andre.chambarel@univ-avignon.fr
[2] LHC, Université d'Avignon, 33 rue Pasteur, F-84000 Avignon, France;
evelyne.ferry@univ-avignon.fr
3INRA, Unité de Climat, Sol, Environnement, Avignon, France;
achanzy@avignon.inra.fr
[4]LTHE/CNRS, Grenoble, France; jean-paul.laurent@hmg.inpg.fr
[5]CIRAD, Montpellier, France
[6]Université de Chambéry, Chambéry, France

ABSTRACT

The TDR signal propagation is represented using the electric line approach. The telegraphist equations are resolved in the time domain using a finite element method. The media heterogeneities along the line can be accounted for by distributing the electric properties spatially. The computation gives the temporal evolution of the electric intensity and tension at every location of the line. The TDR signal is extracted from the tension at the entrance end of the line. Then, the simulated signals were compared to measurements made in artificial media (using a multi compartment tank with various well known dielectric media) and in real field conditions. Simulations are in good agreement with measurements but requires to fit the dielectric loss. A discussion is presented on the obtained fitted values and on the possibilities to handle this term in operational application. An inversion procedure of the model is proposed to retrieve soil moisture profiles. Discussion is proposed on the expected accuracy in relation to the TDR technical characteristics as well as to the soil moisture conditions.

INTRODUCTION

A latest generation of instruments (Spaans and Baker, 1995) under development is based on Time Domain Reflectometry -TDR-. These probes come as two or three parallel metal rods driven into the ground down to little over three feet - or 1 m -. An electrical impulse is applied to the end bit above ground surface. The impulse propagates along the rods. Measurement and processing of the signal obtained by reflection should theorically allow the determination of local moisture levels. The 1D model used up to now in the study of our device is that of the electric line represented in Figure 1 (Todoroff, 1998).

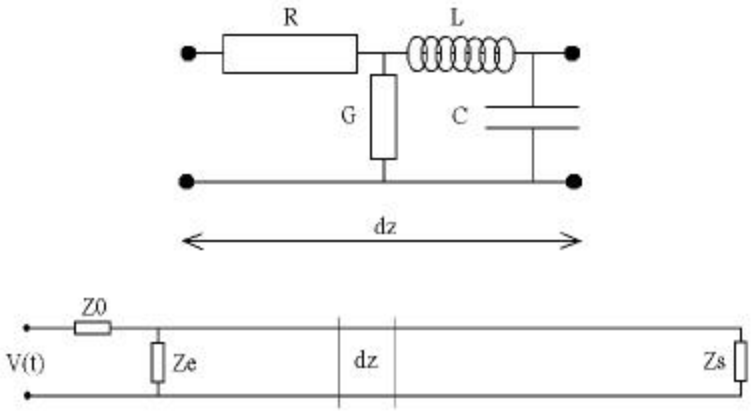

Fig. 1. *The electric line scheme.*

$$\frac{\partial i}{\partial z} = -C.\frac{\partial v}{\partial t} - G.v$$
$$\frac{\partial v}{\partial z} = -L.\frac{\partial i}{\partial t} - R.i$$

The line's 1D mathematical model is governed by a partial differential system called "telegraphists equations". These equations are dealt with in a traditional way through time or frequency approach. In the case of Time Domain Reflectometry though, there is no specific problem. The difficulty in fact lies in the perfect knowledge of the values of parameters (R,L,C,G,Zs), in particular in their relationship with soil moisture profile (Dos Santos, 1997). The impedances Z0 and Ze are given by the electric source properties. Besides, this simplified 1D model neither, for example, takes into account the various propagation modes of electromagnetic waves, nor the cut frequency, nor again the local ratings of soil moisture. The advantage of the 1D model is based on a relative simplicity associated with a fast numerical calculus compatible with the signal inversion process.

MATHEMATICAL MODEL

If ε_r and μ_r are the electromagnetic properties of the medium, the above partial non dimensional differential system can be written :

$$\mu_r.\frac{\partial i}{\partial t} = -\frac{\partial v}{\partial z} - a.i$$
$$\varepsilon_r.\frac{\partial v}{\partial t} = -\frac{\partial i}{\partial z} - b.v$$

Here we have two approaches of the boundary conditions :

- The first case concerns the line only. At the intrance of the line we have a tension f(t) and the end of the line is an open circuit. With these Dirichlet's conditions come the following expressions:

$$z = 0 \quad v = f(t)$$
$$z = 1 \quad i = 0$$

- The second case includes the electric characteristics of the voltage source at the inlet and a known impedance at the outlet. So we have the following conditions :

$$z = 0 \quad D(i, u, t) = 0 \qquad \text{for example} \qquad v = v_0 - Z_0.i$$
$$z = 1 \quad D'(i, u, t) = 0 \qquad\qquad\qquad\quad v = Z_s.i$$

In complex case, D and D' can be differential operators.
In the initial conditions the current and the tension are zero.

FINITE ELEMENT FORMULATION

In our case the advantage of the Finite Element method concern the bondary conditions (Dhatt and Touzot, 1981). In accordance to these we use different formulations. So the boundary conditions can be expressed by Dirichlet's conditions or weak formulation.

Weak Formulation by Direct Integration

With the Galerkin weighting the above partial differential system is written:

$$\int_0^1 \delta i.\mu_r.\frac{\partial i}{\partial t}.dz = -\int_0^1 \delta i.a.\frac{\partial v}{\partial z}.dz - \int_0^1 \delta i.b.i.dz$$
$$\int_0^1 \delta v.\varepsilon_r.\frac{\partial v}{\partial t}.dz = -\int_0^1 \delta v.c.\frac{\partial i}{\partial z}.dz - \int_0^1 \delta i.d.v.dz$$

After the discretization of the segment [0, 1] with ne elements (Ω_e) and using the polynomial base <n(z)> the above integral formulation is:

$$\sum_{ne}\left(\langle \delta i_e \rangle.\int_{(\Omega_e)} \{n\}.\mu_r.\langle n \rangle.dz.\left\{\frac{\partial i_e}{\partial t}\right\}\right) = \sum_{ne}\left(-\langle \delta i_e \rangle.\int_{(\Omega_e)} \{n\}.\left\langle \frac{\partial n}{\partial z} \right\rangle dz.\{v_e\} - \langle \delta i_e \rangle.\int_{(\Omega_e)} \{n\}.a.\langle n \rangle dz.\{i_e\}\right)$$
$$\sum_{ne}\left(\langle \delta v_e \rangle.\int_{(\Omega_e)} \{n\}.\varepsilon_r.\langle n \rangle.dz.\left\{\frac{\partial v_e}{\partial t}\right\}\right) = \sum_{ne}\left(-\langle \delta v_e \rangle.\int_{(\Omega_e)} \{n\}.\left\langle \frac{\partial n}{\partial z} \right\rangle dz.\{i_e\} - \langle \delta i_e \rangle.\int_{(\Omega_e)} \{n\}.b.\langle n \rangle dz.\{v_e\}\right)$$

For the matricial form we obtain :

$$\sum_{ne}\left(\left\langle \delta i_e, \delta v_e \right\rangle . \int_{(\Omega_e)} \begin{bmatrix} \{n\}.\mu_r.\langle n\rangle & 0 \\ 0 & \{n\}.\varepsilon_r.\langle n\rangle \end{bmatrix} .dz. \begin{Bmatrix} \dfrac{\partial i_e}{\partial t} \\ \dfrac{\partial v_e}{\partial t} \end{Bmatrix}\right) =$$

$$\sum_{ne}\left(\left\langle \delta i_e, \delta v_e \right\rangle . \int_{(\Omega_e)} \begin{bmatrix} -\{n\}.a.\langle n\rangle & -\{n\}.\left\langle \dfrac{\partial n}{\partial z}\right\rangle \\ -\{n\}.\left\langle \dfrac{\partial n}{\partial z}\right\rangle & -\{n\}.b.\langle n\rangle \end{bmatrix} .dz. \begin{Bmatrix} i_e \\ v_e \end{Bmatrix}\right)$$

Integration by Parts

We have several possibilities of integration by parts in accordance to the boundary conditions. For example, if we apply a tension v(t) at the inlet to the line and an impedance Z_s at the outlet, we prefer the following formulation :

$$\int_0^1 \delta i.\mu_r.\frac{\partial i}{\partial t}.dz = -\left[\delta i.v\right]_0^1 + \int_0^1 v.\frac{\partial(\delta i)}{\partial z}.dz - \int_0^1 \delta i.a.i.dz$$

$$\int_0^1 \delta v.\varepsilon_r.\frac{\partial v}{\partial t}.dz = -\int_0^1 \delta v.\frac{\partial i}{\partial z}.dz - \int_0^1 \delta i.b.v.dz$$

It is an example of integration. The integration by parts can be applied to the second equation or the both equations. We choose in accordance with the boundary conditions. We built after the matricial formulation.

NUMERICAL METHOD

For all weak formulations, the general formulation of the differential system is (Chambarel and Ferry, 2000):

$$[M].\frac{d}{dt}\{U\} = \{F\} - [K].\{U\} \quad \text{where} \quad \{U\} = \left\{H^{(G)}, E^{(G)}\right\}$$

$$\frac{d}{dt}\{U\} = [M]^{-1}.\{\Psi(U,t)\} \quad \text{where} \quad \{\Psi(U,t)\} = \{F\} - [K].\{U\}$$

For the numerical time-resolution, several methods are tested (Sod, 1978). For numerical quadrature points the nodes of the elements are chosen. Consequently, the mass matrix [M] is *diagonal.* This inversion is an easy procedure. It is a necessary condition for the efficiency of the methods above. Under these conditions we can use the semi implicit methods. In this cases we perform a *matrix-free technique*,

the mass matrix and the stiffness matrix never being built. We note a high performance level for the CPU and the storage costs. For that the following algorithm is used :

$$
\begin{aligned}
&t_n = 0 \\
&\text{while} \quad (t_n \le t_{max}) \\
&\quad \left\{ \begin{array}{l} \left\{\Delta U_n^i\right\} = \Delta t_n . \left[M_n^i\right]^{-1} . \left\{\Psi\left(U_n + \alpha . \Delta U_n^{i-1}, t_n + \alpha . \Delta t_n\right)\right\} \\ \quad i = 1, 2, \ldots \quad \text{until} \quad \left\|\Delta U_n^i - \Delta U_n^{i-1}\right\| \le \text{tolerence} \end{array} \right\} \\
&\quad \left\{U_{n+1}\right\} = \left\{U_n\right\} + \left\{\Delta U_n\right\} \\
&\quad t_{n+1} = t_n + \Delta t_n \\
&\text{end} \quad \text{while}
\end{aligned}
$$

where α is the upward time-parameter.

The semi-implicit method requires inner iterations for each time-step with index i for $\{\Delta U\}$ determination and the convergence criteria can be written (Anderson *et al*., 1984):

$$\alpha . \Delta t . \left\| \frac{\partial}{\partial U} \left\{ [M]^{-1} . \Psi(U, t) \right\} \right\| < 1 \qquad \text{and} \qquad \text{if } (\alpha < 0.5) \text{ then } \Delta t < \Delta t_{CFL}$$

The initial solution of each time step is close to the next solution. For the semi-implicit method the number of iterations is very low, two or three in practice.

NUMERICAL RESULTS

We simulate moisture spots along the line by a space dependent ε values. Several tests are performed using the method above. The numerical results are presented in the following case :

- Length of the line : 1m
- Zo = 50 Ω, Ze = 1000 Ω, Zs = 75 Ω
- Number of elements : 500
- Optimal upward time-parameter α=0.9
- We can used a finite time of tension increasing (1 volt).

Homogeneous Medium ($e_r = 1$)

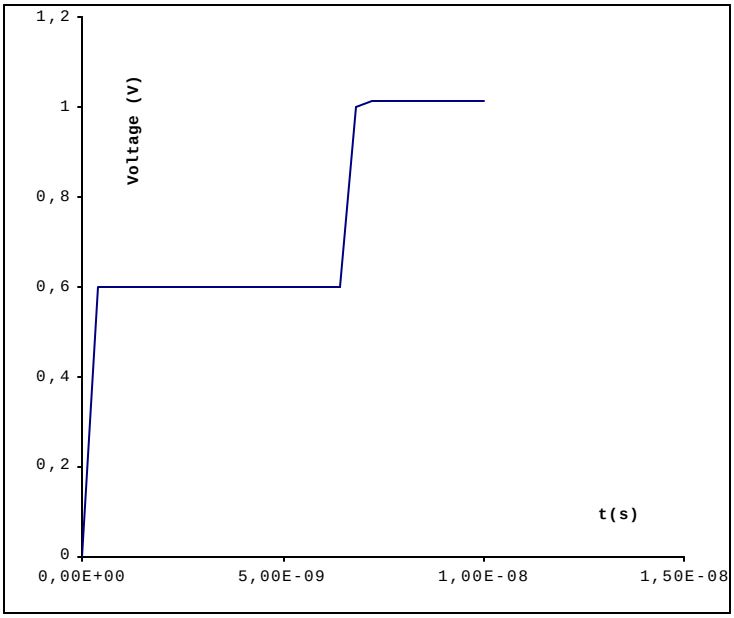

Fig. 2. *Voltage at z=0.*

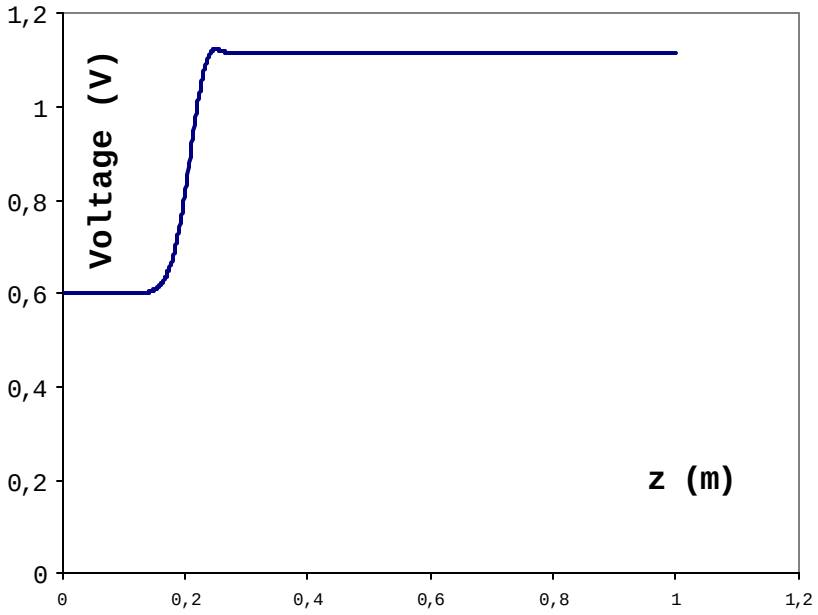

Fig. 3. *Voltage at the time t=6 ns.*

This both results are coherent with the exact solution of the telegraphist's equations.

Inhomogeneous Medium

Discontinuity of e_r

For this case we have the following properties :

$0 \leq z < 0.5m \quad \varepsilon_r = 1$
$0.5m \leq z \leq 1m \quad \varepsilon_r = 10$

For the second case :

$0m \leq z < 0.33m \quad \varepsilon_r = 1$
$0.33m \leq z < 0.66m \quad \varepsilon_r = 10$
$0.66m \leq z \leq 1m \quad \varepsilon_r = 20$

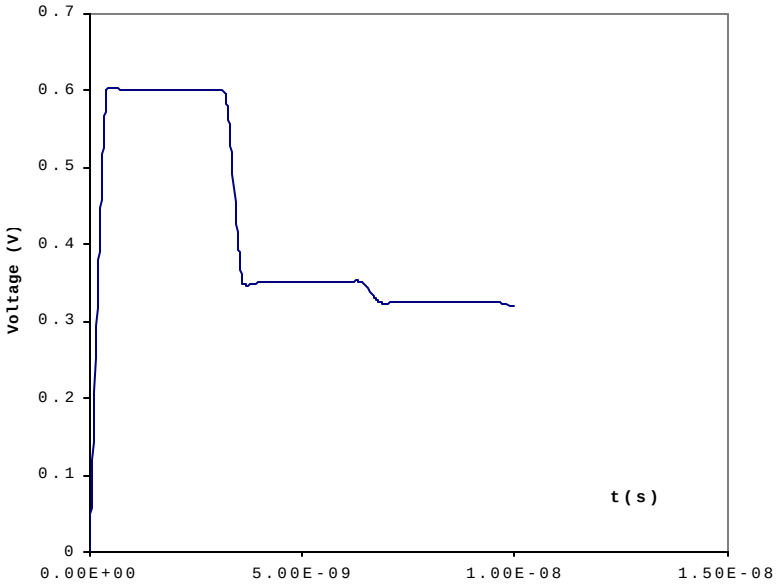

Fig. 4. *Voltage at z=0*

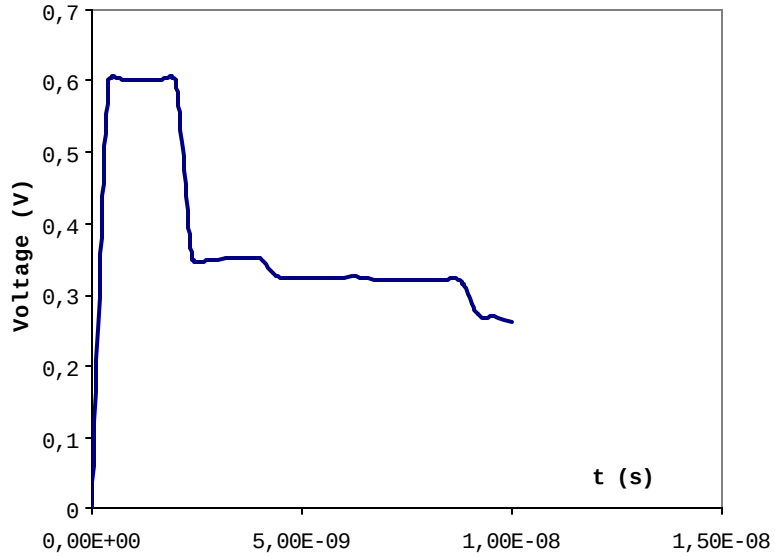

Fig. 5. *Voltage at z=0*

Continuous Variation of e_r.

The first case considers a linear variation of ε_r in Figure 6.

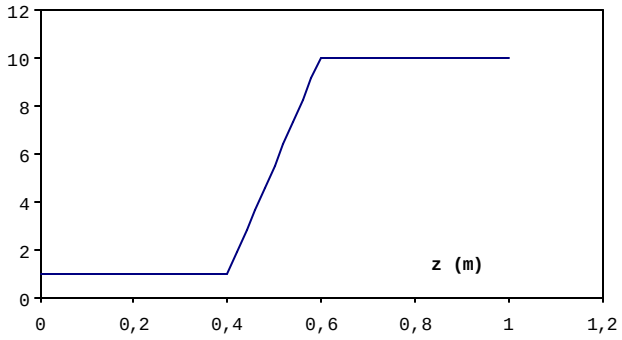

Fig. 6. *Variation of* e_r

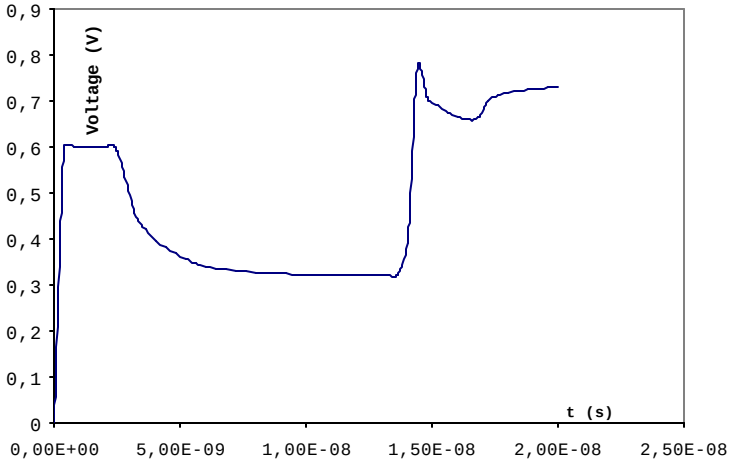

Fig. 7. *The voltage at the intrance of the line* .

COMPARISON WITH THE EXPERIMENT

A first experiment concerns an electric line with five discontinuities of impedance (15-25-35-45-55 Ω). Two cases are presented with increasing impedances and decreasing impedances.

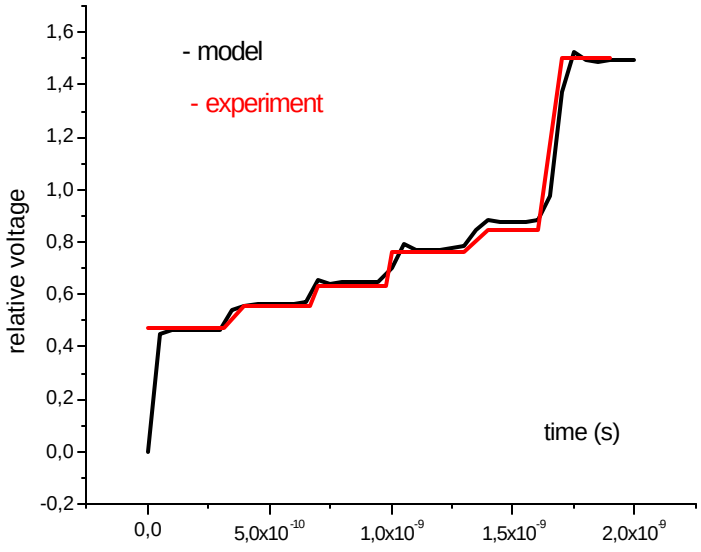

Fig. 8. *Increasing impedances.*

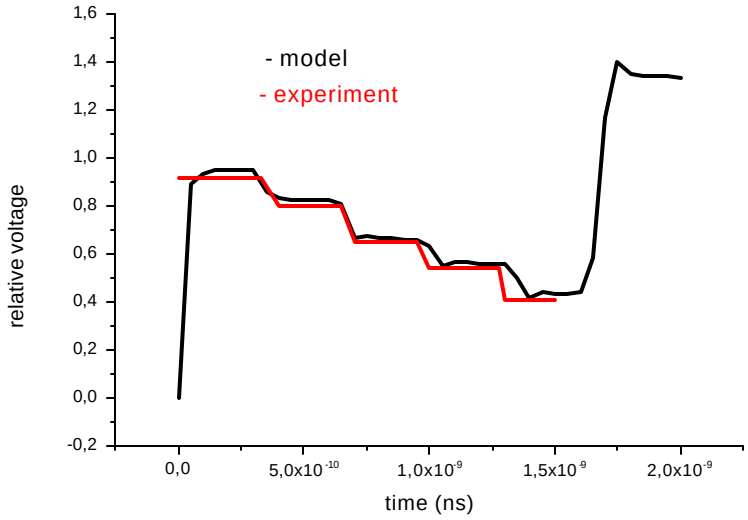

Fig. 9. *Decreasing impedances.*

In the both cases we notice in Figures 8 and 9 a good comparison between the numerical calculus and the experiment.

A second set of experiments use four rectangular plexiglas containers with water (W) or air(A). Figure 10 and 11 compare the experiment and the numerical application. We remark a very good agreement.

For the determination of the medium electric properties, we develop a set of typical tests for identification of the class of profiles.

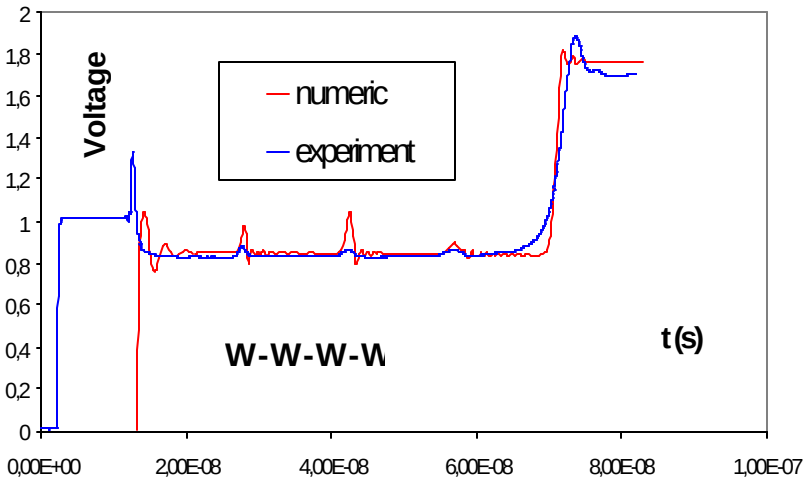

Fig. 10. *Comparison between experimental and numerical results.*

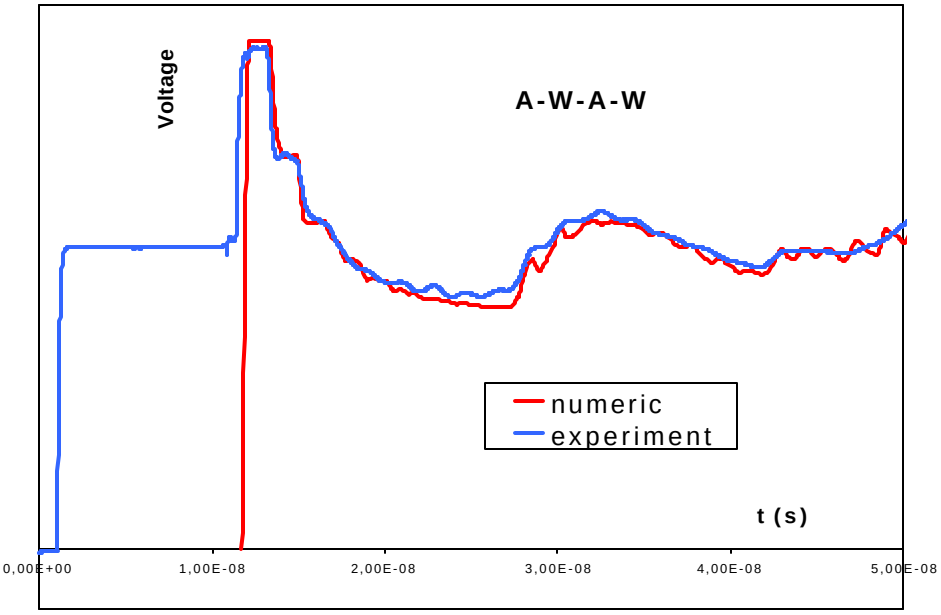

Fig. 11. *Comparison between experimental and numerical results.*

CONCLUSION

The TDR probe can be simulated by electric line Finite Element approach. We present a general Finite Element formulation for telegraphist's equations in the case of propagation phenomenon and introduce the matricial structure of space discretization. Intensity and voltage propagates along the line with the object determining the variable electric properties of the space crossed. The electric loading is given by a known voltage impulse. Generally the wave propagation is always a difficult numerical problem. We do not detect instabilities and this method gives good results. The agreement with the experiment is good. So we have efficient tool for electric line study.

REFERENCES

Anderson, D. A., Tannehill, J. C., and Pletcher, R. H., 1984, Computational Fluid Mechanics and Heat Transfer: Hemisphere Publishing Corporation Editor.

Chambarel, A., and Ferry, E., 2000, Finite Element formulation for Maxwell's equations with space dependent electric properties: Revue Européenne des Eléments Finis, **9**, No. 8, 941-967.

Dhatt, G., and Touzot, G., 1981, Une présentation de la méthode des éléments finis, Editions Maloine S.A.

Dos Santos, L. A., 1997, Développement d'une nouvelle méthode de détermination des profils de teneur en eau dans les sols par inversion d'un signal TDR: Thèse de doctorat, Université Joseph Fourier de Grenoble.

Fleckinger, E., 1991, Electromagnétisme, Editions Masson, Paris.

Gaudu, J. C., Chanzy, A., Mohrath, D., 1993, Mesure de l'humidité des sols par une méthode capacitive: analyse des facteurs influançant la mesure: Agronomie, **13**, No. 1, 57-73.

Luebbers, R., 1993, IEEE Transactions on Antennas and Propagation, **41**, No. 11.

Sod, G. A., 1978, A survey of Several Finite Difference Methods for Systems of Nonlinear Hyperbolic Conservation Laws: Journal of Computational Physics, **27**, 1-31.

Spaans, E. J. A., and Baker, J., 1995, Examining the use of Time Domain Reflectometry for measuring liquid water-content in frozen soil: Water Ressources Research, **31**, No. 12, 2917-2925.

Todoroff, P., 1998, Modélisation de la propagation micro-ondes dans le sol afin d'obtenir un profil hydrique par réflectométrie temporelle: Thèse de doctorat, Université de la Réunion.

TDR SIGNAL SIMULATION USING A WAVE GUIDE 2D MODEL

André Chambarel[1], Hervé Bolvin[2] and Evelyne Ferry[3]

[1]Laboratory of Complex Hydrodynamics 33, rue Louis Pasteur, F-84000 AVIGNON;
andre.chambarel@univ-avignon.fr
[2]Laboratory of Complex Hydrodynamics 33, rue Louis Pasteur, F-84000 AVIGNON;
herve.bolvin@univ-avignon.fr
[3]Laboratory of Complex Hydrodynamics 33, rue Louis Pasteur, F-84000 AVIGNON;
evelyne.ferry@univ-avignon.fr

ABSTRACT

The Time Domain Reflectometry -TDR- probe is a new technique applied to moisture measurement. It is a wave guide constituted by two or three parallel metallic rods stuck in the ground. An electromagnetic wave propagates all along the wave guide and crosses a variable electric properties medium. In that way the reflecting wave is disrupted and we detect the electric singularities. We study the transverse magnetic-mode. We simulate this wave guide in this medium thanks to the Finite Element Method and present the used matricial structure. For time integration we compare a semi-implicit or Runge-Kutta method with variable time-step. This process is driven by the Automatic Multigrid System with an unknown time-dependent number.

INTRODUCTION

Water resource management for plants is becoming an increasingly acute problem. This is associated with pollution phenomena usually caused by fertilizers. It is therefore essential to have a precise idea as to the soil's moisture content, both at surface and underground levels. Various techniques have been used to this effect, e.g. the uneasy technique of sampling. Then in the 60's and 70's neutron probes were used, that - beyond the poor level of accuracy - offered the major drawback of appealing to a radioactive source. The latest generation of instruments (Spaans and Baker, 1995) under development is based on Time Domain Reflectometry -TDR-. These instruments come as two or three parallel metal rods driven into the ground down to little over three feet - or 1 m -. An electrical impulse is applied to the end bit above ground surface. The impulse propagates along the rods. Measurement and processing of the signal obtained by reflection should theorically allow the determination of local moisture levels.

GENERAL PRESENTATION OF MODEL

Geometrical Model of the 2D TDR Probe

The electric line is modelised by two parallel plate electrodes and the electric conductivity of these is infinite. The free space around the electrodes can be an ohmic conductor (Chambarel and Ferry, 2000). In the Transverse Magnetic mode -TM-, the electromagnetic field is :

$$\vec{H} = \begin{Bmatrix} H_x \\ 0 \\ 0 \end{Bmatrix} \quad \text{and} \quad \vec{E} = \begin{Bmatrix} 0 \\ E_y \\ E_z \end{Bmatrix}$$

Maxwell's Equations

With the usual notations the non dimensional Maxwell's equations are formulated as follows (Fleckinger, 1991):

$$[\mu_r].\frac{\partial \vec{H}}{\partial t} = -\overrightarrow{\text{curl}}\,\vec{E} \qquad \text{div}\,([\mu_r].\vec{H}) = 0 \qquad [1]$$

$$[\varepsilon_r].\frac{\partial \vec{E}}{\partial t} = \overrightarrow{\text{curl}}\,\vec{H} - \text{Rm}\,.[\gamma_r].\vec{E} \qquad \text{div}\,([\varepsilon_r].\vec{E}) = 0 \qquad [2]$$

The Maxwell's equations show the non dimensional parameter $Rm = \gamma_0.\mu_0.l.c$ called the *magnetic Reynolds' number*.

The adimensional volumic energy and the Poynting vector (Fleckinger, 1991):

$$w = \left(\frac{\vec{B}.\vec{H}}{2} + \frac{\vec{D}.\vec{E}}{2} \right) \qquad \text{and} \qquad \vec{S} = \vec{E} \times \vec{H} \qquad [3]$$

Boundary Conditions

The boundary conditions at the electric conductor - i.e. electrodes - can be written :

$$\vec{E} \times \vec{n} = \vec{0}$$

At initial time, we apply a constant electric potential difference between the electrodes. The electric loading can be written :

$$\vec{E} = \begin{Bmatrix} 0 \\ E_0(x, y, z = 0, t) \\ 0 \end{Bmatrix}$$

where E_0 is in this case a constant value.

For the other boundary conditions a long way away from the electric line, we must choose :

$$\vec{E} \times \vec{n} = \vec{0}$$

In all cases of TDR procedure, the electromagnetic wave never reaches that boundary because we only study the first reflection in the wave guide for electric properties detection. At the electrodes, we can calculate line current I by the Ampere's theorem.
The initial condition is zero.

FINITE ELEMENT FORMULATION

The Galerkin's Finite Element method is applied to Maxwell's equations in an isotropic medium. In our formulation, the electric properties of the medium can be written :

$$[\mu_r] = \mu_r.[I] \qquad [\varepsilon_r] = \varepsilon_r.[I] \qquad [\gamma_r] = \gamma_r.[I]$$

Weak Formulation (Assous *et al*., 1993)

For the electromagnetic problem we choose the Galerkin's ponderation. We use the vector ($\delta H, \delta E$). The weighted residual method can be written :

$$\int_{(\Omega)} \overrightarrow{\delta H}.\mu_r.\frac{\partial \vec{H}}{\partial t}.d\Omega = -\int_{(\Omega)} \overrightarrow{\delta H}.\overrightarrow{curl}\ \vec{E}.d\Omega \qquad [4]$$

$$\int_{(\Omega)} \overrightarrow{\delta E}.\varepsilon_r.\frac{\partial \vec{E}}{\partial t}.d\Omega = \int_{(\Omega)} \overrightarrow{\delta E}.\overrightarrow{curl}\ \vec{H}.d\Omega - \int_{(\Omega)} \overrightarrow{\delta E}.Rm.\gamma_r.\vec{E}.d\Omega \qquad [5]$$

The equations [11] and [12] constitute the *first formulation*. The integrals of the right hand side of [11] can be transformed by formula [13] :

$$\int_{(\Omega)} \overrightarrow{\delta H}.\overrightarrow{curl}\ \vec{E}.d\Omega = \int_{(\Omega)} \vec{E}.\overrightarrow{curl}\ \overrightarrow{\delta H}.d\Omega - \int_{(\Gamma)} \left(\overrightarrow{\delta H} \times \vec{E}\right).\vec{n}.d\Gamma \qquad [6]$$

We can use this capacity for the introduction of the *natural boundary conditions*. In that way we obtain the *second formulation* by transformation of the equation [4] :

$$\int_{(\Omega)} \overrightarrow{\delta H}.\mu_r.\frac{\partial \vec{H}}{\partial t}.d\Omega = -\int_{(\Omega)} \vec{E}.\overrightarrow{curl}\ \overrightarrow{\delta H}.d\Omega + \int_{(\Gamma)} \left(\overrightarrow{\delta H} \times \vec{E}\right).\vec{n}.d\Gamma \qquad [7]$$

$$\int_{(\Omega)} \overrightarrow{\delta E}.\varepsilon_r.\frac{\partial \vec{E}}{\partial t}.d\Omega = \int_{(\Omega)} \overrightarrow{\delta E}.\overrightarrow{curl}\ \vec{H}.d\Omega - \int_{(\Omega)} \overrightarrow{\delta E}.Rm.\gamma_r.\vec{E}.d\Omega \qquad [8]$$

Finite Element Formulation (Dhatt and Touzot, 1981)

In that way, we can formulate the geometrical discretization. Let $n_i(x)$ a base of work space and index n denotes the elementary nodal values. The approximate function can be written for an isoparametrical element (Dhatt and Touzot, 1981):

$$x_i^h = n_j.x_{ij}^n \quad , \quad H_i^h = n_j.H_{ij}^n \quad \text{and} \quad E_i^h = n_j.E_i^n$$

The discretization of the electric fields is as follows :

$$\{E_h\} = \begin{bmatrix} \langle n_i \rangle & \langle 0 \rangle & \langle 0 \rangle \\ \langle 0 \rangle & \langle n_i \rangle & \langle 0 \rangle \\ \langle 0 \rangle & \langle 0 \rangle & \langle n_i \rangle \end{bmatrix}.\begin{Bmatrix} E_x^n \\ E_y^n \\ E_z^n \end{Bmatrix} = [N].\{E^n\} \qquad [9]$$

So the discretization of the curl operator is easy and we have :

$$\overrightarrow{curl}\ \vec{E_h} = \begin{bmatrix} \langle 0 \rangle & -\left\langle \frac{\partial n_i}{\partial z} \right\rangle & \left\langle \frac{\partial n_i}{\partial y} \right\rangle \\ \left\langle \frac{\partial n_i}{\partial z} \right\rangle & \langle 0 \rangle & -\left\langle \frac{\partial n_i}{\partial x} \right\rangle \\ -\left\langle \frac{\partial n_i}{\partial y} \right\rangle & \left\langle \frac{\partial n_i}{\partial x} \right\rangle & \langle 0 \rangle \end{bmatrix} \begin{Bmatrix} E_x^n \\ E_y^n \\ E_z^n \end{Bmatrix} = [R].\{E^n\} \qquad [10]$$

We have a similar relation for the magnetic field. This curl formulation denotes an anti-symmetrical operator [R]. In the Finite Element Method we try and secure an approximative solution of the weak formulation.

Matricial Formulation

We define the following matrices :

$$[m] = \int_{(\Omega)} N^T.N.d\Omega \quad \text{the mass matrix}$$

$$[m_\mu] = \int_{(\Omega)} N^T.\mu_r.N.d\Omega \quad \text{the magnetic mass matrix}$$

$$[m_\varepsilon] = \int_{(\Omega)} N^T.\varepsilon_r.N.d\Omega \quad \text{the electric mass matrix}$$

$$[k_i] = \int_{(\Omega)} N^T.R.d\Omega \quad \text{the electric stiffness matrix}$$

The elementary electric loading $\{f_i\}$ where the electric field is known and is given by *natural boundary conditions* :

$$\{f_i\} = \int_{(\Gamma_0)} \begin{Bmatrix} \{n_i\}.E_0(y,t) \\ 0 \\ 0 \end{Bmatrix} .d\Gamma$$

For example for the full domain (Ω) the weak formulations [7] and [8] in the first formulation can be written :

$$\sum_{i=1}^{n} \left\langle \delta H^n, \delta E^n \right\rangle . \left(\begin{bmatrix} m_\mu & 0 \\ 0 & m_\varepsilon \end{bmatrix} . \begin{Bmatrix} \dfrac{\partial H^n}{\partial t} \\ \dfrac{\partial E^n}{\partial t} \end{Bmatrix} + \begin{bmatrix} 0 & k_i \\ -k_i & 0 \end{bmatrix} . \begin{Bmatrix} H^n \\ E^n \end{Bmatrix} \right) = 0 \qquad [11]$$

After a classical assembling operation where index (G) denotes the global values, the differential system is as follows :

$$[M] . \frac{d}{dt} \begin{Bmatrix} H^{(G)} \\ E^{(G)} \end{Bmatrix} = \begin{Bmatrix} F_H^{(G)} \\ F_E^{(G)} \end{Bmatrix} - [K] . \begin{Bmatrix} H^{(G)} \\ E^{(G)} \end{Bmatrix} \qquad [12]$$

where global matrix [M] is *symmetrical*. If the *second formulation* is used the global matrix [K] is antisymmetrical. For the first formulation, the global electric loading is provided by the Dirichlet's conditions. Natural boundary conditions are also added for the second formulation.

Numerical Resolution

The general formulation of the differential system is :

$$[M] . \frac{d}{dt} \{U\} = \{F\} - [K] . \{U\} \quad \text{where} \quad \{U\} = \left\{ H^{(G)}, E^{(G)} \right\}$$

$$\frac{d}{dt} \{U\} = [M]^{-1} . \{\Psi(U,t)\} \quad \text{where} \quad \{\Psi(U,t)\} = \{F\} - [K] . \{U\}$$

For the numerical time-resolution, several methods are tested (Sod, 1978).

For numerical quadrature points the nodes of the elements are chosen. Consequently, the mass matrix [M] is diagonal. This inversion is an easy procedure. It is a necessary condition for the efficiency of the methods above. Under these conditions we can test the explicit and implicit methods. In both cases we use a matrix-free technique, the mass matrix and the stiffness matrix never being built. We note a high performance level for the CPU and the storage costs.

Semi-implicit method

The corresponding algorithm is as follows (Chambarel and Ferry, 2000):

$$
\begin{aligned}
&t_n = 0 \\
&\text{while} \quad (t_n \le t_{max}) \\
&\left\{ \begin{array}{c} \left\{\Delta U_n^i\right\} = \Delta t_n . \left[M_n^i\right]^{-1} . \left\{\Psi\left(U_n^i + \alpha.\Delta U_n^{i-1}, t_n + \alpha.\Delta t_n\right)\right\} \\ \left\{U_n^{i+1}\right\} = \left\{U_n^i\right\} + \left\{\Delta U_n^i\right\} \\ i = 1, 2, \ldots \quad \text{until} \quad \left\|\Delta U_n^i - \Delta U_n^{i-1}\right\| \le \text{tolerence} \end{array} \right\} \\
&t_{n+1} = t_n + \Delta t_n \\
&\text{end} \quad \text{while}
\end{aligned}
$$

where α is the upward time-parameter.

The first method requires inner iterations for each time-step with index i for ΔU determination and the convergence criteria can be written (Anderson *et al.*, 1984):

$$\alpha . \Delta t . \left\| \frac{\partial}{\partial U} \left\{ [M]^{-1} . \Psi(U, t) \right\} \right\| < 1 \quad \text{let} \quad \Delta t < \Delta t_0$$

But we always find a time-step value for the convergence of the process. We note the good stability of the scheme in the implicit case. If α<0.5 a CFL condition is also required (Dhatt and Touzot, 1981). In this way we choose a time step as follows :

$$\Delta t \le \text{Min}\left(\Delta t_0, \Delta t_{CFL}\right)$$

The advantage of this method is the matrix free technique associated with an iterative method. The initial solution of each time step is close to the next solution. For the semi-implicit method the number of iterations is very low, two or three in practice.

The Finite Element code

We use efficient C++ Object Oriented Programming for the Finite Element code called FAFEMO (Fast Adaptive Finite Element Modular Object) developed by A. Chambarel (2000). Initially the electromagnetic field is zero. For time t_k, the time step Δt_k can be changed at each step with the CFL condition.

This constitutes a general Finite Element formulation for the Maxwell's equations with an antisymmetrical electric stiffness matrix.

NUMERICAL RESULTS

Space Discretization

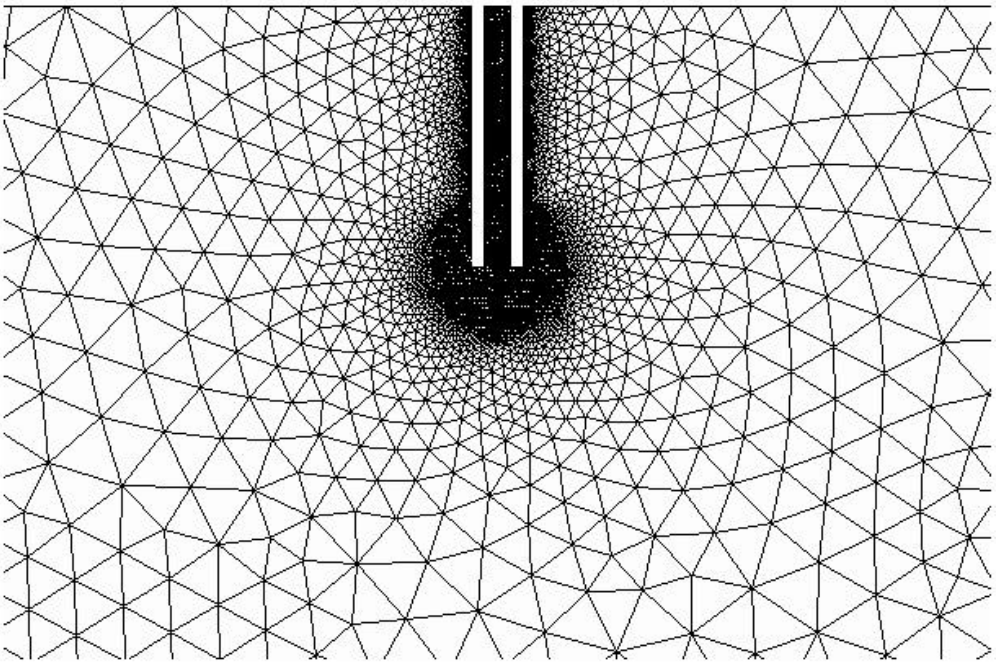

Fig. 1. *Space discretization*.

The 2D model is presented in Figure 1. We discretize with triangular linear elements. They are described in literature references (Dhatt and Touzot, 1981). We refine the mesh near the electrodes, so we have 13,985 triangular elements and 7,300 nodes. 29,200 differential equations are generated by the above Finite Element process. For time integration, we use a semi-implicit scheme for which the better upward parameter is α=0.75. This alpha value is a good compromise for the stability control of the scheme (Sod, 1978).

Numerical Results

Case of Homogeneous Space

In this case, the electric properties are constant and isotropic (ε_0,μ_0). This case is considered as a benchmark for the calculus verification. In the following figures and for different times, the solution of the adimensional magnetic field or the adimensional electromagnetic energy are presented.

At time t=1.5, coming of the electromagnetic wave in the external medium begins. The different results are presented in Figures 2 and 3. We note that the end of the line behaves like an electromagnetic source and the approximate wave front is a circle with a 0.5 radius. We present only the low intensity of the electromagnetic energy and the magnetic field in order to highlight the external electromagnetic field. It

focuses on the numerical values. In these conditions the stationary waves in the wave guide are here not visible.

The electromagnetic energy at the end of the line is presented in Figure 3. We note the well-known point effect at both internal angles because of the high intensity of the electric field.

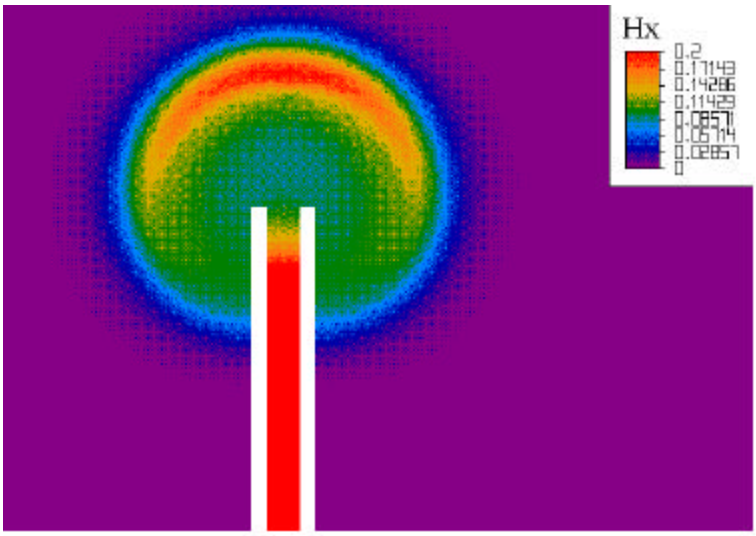

Fig. 2. *Magnetic field.*

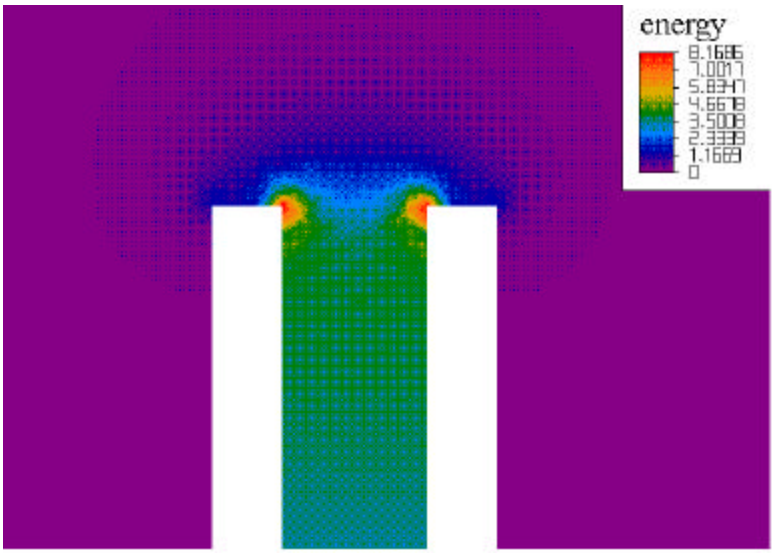

Fig. 3. *Point effect.*

An Example of Variable Electric Properties

In this case, we choose an example of variable electric properties. Around point (y_0, z_0) is a spot of electric singularity and the ε value is modified by the following mathematical model :

$$\varepsilon(y,z) = \varepsilon_0 + \varepsilon_1 . \exp\left(- \frac{(y - y_0)^2 + (z - z_0)^2}{a^2} \right)$$

We also have :

$$\mu_r = 1 \quad \text{and} \quad Rm = 0$$

The gaussian profile of ε is chosen. The example is presented in Figure 4 and we note the asymmetrical dielectric spot. Indeed, we are here considering a mathematical model in which there are no dissipative terms. We stand in the most unfavorable case from the viewpoint of stability of the numerical solution. In this case, there are no diagonal terms for the electric stiffness matrix.

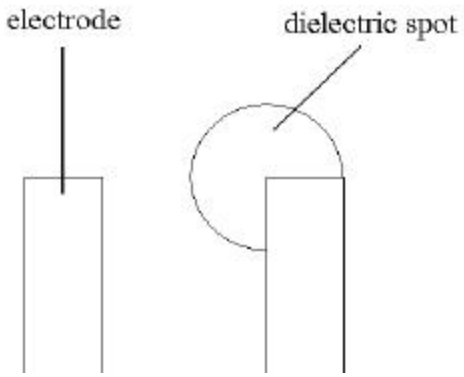

Fig. 4. *Example of electric singularity.*

We present the magnetic field at different times (1.5, 2.0, 3.0). If the time is greater than 1, then the electromagnetic field is at the end of the electric line. We notice stationary waves in the wave guide. The figure show the coming out of the electromagnetic wave in the free space. We note a large dissymmetry because of the electric particularity of the medium. The celerity of the electromagnetic wave decreases strongly in that zone and a more important part of the wave is reflected toward the entrance of the wave guide. It therefore provokes a variation in the impedance of the electric line, in particular, as seen at the entrance.

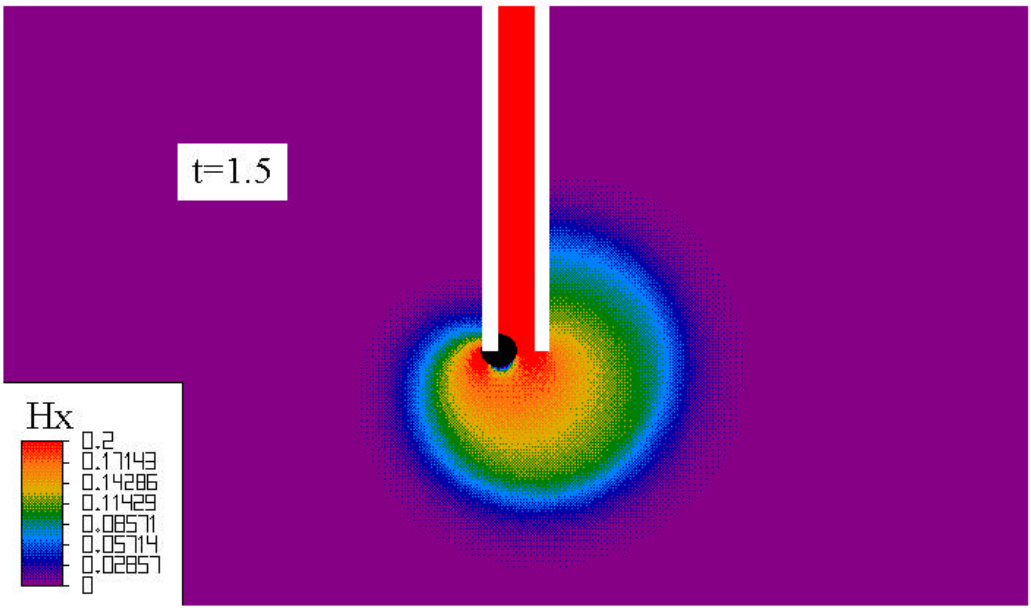

Fig. 5. *First electric singularity*

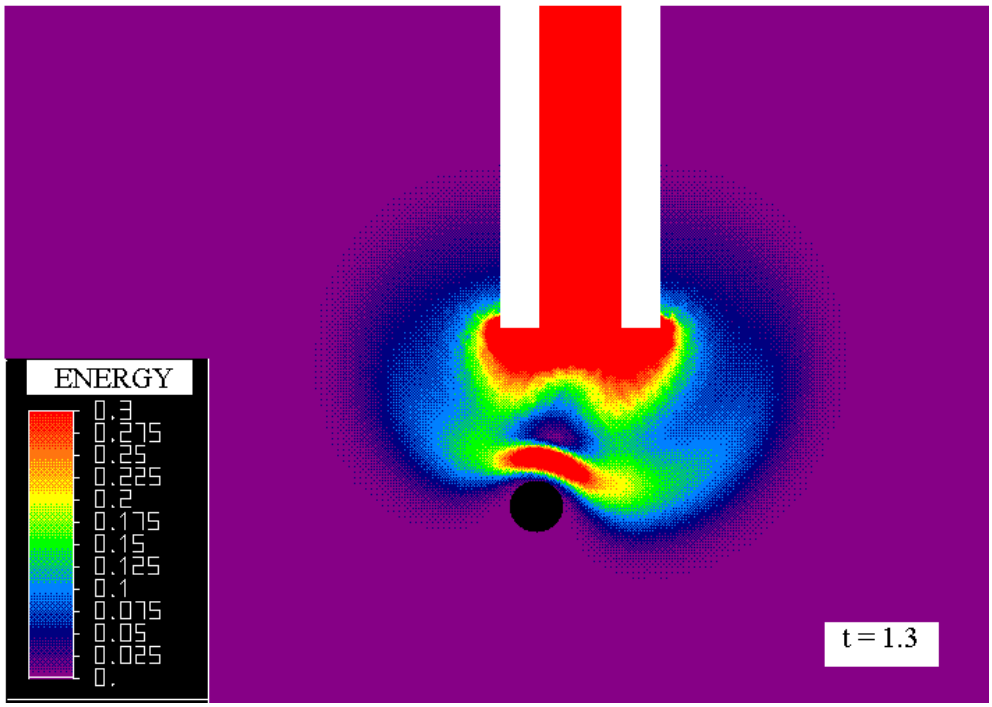

Fig. 6. *Second electric singularity*

For the first case the intensity at the top-end of the line is presented in Figures 5 and 6. The asymmetry of the electromagnetic field is also evident. We compare here the case of homogeneous electric properties with the existence of a dielectric spot. For the homogeneous medium with electric properties of the vacuum we note a spreading of the intensity signal because of the wave guide cut frequency. It is

a low-frequency filter. If the time is lower than 1.5, we have a same line intensity after which the dotted curve shows the gap between the two cases. The two curves are first confounded until the wave, undergoing a reflection from the electric peculiarity comes back to the entrance. Measurement of this time gap allows the determination of the distance of the dielectric singularity. Then, the analysis of the distorsion of the signal completes the knowledge of the peculiarity. At any rate through this analysis we have achieved a tool allowing the determination of a characteristic singularity catalog met in this type of problems.

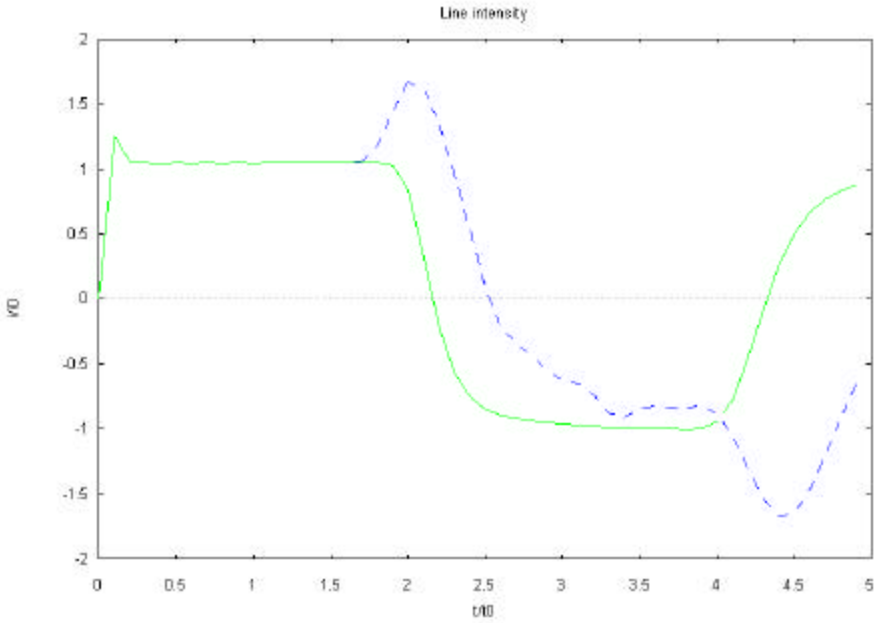

Fig. 7. *Line intensity.*

CONCLUSION

The TDR probe can be simulated by a Galerkin Finite Element approach. We present a general Finite Element formulation for Maxwell's equations in the case of propagation phenomenon and introduce the matricial structure of space discretization.An electromagnetic wave propagates along the wave guide with the object determining the variable electric properties of the space crossed. The electric loading is given by a natural boundary conditions. This process is performed by the AMS with a time dependent number of unknowns. The calculus are performed with a usual PC Pentium 200 MHz. In this way the CPU and memory cost are reasonable. Generally the wave propagation is always a difficult numerical problem. We do not detect instabilities (Assous *et al.*, 1993) and this set of methods gives good results.

REFERENCES

Anderson, D. A., Tannehill, J. C., and Pletcher, R. H., 1984, Computational Fluid Mechanics and Heat Transfer , Hemisphere Publishing Corporation Editor.

Assous, F., Degond, P., Heintze, E., Raviard, P. A., and Segre, J., 1993, On a Finite Element Method for Solving the Three-Dimensional Maxwell Equations: Journal of Computational Physics, **109**, 222-237.

Chambarel, A., and Ferry, E., 2000, Finite Element formulation for Maxwell's equations with space dependent electric properties: Revue Européenne des Eléments Finis, **9**, No. 8, 941-967.

Dhatt, G., and Touzot, G., 1981, Une présentation de la méthode des éléments finis, Editions Maloine S.A.

Dirksen, C. and Dasberg, S., 1993, Improved calibration of time domain reflectometry soil water content measurement: Soil Scien. Am. Soc., **57**, 660-667.

Dos Santos, L. A., 1997, Développement d'une nouvelle méthode de détermination des profils de teneur en eau dans les sols par inversion d'un signal TDR: Thèse de doctorat, Université Joseph Fourier de Grenoble.

Fleckinger, E., 1991, Electromagnétisme, Editions Masson, Paris.

Luebbers, R., 1993, IEEE Transactions on Antennas and Propagation, **41**, No. 11.

Sod, G. A., 1978, A survey of Several Finite Difference Methods for Systems of Nonlinear Hyperbolic Conservation Laws: Journal of Computational Physics, **27**, 1-31.

Spaans, E. J. A., and Baker, J., 1995, Examining the use of Time Domain Reflectometry for measuring liquid water-content in frozen soil: Water Ressources Research, **31**, No. 12, 2917-2925.

A TIME DOMAIN REFLECTOMETRY BOREHOLE PACKER FOR USE IN ROCK

S. W. Truss[1], L. J. West[2], P. Winship[3], M. Nakhkash[4], Y. Huang[5]

[1] School of Earth Sciences, University of Leeds, Leeds LS2 9JT, s.truss@earth.leeds.ac.uk
[2, 3] School of Earth Sciences, University of Leeds, Leeds LS2 9JT,
[4, 5] Department of Electrical and Electronic Engineering, University of Liverpool,
PO Box 147, Liverpool, L69 3BX,

ABSTRACT

A system for the application of time domain reflectometry (TDR) to cemented lithologies has been developed. Specially designed TDR probes will be mounted onto borehole packers that are filled with grout and pressurised to force the probes against the walls of the borehole. The system will allow automatic moisture content and electrical conductivity monitoring in the vadose zone of a sandstone aquifer during both natural rainfall events and infiltration experiments, to provide data for fluid flow and solute transport modelling, and ultimately the assessment of groundwater vulnerability to pollution.

The design, calibration and proof testing of the time domain reflectometry borehole packer probes is described in this paper. The optimisation of the geometry and configuration of the packer-mounted waveguides is described. The aims were to produce good reflections from the start and end of the waveguides over the range of dielectric constants seen in the field, thus allowing the two way travel time to be determined accurately, and to maximise sensitivity to the dielectric constant of the rock. Calibration of the packer-mounted waveguides for both moisture content and electrical conductivity is reported. In both cases the calibration is linear which indicates that the packer influence on the waveguide response is a constant and easily removed from the results. Experimental investigation indicates that most of the sensitivity is within ¼ of the waveguide separation distance from the packer. Proof testing in a sand tank shows that volumetric moisture content accurate to within 0.025 m^3/m^3 can easily be obtained.

INTRODUCTION

Over the previous two decades the technique of time domain reflectometry has been developed for measuring moisture content in soils, and has been widely applied by soil scientists. However, its application for monitoring moisture content in rocks is less well developed, because of the difficulty in inserting the waveguides to the required depths and without air gaps (Hokett *et al*., 1992; Sakaki *et al*.,

1998). Previous attempts to solve this problem have focussed on the use of short borehole packers with TDR waveguides embedded in their walls that are inserted in uncased boreholes on a temporary basis. However, such systems produce significant errors when used to collect time-series moisture content data, due to the repeated repositioning of the TDR waveguides between subsequent readings. Furthermore, open boreholes may act as preferential flow paths for water. A new borehole packer system is being developed in which packers with multiple TDR waveguides are permanently installed in boreholes by filling with grout. The aim is to provide time series of moisture contents and electrical conductivities at a range of depths in boreholes, to track lateral and vertical water and pollutant movements within the vadose zone of the Sherwood Sandstone aquifer in the UK. The Sherwood Sandstone, a consolidated fluvial sandstone of Permo-Triassic age, is the second most important aquifer in the UK in terms of the amount of groundwater abstracted, and improved understanding of its vadose zone is required for land use planning purposes. TDR data will complement those already obtained using cross hole radar to inform groundwater vulnerability assessment and the development of stochastic models of vadose zone flow (Binley *et al*., in press; Binley *et al*., 2001a&b). In this paper, the design of the packers and the TDR waveguides, and the laboratory calibration, spatial sensitivity and proof testing of the waveguides are described.

PACKER DESIGN

The depth to the water table is typically between 10-20m at the proposed packer installation sites (Hatfield and Eggborough in West Yorkshire, UK) and the rock is often poorly cemented and weak, which may lead to caving of the borehole sides. The packer design must therefore:

- Assist in maintaining borehole stability.
- Provide a secure mounting point for accurate location of TDR waveguides.
- Ensure that the waveguides maintain intimate contact with the surrounding rock, and limit air gaps behind and adjacent to the waveguides.
- Seal the borehole so it does not act as a preferential pathway for moisture flow.

Several methods of achieving these aims have been considered, including mechanical devices to force the waveguides into contact with the rock, but the inflatable packer design shown in Figure 1 was selected due to simplicity and ease of manufacture.

Each packer consists of a 12-18 metre long, 125mm diameter tube of impermeable, flexible and elastic material (Chlorino material DP205**,** manufactured by Chlorino Ltd, Italy), sealed at both ends with metal caps, with the upper cap drilled and tapped to allow grout injection and pressurisation. Each packer will be fitted with up to sixteen TDR waveguide assemblies before being lowered into the borehole where it will be filled with cement grout pressurised to force the waveguides into contact with the rock.

Use of large (10m+) inflating packers does present some problems:

- During inflation packers will expands vertically as well as laterally. Any waveguides mounted directly to the packer would be put under tension and risk damage. The spacing between the waveguides could also increase, altering the probe impedance characteristics. Hence, TDR waveguides are mounted on neoprene backing rather than directly on the packers themselves (see Figure 1).

- Cement shrinks upon curing, typically by approximately 0.7%. To prevent the waveguides moving away from the borehole wall and introducing air gaps, a shrinkage reducing agent (Eclipse manufactured by W.R. Grace & Co. Cambridge, Connecticut, USA) is added to the grout mixture. The use of compressible neoprene in the waveguide assemblies also allows some cement shrinkage to be accommodated, while allowing the waveguides to maintain contact with and mould to fit any minor irregularities in the borehole wall.

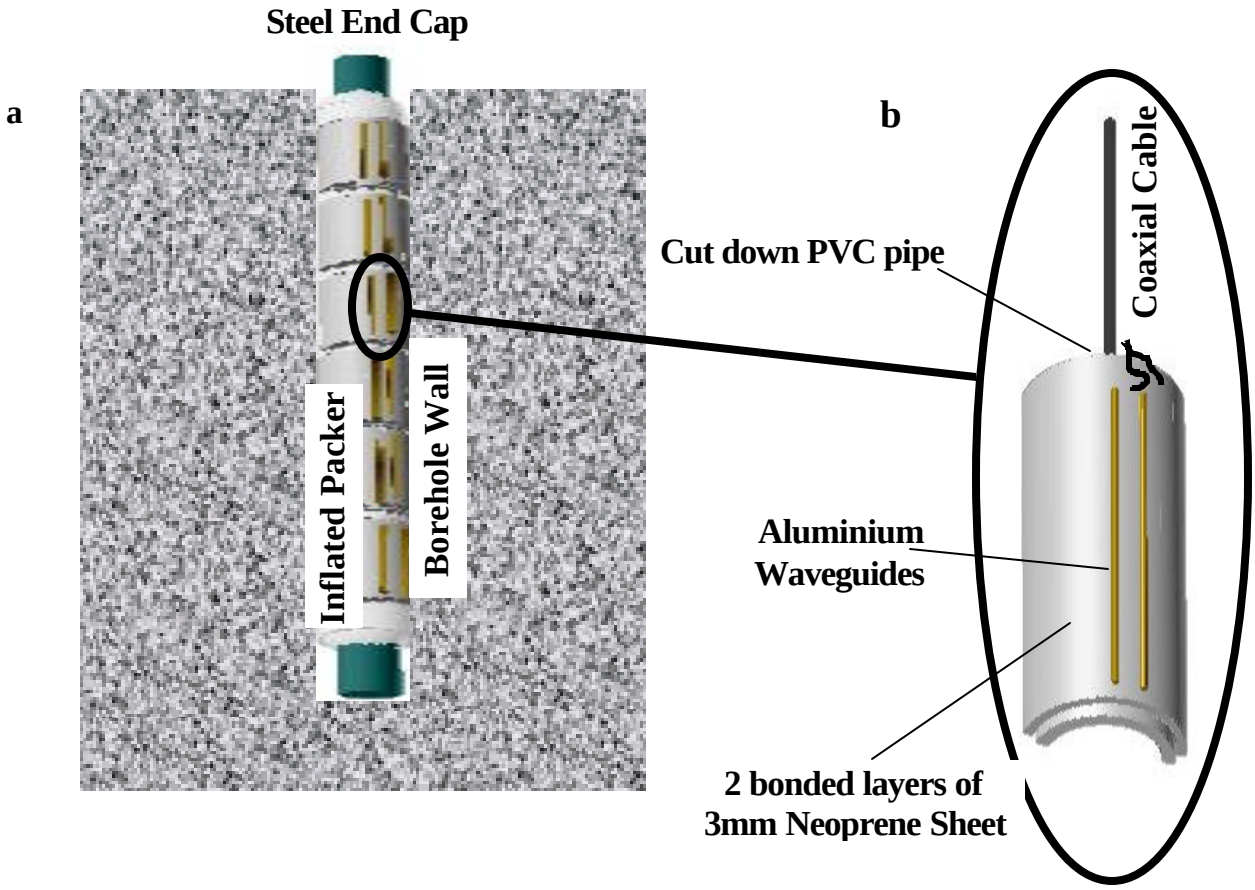

Fig. 1 a) *packer design* **b)** *waveguide assembly design*

WAVEGUIDE ARRANGEMENT

Commonly TDR probes of either a 2 or a 3-waveguide design are used for determination of soil moisture contents. Several probes with flat waveguides suitable for mounting on packers were constructed for testing and it was found that 2-waveguide designs performed well. There was no appreciable differences in moisture content values between a 3-prong Campbell Scientific CS605 probe and the various 2 waveguide designs constructed in house. Therefore, it was decided in the interests of simplicity to utilise a 2-waveguide design for the long packers.

Experimental investigation of both vertically and circumferentially mounted waveguides (Figure 2) was carried out using waveguides width of 3mm, separation of 30mm and width of 4mm, separation of 40mm (in accordance with the optimum separation to width ratio of 10, described below). The

circumferential waveguide configuration posed problems – e.g. difficulties in mounting thin, flexible waveguide assemblies on an expanding packer, limitation of waveguide length to the circumference of the packer, and reduced sensitivity to the dielectric constant of the rock compared with vertically mounted waveguides. The latter effect is the result of the electrical field lines in the circumferential arrangement penetrating further into the packer, and therefore being more influenced by the materials used in packer construction. To avoid these difficulties vertically mounted waveguides were selected.

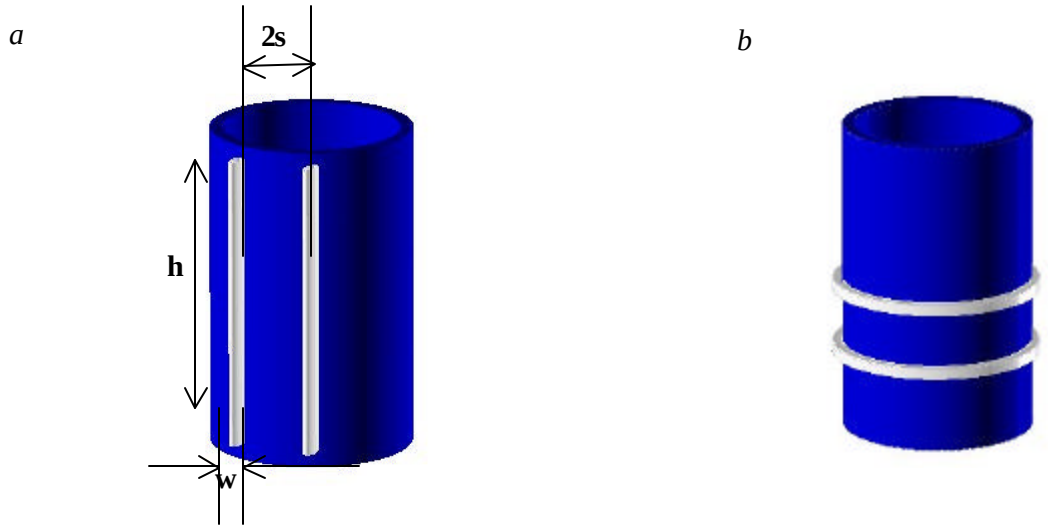

Fig. 2. a) *Vertical electrode arrangement* **b)** *circumferential electrode arrangement*

With the vertical waveguide arrangement, smaller waveguide separations provided better sensitivity to the moisture content of the rock. This is because of the curved nature of the packer surface, which leads to greater influence of the packer materials at greater waveguide separations. In practice, this is not a major problem unless the penetration of the packer by the electric field is sufficient to 'see through' the neoprene layer allowing water content of the cement in the packer to affect the readings. A waveguide separation of 30mm was decided upon as the best compromise between sensitivity to the packer material and adequate penetration into the rock.

Waveguide impedance

Probe impedance needs to be optimised so that both the first and second reflections can be distinguished clearly over the range of moisture content and salinity expected in field conditions, thus facilitating the determination of the two-way travel time for the signal within the waveguides. Assuming that the transmission line formed by the waveguides has zero loss, that changes in impedance happen abruptly where the coaxial cable is joined to the waveguides, and that the coaxial cable has impedance of 50Ω, the reflection co-efficient for the first reflection, R, (see Figure 3) is given by:

$$R = \frac{Z - 50}{Z + 50} \qquad [1]$$

where Z is the impedance of the waveguide. The second reflection co-efficient T, which is a result of two transmissions (cable ⇒ waveguides and waveguides ⇒ cable) plus the reflection from the waveguide tips is given by:

$$T = \frac{200Z}{(Z+50)^2} \qquad [2]$$

The dependence of R and T on Z is illustrated in Figure 3 below.

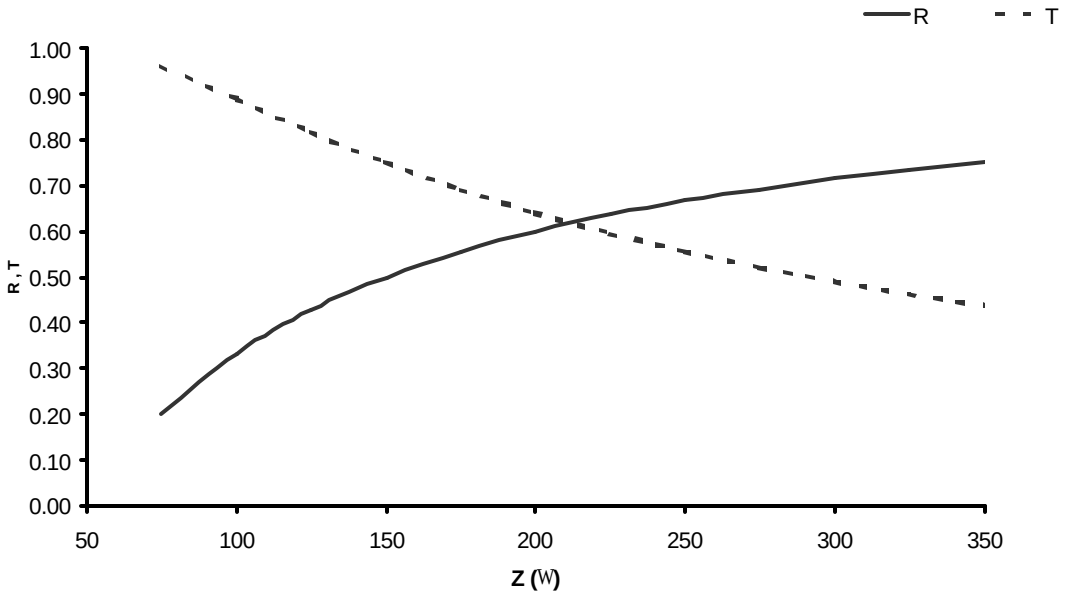

Fig. 3. *Dependence of reflection co-efficients on probe impedance*

Figure 3 shows that as R increases, T decreases. As Z nears 50Ω the first reflection becomes small, hence the TDR waveguides need to have a characteristic impedance greater than 50Ω. The intersection where both jumps are equal can be found by equating (1) with (2) giving a result Z of 211.8Ω. Hence, the optimum probe impedance is 211.8Ω. However, probe impedance depends on the dielectric properties of the medium as well as probe geometry, with increasing dielectric constant leading to reduced probe impedance. Hence in practice a range of probe impedances will occur, according to the dielectric constant of the rock. In order to investigate this, the characteristics of the system were modelled at the Department of Electrical Engineering at the University of Liverpool using LC (Cray, computers USA http://lc.cray.com) software for electromagnetic simulation. The results of this modelling showed that in order to provide detectable first and second reflections over the range of dielectric constants expected in the field (3 for dry rock to 37 for saturated rock), the impedance of the packer-mounted probe in air needs to be greater than 250Ω. This ensures the impedance of the probe remains above 50Ω, and the first reflection, R, remains detectable even in saturated rock conditions. However the Z value in air should not be too large so as to reduce the second reflection, T, to small values. As a compromise an impedance of 275Ω in air was selected.

The next step in waveguide design was to identify a waveguide geometry that would produce a characteristic impedance of 275Ω in air, when placed on an appropriate backing material. Further simulation with the 'LC' software showed that for thin waveguides mounted on thick plastic backing, an impedance of 275Ω in air was attainable when the ratio of waveguide separation to waveguide width was equal to 10, regardless of the actual dimensions of the waveguides.

As equations 1 and 2 do not account for losses in the coaxial cable or the BNC connector, it was considered necessary to measure the impedance of a probe constructed to the above specifications, as a

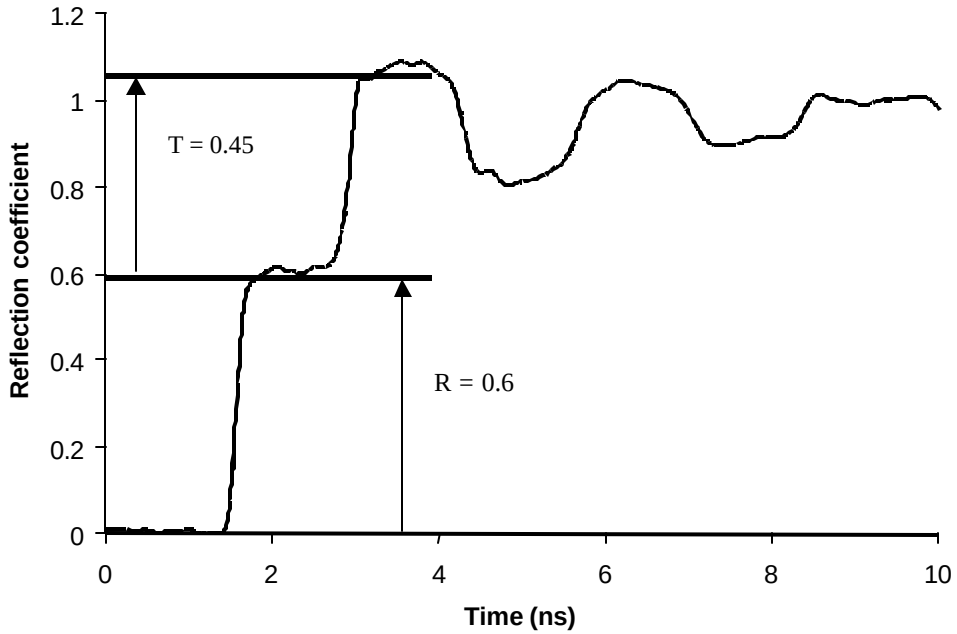

Fig. 4. *TDR trace for prototype probe assembly in air. Probe length is 250mm.*

check. A prototype field probe was constructed from aluminium of thickness 0.5mm, consisting of 250mm long waveguides, 3mm in width, separated by a 3cm gap, and attached to 6mm thick neoprene backing material with adhesive. A typical TDR trace obtained using the Campbell Scientific TDR 100 unit for this probe arrangement in air is shown in Figure 4. Assuming no loss in the probe itself (essentially correct for the air/backing material combination seen by the probe), the impedance may be calculated using the ratio of T/R, which we shall call β.

$$Z = 50\frac{2+\sqrt{4+\beta^2}}{\beta} \qquad [3]$$

From Figure 4, the first reflection co-efficient R is 0.6 and the second T is 0.45, so β is 0.783, and using equation (3) gives Z of 275.73Ω. This is very close to the theoretical value predicted from the LC software (275Ω).

CALIBRATION AND SENSIVITITY ANALYSIS

Moisture content calibration

Probe calibration was undertaken using liquids of known dielectric constant. Cement grout identical to that intended for field use was cast behind a prototype probe assembly to simulate a packer-mounted array. After the cement had set, the probe assembly was removed, voids in the cement were filled, and the cement coated with epoxy resin and silicone sealant to reduce a). voids and b). any tendency of the packer to absorb fluids from its surroundings. The test packer was fixed into a 20-litre container, which was filled with liquids of known permittivity (see Table 1). All calibration tests were carried out at 20°C using a Campbell Scientific TDR 100 unit, using Campbell Scientific PC TDR 2.0 software.

Material	*Relative dielectric constant*	*Source*
Acetone	(20^0C) 21	http://www.ctennant.co.uk/proddata/tp00001a.htm
Methanol	(25^0C) 32.6	http://www.asiinstr.com/dc1.html
Cyclohexane	(20^0C) 2	http://www.asiinstr.com/dc1.html
Water	(20^0C) 80.4	http://www.asiinstr.com/dc1.html
Air	1	http://www.asiinstr.com/dc1.html

Table 1. *Dielectric properties of standard liquids*

As the waveguides are mounted on the packer assembly, the measured dielectric constant will depend partially on the dielectric properties of the neoprene/cement behind the waveguides and partially on the dielectric properties of the measurement medium. The measured relative dielectric constant K_{exp} will thus be given by

$$K_{exp} = K_{medium}(1-w) + K_{packer}.w \qquad [4]$$

where w is a weighting factor between 0 and 1, determining the relative contribution of the packer materials. The weighting factor w for TDR probes attached to a backing material is independent of the dielectric constant of the measurement medium, provided that the backing material is uniform and thick. This assumption is valid here as the neoprene backing contains most of the rearward sensitivity volume of the probe (see below). The purpose of calibration is thus to determine both K_{packer} and the weighting factor w using liquids with a range of dielectric constants.

Figure 5 shows a plot of the relative dielectric constants of the standard liquids against the relative dielectric constants measured by the packer assembly immersed in these liquids. Also shown is a plot of equation (4) with the parameters K_{packer} and w optimised for best fit to the data. The calibrated values of w and K_{packer} for this range are 0.37 and 8.65 respectively.

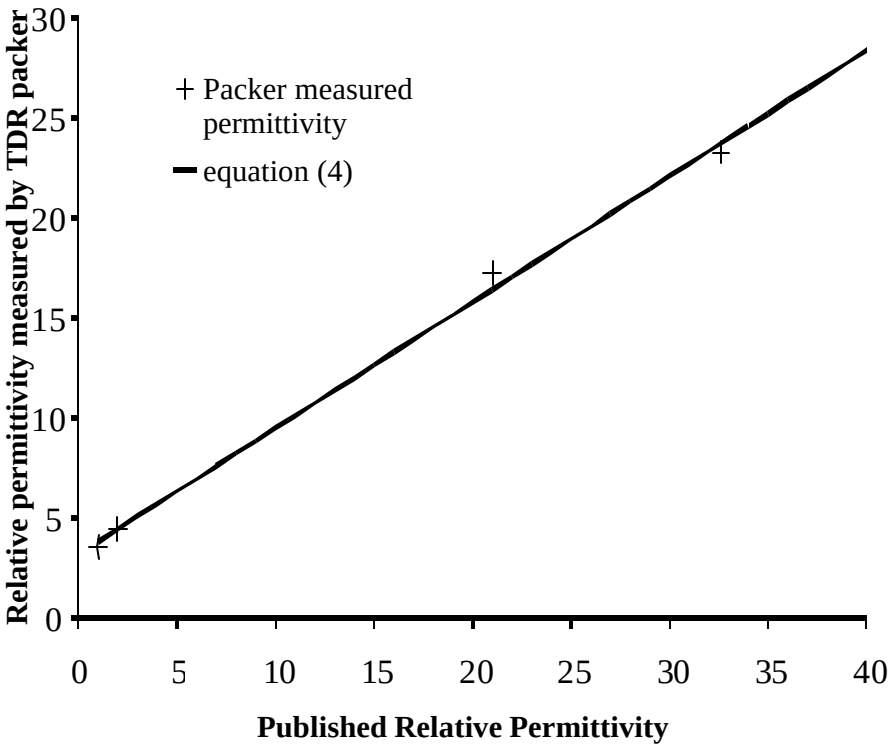

Figure 5. *Packer mounted waveguide calibration using liquids of known dielectric constant*

Electrical conductivity calibration

The electrical conductivity of the medium surrounding a TDR probe can be determined from the ratio of the applied to the reflected voltage after the first reflection from the probe end, ρ,

$$s = \frac{k_p}{Z_c}\frac{1-r}{1+r} \qquad [5]$$

Where Z_c is the cable impedance (50Ω) and k_p is a probe constant (dimensions L^{-1}), taken from TDR100 Instruction Manual, Campbell Scientific inc., 2000. The probe constant depends on the geometry of the waveguides, and in the case of the packer-mounted probe, on the electrical conductivity of the packer assembly. Here, the probe constant was determined for the test packer by measuring ρ in sodium chloride solutions with a range of salinity. The electrical conductivity of the solutions was measured independently using a Jenway 340 Electrochemistry analyser and conductivity probe. Temperatures were monitored throughout the procedure and all conductivities reported are corrected to those at 10°C.

The TDR traces (Figure 6a) show that the signal travel time is independent of ionic concentration, but that the reflected signal is increasingly attenuated at high salinity. Figure 6b shows a plot of TDR measured conductivity (i.e. found using equation 5 with k_p equal to unity) against that measured by the

conductivity probe. Linear regression analysis gives a probe constant of 8.96 m^{-1} for this probe arrangement.

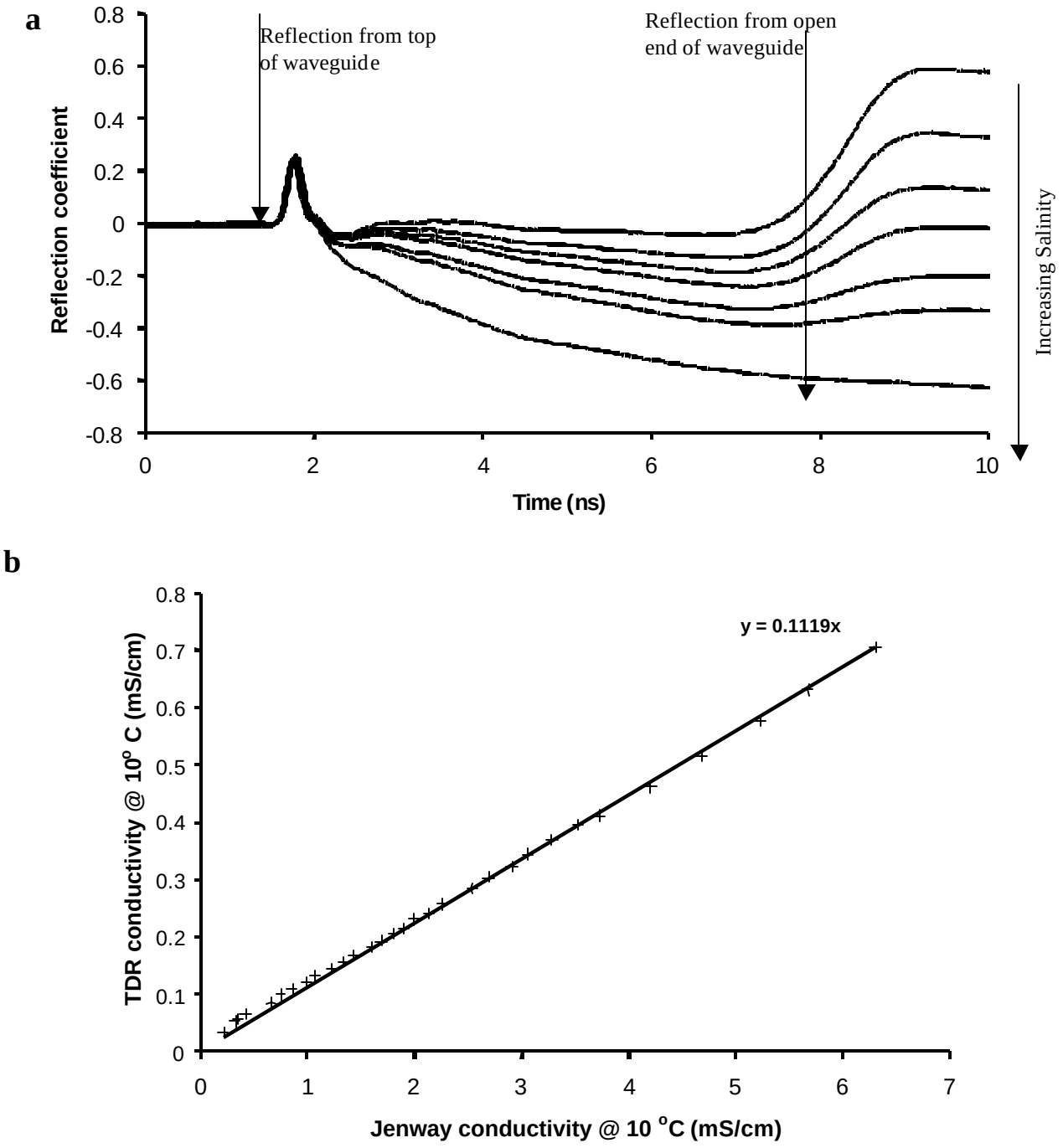

Fig. 6. **a)** *TDR traces from packer mounted probe in salt solutions of various conductivity*
b) *Determination of probe constant for packer mounted probe.*

Spatial sensitivity (moisture content)

Knight (1992) investigated the dependence of the spatial sensitivity of TDR probes on waveguide geometry. For typical waveguide geometries with waveguide separation ratios of around 10, sensitivity is focussed in the immediate proximity to the waveguides, but with some sensitivity in an ellipse around the waveguides in plan. A variation on the method described by Baker and Lascano (1989) was used to investigate the sensitivity of packer-mounted electrodes here. A test waveguide assembly was immersed in a water bath that allowed accurate and controlled movement of a bar of low permittivity material (wood) across the face of the electrode array. This was moved laterally past the waveguides with the two-way travel times in the probe being measured for each position. The bar was then moved away from the waveguides in 1mm steps and the procedure repeated until a 3D picture of spatial sensitivity had been completed. Two-way travel times were converted to apparent moisture content in the sensed volume using the equation of Topp *et al.* (1980). The results were normalised to express sensitivity as a percentage of the highest response along each transect. The results of the sensitivity analysis are shown in Figure 7, over two- thirds of the sensitivity occurs within 3mm of the waveguides (i.e. the thickness of the neoprene).

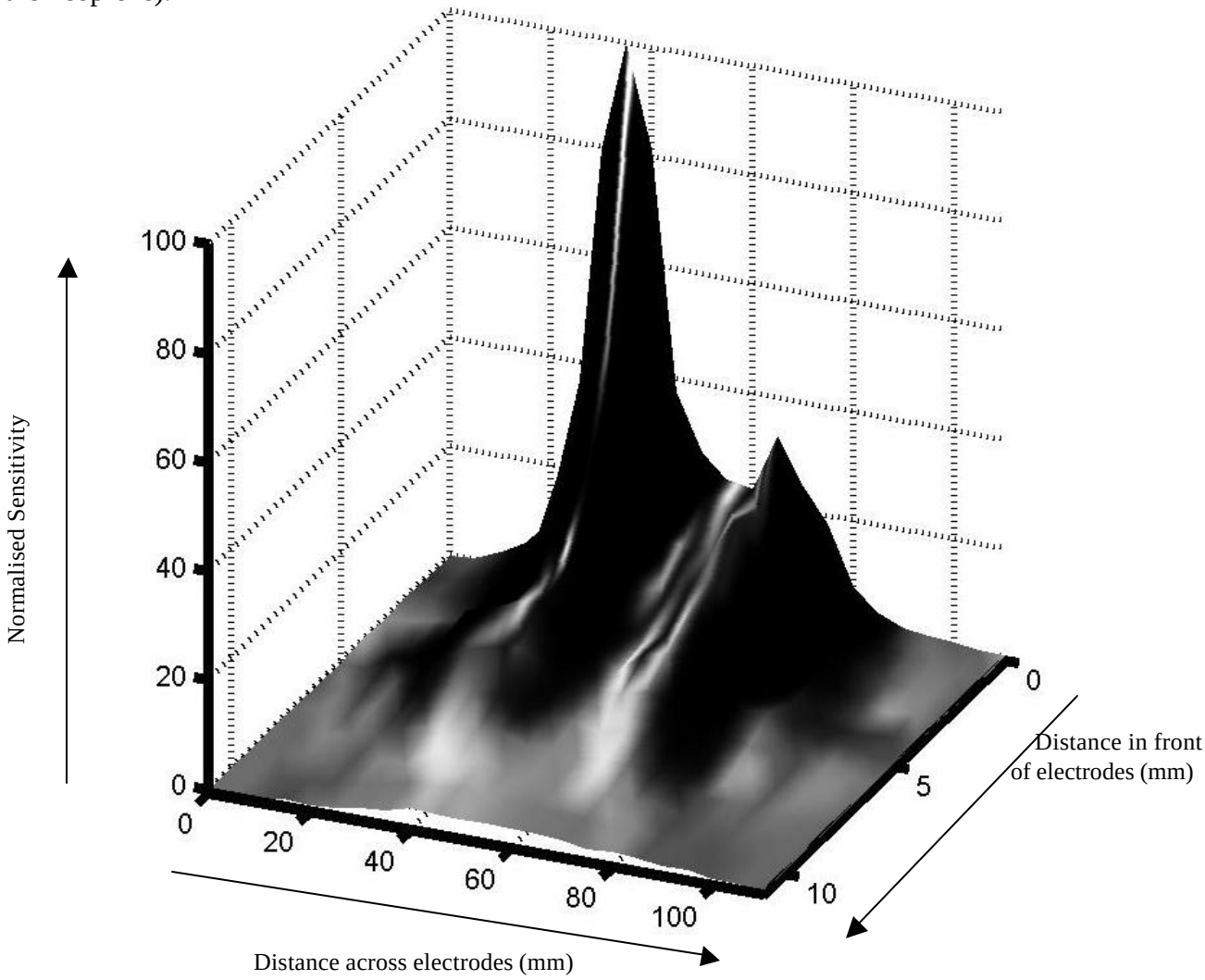

Fig. 7. *Spatial sensitivity of packer mounted probe to moisture content*

PROOF TESTING

The prototype packer-mounted probe was proof tested in sand derived from the Sherwood Sandstone aquifer, to investigate the accuracy in determination of volumetric moisture content using the calibration derived above. A sample of Sherwood Sandstone sand was oven dried at 105^0C for 24 hours, and sieved through a 1.8mm sieve to remove any cemented lumps. Approximately 11kg of oven dried sand was tamped into a large tray (the volume occupied by the sand was recorded in order to obtain the dry density). The volumetric moisture content was determined by pressing the packer-mounted probe onto the surface of the sand. Tap water was progressively added to the sand, 0.5litres at a time, mixing to ensure homogeneity of moisture content and re-tamping as far as possible into the same volume (some difficulties were experienced in compacting the sand down to the same volume., which may have affected the calculation of volumetric moisture content). A TDR volumetric moisture content was recorded for each moisture increment by applying the Topp equation (Topp *et al.*, 1980) to the dielectric permittivity of the sand found using the probe calibration parameters in equation (4). The Topp equation is known to accurately relate dielectric constant to moisture content for Sherwood Sandstone at TDR frequencies (West *et al*., 2001). The results of proof testing are presented in Figure 8 below.

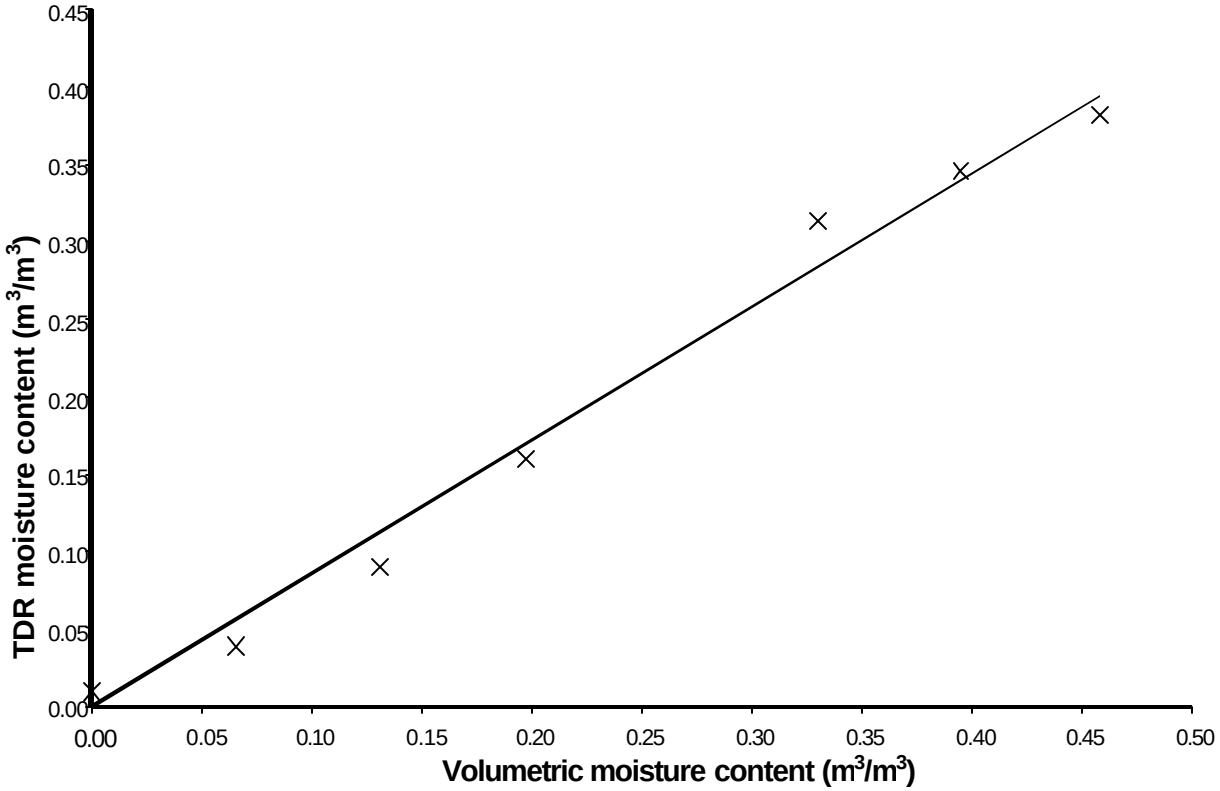

Fig. 8. *Results of proof testing borehole TDR packer in Sherwood Sandstone sand*

The probe mounted packer measures volumetric moisture content remarkably well, to within 0.025 of the values estimated from the mass of water added. The accuracy of the TDR packer itself is probably even better than this, as most of the scatter shown is probably the result of actual volumetric moisture content variation in the sand rather than error.

SUMMARY AND CONCLUSIONS

A borehole packer-mounted TDR system for measuring the moisture content and electrical conductivity of rock has been designed, calibrated and proof tested. The system is designed to be installed in the vadose zone of a consolidated sandstone aquifer, to monitor water and pollutant migration. The packer consists of a flexible plastic tube with metal end caps, which can be grouted into a borehole using non-shrinkable grout. TDR waveguide assemblies are mounted onto the packer and pressed against the borehole walls. The geometry and configuration of the waveguides was selected to ensure that the reflections from the start and end of the waveguides would be significant over the range of dielectric constant values encountered in field conditions, and to maximise sensitivity to the dielectric constant of the borehole walls. The resulting design consisted of waveguides which were 0.5mm thick, 3mm wide and 30mm apart, and 250mm long, mounted vertically on the packer. The measured impedance of the waveguides closely matched that predicted from theoretical modelling.

The packer mounted TDR waveguides were calibrated using liquids of known dielectric constant and aqueous solutions of known electrical conductivity. The calibrations are essentially linear which indicates that the proportion of the sensed volume that resides inside the packer assembly does not depend on the dielectric constant of the surrounding medium. Experimental investigation using a water bath indicates that 90% of the sensitivity to moisture content is focussed within 7.5mm or so of the waveguides, which illustrates the importance of eliminating air gaps between the packer and the borehole walls. It also shows that the probes are not sensitive to the properties of the grout in the packer because of the intervening backing materials. A prototype packer was proof tested in a tank containing sand at varying degrees of saturation. It performed well despite difficulties in maintaining constant sand density, giving moisture content readings within ± 0.025 of the bulk value.

ACKNOWLEDGEMENTS

Financial support for this work has been provided by NERC CONNECT grant NER/D/S/1999/00079 (formerly GR3/CO100), by the Environment Agency, and by a University of Leeds Scholarship awarded to the first author.

REFERENCES

Baker, J.M, Lascano, R.J., 1989, The spatial sensitivity of time-domain reflectometry. Soil Science, **147**, No. 5, 378-384

Binley, A.M., Middleton, R., Pokar, M. and West, L.J., 2001a, Observations of Seasonal Dynamics in the Vadose Zone using Borehole Radar and Resistivity. In: Proc. Symp. Applications of Geophysics to Engineering and Environmental Problems (SAGEEP2001), Environmental and Engineering Geophysical Society, Denver, CO. (VZC-3).

Binley, A.M, Winship, P., Middleton, R, Pokar, M and West, L.J. (in press) High resolution characterisation of vadose zone dynamics in the Sherwood Sandstone using cross-borehole radar. Water Resour. Res.

Binley, A.M., Winship, P and Pokar, M., 2001b, Cross borehole radar and resistivity tomography: a comparison of techniques in unsaturated sandstone. In: Proc. Symp. Applications of Geophysics to Engineering and Environmental Problems (SAGEEP2001), Environmental and Engineering Geophysical Society, Denver, CO. (VZC-1).

Hokett, S.L., Chapman, J.B., and Russell, C.E., 1992, Potential use of time domain reflectometry for measuring water content in rock. Journal of Hydrology, **138**, 89-96.

Knight, J.H., 1992, Sensitivity of time domain reflectometry measurements to lateral variations in soil water content. Water Resour. Res. **28**, 2345-2352.

Sakaki, T., Sugihara, K., Adachi, T, Nishida, K and Lin, W., 1998, Application of time domain reflectometry to determination of volumetric water content in rock. Water Resources Research, **34**, 2623-2631.

Topp, G.C., J.L. Davis and Annan, A.P.,1980, Electromagnetic determination of soil water content: Measurement in coaxial transmission lines, Water Resour. Res., **16**, No. 3, 574-582.

West, L.J., Huang, Y., and Handley, K., 2001, Dependence of sandstone dielectric behaviour on moisture content and lithology, In: Proc. Symp. Applications of Geophysics to Engineering and Environmental Problems (SAGEEP2001), Environmental and Engineering Geophysical Society, Denver, CO. (GTD-5).

THE SAMPLE AREA OF TIME DOMAIN REFLECTOMETRY PROBES IN PROXIMITY TO SHARP DIELECTRIC PERMITTIVITY BOUNDARIES

Paul A. Ferré[1], Henrik H. Nissen[2], Per Moldrup[3] and John H. Knight[4]

[1]Department of Hydrology and Water Resources,
University of Arizona, USA ty@hwr.arizona.edu
[2]Department of Environmental Engineering, Institute of Life Sciences,
Aalborg University, Denmark i5hn@civil.auc.dk,
[3]Department of Environmental Engineering, Institute of Life Sciences,
Aalborg University, Denmark i5pm@civil.auc.dk
[4]Department of Mathematics, Australian National University
and CSIRO Land and Water, Canberra, Australia john.knight@maths.anu.edu.au

THE UNIVERSITY OF ARIZONA.

ABSTRACT

Recent advances in the application of numerical analyses to the spatial sensitivity of conventional two- and three-rod time domain reflectometry (TDR) probes allow for investigation of the response of TDR in spatially heterogeneous media. In this study, we present numerical analyses and laboratory measurements of the effects of steep gradients in relative dielectric permittivity (K) on the spatial sensitivity of TDR probes. Two- and three-rod probes were placed horizontally or vertically within an experimental box. Then, an air/liquid interface was raised upwards from below and past the probe. Three liquids (sunflower seed oil, ethanol and water) with varying K values were used. The same system was analyzed using a numerical model of the spatial sensitivity of TDR probes to lateral variations in K. There was good agreement between measured and modeled K, demonstrating that the spatial sensitivity of TDR probes is biased towards the area of lowest K. Horizontal probes are found to be more appropriate for monitoring across sharp vertical boundaries. The sample area of all designs changes drastically as a function of the dielectric permittivity distribution in the transverse plane.

INTRODUCTION

Time domain reflectometry (TDR) has become a standard method for water content measurement in soils. The method offers rapid, nondestructive, automated measurement of water content in a wide range of soils with minimal soil-specific calibration (Topp *et al.*, 1980). In addition, TDR probes are simple to construct, inexpensive, and allow for modification to tailor the measurement volume and spatial sensitivity of the instrument for specific measurement applications. Knight *et al.* (1997) introduced the use of numerical models to define the spatial sensitivity of TDR probes based on the geometry of the probe and the distribution of dielectric permittivities in the plane transverse to the direction of EM wave propagation. Later work showed how these methods can be used to predict the response (Ferré *et al.*, 1998) and the sensitivity distribution (Ferré *et al.*, 2000) of alternative TDR probe designs that incorporate nonmetallic components in their construction. Recently, the modeling approach has been

used directly in the design of alternative probes, minimizing the construction and testing of prototype probes (Nissen *et al.*, 2001).

Despite the success of the numerical modeling approach in predicting the response of alternative TDR probes, a definitive, measurement-based test of the ability of numerical models to describe the spatial sensitivity of TDR probes has not been presented. Conditions that include sharp contrasts in dielectric permittivity within the sample volume of a TDR probe are the most difficult to represent numerically. Therefore, the ideal test of the ability of the model to predict probe responses will involve measurement in the vicinity of sharp dielectric permittivity contrasts. These conditions are not uncommon for field and laboratory applications of TDR. Examples include measurements made with TDR probes placed near wetting fronts, the soil surface, or the nonmetallic walls of soil columns.

THEORY

Early efforts to define the sample area of TDR probes relied on direct measurements of the change in the measured dielectric permittivity with changes in the distribution of dielectric permittivity in the plane transverse to the long axis of TDR probes (Baker and Lascano, 1989). Knight (1992) took a similar approach in developing an analytical description of the sensitivity of two-rod TDR probes placed in a homogeneous medium subjected to small perturbations in the permittivity field. Petersen *et al.* (1995) showed that this approach was able to predict the response of TDR probes buried at shallow depths near the ground surface. However, although this approach gives a direct measure of the sample area of a TDR probe in a homogeneous field, it does not allow for prediction of the spatial sensitivity of TDR probes under heterogeneous conditions. Therefore, Knight *et al.* (1997) extended the spatial weighting function concept underlying the earlier analytical solution to construct a numerical approach capable of predicting the response of TDR probes of any geometry to any spatial distribution of dielectric permittivity in the plane transverse to wave propagation.

Full development of the theory underlying the numerical analysis is provided in Knight *et al.* (1997). The approach is based on a finite element solution of the two-dimensional Laplace equation in the transverse plane. Rods are internal boundaries to the domain and are set to constant potentials. The domain is chosen to be sufficiently large that a zero potential and a zero flux boundary condition give the same result. The potential distribution within the domain, $\Phi(x,y)$, is determined for a given dielectric permittivity distribution $K(x,y)$. The spatial weighting function $w(x,y)$ is defined for each element within the domain based on the square of the gradient of the potential across that element.

$$w(x,y) = \frac{\left|\nabla\Phi(x,y)\right|^2}{\iint_\Omega \left|\nabla\Phi_0(x,y)\right|^2 dA} \qquad [1]$$

where $\Phi_0(x,y)$ is the potential in a given element for a homogeneous K distribution, Ω is the domain of integration, and dA is the area of the element. The predicted measured dielectric permittivity is then,

$$K_a = \iint_\Omega K(x,y)w(x,y)dA \qquad [2]$$

The spatial weighting function describes the sensitivity of the instrument to any given point in the domain. The weighting function is defined such that,

$$\iint_{\Omega} w(x, y)dA = 1 \qquad [3]$$

Therefore, using this quantity, a sample area can be defined for the modeled TDR probes that, for instance, contains 50% of the total sensitivity,

$$\iint_{50\%} w(x, y)dA = 0.5 \qquad [4]$$

Furthermore, the area can be uniquely defined such that it includes only those areas of highest sensitivity. This is achieved by summing the product of the elemental weighting function and the elemental area in order of decreasing spatial weighting factor until 50% of the total weighting is reached. In this manner, the sample area is a true reflection of the sensitivity distribution, rather than being constrained to a predefined shape.

The equivalent dielectric permittivity can also be determined for the entire domain based solely on the total electrical flux into or out of the interior constant potential boundaries. In other words, the flux into the domain is a function of the geometry of the system, the boundary conditions, and the dielectric permittivity distribution. The flux out of the domain can be calculated for a uniform medium as q_0, with the dielectric permittivity set to a constant value of K_0. The flux out of the domain can be calculated for any dielectric permittivity distribution as q. Given that the domain geometry and the boundary conditions are unchanged, the effective dielectric permittivity of the heterogeneous system is defined as,

$$K_a = \frac{q_0}{qK_0} \qquad [5]$$

This method has the advantage that it is less sensitive to the discretization of the domain than the spatial weighting approach. That is, the spatial weighting factor for each element is a single value defined by the average gradient across that element. This necessarily leads to some inaccuracy in the approximation of the effective dielectric permittivity from the spatial weighting of distributed dielectric permittivities. To minimize these errors, it is standard practice to compare the effective dielectric permittivity determined by both methods to ensure that they do not differ significantly. If differences are too great, the finite element grid should be refined, especially in areas of high sensitivity.

The spatial weighting concept and the associated sample area definitions are very useful in describing the behavior of TDR probes. However, there is no direct means to measure the spatial weighting function or spatial sensitivity of a probe. The method of Baker and Lascano (1989) cannot be used because any change in the dielectric permittivity distribution in the transverse plane changes the spatial sensitivity. Therefore, the only available method to confirm these sample areas is the comparison of the dielectric permittivities predicted using the internal boundary fluxes and those determined using the spatial weighting factors. Agreement of both of these predicted values with measured values for known

dielectric permittivity distributions constitutes an indirect validation of the spatial sensitivity determined using the numerical analysis.

OBJECTIVES

The objectives of this investigation were: (i) to measure the effects of sharp gradients in dielectric permittivity on the TDR-measured dielectric permittivity for a range of two- and three-rod probes; (ii) to validate the numerical analysis of TDR spatial sensitivity and sample area by comparing the numerically predicted responses of TDR probes in the vicinity of sharp dielectric permittivity gradients with measured responses; and (iii) to use model-derived sample areas of TDR probes to explain the observed behavior of TDR probes subjected to sharp dielectric permittivity gradients within their sample areas.

EXPERIMENTAL AND NUMERICAL METHODS

A box was constructed to allow for the controlled advance of a sharp dielectric permittivity boundary into and through the sample area of TDR probes (Figure 1).

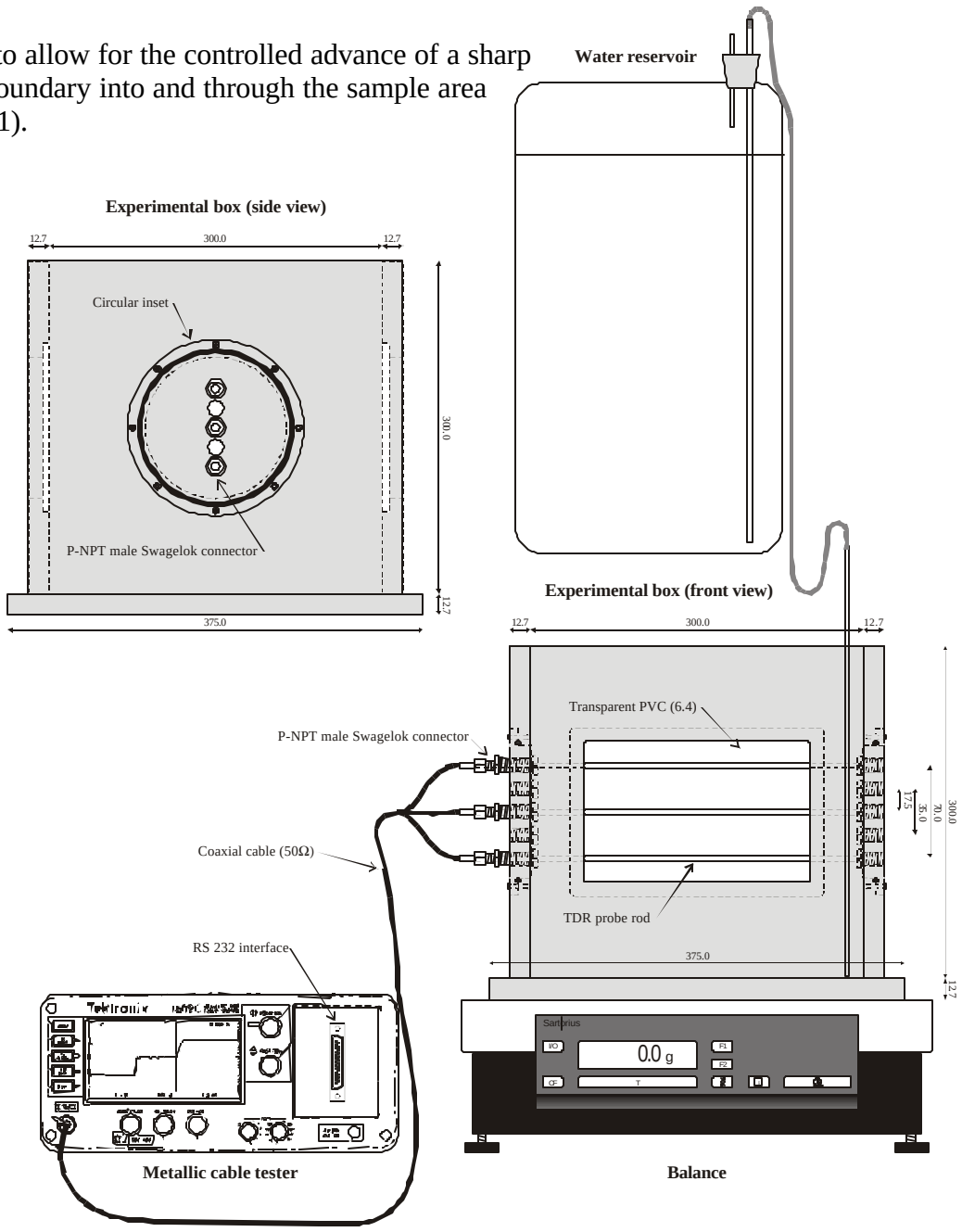

Fig. 1. *The experimental setup including the box, fluid delivery system, cable tester and balance. The balance and cable tester are both connected to a PC for automatic data acquisition. The setup is shown for a three-rod vertical probe configuration (70.0-mm rod separation). Turning the insets 90° will change the setup to the horizontal case.*

The box was constructed of a PVC base and four PVC walls. The inner dimensions of the completed box were 0.3 x 0.3 x 0.3 m. Two opposite walls included a transparent PVC window to allow for visual location of a liquid-air interface within the box. The remaining two opposite walls included a circular inset with five NPT threaded holes capable of accommodating Swagelok male connector tube fittings. Using these fittings, rods of diameters equal to 3.2, 4.6 and 6.4 mm can be inserted through the box walls. The effective length of the probe rods inside the box is approximately 285 mm. Two and three-rod probes can be formed with outer rod spacings equal to 17.5, 35.0, 52.5, and 70.0 mm for the two-rod probe and 35.0 and 70.0 mm for the three-rod probe, respectively. The circular insets can rotate to six different positions, allowing the probe axis passing through the center of the probe rods to lie in the horizontal plane, the vertical plane, or 45^o from the horizontal. For these experiments, we used probes formed by placing horizontal rods in the horizontal plane (referred to as horizontal probes) and horizontal rods placed in the vertical plane (referred to as vertical probes). Figure 2 shows a representative cross section through a vertical two-rod probe and through a horizontal three-rod probe.

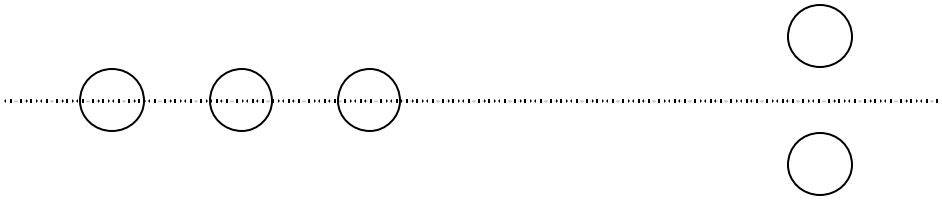

Fig. 2. *Schematic diagram of a three-rod horizontal probe (left) and a two-rod vertical probe (right). The horizontal line shows the height of the midpoint of the probes. All measurements are related to this midpoint.*

Legend	Number of Rods	Rod Diam. [mm]	Rod Sep. [mm]	Fluid	Orientation
A	2	4.6	35	Water	Horizontal
B	2	4.6	35	Oil	Horizontal
C	2	4.6	35	Ethanol	Horizontal
D	2	4.6	35	Water	Vertical
E	2	4.6	35	Oil	Vertical
F	2	4.6	35	Ethanol	Vertical
G	3	4.6	70	Water	Horizontal
H	3	4.6	70	Oil	Horizontal
I	3	4.6	70	Ethanol	Horizontal
J	3	4.6	70	Water	Vertical
K	3	4.6	70	Oil	Vertical
L	3	4.6	70	Ethanol	Vertical

Table 1: *Legend describing the rod geometries and fluids used for all 12 experiments.*

The box was placed on a Sartorius IC 34000 P balance with 0.5 g precision, which was interrogated every 10 seconds. A Tektronix 1502B cable tester was connected to the TDR probe and a waveform was collected every 10 seconds using TACQ software from Dynamax. Three liquids were used for testing: deionized water, ethanol, and sunflower oil. Water, with a relative dielectric permittivity of 80 (Musil and Zacek, 1986) provides the strongest contrast with air (K = 1) across the fluid-air interface. Ethanol has a relative dielectric permittivity similar to that of most soils under saturated conditions, K = 25 (Musil and Zacek, 1986). Oil, with a relative dielectric permittivity of 3 (Musil and Zacek, 1986), produces a very subtle dielectric permittivity contrast with air. Each liquid was tested separately. Liquid was added slowly at the bottom of the box through a vertical tube. The distance between the liquid-air interface was determined from the change in mass, the fluid density added and the cross sectional area of the box. This was checked visually at the time at which the interface reached the bottom and top of the probe rods.

A finite element grid was constructed for each probe geometry. For this investigation the model was defined for 12 probe/fluid combinations, as described in Table 1. For each simulation, the domain was divided into 60 layers to model a series of liquid-air interfaces. However, in most cases some of the layers were pooled in areas of low sensitivity to reduce the modeling task. Approximately 16000 elements were used to discretize the domain. The run time for each liquid-air interface location was approximately 1 minute.

RESULTS AND DISCUSSION

The experimental and numerical results will be presented in three sections: directly measured influences of sharp dielectric boundaries on probe responses; comparisons of the measured and predicted probe responses; and the effects of sharp dielectric boundaries on probe sample areas.

MEASURED PROBE RESPONSES

The dielectric permittivities determined directly from TDR measured travel times are shown as a function of the distance of the interface above the center of the probe in Figure 3. Negative values indicate that the interface is located below the center of the probe. Each data series represents the measured dielectric permittivity at a series of interface heights for a single probe geometry. The data series label refers to Table 1. The probe geometry is shown graphically above the legend as a representative cross section of the probe. For each probe geometry there is a clear distinction between the dielectric permittivity responses when the probes are entirely immersed in air, oil, ethanol, or water. The two- and three- rod horizontal probes show a sharp increase in dielectric permittivity when the fluid makes contact with the lowest edge of the rods. As predicted from numerical and analytical solutions (Knight *et al.*, 1994), the measured dielectric permittivity is the arithmetic mean of the dielectric permittivities of the fluid and air when the interface reaches the midpoint of the rods. The probe response is more complex for the vertical probe orientations. For the two-rod vertical probe, the observed sharp rise in dielectric permittivity does not occur until the interface reaches the lowest edge of the uppermost rod. As predicted from numerical and analytical solutions (Knight *et al.*, 1994), the measured dielectric permittivity is the harmonic mean of the dielectric permittivities of the fluid and air when the interface reaches the midpoint of the two-rod vertical probe. The response of the three-rod vertical probe shows two discontinuous regions. The first discontinuity occurs when the interface contacts the lowest edge of the center rod. A second discontinuity occurs when the interface contacts the base of the uppermost rod. Waveforms between these discontinuities show multiple peaks, making automated analysis difficult.

COMPARISON OF PREDICTED AND MEASURED PROBE RESPONSES

The dielectric permittivities determined directly from measured travel times are shown as symbols in Figures 3 through 5 for the oil, ethanol and water experiments, respectively. The solid lines represent the model-predicted probe responses. Discussions will be grouped as follows: i) two- and three-rod horizontal probes; ii) two-rod vertical probes; and iii) three rod vertical probes.
It is important to note that the measurements with two-rod probes were made with unbalanced probes, i.e. no balun was inserted between the cable tester and the probe. To examine if there is any difference in the response between balanced and unbalanced two-rod probes model runs were conducted with the potentials at the surface of the rods set to equal and opposite values to represent a balanced probe. In

addition, an unbalanced probe configuration was modeled with the upper rod potential set to one and the lower to zero. Finally, the probe was modeled with the upper rod set to a constant potential of zero and the lower to one. The modeled responses of these configurations were identical when subjected to a rising air-water interface. The measured data were independent of the location of the grounded rod (data not shown) and there was a very good agreement between the measured and modeled response (Figure 6, Case D). This constitutes direct evidence that the use of unbalanced two-rod probes does not affect the spatial sensitivity of TDR probes.

HORIZONTAL PROBES

The model provides excellent predictions of the measured travel times for the horizontal probe geometries in oil (Figure 4, case B) and ethanol (Figure 5, case C), and good fits to the measurements made in water (Figure 6, case A). Of specific interest is the increasing asymmetry of the response about the midpoint of the horizontal probes with increasing dielectric permittivity contrasts. This demonstrates that the specific probe response is a function not only of the distribution of dielectric permittivities, but also of the magnitude of dielectric permittivity contrasts and that the sensitivity is biased towards the low conductivity region.

TWO-ROD VERTICAL PROBES

For the two-rod probes with a vertical orientation, the model predictions improve with increasing fluid dielectric permittivity. The measured and predicted results for the air-water case are indistinguishable, with both showing the displacement of measured increase in dielectric permittivity until the liquid interface was located well above the midpoint of the probe. For the oil and ethanol experiments, the model predicts an initial increase in the measured dielectric permittivity as the interface approaches the center of the probe ($z = 0$). A region of relative insensitivity follows shown by a minimal increase in the apparent K as the interface rises above the center of the probe. There is a second region of rapid increase in measured K with interface height as the interface approaches the upper rod. In contrast, the measured and modeled dielectric permittivities for the air-water case show a monotonic increase that is displaced to a location above the midpoint of the probe. That is, there is very little response until the air-water interface reaches the bottom of the upper rod.

THREE-ROD VERTICAL PROBES

The model predicts three sensitivity regions for the three-rod vertical probes. There are regions of rapid increase in measured K with interface height as the interface approaches and passes the center and upper rods. The predicted probe response shows regions of relative insensitivity when the interface is beneath the center rod, between the center and upper rods, and above the upper rod. The measured response in oil is in good agreement with this predicted behavior. In ethanol, the waveforms collected with the interface between the middle and upper rods make accurate travel time determination difficult, obscuring the probe response. Similarly, the waveforms collected with the air-water interface located between the lower and upper rods make comparison with the predicted response difficult. Further work is necessary to improve the identification of final reflections from these waveforms.

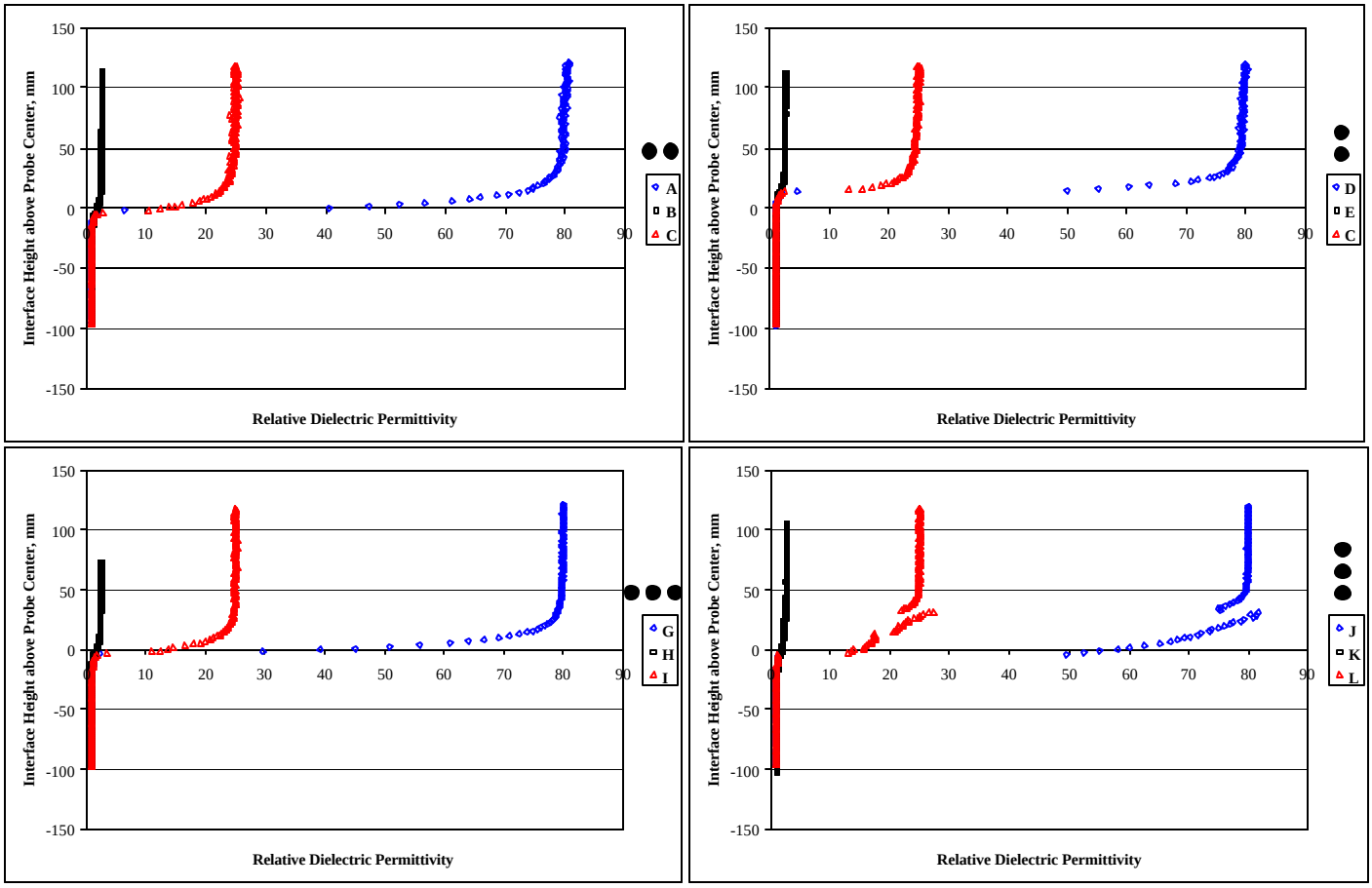

Fig. 3. *Measured relative dielectric permittivity as a function of the distance of the air-liquid interface above the probe midpoint. Three fluids were used: oil (squares), ethanol (triangles) and water (diamonds). Four probe geometries were tested, as shown schematically as a representative cross section above each legend. The probe/fluid combinations are referenced in the legend to Table 1.*

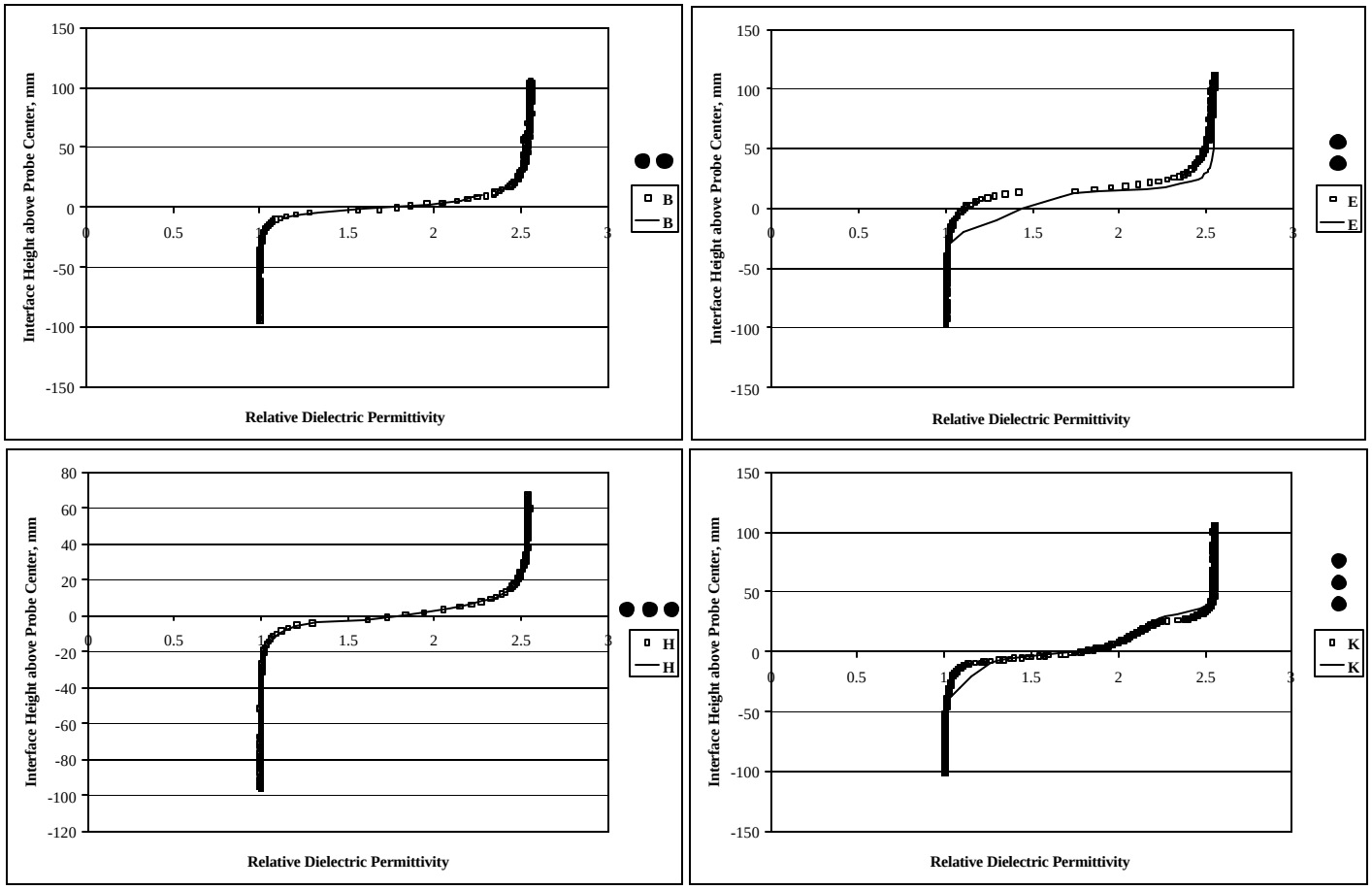

Fig. 4. *Measured (symbols) and modeled (lines) relative dielectric permittivity as a function of the distance of the air-oil interface above the probe midpoint. Four probe geometries were tested, as shown schematically as a representative cross section above each legend. The probe/fluid combinations are referenced in the legend to Table 1.*

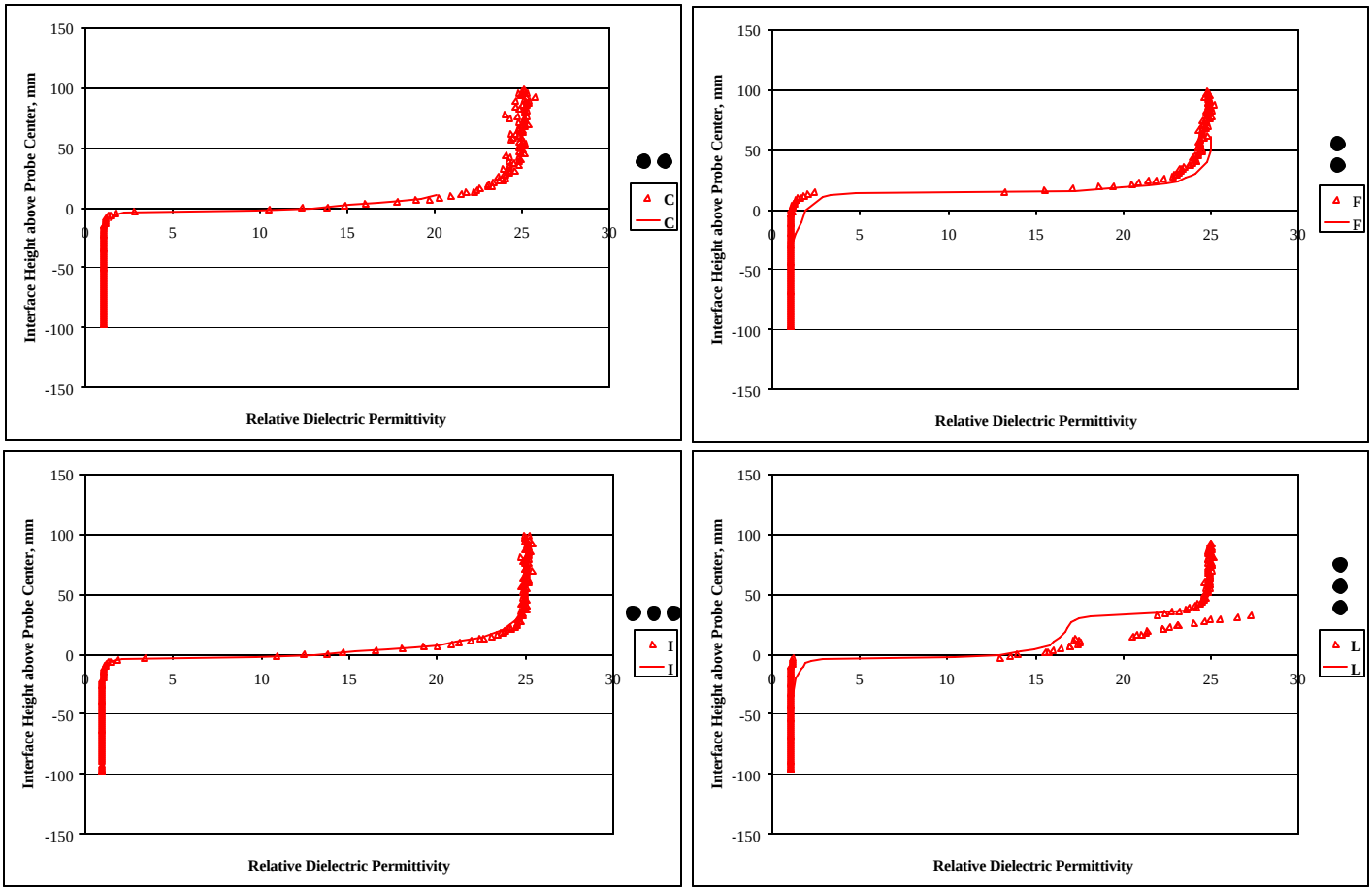

Fig. 5. *Measured (symbols) and modeled (lines) relative dielectric permittivity as a function of the distance of the air-ethanol interface above the probe midpoint. Four probe geometries were tested, as shown schematically as a representative cross section above each legend. The probe/fluid combinations are referenced in the legend to Table 1.*

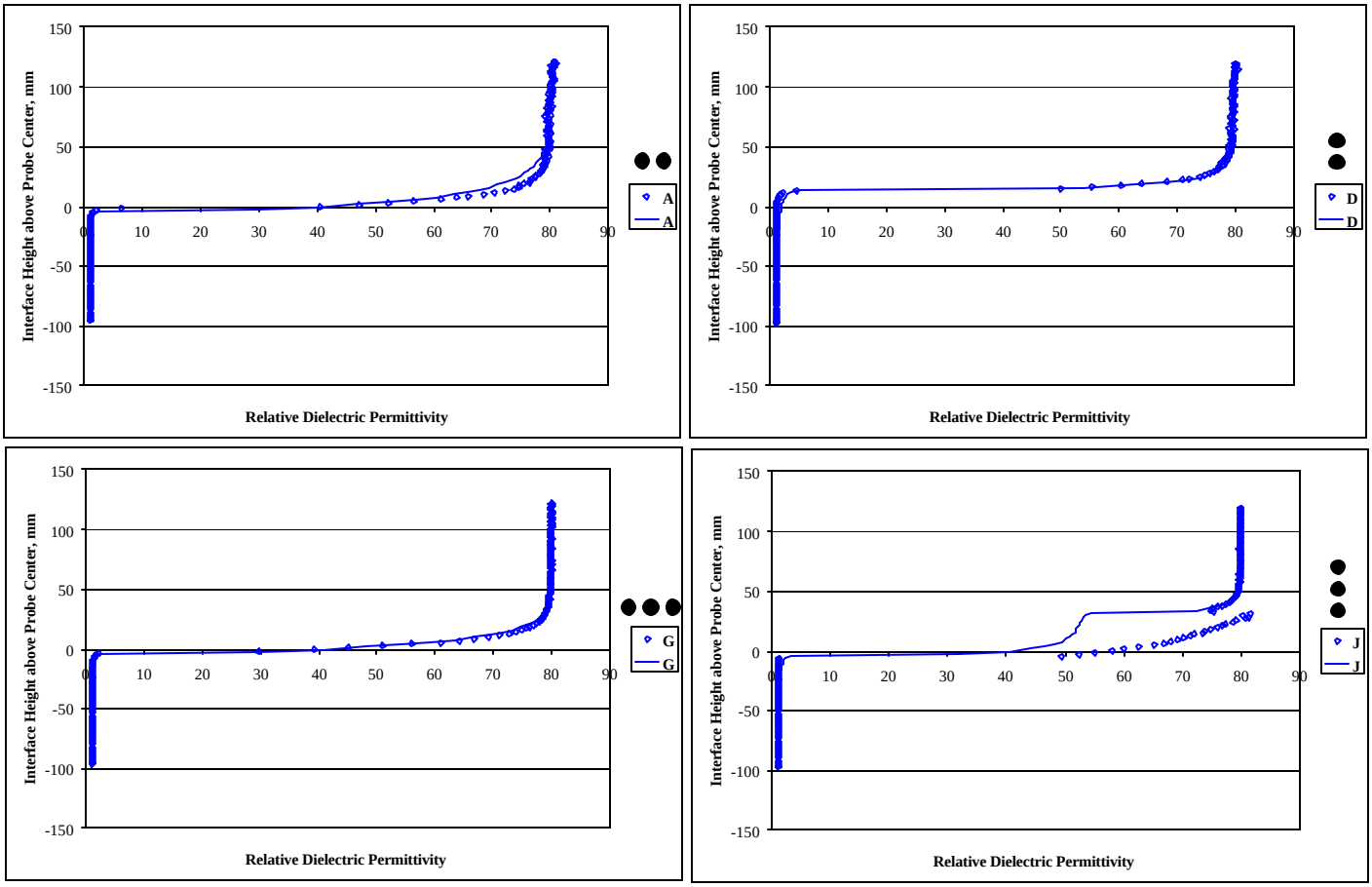

Fig. 6. *Measured (symbols) and modeled (lines) relative dielectric permittivity as a function of the distance of the air-water interface above the probe midpoint. Four probe geometries were tested, as shown schematically as a representative cross section above each legend. The probe/fluid combinations are referenced in the legend to Table 1.*

EFFECTS OF LIQUID INTERFACE LOCATION ON PROBE SAMPLE AREAS

Using the numerical approach, the weighting factors are calculated throughout the domain for each liquid interface location for each probe geometry. Figures 6-i through 6-vi show the sample areas as a function of interface location for all four probe geometries as defined by Ferré *et al.* (1998). A region is shown for each probe that encloses 90% of the total probe sensitivity. Four probe geometries are shown on each plot. The left half of the plot shows the sample areas of the two-rod (solid lines) and three-rod (filled area) horizontal probe orientations; the right half shows the two-rod (solid lines) and three-rod (filled area) vertical probe orientations. Each orientation is symmetric about the vertical midline. Sample area plots are shown for the liquid interface located: i) a distance of 1/8th of the outer rod spacing below the lowest rod; ii) 1/4 of the outer rod spacing above the lowest rod; iii) at the probe midpoint; iv) 1/4 of the outer rod spacing below the uppermost rod; v) a distance of 1/8th of the outer rod spacing above the uppermost rod, and vi) at the top of the box (homogeneous case).

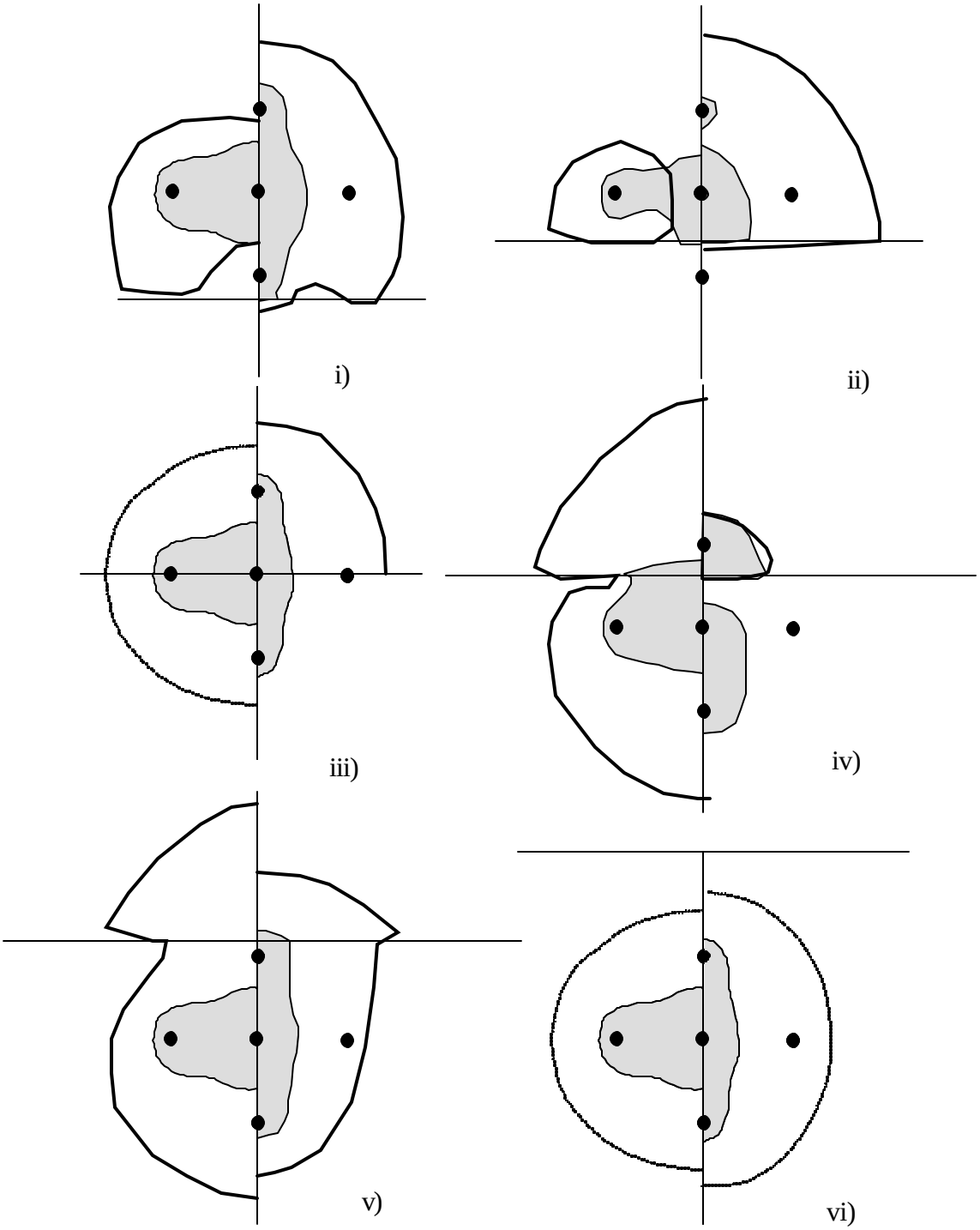

Fig. 7. *The 90% sample areas of four probe geometries (Cases A, D, G, and J in Table 1) as the function of the height of an air-water interface (shown as a vertical line). Four geometries are compared on each panel. The left half of each panel shows the two- and three-rod horizontal orientations. The right shows the vertical orientations. All orientations are symmetric about the central vertical line. The sample areas of three-rod probes are shown as shaded regions; two-rod probe areas are shown as solid lines.*

In the homogeneous case, the three-rod probes have smaller sample areas than the two-rod probes. The sample area is unchanged when the air-water interface is located at the probe center (iii) except for the two-rod case vertical case, which shows a restriction of the sample area to the overlying air. In fact, this probe shows very little sensitivity within the water until the interface reaches the upper rod (v). This explains the displacement of the response of this geometry to the rising interface as seen in Figures 2 through 5. Similarly, sample areas of the two- and three-rod horizontal cases show sample areas that are highly restricted to within the air until the interface reaches the rods (i and ii). When the interface is located at the center of the probe, the sample areas are equally distributed in both liquids. As the interface rises, the sensitivity is predominantly located in the water. This explains the sharp rise in measured dielectric permittivity as the interface reaches the probe center followed by a slightly slower rise as seen for this geometry in Figures 2 through 5. The three-rod vertical geometry shows sharp changes in the sample area as the interface passes the middle (ii, iii) and upper (iv, v) rods. There is little change between these states. These sharp changes explain the three-region response as shown on Figures 2 through 5. We expect that the separate, nonoverlapping sample areas in air and water shown for the three-rod vertical probes (iv) may explain the complex waveforms collected when the interface lies between the middle and uppermost rods.

CONCLUSIONS

The results of this study demonstrate the utility of the numerical approach to predicting the responses of TDR probes placed in highly heterogeneous media even in the presence of strong dielectric contrasts. The measured and predicted responses were in good agreement for most probes, although there remain discrepancies that will require refinement of both the laboratory and numerical methods. In addition, the spatial weighting factors are shown to provide a unique description of the spatial sensitivity of the probes that can help to explain the probe responses.

Four probe geometries were tested to observe their responses in the vicinity of sharp dielectric boundaries. The two- and three- rod horizontal configurations use horizontal rods placed in the horizontal plane; the two- and three-rod vertical probes used horizontal probes placed in a vertical plane (Figure 1).

The responses of the horizontal probes to the advance of a horizontal liquid interface showed a bias toward the lower dielectric permittivity fluid. The sample areas of these probes were almost entirely restricted to the lower dielectric permittivity fluid until the fluid level reach the midpoint of the probe. As the interface approached the bottom of the rods, the sample area of the three-rod horizontal probes became extremely concentrated in the immediate vicinity of the probes.

The measurements made with two-rod vertical probes showed little change until the interface reached the uppermost rod. This would result in a displacement of an observed wetting front by a distance equal to the rod separation. There was no difference seen between the responses of a two-rod vertical probe with the shield connected to the upper rod and the center conductor connected to the lower rod compared with those of probes with the opposite polarity. The three-rod vertical probes showed a three-region sensitivity. The probes were sensitive to the advance of the liquid interface as the interface approached the middle and upper rods. The change in measured response with the change in interface location was less pronounced in all other regions. The three-rod vertical probe design resulted in poor quality waveforms when the interface was located between the central and upper rods. The sample area

analysis suggests that this may be due to the separation of the sample area into two, non-overlapping regions, with one area residing in each fluid. Further work is necessary to address these problematic waveforms.

REFERENCES

Baker, J. M. and Lascano, R. J., 1988, The spatial sensitivity of time domain reflectometry: Soil Science, **147**, 378-384.

Ferré, P.A., Knight, J. H., Rudolph, D. L., and Kachanoski, R. G., 1998, The sample area of conventional and alternative time domain reflectometry probes: Water Resources Research, **34**, 2971-2979.

----------, 2000, The sensitivity of conventional and alternative time domain reflectometry probes: Water Resources Research, **36**, 2461-2468.

Knight, J.H., 1992, Sensitivity of time domain reflectometry measurements to lateral variations in soil water content: Water Resources Research, **28**, 2345-2352.

Knight, J.H., Ferré, P. A., Rudolph, D. L., and Kachanoski, R. G., 1997, A numerical analysis of the effects of coatings and gaps upon relative dielectric permittivity measurement time domain reflectometry probes: Water Resources Research, **33**, 1455-1460.

Knight, J.H., White, I., and Zegelin, S.J., 1994, Sampling volume of TDR probes used for water content monitoring: Proceedings of the Symposium and Workshop on Time Domain Reflectometry in Environmental, Infrastructure and Mining Applications, 93-104.

Musil, J. and Zacek, F., 1986, Microwave measurement of complex permittivity by free space methods and their application: Elsevier, Amsterdam, 275 pp.

Nissen, H.H., Ferré, P.A., and Moldrup, P., 2001, Metal-coated printed circuit board time domain reflectometry probes for measuring water and solute transport in soil. Submitted for publication in Water Resources Research.

Petersen, L.W., Thomsen, A., Moldrup, P., Jacobsen, O.H., and Rolston, D.E., 1995, High resolution time domain reflectometry - sensitivity dependence on probe design: Soil Science, **159**, 149-154.

Topp, G.C., Davis, J.L., and Annan, A.P., 1980, Electromagnetic determination of soil water content: measurement in coaxial transmission lines: Water Resources Research, **16**, 574-582.

THE SENSITIVITY OF TIME DOMAIN REFLECTOMETRY PROBES TO SPATIALLY HETEROGENEOUS ELECTRICAL CONDUCTIVITIES

Paul A. Ferré[1], Henrik H. Nissen[2], Per Moldrup[3] and John H. Knight[4]

[1]Department of Hydrology and Water Resources,
University of Arizona, USA ty@hwr.arizona.edu
[2]Department of Environmental Engineering, Institute of Life Sciences,
Aalborg University, Denmark i5hn@civil.auc.dk,
[3]Department of Environmental Engineering, Institute of Life Sciences,
Aalborg University, Denmark i5pm@civil.auc.dk
[4]Department of Mathematics, Australian National University
and CSIRO Land and Water, Canberra, Australia john.knight@maths.anu.edu.au

THE UNIVERSITY OF ARIZONA.

ABSTRACT

Numerical models have been applied successfully to the analysis of the sensitivity and spatial sample areas of both conventional and alternative time domain reflectometry (TDR) probes. However, no similar treatment has been presented for the spatial sensitivity of TDR to lateral variations in electrical conductivity, (σ). The objective of this investigation was to examine the response of conventional two- and three-rod probes to sharp changes in σ of the media within their sample areas. Numerical analyses were performed for probes of varying rod diameters and separations for sharp interfaces both parallel to and perpendicular to the plane containing the rods. The results show clear effects of the σ distribution on the probe response that are well described by a numerical model developed to predict the response of TDR probes to laterally heterogeneous dielectric permittivity, K, distributions. We show that if the pore water σ is spatially uniform in the transverse plane then the TDR sample area for K and σ will be nearly identical for standard, uncoated parallel rod probes.

INTRODUCTION

Time domain reflectometry (TDR) is a widely accepted method for volumetric water content (θ) measurement in soils due to its ability to make rapid, nondestructive, automated measurements of θ in a wide range of soils with minimal soil-specific calibration (Topp *et al.*, 1980). In addition, TDR waveforms contain information that can be used to infer the electrical conductivity, σ. of the surrounding medium (Dalton *et al.*, 1984; Dalton and Poss, 1990), allowing for solute transport monitoring in variably saturated media (e.g. Elrick *et al.*, 1992; Kachanoski *et al.*, 1992; Nissen *et al.*, 1998). The ability to monitor volumetric water content and electrolytic solute concentration with a single instrument suggests that TDR can be used to monitor solute transport during transient unsaturated flow (Persson, 1997; Risler *et al.*, 1996). Ferré *et al.* (2000b) point out potential limitations to this approach if θ varies along the TDR probes. A further potential limitation lies in the underlying

assumption that θ and bulk electrical conductivity (σ_a) are measured within the same sample volume for a given probe.

Given that TDR probes are simple and inexpensive to construct and that the flexibility of their design allows for a wide range of modifications, probes can be designed to best-fit specific measurement needs. However, the probe geometry (defined by the number, size, and spacing of the rods), the presence of nonmetallic probe components within the sample area (e.g. resistive coatings), and the distribution of soil electrical properties all influence the spatial sensitivity of a given TDR probe. Knight *et al.* (1997) introduced the use of numerical models to define the spatial sensitivity of TDR probes based on the geometry of the probe and the distribution of dielectric permittivities in the plane transverse to the direction of electromagnetic (EM) wave propagation. Later work showed how these methods can be used to predict the response (Ferré *et al.*, 1998) and the sensitivity distribution (Ferré *et al.*, 2000a) of alternative TDR probe designs that incorporate nonmetallic components in their construction. Recently, the modeling approach has been used directly in the design of alternative probes, minimizing the construction and testing of prototype probes (Nissen *et al.*, 2001). In a companion article in these proceedings, this modeling approach is shown to describe the spatial sensitivity of TDR probes adjacent to sharp dielectric boundaries. While this numerical modeling approach has been shown to be highly effective for predicting the response of alternative TDR probes to variations in K in the plane transverse to the direction of EM wave propagation, no similar analyses have been performed to determine the spatial sensitivity of TDR to variations in the σ_a of the surrounding medium.

OBJECTIVES

The objectives of this investigation were: (i) to develop a theoretical framework for the analysis of the spatial sensitivity of TDR to variations in σ in the plane transverse to the direction of EM wave propagation; (ii) to measure the effects of sharp horizontal gradients in σ in the plane transverse to the direction of EM wave propagation on the TDR-measured σ_a for a range of two- and three-rod probes; (iii) to apply the numerical analyses developed by Knight *et al.* (1997) to describe the spatial sensitivity of TDR to heterogeneous σ distributions in the plane transverse to the direction of EM wave propagation; and (iv) to compare the spatial sensitivity of TDR to dielectric permittivity and electrical conductivity to identify potential limitations to the simultaneous measurement of water content and solute transport with TDR.

THEORY

We present a theoretical basis for the analysis of the spatial sensitivity of TDR to variations in σ in the plane transverse to the direction of EM wave propagation under spatially uniform θ and hence K conditions. The development of this method of analysis draws on parallels to similar developments presented for the spatial sensitivity of TDR to variations in dielectric permittivity in the plane transverse to the direction of EM wave propagation. A more complete description of the latter development is presented in Knight (1992).

THE ELECTRICAL CONDUCTIVITY RESPONSE OF TDR

Dalton *et al.* (1984) first demonstrated that the attenuation of a TDR pulse could be used to estimate σ simultaneously with estimation of soil water content from the pulse speed. Dalton and van Genuchten

(1986) presented an analysis of the physical principles underlying the TDR method for measuring both θ and σ in porous media. We will extend their analysis to investigate the spatial sensitivity of TDR to lateral variations of σ for spatially uniform θ and hence K conditions. Our development will follow that of Knight (1992) for the spatial sensitivity of TDR measurements to small variations of K in the plane transverse to the direction of EM wave propagation.

In an ideal lossless transmission line a wave or pulse propagates at constant speed without energy loss or change of shape. In lossy media, energy loss occurs if there is a series resistance in the direction of propagation, or if there is a shunt conductance through the medium between the conductors. In general the wave speed and attenuation rate are frequency dependent. If the medium between the conductors has an electrical conductivity of s per unit length of material, then this will cause a shunt electrical conductivity G per unit length of transmission line between the conductors. The relationship between G and s depends on the voltage distribution around the conductors, which is determined by their geometrical configuration and the voltages on the conductors. G represents a spatial average of the s distribution around the probe. The spatial weighting function that describes this spatial averaging of s determines the spatial sensitivity of the TDR probe to the σ distribution in the plane transverse to the direction of propagation.

The theory of the wave propagation along lossy transmission lines with spatially uniform parameters is well developed (e.g. Liboff and Dalman, 1985; and Smythe and Yeh, 1972). The voltage $V(z, t)$ and current $I(z, t)$ on the transmission line are assumed to be functions of the time of propagation, t, and the distance along the transmission line, z. Then $V(z, t)$ and $I(z, t)$ satisfy the system of partial differential equations

$$\begin{aligned} \frac{\partial V}{\partial z} &= - RI - L\frac{\partial I}{\partial t} \\ \frac{\partial I}{\partial z} &= - GV - C\frac{\partial V}{\partial t} \end{aligned} \quad , \qquad [1]$$

where L is inductance, R is series resistance, C is capacitance and G is shunt conductance, all expressed per unit length. These equations can be solved readily in the frequency domain if it is assumed that the solutions are periodic with time, t, dependence proportional to the frequency, w, and the imaginary variable, i, as $\exp(iwt)$,

$$\begin{aligned} \frac{\partial V}{\partial z} &= - RI - iwLI \\ \frac{\partial I}{\partial z} &= - GV - iwCV \end{aligned} \qquad [2]$$

Differentiating and combining these equations gives,

$$\frac{\partial^2 V}{\partial z^2} = l^2 V \qquad [3]$$

where the complex propagation constant, l, satisfies

$$l^2 = (R + iwL)(G + iwC) \qquad [4]$$

The general solution of (3) is

$$V(z) = A\exp(-l\,z) + B\exp(l\,z) \qquad [5]$$

where A and B are constants chosen to satisfy the boundary conditions. The propagation constant, l, is usually written in terms of its real and imaginary parts as

$$l = a + ib \qquad [6]$$

The solution of Eq. [1] that decays in the positive z direction is then,

$$V(z,t) = A\exp(-a\,z)\exp i(wt - b\,z) \qquad [7]$$

An EM wave propagating along the transmission line in the direction of positive z is attenuated as exp($-az$) and has speed w/b. In general both the attenuation rate and the wave speed are frequency dependent, giving rise to dispersion for a multiple frequency pulse. In the time domain, a pulse will change shape as the components of different frequencies move at different speeds and experience different attenuation.

If R and G are both zero then there is no energy loss and

$$a = 0 \quad b = w(LC)^{0.5} \qquad [8]$$

and the wave speed is $v = (LC)^{-1/2}$ as is generally assumed in TDR analysis.

The low-loss approximation holds in the lower frequency region in which

$$R << wL \qquad G << wC \qquad [9]$$

For these conditions, the propagation constant can be expanded as a Taylor series to give

$$a = \frac{(LC)^{0.5}}{2}\left(\frac{R}{L} + \frac{G}{C}\right) \quad b = w(LC)^{0.5} \quad v = (LC)^{-0.5} \qquad [10]$$

Previous analyses of the σ response of TDR (e.g. Dalton *et al*., 1984; Yanuka *et al*., 1988; and Topp *et al*., 1988) implicitly use the low-loss approximation. The measured or estimated value of the attenuation

coefficient, a, is used to infer the shunt conductance, G, from Eq. [10]. Then the appropriate formula for the shunt conductance of a transmission line is used to infer the bulk electrical conductivity, s_a.

Equation [10] shows that the wave speed for conditions satisfying the low-loss assumption is the same as the wave speed in the no-loss case. Furthermore, the wave speed and attenuation rate are independent of frequency for the lower frequency band satisfying Eq. [9]. Equation [10] shows further that the losses due to series resistance R and shunt conductance G are additive. As a result, losses due to the imaginary part of the dielectric permittivity and of the σ_a cannot readily be distinguished, as found by Topp *et al*. (2000).

SPATIAL WEIGHTING OF PERMITTIVITY AND ELECTRICAL CONDUCTIVITY BY TDR

The concept of a spatial weighting function was introduced by Baveye and Sposito (1984) and further explored by Cushman (1986). Knight (1992) calculated an approximate spatial weighting function for the response of a TDR probe to small departures from uniformity of the distribution of dielectric permittivity $K(x, y)$ in the lateral (x, y) plane, which is oriented transverse to the direction of propagation. The voltage distribution $V(x, y)$ in the lateral plane satisfies the equation

$$\nabla(K\nabla V) = 0 \qquad [11]$$

with the boundary conditions of constant voltage V_1 on one conductor of a two-rod probe and - V_1 on the other rod. The rod size and separation is chosen to form a representative cross section of a given probe geometry. The spatial weighting function is determined by the normalised energy distribution, which is proportional to the square of the gradient of the voltage distribution satisfying Eq. [11]. The spatial weighting function can be considered as the weighting function that the probe uses to average the spatially heterogeneous $K(x, y)$ distribution to arrive at the transmission line capacitance C in Eq. [1]. Alternatively, the spatially-weighted $K(x, y)$ represents the dielectric permittivity that would be measured with the modeled TDR probe.

Likewise, we can consider a system with uniform K, and examine the effects of small departures from uniformity of the distribution of electrical conductivity s (x, y) in the lateral plane. The voltage distribution $V(x, y)$ in the lateral plane satisfies the equation

$$\nabla(s\nabla V) = 0 \qquad [12]$$

with the boundary conditions of constant voltage V_1 on one conductor of a two-rod probe and - V_1 on the other rod. By analogy with the solution of *Knight* [1992], the apparent measured value of s in the lateral plane then is determined by the same spatial weighting function, which is proportional to the square of the gradient of the voltage distribution. Therefore, the probe can be considered to apply the same spatial weighting function that it used to determine an equivalent C to "average" the electric conductivity distribution to arrive at the transmission line shunt conductance G in equation (1).

For example, the capacitance per unit length, C, of a two-wire transmission line is (Table 5b-3, Smythe and Yeh ,1972),

$$C = \frac{p e_o K}{\cosh^{-1}\left(\frac{s}{d}\right)} \qquad [13]$$

where e_0 is the dielectric permittivity of free space, d is the diameter of each wire, and s is the separation of their axes. Likewise, the conductance per unit length, G, of a two-wire transmission line is (Table 5b-3, Smythe and Yeh,1972),

$$G = \frac{p s}{\cosh^{-1}\left(\frac{s}{d}\right)} \qquad [14]$$

Comparison of equations (13) and (14) shows the equivalence of the geometrical factors applied to the spatial averaging of dielectric permittivity (e_0K) and electrical conductivity (s) by TDR. Based on the similarity of these transmission line responses, we propose that TDR will show identical σ and K responses to equivalent K and s distributions in the transverse plane. Therefore, we present a modified form of the spatial weighting analysis to describe the spatial sensitivity of TDR to σ.

NUMERICAL ANALYSIS OF THE SPATIAL WEIGHTING OF s BY TDR

Early efforts to define the sample area of TDR probes relied on direct measurements of the change in the measured K with changes in the distribution of $K(x, y)$ in the plane transverse to the long axis of TDR probes (Baker and Lascano, 1989). Petersen *et al.* (1995) showed that this approach was able to predict the response of TDR probes buried at shallow depths near the ground surface. No similar investigations have been presented to determine the spatial sensitivity of TDR to lateral σ variations.

Following the development of Knight (1992) and Knight *et al.* (1997), we present a numerical analysis of the spatial weighting function for a given TDR probe geometry. From the preceding development, we propose that this analysis can be used to predict the σC response of TDR probes of any geometry to any spatial distribution of σ in the plane transverse to wave propagation. Full development of the theory underlying the numerical analysis is provided in Knight *et al.* (1997). The approach is based on a finite element solution of the two-dimensional Laplace equation in the transverse plane. Rods are internal boundaries to the domain and are set to constant potentials. The domain is chosen to be sufficiently large that a zero potential and a zero flux boundary condition give the same result. The potential distribution within the domain, $F(x, y)$, is determined for a given $s(x, y)$ distribution. The spatial weighting function, $w(x, y)$, is defined for each element within the domain based on the square of the gradient of the potential across that element.

$$w(x, y) = \frac{\left|\nabla\Phi(x, y)\right|^2}{\iint_\Omega \left|\nabla\Phi_0(x, y)\right|^2 dA}$$

where $F_0(x, y)$ is the potential in a given element for a homogeneous s distribution, Ω is the domain of integration, and dA is the area of the element. The predicted measured σ_a is then,

$$s_a = \iint_\Omega s(x, y) w(x, y) dA$$

The spatial weighting function describes the sensitivity of the instrument to any given point in the domain. The weighting function is defined such that,

$$\iint_\Omega w(x, y) dA = 1$$

The equivalent σ can also be determined for the entire domain based solely on the total electrical flux into or out of the interior constant potential boundaries. In other words, the flux into the domain is a function of the geometry of the system, the boundary conditions, and the $\sigma(x, y)$ distribution. The flux out of the domain can be calculated for a uniform medium as q_0, with the electrical conductivity set to a constant value of s_0. The flux out of the domain can be calculated for any electrical conductivity distribution, $s(x, y)$ as q. Given that the domain geometry and the boundary conditions are unchanged, the effective electrical conductivity of the heterogeneous system is defined as,

$$s_a = \frac{q_0}{q s_0}$$

EXPERIMENTAL AND NUMERICAL METHODS

A box was constructed to allow for the controlled advance of a sharp fluid boundary into and through the sample volume of TDR probes (Figure 1).

The box was constructed of a PVC base and four PVC walls. The inner dimensions of the completed box were 0.3 x 0.3 x 0.3 m. Two opposite walls included a transparent PVC window to allow for visual location of a liquid-air interface within the box. The remaining two opposite

Figure 1: *Photograph of the experimental setup showing the box, fluid delivery system, cable tester and balance. The balance and cable tester are both connected to a PC for automatic data acquisition. The setup is shown for a two-rod vertical probe configuration (35.0-mm rod separation). Turning the insets 90 ° will change the setup to the horizontal case. Note that the air-fluid interface has just passed the upper rod.*

walls included a circular inset with five NPT threaded holes capable of accommodating Swagelok male connector tube fittings. Using these fittings, rods of diameters equal to 3.2, 4.6 and 6.4 mm can be inserted through the box walls. The effective length of the probe rods inside the box is approximately 285 mm. Two and three-rod probes can be formed with outer rod spacings equal to 17.5, 35.0, 52.5, and 70.0 mm for the two-rod probe and 35.0 and 70.0 mm for the three-rod probe, respectively. The circular insets can rotate to six different positions, allowing the probe axis passing through the center of the probe rods to lie in the horizontal plane, the vertical plane, or 45^o from the horizontal. For these experiments, we used probes formed by placing horizontal rods in the horizontal plane (referred to as horizontal probes) and horizontal rods placed in the vertical plane (referred to as vertical probes). Figure 2 shows a representative cross section through a vertical two-rod probe and through a horizontal three-rod probe.

The box was placed on a Sartorius IC 34000 P balance with 0.5 g precision, which was interrogated every 19 seconds. A Tektronix 1502B cable tester was connected to the TDR probe and a waveform was collected every 19 seconds using TACQ software from Dynamax. Demineralized water was used for testing. To alter σof the water, KCl was added to 0.001M and 0.005 M. Each solution was tested separately. Solution was added slowly at the bottom of the box through a vertical tube. The distance between the liquid-air interface was determined from the change in mass, the fluid density added and the cross sectional area of the box. This was checked visually at the time at which the interface reached the bottom and top of the probe rods.

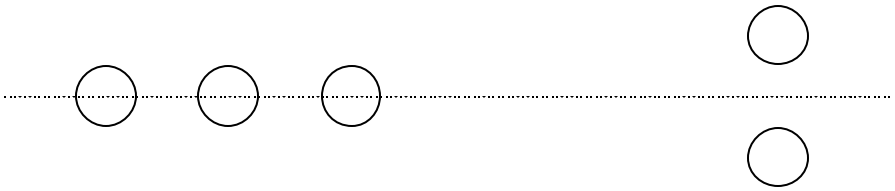

Fig. 2. *Schematic diagram of a three-rod horizontal probe (left) and a two-rod vertical probe (right). The horizontal line shows the height of the midpoint of the probes. All measurements are related to this midpoint.*

Legend	Number of Rods	Rod Diam. [mm]	Rod Sep. [mm]	Fluid	Orientation
A	2	6.35	70	Dem. water	Horizontal
B	2	6.35	70	0.001 KCl	Horizontal
C	2	6.35	70	0.005 KCl	Horizontal
D	2	6.35	70	Dem. water	Vertical
E	2	6.35	70	0.001 KCl	Vertical
F1	2	6.35	70	0.005 KCl	Vertical
F2	2	6.35	70	0.005 KCl	Vertical
G	3	6.35	70	Dem. water	Horizontal
H	3	6.35	70	0.001 KCl	Horizontal
I	3	6.35	70	0.005 KCl	Horizontal
J	3	6.35	70	Dem. water	Vertical
K	3	6.35	70	0.001 KCl	Vertical
L	3	6.35	70	0.005 KCl	Vertical

Table 1. *Legend describing the rod geometrics and fluids used for all 13 experiments. Note that for experiment F1 the shield was connected to the upper rod; for experiment F2 these connections were reversed.*

A finite element grid was constructed for each probe geometry. For this investigation the model was defined for 13 probe/fluid combinations, as described in Table 1. For each simulation, the domain was divided into 60 layers to model a series of liquid-air interfaces. However, in most cases some of the layers were pooled in areas of low sensitivity to reduce the modeling task. Approximately 16000 elements were used to discretize the domain. The run time for each liquid-air interface location was approximately 1 minute.

RESULTS AND DISCUSSION

The experimental and numerical results will be presented in two sections: directly measured influences of sharp electrical conductivity boundaries on probe responses, and comparisons of the measured and predicted probe responses.

MEASURED PROBE RESPONSES

The electrical conductivities determined directly from TDR measured signal loss are shown as a function of the depth of water in the box in Figure 3. The center height of the top and bottom rods are shown for vertical configurations. The center height of the probe is shown for all configurations. Each data series represents the measured σ at a series of interface heights for a single probe geometry. The data series label refers to Table 1. The probe geometry is shown graphically above the legend as a representative cross section of the probe.

For each probe geometry there is a clear distinction between the σ responses when they are immersed in air, 0.001M KCl and 0.005 M KCl. However, there is very little difference between the σ response in air and in demineralized water. The two- and three- rod horizontal probes show a sharp increase in σ when the fluid makes contact with the lowest edge of the rods. The probe response is more complex for the vertical probe orientations. For the two-rod vertical probe, the observed sharp rise in σ does not occur until the interface reaches the lowest edge of the uppermost rod. The response of the three-rod vertical probe shows two distinct regions. The first rise in measured σ occurs when the fluid interface contacts the lowest edge of the center rod. A second increase occurs when the interface contacts the base of the uppermost rod. Although the waveforms between these discontinuities show multiple peaks, making automated travel time analysis difficult, there was no difficulty in identifying the final amplitude from the waveforms. Therefore, the σ response is well behaved for all interface locations.

COMPARISON OF PREDICTED AND MEASURED PROBE RESPONSES

To compare the predicted response with the measured σ and K responses, all responses and predictions were normalized using the values corresponding to measurements in air and the advancing fluid. The normalized measured dielectric permittivities for the 0.001M KCl are shown as squares in Figures 4 and 5; the 0.005M KCl solution results are shown as triangles. There was no significant difference in the σ of air and demineralized water; therefore, the normalization led to large relative errors in the measurements. The solid lines represent the model-predicted cumulative weighting function summed from the base of the box to a given height. Discussions will be grouped as follows: (i) two- and three-rod horizontal probes (B, C, H, I), (ii) two-rod vertical probes (E, F1, F2), and (iii) three-rod vertical probes (K, L).

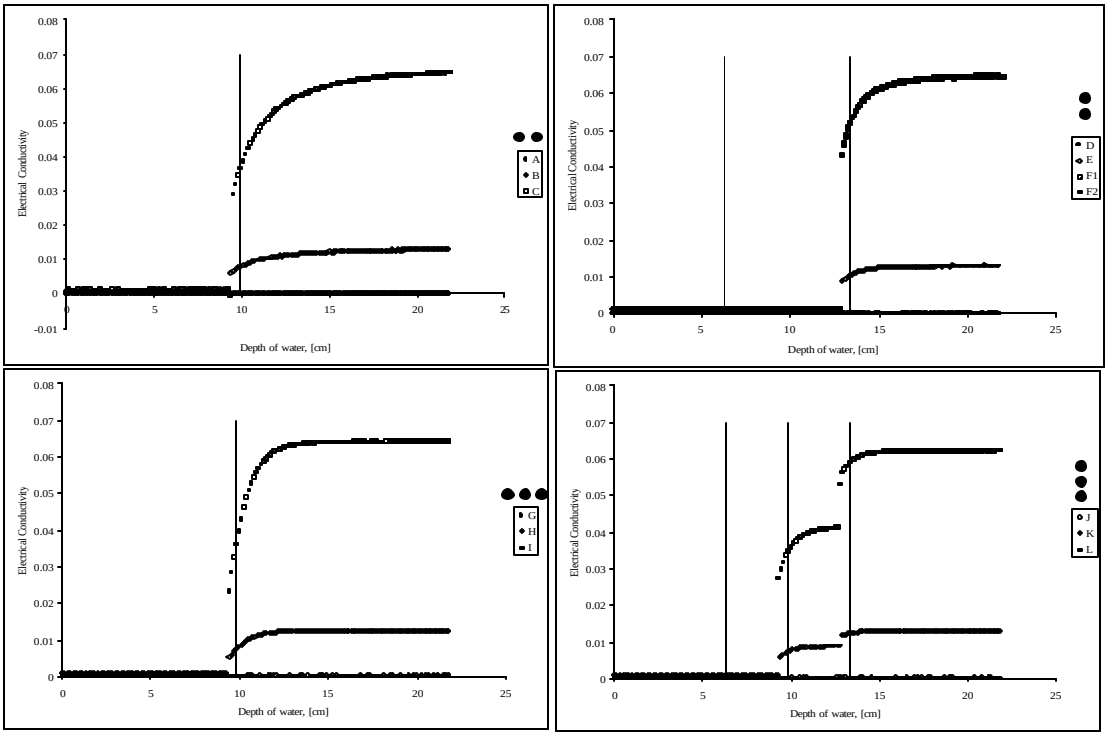

Fig. 3. *Measured electrical conductivity (s) as a function of the depth of solution in the box. Three fluids were used: demineralized water (circles), 0.001M KCl (diamonds) and 0.005M KCl (squares). Four probe geometries were tested, as shown schematically as a representative cross section above each legend. The probe/fluid combinations are referenced in the legend to Table 1. For vertical geometries, the midheights of the rods are shown as vertical lines. The elevation of the center of all of the rods is shown as a single line for the horizontal configurations.*

HORIZONTAL PROBES

The model and all of the measurements (B, C, H, I) show a response that is skewed about the height of the middle of the probe with a sharper response as the interface approaches the probe midpoint from below followed by a slower response as the interface continues to rise. This indicates that both the σ and the K responses are more sensitive to the medium with a lower *K* or *s* when the interface is between the rods. The three-rod probe response is sharper than the two-rod response.

For the two-rod cases (B and C) the modeled cumulative weighting function shows better agreement with the measured *K* than with the measured σ. For the three-rod cases (H and I) there is very little difference among the measured and modeled responses. This agreement demonstrates that the spatial weighting approach based on the energy distribution describes the spatial sensitivity of TDR to both the dielectric permittivity and the electrical conductivity even in the presence of sharp contrasts in *K* and *s* in the transverse plane.

TWO-ROD VERTICAL PROBES

The measured *K* and σ both show very good agreement with the model predictions for this probe geometry. The probe showed very little response until the interface reached the base of the upper rod. Furthermore, the polarity of the probe (connection of either the upper or lower to the shield) had no

effect on either the *K* or the σ response, demonstrating that two-rod probes can be used without a balun with no effect on their response or sample area.

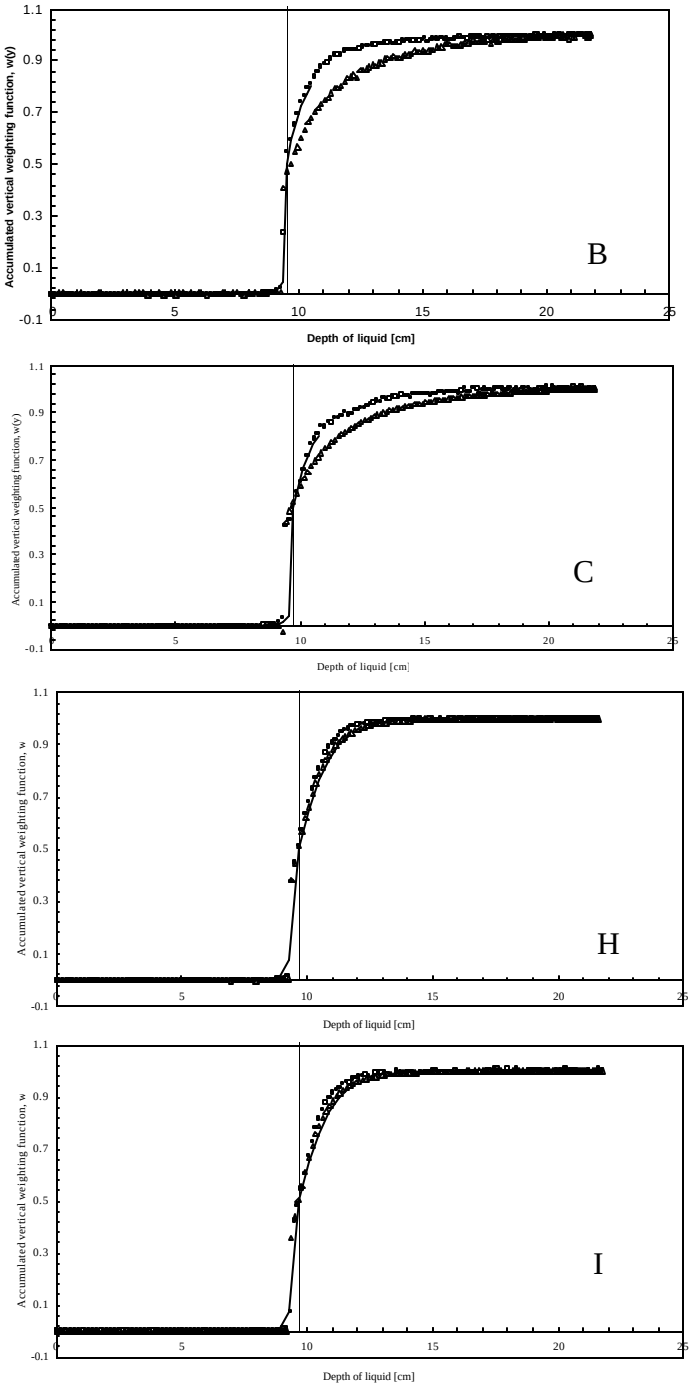

Fig. 4. *Normalized measured dielectric permittivity, K, (squares) and electrical conductivity, s, (triangles) and model predicted cumulative weighting functions (line) as a function of the depth of solution. The probe center height is shown as a vertical line. Probe geometries and fluid compositions are referenced to Table 1.*

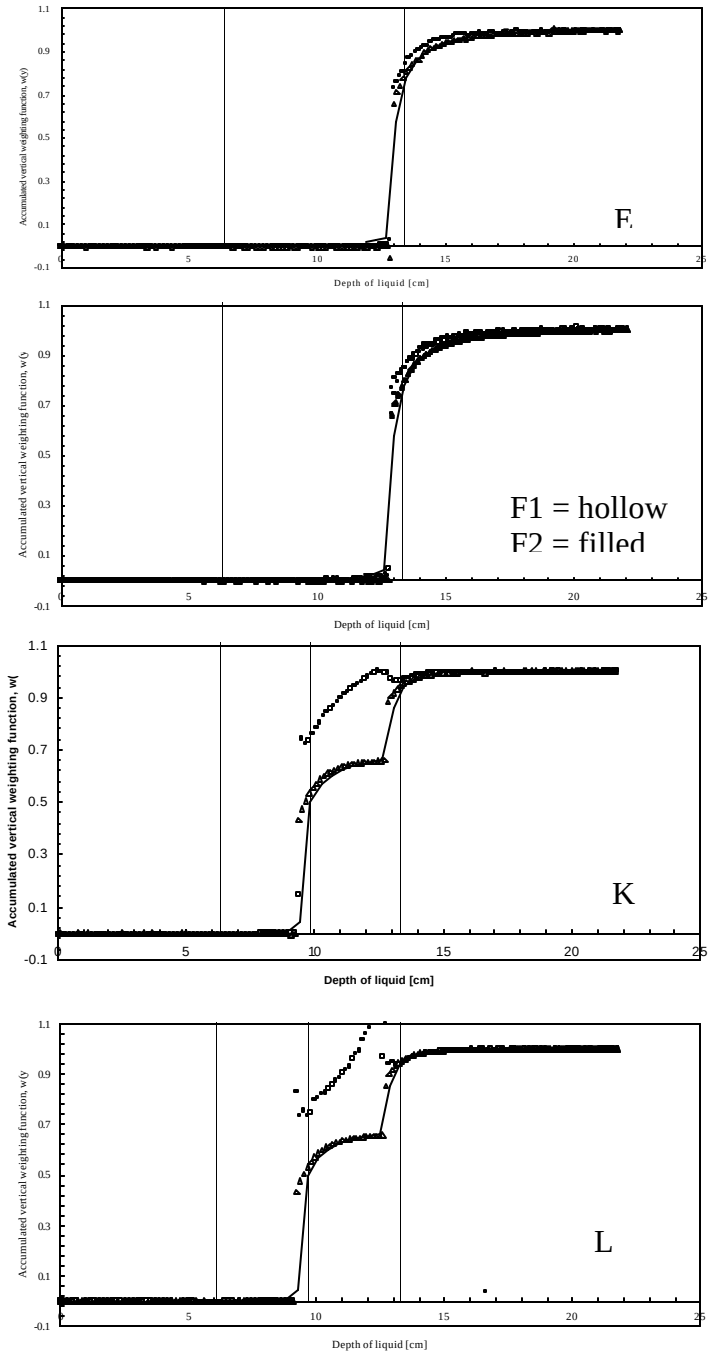

Fig. 5. *Normalized measured dielectric permittivity, K, (squares) and electrical conductivity, s, (triangles) and model predicted cumulative weighting functions (line) as a function of the depth of solution. The uppermost and lowermost rod center heights are shown as vertical lines for all probes. A vertical line also indicate the center height of the middle rod for the three-rod probe. Probe geometries and fluid compositions are referenced to Table 1.*

THREE-ROD VERTICAL PROBES

As shown in a companion article in these proceedings, the measured *K* response of vertical three-rod probes shows poor agreement with the model predictions when the interface is located between the middle and uppermost probes. They conclude that this is due to difficulties in interpreting the complex waveforms that arise with the interface in these locations. This conclusion is supported by the excellent agreement between the model prediction and the measured σ response. The preceding discussion demonstrates that the *K* and σ sample areas of TDR probes are nearly identical for similar *K* and *s* distributions in the plane transverse to the direction of EM wave propagation. This suggests further that the *K* response should follow the model prediction for the three-rod vertical case, as does the *s* response, and that the disagreement is due to errors in waveform interpretation.

CONCLUSIONS

The measured probe responses demonstrate that the σ of a high conductivity medium cannot be measured without making physical contact with that medium. However, σ of a low conductivity medium can be measured through a high conducting medium. One result of this is that air gaps around probes may have a more pronounced effect on the σ reasponse than on the K response.

There is good agreement between the normalized measured σ and the model-predicted cumulative weighting function. The only exception is the two-rod horizontal geometry. For some cases, such as three-rod vertical probes, the σ response shows better agreement with the model predictions than does the *K* response. This general agreement demonstrates that the spatial weighting approach developed to predict the response of TDR probes to laterally heterogeneous dielectric permittivities can be used to predict the σ response as well. Furthermore, this indicates that the spatial sensitivity of TDR to K and σ are very similar for similar *K* and *s* distributions in the plane transverse to the direction of EM wave propagation. Given that both K and σ show a second order dependence on θ, this suggests that the *K* and σ sample areas may be very similar even if θ varies in the transverse plane. However, if the pore water σ varies laterally, these sample areas will be different.

REFERENCES

Baker, J. M. and Lascano, R. J., 1988, The spatial sensitivity of time domain reflectometry: Soil Science, **147**, 378-384.

Baveye, P., and Sposito, G., 1984, The operational significance of the continuum hypothesis in the theory of water movement through soils and aquifers: Water Resources Research, **20**, 521-530.

Cushman, J.L., 1986, On measurement, scale, and scaling: Water Resources Research, **22**, 129-134.

Dalton, F. N., Herkelrath, W. N., Rawlins, D. S., and Rhoades, J. D., 1984, Time domain reflectometry: Simultaneous measurement of soil water content and electrical conductivity with a single probe: Science, **224**, 989-990.

Dalton, F.N., and van Genuchten, M.Th., 1986, The time-domain reflectometry method for measuring soil water content and salinity: Geoderma, **38**, 237-250.

Dalton, F. N. and Poss, J. A., 1990, Soil water content and salinity assessment for irrigation scheduling using time domain reflectometry: Principles and application: Acta Horticulturae, **278**, 381-392.

Elrick, D. E., Kachanoski, R. G., Pringle, E. A., and Ward, A., 1992, Parameter estimates of field solute transport models based on time domain reflectometry measurements: Soil Science Society of America Journal, **56**, 1663-1666.

Ferré, P.A., Knight, J.H., Rudolph, D.L., and Kachanoski, R.G., 1998, The sample area of conventional and alternative time domain reflectometry probes: Water Resources Research, **34**, 2971-2979.

----------, 2000a, The sensitivity of conventional and alternative time domain reflectometry probes: Water Resources Research, **36**, 2461-2468.

Ferré, P.A., Rudolph, D.L., and Kachanoski, R.G., 2000b, Identifying the Conditions Amenable to the Determination of Solute Concentrations with Time Domain Reflectometry: Water Resources Research, **36**, 633-636.

Kachanoski, R. G., Pringle, E., and Ward, A., 1992, Field measurement of solute travel times using time domain reflectometry: Soil Science Society of America Journal, **56**, 47-52.

Knight, J.H., 1992, Sensitivity of time domain reflectometry measurements to lateral variations in soil water content: Water Resources Research, **28**, 2345-2352.

Knight, J.H., Ferré, P.A., Rudolph D.L., and Kachanoski, R.G., 1997, A numerical analysis of the effects of coatings and gaps upon relative dielectric permittivity measurement time domain reflectometry probes: Water Resources Research, **33**, 1455-1460.

Liboff, R.L., and Dalman, G.C., 1985, Transmission lines, waveguides, and Smith charts. Macmillan, New York, 269 pp.

Nissen, H. H., Moldrup, P., and Henriksen, K., 1998, Time domain reflectometry measurements of nitrate transport in manure-amended soil: Soil Science Society of America Journal, **62**, 99-109.

Nissen, H.H., Ferré, P.A., and Moldrup, P., 2001. Metal-coated printed circuit board time domain reflectometry probes for measuring water and solute transport in soil. Submitted for publication in Water Resources Research.

Persson, M., 1997, Soil solution electrical conductivity measurements under transient conditions using time domain reflectometry: Soil Science Society of America Journal, **61**, 997-1003.

Petersen, L.W., Thomsen, A., Moldrup, P., Jacobsen O.H., and Rolston, D.E., 1995, High resolution time domain reflectometry - sensitivity dependence on probe design: Soil Science, **159**, 149-154.

Risler, P. D., Wraith, J. M., and Gaber, H. M., 1996, Solute transport under transient flow conditions estimated using time domain reflectometry: Soil Science Society of America Journal, **60**, 1297-1305.

Smythe, W.R., and Yeh, C., Section 5b: Formulas. In "American Institute of Physics Handbook", edited by D.E. Gray, 3rd edition, McGraw-Hill Book Company, New York, 5-106, 1972.

Topp, G.C., Davis, J.L., and Annan, A.P., 1980, Electromagnetic determination of soil water content: measurement in coaxial transmission lines: Water Resources Research, **16**, 574-582.

Topp, G.C., Zegelin, S., and White, I., 2000, Impacts of the real and imaginary components of relative permittivity on time domain reflectometry measurements in soils: Soil Science Society of America Journal, **64**, 1244-1252.

Topp, G.C., Yanuka, M., Zebchuk, W.D., and Zegelin, S., 1988, Determination of electrical conductivity using time domain reflectometry: soil and water experiments in coaxial lines: Water Resources Research, **24**, 945-952.

----------, 1988, Multiple reflections and attenuation of time domain reflectometry pulses: Theoretical considerations for applications to soil and water: Water Resources Research, **24**, 939-944.

SALINE CLAYEY SOIL MOISTURE MEASUREMENT USING TIME-DOMAIN REFLECTOMERY

Z.J. Sun[1] and G.D. Young[2]

[1]E.S.I. Environmental Sensors Inc., 100-4243 Glanford Avenue, Victoria, British Columbia, Canada. V8Z 4B9; jason@esica.com
[2]E.S.I. Environmental Sensors Inc., 100-4243 Glanford Avenue, Victoria, British Columbia, Canada. V8Z 4B9; jyoung@esica.com

ABSTRACT

Laboratory experiments were conducted to explore the effects of bound water and soil electrical conductivity (EC) on soil moisture determination using time-domain reflectometry (TDR) in saline clayey soil. The elevated soil EC increases both the rise time of the reflected signal and the total time delay, resulting in overestimation of soil moisture. The bound water in clayey soil reduces the time delay because of its lower dielectric constant, resulting in underestimation of soil water content. There is a turning point moisture, at which, the effect of bound water is balanced by the effect of soil electrical conductivity. Below this point bound water effect dominates and TDR underestimates soil moisture. Above this point the effect of soil EC dominates and TDR overestimates soil moisture. This turning point moisture decreases as the soil salinity increases. The linear calibration (T/T_{air} *vs*. volumetric water where T/T_{air} is the ratio of propagation time in soil to that in air over the same distance) is no longer valid for saline clayey soil. A logarithm calibration has been developed and this relation includes soil EC as a parameter. It is also possible to estimate the amount of bound water in a soil sample from the turning point moisture. The dielectric constant of bound water and number of water molecular layers are attached to the soil particle surface are estimated. A four-phase dielectric-mixing model works well for non-saline Rideau Clay.

INTRODUCTION

Time-domain reflectometry (TDR) has been used to measure moisture of non-saline sandy and loamy soils with great successes (Topp *et al*., 1980; Hook *et al*., 1992; Topp and Ferre, 1998; Sun *et al*., 2000). The semi-empirical relationship between the time delay and volumetric soil water content has been established (Alharthi and Lange, 1987; Roth *et al*., 1990; Sun, 1995). For example, linear equation (1) presented below is widely used to convert time delay (T/T_{air}) to volumetric water content θ.

$$\theta = (T/T_{air} - T_s/T_{air})/(\sqrt{\varepsilon_w}-1) \quad [1]$$

where ε_w is the dielectric constant of free water and T_s/T_{air} is soil type related parameter, for loamy soil, $T_s/T_{air} = 1.55$ (Hook and Livingston, 1996). T/T_{air} is the ratio of propagation time in soil being tested to that in air over the same distance. It is not difficult to prove that T/T_{air} equals the square root of the dielectric constant of the medium, in which the signal is travelling. This equation is based on a three-phase dielectric-mixing model with a geometry related parameter $\alpha = 0.5$. However numerous reports have revealed that in clay soil there is a discrepancy in measured soil moisture between TDR and standard oven-drying method. The relationship between volumetric soil water content measured apparent dielectric constant also deviates from the established relationships, i.e. Topp's polynomial universal equation and some linear equations (Dasberg and Hopmans, 1992; Whalley, 1993; Hook and Livingston, 1996; Yu *et al*., 1999). The source of the discrepancy and deviation has not been completely identified and understood.

There are several possible causes:

(1) Bound water

The polarization of bound water molecules is impeded by high electrostatic attraction from the negatively charged clay particle surface (Shang, 1994). Reduced polarization will result in much lower dielectric constant. For bound water that is directly attached to the soil particle surface, the dielectric constant is only 3.2, which will lead to a faster propagating velocity and shorter time delay. Therefore, the effect of bound water tends to underestimate soil water content. In sandy and loamy soil, the specific surface and the bonding force for water molecules are too small to have significant consequence. However in clayey soil, the specific surface is large and the affinity towards water molecules is strong, therefore the effect of bound water has to be taken into consideration.

(2) The bulk soil electrical conductivity (EC_b).

EC_b consists of soil particle surface electrical conductivity (EC_s) and soil solution conductivity (EC_w). The effect of EC_b on TDR moisture measurement has long been observed (Topp *et al*., 1980, White *et al*., 1994, Malicki *et al*., 1994, Sun *et al*., 2000). The elevated EC_b causes dispersion of the reflected signal, resulting in longer rise time, and evidence showed that there is a rise time related measurement error (Hook and Livingston, 1995). Meanwhile the signal is attenuated by energy dissipation through current flow making the detection of final reflection signal very difficult, if it is still possible. The elevated EC_b also increases the apparent dielectric constant (White *et al*., 1994, Sun *et al*., 2000), leading to an overestimated soil water content. Early in 1955, O'Konski described that in a colloid a semi-conducting surface can arise due to a distribution of charge density and induce extra polarization (O'Konski, 1955). This interfacial polarization may interact with TDR signal and impede its propagation.

Clearly there are two major challenges in using TDR to measure soil water content in soils with large clay content. The bound water effect leads to underestimate soil water content because of its lower dielectric constant, and the soil electrical conductivity leads to overestimating soil water content. At lower soil water content, the volume fraction of bound water to total water is higher and the EC_b is low (Rhoads *et al*., 1989), resulting in an underestimation of water content. At high soil water content, the ratio of bound water to total water is small and EC_b is large, then, the overestimation dominates the

measurement. For a specific soil, there should be a turning point, at this water content, the effect of bound water is balanced by that of soil electrical conductivity. This turning point water content varies according to soil texture (especially clay content) and soil salinity. The purpose of this study is to explore the combination effects of bound water and soil electrical conductivity on water content measurement using TDR in clayey soils. This study is the second part of a series study of the effect of soil salinity on TDR soil water content measurement (Sun *et al*., 2000). We hope that the experimental results presented here could be useful for further improvement of the performance of TDR soil moisture measurement in clayey soils.

MATERIALS AND METHODS

Rideau Clay from Ottawa area, Canada was used in the experiment. The soil consists of approximately 50% of clay, 46% of silt and 4% of sand. Meanwhile a clayey loam collected from Saanich, Victoria, BC, Canada was used for comparison. The TDR instrument used for soil moisture and time delay measurements was Moisture Point MP-917 (E.S.I. Environmental Sensors Inc., Victoria, BC, Canada) with a 30 cm long probe having switching diodes mounted at both ends of the probe (Hook *et al*., 1992). The oven-dry method determined volumetric soil water content was used as the standard reference. The details of the experimental arrangement were outlined in a previous paper (Sun *et al*., 2000). The moisture equilibrium time for clayey soil is very long because of its low hydraulic conductivity. Therefore the soil was mixed throughout with added water in a plastic box before re-packing back into a PVC cylinder each time. The tested volumetric water content ranged from zero to 0.50 m^3/m^3 with approximately 0.05 m^3/m^3 increment.

Adding solution with different KCl concentration to the testing soil generated different soil salinity. The amount of KCl added each time was calculated in a way that makes the electrical conductivity of soil saturated extract (EC_e) having the value of 1 dS/m, 4 dS/m, 6 dS/m, 8 dS/m and 16 dS/m. The salt concentration of soil solution was high when soil moisture was low, however the amount of KCl remained the same for each designed EC_e at different moisture levels. A K320 Microcomputer Conductometer (Consort pvba, Turnhout, Belgium) was used to measure EC_e.

RESULTS AND DISCUSSION

The Effects of Bound Water

Figure 1 shows the relationship between time delay (expressed as T/T_{air}) and gravimetric method determined reference volumetric soil water content for non-saline Rideau Clay. It substantially deviates from the linear pattern as predicted by equation (1). For each measured time delay, the displayed moisture that was calculated using a three phase, square root dielectric mixing model is small than the reference moisture. This underestimation is the result of the existence of large amount of bound water. Only at very high moisture level, when the volume fraction of bound water to total water is very small, then the effect of bound water can be neglected. When Topp's universal calibration (Topp *et al*. 1980) was applied, the underestimation is almost as the same as using three phases, square root dielectric mixing model.

In non-saline soil, the clay content determines the extent of underestimation of soil water content. In Figure 2, a Saanich clay loam with 35% of clay content shows much less underestimation and the effect of bound water can be neglected when soil moisture is just above 0.20 m^3/m^3.

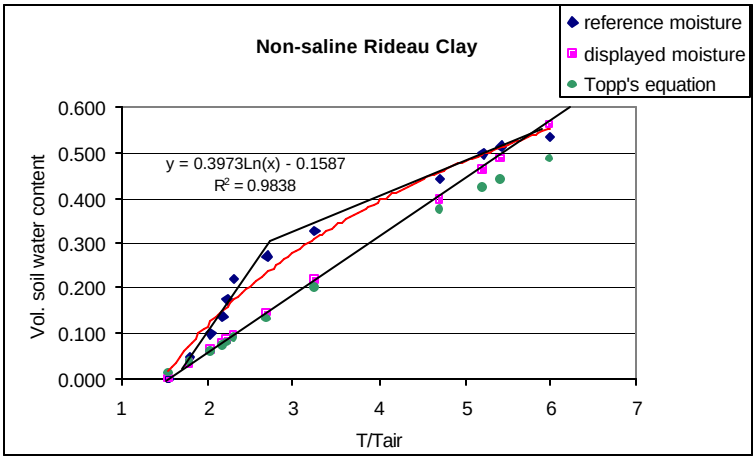

Fig. 1. *The relationship between time delay (T/Tair) and volumetric Water content for Rideau Clay. The displayed moisture was calculated from measured T/Tair using three-phase square root dielectric mixing model.*

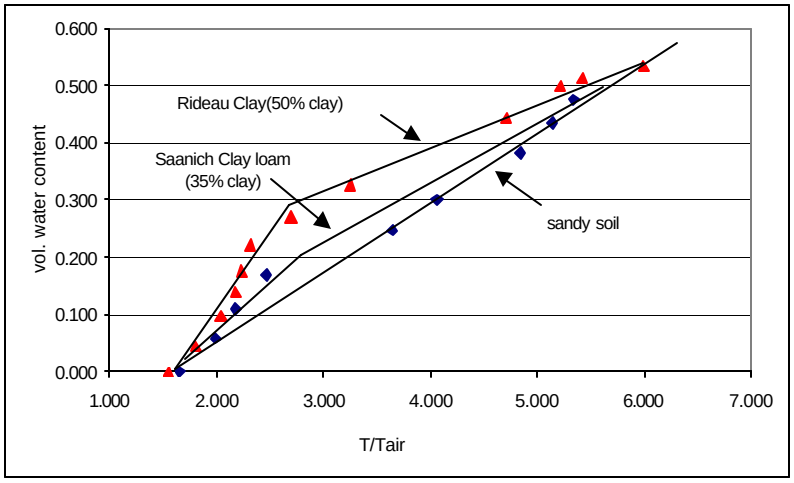

Fig. 2. *The comparison of the relationship between T/T_{air} and volumetric Water content between Rideau Clay and Saanich clay loam*

The effect of soil electrical conductivity

Figure 3 show the relationship between time delay and volumetric water content at different soil saturated extract electrical conductivity (EC_e). At the same volumetric water content, the time delay increases as EC_e increasing. At saturation (0.50 m^3/m^3), the time delay (T/Tair) increased from 5.544 to 6.854 to 7.872 as EC_e increased from 4 dS/m to 8 dS/m to 16 dS/m. If equation (1) is applied the calculated soil water content will be 0.496 m^3/m^3, 0.661 m^3/m^3 and 0.785 m^3/m^3 correspondingly. Therefore, the effect of soil salinity has to be taken into account when EC_e exceeds 4 dS/m in clayey soil condition.

The soil electrical conductivity also causes signal attenuation and dispersion, resulting in smaller signal amplitude and longer rise time. Figure 4 shows the recorded 255-points waveforms. When the EC_e increased from 4 dS/m to 16 dS/m, the signal amplitude is reduced more than 50%. The rise time was tripled when EC_e increased from less than 1dS/m to 4 dS/m.

It is better to use logarithm regression instead of a linear one to describe the relationship between time delay (T/T_{air}) and volumetric water content for saline Rideau Clay. The general form of the logarithm calibration is given as: $\theta_v = C_1 \ln(T/T_{air}) + C_2$, where C_1 and C_2 are EC_e related parameters and they can be determined experimentally. This is the same expression used for saline sandy soil (Sun et. al. 2000).

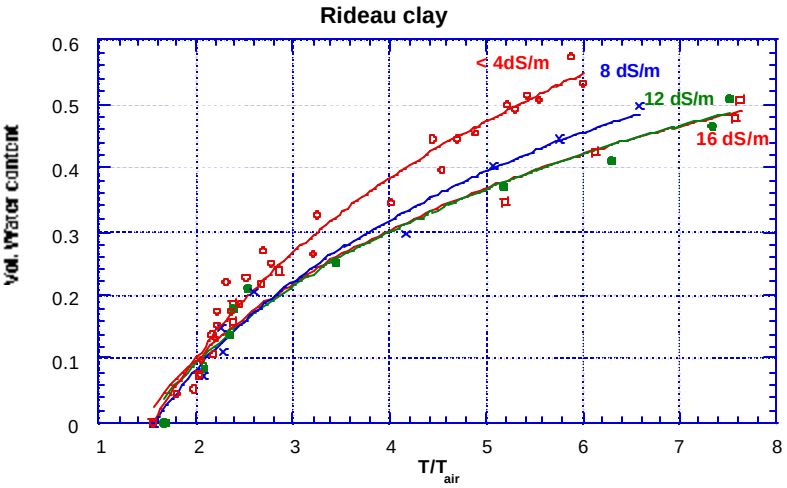

Fig.3 *The relationship between T/T_{air} and volumetric soil water content for Rideau Clay at different electrical conductivity. Lines are by regression - see text.*

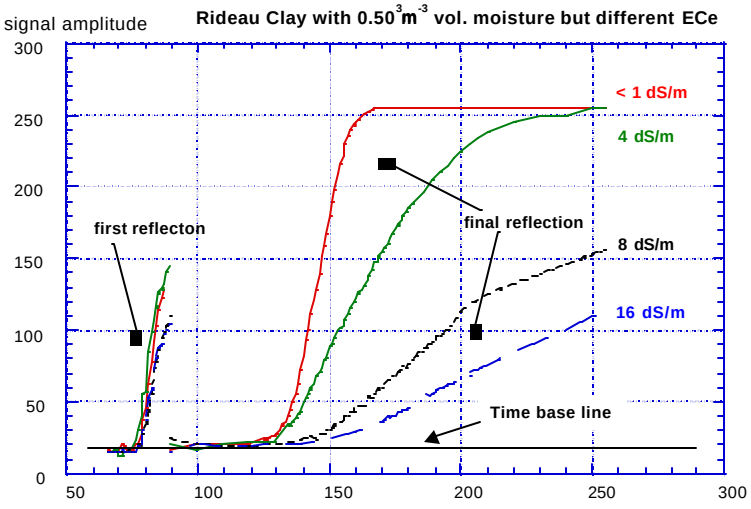

Fig. 4. *The amplitude and rise time of the first and final reflections of TDR signal in Rideau Clay at different electrical conductivity.*

The Combination Effect of Bound Water and Soil Electrical Conductivity in Clay Soil

Table 1 shows the calculated soil water content using logarithm calibration and measured T/T_{air} value for saline sand and saline Rideau clay both are having EC_e of 12 dS/m.

The logarithm calibration equations for saline sand and Rideau Clay are empirically fits using the measured time delays and standard moisture references with 0.98 and 0.99 regression coefficient. So it is reasonable to assume that the water contents presented in column two and four are very close to the actual soil water content at each T/T_{air} value.

When EC_e at 12 dS/m the water content calculated using linear calibration (third column) is larger than the actual water content in sandy soil for moisture range from less than 0.03 m^3/m^3 to 0.34 m^3/m^3. It is interesting to find that for Rideau Clay there is a turning point water content, below this level, the linear calibration UNDERESTIMATES water content, and it switches to OVERESTIMATES when soil moisture exceeds this level. For Rideau clay with EC_e of 12 dS/m, this turning point soil water content is at approximately 0.30 m^3/m^3. Below this point, bound water effect dominates, leading to an underestimation of water content when using the linear equation that doesn't include the bound water as an independent phase. Beyond this point, soil electrical conductivity effect dominates, leading to overestimation of water content. At 0.30 m^3/m^3 water content, the effect of bound water is balanced by the effect of soil electrical conductivity. The linear equation can only give correct water content at this point. This turning point will move to high moisture range when soil clay content increases and/or soil salinity decreases, and move to lower moisture range when clay content decreases and/or soil salinity increases. For example, the turning point for a clayey loam from Regain, Sask. Canada (approximately 39 % of clay), the turning point is 0.232 m^3/m^3 and it moves to 0.525m^3/m^3 for non-saline Rideau Clay (50% of clay).

Figure 5 shows how the turning point soil water content changes with soil electrical conductivity. It is noticed that there are two plateaus in the curve, one is at low EC_e (< 4.0 dS/m) but high moisture (0.50-0.52 m^3/m^3) range and the other is in high EC_e (>15 dS/m) but low moisture (0.21-0.22 m^3/m^3) range. Previous experimental results in sandy soil indicated that there is no noticeable overestimation of soil water content measured by TDR for EC_e up to 3.27 dS/m. For clay soil, the electrical conductivity of soil particle surface (EC_s) is an extra, however the EC_s calculated using the formula suggested by Rhoades (Rhoades *et al*. 1989) turned to be only 1.1 dS/m. The low total electrical conductivity doesn't cause a noticeable overestimation of soil water content, meanwhile, the negligible bound water effect at high moisture range doesn't cause a significant underestimation of soil water content. This explains why the turning point soil water content didn't change, resulting in the first plateau. On the other hand, if the soil moisture is low and most remaining water molecules are those being bound to particle surface, and they contribute little to ionic current flow. The migration of ions in soil meets great resistance, so there is no significant signal attenuation even EC_e is high. This may be the reason for the appearance of the second plateau at low moisture range. Therefore the second plateau can only be formed when all the remaining water molecules in soil are being bound to soil particle surface to some extent. One may infer from Fig.5 that the remaining bound water is at volume fraction of 0.21-0.22 m^3/m^3 range for the test Rideau Clay.

In general, the volume fraction of bound water can be estimated by (Dirksen and Dasberg, 1993)

$$\theta_b = l\delta\rho_b S \qquad [2]$$

where l is the number of molecular water layers of tightly bound water; $\delta = 3 \times 10^{-10}$ m is the thickness of one molecular water layer, ρ_b is the bulk density, and S is the specific surface. The tested Rideau clay has the bulk density of 1.20 g/cm^3 and specific surface of 150 m^2/g. If the volume fraction of tightly bound water molecules is 0.215 m^3/m^3 as inferred from the second plateau in Figure 5, then the

T/T_{air}	Sand EC_e=12 dS/m $\theta = 0.2796\ln(T/T_{air})-0.1597$ R^2=0.99	General linear calibration $\theta = (T/T_{air}- T_s/T_{air})/(\sqrt{\varepsilon_w}-1)$	Rideau Clay EC_e=12 dS/m $\theta = 0.2981\ln(T/T_{air})-0.1136$ R^2=0.98
2.00	0.034	0.050	0.093
2.50	0.096	0.113	0.160
3.00	0.147	0.176	0.214
3.50	0.191	0.239	0.260
4.00	0.228	0.302	0.300
4.50	0.261	0.365	0.335
5.00	0.290	0.428	0.366
5.50	0.317	0.491	0.395
6.00	0.341	0.554	0.420

- Ts/T_{air} =1.60 and ε_w = 80 are used in linear calibration.
- The third column shows the water content that would be calculated from T/Tair measurement using three-phase square root dielectric mixing model.

Table 1. *The calculated volumetric water content using linear regression and logarithm regression for sandy soil and Rideau Clay both having12 dS/m EC_e*

EC_e (dS/m)	Water content m^3/m^3	Time delay T/T_{air}	Standard deviation (n ≥100)
4	0.225	2.687	0.034
8	0.214	2.603	0.021
16	0.200	2.750	0.025

Table 2. *The measured time delay at 0.21-0.22 m^3/m^3 water content but different EC_e*

calculated number of molecular water layer *l* is 3.9 using equation (2). This indicates that the four layers of water molecules that are closes to the particle surface contribute little to ion migration. This is further proved by the measured time delay. Table 2 shows that in 0.21-0.22 m^3/m^3 soil water content range, the measured time delays have no significant difference for EC_e from 4 dS/m up to 16 dS/m.

It cannot be over-emphasized that clay mineral plays an important role in water content measurement using TDR because (a) Different clay minerals have different specific surface that determines the volume fraction of bound water, and (b) Different clay minerals have different surface electrical charge density, surface electrical potential and ionic holding capacity that determines the numbers of ions held by particle surfaces that can be released into soil solution when the soil become wet. The effect of clay mineral types on TDR soil moisture determination is currently under investigation at ESI.

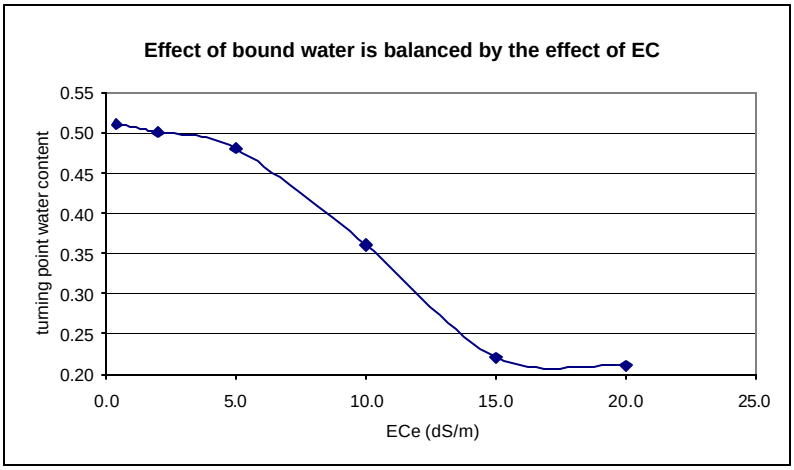

Fig. 5. *The turning point soil water content, at which the effect of bound water is balanced by the effect of soil electrical conductivity decreases as (EC_e) increasing.*

Bound Water Estimation

In Rideau clay, we assume that the bound water consists of four water molecular layers. The dielectric constant of bound water attached directly on the particle surfaces equals that of ice, or $\varepsilon_b = 3.2$ (Dirken and Dasberg 1993). The water molecules outside the fourth layer belong to the bulk water and have the dielectric constant of 80.2. Gur *et al*. (1978) and Israelachvili and Pashley (1984) reported that the dielectric constant increases exponentially with distance from the surface. Figure 6 shows how $\varepsilon_b(L)$ increases with L - the distance from soil particle surface. The distance weighted average ε_b for four water molecular layers can calculated by

$$\varepsilon_b = \int \varepsilon_b(L)dL \,/\, \int dL \qquad [3]$$

where $\varepsilon_b(L) = 2.14 \exp(2.68 \times 10^{-9} L)$, and the integration is from $L_1 = 1.5 \times 10^{-10}$ m (distance form the center of the first layer to surface,) to $L_2 = 10.5 \times 10^{-10}$ m (distance of the center of 4th layer to surface). The calculated $\varepsilon_b = 32.5$. Dobson *et al*. (1985) also found a good correspondence between theory and

experiment for ε_b value between 20 and 40. Therefore, for the Rideau clay tested, it is reasonable to assume (a) the volume fraction of bound water is 0.21 m^3/m^3 (b) the bound water consists of four water molecular layers and (c) the distance weighted average dielectric constant of bound water is 32.5. Based on the above assumptions, we calculated the time lay (T/Tair) in non-saline Rideau Clay at different water contents using a four-phase dielectric mixing model

$$\varepsilon^{\alpha} = f_1 \varepsilon_{air}^{\alpha} + f_2 \varepsilon_{solid}^{\alpha} + f_3 \varepsilon_w^{\alpha} + f_4 \varepsilon_b^{\alpha} \quad [4]$$

where f_1, f_2, f_3 and f_4 are the fraction of air, solid, free water and bound water.

The numbers in table 3 were calculated using $\varepsilon_{air} = 1, \varepsilon_{solid} = 2.56, \varepsilon_w = 80.2$ and $\varepsilon_b = 32.5$ for dielectric constant of air, soil solid, free water and bound water. The geometric parameter α is 0.5.

.

Vol. Water content	Measured T/T_{air}	Calculated T/T_{air} using equation (4)	Difference in T/T_{air} between measured and calculated	Difference in water content m^3/m^3
0.10	1.941	1.775	0.166	0.035
0.17	2.228	2.119	0.109	0.020
0.27	2.695	2.795	-0.098	-0.014
0.35	3.254	3.432	-0.178	-0.021
0.44	4.612	4.148	0.364	0.042
0.53	5.420	4.864	0.456	0.043

Table 3. *The measured time and calculated time delay based on four-phase dielectric-mixing model*

When soil water content is less than 0.21 m^3/m^3, f_3 (fraction for free water) equals to zero. At saturation (0.53 m^3/m^3), f_4 (fraction for air) equals to zero. The difference in soil water content presented in column five was calculated using logarithm regression (Fig.1).

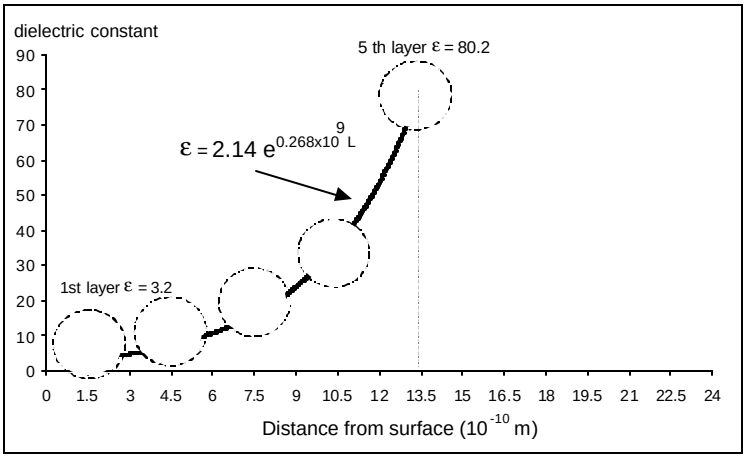

Fig. 6. *The dielectric constant of bound water increases exponentially with the increase of the distance from soil particle surface*

The maximum discrepancy in water content between the measured and calculated is 0.043 m^3/m^3. Considering the accuracy of the instrument of 0.013 m^3/m^3 (Moisture. Point Manual, ESI Environmental Sensors Inc. Victoria, BC, Canada), the four-phase dielectric mixing model with $\alpha = 0.5$ works reasonable well for non-saline Rideau Clay.

SUMMARY

A detailed study on clayey soil moisture measurement using TDR shows that clay content and soil electrical conductivity are the two most important factors that influence the time delay measurement. The bound water leads to a shorter time delay and soil electrical conductivity leads to a longer time delay. The three-phase, square root dielectric mixing model is not valid for saline clayey soil. An empirical logarithm calibration containing two soil electrical conductivity related parameters fits the experimental data well. The effect of bound water will be balanced by the effect of soil electrical conductivity at a so-called turning point moisture and this turning point varies with soil clay content and electrical conductivity. The volume fraction of bound water in a clayey soil can be estimated from the relationship between turning point moisture and EC_e. The volume fraction of bound water for Rideau Clay is estimated at 0.21 m^3/m^3, which consists of 4 water molecular layers. The calculated distance weighted average dielectric constant for 4 water molecular layers is 32.5. The four-phase dielectric-mixing model with $\alpha = 0.5$ works well for Rideau Clay. Clay mineral plays an important role in soil moisture measurement using TDR attributing its specific surface, electrical charge density and ion holding capacity. An investigation of the effect of different clay mineral is needed for understanding how the TDR signal is affected in clayey soil and further improve the performance of TDR instrument in challenging soil conditions.

REFERENCES

Alharthi, A. and Lange, J., 1987, Soil Water Saturation: Dielectric Determination.Water Resour. Res. **23**, No. 4, 591-595

Dasberg, S. and Hopmans, J.W., 1992, Time Domain reflectometry Calibration for Uniformly and Nonuniformly Wetted Sandy and Clayey Loam Soils. Soil Sci. Soc. Am. J. **56**, 1341-1345

Dirksen, C. and Dasberg, S., 1993, Improved Calibration of Time Domain Reflectomery Soil Water Content Measurements. Soil Sci. Soc. Am. J. **57**, 660-667

Gur, Y.I, Ravina, I. and Babchin, A. J., 1978, On the Electric Double Layer Theory. II. The Poisson – Boltzmann Equation Including Hydration Forces. J. Colloid Interface Sci. **64**,333-341

Hook, W.R., Livingston, N.J., Sun, Z.J. and Hook, P.B., 1992, Remote Diode Shorting Improves Measurement Soil Water by Time Domain Reflectometry. Soil Sci. Soc. Am. J. **56**, 1383-1391

Hook, W.R. and Livingston, N.J., 1995, Propagating Velocity Errors in Time Domain Reflectometry Measurement of Soil Water. Soil Sci. Soc. Am. J. **59**, 92-96

Hook, W.R. and Livingston, N.J., 1996, Errors in Converting Time Domain Reflectometry Measurements of Propagation Velocity to Estimates of Soil Water Content. Soil Sci. Soc. Am. J. **60**, 35-41

Isarelachvili, J.N., and Pashley, R.M., 1984, Measurement of the Hydrophobic Interaction between two Hydrophobic surfaces in Aqueous Electrolyte Solutions. J. Colloid Interface Sci. **98**, 500-514

Malicki, M.A., Walczak, R.T., Koch, S. and Fluhler, H., 1994, Determining Soil salinity from Simultaneous Readings of Its Electrical Conductivity and Permittivity Using TDR. Pages 328-336. in Symposium and Workshop on Time Domain Reflectometry in Environmental, Infrastructure, and Mining Applications. United States Department of Interior Bureau of Mines.

O'Konski, C.T., 1955, Effect of Interfacial Conductivity on Dielectric Properties. J. Chem. Phy. **23**, 1559

Rhoades, J.D., Manteghi, N.A., Shouse, P.J., and Alves, W.J., 1989, Soil electrical conductivity and soil salinity: New formulations and calibrations. Soil Sci. Soc. Am. J. **53**, 433-439.

Roth, K., Schulin, R., Fluhler, H. and and Attinger, W., 1990, Calibration of time domain reflectometry for water content measurement using a composite dielectric approach.Water Resour. Res. **26**, 2267-2273

Shang, J. Q., 1994, Quantitative Determination of Potential Distribution in Stern-Gouy Double-layer Model. Can. Geotech. J. **31**, 624-636

Sposito, G., 1984, The Surface Chemistry of Soils. Oxford University Press. Inc. New York

Sun, Z.J., 1995, in Stable Carbon Isotopes as Indicators of Increased Water Use Efficiency and Biomass Production in White Spruce (picea glauca (moench) voss) Seedlings Grown under Different Water and Nitrogen Regimes. 33-55. Ph.D. Dissertation, Biology Department, University of Victoria, Victoria, BC, Canada

Sun, Z. J., Young, G.D., McFarlane, and Chambers, B.M., 2000, The Effect of Soil Electrical Conductivity on Moisture Determination using Time-domain-Reflectometry in Sandy Soil. Can. J. Soil Sci. **80-1**, 13-22

Topp, G.C., Davis, J.L. and Annan, A.P., 1980, Electromagnetic Determination of Soil Water Content: Measurements in Coaxial Transmission Lines. Water Resour. Res. **16**, 574-582

Topp, G.C. and P.A. Ferré, P.A., 2000, Measuring Water Content in Soil using TDR: A State-of-the-Art in 1998. In Comparison of soil water measurement using the neutron scattering, time domain reflectometry and capacitance methods. International Atomic Energy Agency, Vienna, Austria. IAEA-TECDOC-1137, 111-124.

Van Olphen, H., 1977, An Introduction to Clay Colloid Chemistry. Interscience, New York

Whalley, W.R., 1993, Considerations on the Use of Time-domain Reflectometry (TDR) for Measuring Soil Water Content. J. Soil Sci., **44**, 1-9

White, I., Zegelin, S.J., Topp, G.C., and Fish, A., 1994, Effect of Bulk Electrical Conductivity on TDR Measurement of Water Content in Porous Media. in Symposium and Workshop on Time Domain Reflectometry in Environmental, Infrastructure, and Mining Applications. United States Department of Interior Bureau of Mines, 294-308.

White, I., Knight, J.H., Zegelin, S.J. and Topp, G.C., 1994, Comments on 'Consideration on the use of time-domain reflectometry (TDR) for measuring soil water content' by W.R. Whalley. Euro. J. Soil Sci. **45**, 503-508

Yu, C., Warrick, W. and Conklin, M.H., 1999, Derived Functions of Time Domain Reflectometry for Soil Moisture Measurement. Water Resour. Res. **35-6**, 1789-1796

DEVELOPMENT AND APPLICATION OF TDR INVERSION ALGORITHMS WITH HIGH SPATIAL RESOLUTION FOR MOISTURE PROFILE DETERMINATION

Stefan Schlaeger[1], Christof Huebner[2], Alexander Scheuermann[3] and Johannes Gottlieb[4]

[1]Evironmental Research Center, University of Karlsruhe
D-76128 Karlsruhe, Germany; Stefan.Schlaeger@fzu.uni-karlsruhe.de
[2]Institute for Meteorology and Climate Research, Karlsruhe Research Center
D-76021 Karlsruhe, Germany; Christof.Huebner@imk.fzk.de
[3]Institute of Soil Mechanics and Rock Mechanics, University of Karlsruhe
D-76128 Karlsruhe, Germany; Alexander.Scheuermann@bau-verm.uni-karlsruhe.de
[4]Institute of Soil Mechanics and Rock Mechanics, University of Karlsruhe
D-76128 Karlsruhe, Germany; Gottlieb@HotRock.de

Karlsruhe Research Center
Technology and Environment

ABSTRACT

Many applications in hydrology, agriculture and civil engineering ask for the moisture profile in soils or buildings. So far TDR technology was limited to integral or very coarse resolved water content determination along the transmission line. A new inversion algorithm has been developed which uses the full information content of the TDR reflection data from both sides of an embedded flat band cable. It is based on the telegraph equations for nonuniform transmission lines and an optimization approach to reconstruct simultaneously two line parameters with high spatial resolution. These parameters are converted to dielectric coefficients respectively water content by the help of a cable model and dielectric mixing rules. Field investigations on a full-scale dike model demonstrate how the algorithm works with real data. One cross section was equipped with 12 vertically installed flat band cables between 0.8 and 3.0 meters. A permanent monitoring with high resolution in space and time of transient hydrological processes e.g. the infiltration into the dike by precipitation or the percolation due to simulated flood events could be realized for the first time.

INTRODUCTION

Time domain reflectometry (TDR) is a widley used tool for measuring water content in materials like soils (Ferre and Topp, 2000). The sensing device is a transmission line, which is inserted or buried in the material. An electromagnetic pulse is applied to the transmission line and the reflections are recorded. The standard procedure is based on the measurement of the travel time of the electromagnetic pulse, which induces an electromagnetic wave on a transmission line of known length. For homogeneous materials the travel time is directly related to the dielectric constant, which is in moist porous materials mainly a function of water content (Topp *et al.*, 1980). One approach for spatial resolution has been developed by Hook *et al.* (1992). The transmission line is divided in several sections by remote controlled switches. The switches can short circuit their corresponding section and allow a very coarse spatial resolution of the water content distribution.

Other inversion strategies to reconstruct the spatial distribution of the line parameters make use of optimization approaches, but haven't proofed their practicability with real data yet. Norgren and He, 1996, use frequency-dependent reflection and transmission coefficients to calculate several pairs of the nonuniform transmission line parameters. They show that the reconstruction of any line parameters using only transmission data is in general not unique. The best results were obtained when choosing two-sided reflection data. One disadvantage of this method is the restriction to a limited frequency range. Lundstedt and He, 1996, use the transient response as a function of time which must be calculated from the measured reflection data. Their algorithm is based on a time domain wave-splitting technique and the compact Green function technique since that is efficient in describing the transient response.

TRANSMISSION LINE DESIGN

The typical TDR transmission line is a metallic fork, which is inserted in the material. The maximum length is limited, because the electromagnetic pulse is attenuated and disappears on longer lines. In the case of soils the upper limit is about 1 m depending on the conductivity (Dalton *et al.*, 1986). For longer transmission lines insulated flat band cables are proposed. They exhibit much less pulse attenuation than non-insulated metallic forks in the same media. Several cables with different geometries have been developed and manufactured, from simple concentric insulation to sophisticated multiwire structures with one-side sensitivity (Huebner and Brandelik, 2000). The flat band cable used for the experiments in this work is shown in Fig. 1 together with its electrical field distribution. The cable consists of three flat band copper wires covered with polyethylene insulation with polyethylene insulation.

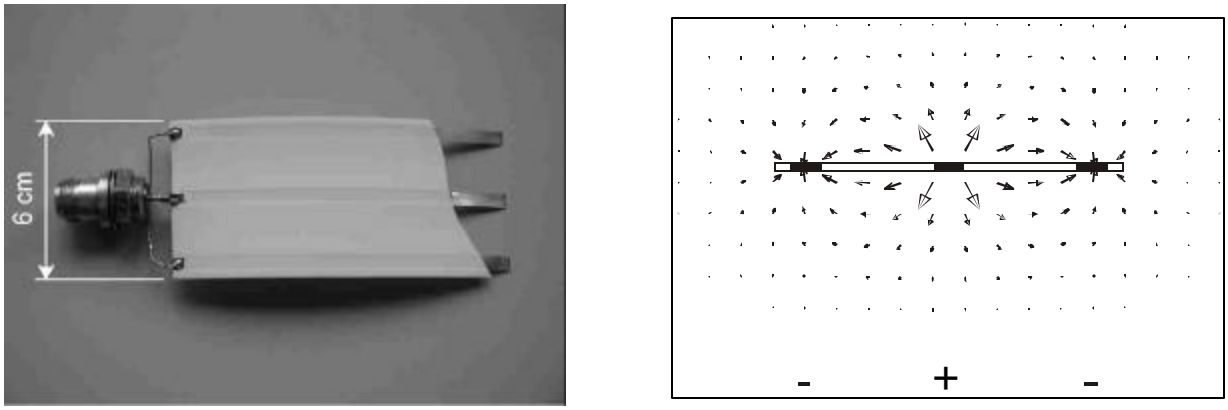

Fig. 1. *The insulated flat band cable and the electric field distribution of the cross section.*

The electrical field concentrates around the conductors and defines the sensitive area of 3 to 5 cm around the cable. The spatial weighting of the measurements in the cross section of the cable is directly related to the energy density distribution. The electric properties of the flat band cable used in this work can be calculated and measured (cf. Fig. 3 and Tab. 1). One can assume that the well-known equivalent circuit for the infinitesimal line section as shown in Fig. 2 fully describes the electric properties of the line.

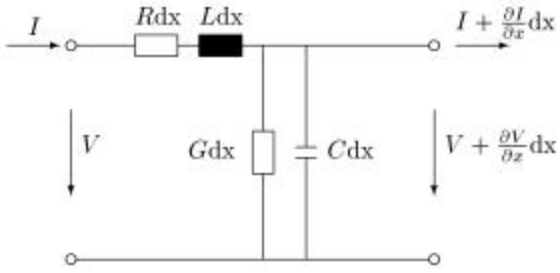

Fig. 2. *Electric equivalent circuit of an infinitesimal section of a TEM transmission line.*

This model is only true for pure transverse electromagnetic (TEM) propagation. Nevertheless, it is a good approximation of the so-called quasi-TEM mode of the cable with stratified cross section used here. In most cases the line resistance *R* can be neglected. The same is true for the conductance *G* in case of lossless material surrounding the line. Transmission lines embedded in soils have conductivity values that cannot be neglected. *G(x)* depends on soil type, water content and frequency. Usually clayey and loamy soils have much higher conductivity than sands. The remaining capacitance *C* and inductance *L* can be determined by solving the Laplace equation for electrostatic fields in the cross section of the transmission line.

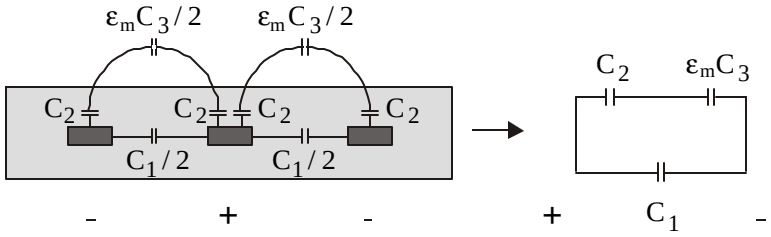

Fig. 3. *Capacitance model of the insulated flat band cable.*

The total capacitance *C* may be replaced by three capacitances C_1, C_2, and $e_m C_3$ as shown in Fig. 3 and can be transformed into a direct relation between the dielectric coefficient e_m of the surrounding material and the total capacitance:

$$C(e_m) = C_1 + \frac{C_2 e_m C_3}{C_2 + e_m C_3} \qquad [1]$$

The three unknown capacitances C_1, C_2, and C_3 were derived from calibration measurements of three different materials with well-known dielectric properties. The inductance was determined by measuring the wave impedance with a variable resistor at the end of the cable adjusted for minimum reflection. The values for the cable of Fig. 1 are given below.

Circuit element	C_1	C_2	C_3	L
Measured value	3.4 pF/m	323 pF/m	14.8 pF/m	756 nH/m

Table 1. Cable parameters for the flat band cable in Fig. 1.

THE TELEGRAPH EQUATIONS

A three step algorithm for reconstructing the water content profile along a given profile has been developed. In the first step the transmission line parameters *C(x)* and *G(x)* are reconstructed with two independent time domain measurements from both sides of the flat cable by solving the inverse problem for the telegraph equations. The second step transforms *C(x)* into the dielectric coefficient $e_m(x)$ by the inversion of (1). In the third step $e_m(x)$ is converted into the water content profile $T_v(x)$ by standard transformations (Topp *et al.*, 1980) or material specific calibration functions. The first step as key component for the reconstruction will be discussed in detail.

The telegraph equations describe the variation of the voltage *V(x,t)* and the current *I(x,t)* in time along the transmission line. By applying the Kirchhoff's voltage and current laws to the equivalent circuit in Fig. 2 one obtains:

$$\frac{\partial}{\partial x}V(x,t) = -R(x)I(x,t) - L(x)\frac{\partial}{\partial t}I(x,t)$$
$$\frac{\partial}{\partial x}I(x,t) = -G(x)V(x,t) - C(x)\frac{\partial}{\partial t}V(x,t) \qquad [2]$$

In order to reconstruct the two parameters *C(x)* and *G(x)*, two independent measurements are needed. Consequently, the task is divided into two parts, one part that deals with an incident wave from one side and another part dealing with an incident wave from the other side of the cable.

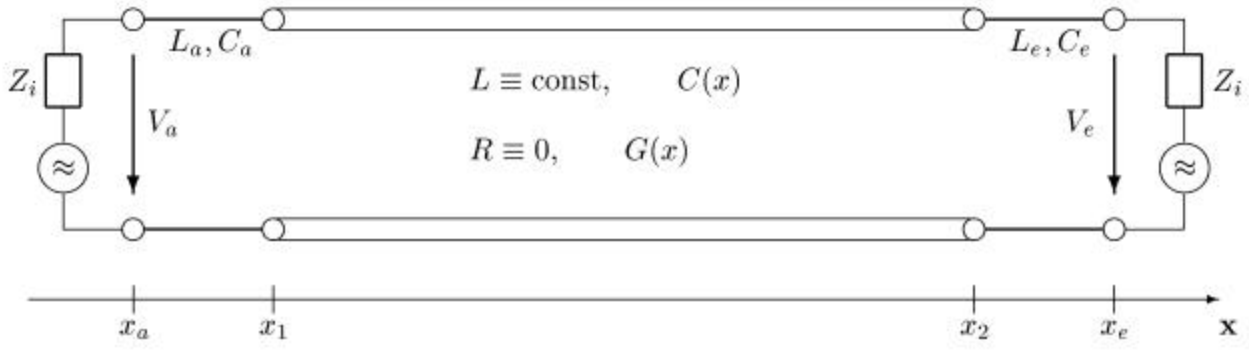

Fig. 4. *The uniform flat band cable, situated between x_1 and x_2, is connected to two lossless uniform coaxial cables with matched impedances Z_i at their endpoints.*

Fig. 4 describes the setup for receiving the reflection data from both sides of the unknown material. Therefore two separate measurements must be carried out with the external currents $F_{ex}^1 = d(x-x_a)f(t)$ and $F_{ex}^2 = d(x-x_e)f(t)$, respectively.

The inverse method we present in the next section is based on an iterative search for the electrical parameters of the nonuniform flat band cable with the full wave solution of both direct problems. During the search the solutions of the line need to be calculated repetitively. It is therefore important to use a technique that is computationally efficient, and which provides a simple mapping from the parameters to

the direct solution, to guarantee a fast convergence. Equations (2) and (3) can be easily transformed into a partial differential equation (PDE) for $V_i(x,t)$ representing the voltages of each separate experiment with regard to $F_{ex}^{\,i}$, i=1,2

$$\left[LC\frac{\partial^2}{\partial t^2} + LG\frac{\partial}{\partial t} + \frac{\frac{\partial}{\partial x}L}{L}\frac{\partial}{\partial x} - \frac{\partial^2}{\partial x^2} \right] V_i(x,t) = 0, \qquad i = 1,2 \qquad [3]$$

with the initial conditions

$$V_i(x,t)\big|_{t\le 0} = 0, \qquad \frac{\partial}{\partial t}V_i(x,t)\bigg|_{t\le 0} = 0 \qquad x_a \le x \le x_e \qquad i = 1,2. \qquad [4]$$

The boundary conditions depend on the location of the external current $F_{ex}^{\,i}(x,t)$, i=1,2. For the source at $x = x_a$, there is an absorbing boundary condition at $x = x_e$

$$\left[\frac{\partial}{\partial x} + \sqrt{L_e C_e}\,\frac{\partial}{\partial t} \right] V_1(x,t)\bigg|_{x=x_e} = 0, \qquad t \ge 0, \qquad [5]$$

and an absorbing boundary for the reflected wave at $x = x_a$ in connection with the external current:

$$\left[\frac{\partial}{\partial x} - \sqrt{L_a C_a}\,\frac{\partial}{\partial t} \right] V_1(x,t)\bigg|_{x=x_a} = L_a \frac{\partial}{\partial t} F_{ex}^{1}(x,t)\bigg|_{x=x_a}, \qquad t \ge 0. \qquad [6]$$

For the other PDE for $V_2(x,t)$ with external current $F_{ex}^{\,2}(x,t)$ the boundary conditions are exchanged.

THE OPTIMIZATION APPROACH

The aim of the investigation is the determination of the unknown distributions of $C(x)$ and $G(x)$ with measurements of input and output data in the time domain. The input data $f(t)$, which describes the incident pulse, can be easily extracted from the measurements $V_a(t)$ of the coaxial cable between x_a and x_1 with an open end at x_1. The output data $?_i(t)$, i=1,2, can be received from the two separate measurements with the external current $F_{ex}^{\,1}$ and $F_{ex}^{\,2}$, respectively.
Define a cost function $J(C,G)$ which measures the difference in the L_2-norm between the solutions $V_i(x_i,t)$, i=1,2, of the direct problems (4)-(7) corresponding to the parameters $C(x)$ and $G(x)$ and the given measurements

$$J(C,G) = \sum_{i=1}^{2} \int_0^T \left[V_i(x_i,t) - l_i(t) \right]^2 dt \qquad [7]$$

with $T>2t(x_1,x_2)$, where $t(x_1,x_2)$ is the travel time between x_1 and x_2. The cost function refers to the error in the solution $V_1(x_1,t)$ and $V_2(x_2,t)$, respectively. The concept of the method is to find the parameters that minimize the cost functional J. If the inverse problem has a solution the theoretical minimum of J is zero. One more important reason for choosing the L_2-norm is that this makes it possible to derive exact expressions for the gradient of J.

Exact expression for the gradient of the cost function

It is convenient to derive the gradient of J with respect to C, J_C, by $lim_{||dC(x)||? 0} (J(C+dC)-J(C)) =: (J_C , dC(x))$ where $dC(x)$ denotes the differential of $C(x)$ and (f,g) is the inner product defined by

$$\big(f(x), g(x)\big) = \int_{x_1}^{x_2} f(x)\, g(x)\, dx \ . \qquad [8]$$

Thus, the gradient $J_C(x)$ is the direction in which J increases most rapidly with respect to the norm of the change of the function $C(x)$. $J_C(x)$ and $J_G(x)$ are given by

$$J_C(C,G) = -\sum_{i=1}^{2} \int_0^T \left(\frac{\partial}{\partial t} \Psi_i \right) \left(L \frac{\partial}{\partial t} V_i \right) dt \ , \qquad J_G(C,G) = \sum_{i=1}^{2} \int_0^T \Psi_i \left(L \frac{\partial}{\partial t} V_i \right) dt \ , \qquad [9]$$

where the dual functions ? $_1$ and ? $_2$ satisfy the following PDEs

$$\left[LC \frac{\partial^2}{\partial t^2} - LG \frac{\partial}{\partial t} - \frac{\frac{\partial}{\partial x} L}{L} \frac{\partial}{\partial x} - \frac{\partial^2}{\partial x^2} \right] \Psi_i(x,t) = 2d(x - x_i)\big[V_i(x,t) - l_i(t)\big], \quad i = 1,2 \ \ [10]$$

with the initial conditions for $t > T$ and boundary conditions similar to (5)-(7).

Reconstruction of the parameters

Only reflection data are used to determine uniquely the parameters $C(x)$ and $G(x)$ (He *et al.*, 1994). The optimization is done with a conjugate gradient method using Fletcher-Reeves update formulas (Fletcher and Reeves, 1964). To determine the optimal step size for the search direction a parabolic approximation technique is used in each conjugate gradient step. The result of the minimization of (8) is the distribution of the total capacitance C and total conductance G. $C(x)$ can be easily transformed into the dielectric properties $e(x)$ of the surrounding material. Furthermore the volumetric water content $T_v(x)$ can be determined using standard transformations (Topp *et al.*, 1980) or a special calibration function for the material used (see Fig. 5). The total conductance $G(x)$ describes the conductivity of the material between the copper wires, i.e. of the system of the polyethylene insulation and the surrounding material. The conductivity of the material around the cable cannot be calculated as simple as the dielectric coefficient. The determination of the water content distribution of the surrounding material does not require the knowledge of the conductivity distribution of the material, but it cannot be neglected during the reconstruction of $C(x)$.

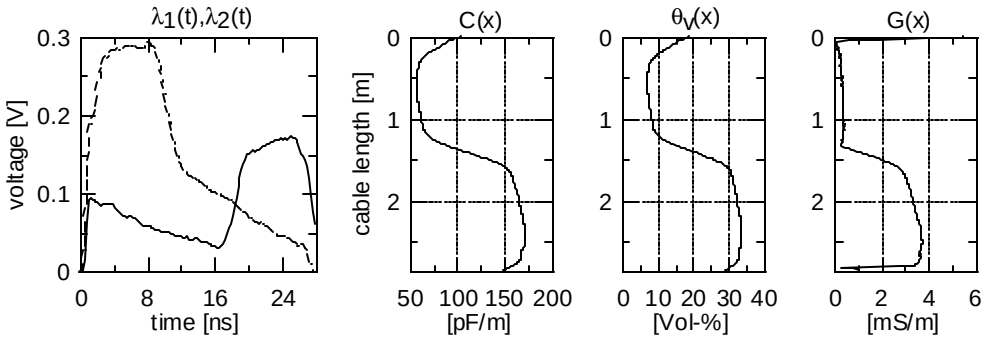

Fig. 5a – 5d. *Measured time domain reflection data from both sides of the cable* **(a)** *and the spatial distribution of the capacitance* **(b)**, *the volumetric water content* **(c)** *and the conductance* **(d)** *as a function of the cable length.*

FIELD EXPERIMENTS

The seepage through dikes due to a hydraulic load in dependency of an initial distribution of water content is currently investigated. Therefore a full-scale dike model is available at the Federal Waterways and Research Institute in Karlsruhe (Fig. 6). The dike is built up homogeneously with uniform sand (grain size 0.2 – 2 mm) and it is based on a waterproof sealing of plastic, so that the water within the dike body will flow to a drain at the toe of the landside slope. In order to simulate flood events a basin is included in the construction. The dike is equipped with pore water gauges at the base to measure the hydraulic head inside the dike and the new water content monitoring system with flat band cables. The advantage of this system is its high resolution in space and time. The system consists of 12 vertically installed flat band cables between 0.8 and 3 m length. The connection between the coaxial and the flat band cable at one side of the cable at position 4.65 m was damaged so it was ignored for the representation of the results (cf. Fig. 7). The data collection and controlling equipment are placed in a measuring container at the toe of the landside slope.

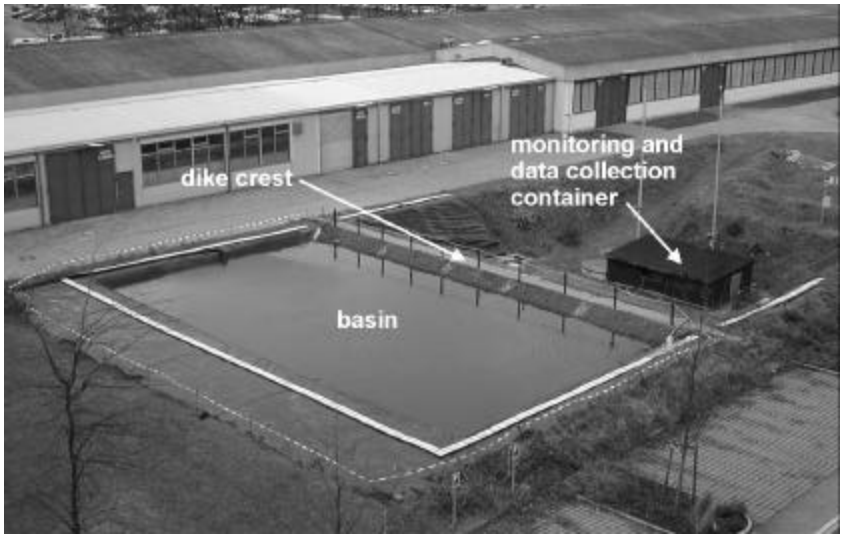

Fig. 6. *Full-scale dike model at the Federal Waterways and Research Institute in Karlsruhe during a flood simulation test (steady state of seepage condition).*

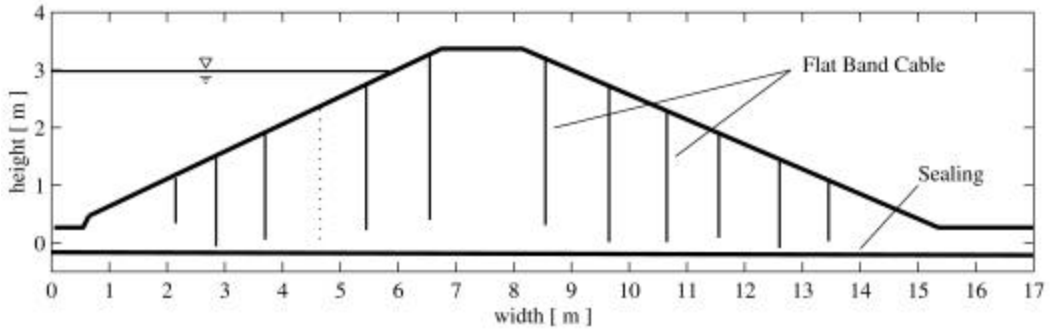

Fig. 7. *Location and length of the flat band cables in the cross section of the dike.*

A simulation of an extreme precipitation event has been carried out at the dike model. Fig. 8 shows the hydrograph of the sprinkler irrigation with 21.7 l/min on a horizontal area of 270 m^2 and the resulting flow rate of seepage water. This three-day experiment represents a precipitation event of 125 mm which is assumed to occur every 100 years in Karlsruhe.

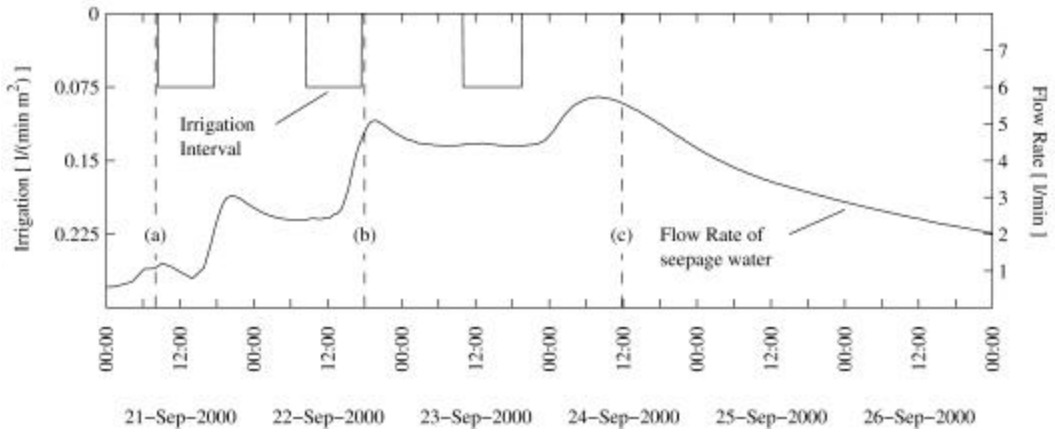

Fig. 8. *Hydrograph of sprinkler irrigation at the dike surface and the flow rate of the seepage water during the extreme precipitation event.*

The results of the measurements of the water content are given in Fig. 9. For better visualisation the single measurements of each cable were interpolated over the observed area in the cross section. The blue colors show wet zones whereas the red and yellow colors represent the more dry zones.

Fig. 9(a) shows the water content distribution at the beginning of the irrigation. After the second irrigation interval the water content distribution has rised from 9 to 14 Vol-% in the first 50 cm of the subsurface (Fig. 9(b)). The water percolates through the material according to the gravity. It accumulates on top of the sealing in the base of the dike (Fig. 9(c)) and flows slowly to a drain at the toe of the landside slope. As one can see at the pictures in Fig. 9 the new measurement system allows the verification of even small changes in the water content.

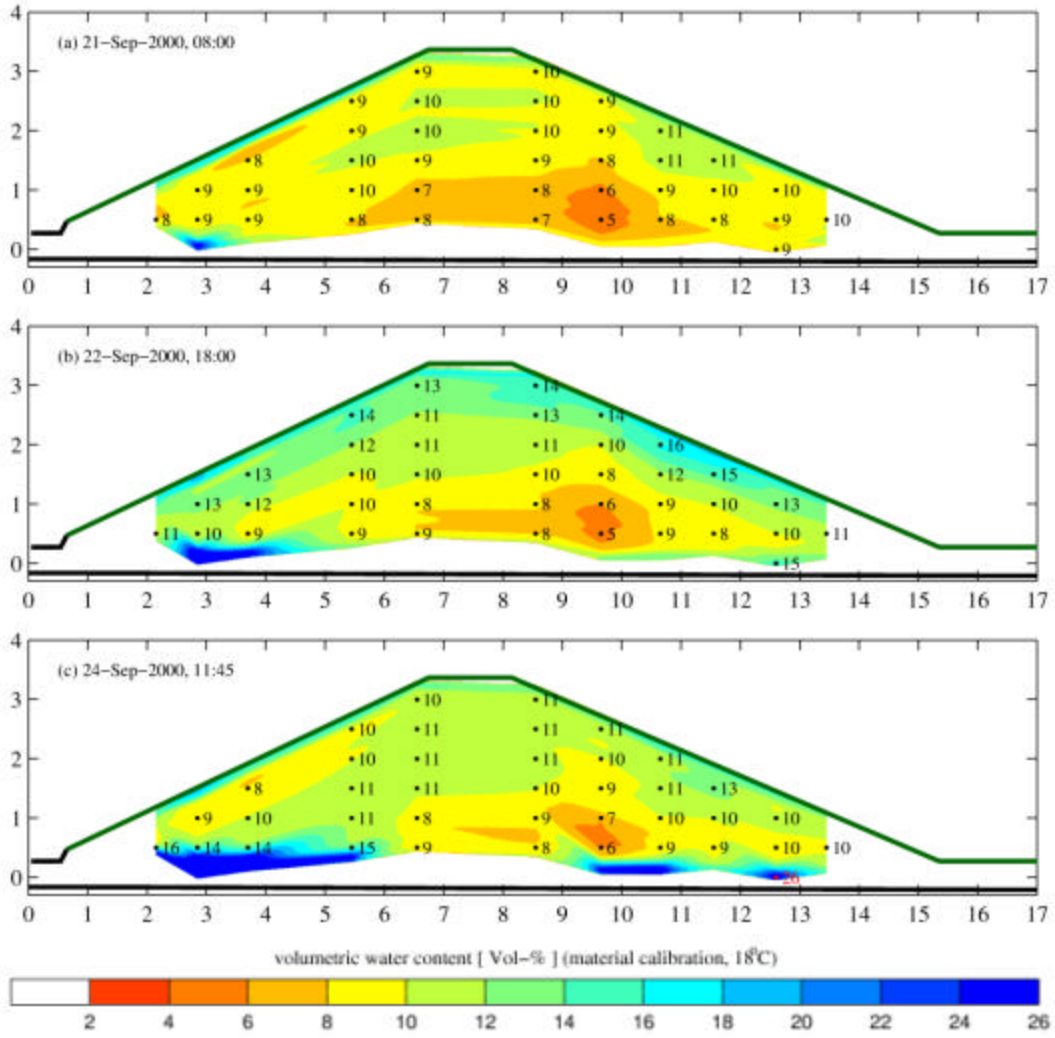

Fig. 9a – 9c. *Volumetric water content T_v at the dike model during the extreme precipitation event.*

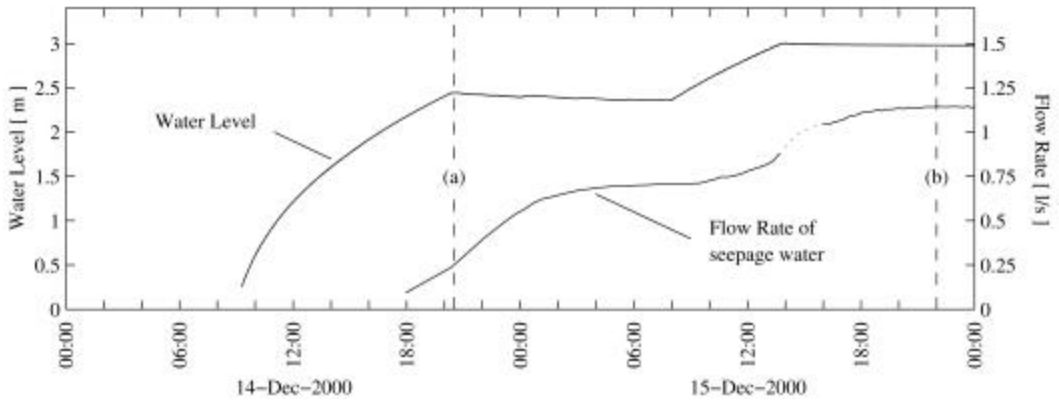

Fig. 10. *Hydrograph of the waterlevel in the basin and the flow rate of the seepage water during the flood simulation.*

A simulation of a flood event has been carried out at the same dike model as well (Scheuermann *et al.*, 2001). Fig. 10 shows the hydrograph of the water level and the resulting flow rate of the seepage water for the phase of increasing water level up to the steady state of seepage condition.

The measurements of the water content and the total conductance are given in Fig. 11 and Fig. 12, respectively. In addition, levels of the hydraulic head are given in the figures representing the approximate position of the phreatic line inside the dike body. The independently measured water level in the basin is also marked.

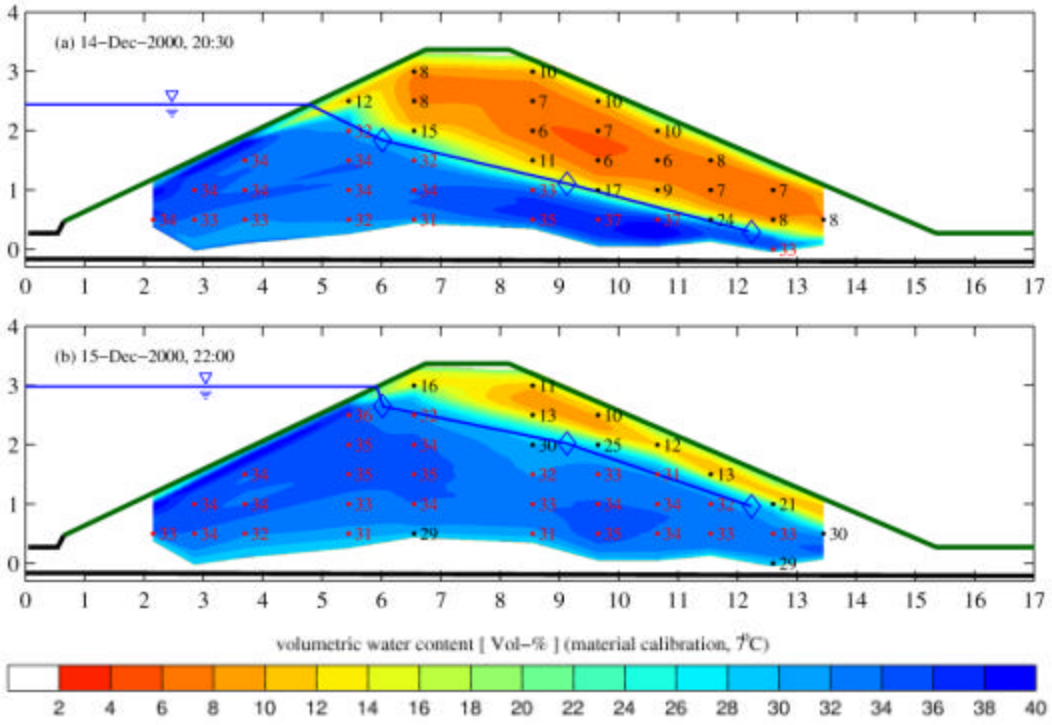

Fig. 11a – 11b. *Volumetric water content T_v at the dike model during the flood simulation.*

Fig. 11(a) represents the water content distribution after 11 hours of charging. The distribution of the total conductance at the same time is shown in Fig. 12(a). Fig. 11(b) and Fig. 12(b) show the volumetric water content distribution and the total conductance distribution of the steady state of seepage condition. As one can see in Fig. 11 the measured phreatic line and the location of the transient of the wet to the dry zone correspond well. One can also recognize a gradual transient from the wet to the dry zone on a small area above the blue zone representing the capillary border. The observation of the water content distribution during the steady state condition was verified by independent measurements.

During a laboratory investigation the water content distribution in the subsurface from groundwater to unsaturated zone has been measured in a medium sand. The changes in water content were reconstructed with a spatial accuracy <1 cm and an average deviation of ±2.3 Vol-% compared to oven-drying measurements (Schlaeger *et al.*, 2001).

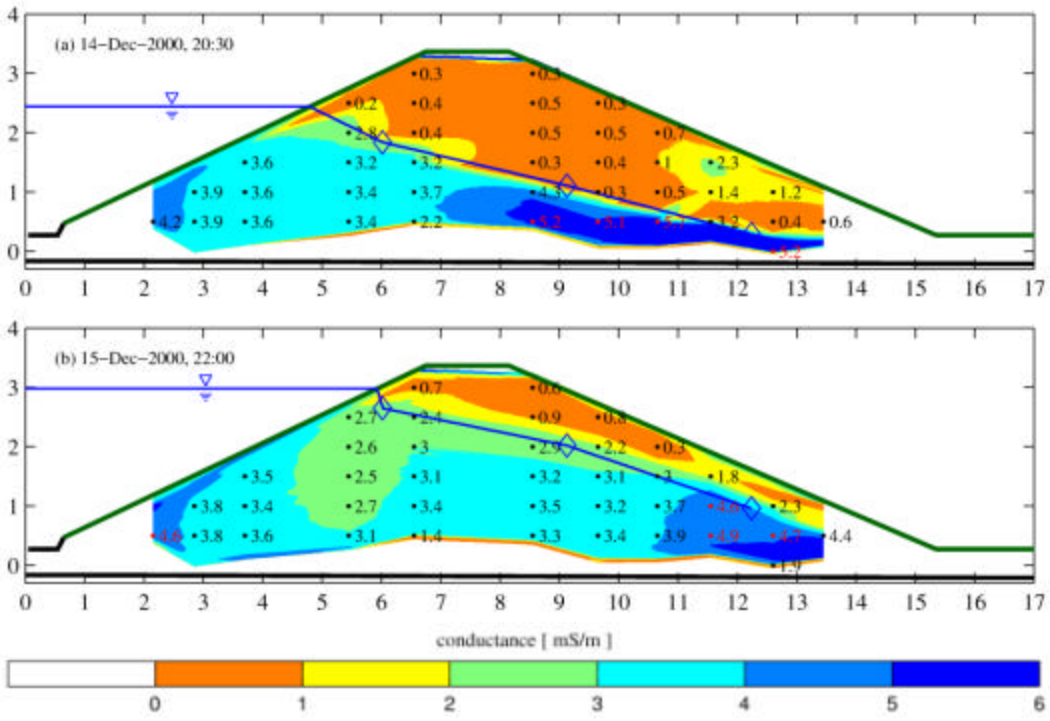

Fig. 12a – 12b. *Conductance G at the dike model during the flood simulation.*

SUMMARY

In this paper a new algorithm for determining the moisture profile in porous materials with high resolution in space and time is presented. It is based on TDR measurements from both sides of the transmission line and an optimization approach for solving the inverse problem of the telegraph equations. For the first time the new algorithm has been integrated into a water content measurement system for investigating the water transport processes in a full-scale dike model. For this purpose 12 flat band sensor cables were installed in the dike and connected to a TDR device and data acquisition equipment. Simulations of an extreme precipitation event and a flood event were carried out. This way the spatial resolution has an accuracy of about 3 cm and the volumetric water content profiles along the sensor cables were determined with an average deviation of ±2.3 Vol-% compared to independent measurements. Due to the data acquisition time for the TDR data of about 5 minutes for the complete cross section of the dike, fast running water transport processes could be monitored for the first time in this spatial resolution. The processing of the time-dependent TDR data into a spatial resolution is still very time consuming and subject to future improvements. Furthermore, the calibration of the system on a special soil has not been solved satisfactorily. For the present study a material dependent calibration between dielectric properties and water content was carried out in the laboratory. Further investigations should be conducted in this field in order to find a more manageable method of calibration.

ACKNOWLEDGEMENTS

The authors are indebted to many people for discussions and suggestions. In particular, thanks go to J. Gottlieb who has initiated the research group "Fundamentals of Electromagnetic Soil Moisture Measurement – The Inverse Problem of Electromagnetic Wave Propagation in the Three-Phase Medium

Soil". We would also like to thank the Deutsche Forschungsgemeinschaft (DFG-Go-742/2-4) for the financial support and the Federal Waterways and Research Institute for the appropriation of the full-scale dike model.

REFERENCES

Dalton, F.N., and Van Genuchten, M.Th., 1986, The time domain reflectometry method for measuring soil water content and salinity, Geoderma, **38**, 237-250.

Ferre, P.A., and Topp, G.C., 2000, Time-domain reflectometry techniques for soil and water content and electrical conductivity measurements, in Baltes, H., Goepel, W., and Hesse, J. (eds.), Sensors Update 7: Wiley-VCH, 277-300.

Fletcher, R., and Reeves, C.M., 1964, Function minimization by conjugate gradients: Computer Journal, **7**, 163-168.

He, S., Romanov, V.G., and Stroem, S., 1994, Analysis of the Green function approach to one-dimensional inverse problems. Part II: Simultaneous reconstruction of two parameters: Journal of Mathematical Physics, **35**, No. 5, 2315-2335.

Hook, W.R., Livingston, N.J., Sun, Z.J., and Hook, P.B., 1992, Romote diode shorting improves measurement of soil water by time domain reflectometry: Soil Science Society American Journal, **56**, 1384-1391.

Huebner, Ch., and Brandelik, A., 2000, Distinguished problems in soil and snow aquametry, in Baltes, H., Goepel, W., and Hesse, J. (eds.), Sensors Update 7: Wiley-VCH, 317-340.

Lundstedt, J., and He, S., 1996, A time-domain optimization technique for the simultaneous reconstruction of the characteristic impedance, resistance, and conductance of a transmission line: Journal of Electromagnetic Waves and Applications, **10**, No. 4, 581-602.

Norgren, M., and He, S., 1996, An optimization approach to the frequency domain inverse problem for a nonuniform LCRG transmission line: IEEE Transactions on Microwave Theory and Techniques, **44**, No. 8, 1503-1507.

Scheuermann, A., Schlaeger, S., Huebner, Ch., Brandelik, A., and Brauns, J., 2001, Monitoring of the spatial soil water distribution on a full-scale dike model, in Kupfer, K. *et al.* (eds.) Proceedings of the Fourth International Conference on Electromagnetic Wave Interaction with Water and Moist Substances: 343-350.

Schlaeger, S., Huebner, Ch., and Weber, K., 2001, Moisture profile determination with TDR, in Breh W. *et al.* (eds.) Proceedings of the Second International Conference on Strategies and Techniques for On-Site Investigation and Monitoring of Contaminated Soil, Water, Air and Waste: Field Screening 2001, Dordrecht, Kluwer Academic Publishers, 341-346.

Topp, G.C., Davis, J.L., and Annan, A.P., 1980, Electromagnetic determination of soil water content: Measurement in coaxial transmission lines: Water Resources Research, **16**, No. 3, 574-582.

Soil Moisture Monitoring

Long-Term Stability of Time Domain Reflectometry Measurements in a Multi-Year Field Experiment
T. G. Schofield, *Los Alamos National Laboratory*

Long-Term Monitoring of Soil Moisture in a Harsh Climate Using Reflectometer and TDR Probes
G. N. Delin, and W. N. Herkelrath, *U.S. Geological Survey*

Application of the TDR Technique in Tropical Soil
E. E. Matsura, C. F. Souza and R. Testezlaf, *UNICAMP/Feagri - Departamento de Água e Solo, Brazil*

Temperature Effect on TDR Measurement of Water Content of Unbound Materials
G. Zuo, W. C. Wright, R. E. Yoder, E. C. Drumm and N. R. Rainwater, *University of Tennessee*

Using the Formation Factor to Calibrate TDR for Water Content and Salinity Measurements in Drip Irrigated Fields*
Arie Nadler, *Soil and Water Institute, The Volcani Center, Israel*; A. L. Ward, *Pacific Northwest National Laboratory*

*NOT PRESENTED AT TDR 2001

Back to Table of Contents

LONG-TERM STABILITY OF TIME DOMAIN REFLECTOMETRY MEASUREMENTS IN A MULTI-YEAR FIELD EXPERIMENT

Tracy G. Schofield

Environmental Science Group, Los Alamos National Laboratory,
Los Alamos, New Mexico 87545; tgs@lanl.gov

Los Alamos
NATIONAL LABORATORY

ABSTRACT

Time Domain Reflectometry (TDR) measurements from a field demonstration of landfill covers at Los Alamos, New Mexico, USA were analyzed in an attempt to determine the long-term stability of the TDR system. The demonstration was comprised of four landfill cover designs: Conventional, EPA, Loam Capillary Barrier and Clay Loam Capillary Barrier with each design replicated at slopes of 5%, 10%, 15%, and 25% for a total of 16 plots. A total of 212 locations in the plots were instrumented with 2 rod TDR pairs and each location was interrogated at 7 hour intervals for seven years using an automated and multiplexed measurement system. The TDRs were located in a variety of soil types and at differing depths from the soil surface. Measurements from differing soil types were considered separately and seasonal changes in soil water content due to precipitation were minimized by annual averaging. Statistical and graphical analyses were performed to assess the stability of the measurements over the life of the demonstration.

INTRODUCTION

Federal and state regulations governing landfill closures specify long-term monitoring (30 years or more) of the performance of the landfill cover. Time Domain Reflectometry (TDR) measurements are a likely candidate for fulfilling this requirement since they are easily automated and a proven technology. Soil moisture content of the cover will be an important variable because it affects seepage through the cover to the waste and surface runoff. Regulators will request data that demonstrates the stability of the measurement technique over the long post closure monitoring period. Without such evidence, regulators are unlikely to accept a monitoring method. The objective of this presentation is to develop the basis for accepting TDR as a long-term monitoring technique for soil water content at Los Alamos.

Seven years of TDR measurements from a field experiment evaluating the performance of various landfill covers were analyzed in an attempt to identify any long-term degradation in performance by the

TDR system. Data from 212 locations in the experimental design were taken at approximately 7-hour intervals from January 1992 through December 1998 at the Protective Barrier Landfill Cover Demonstration at Los Alamos National Laboratory, Los Alamos, New Mexico (Nyhan, *et al*., 1997).

The TDRs in this field experiment were installed at various depths and in different soil types for purposes of evaluating the landfill cover performance. For the purposes of this analysis the TDR data from differing soil types were segregated to identify performance effects caused by soil characteristics and because the environmental conditions presented to each soil type varied widely due to positioning in the cover profile.

An analysis of each TDR in a soil type was performed in which the mean annual soil water content was determined for each year to minimize seasonal water content fluctuations. The mean for each year was compared to the mean soil water content for all the years (Grand Mean). A preliminary analysis using the time stability concept proposed by Vauchaud, *et al*. 1985, was performed to compare TDR data from two different soil types.

MATERIALS AND METHODS

The purpose of the Protective Barrier Landfill Cover Demonstration was to monitor and compare water balance for the conventional landfill cover design, similar to that used in Los Alamos and the waste management industry for waste disposal, with that of three other designs containing engineered barriers. The performance of all four designs was evaluated at dominant downhill slopes of 5, 10, 15 and 25%, giving a total of 16 plots. Each of the 16 plots consist of 4 metal pans in the bottom for seepage collection overlain by layers of soil which vary in type and thickness depending on the cover design. The plot profiles are seen in Figures 1a through 1d and detail the soil type used for each layer and the layer's thickness. The experiment used six different soil types in all. A full description of the plot construction has been previously provided by Nyhan, *et al.,* (1994).

Volumetric water content was measured with a pair of stainless steel wave guides (60-cm long, 3-mm diam soil moisture probes; Campbell Scientific, Logan, UT) which are buried parallel and 5 cm apart in the soil. One set of wave guides was emplaced vertically in every soil layer above the bottom center of each metal pan in the seepage collection system; these wave guides allowed us to determine soil water inventory in four locations in each field plot. A second set of wave guides was emplaced horizontally in several soil layers to provide us with a more detailed picture of soil water dynamics close to the interfaces of certain key soil layers. Positioning of the TDRs in the cover profile are shown in Figures 1a through 1d. These figures are for the four different cover types with a 5% slope but are representative of the positioning in corresponding cover types with higher slopes.

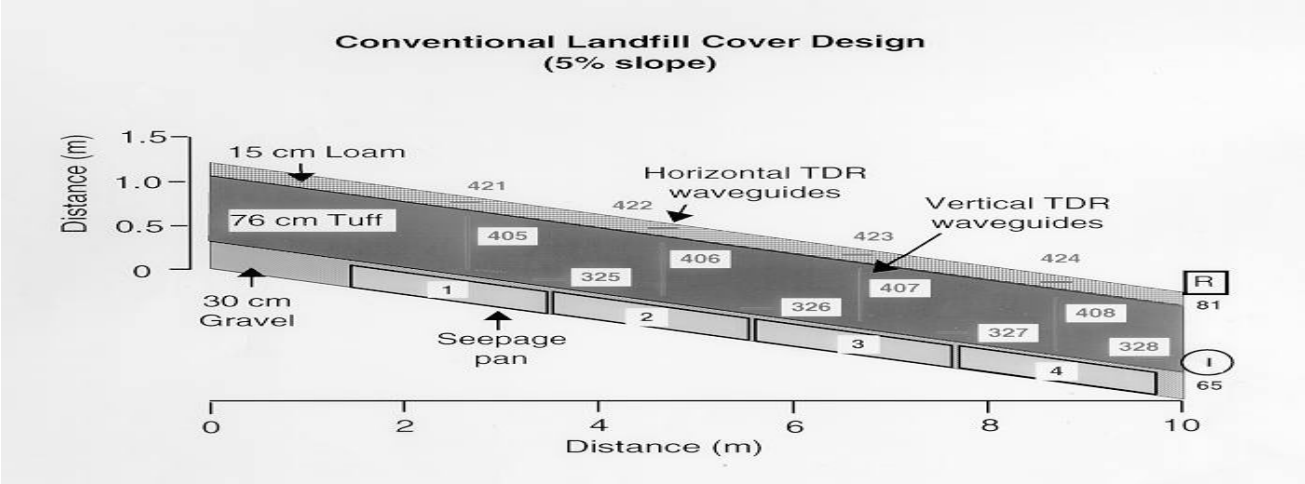

Fig. 1a *Plot profile of Conventional Cover Design*

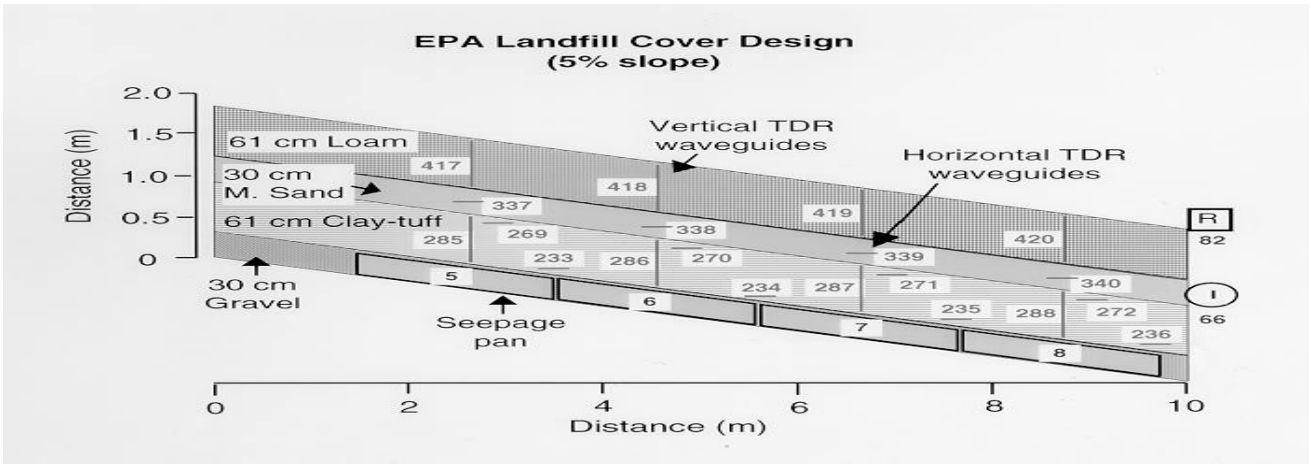

Fig. 1b. *Plot profile of EPA Cover Design*

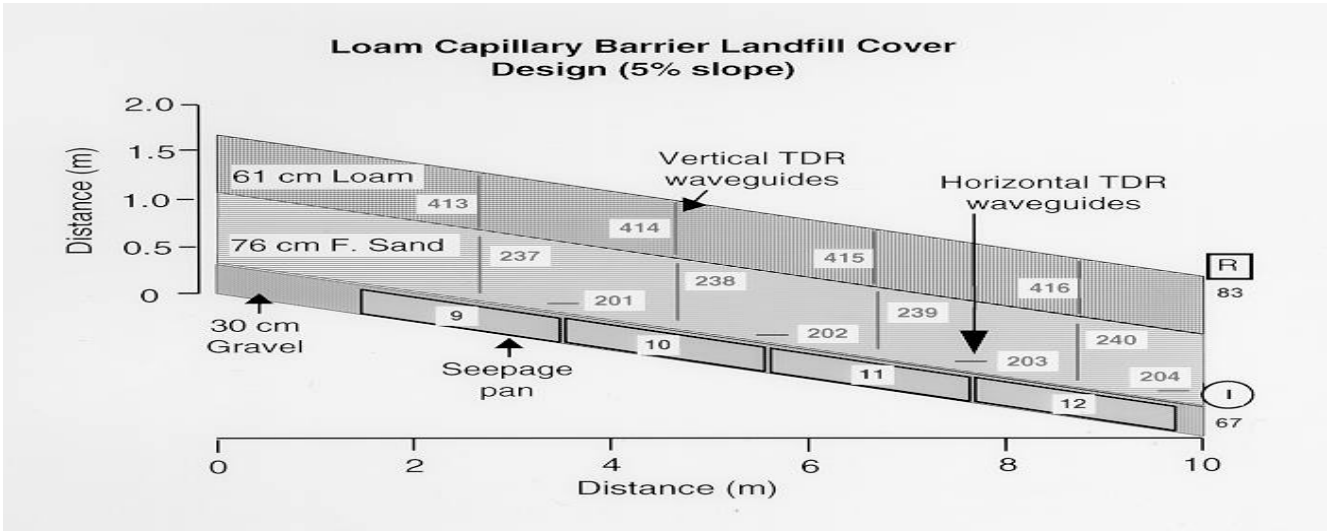

Fig. 1c. *Plot profile of Loam Capillary Barrier Design*

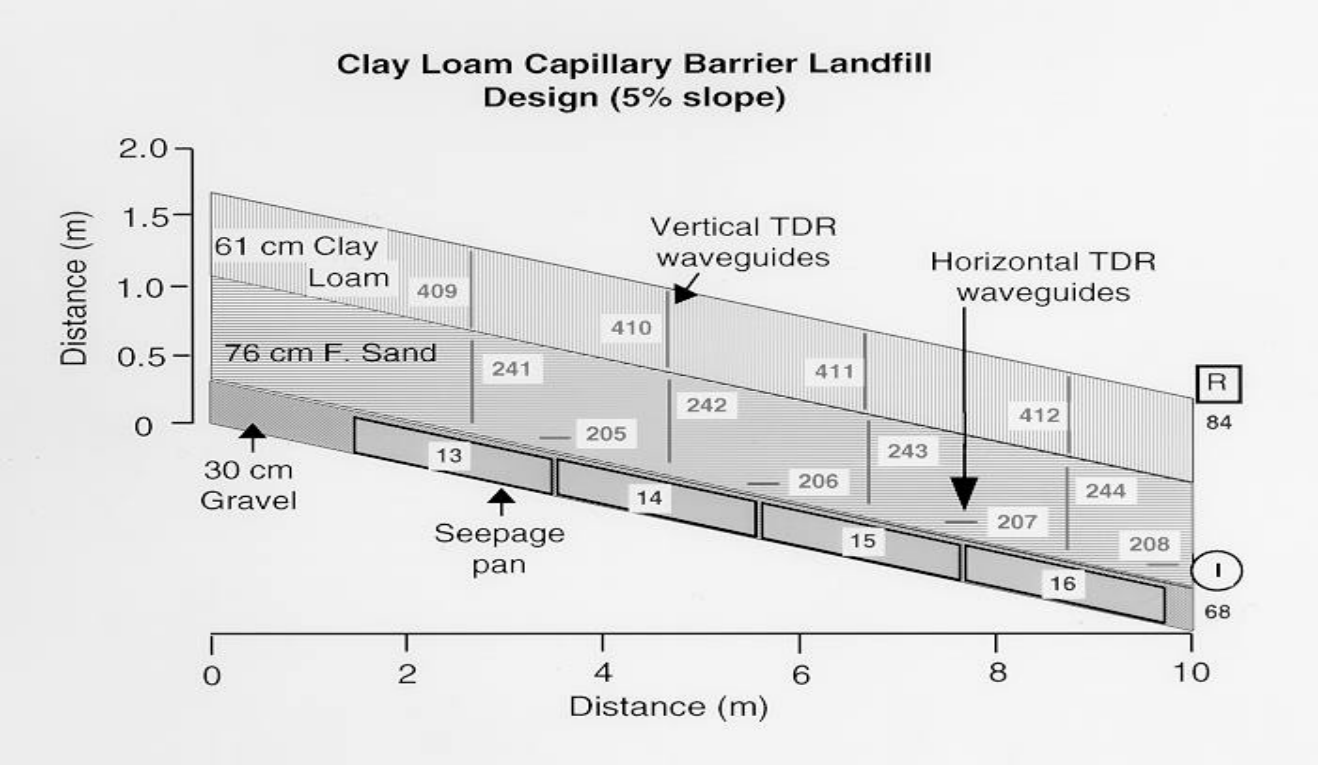

Fig. 1d. *Plot profile of Clay Loam Capillary Barrier Design*

Each set of wave guides was connected to 4.6-m of shielded twin-lead antenna cable that was connected to a molded balun connected to a 26-m length of RG-8/U coaxial cable. An instrument trailer housed a 256-to-1 coaxial switch that connected one set of wave guides at a time to a TDR cable tester (model 1502B, Tektronix Inc., Beaverton, OR) through a system of 37 8-to-1 coaxial switches (model 610-007A, Autek Systems Corp., Santa Clara, CA). The computerized TDR system captured and stored the information from each pair of wave guides as a 220-point waveform (which represented an average of 16 waveform determinations). A personal computer (model 386-20, Compaq Computer Co., Austin TX) stored the waveform data on a hard disk, which was then used to determine the water content of the soils using the calibration described by Topp, *et al*., (1980).

APPROACH

The TDR data were segregated by soil type to see if any observable effects were related to a soil type and because each soil type experienced very different soil water content levels and fluctuations due to their physical location within the plots.

Two approaches were used for this analysis. In the first, data from each TDR was compared only to data from the same TDR for each of the years. Annual averaging of the measurements for each TDR was performed which contributed to smoothing variations from seasonal changes in soil water content. While year to year variations in soil water content will still have an effect on the annual means, the mean for any one year can be compared to the mean of all the years (Grand Mean). The comparison of the final year's mean to the grand mean should be in the same range as the comparison of the other years means to the grand mean if there has been no appreciable degradation of the measurement system.

The first technique used thus becomes:

1. segregate TDR measurements by soil type
2. determine failure rate of TDRs in each soil type and overall failure rate
3. determine the annual mean for each TDR in a soil type for all years
4. compare each TDR annual mean for a particular year to the Grand mean.
5. compare annual means from year to year for each TDR to determine if the final year indicates any trend that is noticeably different from the other years. The final year of the experiment should be the strongest indicator of a system that is degrading over time.

The second approach is based on the time stability concept described by Vachaud, *et al*., (1985), in which the difference Δ_{ij} between individual determinations of soil water content S_{ij} at location i (i =1-L) at time j (j =1-2486) and the mean soil water content S_j at the same sampling time is calculated:

$$\Delta_{ij} = S_{ij} - \overline{S}_j$$

with

$$\overline{S}_j = (1/L)\sum_{i=1}^{i=L} S_{ij}$$

where

L= number of locations for a soil type

This corresponds to a relative difference:

$$Rd = \Delta_{ij} / S_j$$

Our multiple daily measurements were averaged on a daily basis to provide a uniform sampling interval for this analysis. By determining the annual mean of these daily differences any large spread in the grouping around the mean should be apparent which would indicate that some of the TDRs are behaving abnormally. We employed this approach on two of the soil types. The medium sand was chosen because it was impacted very little by precipitation, and clay loam topsoil was chosen because it was used as a topsoil and experienced large fluctuations in water content.

ANALYSIS

The failure rate of the TDRs was determined for each soil type as well as for the experiment overall. Out of the 212 TDRs in the experiment 10 had failed by the time data collection had stopped, giving an overall failure rate of 4.7%. Table 1 shows the total number of TDRs in each soil type and failure rates for each. There has been no post mortem performed to identify the exact failure mechanism.

SOIL TYPE	TOTAL	FAILED	FAILURE RATE (%)
Medium Sand	16	0	0%
Fine Sand	64	2	3.1%
Tuff	32	3	9.4%
Clay Loam	16	1	6.3%
Loam	48	0	0%
Clay/Tuff	36	4	11.1%

Table 1. *TDR Failure Rates By Soil Type*

Analyses were performed on five (medium sand, fine sand, tuff, clay loam, loam) of the six soil types in the experiment. The clay/tuff soil was not included due to this soil's high electrical conductivity, which made soil water content determinations difficult. Regulatory requirements for long-term monitoring of covers with a clay layer of this type may require use of alternative monitoring technologies. Since the aim of our efforts is an attempt to determine stability it was decided to only consider data from soils that are good candidates for TDR measurements. Figures 2 through 6 show representative examples of soil water content over time for TDRs in each of the soil types. These plots demonstrate the wide range of soil water content regimes between soil types. Also plotted are the annual means and the grand mean for that probe. As the degradation of a system should be most apparent over longer periods of time it is instructive to compare the data from the last year of the experiment to data from earlier years. Time series plots for all the TDRs show no obvious differences for 1998 as compared to the other years.

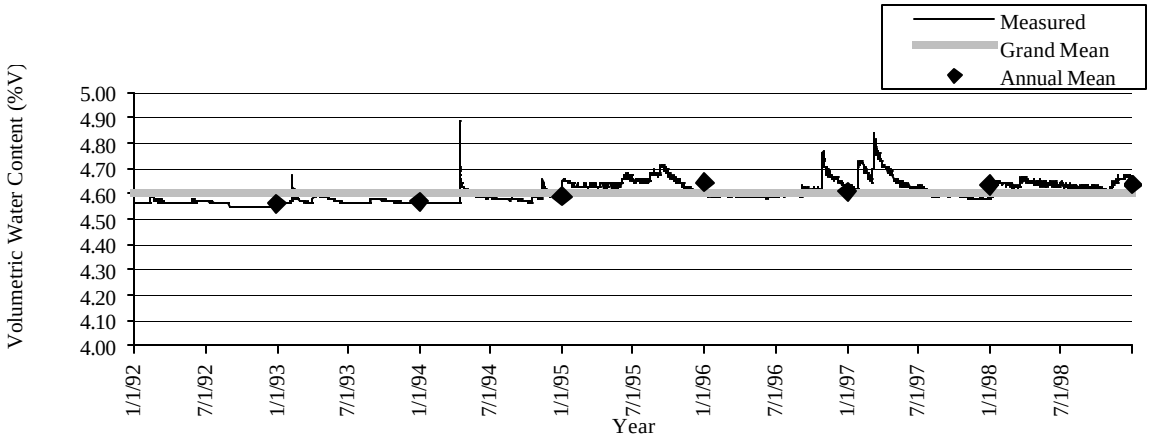

Fig. 2. *Typical TDR in Medium Sand*

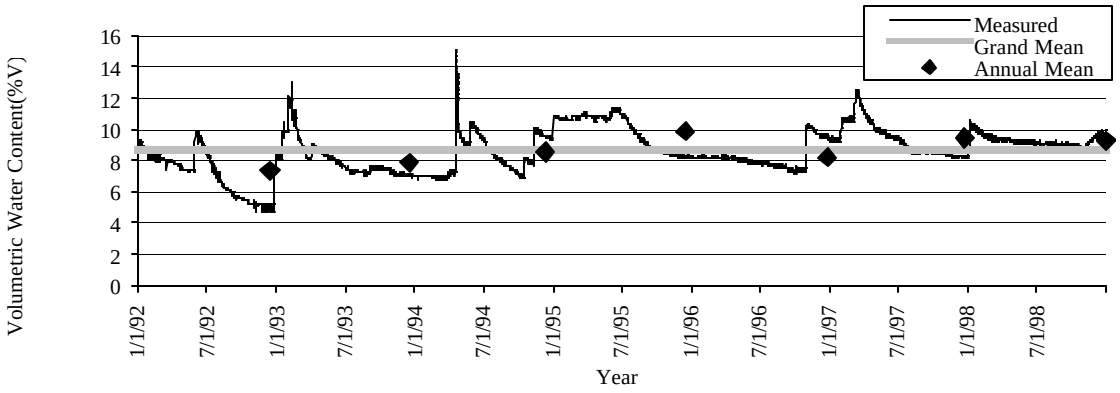

Fig. 3. *Typical TDR in Fine Sand*

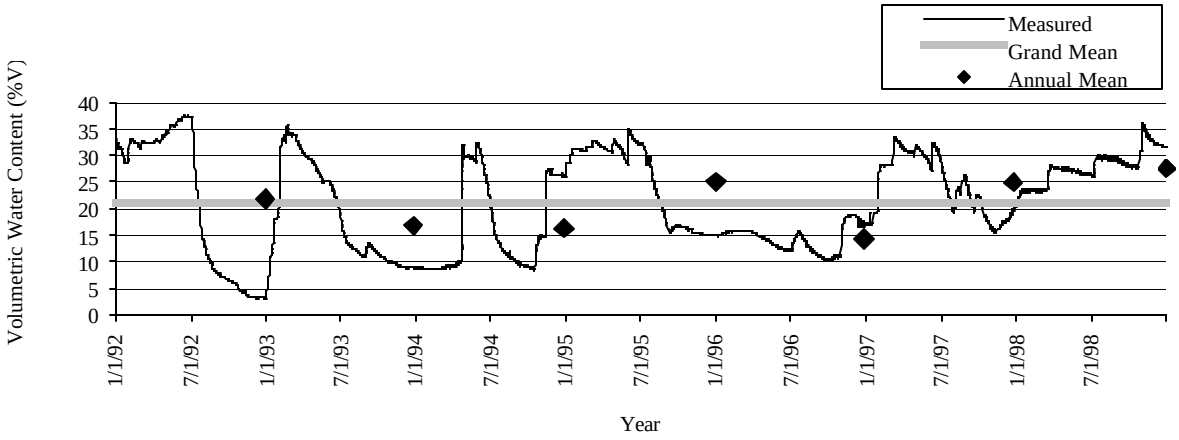

Fig. 4. *Typical TDR in Tuff*

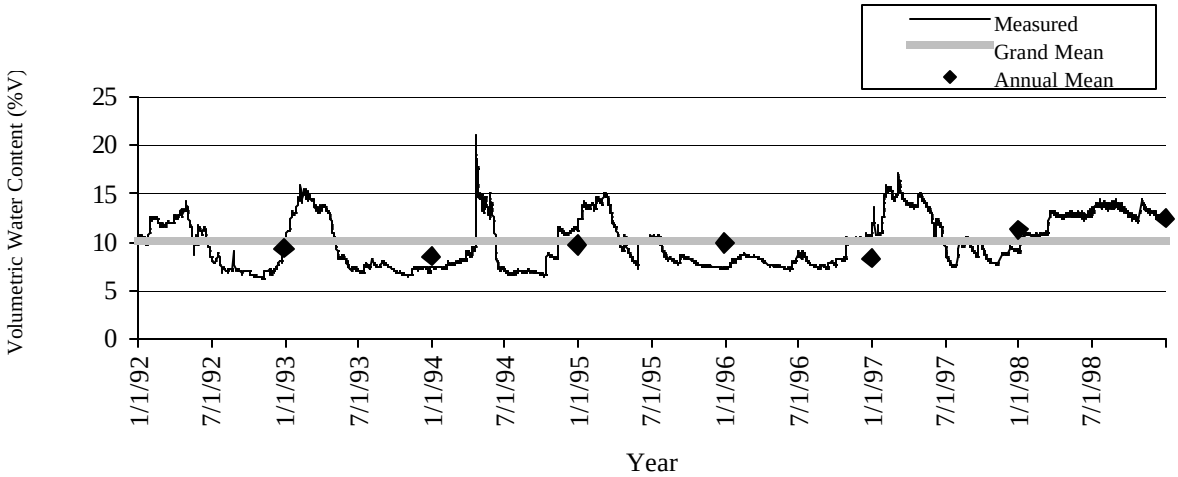

Fig. 5. *Typical TDR in Clay Loam*

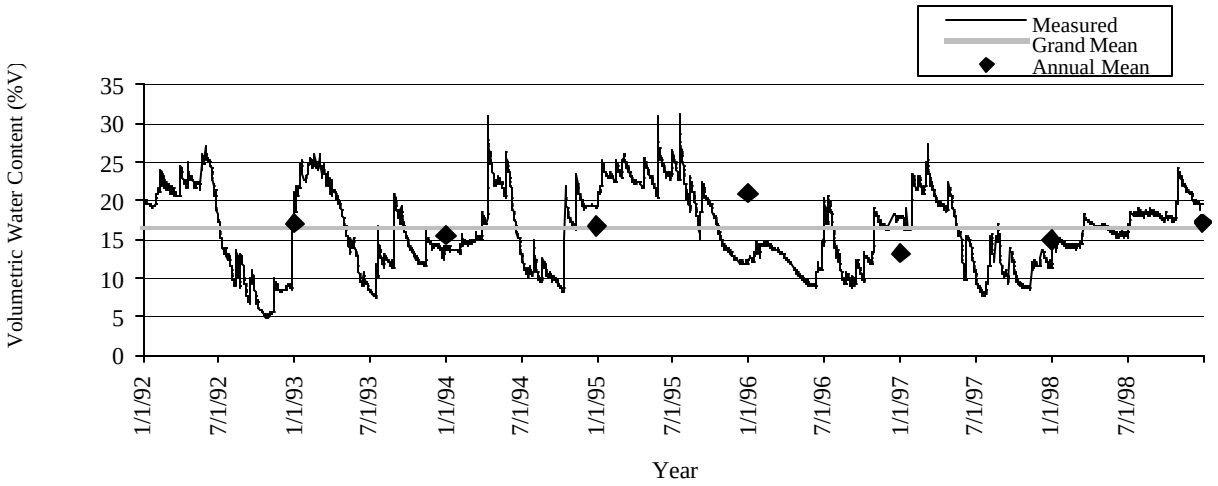

Fig. 6. *Typical TDR in Loam Topsoil*

The annual mean water content for every probe was calculated and plotted by soil type (Figures 7 through 11). Considering the spread of the data points for each year it is seen that the 1998 data falls within the range of the data from the earlier years. The medium sand layer (Figure 7) maintained very stable water contents for the length of the experiment. Response to precipitation can be seen in the time series plot for this probe (Figure 2) but the change in values were on the order of less than half of a per cent volumetric water content. While this change is certainly caused by precipitation it shows that if there is any trend to instability in the system it is not observable even on a water content scale this fine.

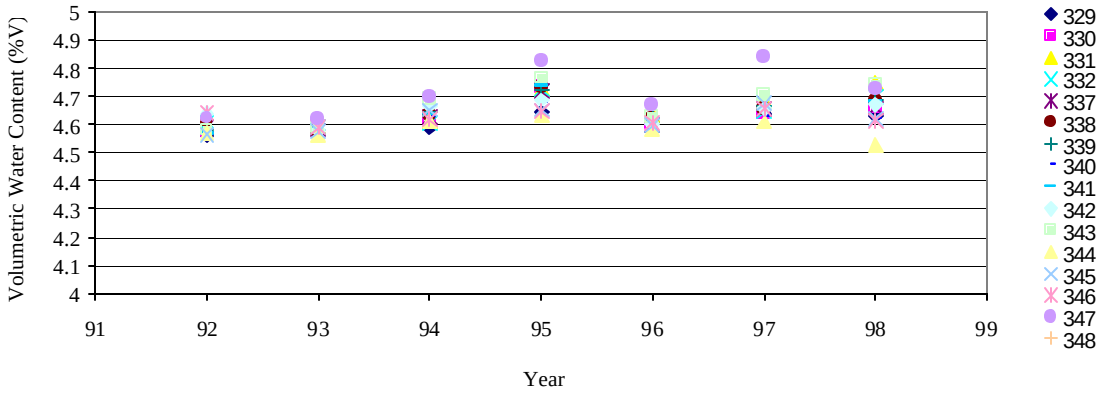

Fig. 7. *Medium Sand Annual Means By Probe*

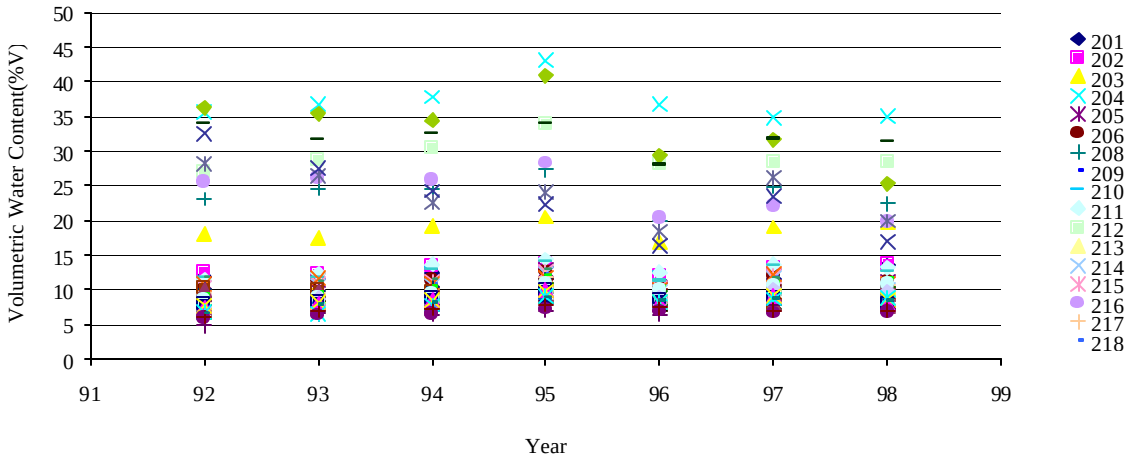

Fig. 8. *Fine Sand Annual Means By Probe*

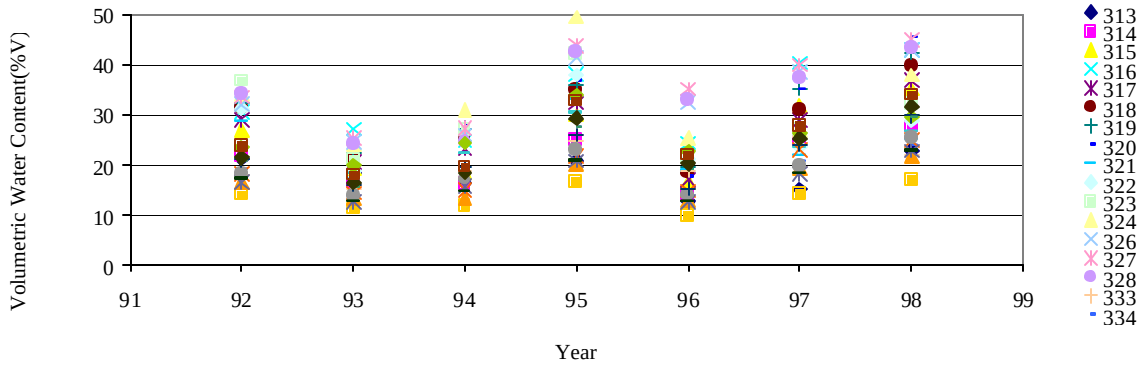

Fig. 9. *Tuff Annual Means By Probe*

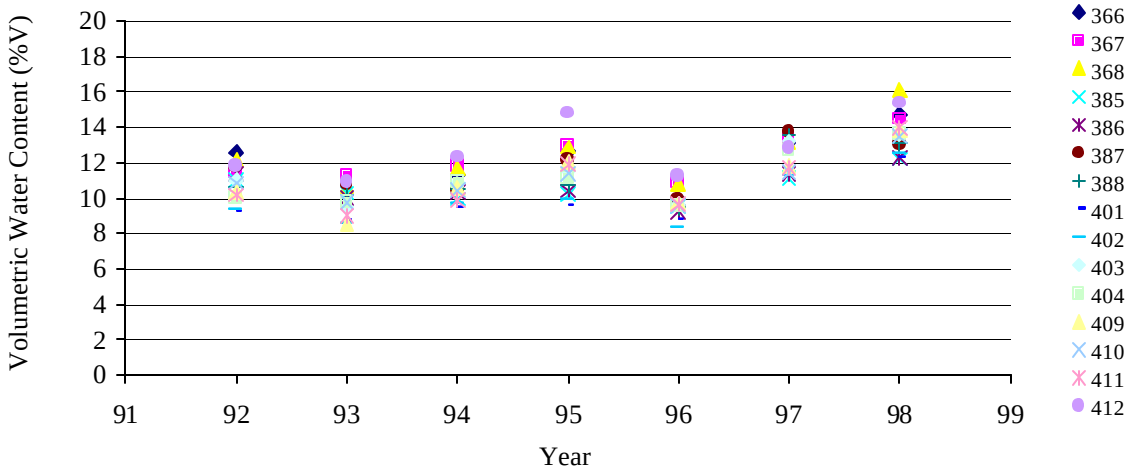

Fig. 10. *Clay Loam Annual Means By Probe*

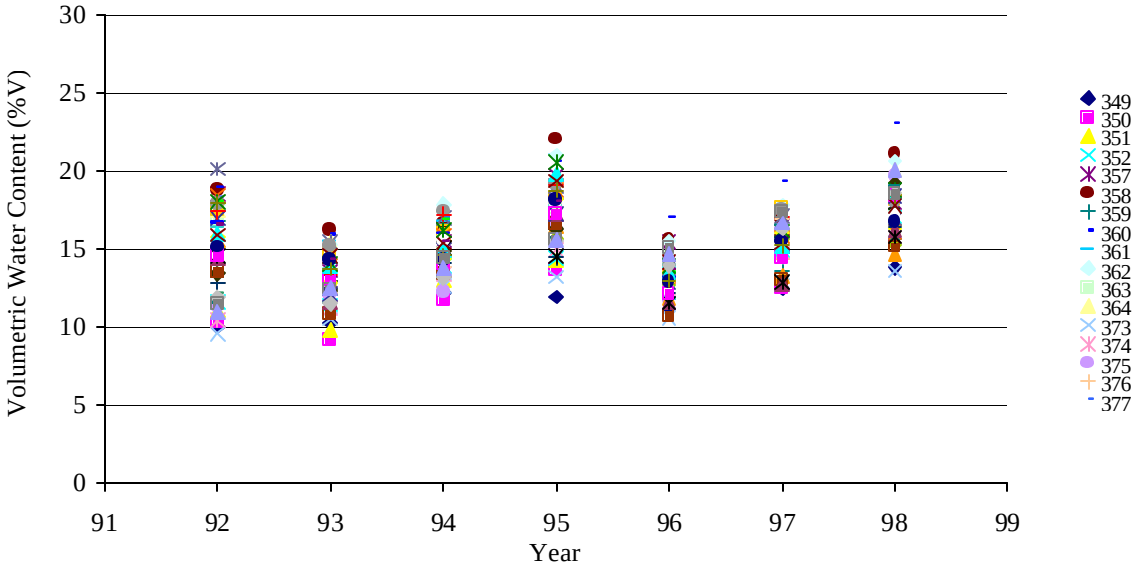

Fig. 11. *Loam Topsoil Annual Means By Probe*

The mean relative difference calculation of the medium sand data, which is presented by year, is shown in Figure 12. While there is slightly more spread in the values around the mean in the 1998 data, the maximum mean relative difference for any of the TDRs is less than 4% and the 1998 data are not largely different than the previous years. The results of the same calculation of the clay loam data are shown in Figure 13. The spread around the mean is on the order of + or – 15% reflecting the greater fluctuations in water content seen by these TDRs. However, the overall spread of the data around the mean is basically the same for all years.

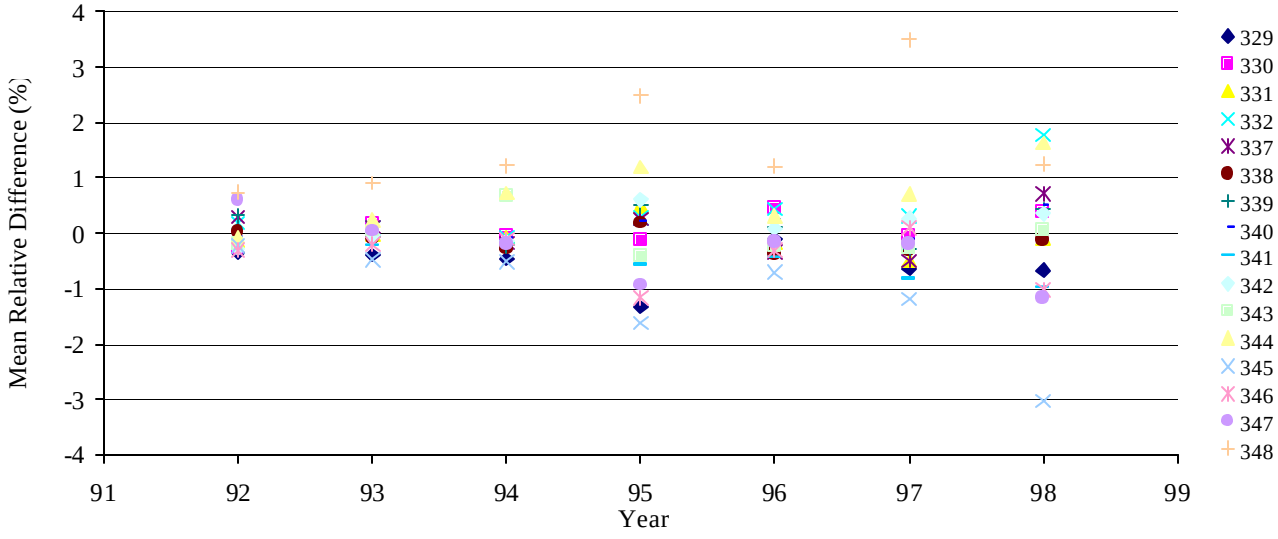

Fig. 12. *Mean Relative Difference By Year in Medium Sand*

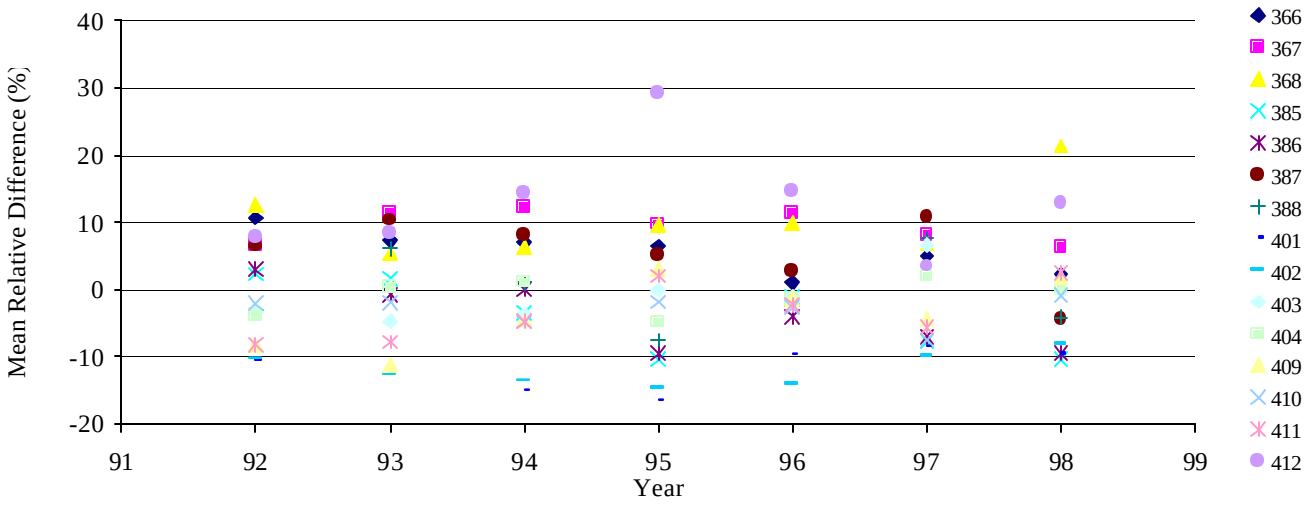

Fig. 13. *Mean Relative Difference By Year in Clay Loam*

CONCLUSIONS

Preliminary analysis of seven years of data from 212 TDR locations emplaced in various soil materials at Los Alamos showed no discernable evidence of drift in water content measurements. Changes in soil water content due to precipitation make an analysis of signal stability difficult. Even in a soil that has very little change in water content over long time periods and changes by only small increments, no discernable trend in the data could be identified. Comparing annual averages from year to year for each TDR showed no large in difference in the final year of data compared to previous years which should have given an indication of overall signal drift. Also, comparing the relative mean difference of each TDR compared to all other TDRs at any one sampling time showed no evidence that there was a trend in the data from one year to the next. This leaves us with only two possible conclusions. Either there is no stability problem with this technology in the time frame involved in this experiment or any trend to instability is of such a small value that it was not evident even in our most stable soil. The robustness of the TDR system is evident in the low failure rate we experienced over the seven years of data collection.

ACKNOWLEDGEMENTS

The author would like to thank Dr. John Nyhan for his contribution to the experimental design and project oversight. Thanks also to Dr. Everett Springer for his invaluable guidance in the analytical approach and for his editorial contribution. The data collection effort for this study was supported by the Environmental Restoration Program at Los Alamos National Laboratory. Los Alamos National Laboratory is operated by the University of California for the U.S. Department of Energy under contract W-7405-ENG-36.

REFERENCES

Nyhan, J.W., Schofield, T., Martin, C., Use of Time Domain Reflectometry in hydrologic studies of multi-layered landfill covers for closure of waste landfills at Los Alamos, New Mexico, Proceedings of the Symposium on Time Domain Reflectometry in Environmental, Infrastructure, and Mining

Applications, Evanston, Illinois, Sept 7-9, U.S. Bureau of Mines, Special Publication SP 19-94, 1994, NTIS PB95-105789, 193-206.

Nyhan, J.W., Schofield, T., Starmer, R., A water balance study of four landfill cover designs varying in slope for semiarid regions, Journal of Environmental Quality, **26**, No. 5, Sept. – Oct. 1997, 1385-1392.

Topp, G.C., Davis, J., Annan, A., Electromagnetic Determination of Soil Water Content: Measurements in Coaxial Transmission Lines. Water Resources Research, **16**, No.3, 1980, 574-582.

Vachaud, G., Passerat De Silane, A., Balabanis, P., and Vauclin, M., Temporal stability of spatially measured soil water probability density function, Soil Science Society of America Journal, **49**, 822-827, 1985.

LONG-TERM MONITORING OF SOIL-MOISTURE IN A HARSH CLIMATE USING REFLECTOMETER AND TDR PROBES

William N. Herkelrath[1] and Geoffrey N. Delin[2]

[1] U.S. Geological Survey, Menlo Park, CA 94025; wnherkel@usgs.gov
[2] U.S. Geological Survey, Mounds View, MN 55112; delin@usgs.gov

ABSTRACT

An automated data logging system was used to measure unsaturated zone hydraulic properties relevant to evaluating the effects of recharge on dissolution of crude oil at a research site near Bemidji, Minnesota. Laboratory and field testing of several soil-moisture probes indicated that the CS615 "reflectometer" probe was better suited than the CS605 time-domain reflectometry (TDR) probe to the field conditions of having a limited power supply and extreme weather typical of northern Minnesota. All probes were manufactured by Campbell Scientific Inc. The reflectometer probes provided dependable and accurate data over long time periods, were somewhat easier to install, and had less data fluctuation than the TDR probes. However, there were problems, both with the reflectometer and TDR probes. Many of the probes that were installed beneath the water table or within the capillary fringe eventually failed. Also, laboratory calibrations run using soil from the field site differed significantly from the calibrations provided by the manufacturer. Recharge estimates based on the horizontal soil-moisture probe measurements varied by about ±25%, possibly because of uncertainty in the calibration curves. The most serious problem with the reflectometer probes occurred when a severe electrical storm apparently caused a permanent shift in the probe calibrations. Some TDR probes that were installed vertically in the unsaturated zone at the bottom of boreholes yielded anomalously high values of soil moisture. It is possible that installation of the vertical probes created a preferential pathway that caused moisture content to increase in the vicinity of the probes.

INTRODUCTION

Long-term monitoring of soil moisture has become routine in the past two decades with the emergence of dataloggers and electronic monitoring equipment (Baker and Allmaras, 1990; Herkelrath *et al*., 1991; Delin *et al*., 1997). These types of automated electronic soil-moisture monitoring systems have distinct advantages over

the widely used neutron probe method in that they can be automated to collect data unattended, can collect numerous measurements each day, and do not require a radioactive source. Long-term monitoring of soil moisture in cold climates, where temperatures during the winter commonly reach –30°C, can be problematic, particularly when cable testers are required for making time-domain reflectometry (TDR) measurements (Herkelrath *et al*., 1991; Delin and Herkelrath, 1999). Additional research is needed to evaluate how these types of automated soil-moisture monitoring systems perform over long periods of time in cold climates.

The primary goal of the investigation described in this paper was to determine which of three probes was most appropriate for long-term monitoring of soil moisture at a crude-oil research site near Bemidji, Minnesota. A wide variety of different soil-moisture probes are available. Three Campbell Scientific Inc. probes were used in this study primarily because of a preponderance of compatible equipment already installed at the site (use of trade names does not constitute endorsement by the U.S. Geological Survey). Probe length is a factor that has been evaluated in previous studies. Zegelin *et al*. (1992) found that measurement of travel times becomes inexact for shorter probe lengths. We evaluated the effects of a 50-cm long probe versus the more standard 30-cm long probe.

A secondary goal was to investigate the effects of probe orientation on soil-moisture measurements and ground-water recharge estimation. Soil-moisture probes used for long-term monitoring typically are installed horizontally in the wall of a shallow pit or trench. One of the primary reasons for using a horizontally oriented probe is to measure soil moisture at a single elevation in the soil profile. However, this method of installation is highly invasive and is generally limited to about the upper 2 m of the unsaturated zone. Another method of installation is to place the probes vertically in a borehole. This allows installation of the soil-moisture probes at any depth within the unsaturated zone. A disadvantage of this type of installation is that the collected data do not represent a single depth but rather the average soil-moisture measured over the entire vertical length of the probe. Another disadvantage is that the borehole above the probe is backfilled with soil that may be poorly compacted, which could alter the vertical flow of water. Thus, the soil-moisture measurements using a vertical installation may not be representative of the undisturbed native soil. Little is known of how probe orientation affects soil-moisture measurements.

This research was part of a larger study designed to better understand the effects of recharge on the dissolution and movement of oil through the unsaturated and saturated zones at the research site. The soil-moisture data were used to estimate recharge during 1999 based on an unsaturated-zone water balance method.

Location And Description Of Research Area

On August 20, 1979, approximately 16 kilometers northwest of Bemidji, Minnesota, the land surface and shallow subsurface were contaminated with crude oil when a pipeline burst, spilling about 1,700,000 L of crude oil onto a glacial outwash deposit. After cleanup efforts were completed, about 400,000 L of crude oil remained at the site. Some crude oil percolated through the unsaturated zone to the water table near the rupture site (north oil pool, fig. 1). Some of the oil flowed over the land surface toward a small wetland forming two other areas of oil infiltration (middle and south oil pools).

Sediments at the site consist of poorly sorted glacial outwash sand of fine to very coarse grain size, with some fine gravel and cobbles. One- to 10-mm thick iron-cemented laminations occur between depths of 0.3 and 1.0 m at the south oil pool. Crude oil (about 0.1-0.5- m thick) floats on the water table, which is about 2.7 m below land surface at the south oil pool. At a depth of about 25 m, a regionally persistent and uniform layer of low permeability till restricts vertical ground-water movement.

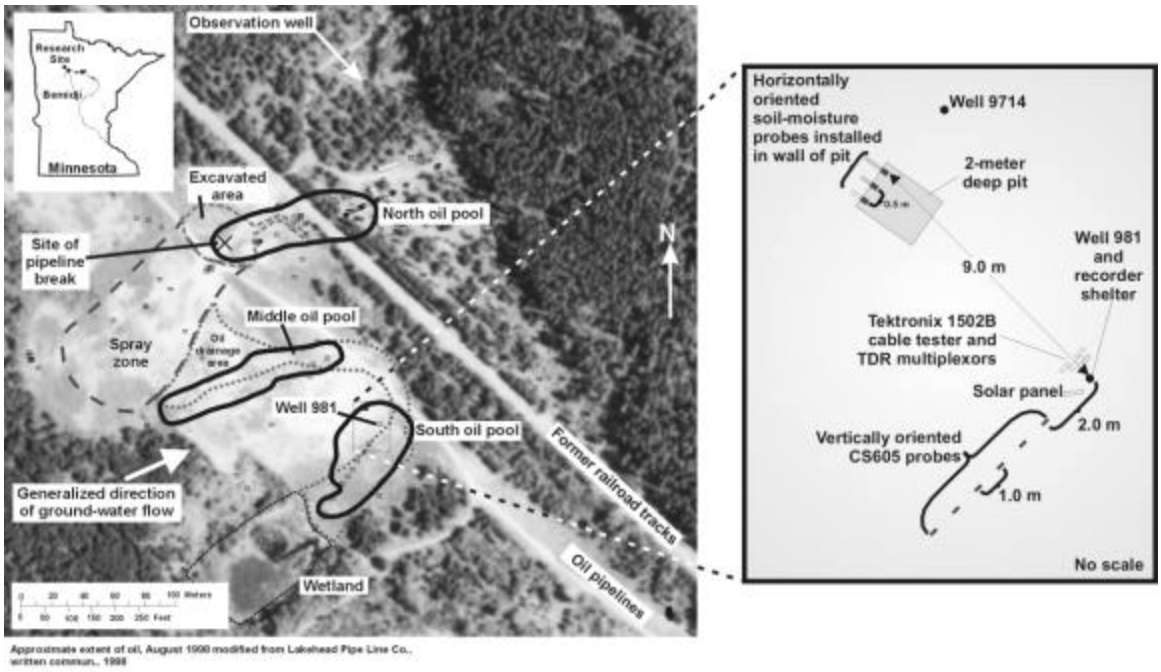

Fig. 1. *Features of the Bemidji, Minnesota crude-oil spill research site superimposed on a 1991 aerial photograph and layout of instrumentation near Well 981.*

Methods

An automated data-logging system was installed near Well 981 (south oil pool; fig. 1) in late 1996 to compare the performance of several different soil-moisture probes used to estimate recharge at the site. Other data measured continuously at the site included soil temperature (at 50-cm depth intervals), ground water level in nearby Well 9714, and precipitation. The soil moisture and other data were collected every four hours from late 1996 to July, 2000. Data logger water levels were calibrated monthly using an electric contact gauge. Solar-charged batteries initially powered the Campbell Scientific CR10X data logger and the TDR system. The batteries were replaced in the fall of 1997 with 110-volt AC power supply.

Three types of Campbell Scientific soil-moisture probes were installed at the Well 981 site. The CS615 probes were 30-cm long and had 2 prongs (Bilskie, 1997). The CS615 is a self-contained “reflectometer” that does not require a TDR cable tester to determine water content. This probe was compared to 30-cm long and 50-cm long TDR probes that require a cable tester. A two-meter-deep pit was dug, and 3 vertical profiles of probes were installed in the pit. Each profile consisted of 6 probes of the same type. A total of 18 probes were

installed in the pit. The three vertical profiles were separated laterally by about 0.5 meters. The uppermost 4 probes were pushed horizontally into the undisturbed soil in the pit wall at depths of 50, 100, 150, and 200 cm. Small boreholes were dug in the bottom of the pit, and the lowermost two probes were installed vertically into the soil at the bottom of the boreholes at depths of 250 and 300 cm below land surface. The pit and boreholes were backfilled with soil after the probes were installed. An array of 6 vertically oriented, 30-cm long TDR probes was also installed at 50-cm depth intervals in small-diameter boreholes located about 2 m southwest of Well 981 (fig. 1). The boreholes were backfilled with soil after the vertical probes were installed.

Using the methods described in Herkelrath *et al*. (1991), the three types of soil-moisture probes were calibrated in the laboratory using repacked, 10-cm-diameter columns of sandy sediments obtained from the field site. Each probe was inserted into the top of its own dry column. The columns were kept vertical throughout the calibration. After the probes were installed, each column was saturated with water from the bottom through a tube. Relative permittivity of the sediments was determined for the saturated sample using each soil-moisture probe. Each column was drained in a series of steps by suction of water out the bottom. Soil permittivity and column mass was measured at each moisture-content step. At the end of the experiment the soil was removed and oven dried. Total water content corresponding to each measurement was calculated from the difference between the measured column mass and the oven-dry mass. Volumetric water contents were assumed to equal the ratio of total water content to soil volume.

Ground-water recharge estimation using the soil-moisture data was based on the zero-flux plane (ZFP) water-balance method (Richards *et al*., 1956). The ZFP is defined as the horizontal plane in the unsaturated zone where the vertical hydraulic gradient is equal to zero. According to this hypothesis, water in the soil above the ZFP moves upward in response to evapotranspiration, and water below the ZFP drains downward to the water table. We assumed that water that infiltrates into the "recharge zone" below the ZFP is unavailable for evapotranspiration and results in "recharge."

The elevation of the ZFP changes during the year. The ZFP is near land surface during the winter months when evapotranspiration is low, and then moves downward as evapotranspiration demand increases in summer. Unfortunately, our knowledge of the location of the ZFP in this study was limited. Tensiometers were installed at the Well 981 site to measure the soil-water potential profile and estimate the ZFP elevation, but the instruments failed and the measured data could not be used. However, tensiometer data obtained at a nearby location at the north oil pool (fig. 1) indicated that the ZFP depth was above a depth of 1.0 meter throughout the year. We assumed that similar ZFP depths existed at the south pool.

To estimate recharge using the soil-moisture probe measurements, we calculated the maximum increase in the total volume of water present in the recharge zone that occurred during each recharge event:

$$R_j = V_{jmax} - V_{jant} . \qquad [1]$$

R_j is the recharge per unit cross section that occurred during recharge event j, V_{jant} is the total volume (per unit cross section) of moisture present antecedent to the event, and V_{jmax} is the maximum moisture volume measured during the recharge event. The total volume of moisture in the recharge zone, per unit cross section, was estimated by

$$V = \sum_{i=1}^{M} q_i \Delta z_i \,, \qquad [2]$$

where i is an index to the soil-moisture probes (equal to one for the probe nearest the water table and increasing upward to a value of M for the probe nearest the ZFP), q_i is the soil moisture content measured by probe i, and Δz_i is the vertical thickness of the unsaturated zone associated with probe i. The annual recharge is assumed to equal the sum of the individual recharge events during the year.

Recharge was also estimated by applying the method of hydrograph analysis (Rasmussen and Andreason, 1959) to water-level data from nearby Well 9714. In this method, the measured change in water-table elevation in a well was used to estimate the change in the amount of water stored in the aquifer. The change in storage was attributed to recharge. At the study site, recharge was assumed to equal the water table rise multiplied by the assumed aquifer specific yield of 0.3.

RESULTS AND DISCUSSION

Probe calibration

Results of laboratory calibration tests indicated that the volumetric water content calculated using the factory-supplied calibration for the CS615 "reflectometer" probe was accurate to within about +/- 0.02 cm^3/cm^3 of the volumetric water content based on gravimetric analyses over the entire moisture-content range (fig. 2). On the other hand, the volumetric water content based on the factory-supplied software for the TDR probes was consistently greater than the volumetric water content based on gravimetric analyses. The lab calibration for each probe type was assumed to apply to all field probes of the same type. Water content measurements obtained in the field using the factory-supplied software were corrected using the functional relationships graphed in figure 2. Each curve was fit to a polynomial function that was used to calculate "actual" moisture content from the "factory" value.

Comparison of soil-moisture probe performance in the field

The two-pronged reflectometer probe was easier to install than the three-pronged TDR probe, largely because of increased friction and the enhanced likelihood of hitting gravel with three prongs. However, care was required during installation of the reflectometer probes to ensure that the internal circuitry of the reflectometer was not damaged. The 50-cm long TDR probes were most difficult to install because of their greater length, which increased friction and the likelihood of hitting gravel.

As an example of the data collected during this study, soil-moisture measurements collected during 1999 from the probes located at the 100 and 150 cm depths are shown in figures 3 and 4. Data were lost as a result of an electrical storm on July 3, 1999 and also during a period of time in December 1999. These periods of record are labeled "Missing data" in the figures.

The 3 horizontal soil-moisture probes at each depth detected wetting front arrival at approximately the same time following precipitation events. However, the magnitude of the response of horizontal probes installed at the same depth differed by as much as 0.07 cm^3/cm^3. It is possible that spatial variability in particle size and soil structure resulted in this much variability in soil moisture. However, it is also possible that most of the measured variability was an artifact caused by the fact that the calibration curve varies from probe to probe, and as a function of soil structure.

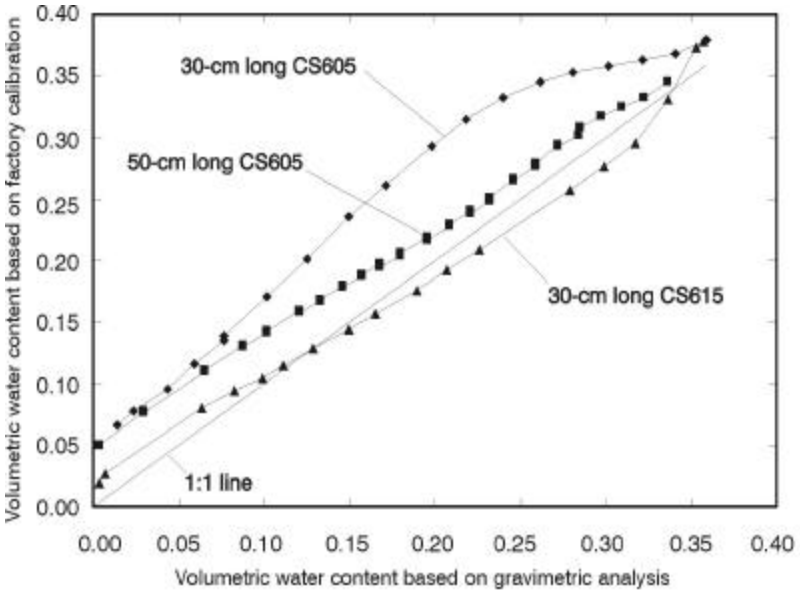

Fig. 2. *Calibration results for Campbell Scientific soil moisture probes at the Bemidji crude-oil spill site.*

There was an anomalous change in measured soil moisture for the reflectometer probes, which resulted from damage caused by the severe storm on July 3, 1999. Day-to-day changes in soil moisture measured by these probes from July through December 1999 are reasonable. However, the moisture-content vs. time curve for each probe (figs. 3 and 4) appears to be shifted by a constant amount after the storm. We hypothesize that an element of the reflectometer circuit in each probe was permanently damaged by the lightning strike. We estimated the amount of the curve shift caused by the storm by comparing steady soil moisture content values obtained using the reflectometer probes in winter before and after the storm. The shifts in the measured soil moisture content varied from +0.11 to -0.03 cm3/cm3. We plan to retrieve the probes at the end of the experiment and investigate the nature of the damage.

Soil-moisture values measured with the reflectometer probes were more stable and had less data fluctuation ("noise") than those measured with the TDR probes. The background noise level for probes in the upper 200 cm of the unsaturated zone was estimated using the soil moisture measurements taken during the winter months of January through March 1999. During this period, the soil was frozen to a depth of about 60 cm and the soil moisture was relatively constant at all depths. The first step in estimating the noise in the moisture content vs. time data was to smooth the data by calculating the running median of each group of five consecutive measured values. The noise was then estimated by calculating the root-mean-square difference between the raw moisture content vs. time curve and the smoothed curve for the entire winter. The noise in the reflectometer probe data ($\sim 6 \times 10^{-5}$) was much less than for the TDR probes ($\sim 1 \times 10^{-3}$).

Data loss for the reflectometer probes were much less than for the TDR probes in the upper 200 cm of the unsaturated zone. Loss of data could critically affect recharge estimates resulting in inaccurate or missing estimates. Only 0.7, 0.0, and 0.4 percent of the reflectometer data were lost during 1997, 1998, and 1999, respectively. Average data loss for the TDR probes was 17.9, 11.3, and 4.9 percent, respectively, in 1997, 1998, and 1999. Data losses as a result of the July 3, 1999 electrical storm were not included in the calculation

of losses for 1999. Most of the data loss for the TDR probes occurred when the cable tester could not detect the end of the soil-moisture probe, which resulted in out-of-range values. Apparently, the signal reflected from the end of the TDR probe was not of sufficient amplitude. A minimal amount of the data loss for the TDR probes resulted from variations in power supply voltage and line noise that caused out-of-range values.

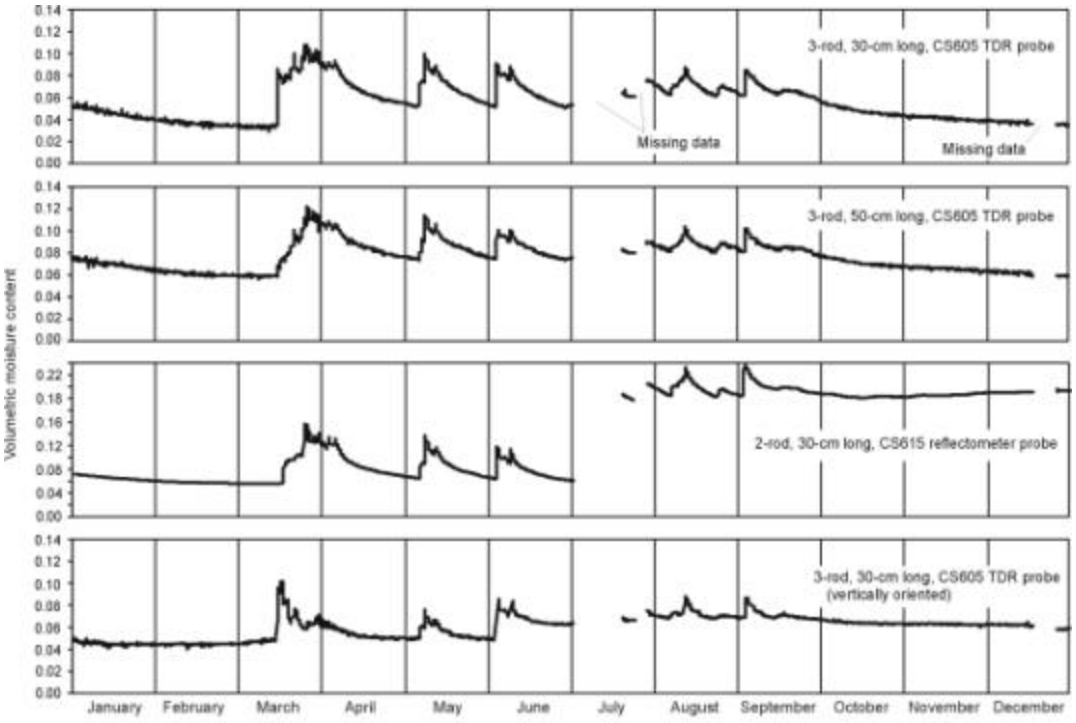

Fig. 3. *Measured soil moisture content during 1999 at the 100-centimeter depth.*

Data losses for the TDR probes in the capillary fringe (250-cm depth) and below the water table (300-cm depth) were significant, averaging 31 and 52 percent of the time, respectively, during 1999. In many of these cases, the cable tester failed to detect the end of the parallel rods in the saturated or near-saturated moisture conditions, resulting in an over range soil-moisture value. Unrealistically large values (greater than aquifer porosity) were also recorded by the TDR probes. Data losses for the reflectometer probe at the 250-cm depth were 29 percent prior to the July lightning strike. Data losses for the reflectometer probe at the 200-cm depth were zero before the July lightning strike, but the probe failed to collect any accurate data following the storm. In addition to overrange values, the reflectometer probes at these depths also recorded erroneously large and small soil moisture values. Long-term data collection in the capillary fringe and below the water table was erratic using both the TDR and reflectometer probes. Many of the TDR and reflectometer probes in the capillary fringe and below the water table eventually failed completely. Apparently, the poor performance and failure of the probes was caused by long-term exposure to saturated or nearly saturated conditions.

During the time when the monitoring system was powered by solar-charged batteries, data losses for the TDR probes increased during the winter months when air temperatures were below -10°C. This increased data loss was likely due to insufficient solar radiation during the winter to charge the batteries to power the cable tester. On the other hand, the reflectometer probes had sufficient power to make measurements during the winter months. This problem of insufficient battery power for the cable tester was corrected by installation of 110-volt power supply in November 1997.

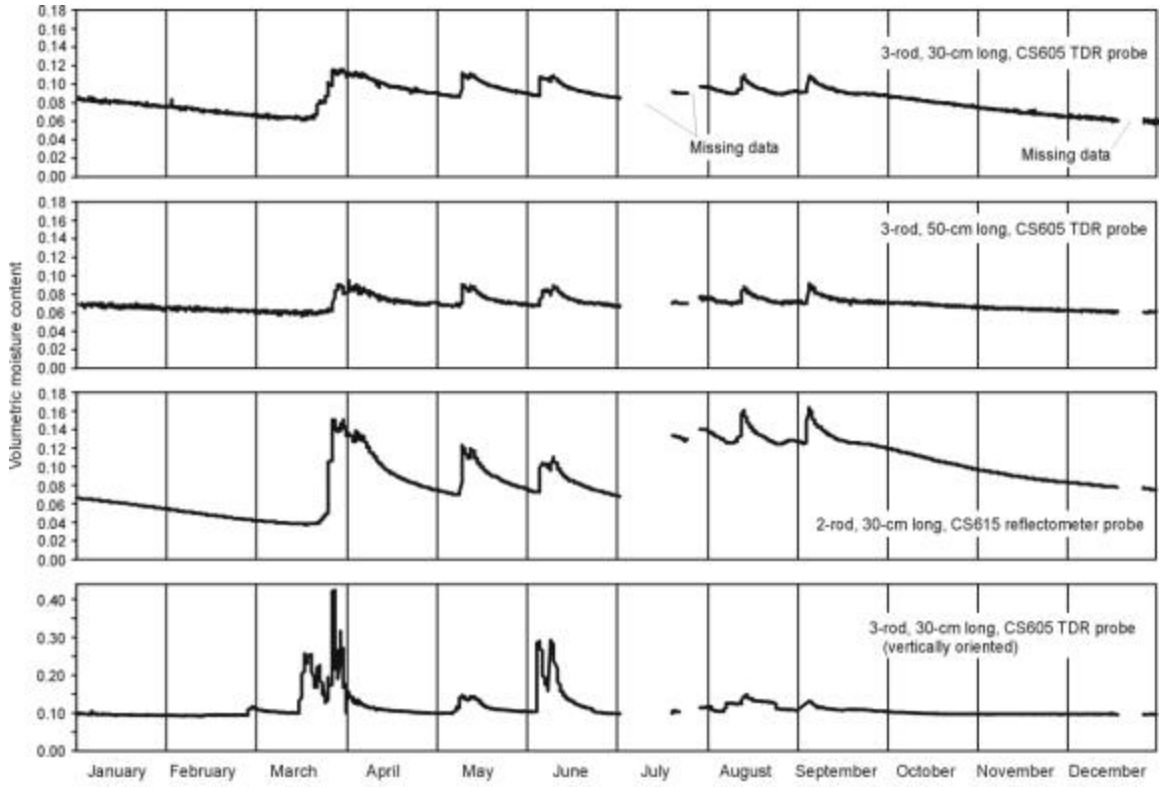

Fig. 4. *Measured soil moisture content during 1999 at the 150-centimeter depth.*

Ground-water recharge estimates

Ground-water recharge based on the zero-flux plane (ZFP) method was estimated at the Well 981 site for the six primary events in 1999 in which precipitation exceeded 2.0 cm. Recharge was not detected by the probes for rainfall events of less than 2.0 cm. As shown in Table 1, the estimated recharge decreased as the assumed depth of the ZFP increased. For a given assumed ZFP depth, there was good agreement between the recharge estimates obtained using the horizontal TDR probe data. However, the recharge estimates for both the horizontal reflectometer probes and the vertical TDR probes were higher than the estimates for the horizontal TDR probes. The recharge estimates were significantly affected by changes in the calibration curve used to interpret the probe data. For example, as shown in Table 2, recharge estimates based on the factory calibration curves changed as much as ±25% compared to estimates obtained using the laboratory calibrations (Table 1).

The annual recharge estimated using the horizontal reflectometer and TDR probe data varied from about 25% to about 60% of 1999 precipitation, which was 82 cm. These results are similar to measurements obtained in other sand plain areas of the region, which indicate recharge typically ranges between 10 and 40 percent of total annual precipitation (Delin *et al*., 2000). On the other hand, the annual recharge estimated using the vertically oriented TDR probes was about 90% of precipitation, which is unreasonably high. Recharge estimated using hydrograph analysis (Rasmussen and Andreason, 1959) was about 20 cm, which compares most favorably with the horizontally oriented TDR probes with the ZFP at a depth of about 75 cm.

	1999 estimated recharge in cm for each probe (lab calibration)			
Assumed ZFP depth in cm	CS605-30 (Horiz. TDR)	CS605-50 (Horiz. TDR)	CS615 (Horiz. Reflectometer)	CS605-30 (Vertical TDR)
25	30	30	49	76
50	26	25	44	74
75	22	21	41	71

Table 1. *Recharge estimates based on soil-moisture measurements. Probe calibrations were based on laboratory experiments carried out using soil from the field site.*

	1999 estimated recharge in cm for each probe (factory calibration)			
Assumed ZFP depth in cm	CS605-30 (Horiz. TDR)	CS605-50 (Horiz. TDR)	CS615 (Horiz. Reflectometer)	CS605-30 (Vertical TDR)
25	38	27	39	69
50	33	22	35	65
75	29	18	33	62

Table 2. *Recharge estimates based on soil-moisture measurements. Factory probe calibrations were used in these estimates.*

Effects of Probe Orientation

Vertical probe orientation did not affect the noise in the data. The root mean square variance for the vertically oriented TDR probes was about the same as for the 50-cm long horizontally oriented probes. Data losses were nearly identical for all of the TDR probes in 1997, 1998, and 1999 irrespective of probe orientation. The magnitude of change in measured soil moisture in response to recharge events was not affected by probe orientation at the 50- and 100-cm depths (fig. 3), where changes were very similar for the horizontally and vertically orientated probes. However, at the 150- and 200-cm depths the magnitude of change in measured soil moisture for the vertically oriented TDR probes generally was two to six times greater in response to the recharge events (fig. 4). The vertically oriented TDR probes at the 150- and 200-cm depths typically detected wetting front movement hours to days earlier than the other probes at similar depths.

A likely factor contributing to the anomalously large changes in soil moisture at the 150- and 200-cm depths is the presence of crude oil. Crude oil was detected in the ground during installation of these vertically oriented probes. The oil may have caused a hydrophobic condition in the surrounding soil matrix. The installation of a vertical probe may have created a preferential pathway for flow of water. The preferential pathway could result in increased soil moisture content adjacent to the probe over a prolonged period of time. “Fingering” or “funnel flow” of water through hydrophobic soils is well documented (Wallis and Horne, 1992). In addition, the presence of crude oil in direct contact with the probes could have caused a change in the calibration curve.

Soil heterogeneity could also contribute to inconsistent response of the vertically oriented probes at the different depths. Although the soil at the site is mostly sand, there are isolated layers of silt, which have lower permeability and tend to impede infiltration. If the 150- and 200-cm probes penetrated silt layers, the probe electrodes could have created a localized preferential pathway through the silt, resulting in increased vertical movement of water.

Variability in the material filling the borehole above the vertically oriented probes may also have been a contributing factor to the inconsistent response of these probes. If the soil is nearly saturated, poorly compacted fill material in a borehole may have a high permeability and provide a preferential pathway for moisture. On the other hand, under dry conditions, poorly compacted fill material may be drier than the surrounding soil. Relatively dry fill material would tend to reduce soil moisture flow. Drilling and refilling of boreholes also destroys the layered soil structure in the borehole. Infiltrating water can be diverted laterally by silt layers in the unsaturated zone, and then "funneled" rapidly downward when a borehole filled with homogeneous sand is encountered (Kung, 1990). Further research into the effect of probe orientation on TDR measurements is warranted.

SUMMARY AND CONCLUSIONS

Laboratory and field testing of the soil-moisture probes indicated that the Campbell Scientific CS615 "reflectometer" probe was better suited than TDR probes to the field conditions of having a limited power supply and extreme weather typical of northern Minnesota. Field testing also indicated that (1) the reflectometer probes provided a dependable and accurate means for long-term monitoring of soil moisture in the glacial outwash being studied; (2) the reflectometer probe was somewhat easier to install in sandy soils than the standard TDR probe; and (3) data from the reflectometer probes had less "noise" than data from the standard TDR probes.

However, there were problems with both the reflectometer and TDR probes. Many of the probes that were installed beneath the water table or within the capillary fringe eventually failed. Also, laboratory calibrations run using soil from the field site differed significantly from the calibrations provided by the manufacturer. Recharge estimates based on the horizontal soil-moisture probe measurements varied about ±25%, possibly because of uncertainty in the calibration curves. The most serious problem with the reflectometer probes occurred when a severe electrical storm caused a permanent shift in the probe response. After the storm, day-to-day changes in the moisture content values obtained using the reflectometer probes were reasonable, but the moisture-content vs. time curves appeared to be shifted by a constant amount. Some TDR probes that were installed vertically in the unsaturated zone at the bottom of boreholes yielded anomalously high values of soil moisture. It is possible that installation of the vertical probes created a preferential pathway that caused moisture content to increase in the vicinity of the probes. It is also possible that the anomalous response of the vertical probes was caused by crude oil or hydrophobic soil contacting the probes.

REFERENCES

Baker, J.M, and Allmaras, R.R., 1990, System for automating and multiplexing soil moisture measurement by time-domain reflectometry: Soil Sci. Soc. Am. J., **54**,1-6.

Bilskie, Jim, 1997, Using dielectric properties to measure soil water content: Sensors, **14**, 26-32.

Delin, G.N., Healy, R.W., Landon, M.K., and Böhlke, J.K., 2000, Effects of topography and soil properties on recharge at two sites in an agricultural field: Am. Water Res. Assoc. J., **36**, 1401-1416.

Delin, G.N., Landon, M.K., Nelson, K.J., Wanty, R.B., Healy, R.W., Olsen, H.W., Böhlke, J.K., Schroyer, B.R., and Capel, P.D., 1997, Hydrogeologic and water-quality data used to evaluate the effects of focused recharge on ground-water quality near Princeton, Minnesota: 1991-95: U.S. Geological Survey Open-File Report 97-21, 30 p.

Delin, G.N., and Herkelrath, W.N., 1999, Long-term monitoring of unsaturated-zone properties to estimate recharge at the Bemidji crude-oil spill site: U.S. Geological Survey Water Resources Investigations Report WRIR 99-4018C, 143-151.

Herkelrath, W.N., Hamburg, S.P., and Murphy, Fred, 1991, Automatic, real-time monitoring of soil moisture in a remote field area with time-domain reflectometry: Water Resources Research, **27**, 857-864.

Kung, K. –J.S., 1990, Preferential flow in a sandy vadose zone: field observation: Geoderma, **46**, 51-58.

Rasmussen, W.C., and Andreason, G.G., 1959, Hydrologic budget of the Beaver Dam Creek Basin Maryland: U.S. Geological Survey Water-Supply Paper 1472, 106 p.

Richards, L.A., Gardner, W.R., and Ogata, G., 1956, Physical processes determining water loss from soil: Soil Sci. Soc. Amer. Proc., **20**, 310-314.

Wallis, M.G., and Horne, D.J., 1992, Soil water repellency: Advances in Soil Science, **20**, 91-146.

Zegelin, S.J., White, Ian, and Russell, G.F., 1992, A critique of the time domain reflectometry technique for determining field soil-water content: Proceedings of Soil Science Society of America symposium Advances in Measurement of Soil Physical Properties – Bringing Theory into Practice, SSSA Special Publication no. **30**, 187-208.

APPLICATION OF THE TDR TECHNIQUE IN TROPICAL SOIL

C. F. Souza[1], E. E. Matsura[2], and R. Testezlaf[3]

[1]UNICAMP/FEAGRI – Departamento de Água e Solo
Cx. Postal 6011, 13081-970, Campinas-SP-Brazil; cfsouza@agr.unicamp.br
[2]UNICAMP/FEAGRI – Departamento de Água e Solo
Cx. Postal 6011, 13081-970, Campinas-SP-Brazil;
[3]UNICAMP/FEAGRI – Departamento de Água e Solo
Cx. Postal 6011, 13081-970, Campinas-SP-Brazil; bob@agr.unicamp.br

ABSTRACT

One recent technology developed to estimate soil water content is the TDR technique (Time Domain Reflectometry), where the determination of a calibration curve is recommended (volumetric water content (θ) *versus* apparent dielectric constant (e_b)) for each soil type. The intensity of this limitation is more pronounced in tropical soils, because the equations available in the literature do not appear to take into account the differences of this type of soil. Silva (1998) concluded that it could affect the magnetic field created by electric pulse, and consequently affect the time of displacement of the emitted wave. The objective of this study is to discuss the limitations of Dusky Red Latosol calibration equation and to develop modifications which would overawe these limitations. Two methodologies to determine the calibration equation are used: the first one, described by Tommaselli (1997), for laboratory condition using deformed soil sample, and the second for field condition. The advantages and disadvantages of each procedure are analyzed and important recommendations are given. The found calibration equations are compared with the Topp *et al*. (1980) equation. The results show that the joining of the laboratory and field experimental data help to explain satisfactorily the water content variation when compared with the water content determined by the gravimetric method.

INTRODUCTION

The knowledge of soil water content is important for agriculture, mainly the determination of its variation in the soil profile to optimize irrigation management. The tendency to use the TDR technique to measure the soil water content is relatively new in Brazil. Its outstanding advantages are accuracy, speed, reproducibility, good theoretical basis, a well-defined and selected sampled volume, and the fact that θ and salinity are measured in exactly the same volume. The method is based on the sensitive effect of the θ in the microwaves pulses propagation speed in conductive cables in soil, caused by the large differences in the relative dielectric permittivities of water (81), air (1), and soil particles (3-5). Basically, a cable test and a sensor with metallic rods tied by coaxial cable are needed.

In TDR, the propagation velocity of a high-frequency electromagnetic signal is determined by:

$$v = c/\sqrt{\varepsilon_b}$$

Where v is the propagation velocity, c is the propagation velocity of electrical signals in vacuum or free space ($3x10^8$ m/s), and e_b is the apparent dielectric constant of the soil. In the application of TDR to soil water measurement, a fast rise-time voltage pulse travels in the soil guided by a transmission line or wave guide of length, L, and the pulse reflects back from the end. By determining the travel time, t, of the pulse sent through the transmission line, it is possible to obtain the velocity during the two-way travel as $v = 2L/t$. Combining the two mathematical expressions, the ε_b of the measured soil can be calculated by:

$$\varepsilon_b = (ct/2L)$$

The TDR technique is an indirect form to determine the water content; therefore it needs a calibration curve to convert apparent dielectric constant to water content. Topp *et al*. (1980) proposed an empirical method for the relationships between apparent dielectric and water content based on a third-order polynomial fitted:

$$q = -5.3x10^{-2} + 2.92x10^{-2} * e_b - 5.5x10^{-4} * e^2_b + 4.3x10^{-6} * e^3_b$$

According to these authors, this equation can be used as a universal calibration curve for TDR water content determination. But, this equation fitted well with the experimental data for some soil. However, it did not fit for fine-textured mineral soils, organic soils, and clays (Dirksen & Dasberg, 1993; Jacobsen & Schjonning, 1993). Dirksen & Dasberg (1993) found that two Brazilian ferralsols had substantially different calibrations from that of Topp *et al*. (1980), which they attributed to the presence of gibbsite.

The results showed by Robinson *et al*. (1994) would indicate that soil mineralogy might well have a substantial influence on calibrations of apparent dielectric constant *versus* water content. The presence of 15 % goethite is unlikely to alter estimations of θ achieved through Topp's equation. The presence of 15 % hematite may increase to determined θ from Topp's equation in both dry and wet conditions by about 6 %.

High clay content leads to a higher specific surface area, and because layers of water molecules around the soil particles are thought to have a restricted rotational freedom, the ε_b of these molecules is lower than that of bulk water (Roth *et al*. 1990).

These phenomena are usually explained by an increase in the content of bound water with an increasing content of free iron oxide, organic matter and clay, since the ε_b of bound water is much lower than the ε_b in free water. Grohmann (1970) showed that the specific surface for Dusky Red Latossol presented decreased by 50% when the free iron oxide and organic matter were removed.

Ponizovsky *et al*. (1999) introduced the term "bound water"; the term "confined water" is also employed hereafter to designate the portion of soil water that is close to soil particles, is affected by the surface forces, and thus has a ε_b distinctly different from that of free water. The relative dielectric constant (ε) of

free water is $\varepsilon = 81$ at 18 ^{o}C, and it decreases by 0.37 per 1 ^{o}C (Wobschall, 1977). The lower limit of the ε_b of the tightly bound water is likely to be similar to that of ice, or $\varepsilon = 3.2$.

This limitation is more pronounced in tropical soils because the available equations do not consider the differences of these soils, mainly the presence of iron oxide. Silva (1998) concluded that its presence could affect the magnetic field created by electric pulse, and consequently affect the time of displacement of the emitted wave. The objective of this work is to study the limitations in order to develop a Dusky Red Latosol calibration equation. Two methodologies to determine the calibration equation were used: the first one, described by Tommaselli (1997), for laboratory condition using deformed soil sample, and the second for field condition.

MATERIALS AND METHODS

Experiments were conducted in the Hydraulic, Irrigation and Drainage Laboratory of the Agricultural Engineering College (State University of Campinas/Unicamp). Two methodologies were used to determine the calibration equation: the first one, described by Tommaselli (1997), for laboratory condition using deformed soil sample, and the second for field condition. The ε_b was measured by Trase System I[1], model 6050X1 (Soilmoisture Equipment Corp., Santa Barbara, CA, USA). Parallel steel 3-wire probes (200 mm length and 3 mm diameter) were used in the experiments. The interpretation of the TDR waveforms was made by internal automatic software of the Trase System I.

The soil type studied was Dusky Red Latosol, and some soil physical and chemistry characteristics are presented in the Table 1.

Physical											
Depth (m)	Bulk density (Kg/m^3)		Total porosity (%)			Texture (%)					
						Clay		Silt		Sand	
0-0.25	1,240		53.2			56		9		35	
Chemistry											
Depth (m)	PH $CaCl_2$	P $\mu g/cm^3$	O. M.	F_3O_2	H+Al	K	Ca	Mg	S	CTC	V (%)
			(%)		e. mg/100 g of soil						
0-0.25	5.7	120	3.9	21.3	2.8	0.4	7.9	2.0	10.3	13.1	79

Lucarelli, 1997

Table 1. *Soil physical and chemistry characteristics.*

The methodologies used to determine calibration equation are described below.

Laboratory condition methodology

Air-dry soil sample was grounded and then passed through a 2 mm sieve. The sample was divided in two parts and strewn in a thin layer on the plastic plate and brought to the desired water content using a

[1] Reference to registered mark does not constitute endorsement for the authors.

water spray. Then, the sample was thoroughly mixed and placed into a cylindrical plastic recipient, 0.18 m in diameter and 0.25 m in height. The recipient was tightly shut and left to rest for 24 hours to reach equilibrium between water and solid phases. Thereafter, the apparent dielectric constant of the sample was measured by means of the TDR technique. The recipient was weighed. The weight of sample was used to estimate the water content and bulk density. Finally, the soil sample was removed from the recipient, divided in two parts and strewn in a thin layer again, and brought to new water content (Tommaselli, 1997).

Field condition methodology

The experiment was conducted during the period of low pluviometric precipitation in Campinas-SP (June to September), with a duration of around 70 days. An area of 25 m^2 was selected inside the experimental field of Feagri/Unicamp and irrigated until it reached approximately the field capacity of the soil. This area was representative of the soil under study and its characteristics are shown in the Table 1. Thus, using 3-wire TDR probes, installed at the depth of 0–0.20 m, the apparent dielectric constant was measured for different values of soil water content. Simultaneously, 5 soil samples were collected from around the installed probes to determine of the water content through of the gravimetric method.

Validation of the equations

The estimated equations were compared with the gravimetric method, determining the wetting front in drip irrigation. The experiment was accomplished inside two soil columns (0.9 m of length and 0.6 m of diameter) filled with soil (Dusky Red Latossol). Each recipient was irrigated (15 mm of depth) with an emitter of rate 2 and 4 L/h, separately. For wetting front measurements 10 TDR multi-wire probes with 3 segments of 0.20 m and spaced 0.08 m were installed inside the recipients, as described by Souza *et al*., 1999. The wetting front was monitored and measured by the probes, and soil samples were collected after 48 hours to estimate the water content by the gravimetric method.

RESULTS AND DISCUSSION

The experimental data obtained by both procedures is presented in Table 2. In this table, it is possible to verify that in both methodologies the desirable range of soil moisture values was not obtained. In the laboratory procedure, it was difficult to make apparent dielectric constant readings for water content values above 0.20 m^3/m^3 due to the occurrence of soil compaction. This problem occurred due to the high clay concentration (56%) and porosity (53.2%). The structure of the Dusky Red Latossol collapsed due to soil compaction phenomenon. The critical water content for the soil compaction was above 0.20 m^3/m^3 for the soil-deformed samples used in the study. This effect was caused by the compression of an unsaturated soil during which an increase of the bulk density of soil occurs as a consequence of the reduction of its volume, due to the expulsion of the air caused by inadequate management.

The field methodology showed some reading problems for soil water content values below 0.21 m^3/m^3. Apparent dielectric constant readings decreased abruptly for a range below this point, where the soil water content presence was visible. The observed results indicated that soil mineralogy has a substantial influence on the apparent dielectric constant readings. It is believed that the greatest influence was

q **(m^3/m^3)**	e_b	q **(m^3/m^3)**	e_b
0.027	**2.8**	0.276	16.3
0.043	**3.2**	0.283	16.8
0.063	**3.8**	0.286	18.1
0.094	**4.5**	0.349	19.2
0.109	**5.1**	0.327	19.9
0.126	**5.5**	0.317	20.2
0.151	**5.9**	0.317	20.3
0.173	**6.5**	0.363	24.4
0.206	8.7	0.392	25.8
0.224	11.0	0.425	27.0
0.232	14.1	0.398	27.4
0.271	15.2	0.419	29.8

Bold letter data were obtained in laboratory condition and others in field conditions

Table 2. *Observed results in field and laboratory condition*

caused by the high presence of iron oxide and clay, which increases the specific surface activity effect of the particles of the soil in the water retention. This phenomenon reduces the free water in the soil, which consequently promotes low apparent dielectric constant values.

The difficulties found in both procedures (lab and field conditions) showed that the calibration curve determination is not an easy task, but involves a series of details that could result in imprecise results. Thus, it was decided to check the possibility of joining the experimental data of the methodologies used, (Table 2). The third-order polynomial model was adopted, because a superiority of this mathematical model when compared with other models, which presented the largest correlation coefficient values for clay soils, is observed in the literature. Tommaselli (1997) observed that third-order polynomial term of θ stops being important when soil texture becomes thicker.

Using the results presented in Table 2, it was possible to estimate the equation represented by Figure 1, which was compared with Topp's equation. The water content estimated by using by Topp's equation was underestimated by 20 % and overestimated by 10 % for the great differences when compared with gravimetric method. The comparison confirms the tendency observed by Tommaselli (1997) and Silva (1998). The authors observed that Topp's equation could underestimate or overestimate water content for Brazilian conditions soils.

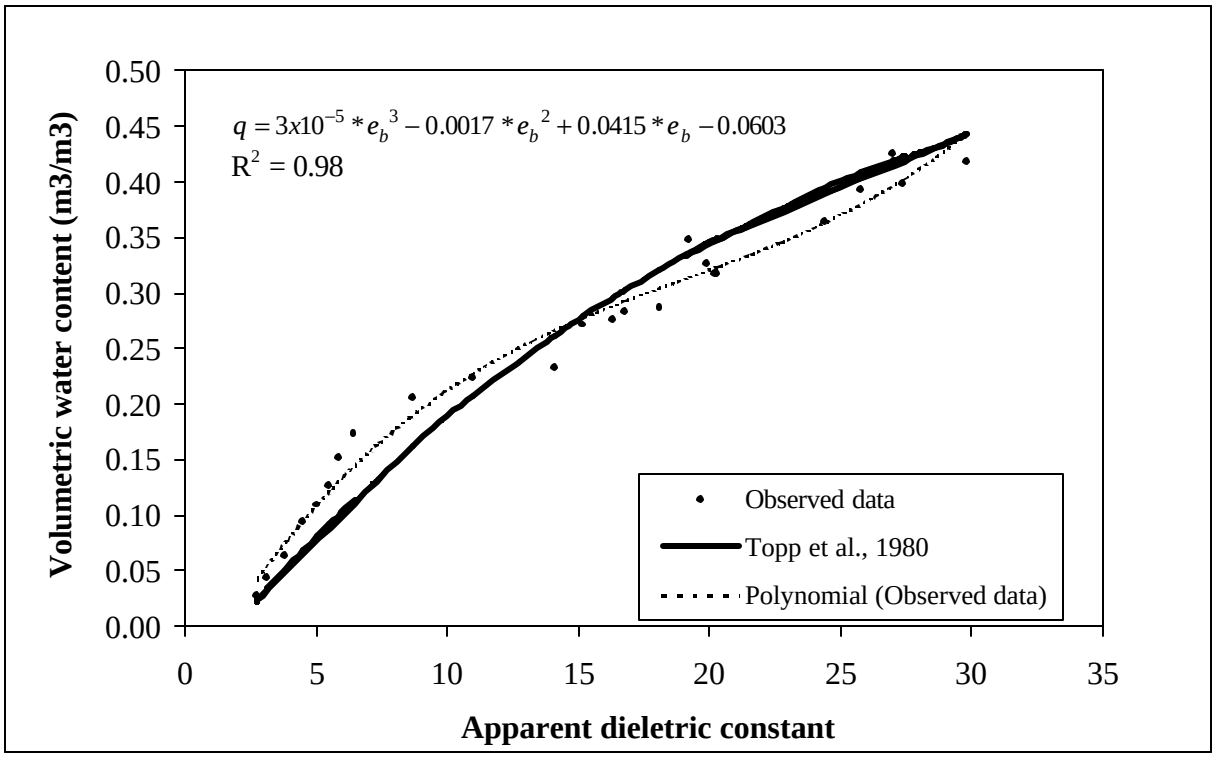

Fig. 1. *Calibration equation found for studied conditions.*

The precision of the equation we developed was tested in a laboratory experiment which determined the evolution of the wetting front. It was then compared with the wetting front determination, achieved by using gravimetric method (Figure 2). The results were satisfactory.

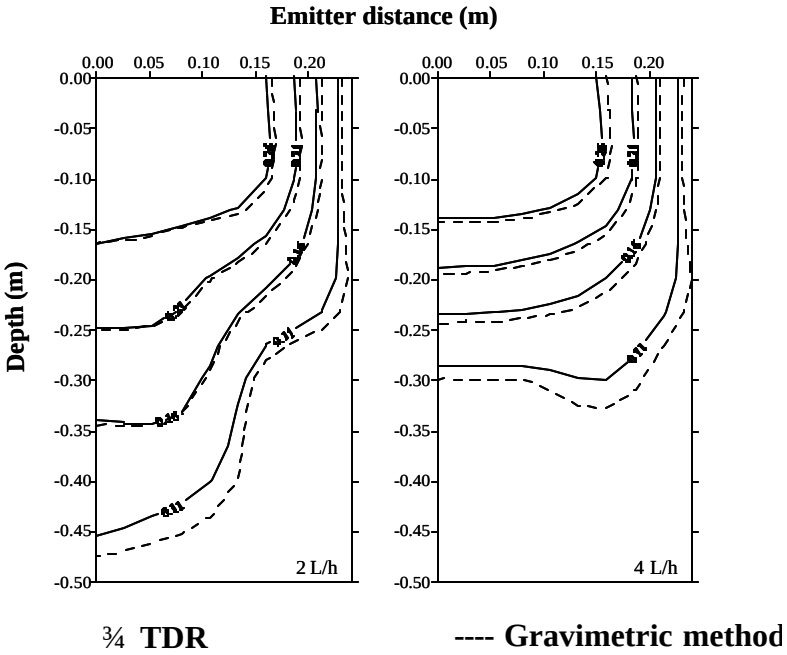

Fig. 2. *Comparison between q measured by gravimetric method and TDR after 48 h of the water application.*

The experiment showed that the determination of the calibration equations for clay soils should be accomplished carefully, mainly when these soils contain high free iron oxide concentration. The possibility of making calibrations in laboratory conditions using for soil-deformed samples was discarded. For calibrations, whose the objective is the irrigation management the equation obtained in field conditions is recommended, because the moisture storage range could be estimated.

CONCLUSION

Although Topp's equation has been adopted universally, it was found to be inadequate for the studied soil type, because it underestimated or overestimated observed water content.

It was difficult in lab conditions to obtain a TDR calibration curve that contains the total range of the water content used for irrigation management, using soil-deformed samples.

In field conditions, the soil bounded water affects abruptly the readings of the apparent dielectric constant.

When the experimental data for lab and field methodology were put together, the results obtained were more satisfactory, even when used for water content measurements in air-dry soil conditions.

More studies using non-deformed soil samples in laboratory to determine the calibration curve are recommended.

REFERENCES

Dirksen, C. & Dasberg, S., 1993, Improved calibration of Time Domain Reflectometry soil water content measurements, Soil Sci. Soc. Am. J., **57**, 660-667.

Grohmann, F., 1970, A superfície específica e sua correlação com propriedades físicas e físico-químicas do solo, Piracicaba, Tese de Doutorado - ESALQ/USP, 52 p.

Jacobsen, O. H. & Schojonning, P., 1993, A laboratory calibration of time domain reflectometry for soil water measurement including effects of bulk density and texture, Journal of Hydrology, **151**, 147-157.

Lucarelli, J. R. F., 1997, Alterações em características de um Latossolo Roxo submetido a diferentes sistemas de manejo. Campinas, Tese de Mestrado – Feagri/UNICAMP, 86 p.

Ponizovsky, A. A.; Chudinova, S. M.; Pachepsky, Y. A., 1999, Performance of TDR calibration models as affected by soil texture, Journal of Hydrology, **218**, 35-43.

Robinson, D. A.; Bell, J. P.; Batchelor, C. H., 1994, Influence of iron and titanium on water content determination by TDR, In: TDR symposium, 16, Foulum. *Proceedings*... Foulom, Denmark: Danish Institute for Plant and Soil Science, 63- 70.

Roth, K.; Schulin, R.; Fluhler, H.; Attinger, W., 1990, Calibration ot time domain reflectometry for water content measurement using a composite dielectric approach, Water Resources Res., **26**, 2267-2273.

Silva, E. L., 1998, Determinação automática de teor de água em Latossolo Roxo Distrófico com uso de reflectometria de onda. In: CONGRESSO BRASILEIRO DE ENGENHARIA AGRÍCOLA, 27, Poços de Caldas. *Anais*... Lavras: SBEA/UFLA, 154- 156.

Souza, C. F.; Matsura, E. E.; Testezlaf, R., 1999, Desempenho de sondas multihaste segmentada para o monitoramento da umidade do solo por meio da técnica de TDR. In: CONGRESSO BRASILEIRO DE ENGENHARIA AGRÍCOLA, 28, Pelotas. *Anais*... Pelotas: SBEA/UFPel,. [CD ROM]

Tommaselli, J. T. G., 1997, Influência de algumas características do solo sobre a calibração de um aparelho de TDR (Time Domain Reflectometry), Piracicaba, Tese de Doutorado - CENA/USP, 167 p.

Topp, G. C., Davis, J. L., and Annan, A. P., 1980, Electromagnetic determination of soil water content: measurements in coaxial transmission lines, Water Resources Res., **16**, 574-582.

Wobschall, D., 1977. A theory of the complex dielectric permittivity of soil containing water: The semi-disperse model, Trans Geosci. Electron, **15**, 49-58.

TEMPERATURE EFFECT ON TDR MEASUREMENT OF WATER CONTENT OF UNBOUND MATERIALS

Gang Zuo[1], N. Randy Rainwater[2], Wesley C. Wright[3], Ronald E. Yoder[4], and Eric C. Drumm[5]

[1] Department of Civil & Environmental Engineering, University of Tennessee, Knoxville, TN 37996-2010; gzuo@engr.utk.edu
[2] Department of Civil & Environmental Engineering, University of Tennessee, Knoxville, TN 37996-2010; nrainwat@utk.edu
[3] Department of Agricultural and Biosystems Engineering, University of Tennessee, Knoxville, TN 37901-1071; wright1@utk.edu
[4] Department of Agricultural and Biosystems Engineering, University of Tennessee, Knoxville, TN 37901-1071; ryoder@utk.edu
[5] Department of Civil & Environmental Engineering, University of Tennessee, Knoxville, TN 37996-2010; edrumm@utk.edu

ABSTRACT

A seasonal monitoring program of flexible pavement performance has been performed in Tennessee since 1996, in which the water content of the subgrade is measured by Time Domain Reflectometry (TDR) probes. Five-segment probes were chosen to increase the number of measurements and volume of soil monitored. The variations of water content measured in the subgrade and the base course closely follow the temperature trends. This finding suggests the significance of temperature effects on TDR measurement. A laboratory calibration program was thus carried out to study the temperature effects on TDR measurement of volumetric water content. Temperature effects on TDR measurement are related to the energy of the signal. After correcting for temperature effects, the field TDR measurements of volumetric water content appear to track a seasonal variation.

INTRODUCTION

As part of the pavement instrumentation conducted by the Tennessee Department of Transportation (TDOT), Time Domain Reflectometry (TDR) probes were installed to measure volumetric water content (VWC) of subgrade soil and unbound aggregate at four sites in Tennessee. Moisture Point type III five-segment TDR probes (Figure 1) produced by Environmental Sensors ® were used in the project. The length of each segment is 300 mm. The probe is made of two stainless steel plates approximately 12.7 mm wide by 3.2 mm thick, separated by 12.7 mm of high density plastic and epoxy. The Moisture Point MP-917 is used to measure signal propagation time. A pulse signal is emitted at the center of the probe, between segment 3 and segment 4. The signal then travels through segment 3 – 2 –1, and 4 – 5, respectively. Due to the signal attenuation, the propagation time measured by segment 3 and segment 4 are the most precise. Segment 2 and segment 5 propagation times are less precise than 3 and 4, while segment 1 is the least precise.

Because the waveguides are separated by plastic and epoxy, part of the waveguides are in contact with plastic and epoxy, instead of soil. Thus, the measured propagation time should be corrected for this incomplete contact, before it is used to calculate volumetric water content. A linear model was recommended by the manufacturer (Young, 1995) to correct for the effect of the plastic and epoxy on the propagation time. To develop a soil specific correction, slopes and intercepts of the linear model for different segments were obtained from calibration tests on Blount County soil (Wright, 1998 and Wright *et al*., 2001).

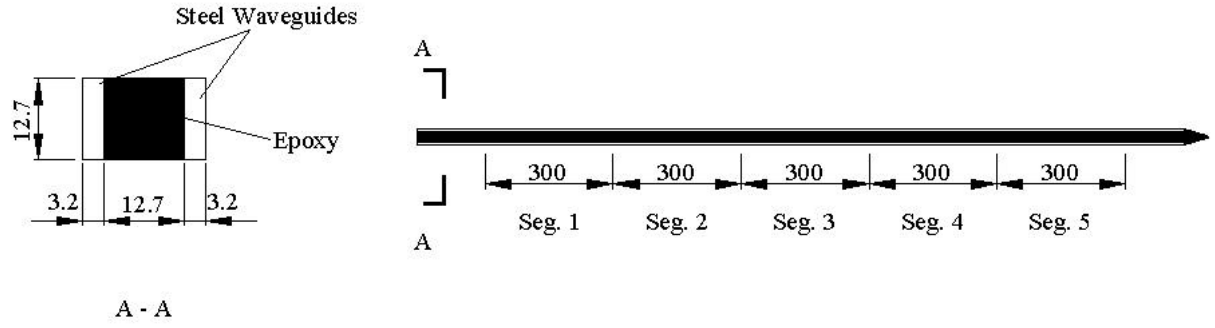

Fig. 1. *Moisture Point Type III Five-Segment TDR Probe (Unit: mm)*

The linear model proposed by Young (1995) is

$$T_{MC} = \frac{T_M}{B} - A \qquad [1]$$

where

T_M = measured roundtrip propagation time;
T_{MC} = corrected roundtrip propagation time;
A = time-offset correction constant;
B = incomplete-contact correction constant.

Herkelrath's (1991) equation, Equation (2), was adopted for the calculation of VWC, based on the results of the 10 models assessed by Wright *et al*. (2001).

$$q_V = Slope(1/v) + Intercept \qquad [2]$$

where q_V = volumetric water content of soil;

v = signal velocity;
Slope and *Intercept* = constants.

Data has been collected from four instrumented pavement sites for more than three years. Figure 2 shows the subgrade volumetric water contents measured by the TDR probe at the Blount County Site without any temperature correction. Also shown in Figure 2 is the temperature of the subgrade soil measured by thermistors at the same depth as the TDR Probe. This data is typical for all the test sites.

The variation in volumetric water contents measured by segments 1, 2 and 5 of the TDR probe are surprisingly consistent with the temperature variation. A temperature correction equation was proposed by the manufacturer (Young, 1996) to account for the decrease of dielectric constant of water with increasing temperature. But the volumetric water contents measured by segments 1, 2, and 5 were opposite to this correction. This phenomenon indicates that either volumetric water content is affected by temperature or the calibration equation needs to be improved to better account for the temperature effect on the dielectric properties of the soil-water medium or on the equipment.

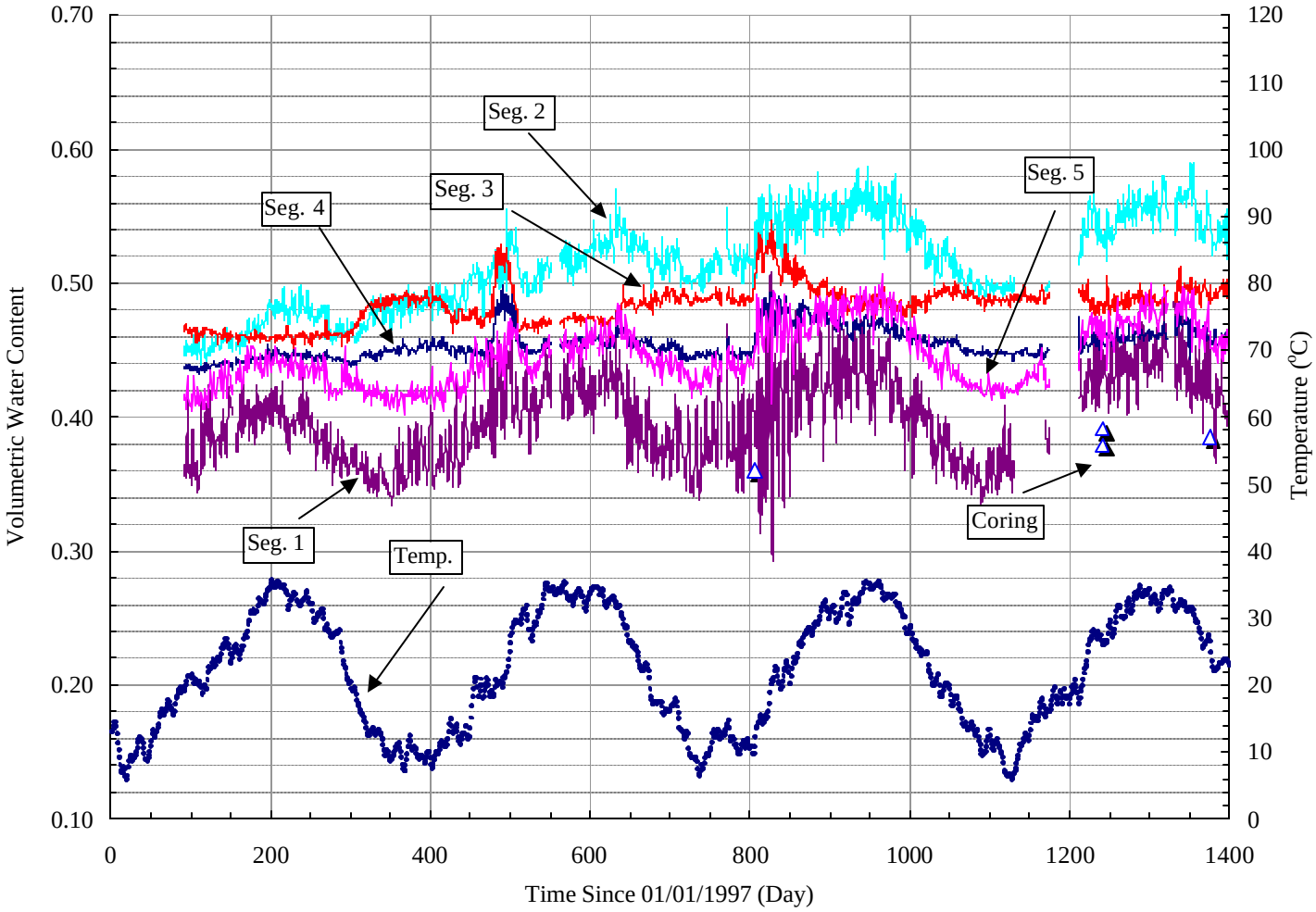

Fig. 2. *Volumetric Water Content and Soil Temperature of Blount County*

Research has shown contradictory trends in regard to the magnitude and direction of temperature effect on TDR measurement in soil (Halbertsma *et al*., 1995; Verstricht *et al*., 1994; Alvenas and Stenberg 1995; Pepin *et al*., 1995). The effect of temperature on the dielectric properties of soil-water medium can be different for different soils, and even for the same soil the effect can be different at significantly different water contents. A comprehensive review on this topic can be found in the paper by Wraith and Or (1999), in which the contradictory effects of temperature on TDR measurement of soil water content were explained by the interplay of two competing phenomena: (1) the reduction in the dielectric

constant of free water with increased temperature; and (2) the increase in the amount of released bound water with increased temperature.

SETUP AND PROCEDURES OF LABORATORY TEST

The most accurate way to determine what effect temperature has on a specific soil is to perform a calibration test with the soil. This paper describes the procedure and analysis used to determine the effect of temperature on VWC measurements using the Moisture Point Type III five-segment TDR probe.

Soil was first mixed to a typical water content corresponding to that determined from gravimetric samples obtained by coring at the field sites. De-ionized water was sprayed into the air-dried soil, which was mixed by hand as evenly as possible, and the soil was then placed in a sealed container. After the moisture in the soil equilibrated for at least 24 hours, a specific mass of soil was placed into an aluminum box with inside dimensions of 6.35 cm (2.5 in.) wide by 8.9 cm (3.5 in.) high by 182.88 cm (72 in.) long. The amount of soil placed into the box was based on the dry density of the soil samples obtained by coring at the site. The TDR probe was placed in the middle layer of the soil while packing. The box was set in a steel frame, which constrained the horizontal expansion during compression, and a steel lid was placed on the soil surface. Seven C-clamps were used to compress the lid down until the depth of soil in the box was reduced to 6.35 cm (2.5 in.), so that the density in the box was similar to that of the field. The box was left in the frame with the C-clamps applied long enough to ensure that the soil did not swell significantly when the frame and clamps were removed. The loading lid was removed and three thermistors were inserted into the soil. The box was then wrapped in plastic wrap to prevent moisture loss and moved into an environmental chamber where the temperature and humidity were strictly controlled.

The temperature in the environmental chamber was increased by 5 $^{\circ}C$ every 24 hours ranging from 5 $^{\circ}C$ to 40 $^{\circ}C$, the typical temperature range in the soil subgrades at the research sites. TDR propagation time was collected by the MP-917 automatically every 30 minutes, and soil temperature which was measured by thermistors was collected by a data logger simultaneously with TDR propagation time.

DATA PROCESS

Slopes and Intercepts of Herkelrath's Equation

The slope and intercept of Herkelrath's equation for Blount County soil were derived by Wright *et al*. (2001), over a volumetric water content range of 0.05 to 0.45. A scatter plot of the data used in their derivation (Figure 3-a) suggests that there is a break point at VWC = 0.20. The slope of the volumetric water content data below 0.20 is greater than the slope above VWC = 0.20. This is consistent with the characteristics of TDR measurement in clayey soil as discussed by Hook and Livingston (1996). Both the TDR measurement from the field and the water content obtained from field coring samples indicate that the volumetric water content of the subgrade soil at the Blount County Site is consistently higher than 0.20. Therefore, a new slope and intercept was derived from data with high water content for each segment of the five-segment probe. The newly derived slopes and intercepts are listed in Table 1 together with the slope and intercept derived by Wright *et al*. (2001). The new segment-specific model and the Wright's model (2001) are compared with the data in Figure 3.

	Wright *et al.* (2001)	Proposed Segment Specific				
		1	2	3	4	5
Slope	37.396	30.913	33.558	44.680	39.844	34.535
Intercept	-0.193	-0.067	-0.102	-0.258	-0.182	-0.106

Table 1. *Slopes and Intercepts for the Herkelrath Equation*

Relationship between TDR Measurement and Temperature

The segment-specific constants for the Herkelrath equation were used to determine the volumetric water content of the Blount County soil in the environmental chamber (Figure 4). The soil was maintained at VWC = 0.41. Measurements by Segment 3 and 4 show little variation with change in temperature. Segments 2 and 5 show significant increase both in the mean value and the deviation of measured volumetric water content at each temperature step as the temperature increases. Segment 1 shows even more increase in the mean value and the deviation of measured volumetric water content with increasing temperature. The following procedures were used to determine the relationship between measured volumetric water content and temperature:

1) Delete the intermediate data points collected before the temperature stabilized at each temperature step.
2) Find the median volumetric water content for each temperature.
3) Fit the medians to appropriate functions.

The volumetric water content data at each temperature step is very scattered. It can be deduced that the intermediate data should also have a lot of noise. If the sampling rate were high enough, similar scattering as shown in the stabilized temperature would also be exhibited in the intermediate data. Since there were not enough data points to calculate the mean or median at each intermediate temperature, the inclusion of intermediate data in the curve fitting would only increase the error. The sample size of the data at some stabilized temperature is not large enough to determine an accurate mean, and the data is quite noisy. Median is used rather than mean, because it is not as sensitive to outliers as mean.

Medians of the measured volumetric water content at stabilized temperatures are shown in Figure 5. Linear or second order polynomials used to fit the curves are shown in the same figure. The volumetric water contents measured by segments 3 and 4 exhibit small linear decrease with increasing temperature. Measurements from segments 2 and 5 do not show a significant increase when the temperature is below $11\ ^{\circ}C$, but increase quickly as temperature rises beyond $11\ ^{\circ}C$. The equations in Figure 5 were used to adjust field measurements of volumetric water content from each segment.

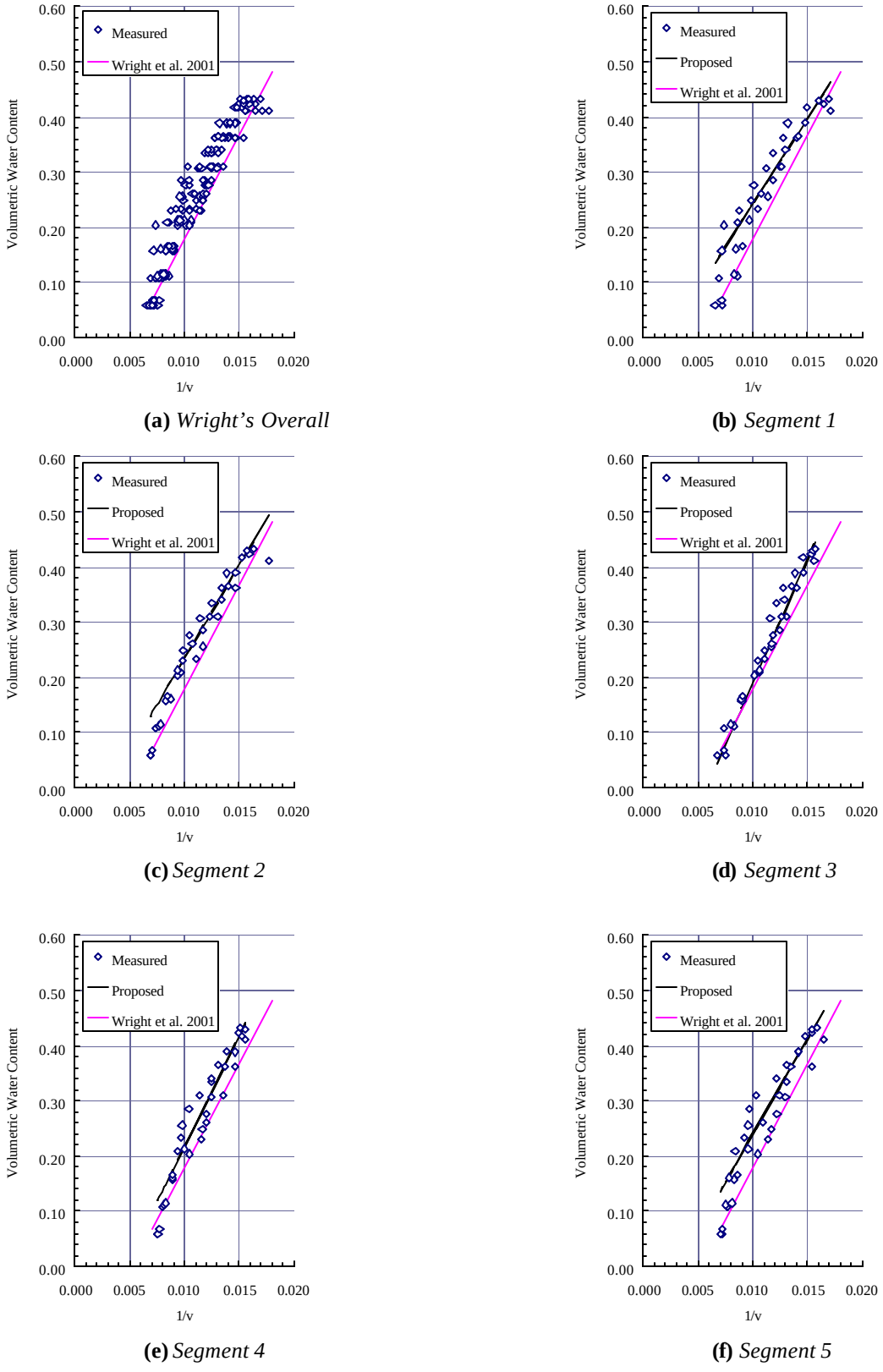

(a) *Wright's Overall* **(b)** *Segment 1*

(c) *Segment 2* **(d)** *Segment 3*

(e) *Segment 4* **(f)** *Segment 5*

Fig. 3. *Comparison of Wright's Model and Proposed Segment-Specific Model for Blount County Soil*

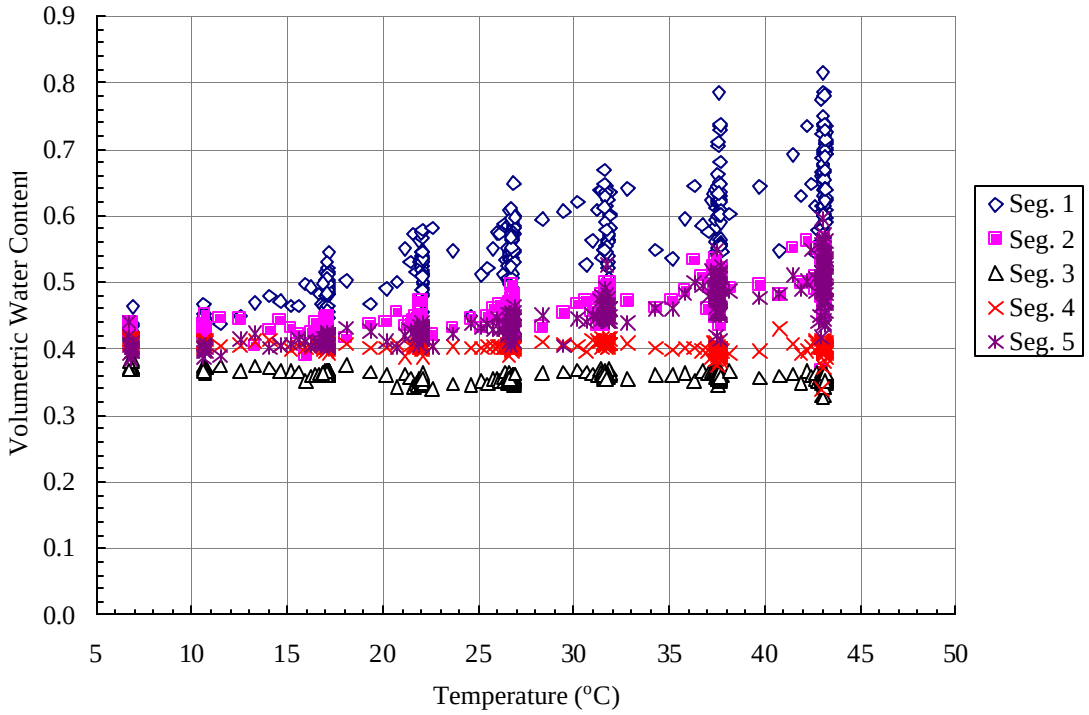

Fig. 4. *Volumetric Water Content Meausured by TDR vs. Temperature (Lab Data of Blount County Soil)*

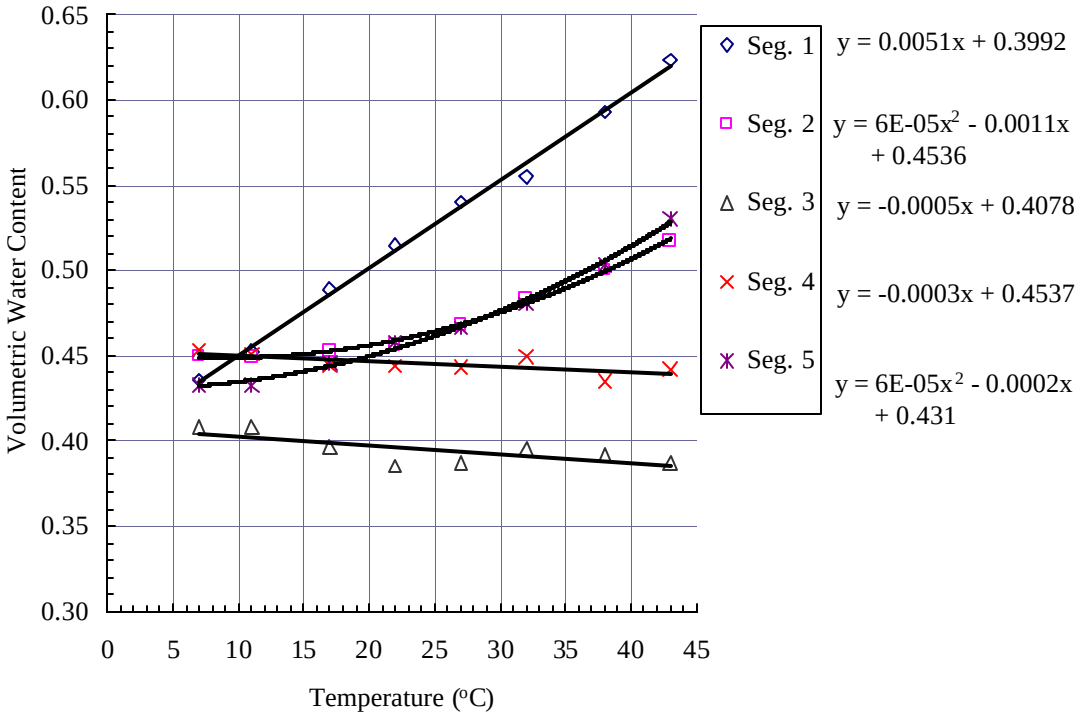

Fig. 5. *Volumetric Water Content Measured by TDR at Stabilized Temperature*

RESULT AND DISCUSSION

The different temperature dependence of each segment shown in Figure 5 reveals a possible relationship between signal energy level and the TDR measurement. The signal is emitted between segment 3 and segment 4. Energy propagated through segments 3 and 4 is the strongest. When the signal reaches segments 2 and 5, it is not as strong. By the time it reaches segment 1, much of the voltage pulse energy has dissipated. Perhaps, measured VWC tends to decrease with increasing temperature for strong signals and increase with increasing temperature for weak signals (Figure 5). This may offer some additional explanation to the contradictory effects of temperature found by various researchers.

The corrected volumetric water content for each segment of the TDR probe in the subgrade of the Blount County site is shown in Figure 6. Also shown in the figure are subgrade temperature and rainfall data collected at the on-site weather station. Volumetric water contents measured by segments 3 and 4 are relatively constant for most of the time except for brief periods after high rainfall in spring and winter seasons. Segments 2 and 5 have similar characteristics as segments 3 and 4, but show some variation opposite to the temperature trends. Segment 1 shows significant variation opposite to the temperature, which makes the peaks in water content after excess rainfall in spring and winter seasons not as easily discernable as in the other four segments. However, as suggested by the lab data (Figure 4), volumetric water content measured by segment 1 is the least precise. It is very possible that the inverse relationship between VWC measurement of segment 1 and temperature are caused by over-correction.

The field coring samples show that the subgrade is a little drier than saturation (Figure 6), but the volumetric water content measured by the TDR probe is always unreasonably higher than the saturation ratio (0.42) of the material, except for the measurement of segment 1 during hot dry days. Several field investigations and alternate instrumentation are planned to verify and aid in interpreting the field data in light of the temperature effect calibration study.

CONCLUSION

The laboratory calibration of Moisture Point Type III TDR probes using the Blount County soil demonstrate that temperature effects on TDR measurement of VWC may be dependent on the energy of the signal propagated through the probe. Therefore, any temperature correction will be dependent on the TDR probe and instrumentation design as well as soil characteristics. For instance, TDR systems with long cable lengths will likely experience a greater temperature effect than short cable lengths, due to signal attenuation. Thus, in addition to Wraith and Or's (1999) explanation of the contradictory effects of temperature, i.e., (1) the reduction in the dielectric constant of free water with increased temperature; and (2) the increase in the amount of released bound water with increased temperature, a third explanation may be added as (3) TDR probe and instrumentation design and the resulting energy of the signal. The study of temperature effects on TDR measurements of VWC warrants additional investigation.

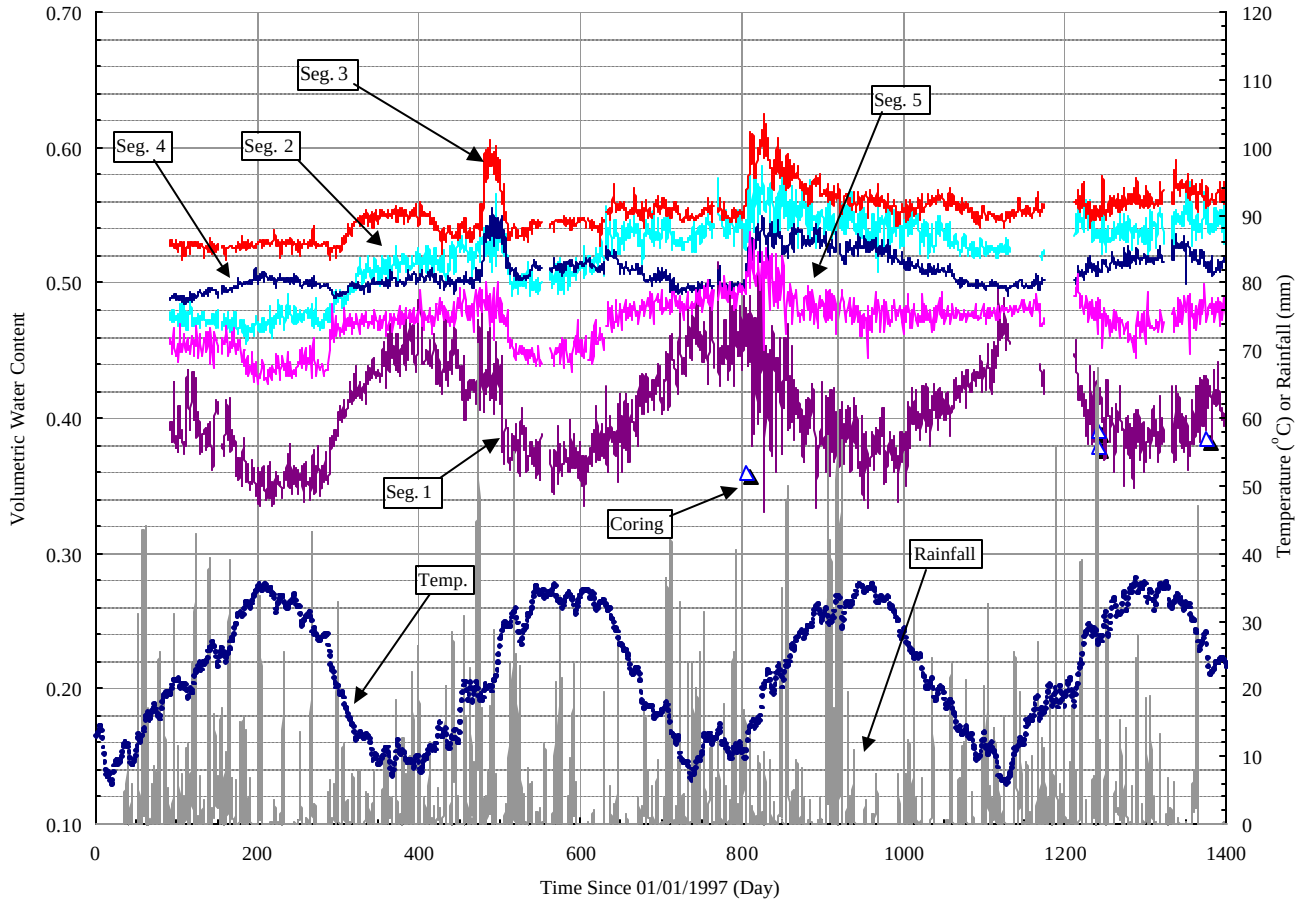

Fig. 6. *Corrected Volumetric Water Content of Blout County Site Subgrade*

SUMMARY

Laboratory calibration was performed to study the temperature effect on measuring the volumetric water content of soil using the Moisture Point Type III five-segment TDR probe. Temperature affected TDR measurements for each segment differently, with segments 3 and 4 showing little variation with temperature, while segment 1 shows the most significant dependence on temperature. The difference in temperature effects of TDR measurements of different segments may be attributed to the change in energy of the signal as a result of signal attenuation. Field data corrected for temperature effects reveal that rainfall during the cold season is a major source of subgrade moisture increase.

REFERENCES

Alvenas, G., and Stenberg, M., 1995, Problems in Estimating Soil Water Content by TDR Measurements, Paper in the Proceedings of the Symposium: Time-Domain Reflectometry Applications in Soil Science (Foulum, Denmark, Sept. 16, 1994); SP Report No. 11, June, **3**, 121-123.

Halbertsma, J., van den Elsen, E., Bohl, H., Skierucha, W., 1995, Temperature Effects on TDR Determinated Soil Water Content, Paper in the Proceedings of the Symposium: Time-Domain

Reflectometry Applications in Soil Science (Foulum, Denmark, Sept. 16, 1994); SP Report No. 11, June, **3**, 35-37.
Herkelrath, W. N., Hamburg, S. P., and Murphy, F., 1991, Automatic, Real-Time Monitoring in a Remote Field Area with Time Domain Reflectometry; Water Resources Research, **27**, No. 5, 857-864.

Hook, W. R. and Livingston, N. J., 1996, Errors in Converting in Time Domain Reflectometry Measurements of Propagation Velocity to Estimate Soil Water Content; Soil Science Society of America Journal, **60**, No. 1, 35-41.

Pepin, S., Livingston, N. J., and Hook, W. R., 1995, Temperature-Dependent Measurement Errors in Time Domain Reflectometry Determinations of Soil Water, Soil Science Society of America Journal, **59**, 38-43.

Verstricht, J., Neerdael, B., and Volckaert, G., 1994, Clay Moisture Measurements in Radioactive Waste Disposal Research, Proceedings of the Symposium on Time Domain Reflectometry in Environmental, Infrastracture, and Mining Applications, Evanston, Illinois, Sept. 7-9, U.S. Bureau of Mines; Special Publication SP 19-94, NTIS PB95-105789, 337-348.

Wraith, J. M., and Or, D., 1999, Temperature Effects on Soil Bulk Dielectric Permittivity Measured by Time Domain Reflectometry: Experimental Evidence and Hypothesis Development; Water Resources Research, **35**, No. 2, 361-369.

Wright, W. C., 1998, In Situ Water Content Measurement of Compacted Highway Subgrade Using Time Domain Reflectometry, A Thesis Presented for the Master of Science Degree, The University of Tennessee, Knoxville, 247 p.

Wright, W. C., Yoder, R. E., Rainwater, N. R. and Drumm, E. C., 2001, Calibration of Five-Segment Time Domain Reflectometry Probes for Water Content Measurement in High Density Materials; ASTM Geotechnical Testing Journal, GTJODJ, **24**, No. 2, 172-184.

Young, G. D., 1995, Single-Diode Probes; Moisture Point MP-917 Technical Brief 13, Environmental Sensors, Inc., San Diego, California, 18 p.

---------- 1996, Calibration of Profiling Probes; Moisture Point MP-917 Technical Brief 17, Environmental Sensors, Inc., San Diego, California, 11 p.

USING THE FORMATION FACTOR TO CALIBRATE TDR FOR WATER CONTENT AND SALINITY MEASUREMENTS IN DRIP IRRIGATED FIELDS

Arie Nadler[1] and A. L. Ward[2]

[1]Soil and Water Institute, Agricultural Research Organization, the Volcani Center, Bet-Dagan, 50250, Israel; vwnad@agri.gov.il
[2]Pacific Northwest National Laboratory, Richland, WA; andy.ward@pnl.gov

ABSTRACT

Effective irrigation scheduling, especially when using saline waters, requires frequent, preferably non-destructive, measurements of soil water content and soil salinity levels because crop yield is affected by the osmotic potential of the soil solution in the root zone. Resolving the field calibration problem may help to apply the TDR technique for monitoring drip-irrigated fields. Therefore, salinity values were calculated from TDR measured soil water content (θ) and bulk soil electrical conductivity (σ_a) in a commercial, drip irrigated, cotton (Gossypium hirsutum) field. Saline-sodic (EC=3.8 dS m^{-1}, SAR=19.7) irrigation waters were applied in three levels (4580, 3850, and 3010 m^3 ha^{-1}) on a loamy soil (Calcic Palexeralf) in a semi arid region (Northern Negev, Israel). EC of the soil solution (σ_w) was derived from σ_a by using a previously established σ_a-σ_w calibration procedure that considers the soil type, formation factor, σ of the soil solids surfaces, and their mutual interactions. Resulting σ_w values ranged 5-25 dS m^{-1} with an estimated accuracy of ±25%. The inevitable uncertainty in σ_w measurement originates from both the continuous changes in water contents and dimensions of the wetted soil volume (dynamic heterogeneity), and the attenuation of the energy of the TDR pulse by the conductive soil. These restrictive conditions were partially overcome by (i) moving the TDR probes 0.25 m away from the drip laterals to enable water redistribution, thereby reducing extreme spatial variability, and a careful, manual analysis of the TDR trace. Resulting σ_w values were verified by a salt mass balance (uncertainty = ±25%) and a calculation procedure based on a model which used the tortuosity to predict σ_w from θ and σ_a.

INTRODUCTION

With the growing need for irrigation and an increasing tendency to use recycled water, particularly treated sewage, the practice of irrigating with saline waters is becoming more common. Drip systems are well suited to irrigating with saline waters. Under drip irrigation, there is a greater economy of water use

since soil evaporation and deep percolation losses are reduced. Because the root zone is kept at a high moisture level and the water does not contact the plant, use of more saline water is possible with less stress and damage to the plant. While this practice allows use of currently discarded marginal waters, there is still a risk of increased soil salinity, which can restrict plant water uptake, stunt growth, and reduce yield. Therefore, maintaining crop productivity while controlling soil salinity is dependent on proper irrigation management, which can be achieved through optimal irrigation scheduling.

Effective irrigation scheduling requires frequent, preferably non-destructive, measurements of soil water content (θ) and soil salinity levels. Soil salinity, which is often expressed in terms of the electrical conductivity of the pore water (σ_w) is difficult to measure in situ. Estimates of σ_w can be obtained from simultaneous measurements of θ and the bulk electrical conductivity, σ_a, for any soil with known values of the mineral phase surface conductivity, σ_s, and tortuosity (Rhoades, *et al.*, 1976) or formation factor (Cremers *et al.*, 1966; Nadler and Frenkel, 1980). Bulk electrical conductivity can be measured by several techniques, such as electromagnetic induction, and electrical resistivity probes, including the four electrode probe, and the Wenner array which is an in-line sequence of conductive pegs of which different combinations of quadruplets are selected to gradually form an increasing inter-electrode spacing (Rhoades and Ingvalson, 1971; Nadler and Frenkel, 1980; Rhoades *et al.*, 1990; Slavich 1990). Electromagnetic induction methods have also been used to infer mean ? as well as depth profiles of ? in the field (Kachanoski *et al.*, 1988; Sheets and Hendrix, 1995). The dilemma is that with these techniques there is no simple way to separate the effects of σ_w, σ_s, and θ on σ_a.

Time domain reflectometry (TDR) is now a primary tool for measuring θ in soils and has been successfully demonstrated in the field and laboratory (Topp *et al.*, 1982; van Wesenbeeck and Kachanoski, 1988; Ward *et al.*, 1994). The TDR technique has also been used for simultaneous measurements of θ and salinity (Dasberg and Dalton, 1985; Persson 1997; Nissen *et al.*, 1998; Weerts *et al.*, 1999), as well as θ and solute concentrations with a variety of probe configurations, demonstrating its utility for monitoring θ and σ_a during flow from a point source (Ward and Kachanoski, 1988; Kachanoski *et al.*, 1992; Kachanoski *et al.*, 1994).

Monitoring θ and σ_a under steady-state conditions is relatively straightforward, (Nadler, 1991; Kachanoski *et al.*, 1992). However, during flow from a point source, θ varies approximately with the cube of radial distance creating conditions similar to transient flow conditions and calibration is more complicated (Ward *et al.*, 1994; Wraith *et al.*, 1993). Since calibration constants are extremely sensitive to soil texture and the type of solute used, they are very susceptible to soil spatial variability, limiting their use to conditions identical to those used during calibration. Provided the problem of calibration for field use could be resolved, TDR would be ideal for monitoring θ and soil salinity in drip-irrigated fields.

Nadler *et al.* (1984) showed that the four-probe technique could be used for measuring salinity under extremely variable conditions by making use of the formation factor, which relates σ_a to soil texture through the pore size distribution and θ. It is hypothesized that a similar approach could be used with TDR to overcome the limitations of current calibrations for variable θ and σ_w. Thus, the objective of this study is to evaluate the applicability of the formation factor in calibrating the TDR for in situ measurement of salinity in soils drip irrigated with saline water. The study compares TDR-measured θ

and σ_w values with predictions of a conceptual model and with values obtained from the analysis of soil cores obtained under a range of θ and σ_w.

THEORY

If it is assumed that the electrical conductivity of the bulk soil (σ_a) is made up only of the conductivity of the liquid phase (σ_w) and the solid phase (σ_s), a theoretical relationship for σ_a may be defined as (Waxman and Smits, 1968; Nadler and Frenkel, 1980)

$$\sigma_a = (\sigma_w + \delta(\sigma_w) * \sigma_s)/F(\theta) = \sigma_w/F + \delta(\sigma_w) * In \quad [1]$$

In Eq. (1) σ_a, σ_s, and σ_w are as previously defined, δ is the salinity-dependent empirical ratio of the equivalent conductance of clay counter ions to their maximal value, F is the formation factor and In ($=\sigma_s/F$) is the intercept of the linear part of the σ_a-σ_w curve at σ_w=0. The formation factor relates σ_a to soil texture through the pore size distribution and θ and is a measure of the tortuosity of the soil with a nonconductive solid phase. The inverse of F is equivalent to the product of $\theta * T$ (T being the transmission coefficient, Rhoades *et al.*, 1976). In the field, F therefore encompasses the variability in θ and tortuosity. Generally at $\sigma_w < 4$ dS m^{-1}, the second term in Eq.(1) determines the shape of the σ_a- σ_w curve. At $\sigma_w > 4$ dS m^{-1}, the relationships are linear and an intercept equal to In can be derived as δ is then equal to unity. In soils irrigated with saline waters, σ_w generally exceeds 4 dS m^{-1} and σ_w can be inferred from σ_a, provided there is an F (?) function for the soil of interest.
Rearranging Eq. 1 gives

$$\sigma_w = (\sigma_a - \delta(\sigma_w) * In) * F(?) \quad [2]$$

where σ_w can be calculated from F and In. Because the salinity term appears in both sides of the equation, repeated iterations are needed until the calculated δ introduced in Eq. 2 results in a σ_w value which gives a δ value similar to the one used in the previous iteration.

Although F is critical for σ_w calculation, it cannot be determined directly on a pure theoretical basis because there is no way to have an exact mathematical description of the pore water geometry due to the interdependence of several soil- and liquid-phase parameters. Nadler (1982) has developed an empirical procedure to calculate F-θ for different soil types by superimposing the complete suction water retention relationship on two F-θ measurements at the same θ values resulting in a family of curves (see Fig. 2, Nadler *et al.*, 1984).

Based on the similarity between electrical and groundwater flow, a conceptual model to describe the relationship between F and the pore water geometry has been proposed by Mualem and Friedman (1991). Their hypothesis is that the flow lines of the water molecules under the hydraulic gradient in a given soil water content are similar to the flow lines of the electric current in the same soil and the same water content under electrical potential gradient. This relation can be used in the definition of σ_w in terms of F as

$$\sigma_a = \sigma_w * F(?) * (\theta^{n+2}/\theta_{sat}) \quad [3]$$

where F(?) =(1+2/ ?)/(1+1/ ?)^2. They obtained ? from the approximation $\theta = \theta_{sat}*(?/?_{cr})^{-?}$ in which θ_{sat} is the saturated water content, and ? is the capillary head. When the soil water retention and hydraulic conductivity functions are not available for calibration of the model, the empirical value for n is optimally set equal to 0.5, resulting in relative σ_a , for unsaturated conditions, being equal to

$$\sigma_{a,\,rel} = (\theta/\theta_{sat})^{2.5} \qquad [4]$$

In this study, since $\sigma_w > 4$ dS m^{-1}, the relationship between σ_a and σ_w is linear and a constant In is assumed, thus the only requirement is to measure σ_a and θ.

Both σ_a and θ can be determined from in situ measurements of the dielectric constant (ε), and the soil electrical resistance (R_s). For a probe of length L, ε is given by

$$e = (c\,\Delta t / 2L)^2 \qquad [5]$$

in which c is the velocity of light in free space, and t is the transit time. By defining an apparent length L_a as $c\Delta t/2$, Eq (5) can be rearranged to express ε as $(L_a/L)^2$ from which θ is calculated as (Topp *et al.*, 1980)

$$q = -5.3 \cdot 10^{-2} + 2.92 \cdot 10^{-2} e - 5.5 \cdot 10^{-4} e^2 + 4.3 \cdot 10^{-6} e^3 \qquad [6]$$

The bulk electrical conductivity of a sample at 25^{o}C can be calculated from (Nadler *et al.*,1991)

$$s_{25} = (K_p / R_s) f_T \qquad [7]$$

in which K_p is the cell constant of the TDR probe, R_s is the low frequency impedance of the soil sample and f_T is the temperature correction factor.

MATERIALS AND METHODS

The experiments were conducted in a field of cotton (Gossypium hirsutum, cv. Vered) located at Nirim in northern Negev, Israel. Northern Negev is a semi-arid region with a long-term, annual average precipitation of 360 mm. The soil is a loam (Calcic Palexeralf) containing 14% clay, 38% silt, and 48% sand, with a field capacity of 14.6 w/w. The soil also contained 11% $CaCO_3$ and had a cation exchange capacity (CEC) of 11.9 mmol/100 g. During the last 10 years, the studied field has received an average annual application of 4920 m^3 ha^{-1} of irrigation water with σ_w ranging from 1.4 to 4.4 dS m^{-1}. During this time, the field has been planted with either wheat or cotton. In early April 1995, the field was ploughed, disked, and ridged. Paired ridges (0.96 m apart and 16 m long) were seeded with cotton on April 16, 1995 at a rate of 2.25 x 10^6 plants per hectare. The field was fertilized with 230 kg ha^{-1} of N and 70 kg ha^{-1} of P_2O_5 but, like the last three years, received neither manure nor gypsum. There were 6 rows in each plot with the two outer ones being boundary rows.

Drip irrigation laterals, with an emitter spacing of 1 m and a delivery rate of 3.5 L hr^{-1}, were laid in the middle of alternate rows of each bed. Irrigation treatments consisted of three application rates of saline-sodic water (σ=3.6-4.0 dS m^{-1}, SAR=19.7) from a local well. Each treatment was duplicated in two plots.

The lowest rate, treatment A, applied water at 3010 m^3 ha^{-1}; the intermediate rate, treatment B, applied water at 3850 m^3 ha^{-1}; and the highest rate, treatment C, applied water at 4580 m^3 ha^{-1}. Treatment C was only slightly below the 4800 m^3 ha^{-1} normally applied in the area. During the first 3 weeks, irrigation frequency was once per week, after which it was increased to twice per week and maintained at this level for the next 10 weeks.

Instrumentation was installed only in the two inner rows of each plot. A pair of three-rod TDR probes (3 mm o.d., 0.20 m long, 0.05 m spacing) was installed horizontally at 12 different drippers. To install the probes, a pit (0.4 m x 0.4 m x 0.7 m) was first constructed and its walls gently smoothed. A pair of probes was then installed at depths of 0.3 m and 0.6 m in each pit. A thermistor was installed at each depth to measure soil temperature. Soil from the pits was back filled in the reverse order of removal, slightly compressed and wetted.

Soil solution samplers were installed at depths of 0.3 m, 0.6 m and 0.9 m. Instruments were installed 0.25 m away from the dripper. Each instrument site was wetted every 3 days for 2 weeks during which no measurements were taken. In each plot, a 1.05-m long neutron probe (NP) access tube was installed to permit independent measurements of ?.

All measurements were made at weekly intervals, just before the start of the each irrigation event, i.e. when ? values were the lowest and F values were threrefore harder to get. A Tektronix 1502 cable tester was used to obtain manual measurements of L_a and R_s. Soil water content, ?, was calculated using Eq. (6). The pore water conductivity, σ_w, was calculated from σ_a using Eq. (1) and the F(?) relationship (Nadler *et al.*, 1984). Clay content, estimated from the hygroscopic water (Banin and Amiel, 1969), was used to calculate In and to interpolate between textures and ? values.
A single core was obtained from each plot, on three different occasions during the growing season, by coring down to a depth of 0.9 m in 0.15-m increments. Independent measurements of θ were obtained by gravimetry and the salinity of 1:1 aqueous extracts measured. The ratio $?_{1:1}$/? was used to adjust the σ_w of the aqueous extracts. A neutron probe (NP) was used to measure θ to a depth of 1.05 m (one access tube per plot). Thermistors at 0.3 and 0.6 m were used to measure soil temperature throughout the study. Soil temperature was used to normalize TDR-measured σ_a. The applicability of the approach using the formation factor has been demonstrated in homogenous soils wetted with solutions of known σ_w by Nadler (1991).

RESULTS AND DISCUSSION

There are certain physical processes that can be expected to occur during irrigation with saline waters. For example, as more water is applied, salts are leached deeper into the soil profile causing σ_a and σ_w to increase at depth. Monitoring the evolution of these processes is therefore a good way to evaluate the applicability of the methodology developed above, but proper interpretation of the results require an understanding of the limitations of the technique. The first issue concerns placement of the monitoring devices under the dripper.

The dripper is a point source and the placement of sampling devices to ensure identical conditions is not simple. Therefore, when comparing the σ_w values obtained by different techniques (TDR, soil cores) at different locations, soil spatial variability may impose some limits. The effect of variability may be compounded by temporal variations in the volume of the wetted and saline soil during each irrigation cycle. In an evaluation of the placement of TDR probes relative to drippers, Or (1995) concluded that large differences in θ were due to the nonlinear relationships between relative θ and matric potential and attributed 12 to 24% of the variance to spatial variability. Thus, small-scale changes in soil texture, such as might occur between drippers, could increase the variance in θ. The increase in variance is also influenced by the dimensions of the TDR probe. Under quasi-steady state conditions, averaging of θ over the length of the probe could increase the variance as is characteristic to drip irrigation. To overcome these problems and to reduce the extent of the rapid fluctuations caused by the irrigation events, instruments were installed at 0.25 m away from the dripper. By avoiding the area most susceptible to spatial errors, i.e., under the dripper, 12 to 24 % estimate observed by Or (1995) is a conservative estimate for this experiment.

Figure 1 shows the field-averaged σ_w values calculated from TDR-measured σ_a at the 0.3-m and 0.6-m depths for the three irrigation treatments with clay-content estimated In=0.28 dS m^{-1} (Nadler *et al.*, 1984). For the first 80 days, σ_w showed a steady increase. Failure of a pump on day 86 caused a switch to less saline waters (σ=3.1 dS m^{-1}) for a 2-week period. During that period, local well water (σ = 3.4 dS m^{-1}) was mixed in a 1:1 ratio with treated sewage water (σ = 1.6 dS m^{-1}) from the Dan region activated sludge plant. The decrease in salinity observed after day 86 was due to the use of the less saline water. The differences in timing and amount of irrigation (treatments C and A) and the switch in schedule of treatment B are clearly reflected in σ_w.

Salinity in A was generally higher than C for most of the season. This can be expected because at such low irrigation rates, there is little possibility for leaching and salts tend to accumulate in the root zone causing an increase in σ_w. The difference between treatments showed a further increase after day 94. On day 94, treatment B started to receive larger returns of water inputs relative to evapotranspiration (ET). During this period, the plants consumed less

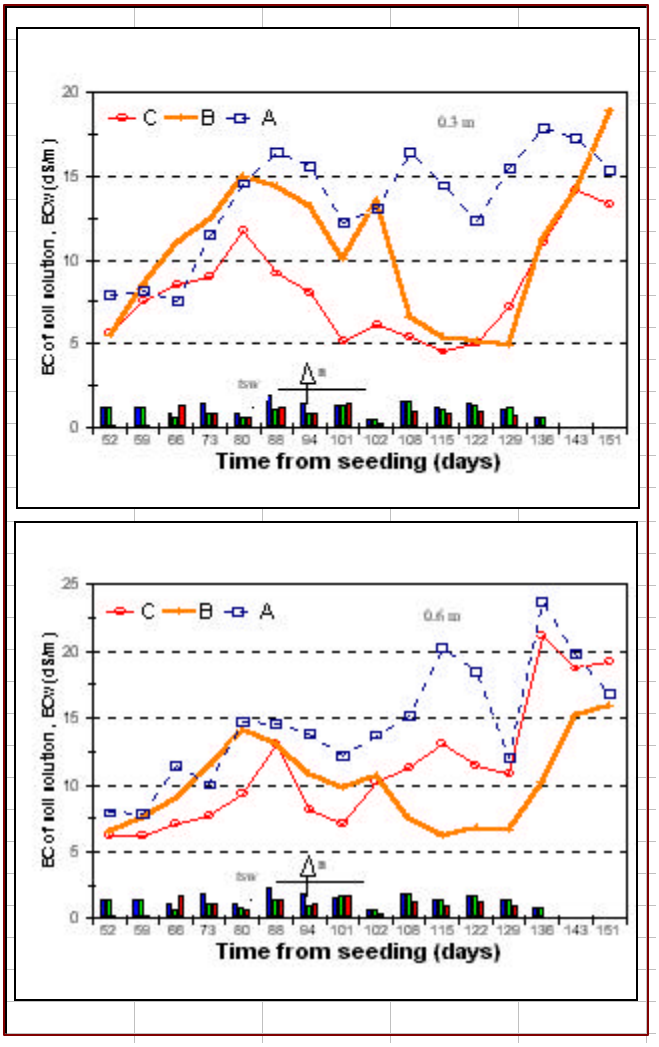

Fig. 1. *Averaged values of soil solution salinity, s_w (dS m^{-1}), calculated from TDR measurements, at 0.3 and 0.6 m depths, for the three levels of applied irrigation waters (A, B, C) vs. time. The bars triplets along the ordinate indicate time and amount of applied irrigation.*

water and irrigation water was also less saline. σ_w values approached and eventually became equal to that of treatment C, which received the highest amount of water. Thus, the increased water led to an increase in leaching, which removed accumulated salts and resulted in a reduction in salinity. With the salinity of irrigation water being 4.0 dS m^{-1}, and the expected dissolution of precipitated salts, final σ_w values of 4.5 dS m^{-1} at the 0.3-m depth (Fig. 1a) and 6.0 dS m^{-1} at the 0.6-m depth (Fig.1b) are quite reasonable.

Depth range (m):	**0 – 0.9**				**0 –0.6**	
		Irrigation Input				
Method:	Aqueous Extracts	irrigation	initial	total	Extracts	TDR
C	26.2*	20.0	3.6	23.6	19	14.9
B	19.4	16.5	3.6	20.1	13	10.6
A	17.3	13.0	3.6	16.6	13.5	16.2

*) mole charge m^{-2}

Table 1. *Mass balance of salt content (mole charge m^{-2}) based on aqueous extracts, input by irrigation water (for the upper 0.9 m profile) and TDR measurements (for the 0.6 m profile) for the three irrigation treatments.*

Following the initial decline in σ_w, there was a large increase at both depths after irrigation was terminated. Since plant water uptake continued, there was an increase in salinity raising it to more than six times that of the irrigation water. While the observed changes in σ_w are consistent with observed ? and the salinity of the irrigation water, it is known that the error in measured σ_w may increase at low ? (Rhoades *et al.*, 1976).

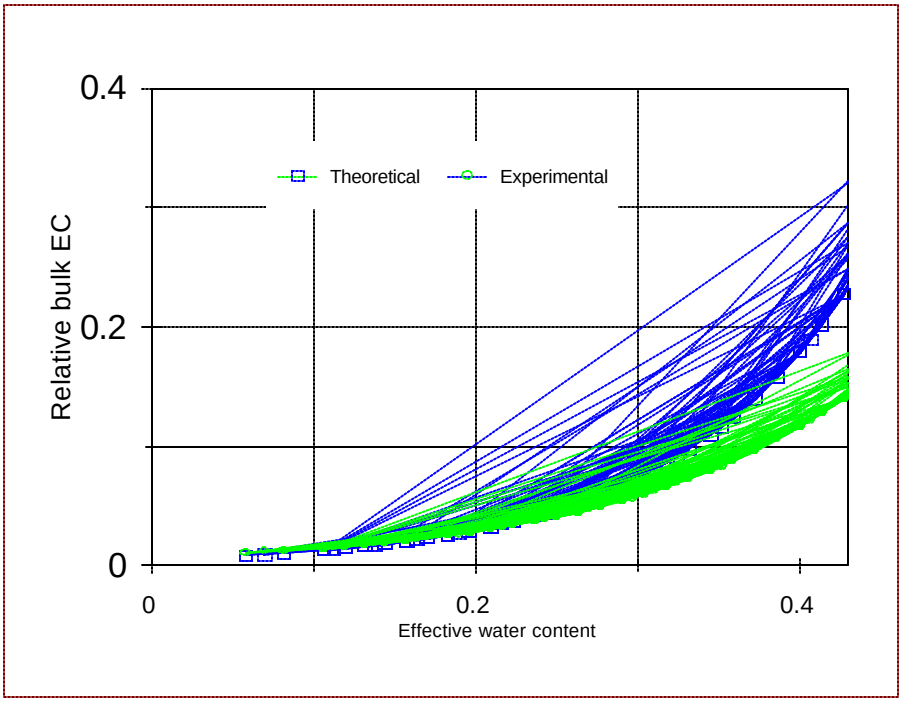

Fig. 2. *Comparison of measured and theoretically calculated relative bulk s_a vs. effective water content.*

An analysis of variance between σ_w, depth, irrigation rate, and time since seeding showed the effects of these variables and their interactions to be significant at $p < 0.012$.

The validity of the TDR-measured σ_w results can be determined directly by simply making independent measures of σ_w on soil cores. However, such an approach would render the sampling site useless for further analysis. Verification can also be done indirectly and semi-quantitatively using three different approaches: (1) salt mass balance; (2) a theoretical approach; or (3) comparison with data collected during previous studies on similar soils and under similar boundary conditions.

Results of the salt mass balance are presented in Table 1. The left columns of the table shows a ± 5%

match in the soil profile (upper 0.9 m) between the salt content by extraction (calculated from the product of θ and σ_w of the soil extracts) with that calculated from the irrigation input. The last two columns of Table 1 compare salt content in the upper 0.6 m of the profile from aqueous extracts and TDR measurements. This TDR estimation is based on the assumption that the size of the soil region that influences the TDR measurement (≈ 0.04 m) represents the 0.30 m section of the soil profile.

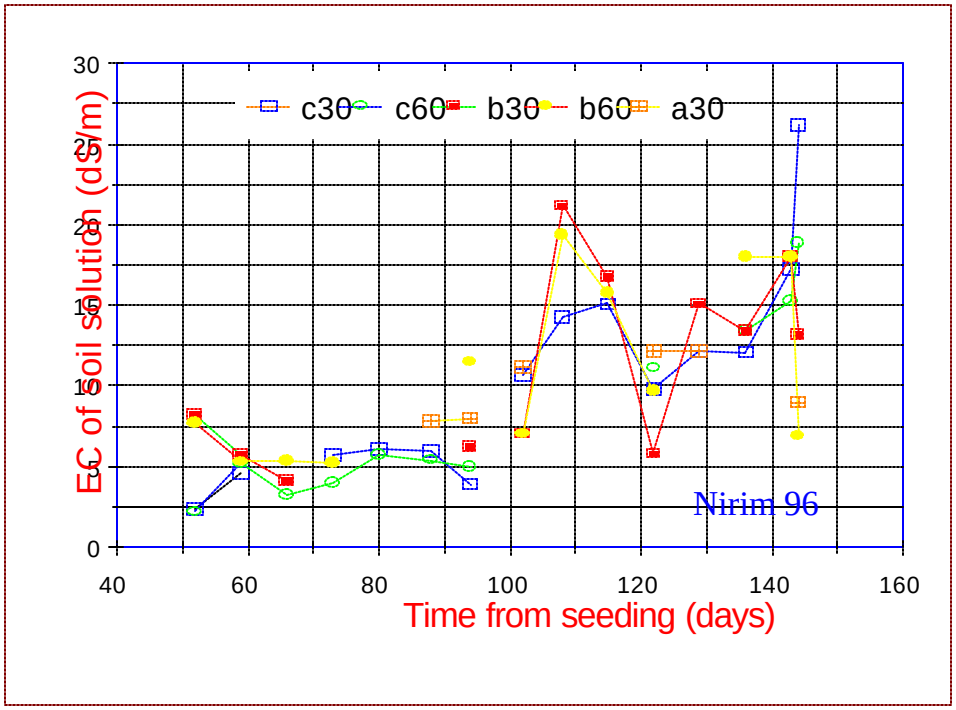

Fig. 3. *General range of soil solutions s_w for similar studies in the area (After Mantel* et al.*, 1991, 1992, 1993, Nadler and Heuer 1995).*

Another approach is to compare the theoretical relative σ_a from Eq. 4 with those calculated from the measurements in this study. For unsaturated conditions Mualem and Friedman (1991) used Eq.4 where σ_a was converted to relative σ_a by dividing it by $\sigma_{a,sat}$ and θ was converted to effective water content by dividing it by θ_{sat}. For this comparison we have calculated the experimental relative σ_a for σ_w = 3.3 at different water content by using θ_s=0.50 m^3 m^{-3}, θ_r = 0.05 m^3 m^{-3}, and $\sigma_{a,sat}$ =1.7 dS m^{-1} from direct measurements and In=0.28 dS m^{-1}, and F_{sat} = 4.4 from Nadler *et al.*, (1984). Figure 2 compares the measured and predicted relative σ_a as a function of effective water content. Over the θ range 0.08 to 0.21 m^3 m^{-3}, (most of the relevant θ values), predicted and measured values are essentially equal. However, for θ greater than 0.21 m^3 m^{-3}, predicted relative σ_a show increasing deviation from the measured values.

An examination of the results of previous studies (Fig. 3) may also help to validate the observed salinity levels. A summary of σ_w at the 0.3 and 0.6-m depths has been compiled (Fig. 3) from previous studies in neighboring locations (Mantel *et al.*, 1991, 1992, and 1993; Nadler and Heuer 1995). Based on the historical data and the present studies (excluding the TDR results), it can be expected that, during the growing season, salinity levels at the 0.3 and 0.6 m depths will increase, according to water management and quality. The expected limits are: (i) lower limit, from 3 to 7 dS m^{-1}, under optimal irrigation management (4800 to 5500 m^3 ha^{-1}) and water quality of 1.5 dS m^{-1}, ('imported' treated sewage) (ii) upper limit, from 7.5 to 25 dS m^{-1}, with restricted water amounts (3800-4800 m^3 ha^{-1}) and σ=4 to 5 dS m^{-1} (local well waters). This wide scatter in salinity among the studies is attributed to drip irrigation, previous salinization and leaching, deviation in measuring devices location relative to drippers, variability of the natural soil and fluctuations in wetted volumes. While these factors can be expected to reduce the accuracy of absolute numbers, they should not change the trends. Figure 3 shows the range of

σ_w for similar studies conducted in the area of this experiment. Data points of the present and previous studies show a similar distribution. The bias towards the lower limit between days 88 to 100 of the present study data was caused by the temporary decrease in soil solution salinity due to a decrease in σ of the irrigation water.

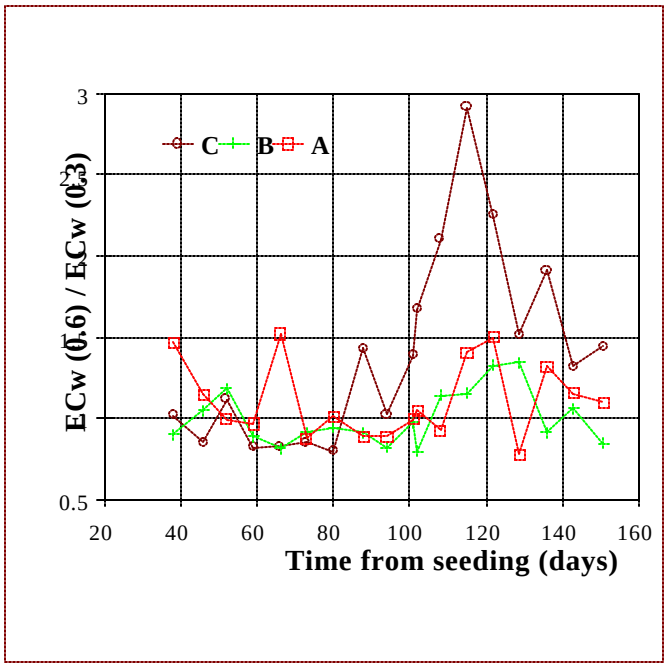

Fig. 4. *Ratio of s_w at the two monitored depths ($s_{w.6\,m}/s_{w.3m}$) for the three levels of applied irrigation, vs. time.*

In the last comparison, we focus on the ratio of σ_w at the 0.6-m depth ($\sigma_{w0.6}$) to that at the 0.3-m depth ($\sigma_{w0.3}$). Figure 4 shows a temporal plot of the ratio $\sigma_{w0.6}/\sigma_{w0.3}$ for the three treatments. The ratios show that over time, there was an increase in σ_w at 0.6 m and treatment C showed the greatest increase. This results are not surprising as water infiltration and redistribution at the greater depth would be accompanied by an increase in salinity; since treatment C received the highest rate of water, leaching of salt from the 0.3-m depth to 0.6 m could be expected to be higher. The observed ratios are consistent with other observations including plant size and the quality and timing of water application (Nadler and Heuer, 1997). The effect of the change in water quality after day 94 is clearly reflected in the response of treatments A and B. The two treatments become more similar and are essentially identical by the end of the experiment.

In a limited number of cases, this ratio decreases to 0.8 (within experimental error) but in most cases, the soil solution of the deeper layer was more saline. The highest ratio was observed during days 100 to 130 under treatment C. The larger amount of water applied under C (and a better shading of the soil surface due to larger plants) helped retain lower salinity levels at the 0.3 m depth. The ratio is therefore high because of the low σ_w at 0.3 m rather than high values in 0.6 m. A similar situation could be expected for treatment B but was suppressed by a larger difference between the applied and consumed water. The plants in this treatment were generally smaller and therefore consumed less water during days 100 to 130, resulting in an improved leaching that kept the ratio low.

Figure 5 shows a plot of TDR-measured θ as a function of time. The difference between treatments is quite clear and corresponds to changes in the irrigation schedules. The differences appear quite moderate mainly because of the monitoring protocol. Measurements were generally taken about 72 h after each irrigation event rather than immediately after the event. This protocol was followed to enable redistribution (by drainage and evapotranspiration) and enough time for plants to adjust to irrigation events.

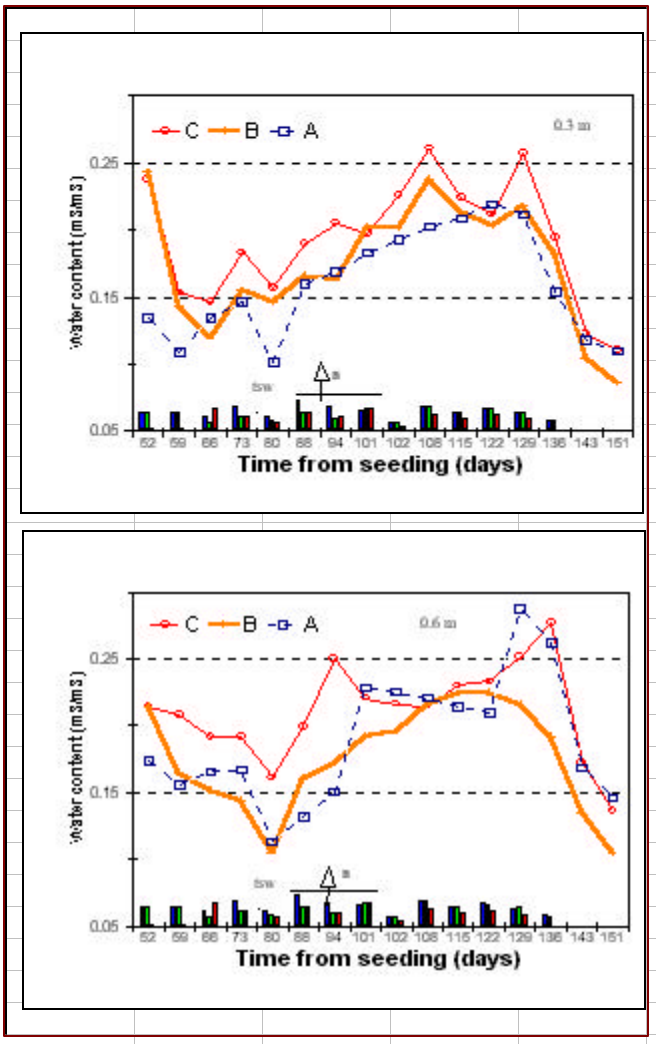

Fig. 5. *Averaged q values, calculated from TDR measurements, at 0.3 and 0.6 m depth, for the three levels of applied irrigation waters vs. time. The bars triplets along the ordinate indicate time and amount of applied irrigation.*

CONCLUSION

The relationship between the formation factor, volumetric water content, and salinity can be used, in combination with TDR measured ? and σ_a, to estimate σ_w. The TDR-measured σ_w showed reasonably good agreement with independent estimates of σ_w obtained from an analysis of irrigation inputs and using a conceptual model. The errors in the predictions appear to be rather high but may be expected given the effects of temporal and spatial variable in the soil. Under the conditions of this study the error in estimating σ_w is roughly ± 25%. It is speculated that the improvement in the accuracy of the σ_w values may be partly attributed to use of a manual rather than automated method for analyzing the TDR waveforms. Under the prevailing salinity, an experienced operator may have an advantage over the currently available numerical algorithms used for finding the travel time and hence ε in Eq (5). Recent developments in probe design, such as remote diode shorting (Hook *et al.*, 1992), may allow more accurate measurement of ? in saline soils. However, a limitation of the remote diode shorting is that it does not permit simultaneous measurement of σ_a. Since estimating soil variability and its influence on accuracy of σ_w measurements was not the sole purpose of this study, an attempt was made to quantify the effects of spatial variability on the required model parameters. However, in the literature, there was no information on a simple, practical method for estimating the degree of variability related to the parameters involved, or a simply applicable equation for evaluating the errors introduced by these sources. An improvement would be expected by increasing the number of replicates in more homogeneously irrigated soil.

REFERENCES

Banin, A., and Amiel, A., 1969, A correlative study of the chemical and physical properties of a group of natural soils of Israel: Geoderma, **3**, 185-198.

Cremers, A., van Loon, J., and Laudelout, H., 1966, Geometry effects for specific electrical conductance in clays and soils. Proceedings of the 14th National Conference of clays and clay minerals, p. 149-162.

Dasberg, S., and Dalton, F. N., 1985, Field measurement of soil water content and bulk electrical conductivity with time-domain reflectometry: Soil Science Society America Journal, **49**, 293-297.

Hook, W. R., Livingston, N. J., Sun, Z. R., and Hook, P. B.. 1992, Remote diode shorting improves measurement of soil water by time domain reflectometry: Soil Science Society America Journal, **56**, 1384-1391.

Kachanoski, R.G., Gregorich, E.G., and van Wesenbeeck, I. J., 1988, Estimating spatial variations of soil water content using non-contacting electromagnetic induction methods: Canadian Journal of Soil Science, **68**, 715-722.

Kachanoski, R. G., Pringle, E., and Ward, A., 1992, Field measurements of solute travel times using Time Domain Reflectometry: Soil Science Society America Journal, **56**, 47-52.

Kachanoski, R.G., Thony, J. L., Vaulcin, M., Vachaud, G., and Laty, R., 1994, Measurement of solute transport during constant infiltration from a point source: Soil Science Society America Journal, **58**, 304-309.

Mantell, A., Meiri, A., Frenkel, H., Issachar, I., and Sharabani, N..1991, 1992, 1993. Response of drip-irrigated cotton to water management, soil and water salinity, and long-range balance of soil salinity, In, Annual reports, 1990/91, 1991/92, 1992/93 Project No. 307/190, Agr. Res. Org., The Volcani Center, Institute of Soils and Water, Min. Agric., Israel (in Hebrew).

Mualem, Y., and Friedman, S. P., 1991, Theoretical prediction of electrical conductivity in saturated and unsaturated soil: Water Research Resources: **27**, 2771-2777.

Nadler, A., and Frenkel, H., 1980, Determination of soil solution electrical conductivity from bulk soil electrical conductivity measurements by the four-electrode method: Soil Science Society America Journal, **44**, 1216-1221.

Nadler, A., 1982, Estimating the soil water dependence of the elctrical conductivity soil solution/electrical conductivity bulk soil ratio: Soil Science Society America Journal, **46**, 722-726.

----------, 1991, Effect of soil structure on bulk soil electrical conductivity (ECa) using the TDR and the 4P techniques: Soil Science, **152**, 199-203.

Nadler, A., Frenkel, H., and Mantell, A., 1984, Applicability of the four-probe technique under extremely variable water contents and salinity distribution: Soil Science Society America Journal, **48**, 1258-1261.

Nadler, A., Dasberg, S. and Lapid, I., 1991, Time domain reflectometry measurements of water content and electrical conductivity of layered soil columns: Soil Science Society America Journal, **55** ,998-943.

Nadler, A., and Heuer, B., 1995, Effect of saline irrigation and water deficit on tuber quality: Potato Research, **38**, 119-123.

----------, 1997, Soil moisture levels and their relation to water potential of cotton leaves. Australian Journal of Agricultural Research: **48**, 923-932.

Nissen, H. H., Moldrup, P., and Henriksen, K., 1998, Time domain reflectometry measurements of nitrate transport in manure-amended soil: Soil Science Society America Journal, **62**, 99-109.

Persson, M., 1997, Soil solution electrical conductivity measurements under transient conditions using time domain reflectometry: Soil Science Society America Journal, **61**, 997-1003.

Or, D., 1995, Stochastic analysis of soil water monitoring for drip irrigation management in heterogeneous soils: Soil Science Society America Journal, **59**, 1222-33.

Rhoades, J. D., and Ingvalson, I., 1971, Determining salinity in field soils with soil resistance measurements: Soil Science Society America Journal, **35**, 54-60.

Rhoades, J. D., Raats, P. A. C., and Prather, R. J., 1976, Effects of liquid-phase electrical conductivity, water content, and surface conductivity on bulk soil electrical conductivity: Soil Science Society America Journal, **40**, 651-655.

Rhoades, J. D., Shouse, P. J., Alves, W. J., Manteghi, N. A., and Lesch, M., 1990, Determining soil salinity from electrical conductivity using different models and estimates: Soil Science Society America Journal, **54**, 46-54.

Sheets, K. R., and Hendrix, J. M. H., 1995, Noninvasive soil water content measurement using electromagnetic induction. Water Research. Resources: **31**, 2401-2409.

Slavich, R. G., 1990, Determining ECa-depth profiles from electromagnetic induction measurements. Australian Journal of Soil Research, **28**, 443-452.

Topp, G. C., Davis, J. L., and Annan, A. P. 1980, Electromagnetic determination of soil water content: Measurement in coaxial transmission lines: Water Research. Resources, **16**, 574-582.

----------, 1982, Electromagnetic determination of soil water content using TDR: I. Application to wetting fronts and steep gradients: Soil Science Society America Journal, **46**, 672-684.

Ward, A. L., and Kachanoski, R. G., 1988, Solute transport during three-dimensional unsaturated water flow: Axisymmetric measurements using time domain reflectometry. e. c. 192: In Agronomy abstracts. ASA, Madison, WI.

Ward, A. L., Kachanoski, R. G., and Elrick, D. E., 1994, Laboratory measurements of solute transport using time domain reflectometry: Soil Science Society America Journal, **58**, 1031-39.

Waxman, M. H., and Smits, L. J. M., 1968, Electrical conductivities in oil-bearing shaly sand: Society of Petrolium Engineering Journal, **8**, 107-122.

Weerts, A. H., Bouten, W., and Vertraten, J. M., 1999, Simultaneous measurement of water retention and electrical conductivity in soils: Testing the Mualem-Friedman tortuosity model: Water Resources Research, **35**, 1781-1787.

van Wesenbeeck, I. J., and Kachanoski, R. G., 1988, Spatial and temporal distribution of soil water in the tilled layer under a corn crop: Soil Science Society America Journal, **52**, 363-368.

Wraith, J. M., Comfort, S. D., Woodbury, B. L., and Inskeep, W. P., 1993, A simplified waveform analysis approach for monitoring solute transport using time domain reflectometry: Soil Science Society America Journal, **57**, 637-642.

Rock and Soil Deformation Monitoring

Applications of Time Domain Reflectometry to Landslide and Slope Monitoring
W.F.Kane, T.J.Beck, J.J.Hughes, *KANE GeoTech Inc., USA*

Calibration of Small-Diameter TDR Cables for Measuring Displacement in Physical Soil Models
C. E. Pierce and C. M. McAlister, *University of South Carolina*

Measurement of Tailings Consolidation Using TDR Technology
K. O'Connor, *GeoTDR, USA*; D. A. Poulter, *The Glasgow Engineering Group*; D. Znidarcic and G. Gjerapic, *University of Colorado at Boulder*

Methodology for Monitoring of Open Pit Slopes Using Time Domain Reflectometry
F. Charette, *Atlas Copco Rock Drills, Canada*; Y. Beauchamp, *LAB Chrysotile, Inc., Canada*

Time Domain Reflectometry to Monitor Tailings Dam Stability
B. P. Gorski, B. Tisch, T. Anderson, K. Judge and K. Tarr, *Mining and Mineral Sciences Laboratories, Canada*

Looping TDR Cables for Increased Sensitivity to Extension
C. E. Pierce, P. Adak and C. M. McAlister, *University of South Carolina*

Back to Table of Contents

APPLICATIONS OF TIME DOMAIN REFLECTOMETRY TO LANDSLIDE AND SLOPE MONITORING

William F. Kane[1], Timothy J. Beck[2], and Jeremy J. Hughes[3]

[1]KANE GeoTech, Inc., P.O. Box 7526, Stockton, CA 95267; wkane@kanegeotech.com
[2]KANE GeoTech, Inc., P.O. Box 7526, Stockton, CA 95267; tbeck@kanegeotech.com
[3]KANE GeoTech, Inc., P.O. Box 7526, Stockton, CA 95267; jhughes@kanegeotech.com

KANE GEOTECH, INC.

ABSTRACT

Time domain reflectometry (TDR) is now an accepted tool for slope and landslide monitoring. As yet, there are no accepted methods or procedures for installing cables or presenting data. Installations, including cable testers, cables, and grout types, vary significantly from job to job, and installer to installer. Applications have included both on-site data collection and remotely accessed systems. In an effort to add to the current knowledge base, this paper summarizes one group's six years of work using TDR for slope and landslide monitoring.

This paper describes case studies documenting TDR installation procedures and the development of software that work in given applications. Experience in California, Nevada, and Illinois included the use of the Tektronix 1502 and Campbell Scientific TDR100 cable testers, both as stand-alone field units and as part of remotely accessed automated monitoring installations.

Local installations included single and multiple TDR cables grouted in boreholes to locate failure planes and delineate the extent of moving areas. Cables were installed on the outside of inclinometer casings as well as grouted inside failed inclinometers in an attempt to gain additional data from otherwise unusable boreholes.

Remote data acquisition was combined with TDR to monitor slope movement. This included coupling TDR with additional instrumentation, such as electrolytic bubble inclinometers and vibrating wire piezometers. TDR also has been used to trigger alarms based on the amount of cable deformation.

Case studies and installation descriptions are included ranging from using TDR as an inexpensive tool to locate shear failure in a slope to implementing it in a sophisticated automated monitoring system.

INTRODUCTION

One of the new developments in landslide monitoring during the 1990's was the use of time domain reflectometry (TDR) to monitor slope and landslide movement. TDR measures the reflective strength of a voltage pulse traveling along a coaxial cable. Originally developed around 1930 to find faults in transmission and power cables, TDR was used in the 1980's to find the limits of caving zones in longwall coal mines. It was not until the mid-1990's that widespread use and general acceptance of this tool for monitoring slope movement took place.

The principal advantage of TDR over other methods of slope monitoring is that it is a quick and economical means of determining the extent of movement of an earth mass. In addition, the digital nature of the data makes it possible to transmit the information by telemetry allowing remote monitoring.

TDR can be easily combined with other electronic instrumentation such as rain gages, vibrating wire piezometers, extensometers, and electrolytic bubble inclinometers to obtain a wide range of information about a particular slope without the necessity of physically traveling to the location. In addition, the entire process can be automated to record and collect data at specific times and intervals.

Following are case studies describing various applications of TDR monitoring installations. Application case studies are divided into field applications using physical on-site data collection and remote installations where TDR signatures are collected automatically and downloaded to a monitoring station.

TIME DOMAIN REFLECTOMETRY (TDR)

Basic Principle of TDR

Radar is a form of time domain reflectometry (TDR). In radar, a radio transmitter sends out a short pulse of energy and measures the time for a reflection, or echo, of the energy from some object. TDR works in much the same way. An electrical pulse is sent along a coaxial cable and an oscilloscope is used to determine the time it takes for the echos to return. The U.S. Bureau of Mines began research with TDR in the 1960's for locating electrical faults in power cables and extended the technology to ground control problems (O'Connor and Wade, 1994).

Time domain reflectometry (TDR) is a relatively new approach to monitoring slope movement (Kane and Beck, 1996; Mikkelsen, 1996; O'Connor and Dowding, 1999). The cable tester sends an electrical pulse down a coaxial cable grouted in a borehole, Figure 1. When the pulse encounters a break or deformation in the cable, it is reflected. The reflection shows as a "spike" in the cable signature, Figure 1. The relative magnitude and rate of

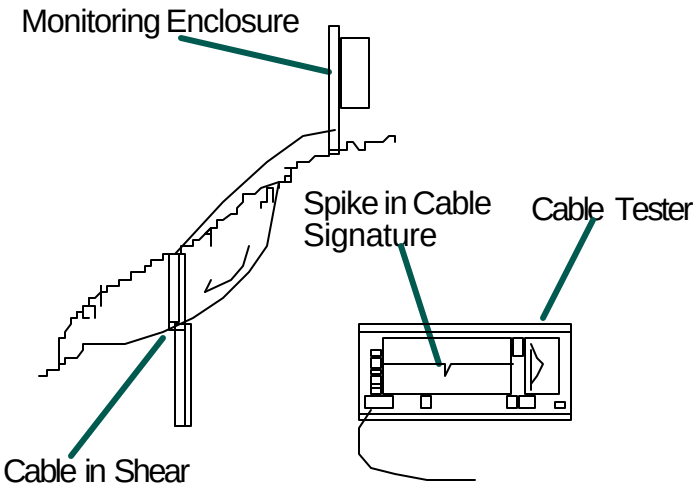

Fig. 1. *Schematic of TDR cable tester operation.*

displacement over time, and the location of the zone of deformation can be determined immediately and accurately.
The size of the spike increase correlates with the magnitude of movement, Figure 2. A laptop computer is connected to the tester and cable signatures are written to disk for future reference.

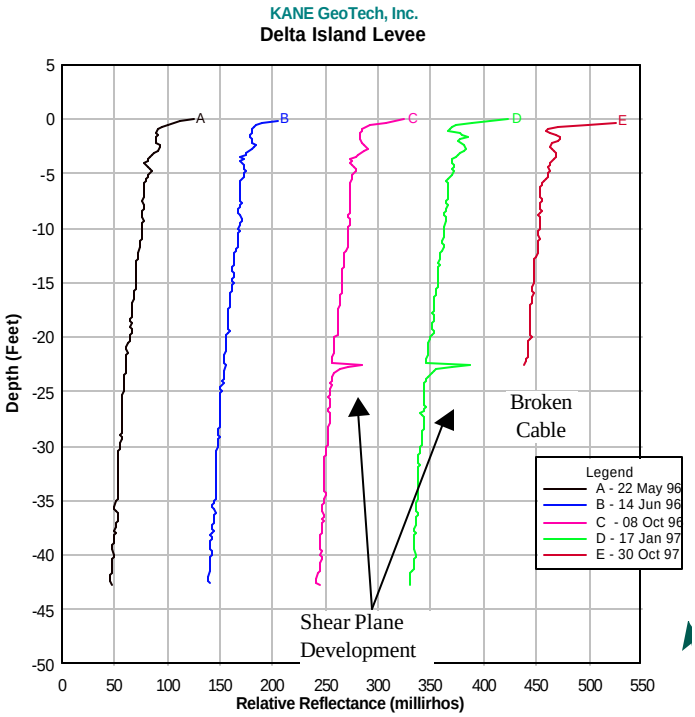

Fig. 2. *Increased TDR signature spike and broken cable with continued slope movement. Cables show shear zone in California Delta levee (see text).*

Equipment and Software

TDR cables generally are read using one of two cable testers: the Tektronix 1502B/C or the Campbell Scientific TDR100. The Tektronix 1502B/C is a heavy, relatively large, rugged cable tester which has a screen to allow viewing of the cable signature. The signature is digitized and transferred to a laptop computer data file in ASCII format using Tektronix SP232 software. SP232 also allows the file to be recalled for viewing. Two signatures can be compared using SP232. The data can be rearranged to plot it using a conventional spreadsheet, or plotted using a program such as TDRPlot2000 (KANE GeoTech, Inc., 2001). Figure 2 was plotted using a Tektronix 1502B, laptop computer, and TDRPlot 2000.

The Campbell Scientific TDR100 is a small lightweight cable tester designed to work with a Campbell Scientific CR10X datalogger in remote automated data acquisitions systems. However, the TDR100 can be incorporated into a field system by placing it in a weatherproof case with a rechargeable battery system. This type of field unit is available commercially. Data output for field monitoring consists of tabular ASCII digitized cable signatures. The output from the remote application is standard datalogger comma-delimited ASCII. This data can be easily plotted using a spreadsheet or with TDRPlot 2000.

Installation

Depending on the application and characteristics of the site, two types of coaxial cables, available from numerous manufacturers, can be used: flexible RG59/U cable television cable or stiffer, higher quality, foam-filled communications cable. RG59/U cable is relatively inferior in quality and suffers from signal attenuation. Graphically, this appears as a slight angle of the cable signatures to one side of the plot. In addition RG cable is elastic and may relax over time making the signature spike appear smaller. For these reasons, it is not recommended for very deep holes, greater than 33-m, or long-term monitoring. However, as long as its limitations are understood, it can be used in these applications. In each of the following case studies, one or both types of TDR cables were grouted in boreholes using a 10% bentonite/90% cement or 100% lean cement grout.

ON-SITE TDR DATA COLLECTION

TDR data can be collected in a manner similar to inclinometer data, that is, personnel can visit the site and interrogate the TDR cable, saving the data to a file. This approach still has significant advantages over using inclinometers. A coaxial cable, no matter how deep, can be read in just a few minutes as opposed to 45 minutes for the shallowest inclinometers and hours for very deep ones. Another advantage is that deformation of the cable, indicating slope movement, can be viewed immediately rather than waiting until data has been downloaded from a logger and plotted on computer.

Levee Embankment San Joaquin/Sacramento River Delta, California

Numerous islands in the California Delta, at the confluence of the San Joaquin and Sacramento Rivers, are below sea level. To protect property from flooding, a system of levees has been developed. Soft peat soil beneath these levees, however, is susceptible to differential settling. The resulting instability may produce small slides on the island side of the levees. Repair is done by the compaction of soil at levee crests and by buttressing the sides of the levees.

In an area that was undergoing slope failure, three cables were installed in boreholes at the top, middle, and bottom of the levee. The purpose of the monitoring was to determine the location of the shear zone so that a buttress repair could be completed above the toe of the slide. The cables were monitored at intervals and the location of the shear plane determined.

Two sections of the levee showed signs of distress including tension cracking and the formation of small scarps in the levee roadway. Settlement of the roadway was as much as eight inches.

Borehole data indicated that the levee profile at this location consisted of 15 feet of medium silty clay. Foundation soils were composed of 10 feet of peat underlain by 7 feet of soft clay followed by a very stiff clay.

Before initiating levee repair, it was necessary to determine the extent of the failure mass. The delineation of the slide mass required at least three monitoring holes as shown in Figure 3. To reduce installation and monitoring costs, TDR cables were installed and run in trenches to a monitoring location on the roadway shoulder. In this way, the boreholes could be read quickly from one location. Six inexpensive RG59/U coaxial cables with twist-on BNC connectors at the ends were installed. Cable lengths ranged from approximately 40 feet at the levee crown to 20 feet on the inboard toe. All cables were grouted in a weak cement grout.

A Tektronix 1502B cable tester was used to collect data using Tektronix SP232 software. TDR signatures were plotted using TDRPlot2000 and signatures arranged to obtain the plot shown in Figure 2.

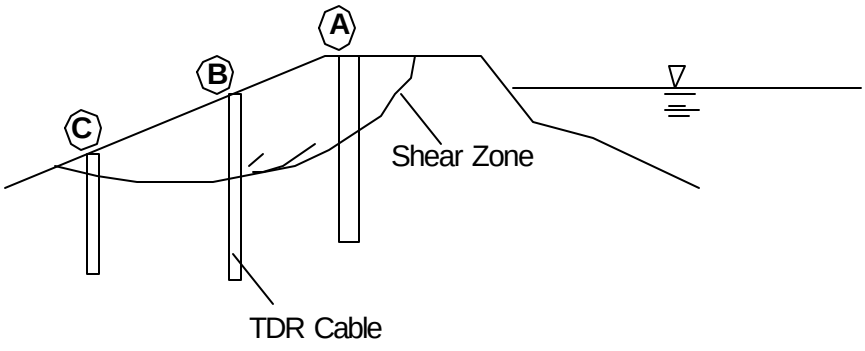

Fig. 3. *Relative locations of TDR cables for levee monitoring.*

TDR monitoring showed that only the cable nearest the roadway in both locations was undergoing slight deformation. Therefore, the failure plane was relatively shallow and could be repaired with an earth buttress.

Small Landslide in Golf Course – San Francisco Bay Area

A small slope failure adjacent to the fairway of a golf course needed repair. Budgetary constraints precluded the installation and labor intensive use of conventional probe inclinometers. Instead, two RG59/U TDR cables were installed, one in the middle and one at the base of the slide. Cables were read using a Tektronix 1502B cable tester. Figure 4 shows the TDR signatures over time. The lower limit of the slide is clearly seen at 48-ft.

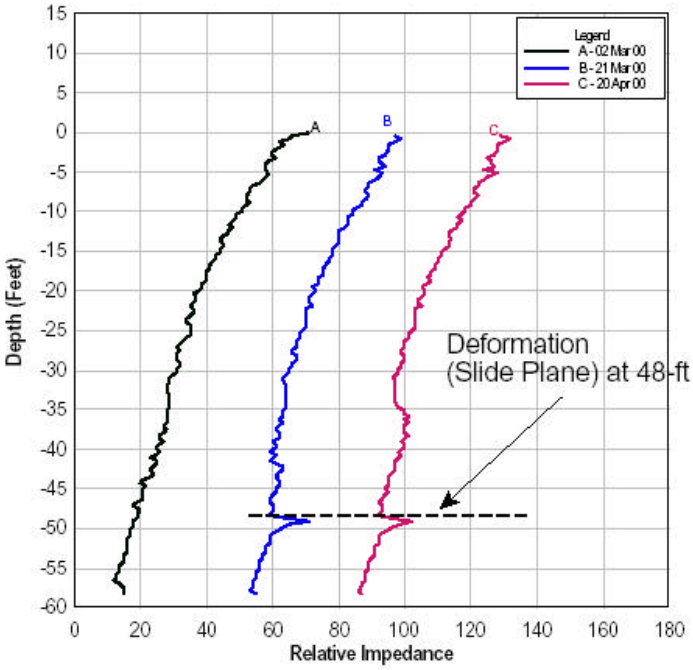

Fig. 4. *TDR signatures over time showing cable deformation due to landslide shear plane.*

Large Landslide in Development – San Francisco Bay Area

Although not generally recommended because of attenuation problems, RG59/U cable can be used in deeper holes, especially when the long-term data outlook is not promising.. Earth moving operations in a valley resulted in a large, relatively fast moving landslide. Inclinometer casing and RG59/U TDR cables were installed in boreholes. The slide quickly rendered the inclinometers unuseable. Figure 5 shows the TDR cable signatures for one of the cables. They were collected using a Tektronix 1502B cable tester. Note the relative rapid development of the TDR signature spike. In this case, movement of the slide was so rapid that the flexible cable had no time to relax. The pronounced slant to the cable signatures is due to attenuation over the relatively deep, 170-ft, cables.

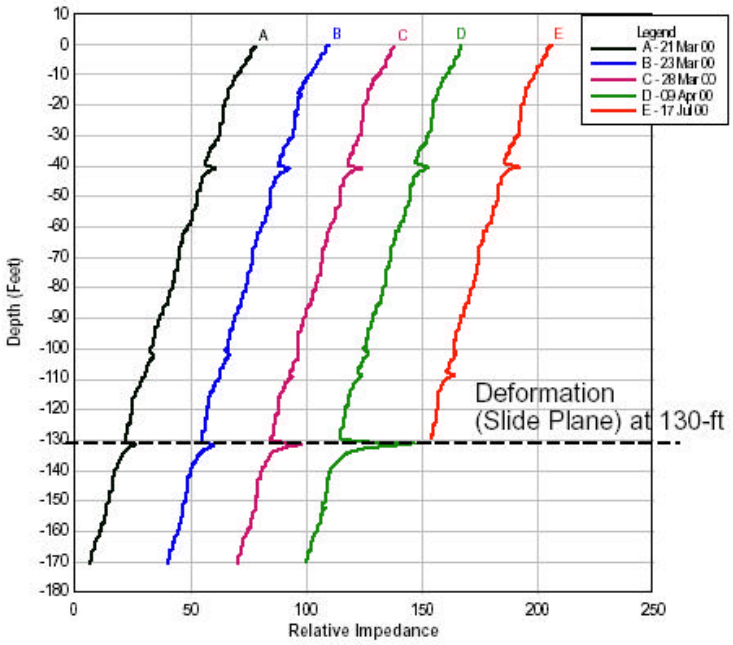

Fig. 5. *Deep RG59/U cables in fast moving landslide.*

Routine Landslide Investigation – San Francisco Bay Area

As part of a routine site investigation for an approximately 25,000 yds^3 landslide, several boreholes were drilled along the centerline of the slide located in a quarry overburden storage area. Evidently material had been added over the years without preparation of the subgrade. The geologic column consisted of about 34-ft of mine overburden overlying a thin 1-ft to 2-ft clay layer, Figure 6. Beneath this clay layer was the siltstone bedrock. The clay layer appeared to be the original topsoil that was buried beneath the overburden waste. An RG59/U TDR cable was installed in the borehole prior to grouting.

The TDR cables were read initially using a Tektronix 1502B tester about one week later. Figure 7 shows the TDR signatures for the borehole between March 21, 2000 and June 19, 2000. The initial reading shows cable deformation at a depth of 23-ft. At this depth, the hole casing jammed and the subsequent effort to remove it damaged the cable. The second reading of April 21, 2000 shows the development of a signature spike at 34-ft. This spike grew during the period from April 21 to June 19, 2000 when repair efforts were begun. Visual observation during that period confirmed that slide movement was continuing. During the repair process, it was determined that the clay layer was indeed the failure plane.

In this instance TDR was used as an inexpensive part of a standard landslide investigation. It supplied valuable data in determining the failure zone without any additional cost.

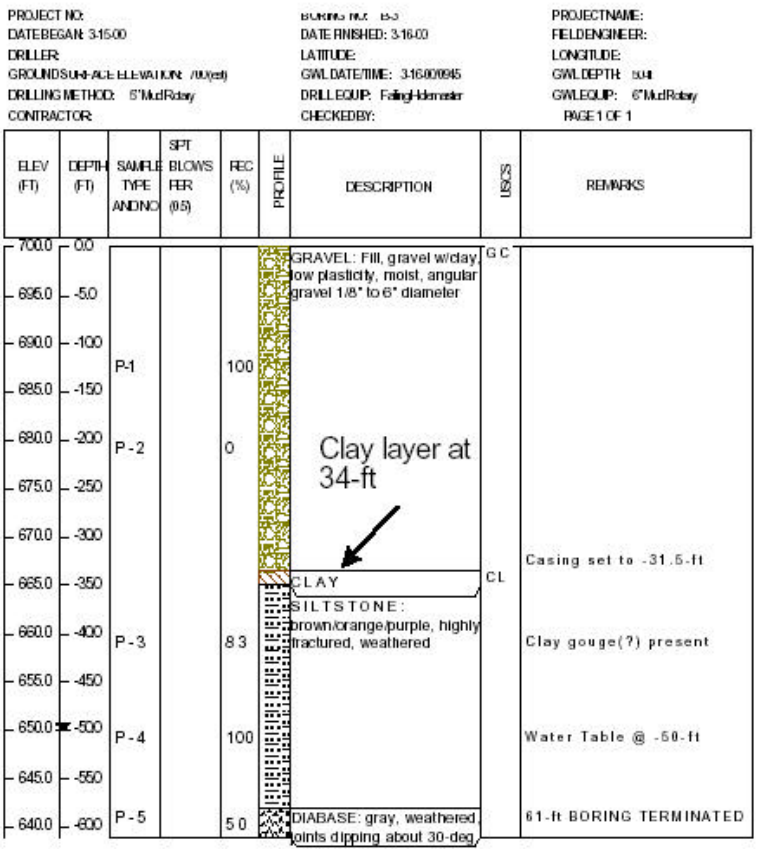

Fig. 6. *Borelog for landslide investigation showing a clay layer at 35-ft.*

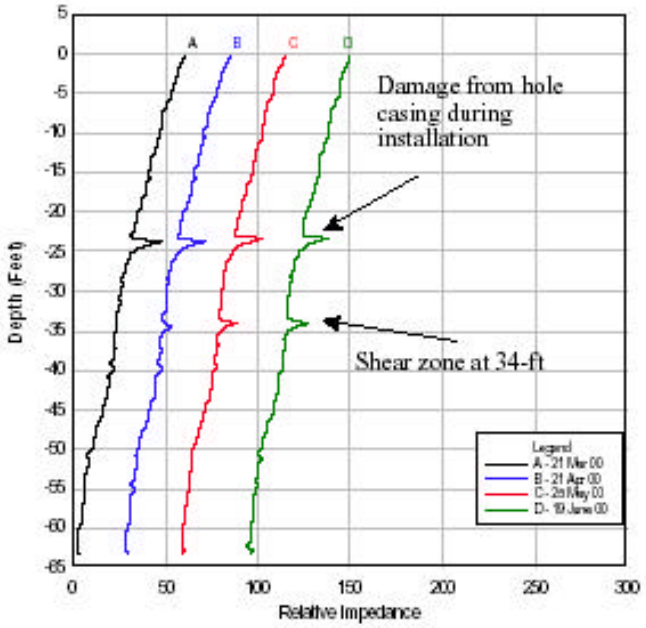

Fig. 7. *TDR signature showing shear zone at top of rock.*

Mining Operation – Nevada

The pit wall of an open-pit gold mine in Nevada experienced significant landsliding and instability. It was desired to locate the shear zone under difficult geologic conditions. The ore body was situated beneath soft volcanic tuff and a thicker, brittle welded tuff. The actual shear zone was believed to be located in the tuffaceous sediments. However, large scale movement of the welded tuff and the deep nature of the shear zone made inclinometers impractical. In addition, it was impossible to position a drill rig close to the head scarp because of large tension cracks in the crest. Consequently, angled boreholes were required, some up to 300 m.

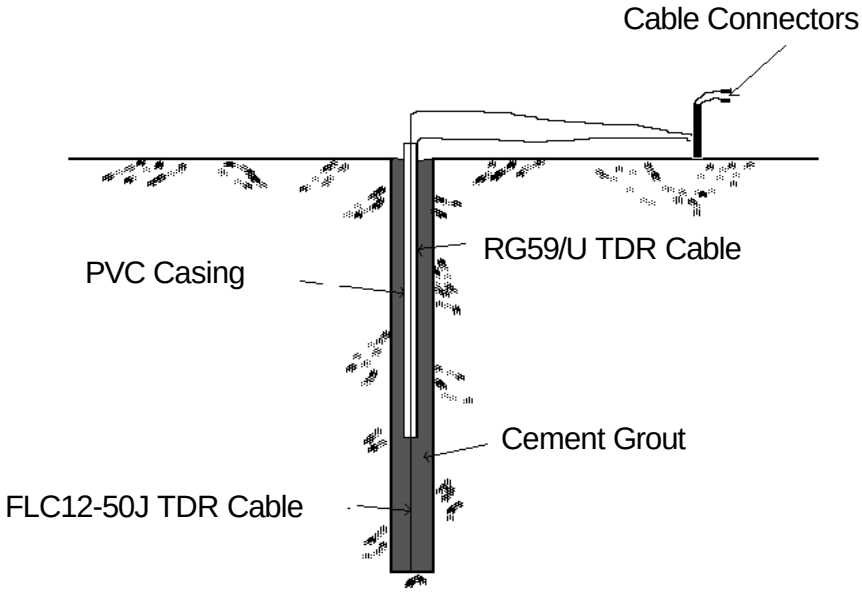

Fig. 8. *TDR installation for Nevada gold mine. Upper portion FLC12-50J cable is protected from slope movement by annular space. RG59/U cable used to monitor for upper slope movement.*

The deep holes, angled borings and the large number of readings that would be required, made inclinometers impractical. It was decided to install six TDR cables initially to monitor continued movement of the pit wall. Cables were read every day to determine locations of deformation.

Another problem at this site was that movement of the upper welded tuff would pinch off any inclinometer or cable before the smaller movements in the tuff sediments member could be monitored. A system was devised to grout a 12.5-mm, corrugated, foam-dielectric coaxial cable into the tuff protecting it by an annular space formed by 150 mm plastic pipe casing in the upper welded tuff unit. This is shown in Figure 8. The casing could take up movement in the welded tuff before movement would affect the cable. A flexible RG59/U cable was attached to the outside of the casing to monitor casing deformation.

Using TDR with Inclinometer Casing – Santa Clara County, California

Many users of TDR prefer to install a TDR cable, usually a flexible RG-type cable, to the outside of an inclinometer or piezometer. The California Department of Transportation (Caltrans) routinely uses this method for a large number of its inclinometer installations. This approach reduces the sensitivity of the TDR cable to movement, but to allow slope monitoring to continue after the inclinometer casing has been sheared off. Figure 9 shows the inclinometer reading for a large landslide in the Coast Range of California, mostly in Franciscan Complex sandstones. The inclinometer was installed with an RG59/U TDR cable attached to the outside of the casing. Slope movement eventually rendered the inclinometer unreadable at 52-ft. Figure 10 is the plot of TDR signatures for the cable obtained with Tektronix 1502B and Campbell Scientific TDR100 cable testers. No movement was detected until after the inclinometer was sheared. Additional movement was also picked up at 18-ft long after the inclinometer was abandoned.

AUTOMATED REMOTE TDR DATA ACQUISITION

TDR is very effective when integrated into a geotechnical instrumentation system with datalogging capabilities. It is relatively easy to program the dataloggers to trigger alarms when a break or deformation in a TDR cable occurs. Telephone lines, cellular telephones, and radios can be used to interface with the system.

TDR/Inclinometers – Monterey County, California

Numerous slides along California Highway 1 in San Luis Obispo and Monterey Counties closed portions of the road throughout the winter of 1998. One slide, known as Grandpa's Elbow landslide, in Monterey County was a reactivation of an older, much larger landslide complex. To protect motorists and clean-up crews, the California Department of Transportation (Caltrans) instrumented the slide with four downhole, electrolytic inclinometers attached to a 12.5-mm, foam dielectric TDR cable in a 61 m borehole. The inclinometers were placed at 46 m, 31 m, 15 m, and 3 m. Any movement of the slide would change the tilt of these inclinometers and trigger the datalogger to issue a warning by phone dialer and hard-wire telephone line. The system could also be monitored remotely by computer and modem.

Soon after installation, slight movement of the inclinometers occurred. The telephone dialer paged personnel who visited the site. TDR cable readings showed the development of a spike in the cable at a depth of 9-m indicating movement, Figure 11. Observation of tension cracks in the ground surface verified the fact that movement had taken place.

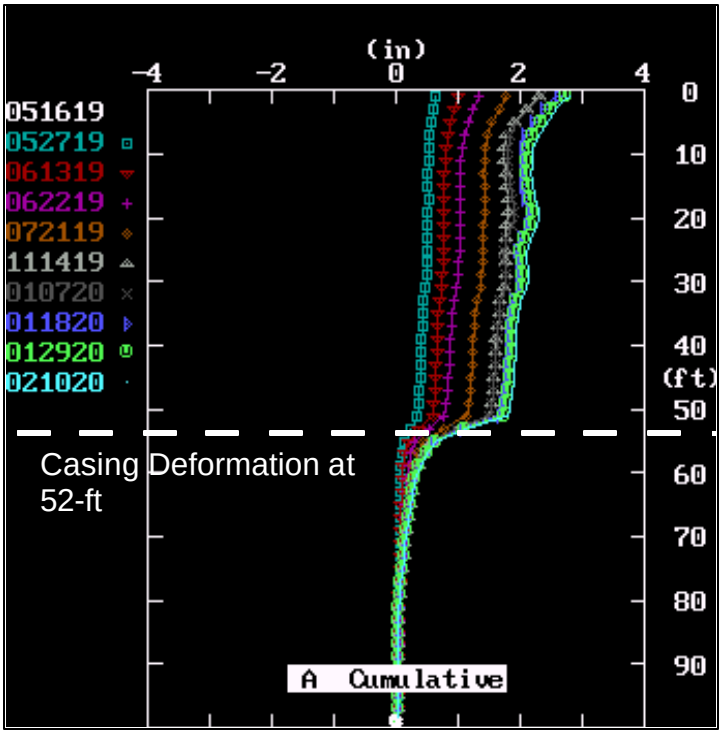

Fig. 9. *Probe inclinometer prior to shearing at 52-ft.*

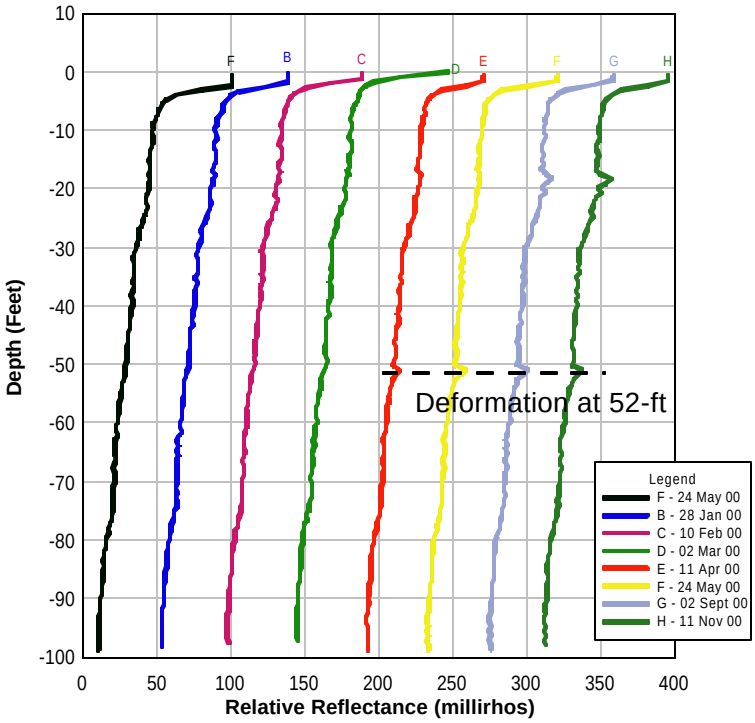

Fig. 10. *TDR signatures from cable attached to the outside of inclinometer casing. Compare with Figure 9.*

TDR/Piezometers/Rain Gage, Morgan County, Illinois

In an effort to determine climatic conditions during slope movement, the Illinois Department of Transportation installed a remote monitoring system adjacent to a highway near Jacksonville, Illinois. The system incorporated five ½" corrugated, foam-dielectric TDR cables and five vibrating wire piezometers to monitor for ground movement and groundwater levels respectively. In addition, a tipping bucket rain gage was installed to record rainfall data, and correlate it with groundwater levels. A datalogger was used. Data collection was performed by manually connecting a laptop computer to the datalogger and downloading the data. The system was powered by a rechargeable battery and solar collector.

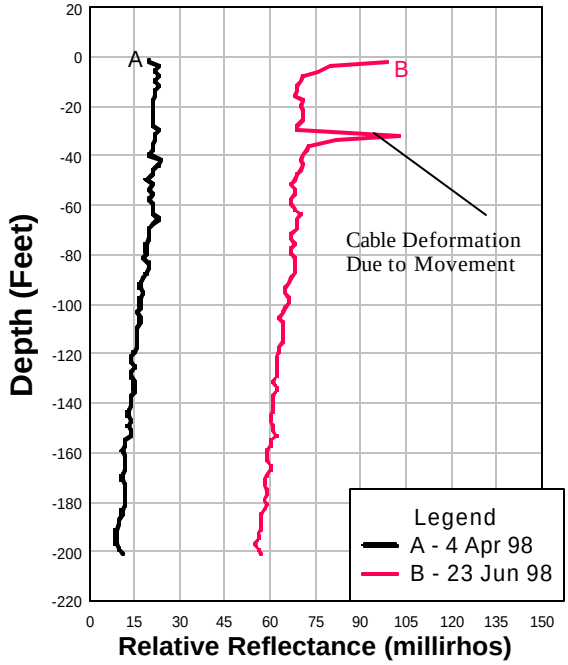

Fig. 11. *TDR signature spike indicating movement at 9-m (30-ft).*

Inclinometers/TDR, Orange County, California (1)

The developer of a coastal property was cautioned by its attorneys that slope movements adjacent to the property could pose a concern. The nearby city of Laguna Niguel, in particular, experienced severe damage from El Niño storms. This included a spectacular failure of a 38-m slope which destroyed several condominium buildings at the base and caused a number of homes at the crest to plummet down the head scarp.

The site, currently under development, contained some weak colluvial material as well as a remnant landslide. Construction plans called for removal of the weak material and construction of an engineered fill shear key. This meant the use of a temporary excavation with steep slopes.

To alleviate fears of litigation by adjacent property owners, and to protect workers and property during construction, an ambitious remote monitoring plan was established. This included the installation of six 33-m conventional cased inclinometer borings and five 33-m, 12.5-mm corrugated, foam-dielectric TDR cables. In addition, each of the six inclinometer casings had a removable electrolytic bubble inclinometer installed to monitor for movement between readings. Data was acquired daily and stored by a datalogger attached to a cellular phone for communications. Alarms were set for each instrument to warn of movement between scheduled automatic readings. A cable tester, modified for automated data collection and a datalogger were used as part of the system. Communications were via cellular telephone. Power was supplied by a solar panel and rechargeable battery.

Inclinometers/TDR, Orange County, California (2)

Another installation in Orange County used a similar set-up as that in Laguna Niguel. On this site, two 12.5-mm, corrugated, foam-dielectric TDR cables were installed in boreholes. Each cable had two inclinometers grouted in place adjacent to a road where a previous landslide had occurred. One

inclinometer was installed above a suspected slide plane and the other below. A datalogger was used but coupled with a cable tester. Communications were via a hardwire telephone. A solar panel and rechargeable battery were used to power the unit.

TDR/Inclinometers/Piezometers/Rain Gage, San Francisco Bay Area, California

A large landslide threatened several residences on a ridge underlain by the Franciscan formation. An ambitious monitoring system was developed. It included two electrolytic tiltmeters attached to two structures close to the head scarp, two electrolytic bubble tiltmeters in inclinometer casings near the scarp, and two tiltmeters attached to a soldier pile retaining wall located at the base of the slide. In addition, three TDR cables were attached to inclinometer casings. To monitor groundwater and rainfall, two vibrating wire piezometers were installed in standpipes and a rain gage mounted near the instrumentation enclosure. A third piezometer was used to determine barometric pressure to correct piezometer readings. A solar collector and rechargeable battery supplied power to the system..

SUMMARY

TDR is an excellent tool for slope monitoring when used properly. TDR cannot reliably provide the amount of slope movement a slope is undergoing. However, it has many uses outlined in this paper. For example,

1. TDR can be used to economically monitor soil embankments. Time can be saved by routing all cables to a central location for data collection.
2. Inexpensive RG59/U cable can be installed as part of routine landslide investigations and can accurately determine the location of slide planes.
3. Coaxial cables can be attached to the outside of inclinometer casing and provide accurate monitoring information as well as extend the life of the monitoring hole.
4. TDR can be used with other electronic instrumentation as part of an automated remote system to monitor many phases of a landslide, including the use of alarms to warn of movement.

REFERENCES

Kane, W.F., and Beck T. J. 1996. Rapid slope monitoring: Civil Engineering, New York: American Society of Civil Engineers, **666**, 56-58.

KANE GeoTech, Inc. 2001. TDRPlot 2000 user's manual: KANE GeoTech, Inc., Stockton, California, 8 p.

Mikkelsen, P.E., 1996, Field instrumentation, in A. K. Turner & R. L. Schuster, Landslides. investigation and mitigation. Washington: Transportation Research Board, ISBN 030906208X.

O'Connor, K. M., and Dowding C. H., 1999, Geomeasurements by pulsing TDR cables and probes: Boca Raton, Florida: CRC Press, ISBN 0-8493-0586-1.

O'Connor, K. M., and Wade, L. V., 1994, Applications of time domain reflectometry in the mining industry: Symposium on time domain reflectometry in environmental, infrastructure, and mining applications, U.S. Bureau of Mines, 494-506, NTIS PB95-105789INZ.

CALIBRATION OF SMALL-DIAMETER TDR CABLES FOR MEASURING DISPLACEMENT IN PHYSICAL SOIL MODELS

C.M. McAlister[1] and C.E. Pierce[2]

[1]Graduate Research Assistant, Department of Civil and Environmental Engineering, University of South Carolina, Columbia, SC 29208; mcaliste@engr.sc.edu
[2]Assistant Professor, Department of Civil and Environmental Engineering, University of South Carolina, Columbia, SC 29208; piercec@engr.sc.edu

ABSTRACT

This paper describes the selection and testing of small-diameter coaxial cables for detecting and measuring shear displacement by time domain reflectometry (TDR). Conceptually, very small diameter TDR cables would enhance the somewhat limited visual methods normally used for measuring soil displacements in centrifuge and other physical soil models. Data can be acquired continuously and rapidly, and data is provided in real time. Coaxial cables that are typically installed in the field are too large and stiff for soil models. Miniature coaxial cables have a lower bending stiffness and are theoretically more conformable to soil deformation patterns. A reduced stiffness allows more accurate measurement of small shear displacements in small-scale models. In this experimental study, three braided coaxial cables were tested in a modified direct shear device. Unjacketed cable diameters range from 2.6 to 7.2 mm, which are significantly smaller than cables normally employed for field measurements. Specialized blocks have been manufactured to fully confine each cable inside a direct shear box, while creating a very thin, fixed shear zone. During direct shearing, voltage reflection and shear load is measured as a function of shear box displacement. The two smallest diameter cables were weaker in shear and demonstrated higher sensitivity to very small displacements. These findings support the development of small compliant sensors for the centrifuge and other physical soil models.

INTRODUCTION

During the 1970s and 1980s, the U.S. Bureau of Mines and Northwestern University pioneered the research and application of time domain reflectometry (TDR) for monitoring rock movements. O'Connor and Wade (1994) provide an excellent summary of case histories involving TDR in mining operations, which dates back to 1969. A typical installation includes manually placing a single cable in a drilled borehole and grouting it in place with a cement grout. Due to the high stiffness of rock, shear displacement along rock joints can be readily detected and quantified with rigid coaxial cables (Dowding *et al.*, 1989). A commercially available, 22.2 mm diameter, solid shielded coaxial cable is

often used for monitoring rock joint displacement. A similarly constructed 12.7 mm diameter, solid shielded cable has been used to measure deformation in weak rock and very stiff soil, but with limited success (O'Connor *et al.*, 1995; Kawamura *et al.*, 1994; McKenna *et al.*, 1994). To identify a cable for measuring localized soil deformation more accurately, Pierce (1998) performed an experimental study on flexible, braided coaxial cables with diameters less than 10 mm. The most compliant cable available was a 75Ω, 7.7 mm diameter, braided cable. Theoretical analyses show that this cable should shear sufficiently to detect and quantify deformation in stiff clay, but not soft clay (Dowding and Pierce, 2001).

To accurately measure subsurface deformation, a cable must conform to movements of the surrounding ground. The ability of a cable to conform is dictated by its bending stiffness, EI, where E is modulus of elasticity and I is moment of inertia. A comparison of bending stiffness for a number of braided and solid shielded cables can be found in Pierce (1998). Decreasing the diameter reduces the bending stiffness of a given cable. For the same diameter, braided cables have a lower bending stiffness than solid shielded cables. A braided shield is designed with negligible stiffness for enhanced flexibility; whereas, a commercial solid shield is constructed of a rigid metallic tube with a relatively thick wall. A coaxial cable with a very small diameter and a braided shield is therefore more compliant and theoretically more conformable to soil movements. Smaller-diameter, braided cables may be advantageous for field measurements and in small-scale physical soil models where a less intrusive, more compliant sensor is needed to measure smaller deformations.

The primary objective of this paper is to describe the shearing response of small-diameter, braided coaxial cables. This work is part of the on-going development of TDR as a usable tool for measuring the location and magnitude of shear displacements occurring in real time within physical soil models. Data on internal displacements would be valuable for any number of geotechnical investigations including slope stability, retaining structures, excavations, tunneling, dam cracking, bearing capacity, and pressure grouting. The advantages of TDR in physical soil models are the same advantages the method provides when employed in the field. Data are provided in real time and because data acquisition is rapid, nearly continuous readings are possible. Shear zone thickness can be more accurately assessed with TDR than with inclinometers and extensometers (Dowding and Pierce, 1994). Successful development of a TDR method to identify the onset of shear displacement in the interior of models, and to measure shear displacement during testing, offers a significant advancement in physical soil model testing.

EXPERIMENTAL PROGRAM

Selected Cables

Sensitivity to shearing differs for every coaxial cable and depends upon its construction. The shear load and voltage reflection response must be measured experimentally to evaluate sensitivity. Three commercially available, coaxial cables were selected for this experimental study: Alpha 9847, Belden 1855A and CommScope 2120k. Table 1 lists the manufacturer specifications for all three cables. Each cable is constructed with a solid bare copper (BC) inner conductor, a foam polymer dielectric, and a braided copper shield that is bare or tinned (T). The first cable, Alpha 9847, was determined to be the most compliant coaxial cable of its size on the market (Dowding and Pierce, 2001). This 75Ω cable has a jacketed diameter of more than 10 mm and is notably larger than the other two cables. With a jacketed

diameter of approximately 4 mm and an unjacketed diameter of less than 3 mm, these two cables can be considered "miniature" cables. Figure 1 illustrates the difference in size between the Alpha 9847 cable and the two miniature cables.

CommScope 2120k and Belden 1855A cables were selected because they are similar in construction except for the size of the inner conductor. The cable with a larger inner conductor has a nominal impedance of 50Ω. Conversely, the cable with a smaller inner conductor has a nominal impedance of 75Ω. The bending stiffness of a 50Ω cable is approximately 75% higher than a similarly sized and constructed 75Ω cable. It is theorized that a 75Ω cable will be more compliant and weaker in shear than a 50Ω cable because of a lower bending stiffness. One drawback to higher impedance cables, however, is that they tend to be lossy (Pierce, 1998). Signal loss is a problem at long distances but is not expected to impact the results of this laboratory investigation of short cables.

Make	Model	Nominal Impedance (Ω)	Inner Conductor		Dielectric		Shield		Jacket	
			Diam (mm)	Material	Diam (mm)	Material	Coverage (%)	Material	Diam (mm)	Material
Alpha	9847	75	1.63	Solid BC	7.24	FPE	81	BC Braid	10.28	PE
CoSc	2120K	50	1.02	Solid BC	2.71	Foam FEP	95	TC Braid	4.10	Cr PVDF
Belden	1855A	75	0.59	Solid BC	2.59	Gas Inj.	95	TC Braid	4.03	PVC

Table 1. *Manufacturer specifications of coaxial cable construction*

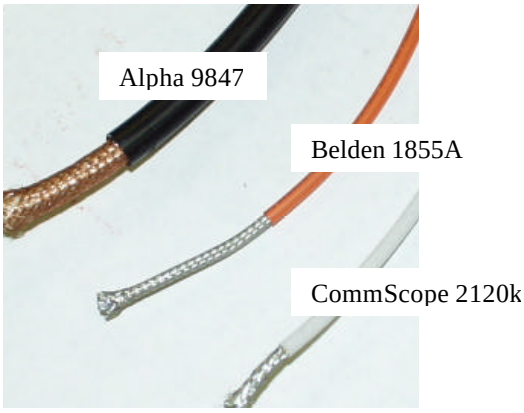

Fig. 1. *Photograph of three selected cables*

Modified Direct Shear

The experimental program was devised to shear cables in a modified direct shear device while recording load-displacement and voltage reflection-displacement response. A pair of aluminum blocks, shown in Figure 2, was manufactured to rest inside a 6.3 cm by 6.3 cm square shear box. The upper block rests directly on the lower block, creating a shear zone of negligible thickness at their interface. Holes were drilled to diameters slightly larger than the cables, making it possible to manually thread the cables through the upper and lower blocks. One limitation with this design is that cables must be slightly smaller than the holes, thus allowing some initial seating movement before the cables physically shear.

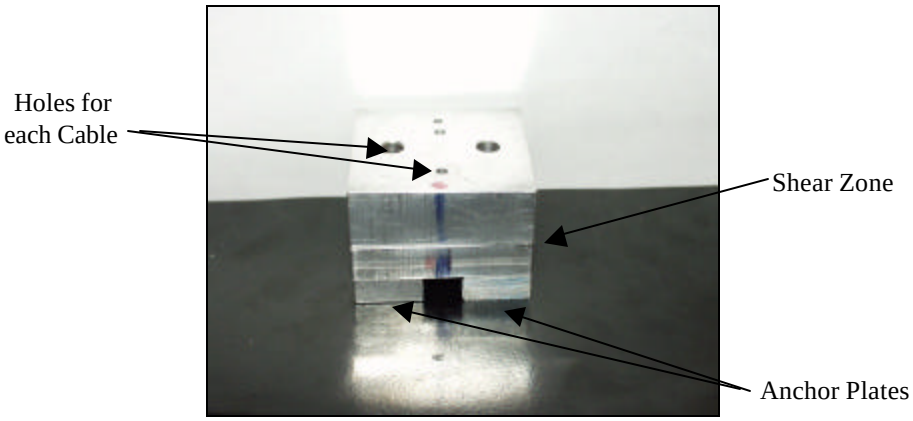

Fig. 2. *Photograph of manufactured blocks used in modified direct shear*

Prior to insertion, the jacket is stripped off the length of cable placed inside the blocks. Anchor plates are equipped with setscrews that tighten on opposing sides of the cable to prevent it from pulling out during shearing. A 20-kg normal load is applied to hold the blocks in place during shearing. The top half of the shear box is raised approximately 2 mm, allowing the blocks to slide. The frictional resistance between sliding blocks was found to be very small; the resistance is subtracted from the measured shear load during each test. Figure 3 shows the final setup prior to testing. A secure cable connection is established and a baseline signal is recorded before shearing starts.

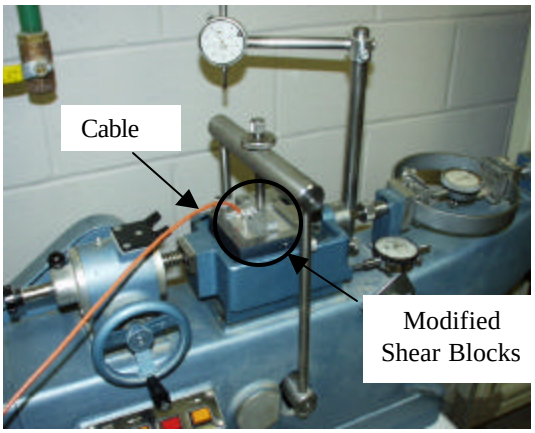

Fig. 3. *Experimental setup in modified direct shear apparatus*

Displacement is set at a constant rate of 0.5 mm per minute for all tests. Shear load is measured from a fixed proving ring and recorded manually. Shear load measurements are recorded until post-peak load is constant for several displacement increments or until the cable severs. Voltage reflection is measured and recorded electronically using a Tektronix 1502C TDR tester interfaced with a desktop computer. Voltage reflection responses are captured at discrete displacement intervals from the start of shearing until the cable short-circuits. Shear load and voltage reflection measurements are recorded every 0.5 mm for Alpha 9847 cables and every 0.25 mm for Belden 1855A and CommScope 2120k cables.

RESULTS AND ANALYSIS

Multiple shear tests are conducted on each of the three cables to assess repeatability of shear load-displacement and voltage reflection-displacement responses. The results from a series of shear tests are presented herein and show that measured responses are unique to each cable. Shear load-displacement and voltage reflection-displacement responses illustrate the stiffness and sensitivity of these cables when sheared along a thin zone.

A real time plot, such as the one shown in Figure 4, is the compilation of voltage reflections recorded at discrete displacement intervals for each test. Each signal shown in Figure 4 represents the voltage difference between the baseline signal and a signal measured at a given displacement. Locations of the downward spikes indicate the shearing zone occurs at about 150 cm. The magnitude of each downward spike represents the amount of voltage reflection, which increases with displacement until the cable short-circuits or severs entirely. In this test, voltage reflection peaks at nearly 115 mp. Immediately after this peak reflection, the cable short-circuits resulting in a voltage signal that drops below the screen at 200 mp. If the entire signal had been captured, this short-circuit would have shown a full 1000 mp reflection.

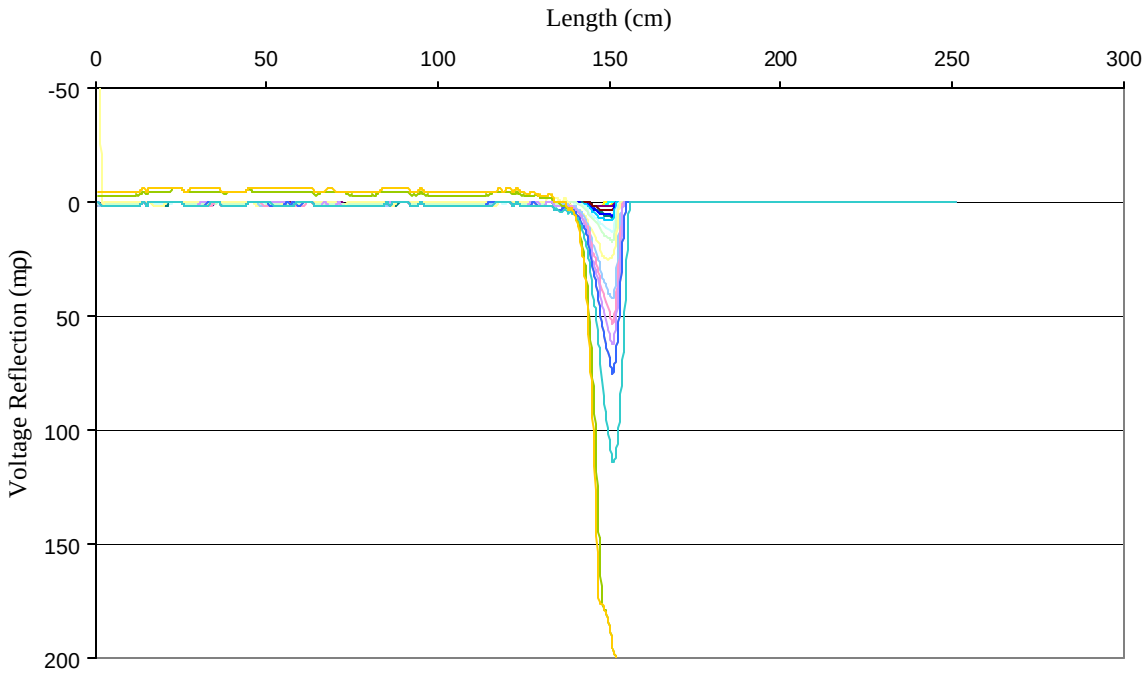

Fig. 4. *Real time recording of voltage reflection responses from shearing Alpha 9847*

For each test on each cable, measured shear loads and voltage reflections are plotted at each displacement interval to evaluate trends in the data. Shear load-displacement and voltage reflection-displacement curves compiled from three direct shear tests of CommScope 2120k cables are shown in Figures 5 and 6. The results from each of the three trial tests on the same cable are consistent and demonstrate repeatability of the method. Consistency in the results was also observed for Alpha 9847

and Belden 1855A cables. Repeatability is important so that voltage reflections can be accurately correlated to shear displacements when cables are embedded in deforming soil.
The trend in Figure 5 appears to be approximately bilinear with a change in stiffness occurring at 2 mm of shear box displacement. It is theorized that this change in stiffness occurs after the cable has fully seated itself inside the drilled hole. The cable physically begins to shear at this point. As illustrated in Figure 6, voltage reflection increases exponentially with shear box displacement. However, voltage reflections are less than 8 mp up to 2 mm of shear box displacement, and do not begin to increase significantly until 2 mm is reached. This observation supports the theory that cables do not begin to shear until the shear box displaces 2 mm.

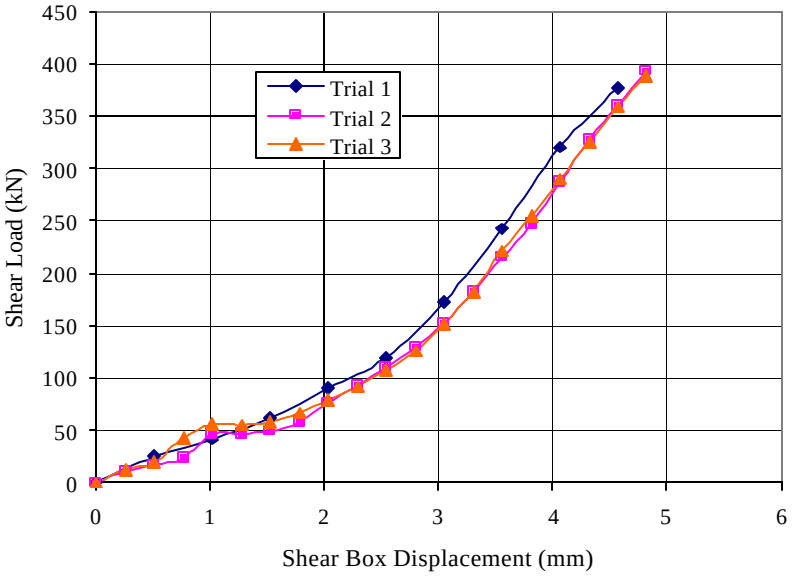

Fig. 5. *Shear load-displacement responses from shearing CommScope 2120k cables*

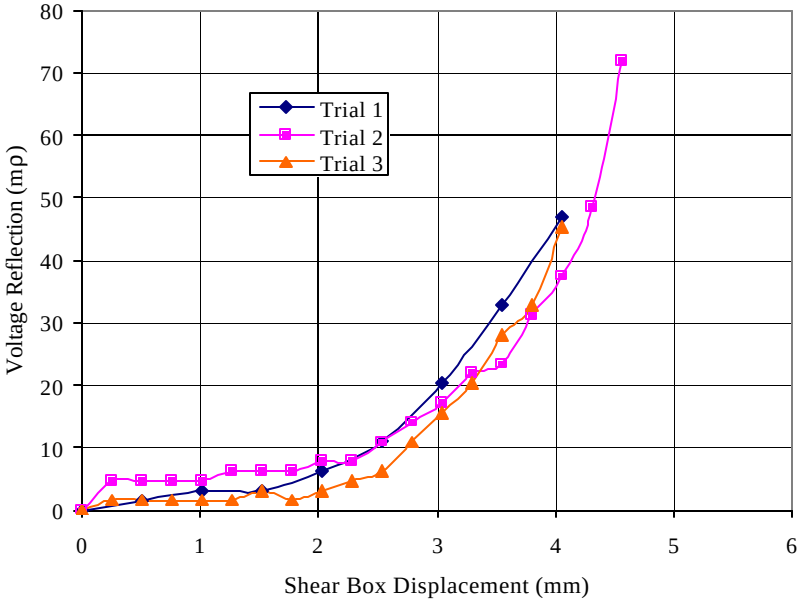

Fig. 6. *Voltage reflection-displacement responses from shearing CommScope 2120k cables*

Figure 7 shows the maximum shear load for both miniature cables is lower than the larger-diameter Alpha 9847 cable, but the shear stiffness appears to be slightly higher beyond 3 mm of shear box displacement. Table 2 summarizes the shear response for all three cables. The maximum shear load sustained by Alpha 9847 ranges from 600 to 678 kN, with an average of 629 kN. Using a different experimental setup, Pierce (1998) reported a slightly lower average of 550 kN. Based on the results shown in Table 2, the maximum shear load varies considerably more with the Alpha 9847 cable than with the miniature cables. Maximum load sustained by the Alpha 9847 cable was reached at a shear box displacement between 10 and 11 mm, which is larger than its unjacketed diameter. In Figure 7, shearing continued to more than 14 mm of displacement. This post-peak response is the result of the dielectric failing and the load being transferred solely to the inner conductor. Upon dismantling the test setup, the cable was observed to have stretched across the shear zone such that its total shear deformation exceeded its diameter.

Make	Model	Dielectric Diameter (mm)	Range of Maximum Shear Box Displacement (mm)	Range of Maximum Shear Load (kN)
Alpha	9847	7.24	10.0-11.0	600-678
Alpha	9847*	7.24	4.6-6.1	461-608
CoSc	2120K	2.71	4.6-4.8	377-392
Belden	1855A	2.59	4.0-4.5	255-275

*** from Pierce (1998)**

Table 2. *Results from modified direct shear tests*

Table 2 and Figure 7 show that the two smaller-diameter cables sustained maximum shear loads at much smaller displacements than Alpha 9847. For example, Belden 1855A sustained an average load of 265 kN, which is less than half of the shear load sustained by Alpha 9847. This load was always reached after 4.5 mm displacement, again less than half of the displacement required for the larger-diameter cable. Both miniature cables displayed brittle failure; when the maximum load was reached, the cable severed completely and the load decreased immediately to zero. Finally, it is observed from Table 2 that the maximum shear box displacements for both miniature cables are approximately 2 mm larger than the cable diameter. This observation further suggests that shearing begins at approximately 2 mm of shear box displacement.

Alpha 9847 produced larger voltage reflections than both miniature cables, as illustrated by three example tests in Figure 8. A peak voltage reflection of nearly 150 mΩ was recorded at 9.6 mm, before the maximum shear load was achieved. This cable short-circuited within 0.5 mm following the peak voltage reflection. Belden 1855A and CommScope 2120k cables display similar exponentially increasing voltage reflection trends, as shown in Figure 8. For these two miniature cables, a short circuit developed immediately after the peak voltage reflection was measured.

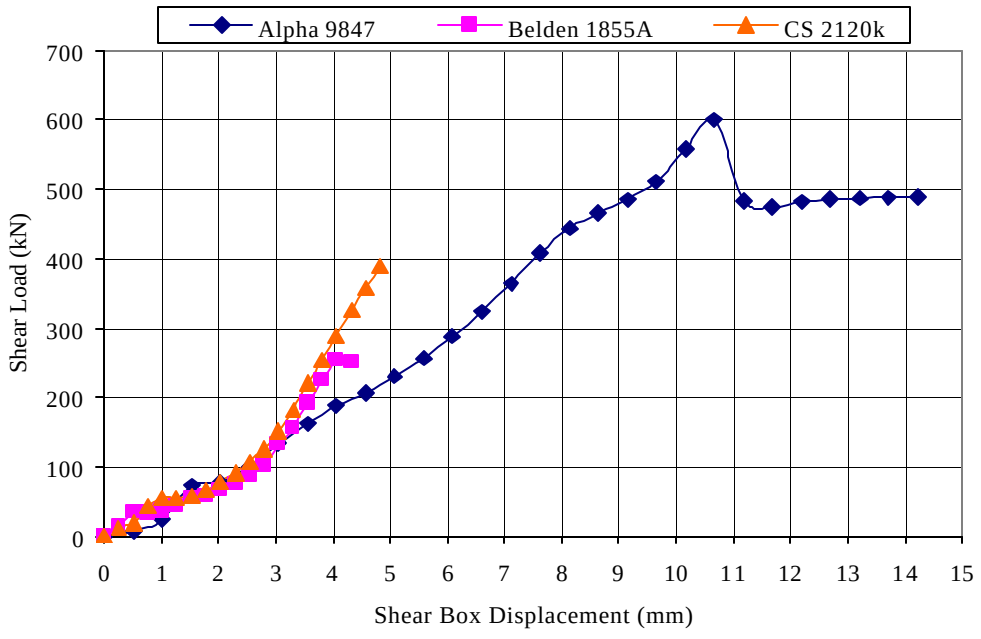

Fig. 7. *Representative shear load-displacement responses from shearing three cables*

The miniature cables produced higher voltage reflections at smaller displacements than Alpha 9847. For example, voltage reflections for both miniature cables are nearly 40 mΩ at 4 mm of displacement, compared to 10 mΩ for Alpha 9847, as shown in Figure 8. These findings show that smaller-diameter cables are more sensitive to very small shear displacements, and more importantly, to very small changes in shear displacement. For

all three cables, there is a rapid increase in voltage reflection as the maximum load approaches. There is an upper limit of shear displacement and voltage reflection for all of the cables, where, within the final displacement increment, the voltage reflections increase quickly until the cable short-circuits.

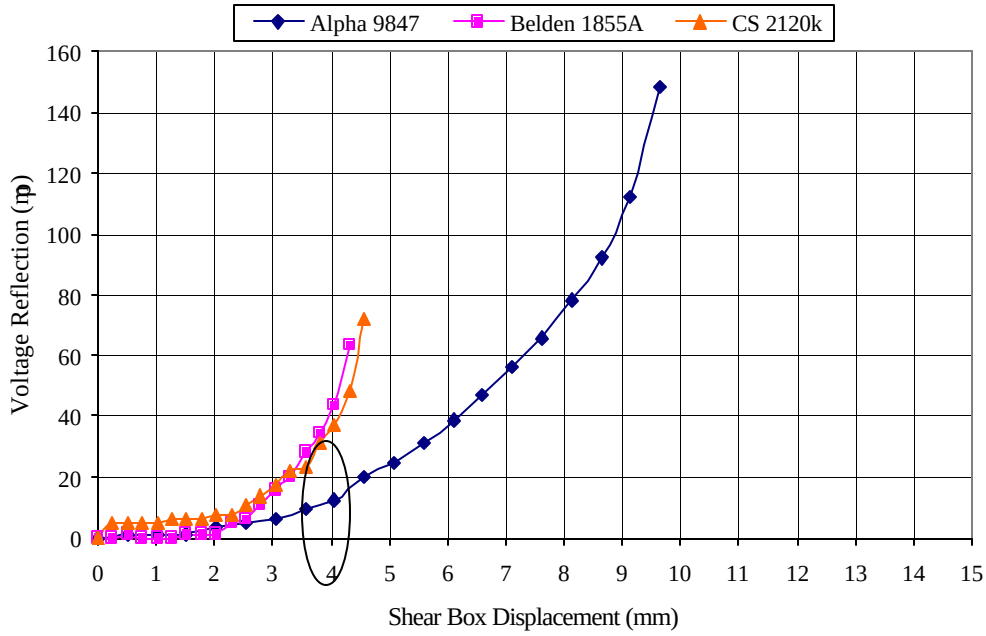

Fig. 8. *Representative voltage reflection-displacement responses from shearing three cables*

CONCEPTUAL APPLICATIONS

At present, there appears to be no available method to measure shear displacement internally during centrifuge testing (Kutter, 1999). Centrifuge researchers often construct plane strain physical soil models and assume that observations at the ends of the model accurately represent internal behavior. Modeling slope stability is an obvious example of this plane strain assumption. Plexiglas sides are typically installed to observe end displacements by marking grids on the Plexiglas, placing spherical markers in the soil, and/or constructing the model with layers of colored sand (Zornberg *et al.*, 1997). These observations can be combined with measurements of the movement of distinct points on the surface of the model by means of LVDTs. The disadvantages of these methods are that friction cannot be entirely eliminated at the boundaries and not all geotechnical problems are plane strain.

Internal displacements are more difficult to identify. In a centrifuge study on face stability of shallow tunnels (Chambon *et al.*, 1991), internal shear displacements could only be determined after the conclusion of the test by investigating displaced patterns of horizontal layers of colored sand. The model soil was moistened and cuts were carefully made to expose various vertical planes. Huat *et al.* (1991) used dry spaghetti strands as displacement markers in their centrifuge models. Moisture from the soil softens the spaghetti and, after the test is completed, the model is cut to expose the deformed shape of the pliable spaghetti, which clearly outlines the final displacement pattern in the soil. The placement of spaghetti strands is the most frequently used method for measuring internal displacements (Phillips, 2001).

These methods, of course, do not allow real time evaluation of shear displacement. Hence, the onset of shear displacement cannot be identified. An ideal TDR sensor would follow the pattern of a deforming soil mass exactly, in the same manner as moist strands of spaghetti. Commercially available, miniature coaxial cables are not as pliable as spaghetti, but the results of this study provide a step in the development of small compliant sensors for the centrifuge and other physical soil models.

SUMMARY

This paper presents the concept of using small-diameter TDR cables in physical soil models to measure small, localized internal displacements. To investigate this concept, three coaxial cables were sheared in a modified direct shear device to acquire shear load and voltage reflection data as a function of shear box displacement. The results displayed the unique shear load and voltage reflection responses of each cable. Although the responses generated by the two miniature cables were similar, they were much different from the larger-diameter Alpha 9847 cable. Shear stiffness of the two miniature cables was slightly higher than the Alpha 9847 cable; however, the shear resistance was much lower. The 75Ω miniature cable, Belden 1855A, was slightly more compliant and weaker in shear than the 50Ω miniature cable, CommScope 2120k. Most importantly, higher voltage reflections were produced at smaller displacements for both miniature cables. Future investigations of this concept include evaluating specially constructed compliant cables in direct shear for potential instrumentation of physical soil models.

ACKNOWLEDGMENTS

This research was funded by the National Science Foundation under NSF Award No. 9908342.

REFERENCES

Chambon, P., Corte, J.-F., Garnier, J. and Konig, D., 1991, "Face Stability of Shallow Tunnels in Granular Soils," Centrifuge 91, Proceedings of the International Conference on Geotechnical Centrifuge Modeling, Boulder, Colorado, 99-105.

Dowding, C.H. and Pierce, C.E., 2001, “Measurement of Localized Soil Deformation with Time Domain Reflectometry,” Journal of Geotechnical and Geoenvironmental Engineering, ASCE, under review.

----------1994, “Measurement of Localized Failure Planes in Soil with Time Domain Reflectometry,” Proceedings of Symposium and Workshop on Time Domain Reflectometry in Environmental, Infrastructure, and Mining Applications, U.S. Bureau of Mines, Special Publication SP19-94, 569-578.

Dowding, C.H., Su, M.B. and O’Connor, K.M., 1989, “Measurement of Rock Mass Deformation with Grouted Coaxial Antenna Cables,” Rock Mechanics and Rock Engineering, **22**, 1-23.

Huat, B.B.K., Craig, W.H. and Merrifield, 1991, "Simulation of a Trial Embankment Structure in Malaysia," Centrifuge 91, Proceedings of the International Conference on Geotechnical Centrifuge Modeling, Boulder, Colorado, 51-57.

Kawamura, N., Bauer, R.A., Mehnert, B. B. and Van Roosendaal, D.J., 1994, "TDR Cables, Inclinometers, and Extensometers to Monitor Coal Mine Subsidence in Illinois," Proceedings of Symposium and Workshop on Time Domain Reflectometry in Environmental, Infrastructure, and Mining Applications, U.S. Bureau of Mines, Special Publication SP 19-94, 528-539.

Kutter, B.L., 1999, Personal communication, Department of Civil and Environmental Engineering, University of California-Davis.

McKenna, G., Livingstone, G. and Lord, T., 1994, "Advances in Slope Monitoring Instrumentation at Syncrude Canada Ltd.," Geotechnical News, September, 66-69.

O'Connor, K.M., Peterson, D.E. and Lord, E.R., 1995, "Development of a Highwall Monitoring System using Time Domain Reflectometry," Proceedings of the 35th U.S. Symposium on Rock Mechanics, Reno, Nevada, 79-84.

O'Connor, K.M. and Wade, L.V., 1994, "Applications of Time Domain Reflectometry in the Mining Industry," Proceedings of Symposium and Workshop on Time Domain Reflectometry in Environmental, Infrastructure, and Mining Applications, U.S. Bureau of Mines, Special Publication SP19-94, 494-506.

Phillips, R., 2001, Personal communication, Centre for Cold Oceans Resources Engineering (C-CORE), Memorial University of Newfoundland, St. John's, Canada.

Pierce, C.E., 1998, "Time Domain Reflectometry Measurements of Localized Soil Deformation," PhD Thesis, Northwestern University, Evanston, Illinois, 237 pp.

Zornberg, J.G., Mitchell, J.K. and Sitar, N., 1997, "Testing of Reinforced Slopes in a Geotechnical Centrifuge," Geotechnical Testing Journal, ASTM, **20**, No. 4, 470-480.

MEASUREMENT OF TAILINGS CONSOLIDATION USING TDR TECHNOLOGY

Dobroslav Znidarcic[1], Gordan Gjerapic[2], Don A. Poulter[3], and Kevin M. O'Connor[4]

[1]Dept of Civil, Environmental and Architectural Eng., Univ of Colorado at Boulder; znidarci@spot.colorado.edu
[2]Dept of Civil, Environmental and Architectural Eng., Univ of Colorado at Boulder
[3]The Glasgow Engineering Group; donp1@mindspring.com
[4] GeoTDR, Inc., 7290 Greencrest Drive, Westerville, Ohio 43082, kevin@geotdr.com

ABSTRACT

TDR is based on the principle of cable radar and is used with a variety of probes and coaxial cables to measure volumetric water content. In the case of saturated tailings, changes in the volumetric fluid content occur as the tailings solids displace pore fluids and recent studies with segmented probes at two mines have shown that TDR may provide a reliable means for monitoring tailings consolidation and the impact on operating storage capacity and long-term closure. Laboratory tests have been performed using a Georgia kaolin slurry. The propagation velocity profile was measured using a MoisturePoint segmented probe during the test. Although the qualitative trend is promising, it will be necessary to do a more fundamental analysis of changes in the TDR waveform rather than simply using the default algorithm in order to improve the sensitivity.

MEASUREMENT OF VOLUMETRIC WATER CONTENT

Time Domain Reflectometry (TDR) was developed by the power and telecommunications industries to locate faults in cables. A cable tester launches a voltage pulse into a coaxial cable, parallel pair wire or twisted pair wire. If a probe consisting of two or more parallel rods is embedded in a porous medium and a voltage pulse is launched along this probe, a reflection is created at the top of the probe and a second reflection is created at the end of the probe so the travel time can be measured. The particular probe shown in Figures 1 and 2 is segmented such that reflections are created at the top and bottom of each segment (ESI, 1997). Since the segment lengths (L_p) are fixed, the pulse velocity along each segment can be computed as twice its length divided by the time (t) required for a pulse to travel along the segment and back. Typically, this velocity is normalized with respect to the speed of light, c (= $3x10^8$ m/s), and expressed as a dimensionless propagation velocity,

$$V_p = 2L_p / ct \, . \qquad [1]$$

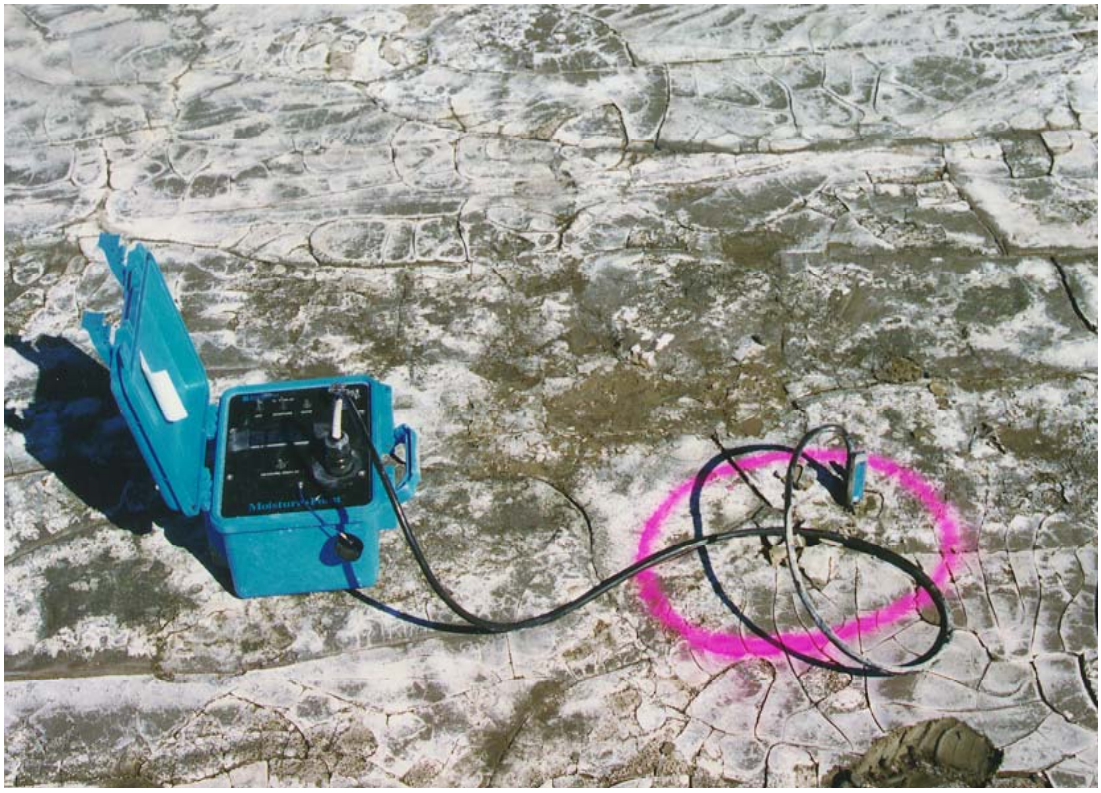

Fig. 1. *Measuring water content of tailings using segmented TDR probe.*

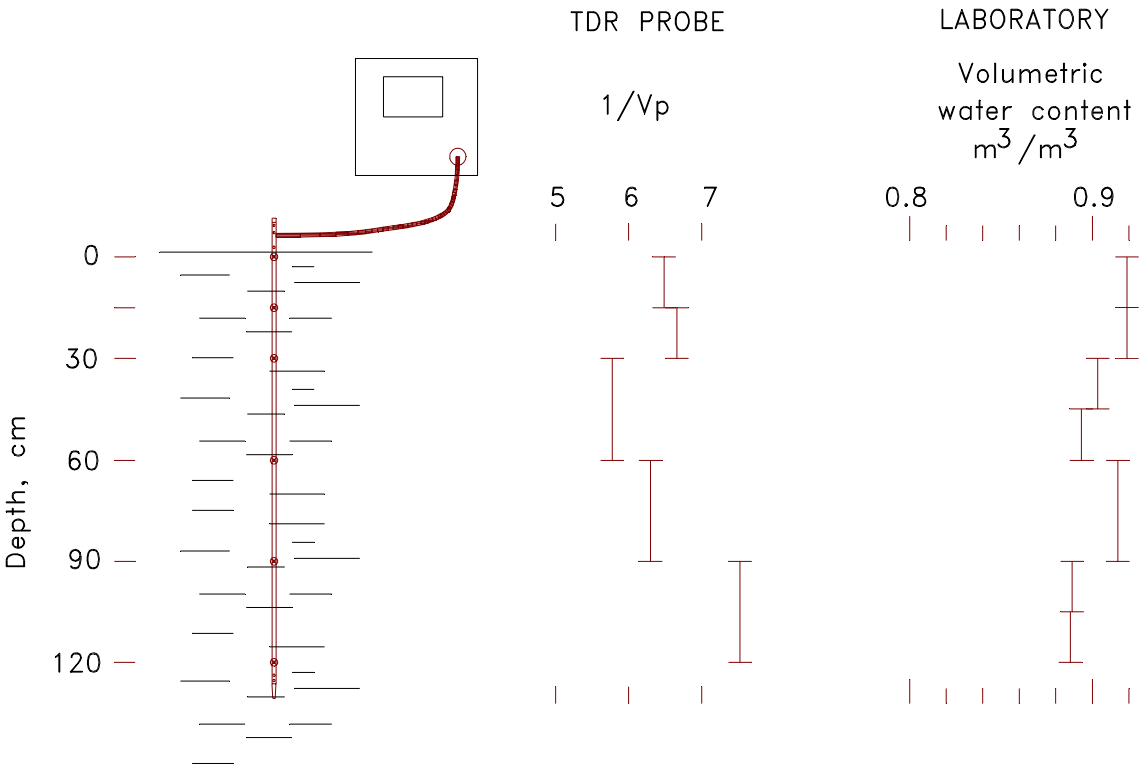

Fig. 2. *Schematic of segmented probe and depth profile of volumetric water content obtained in phosphatic clay tailings.*

This ratio of velocities is approximately equivalent to the dielectric constant of the medium in which the probe is embedded. Since the dielectric constant of water is about 81 while that of mineral soil grains is 3-5, the measured dielectric constant is predominately a function of volumetric water content,

$$2_v = V_w/V_t \qquad [2]$$

where V_w is the volume of water and V_t is the total volume. The relationship between volumetric water content and propagation velocity is linear (Herkelrath *et al*, 1991),

$$2_v = b\,(\,1/V_p\,) \;-\; a \qquad [3]$$

as shown in Figure 3 for clay loam and nickel mine tailings. The slope, b, and offset, a, are functions of the particular porous material, and they are determined by conducting laboratory calibrations (Topp *et al*, 1994; Zegelin and White, 1994)

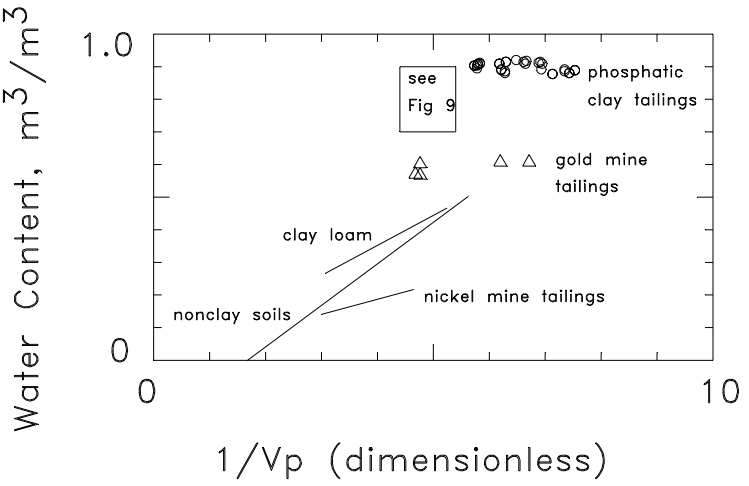

Fig. 3. *Relationship between volumetric water content and propagation velocity for a variety of materials; phosphatic clay and gold mine tailings from present studies; clay loam and nonclay soils (Hook and Livingston, 1996); nickel tailings (Sun, 1996).*

CURRENT DEVELOPMENTS - DIRECT MEASUREMENT OF CONSOLIDATION

As tailings consolidate, there is an increase in the volume and weight of solids,

$$)\,W_s = (\,_w\,G_s\,)\,V_s \qquad [4]$$

where G_s is the specific gravity of the solids. If the tailings are saturated, and there is no change in the total volume, an increase in the solids volume is equal to a decrease in the volume of displaced water, $)\,V_s = -\,)\,V_w$, so

$$)\,W_s = -(\,_w\,G_s\,)\,V_w\,. \qquad [5]$$

Combining with eqtn [2],

$$)\,W_s = -(\,_w\,G_s\,V_t\,)\,2_v \qquad [6]$$

which states that as the tailings consolidate and solids displace water there is a decrease in the volumetric water content. This is measured using TDR technology as discussed earlier.

Preliminary Field Trials

Field trials have been performed in the beach area of a gold mine tailings impoundment in California and a phosphatic clay tailings impoundment in Florida using the segmented probe shown in Figures 1 and 2. This probe was simply pushed into the tailings and measurements made using the push-button TDR unit. For these initial trials, only near-surface profiles in the beach area along the embankment were obtained. Direct samples were also collected for laboratory determination of water content. The profiles in Figure 2 show that the TDR measurements reflect changes in moisture content with depth as did the oven-dried samples.

The compilation in Figure 3 illustrates that the relationship between water content and TDR travel time is materials-specific which is consistent with the experience of all users (Topp *et al*, 1994; Zegelin and White, 1994; Hook and Livingston, 1996). This is a limitation of all techniques used for in situ measurement of water content in clays and organic soils. Among the factors identified by researchers have been the influence of high specific surface, bound water, and the frequency content of the voltage pulse as it travels along the probe (O'Connor and Dowding, 1999)

Use of TDR in loam, sand, and gravel can produce accuracies of "0.03 m^3/m^3 and this can be improved with material-specific calibration. The field trials have highlighted the need for establishing a rigorous calibration protocol for various tailings to assure that the collected data is reliable. As current studies continue, it will be possible to determine the accuracy required for monitoring consolidation.

Use with existing consolidation model

A reliable testing technique to evaluate the highly nonlinear constitutive relations of soft, cohesive soils has been developed (Znidarcic *et al*, 1992; Abu-Hejleh *et al*, 1995). The technique is an enhanced seepage induced consolidation test which eliminates most of the limitations of the previously existing methods and the theory has been implemented in the CONDES finite element program (Yao and Znidarcic, 1997). However, topographic surveys and indirect measurements are still required for field validation, and one of the main shortcomings of this approach to tailings impoundment modeling is the reliance on laboratory testing of slurry samples to obtain consolidation characteristics for the analysis. While the developed laboratory testing methods are reliable they can never address the issue of material variability within a single impoundment. The amount of testing required to properly characterize a typical impoundment would be prohibitively expensive and time consuming. It is also important to note that prior to impoundment filling, there is no way of obtaining representative samples for the tailings. Material segregation is omnipresent during the filling operation and consolidation characteristics change dramatically as the slurry is sorted by grain sizes. The only way of overcoming this major obstacle is to monitor and determine consolidation characteristics as tailings are being deposited in the field. TDR technology in combination with CONDES has the potential to effectively address this need.

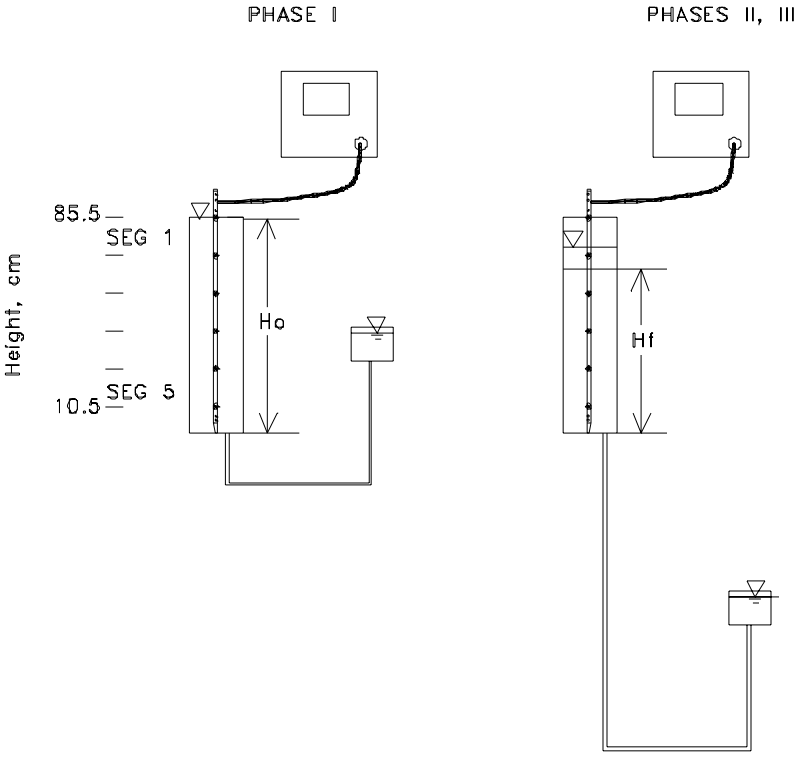

Fig. 4. *Segmented probe in acrylic cylinder for laboratory test of kaolin clay slurry consolidation. The initial solids height Ho was 85.4 cm and the final solids height Hf was 55 cm. Note the change in pore pressure at the bottom of the cvlinder for Phases II and III.*

EXPERIMENTAL SETUP

Sample preparation

Georgia kaolin with the initial void ratio of $e_{00} = 4.7$ and the initial height of $H_o = 85.4$ cm was poured into a transparent acrylic cylinder. The TDR probe manufactured by ESI Environmental Sensors (Figure 4), was placed vertically in the cylinder and fixed into position before the clay was poured in. The probe stayed in this fixed position throughout the test in order to ensure that the TDR test sections stayed in their positions as well as to provide good contact between the probe and the surrounding soil. TDR readings were taken for segments 3, 4 and 5. Since segment 2 was fully submerged into the clay slurry only during the first few days of the consolidation process, readings for this segment were discarded.

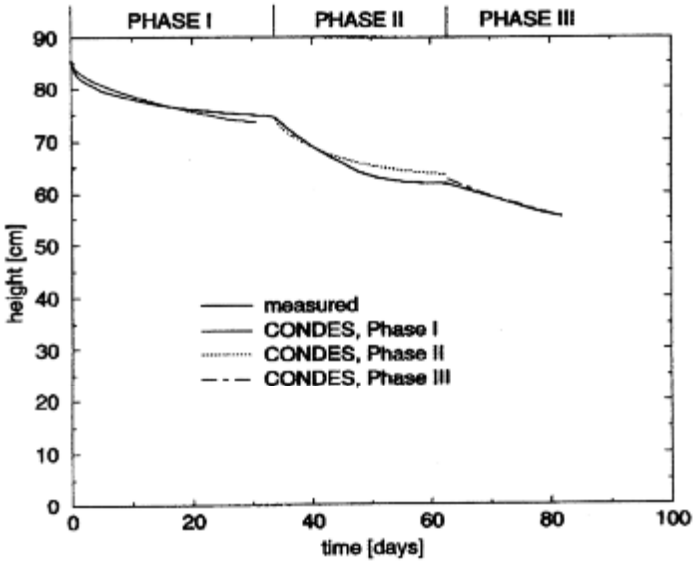

Fig. 5. *Time history of settlement of the top of the solids within the acrylic cylinder.*

Boundary conditions

A consolidation test was conducted in three phases as shown in Figures 4 and 5. The effective stress at the top of the sample was equal to zero during Phase I and Phase II. Phase III commenced with the lowering of the water level below the top surface. This produced negative pore water pressures in the upper layers of the clay column which resulted in the corresponding increase of the effective stress at the top of the soil. The bottom boundary of the sample was subjected to a pressure head of 40 cm during Phase I while a negative pressure of 65 cm of water was imposed at the bottom boundary during Phase II and Phase III.

CONSTITUTIVE MODELS

Constitutive models used in the CONDES program are the relationship between effective stress and void ratio

$$e = A(\sigma' + Z)^B \quad , \qquad [7]$$

and the relationship between hydraulic conductivity and void ratio

$$k = Ce^D \, . \qquad [8]$$

Parameters A, B and Z in equation [7] were obtained by fitting the experimental values of the effective stresses and corresponding void ratios. The void ratio at zero effective stress (i.e., the void ratio of the slurry poured into the container) was found to be 4.7. The void ratio of 2.36 measured at the end of Phase III at the bottom of the soil column corresponded with an effective stress of about 14.3 kPa. Parameters C and D in equation [8] were found by matching the predicted settlement curve with the measured curve as shown in Figure 5.

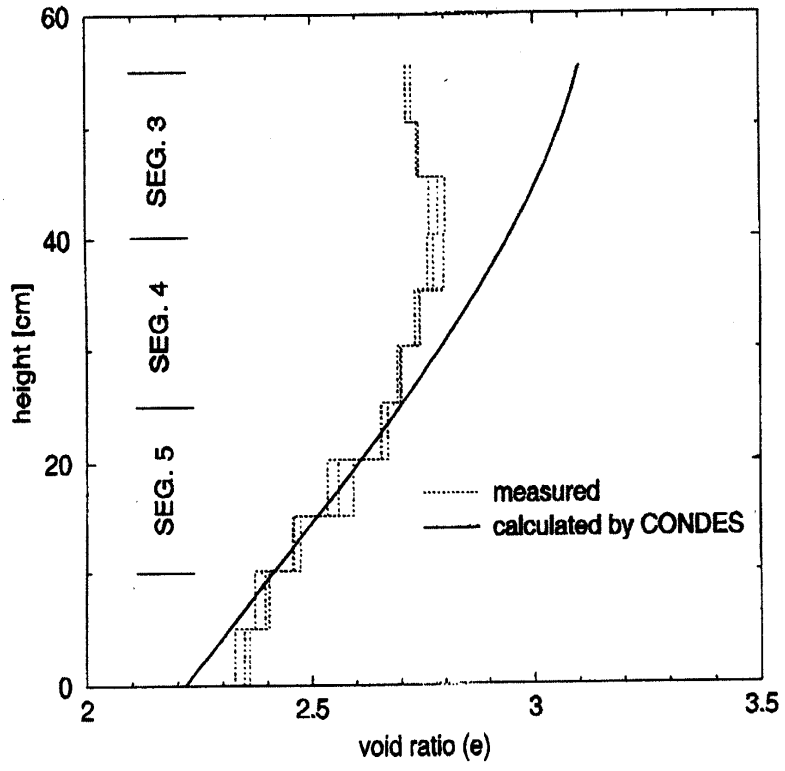

Fig. 6. *Profile of gravimetrically measured void ratio versus depth after completion of Phase III. Note that three (3) gravimetric samples were taken within the depth interval of each TDR probe segment.*

EXPERIMENTAL RESULTS

Final void ratio profiles obtained by sampling the soil column for gravimetric measurement of moisture content are compared with the final void ratio profile calculated by CONDES in Figure 6. The final volumetric water content profile is plotted in Figure 7. The numerical model is consistent with the gravimetric measurements in the lower portion of the slurry column.

The time history in Figure 8 shows that as the solids consolidated, there was a decrease in the travel time, t. Therefore, the velocity V_p was increasing which is consistent with the relationship in equation [6].

In Figure 9, numerically-determined and gravimetrically-determined volumetric water contents are plotted versus TDR measurements of travel time expressed as $1/V_p$. As the slurry consolidated, the water content decreased and the travel time

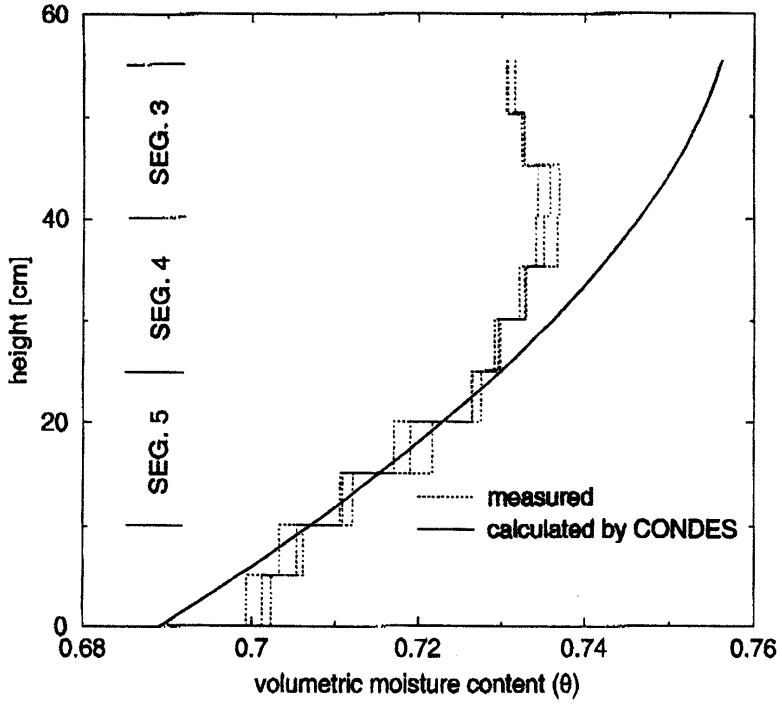

Fig. 7. *Profile of gravimetrically determined volumetric water content versus depth after completion of Phase III.*

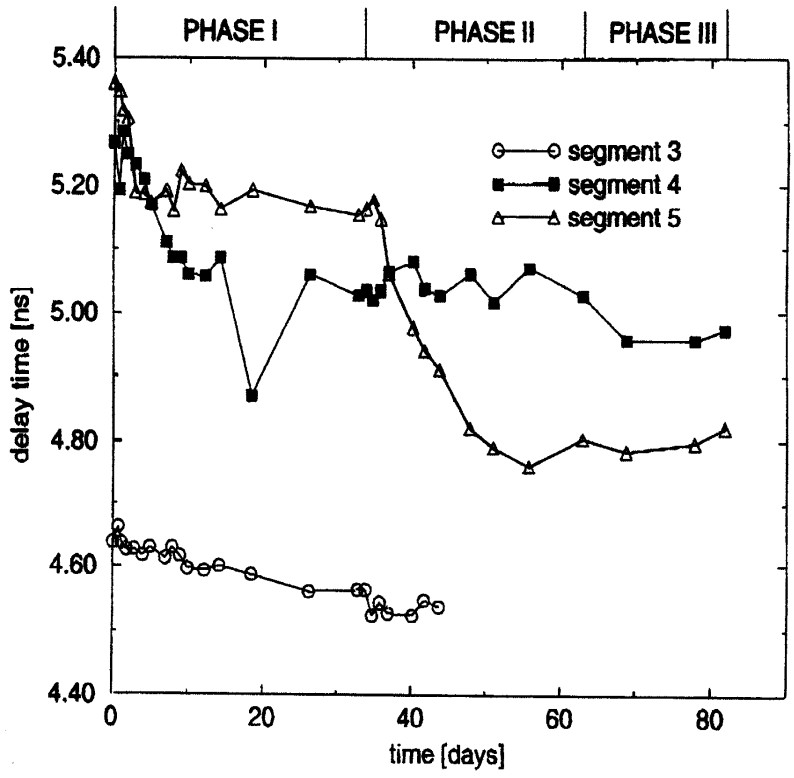

Fig. 8. *Time history of TDR pulse travel time, t, for segments 3, 4, and 5. Each data point is an average of three (3) TDR measurements.*

decreased which is consistent with the relationship in equation [6]. As the volumetric water content decreased from an initial value of 0.825 to a final value of 0.72, $1/V_p$ deceased from 5.2 to 4.8.

DISCUSSION

In Fig 6 and Fig 7, it is apparent that the most consistent numerical results were obtained at the bottom of the soil column. This portion of the column corresponded with the TDR probe segment 4 and segment 5. The results higher in the column diverge from the numerical model, and the TDR measurements in Figure 8 show that within segment 3 the behavior of the slurry must be different. Since the TDR measurements are based on dielectric properties which are highly dependent on free water, it appears that there must be a change in this property for slurry above a height of 40 cm in the column.

This difference is also apparent by comparing Figure 9 and Figure 3. The summary in Figure 3 reiterates the well-known fact that the relationship between volumetric water content and travel time is very dependent on the material dielectric properties. Obviously, there are concerns about the free water content but these studies may help to provide insight into the effect of bulk density on TDR measurements (O'Connor and Dowding, 1999).

The time history in Figure 8 is consistent with the settlement time history in Figure 5 and represents promise for this technique for insitu monitoring of consolidation of

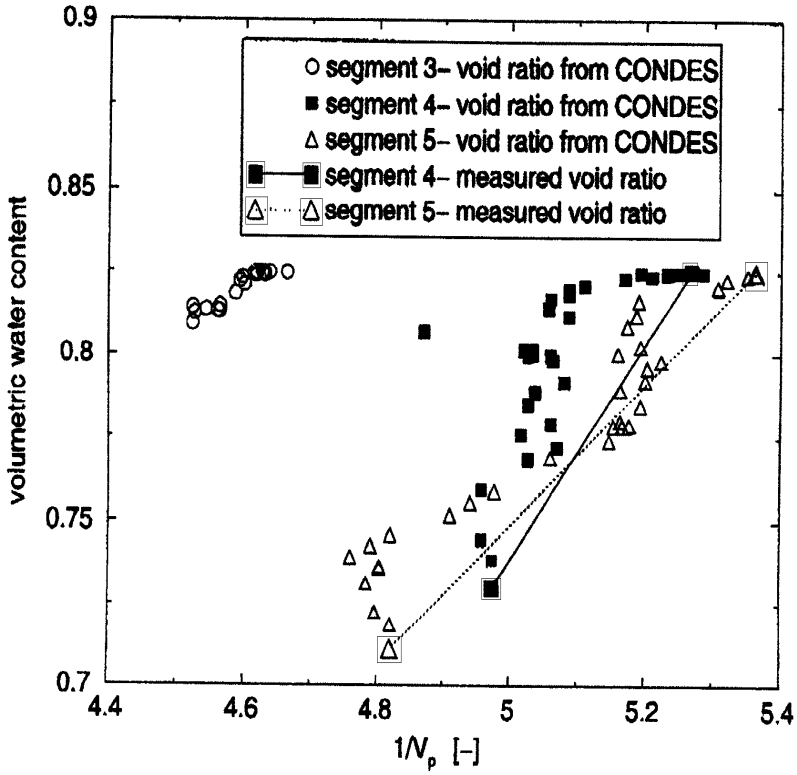

Fig. 9. *Correlation between travel time, $1/V_p$ measured with TDR, and volumetric water content as (a) calculated by CONDES, and (b) measured gravimetrically at the beginning of Phase I and at the completion of Phase III.*

saturated materials. The results in Figure 9, on the other hand, make it apparent that it may not be useful for obtaining measurements that can be used in the CONDES numerical model.

It is important to remember that we are most interested in the CHANGE in volumetric water content versus time. The absolute values plotted in Figure 9 are within the range of +/- 0.03 m^3/m^3 which is consistent with other published results. Perhaps the accuracy in CHANGE in volumetric water content may be +/- 0.003 m^3/m^3

It should also be noted that ESI has updated the firmware algorithm for determining the travel time along each segment of the probe. This algorithm has not been tested in this application.

SUMMARY

Laboratory tests have been performed using a Georgia kaolin slurry with an initial void ratio of 4.7 that was consolidated under self-weight to a final void ratio of 2.35. This corresponds to a decrease in volumetric water content from 0.825 to 0.72. The propagation velocity profile was measured using a MoisturePoint segmented probe during the test and, using the default firmware algorithm for determining travel time along each segment, the measured $1/V_p$ decreased from 5.2 to 4.8. Considering such a small change in $1/V_p$ over a very large change in void ratio, the sensitivity of TDR is much less than that which is possible from gravimetric measurements of water content. Although the qualitative trend is promising, it will be necessary to do a more fundamental analysis of changes in the TDR waveform.

REFERENCES

Abu-Hejleh, A.N. and Znidarcic, D.,1995, Desiccation theory for soft cohesive soils. *Journal of Geotechnical Engineering*, ASCE, **121**, No. 6, 493-502.

ESI Environmental Sensors, Inc., 1997, *MoisturePoint landfill closure monitoring system.* Victoria, British Columbia.

Herkelrath, W.N., Hamburg, S.P., and Murphy, F., 1991, Automatic, real-time monitoring of soil moisture in a remote field area with time domain reflectometry. *Water Resources Research*, **27**, No. 5, 857-864.

Hook, W.R. and Livingston, N.J., 1996, Errors in converting time domain reflectometry measurements of propagation velocity to estimates of soil water content. *Soil Science Society of America Journal*, **60**, No. 1, 35-41.

O'Connor, K.M. and Dowding, C.H., 1999, *GeoMeasurements by pulsing TDR cables and probes*. Boca Raton: CRC Press.

Sun, Z.J., 1996, Feasibility studies for measuring water content in mine tailings using MP-917. ESI Environmental Sensors, Inc., Victoria, 2p.

Topp, G.C., Zegelin, S.J., and White, I., Monitoring soil water content using TDR: an overview of progress. *Proc. Sym. on Time Domain Reflectometry in Envir., Infrastr. and Mining Appl.*, Evanston, IL, September 1994, 67-80; NTIS PB95-105789.

Yao, T.C.D. and Znidarcic, D., 1997, Crust formation and desiccation characteristics for phosphatic clays, users' manual for computer program CONDES0. Florida Institute of Phosphate Research, Publication No. 04-055-134, 115p.

Znidarcic, D., Abu-Hejleh, A.N., Fairbanks, T., and Robertson, A., 1992, Seepage induced consolidation test, equipment description, and users' manual. *Report for Florida Institute of Phosphate Research*, Dept. of Civil Eng., Univ of Colorado, Boulder.

METHODOLOGY FOR MONITORING OF OPEN PIT SLOPES USING TIME DOMAIN REFLECTOMETRY

François Charette[1] and Yves Beauchamp[2]

[1]Atlas Copco Rock Drills, Canada; francois.charette@ca.atlascopco.com
[2] Black Lake Division, LAB Chrysotile Inc, Canada

ABSTRACT

The paper presents a full-scale calibration study aimed at validating a proposed methodology of monitoring of open pit slopes using Time Domain Reflectometry, prism reading and numerical modelling. The monitoring of a major slide in a surface mine was used to obtain a correspondence between slope displacements and TDR reflection readings. Numerical modelling was performed in order to better understand the global behaviour of the slope and to provide a model to predict future performance. Results proved the validity of the methodology and the successful definition of slope deformations and displacements lead to major design decisions.

INTRODUCTION

Time Domain Reflectometry used as a monitoring method for geotechnical applications has been first introduced in 1981 (Panek and Tesch, 1981). Since then, a wide range of geotechnical application has been well documented.

In Canada, Time Domain Reflectometry was first introduced as a mean of monitoring the surface crown pillars of abandoned mines. These shut-down operations were often located under existing urban structures like roads, parks, golf courses or even human dwellings, and the progressive failure of the surface rock cover render these excavations extremely hazardous as well as costly to rehabilitate. Several authors (Aston et al, Charette) reported on the subject of monitoring of old mine workings, mainly through CANMET. Figure 1 shows the location of early works on detection of instability of abandoned mines. Figure 2 presents the monitoring of a road intersection in Timmins, Ontario (1994).

While the use of the technique was successful for following the behaviour of old mine structures, its application to operating mines was not always fully successful. In some cases, where the stiffness of the coaxial cable was too high for the encasing material, the monitoring performance was not outstanding.

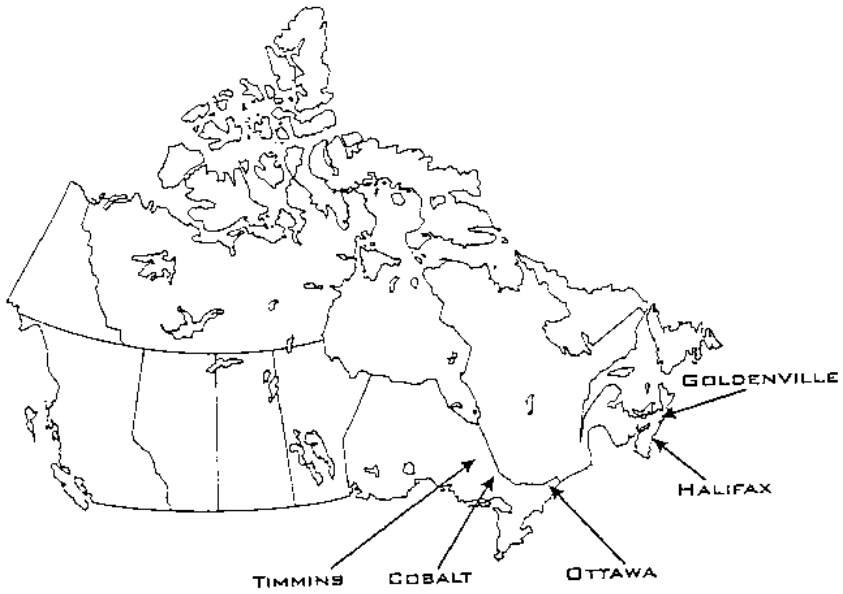

Fig. 1. *Location of monitoring sites of abandoned mine workings in Canada (1995)*

Also, where extension was the main type of movement to detect, the sensitivity could not compete with an extensometer. Finally, where a very long lead between the monitoring zone and the reading box was necessary, the energy loss through the distance was sufficient to mask any small potential deformation (Charette, 1994). In Canada, monitoring of underground mining excavation has also been applied successfully in the cases of Agnico-Eagle (Charette, 1997), Casa Berardi (Leclair, 1998) and Doyon (Charette, 1995) mines, and specifically for block caving operations (Vallée, 1997). Open pit monitoring using Time Domain Reflectometry has been also performed at Doyon, Black Lake Mine, Jeffrey Mine, Selbaie and Syncrude. The monitoring is still performed in the surface operations that are still active.

The use of time domain reflectometry for open pit mines is analysed here for the Black Lake Operations, located in rock of poor quality. The definition of the scale of the movements was instrumental in accelerating the development of the ore body to avoid ramp failure and interruption of mining.

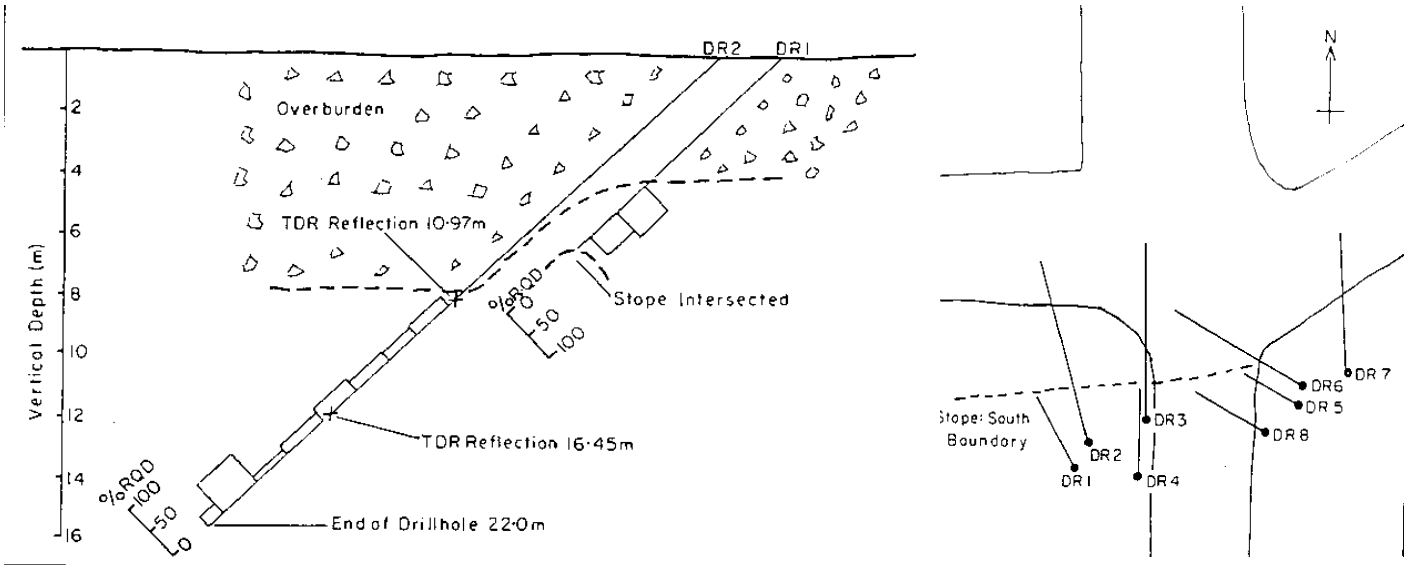

Fig. 2. *Monitoring of a road intersection located above old mine slopes (Timmins, Ontario)*

THEORETICAL ASPECTS

The basis of signal recognition used for this work follows the work performed by Dowding *et al* and O'Connor *et al*, which basically defined the concordance between the main type of ground deformations and reflection signals shape as shown in figure 3.

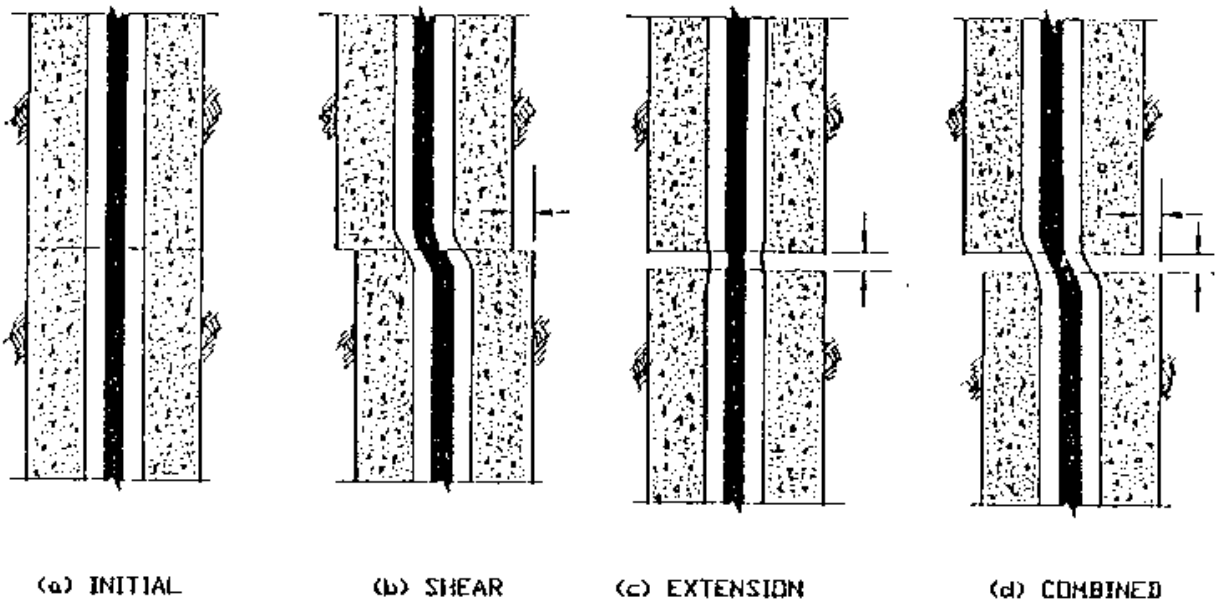

Fig. 3. *Typical movements detected by coaxial cables*

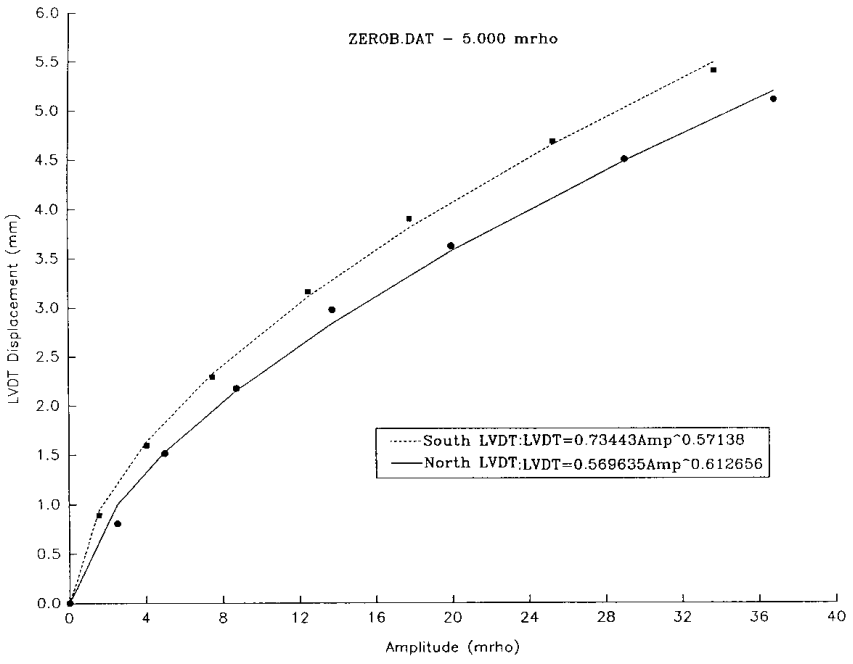

Fig. 4. *Laboratory testing of coaxial cable to assess basic shear signature without grout interference (after Charette, 1993)*

Work performed at the laboratory allowed the definition of signal. Work by Charette (unpublished data, 1994) on coaxial cables sheared by steel blocks, developed the basic relationship between shear movements and reflection signals of a copper clad aluminium cable presented on figure 4. The relation follows a power function of the type $shear = a \times (amplitude^{b})$. For that test, the loss of energy caused by the first shear located 6 inches before the second shear horizon is about 10%. When shear tests are performed with grouted cables, the softness of the grout material allows more deformation to occur

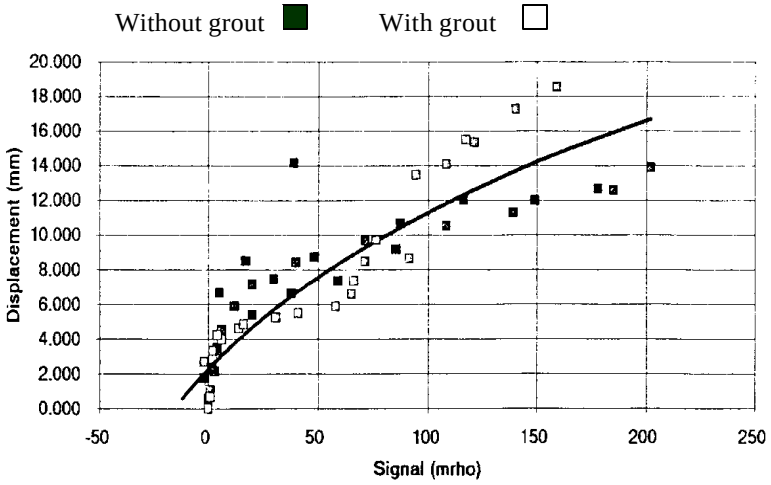

Fig. 5. *Shear testing of coaxial cable*

along the cable, and the reflection signal can reach higher values. For tests performed in grouted material, the complex shear-tensile mechanisms render the analysis more difficult but the reduction of amplitude can also be observed (figure 5).

OPEN-PIT WALLS MONITORING

A complete application study was performed at the surface operations of LAB Chrysotile Ltd, Black Lake Operations Division. Geomechanics evaluation of rock mass slope monitoring with prisms Time Domain Reflectometry, and numerical modelling were used to analyse and follow the behaviour of the South West wall of the main pit, located in Black Lake in the Eastern Township of the province of Quebec, Canada. The objective of the project was to define the applicability of the method for open pit mining operations. Comparison of prism movements, TDR reflections location and intensity as well as numerical simulations showed a direct relationship between the observed movements and the monitoring data.

Geomechanical settings

The Black Lake Division located in the Eastern Township is a major open pit mining operation extracting Chrysotile Asbestos. Following failure of a surface waterline and movements monitored by prisms readings, the Black Lake Division of LAB Chrysotile Inc started a research program to develop a protocol of analysis of slope stability using Time Domain Reflectometry as a monitoring method. Figure 6 presents a view of the area of the pit where the moving zone was delineated through preliminary analysis of prism displacements.

Rock mass property assessment was based on laboratory testing as well as field evaluation. Table 1 shows the intact rock properties for the four major geological domains. Joint properties were computed from laboratory testing and are presented in Table 2. Other data from graduate studies and consulting performed at another Canadian Asbestos mine were also considered, but preliminary modelling runs suggested that these stiffness values were too high for the case studied here; the properties values calculated from shear tests (Golder Associates, 1978) and from back analysis are found in Table 2.

On the main sections where prism movements were measured, core logging was performed in order to define the sheared and broken core intervals. Exploration core drilling was reviewed and the combined data of old holes and new TDR monitoring holes was compiled. The new logs were compared with the older logs and newly damaged zones were also inferred from the observations. Figure 7 shows interval of lower quality rock on section A + 00; this section was chosen for the correlation between prisms monitoring, TDR monitoring and numerical modelling.

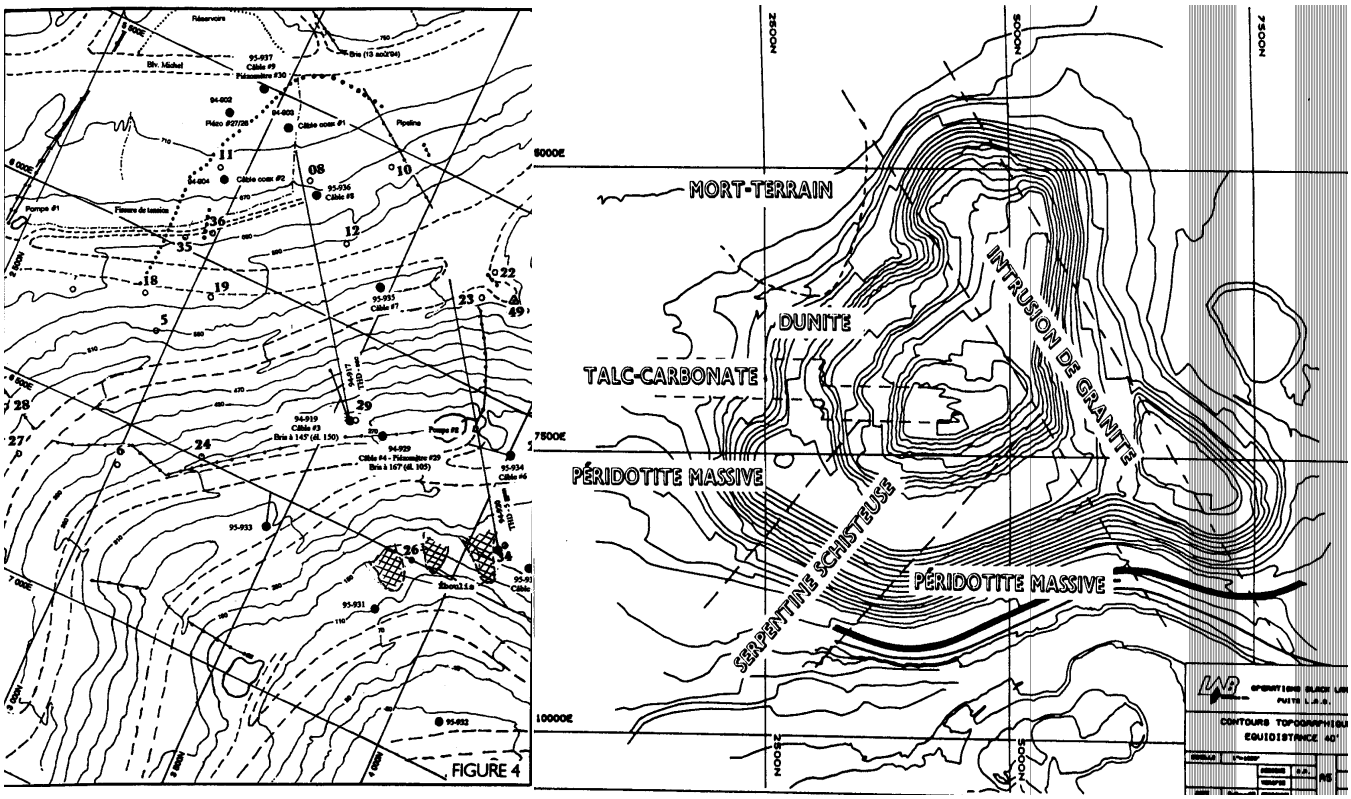

Fig. 6. *Geomechanical situation and monitored pit section*

Rock Type	Young Modulus (Gpa)	Poisson ratio	Specific weight (kN/m^3)	Cohesion (kPa)	Friction angle (^{o})
Over-burden	0.7	0.3	20	0	30
Serpentinised Dunite	7.4	0.22	26	100	30
Shear zone (talc-carbonate and serpentine)	0.65	0.2	20	0	20
Massive Peridotite	13.0	0.25	27	500	35

Table 1. *Intact roc properties (form Golder Associates, 1978)*

Rock Type	Young Modulus (Gpa)	Poisson Ratio	Normal Stiffness (Mpa/m)	Shear Stiffness (Mpa/m)	Cohesion (KPa)	Friction angle (^{o})	Residual friction angle (^{o})
Dunite	1	0.20	100	50	10	27	25
Shear zone	1	0.20	100	50	10	25	20
Peridotite	1	0.20	100	50	50	35	30

Table 2. *Discontinuities mechanical properties*

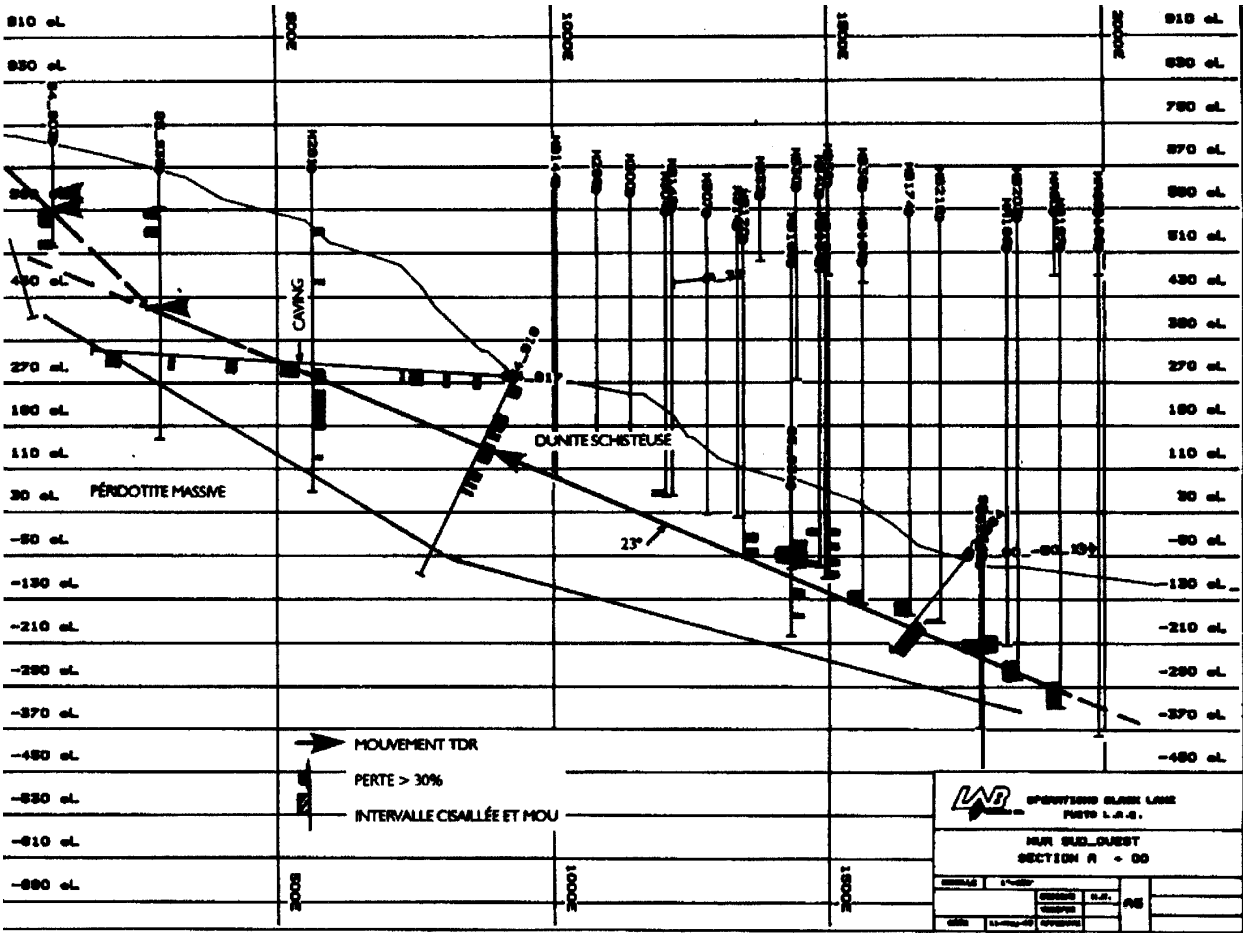

Fig. 7. *Rock quality data from core logging on Section A+00*

Prism monitoring

Figure 8 presents prisms displacements versus time for section A + 00. This section includes prisms P72, P76, P90, P93, P102 and P103. Prisms P72, 76, 90 and 93 show similar rate of movements and a total displacement of 600 mm between September 1994 and May 1995. P72 and P76 are located at the upper end of the wall, while P90 and P93 are located around the middle part of the wall. Rates of movement reached up to 1.4 mm per day between September 1994 and March 1995 (Period I) and peaked at more than 2.5 mm per day between March 1996 and July 1996 (Period II) but averaged 1.1 mm/day from September 1995 to July 1996. Displacements came to a halt in the period March 1995-July 1995 (Period III) and November 1995- February 1996 (Period IV).

Prisms P102 and P103 started to move in May 1995 and the rates of displacement were 0.43 mm/day for the period between May 1995 and January 1996, and 1.11 mm/day for January 1996 to July 1996. Acceleration and stabilisation of displacements occur at the same time for all the prisms in that section. Total displacement rate from September 1994 to July 1996 was about 1 mm/day for P72, P76, P90 and P93.

Prisms located on top and at the middle of the slope move faster than the prisms located at the foot of the slope. The foot of the slope is obviously clamped and the material is crushed just above the base of

the wall. And although the prism P93 is located relatively far from P72, P76 and P90, its displacement pattern is almost exactly the same as P72 and P76.

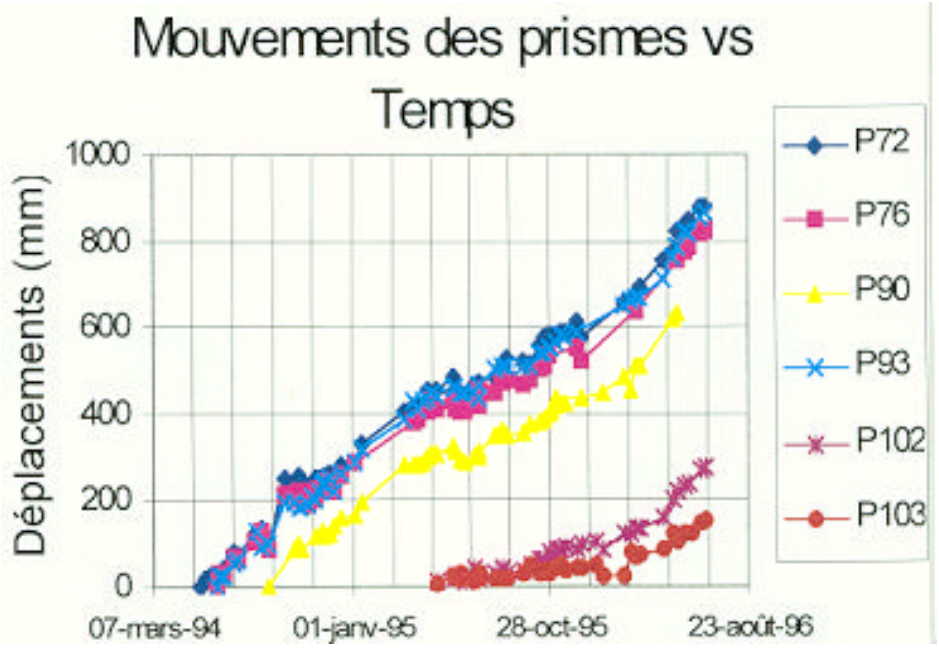

Fig. 8. *Prisms monitoring on Section A + 00*

TDR monitoring

Figure 9 shows the TDR monitoring for Section A + 00. TDR cables 1 and 8 are located around P72 and 76 at the top of the wall, TDR 3 and TDR 4 are located beside P93. The difference in the date of the first measured reflections is caused by a different installation date for cables 1 and 8 and 3. Rate of increase of amplitude for reflection coefficients coincide with the prism readings for the same periods.

TDR-1

The TDR –1 monitoring cable shows a series of reflection (shear type reflection) at depths along the cable ranging from 100 to 142 feet, that can be grouped into two (2) main shearing horizons roughly located at 110 feet and 140 feet. The reflection at 141.5 feet shows the results of large energy loss on the reflection image at the end of the cable: while the reflections located higher on the cable are increasing in size, the reflection at the end is getting smaller because the transmitted pulse is getting much smaller at that point. Finally, this cable was sheared off at 141 feet. The increase of the rate of reflection was around 0.9 mrhos/day for Period I.

TDR-8

This cable was installed almost 8 months after the TDR-1 cable, and was also much longer than the first cable. The history of reflection coefficients presented on figure ** shows that movement deep into the slope are slowly developing. Reflections located at around 250 feet down the cable are more or less at the extension of the potential failure surface delineated by diamond core drilling. Cable was sheared off at 253 feet from reading end. On the main failure surface located at 253 feet, the reflection increase was measured at about 0.3 mrhos/day from June 1995 to July 1996.

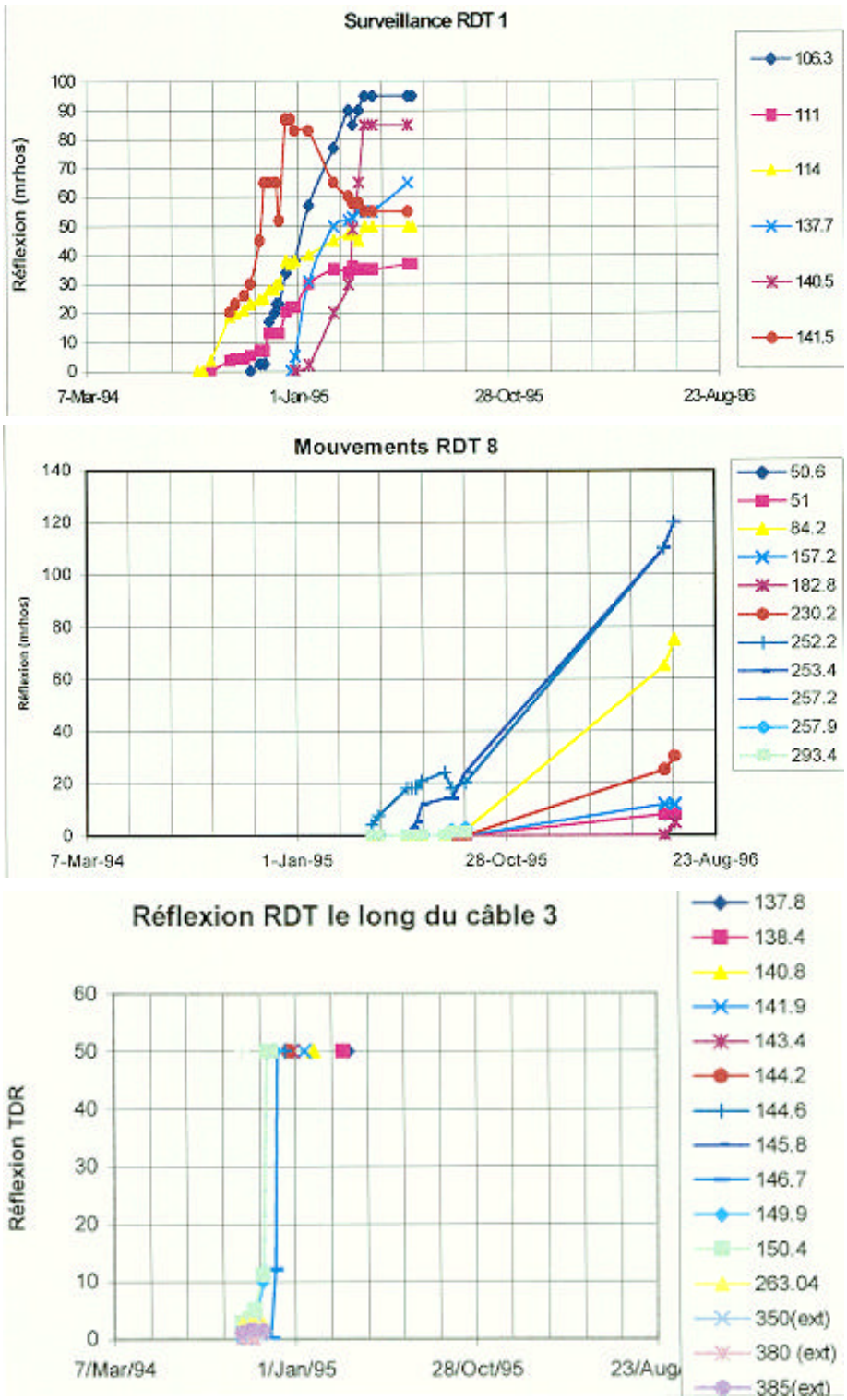

Fig. 9. *TDR monitoring*

TDR-3

This cable, located very close to P93 was cut early in 1995 but showed major shearing around the 145 feet horizon, light shearing around 260 feet and extension at the end (350 to 380 feet). The extension type reflections have not been explained. TDR –3 was ultimately cut at 145 feet from collar.

TDR-4

This cable was not monitored very closely during the period analysed, but it was cut very soon after installation at a depth of 175 feet from reading end.

TDR-16

Cable installed after the monitoring period analysed here.

Correspondence With Prism Movements

Comparison of total displacement and reflection coefficient amplitudes were made for TDR-1 and TDR-8. As the total movement on surface is the sum of all the shear displacements at that point, the corresponding TDR reflection is the sum of all the reflection on the cable during the period analysed. It is somewhat difficult to evaluate the reflection value when there are several large reflections within a small distance along the cable. Multiple reflections closely located tend to mask each other or to reduce the reflected energy in reducing the transmitted pulse to the next shear. It was felt that, although there is a

definite relationship between the change of cable geometry (shear, extension) and the reflected pulse, we did not succeed in accurately quantifying the field correspondence; the presence of masked extension or more simply the attenuation caused by several shear zones may have caused these discrepancies. However, the observed correspondence between surface displacement of slope and total reflected energy (in mrhos) is around 0.86 mm/mrhos. Total reflected energy is the sum of all reflection spikes along any single cable.

Period	Prisms – TDR Cable	Prisms Displacements (mm)	TDR Reflection (mrhos)	Correspondence (mm / mrhos)
Sept. 94 – Jan. 95	P72, P76, P90, P93 – TDR 1	185	198	0.93
Jan. 95 – July 95	P72, P76, P93 – TDR 1	150	217	0.69
Jan. 95 – July 95	P90 – TDR 1	200	217	0.92
Sept. 94 – July 95	P72, P76, P90, P93 – TDR 1	310	380	0.82
April 95 – Nov. 95	P72, P76, P90, P93 – TDR 8	100	55	1.8
Nov. 95 – July 96	P72, P76, P90, P93 – TDR 8	300	345	0.87
April 95 – July 96	P72, P76, P90, P93 – TDR 8	350	385	0.91

Table 3. *Correspondence between prisms displacements and TDR reflections*

Detection Performance

During nearly two (2) years of monitoring, it has been learned that the sensitivity of the detection parameters was of prime importance in the detection and amplitude measurement. To be able to detect adequately the individual large deformations observed during the monitoring period, a horizontal scale of 1 foot/division and a vertical scale of 2 mrhos/division on the Tektronix 1502B was the minimum sensitivity to allow a good and reliable detection and monitoring of ground movements. A general procedure could consist of a first detection using gross parameters. If reflections were found a second scan with high sensitivity would follow to accurately define the reflection. However, this approach could render the early detection of movements almost impossible.

Numerical Modelling

Numerical modelling was another step into building a global procedure for TDR monitoring for surface mining excavations. The possibility of modeling the rock mass behaviour to reproduce measured movements would give more credibility to the methodology, and would also allow use of a model to study mining alternatives with more confidence.

Based on the orientation of the major structures and the location of the broken zones from the core logging, a numerical model was prepared to be run on BSM (Block Spring Model, Wang, 1991) developed and distributed by CANMET. The theoretical description of the model can be found elsewhere (Wang, 1991). Figures 10 and 11 shows the results of numerical modelling for the South West wall. Movements at the tip of the wall were calculated in the order of 20 cm while the central part of the slope reached values of almost 100 cm, and the foot of the wall showed displacements around 30 cm. These numerical modelling results are within the range of the measured prism displacements for the periods studied.

The calibrated model will be used in the future to complete more conventional slope stability analysis such as Janbu methods, that are already used systematically at the Black Lake Operations.

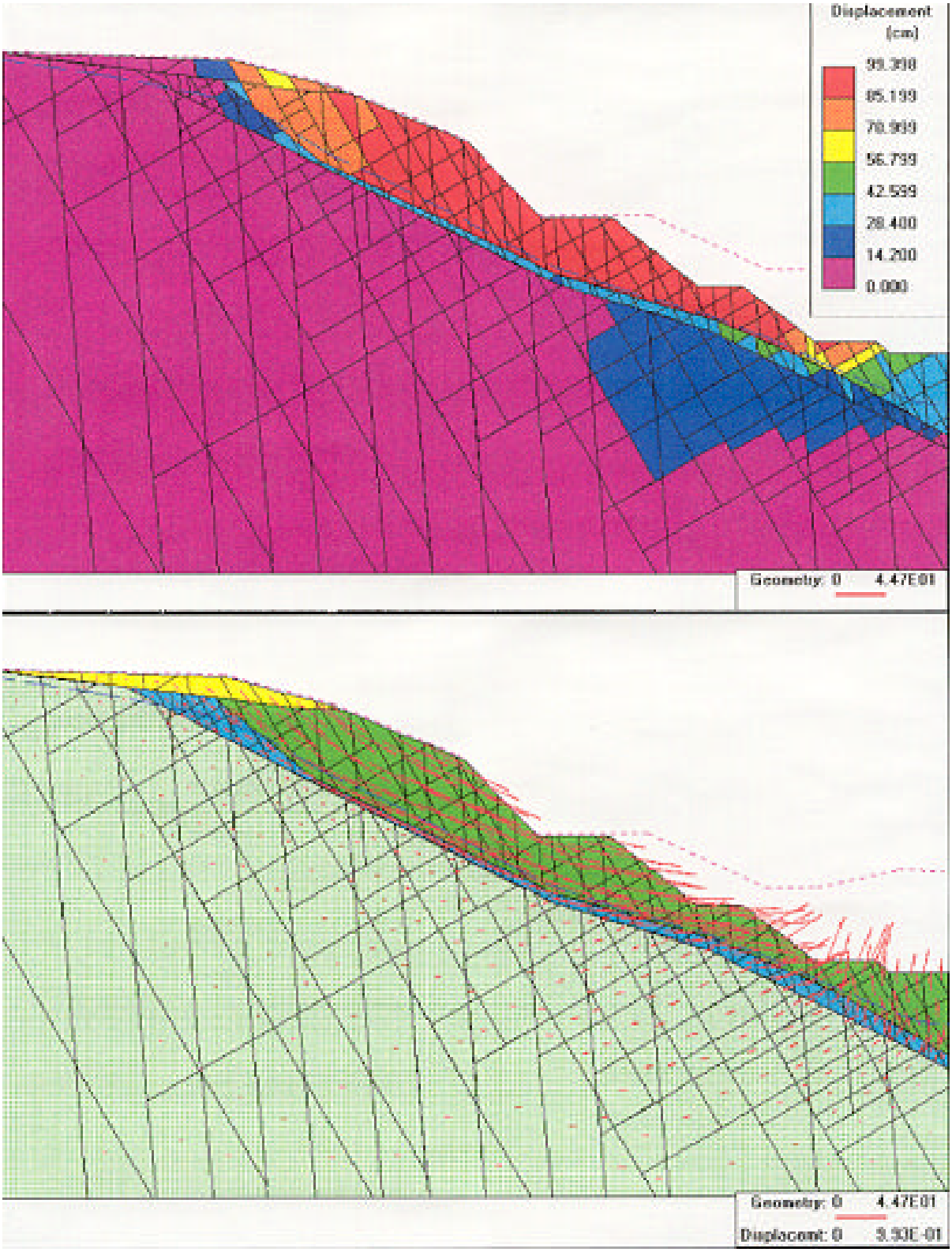

Fig. 10. *Numerical modelling results with BSM*

CONCLUSION

The calibration project has shown the good correlation between the prism movements, numerical modelling and the TDR monitoring results. The methodology of using two monitoring systems in parallel has proven a quantitative approach of monitoring with coaxial cables using Time Domain Reflectometry. Although the accuracy is still not very high, a correspondence between total movement and total reflected energy of 0.86 mm/mrhos was proposed. This is somewhat higher than previously proposed by Aimone-Martin et al. A critical aspect of TDR monitoring is to use parameters that allow accuracy of reading, as much with horizontal definition as with vertical (amplitude) measurements. The project has proven the validity of the method on the based of measured data and simulated data.

REFERENCES

Aimone-Martin, Catherine T., Oravecz, Kalman I., and Nytra, Timothy K. TDR Calibration for Quantifying Rock Mass Deformation at the WIPP Site, Carlsbad, NM. Proceedings of Symposium and Workshop on Time Domain Reflectometry in Environmental, Infrastructure, and Mining Applications, Northwestern Univ., Evanston, Illinois, Sept. 7-9, 1994, 507-517.

Aston, T., and Charette, F., 1993, Installation and Monitoring of Three Abandoned Mine Crown Pillar Sites, Timmins, Ontario: August 1992 to October 1992. CANMETDiv. Rep. MRL 93-020 (CL), Min. Res. Lab., Ottawa, June, 61 pp.

Aston, T.R.C., Bétournay, M.C., Hill, J.D., and Charette, F. Application of TDR For Monitoring the Long Term Behaviour or Canadian Abandoned Metal Mines, Proceedings of Symposium and Workshop on Time Domain Reflectometry in Environmental, Infrastructure, and Mining Applications, Northwestern Univ., Evanston, Illinois, Sept. 7-9, 1994, 518-527.

Charette, F., 1993, Installation and Monitoring of Three Abandoned Mine Crown Pillar Sites, Cobalt, Ontario: February 1992 to July 1992. CANMET Div. Rep. MRL 92-095(CL), Min. Res. Lab., Ottawa, Mar., 64 pp.

Charette, F., 1993, Results of the Monitoring of Three Crown Pillar Sites in Cobalt, Ontario. CANMET Div. Rep. 92-101 (CL), Min. Res. Lab., Ottawa, Mar., 31 pp.

Charette, F., 1985, Monitoring of the South Wall of Mine Doyon Open Pit.

Dowding, C.H., Su, M.B., and O'Connor, K.M., 1989, Measurement of Rock Mass Deformation with Grouted Coaxial Antenna Cable. Rock Mech. And Rock Eng., **22**, 1-23.

Dowding, C.H., and Pierce, C.E., Measurement of Localized Failure Planes in Soil with Time Domain Reflectometry, Proceedings of Symposium and Workshop on Time Domain Reflectometry in Environmental, Infrastructure, and Mining Applications, Northwestern Univ., Evanston, Illinois, Sept. 7-9, 1994, 569-578.

Golder Associates, Southwest and south wall movement, 1996.

Hill, J.D., 1993, Monitoring of surface Crown Pillar Deformation at Goldenville, N.S. using Time Domain Reflectometry. Final Rep., DSS contract 23440-0-9245/01-S2, CANMET, prep. By Dept. Of Min. And Metall. Eng., Tech. Univ. Nova Scotia, Halifax, Mar., 94 pp.

Kawamura, N, Bauer, R.A., Mehnert, B.B., and Van Roosendaal, D.J., TDR Cables, Inclinometers and Extensometers to Monitor Coal Mine Subsidence in Illinois, Proceedings of Symposium and Workshop on Time Domain Reflectometry in Environmental, Infrastructure, and Mining Applications, Northwestern Univ., Evanston, Illinois, Sept. 7-9, 1994, 528-539.

Leclair, J.G., 1984, TDR at Casa Berardi, Personal Communication.

O'Connor, K.M. and Dowding, C.H., Application of Time Domain Reflectometry to Mining, Proceedings of 25th Symposium on Rock Mechanics, Northwestern University, Evanston, Illinois, 1984, 737-746.

O'Connor, K.M. and Zimmerly, T., 1991, Application of Time Domain Reflectometry to Ground Control. Proceedings of the 10th International Conference on Ground Control in Mining (Morgantown, June 1991), WV Univ., 115-121.

Panek, L.A., and Tesch, W.J., 1981, Monitoring Ground Movements near Caving Slopes, Methods and Measurements, RI 8585, U.S. Bureau Mines, Denver, Colorado, 108 p.

Su, M.B., 1987, Quantification of Cable Deformation with Time Domain Reflectometry. Ph.D. Dissertaion, Northwestern Univ., Evanston, IL, 112 p.

Vallée, M., 1985, TDR Monitoring of Bell Mine Crushing Room, Personal Communication.

Wang, B., A Block-Spring model for jointed rocks; Ph.D. thesis, University of Ottawa, Canada, 204 p.

Wang, B., BSM- A Windows application package of the block-spring model for analysis of jointed rocks. Users Manual. MRL 94-012 (TR). 46 p.

TIME DOMAIN REFLECTOMETRY TO MONITOR TAILINGS DAM STABILITY

B. P. Gorski[1], B. Tisch[2], T. Anderson[3], K. Judge[4] and K. Tarr[5]

Natural Resources Canada

[1]Mining and Mineral Sciences Laboratories, Natural Resources Canada, Ottawa, Canada; bgorski@NRCan.gc.ca
[2]Mining and Mineral Sciences Laboratories, Natural Resources Canada, Ottawa, Canada; Btisch@NRCan.gc.ca
[3]Mining and Mineral Sciences Laboratories, Natural Resources Canada, Ottawa, Canada; Tanderso@NRCan.gc.ca
[4]Mining and Mineral Sciences Laboratories, Natural Resources Canada, Ottawa, Canada; Kjudge@NRCan.gc.ca
[5]Mining and Mineral Sciences Laboratories, Natural Resources Canada, Ottawa, Canada; Ktarr@NRCan.gc.ca

ABSTRACT

The Canada Centre for Mineral and Energy Technology (CANMET) is currently monitoring the stability of three tailings dams using Time Domain Reflectometry (TDR) technology. TDR cables 100 metres in length were installed horizontally in all three dams. The first dam was instrumented in October of 1998. Field installation, data acquisition and software modifications will be presented.

INTRODUCTION

Time Domain Reflectometry (TDR) technology has been used successfully for a variety of applications. They include the measurement of soil moisture, rock and soil stability, structural stability, water level, and contaminant leakage. Most applications have utilized vertical or near-vertical placement of the cables, and usually in a grouted borehole (Aston, 1991; Aston and Charette, 1992; and Charette, 1993). Horizontal placement of cables allows for monitoring of movement along the periphery of a tailings dam (Gorski *et al.*, 1996 and Gorski and Anderson, 1998).

Figure 1: *Tailings Embankment Failure*

THEORY

TDR was first developed during the 1950s to locate and identify cable faults in the power and telecommunications industries (O'Connor and Dowding, 1999). A fast rise time electromagnetic pulse is sent down a coaxial cable at a velocity that is specific to the cable. A portion of the pulse will be reflected back to the beginning of the cable if a change in the characteristic impedance of the cable is detected. These "signatures" can be analyzed over time to monitor changes in the cable deformation.

Coaxial cables are composed of a central metallic conductor surrounded by a dielectric, a metallic outer conductor surrounding the dielectric, and a protective jacket. The TDR cables have a characteristic impedance determined by the annulus geometry and dielectric material between the conductors. The dielectric is commonly composed of PVC foam, Teflon, or air (Cablewave Systems, 1999).

If the cable is deformed, the distance between the inner and outer conductors changes, as does the impedance at that point. A change in impedance may be caused by several factors, including a crimp, kink, a change in dielectric material properties (e.g. water), or a break in the cable. Measurement of the amplitude of the reflected waves over time can be used to determine the nature of the observed change in impedance. The time interval between launching of pulses and detection of the reflected pulses provides a measurement of location.

CABLING AND SIGNATURE OPTIMIZATION

Copper coaxial TDR cable type FLC 14-50J, 0.5 inches in diameter was selected for the tailings dams. The cable is manufactured by Cable Wave Systems. The cable consists of a protective polyethylene jacket, corrugated copper outer conductor, foam polyethylene dielectric, and a copper clad aluminum center conductor. The jacketing provides protection against moisture and corrugated copper was considered sufficiently deformable for this field application (Hill *et al.*, 1996).

TDR shear signatures are readily identified as opposed to tensile deformation. The cable will experience tension if dam movement occurs. Movements may occur due to downslope piping, seepage or gullying. The cabling was configured in such a way that tension would be translated to shear signatures by installing “shear inducers” at regular intervals along the length of the cable. The inducer works as a choker loop under tension. In tension the loop tightens up on a double edged wedge. This action leaves a distinctive double shear spike.

INSTRUMENTATION AND SOFTWARE

TDR cable testing was performed using a Tektronix 1502B time domain reflectometer (Tektronix, 1990). The 1502B displays TDR cable waveforms directly on a LCD screen. Tektronix SP232 host application software was used to control the 1502B and transfer data to a laptop. The software was installed in DOS on the laptop.

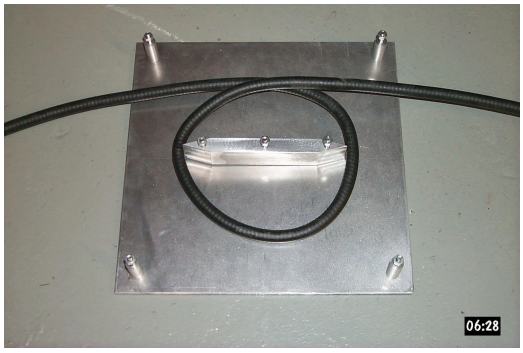

Fig. 2. *Dismantled Choker Plate*

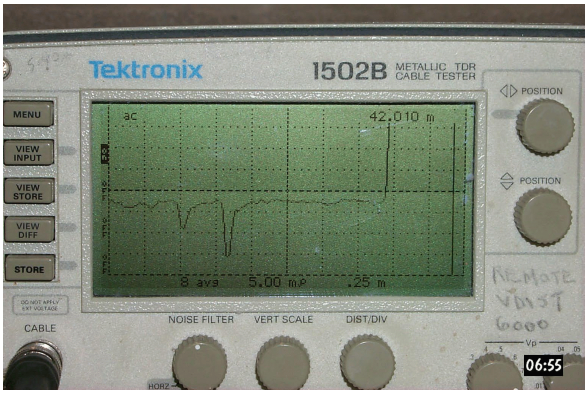

Fig. 3. *TDR Trace on Tektronix 1502B*

New data acquisition software was written six months into the field program of data collection. Labview software was written to collect data from the 1502B in Windows 95 environment.

FIELDWORK

A 100 metre length of TDR cable was installed at each of the three tailings dams. Cabling was placed directly into a trench parallel to the toe of slope and above the toe drain. Shear inducers were installed at 15 metre intervals along the length of the cable. The inducers were wrapped in fine geo-fabric to prevent fill intrusion during backfilling. The free end of the cable was pre-crimped as a distance marker. The cable was backfilled in granular fill material to a maximum depth of one metre. A 30 metre lead cable with BNC connections protected with 25 mm diameter PVC tubing was connected to the TDR cable and run to a secure location for subsequent long-term monthly field measurements.

Fig. 4. *TDR Trench at Toe of Embankment*

DATA RETRIEVAL

Data was initially retrieved at all three sites monthly using SP232 host software. Data was reduced using a Fortran program to units of reflection coefficient (mhro) versus distance (metres). The data was imported into Sigmaplot. Subsequent data sets were offset so that all monthly waveforms could be displayed on the same plot. Data acquired using Labview software was imported directly into Sigmaplot.

DISCUSSION

Data was retrieved at each of the three sites by different CANMET personal using different Tektronix 1502B units and laptops. Tektronix waveform settings were identical for all three sites. The TDR cable and BNC cable lengths and type were identical for all three sites. Personal and equipment changes did not affect the quality or repeatability of field measurements.

Fig. 5. *Acquiring Field Data from TDR Cable*

Site 1: Val d'Or Test Area

The TDR cabling was installed during phase 1 of the construction of this tailings dam. The dam is basically pit run fill with a clay core founded on bedrock. Although the cable was installed in October of 1998, data collection methodology was not finalized until August of 1999. The well defined shear spikes are the result of construction equipment activity over the cable trench during the second lift of the dam construction. Several

noise troughs in the data are attributed to poor field connections to the 1502B. The troughs did not appear in the subsequent sets of readings.

Fig. 6. *Val d'Or Embankment*

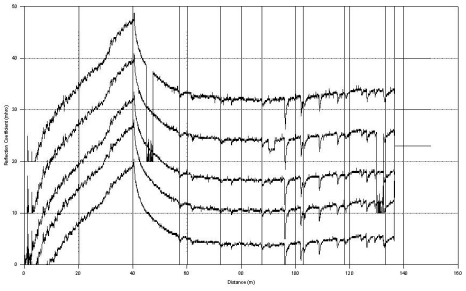

Fig. 7. *Val d'Or Monthly Traces*

Site 2: Elliot Lake Test Area

The TDR cabling was installed in a new toe drain under construction for this tailings dam. The first set of readings show considerable noise in the waveform. This was attributed to a diesel backhoe that was idling at the time of the readings and was located over the backfilled TDR trench. Readings taken in December of 1999 compare data retrieval methods using SP232 software and Labview. The glitches in the Labview curve have since been resolved as erroneous data and the software rewritten.

Fig. 8. *Elliot Lake Embankment*

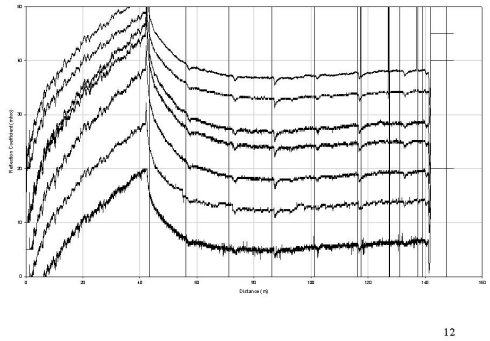

Fig. 9. *Elliot Lake Monthly Traces*

Site 3: Timmins Area

This is our most recent site. The tailings dam is low in height and the tailings are submerged. The site is underlain by New Liskeard clay. The TDR cable was installed in October of 1999. Monthly readings taken to October of 2000 have been consistent at this site.

Fig. 10. *Timmins Embankment*

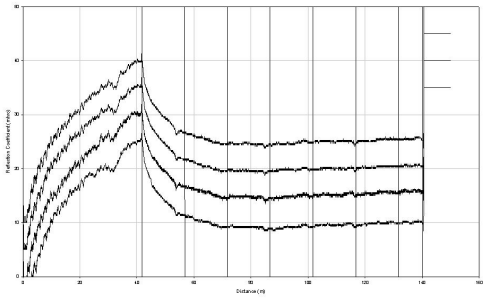

Fig. 11. *Timmins Monthly Traces*

CONCLUSIONS

There are several devices on the market developed specifically to monitor movements of earthfill structures. Movements are detected normally in vertical localized areas of a structure. TDR cable however, may be used to monitor long horizontal segments of earthfill embankments. Embankments may be monitored remotely on-line using a TDR cable as the sensing method is electronic.

Off the shelf Labview is a typical software tool capable of acquiring data and controlling TDR electronics in Windows95 or better. Labview acquires the data at 13 bit resolution versus SP232 8 bit. Data acquired over time is readily compared to baseline readings. Data is acquired at a receive/transmission speed of 19200 baud. SP232 software speed was 1200 baud. Labview may be configured to trigger alarms when embankment movements are detected.

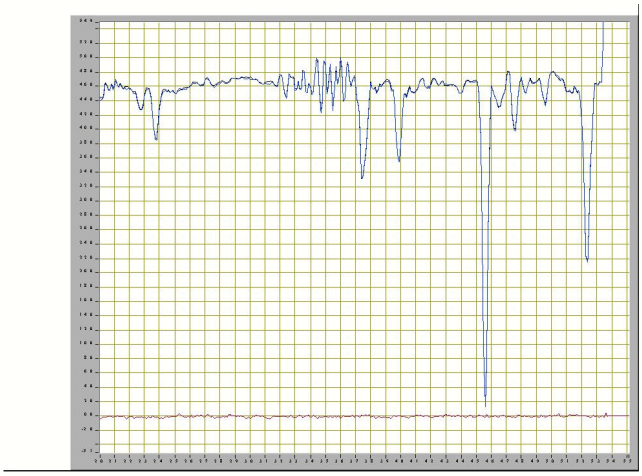

Fig. 12. *TDR Traces using Labview*

REFERENCES

Aston, T., 1991, Installation and Monitoring of Three TDR Cables, Checkerboard Creek Site, Near Revelstoke, B.C.: July 1993 to September 1993: MRL 93-052(CL), Natural Resources Canada, 33 p.

Aston, T., and Charette, F., 1993, Installation and Monitoring of Three Abandoned Mine Crown Pillar Sites, Timmins, Ontario: August 1992 to October 1992: MRL 93-020(CL), Natural Resources Canada, 61 p.

Aston, T., Bétournay, M. C., Hill, J. O., and Charette, F., 1994, Application for Monitoring the Long Term Behaviour of Canadian Abandoned Metal Mines: SP-19-94, U.S. Bureau of Mines, 19 p.

Cablewave Systems Division, 1999, www.cablewave.com/rfs/foam.html: 1 p.

Charette, F., 1993, Installation and Monitoring of Three Abandoned Mine Crown Pillar Sites, Cobalt, Ontario: February 1992 to July 1992*:* MRL 93-095(CL), Natural Resources Canada, 64 p.

Gorski, B., Anderson, T., and Walmsley, J., 1996, Preliminary Visual Geotechnical Assessment: Inactive Tailings Sites, Northern, Ontario*:* MMSL 96-004(TR), Natural Resources Canada, 1-9.

Gorski, B., and Anderson, T., 1998, Geotechnical Assessment and Monitoring: Buffalo-Ankerite Tailings Stack Timmins, Ontario*:* MMSL 98-021(TR), Natural Resources Canada, 31 p.

Hill, J., Maddison, L., and MacConnell, J., 1996, Phase II of Laboratory Evaluation of Time Domain Reflectometry Signal Response to Cable Deformation*:* DSS Contract No. 23440-5-1203/01-SQ, Natural Resources Canada, 132 p.

O'Connor, K. M., and Dowding, C. H., 1999, GeoMeasuremnts by Pulsing TDR Cables and Probes: CRC Press LLC, Florida, USA, 1-2.

Tektronix, Inc., 1990, 1502B Metallic Time Domain Reflectometer: Operator Manual*:* Oregon, USA, 1.1-4.5.

LOOPING TDR CABLES FOR INCREASED SENSITIVITY TO EXTENSION

C.E. Pierce[1], C.M. McAlister[2] and P. Adak[3]

[1]Assistant Professor, Department of Civil and Environmental Engineering, University of South Carolina, Columbia, SC 29208; piercec@engr.sc.edu
[2]Graduate Research Assistant, Department of Civil and Environmental Engineering, University of South Carolina, Columbia, SC 29208; mcaliste@engr.sc.edu
[3]Graduate Research Assistant, Department of Civil and Environmental Engineering, University of South Carolina, Columbia, SC 29208; adak@engr.sc.edu

ABSTRACT

Shearing, crimping, extending or kinking a cable causes it to deform. When a coaxial cable deforms, its characteristic impedance changes locally such that voltage propagating along a cable reflects at the location of deformation. While coaxial cables are often employed as sensors to measure shear deformation with time domain reflectometry (TDR), they are much less responsive to extension. This paper describes a unique approach to enhance the sensitivity of coaxial cables in tension by prescribing loops along the cable length. A series of laboratory tests are performed on two flexible cables with braided shields. These cables have a minimum bending radius less than 20 mm. When cables are bent such that the loop radius is decreased below the minimum bending radius, the cable kinks at the loop. As the loop radius progressively decreases, tests show that the magnitude of voltage reflection exponentially increases. Since the loops are compressed when the cable is pulled from one end, looped cables may be used to measure axial extension. Rigid cables with solid shields require a much larger bending radius to prevent kinking. These cables are not included in this study because they are not considered feasible for field use. Potential applications of looped TDR cables include measuring soil settlement, recording movements in reinforced earth walls, and monitoring movements beneath bridge pier footings that result from bridge scour.

INTRODUCTION

Geotechnical applications of metallic time domain reflectometry (TDR) techniques to measure soil displacement have been somewhat limited by the fact that shearing must be concentrated in a relatively thin zone. O'Connor *et al.* (1995) showed that the magnitude of voltage reflection diminishes as the shear zone thickness increases. While TDR cables can provide more accurate measurements of localized displacement than inclinometers can (Dowding and Pierce, 1994), they cannot detect more general soil movements that occur in a much larger shear zone (O'Connor *et al.*, 1995). The purpose of this paper is to present the concept of looping cables at prescribed locations to increase sensitivity to

extension. Looping cables should permit measurement of more general soil movements and enhance TDR applications in the geotechnical community.

BACKGROUND

Figures 1A and 1B show a TDR cable deforming in a relatively thin shear zone and a relatively thick shear zone, respectively. For a given shear displacement, $*$, the ratio of shear zone thickness to displacement, $t/*$, is smaller in a thin zone than it is in a thick zone. When soil displacements are highly localized, such as along thin slip surfaces in overconsolidated clays, $t/*$ is very small and the TDR cable shears locally. If $t/*$ becomes too large, then the TDR cable will not shear locally and no data can be captured on shear displacements.

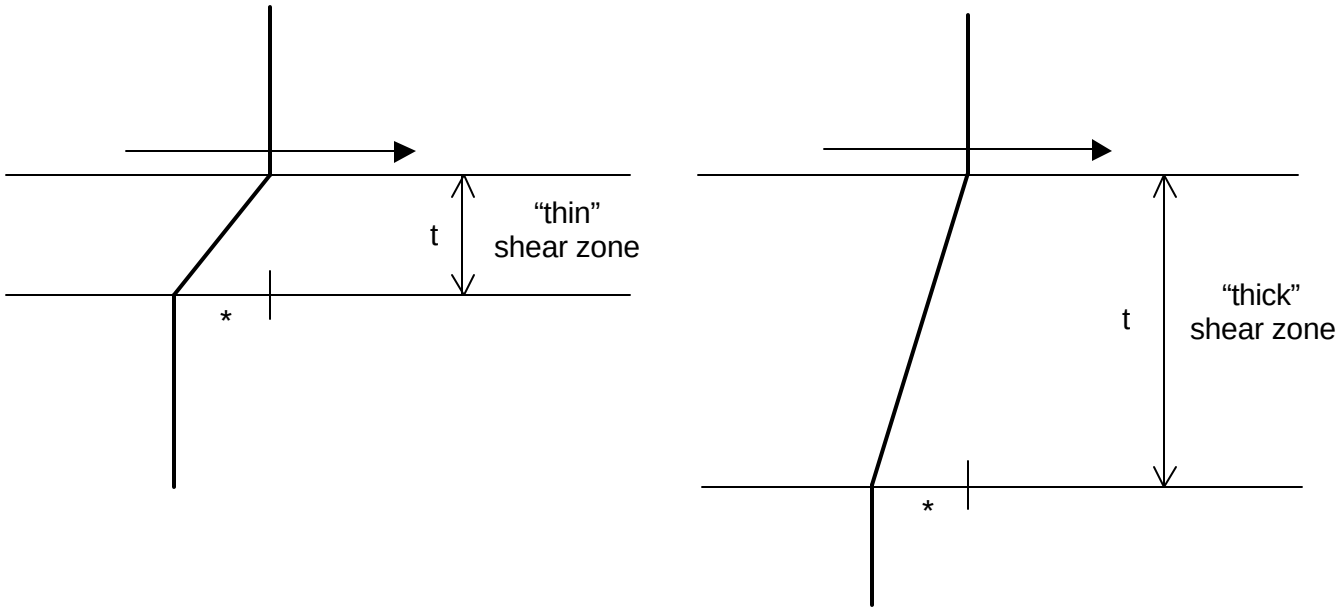

Fig. 1. *Deformed cable profile for given shear displacement in A) "Thin" Shear Zone and B) "Thick" Shear Zone*

Assuming the cable is fixed at the boundaries of the shear zone, the length of cable within the shear zone elongates as soil shear displacement progresses. The change in length, $) L$, is a function of the magnitude of shear zone displacement and thickness. Figure 2 illustrates that cable extension increases as the shear zone displaces for a zone thickness of 10, 20 and 50 mm. For a given shear displacement, the magnitude of cable extension decreases with zone thickness. For example, a cable in a 10-mm zone that displaces 10 mm will theoretically extend more than 4 mm. More than likely, the cable would fail prior to reaching this magnitude of cable extension. However, the same shear displacement in a 50-mm zone would only extend the cable about 1 mm. Thicker shear zones would induce even smaller changes in cable length. If the sensitivity of detecting cable extension with TDR is improved, then it may be possible to capture shear displacement in relatively thick shear zones such as the one illustrated in Figure 1B.

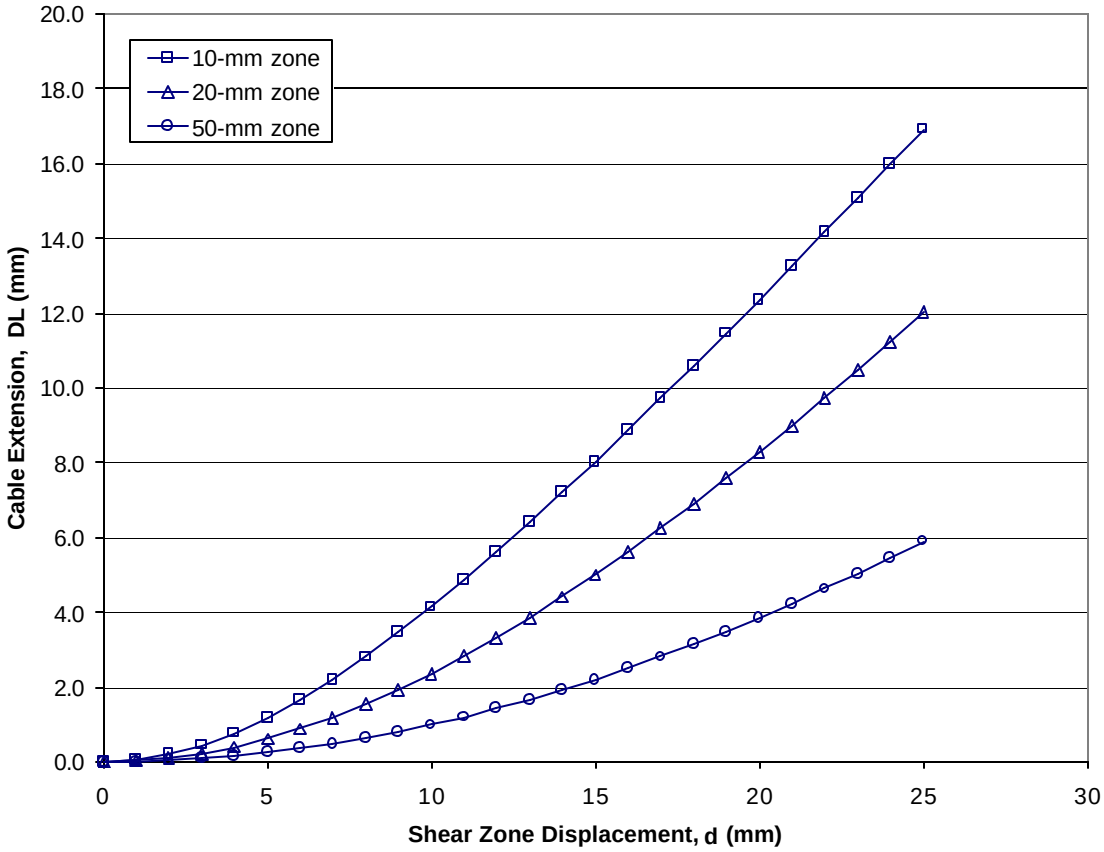

Fig. 2. *Theoretical cable extension as a function of shear zone displacement and thickness*

EXPERIMENTAL PROCEDURES

Selected Cables

Two flexible coaxial cables were selected to demonstrate the effectiveness of looping to increase sensitivity to extension. Alpha 9847 and CommScope 2120k are two common, commercially available cables. Their physical properties can be found in McAlister and Pierce (2001). Both cables have relatively small bending radii that allow small-diameter loops to form in the cable before impeding voltage transmission. Once the loop radius drops below the minimum bending radius, the cable kinks and partially reflects voltage back to the source. Flexible cables inherently have a minimum bending radius that is smaller than rigid cables, as shown in Table 1. CommScope P3 500 and P3 875 are rigid cables that have been frequently used to monitor ground subsidence above abandoned mines (Pierce, 1998; Dowding *et al.*, 1989). Table 1 shows that the minimum bending radius for rigid cables is nearly 10 times its diameter; for flexible cables, the minimum bending radius is only two times its diameter. Kinking rigid cables produces immediate and permanent deformation of its solid shield, whereas kinking flexible cables produces recoverable deformations up to a very small loop radius. For these reasons, no rigid cables were selected for this investigation.

Cable	Shield	Cable Diameter, Jacketed (mm)	Minimum Bending Radius, Jacketed (mm)
Flexible Cables			
CommScope 2120k	Tinned copper braid	4.10	10.7[1]
Alpha 9847	Bare copper braid	10.28	19.5[1]
Rigid Cables			
CommScope P3 500	Solid aluminum tube	14.22	152[2]
CommScope P3 875	Solid aluminum tube	24.00	229[2]

[1] *Determined from laboratory measurements in this investigation.*
[2] *Reported in the manufacturer's catalog (CommScope, 1998).*

Table 1. *Minimum Bending Radius of Select Flexible and Rigid Cables*

Prescribed Circular Loops

The first set of tests involved bending cables in circular loops. This was accomplished by wrapping each cable around progressively smaller pipes, as shown in Figure 3, and other cylindrical items with known diameters. Cables remained jacketed during testing. At least two tests were performed with Alpha 9847 and CommScope 2120k cables to assess repeatability. Cables were wrapped at the same distance every time to produce voltage reflections at a single location on the waveform. Pipes and other items, such as a pen and a screwdriver, were selected so that at least three loop radii were smaller than the minimum bending radius for that cable. For the purpose of this investigation, the minimum bending radius represents the smallest circular loop that can be formed without reflecting voltage.

Fig. 3. *Prescribing circular loops in coaxial cable*

Freely Formed Loops

The second set of tests involved bending cables by prescribing a single, natural loop in the cable and pulling on one end. This loop is referred to as a freely formed loop; in other words, it is formed without the cable being wrapped around a cylindrical object. The cable is pulled until the loop reaches its minimum bending radius, which is designated as the initial condition for testing. The ends of this loop are marked with a pen. The first voltage reflection occurs immediately after the cable is pulled into a loop smaller than its minimum bending radius. Voltage reflections are recorded as the cable is pulled further, which simultaneously reduces the loop radius and extends the cable. For each voltage reflection measurement, the ends of the loop are marked with a pen to acquire the change in length.

Freely formed loops in cables are approximately elliptical, not circular, as illustrated in Figure 4. The perimeter of the loop, P_{loop}, can be approximated as the perimeter of an ellipse,

$$P_{loop} = p\,(a+b)\frac{64-3R^4}{64-16R^2} \qquad [1]$$

where

a = minimum radius of the loop,
b = maximum radius of the loop, and

$$R = \frac{a-b}{a+b} \qquad [2]$$

The smallest loop that can be formed without kinking the cable and reflecting voltage is considered the initial condition. Minimum and maximum loop radii at this initial condition are designated a_0 and b_0, as shown in Figure 4. The apparent cable length at this condition is designated L_0, and is equal to the difference between the physical cable length and the perimeter of the loop. As the cable is pulled with some force, F, the perimeter of the loop decreases causing an extension in the apparent cable length, as illustrated in Figure 4. The resulting cable extension is equal to the change in loop perimeter,

$$\Delta L_0 = \Delta P_{loop} \qquad [3]$$

The maximum achievable cable extension, $\Delta L_{0(max)}$, is some length less than the initial loop perimeter. The magnitude of force required to extend the cable becomes progressively larger as the loop becomes progressively smaller. Forces were not measured in this study and will not be discussed further in the results.

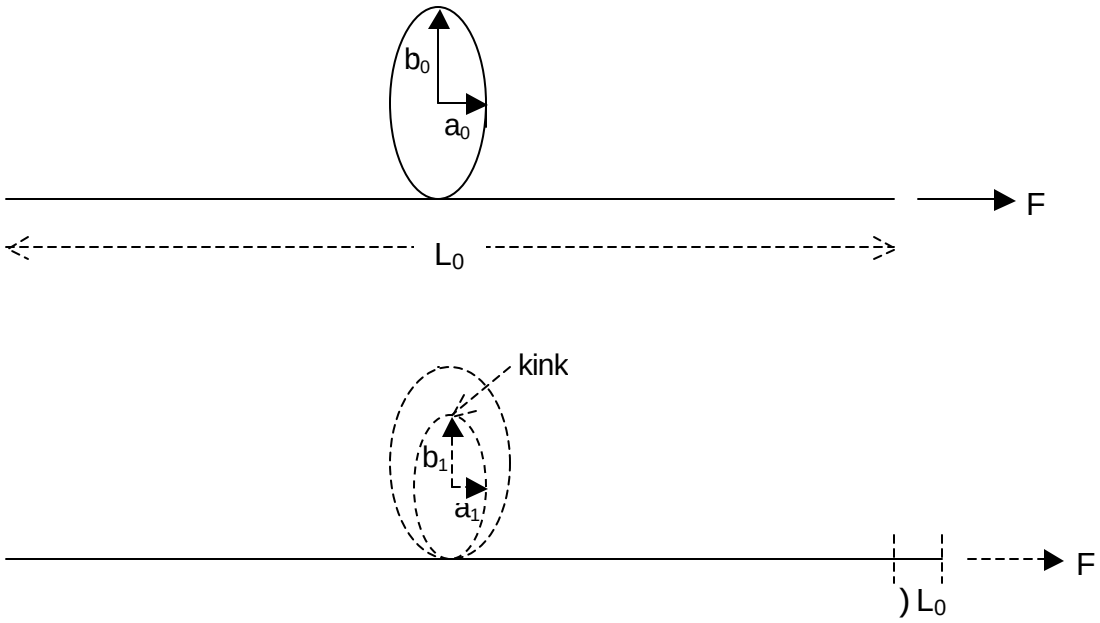

Fig. 4. *Freely formed loops in cable*

RESULTS

An example of cumulative voltage signals for a given bending test is shown in Figure 5. Voltage signals are collected over the entire 200-cm cable length as bending progresses. Voltage data is reduced by taking the difference between each signal and the baseline signal. The resulting signals shown in Figure

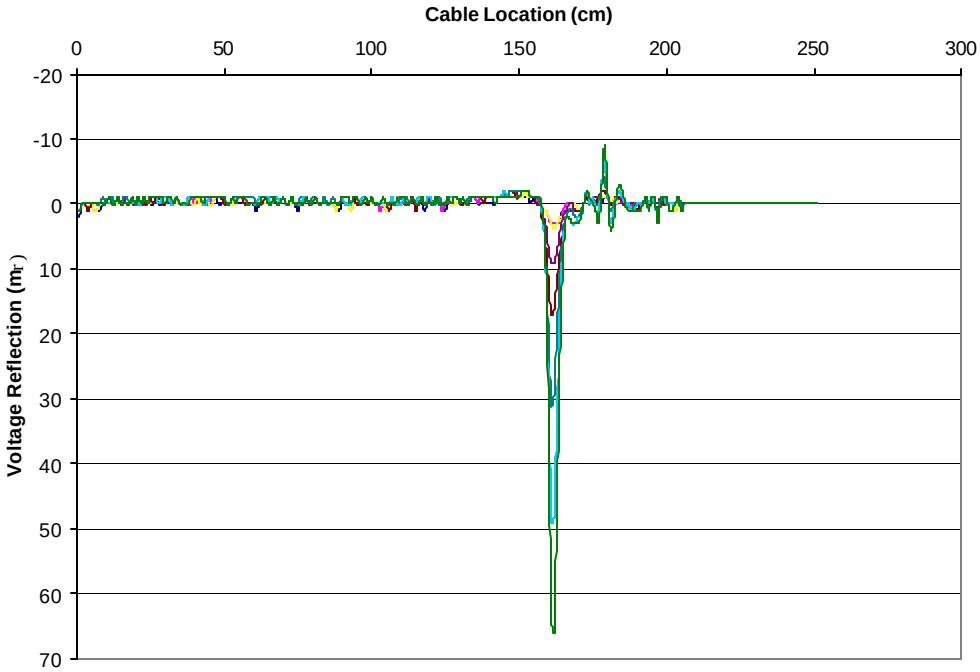

Fig. 5. *Example of cumulative Voltage Reflections Compiled at a Single Loop in Alpha 9847 Cable*

5 are voltage reflection difference signals along the cable. Bending occurs at approximately 160 cm, as indicated by the downward spikes at that location. Reflection magnitude increases to a maximum of 66 mΩ as the loop radius decreases. Noise levels are very low (< 2 mΩ) upstream of the loop but become progressively higher downstream of the loop as bending progresses. In this test, the smallest loop produced noise as high as 9 mΩ at a distance of 180 cm.

Figure 6 compares voltage reflection magnitude as a function of bending radius with prescribed circular loops. First, the smallest loop radius where no voltage is reflected is taken as the minimum bending radius. The values reported previously in Table 1 are somewhat conservative; the actual minimum bending radius is some value between the reported values and the loop radius at first reflection. For the CommScope 2120k cable, the minimum bending radius may in fact be closer to 6 mm than the reported 10.7 mm. Second, bending both cables produces a somewhat gradual increase in voltage reflection initially, but produces a sharp increase in voltage reflection between the final two loops. For example, voltage reflection nearly doubles from 18 mΩ to 32 mΩ when the loop radius on a CommScope 2120k cable is reduced by less than 1 mm. It is theorized that this sharp trend would continue for even smaller loops, until the cable short-circuits or the inner conductor snaps at the kink.

The final set of results demonstrates that looping flexible cables is a potentially viable technique for measuring changes in cable length. Figure 7 compares the trends in voltage reflection as a function of

change in length for both cables. The origin represents the apparent cable length, L_0, with the smallest loop that can be formed without reflecting voltage. As the cable is extended from this initial condition by ΔL_0, voltage is reflected back to the source. Clearly the larger-diameter Alpha 9847 cable can be extended further (to more than 200 mm, in one case) than the smaller-diameter CommScope 2120k (about 40 mm).

Based on these findings, Alpha 9847 cable would be more suitable for monitoring when excessive cable extension is expected. However, the smaller-diameter cable allows more accurate measurement of much smaller changes in length. For example, when ΔL_0 = 30 mm, reflections recorded with the CommScope 2120k cable are nearly 15 mV. Reflections recorded with the Alpha 9847 cable are only 5 mV, which may be indistinguishable from ambient noise levels in the field. Furthermore, a small increase in extension from 30 to 40 mm will be evident with the CommScope 2120k cable, as reflection increases from 15 to 35 mV. The same extension may not be discernible with the Alpha 9847 cable.

Finally, the results in Figure 7 suggest that, if either cable is placed with a loop that is already smaller than the minimum bending radius, and that cable is subject to extension, then a very small change in length will be detectable. For example, if the CommScope 2120k cable is prescribed with a loop that represents the condition when ΔL_0 = 30 mm, even a change in length of only several millimeters should be distinguishable. The same statement can be made for the Alpha 9847 cable, particularly using results from the second test. (It should be noted, however, that the results of the second test are believed to differ from the first test because the same cable was used. This cable may have been damaged internally after the first test, thereby causing a more rapid increase in voltage reflection during the second test.) Based on these observations, small shear displacements occurring in relatively thick shear zones can be measured if cables are looped below the minimum bending radius.

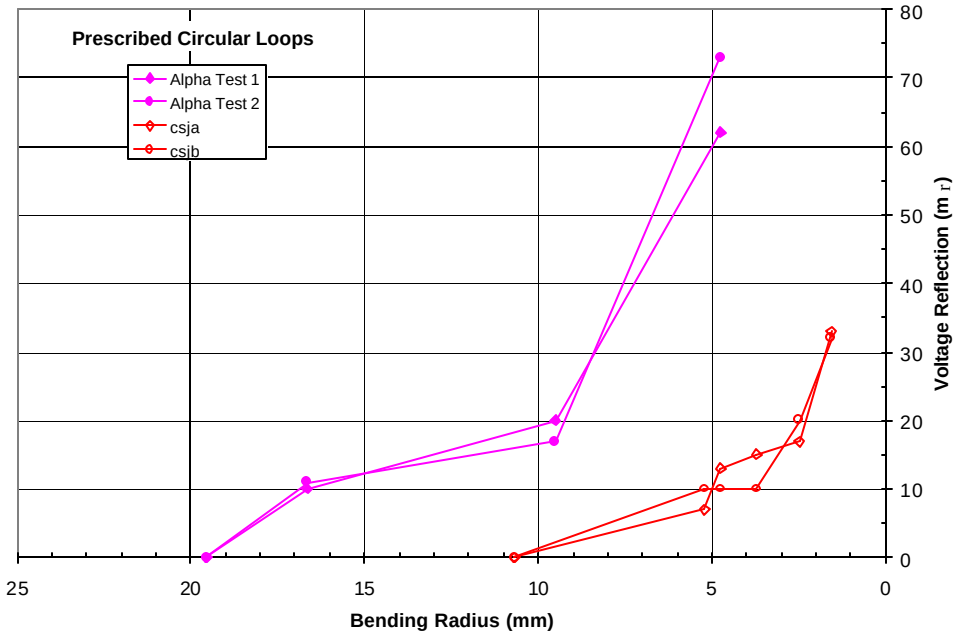

Fig. 6. *Voltage Reflections Measured by Prescribing a Circular Loop in Cables*

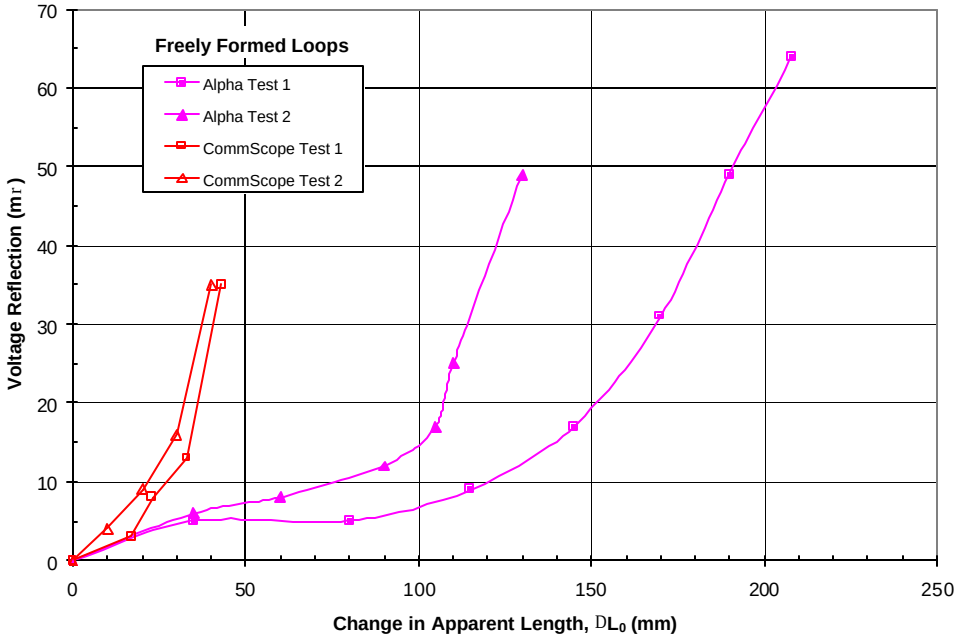

Fig. 7. *Voltage Reflections Measured by Pulling on Cables with a Single, Freely Formed Loop*

SUMMARY

This paper presents a concept for increasing the sensitivity of TDR cables to soil displacements by looping cables at fixed locations. To demonstrate this concept, laboratory tests were conducted on two flexible coaxial cables by prescribing circular loops and freely forming elliptical loops. Loops were formed at the cable's minimum bending radius, which was determined experimentally. The perimeter of the loop was progressively reduced to evaluate voltage reflection response. As the loop perimeter decreases, the apparent cable length directly increases. For both cables in both loop conditions, voltage reflection increases exponentially such that the change in reflection becomes more sensitive to the change in cable length. At least two tests with prescribed circular loops and freely formed elliptical loops were performed for each cable. Voltage reflection responses are relatively consistent, suggesting that the test methods are repeatable. The smaller-diameter cable, CommScope 2120k, has a smaller minimum bending radius and is more responsive (*i.e.*, more voltage is reflected) at smaller changes in cable length. The larger-diameter Alpha 9847 cable can measure larger changes in length simply because it has a larger minimum bending radius. The results suggest that small shear displacements occurring in relatively thick shear zones can be measured if cables are looped initially below the minimum bending radius.

ACKNOWLEDGMENTS

This research was funded by the National Science Foundation under NSF Award No. 9908342 and the University of South Carolina under Research Initiative Grant E155.

REFERENCES

CommScope Inc., 1998, Cable Products Catalog, Hickory, North Carolina, www.commscope.com.

Dowding, C.H. and Pierce, C.E., 1994, "Measurement of Localized Failure Planes in Soil with Time Domain Reflectometry," Proceedings of Symposium and Workshop on Time Domain Reflectometry in Environmental, Infrastructure, and Mining Applications, U.S. Bureau of Mines, Special Publication SP19-94, 569-578.

Dowding, C.H., Su, M.B. and O'Connor, K.M., 1989, "Measurement of Rock Mass Deformation with Grouted Coaxial Antenna Cables," Rock Mechanics and Rock Engineering, **22**, 1-23.

McAlister, C.M. and Pierce, C.E., 2001, "Calibration of Small-Diameter TDR Cables to Measure Displacement in Physical Soil Models," TDR2001, Proceedings of the Second International Conference on Civil Engineering Applications of Time Domain Reflectometry, Evanston, Illinois, 10 pp.

O'Connor, K.M., Peterson, D.E. and Lord, E.R., 1995, "Development of a Highwall Monitoring System using Time Domain Reflectometry," Proceedings of the 35th U.S. Symposium on Rock Mechanics, Reno, Nevada, 79-84.

Pierce, C.E., 1998, "Time Domain Reflectometry Measurements of Localized Soil Deformation," PhD Thesis, Northwestern University, Evanston, Illinois, 237 pp.

Environmental Monitoring

Using Time Domain Reflectometry for Non-Aqueous Phase Liquid Concentration Measurements
M. Persson, *Lund University, Sweden*

A TDR System for Subsurface Pollutants Detection (I): Design & Modeling
A. M. O. Mohamed, R. A. Said and N. K. AlShawawreh, *United Arab Emirates University, UAE*

A TDR System for Subsurface Pollutants Detection (II): Application & Analysis
A. M. O. Mohamed, R. A. Said and N. K. AlShawawreh, *United Arab Emirates University, UAE*

Time Domain Reflectometry for the Characterization of Diesel Contaminated Soils
D. Chenaf and N. Amara, *Royal Military College of Canada*

Use of TDR to Monitor Changes in Ground Water Level and Crude Oil Thickness
K. O'Connor, *GeoTDR , USA*

Measuring Water Table Elevations Within Pavement Systems Using Time Domain Reflectometry
R. Roberson and J. Siekmeier, *Minnesota Dept. Of Transportation*

Salinity compensation of a TDT Instrument Using Slope Correction
R. McFarlane, *Environmental Sensors Inc, Canada*

Back to Table of Contents

USING TIME DOMAIN REFLECTOMETRY FOR NON-AQUEOUS PHASE LIQUID SATURATION MEASUREMENTS

Magnus Persson

Department of Water Resources Engineering, Lund University,
Box 118, SE-221 00 Lund, Sweden; magnus.persson@tvrl.lth.se

ABSTRACT

During recent years, studies have used the apparent dielectric constant (K_a) measured by time domain reflectometry (TDR) for determining the saturation of non-aqueous phase liquids (θ_{NAPL}) in soils. The K_a has been related to θ_{NAPL} using dielectric mixing models. In the unsaturated zone, the water content (θ_w) had to be known (by assumptions or measured using other techniques) to utilize these models. In the present study, unlike previous research, detailed laboratory experiments were conducted to investigate the relationship between TDR measurements and θ_{NAPL}. Calibration was made in homogeneous sand using three different NAPLs. It was shown that the previously used mixing model led to errors up to 0.05 m^3 m^{-3} for saturated soils. In unsaturated soil, it was shown that measurements of only K_a can not be used for estimation of θ_{NAPL} even if θ_w is known. Instead, the TDRs capability of determining both K_a and bulk electrical conductivity (σ_a) was utilized to estimate θ_w and θ_{NAPL}.

INTRODUCTION

The widespread use of hydrocarbons (petroleum products, kerosene, etc) is an increasing environmental threat to natural resources such as soil and water. Organic pollutants like hydrocarbons are typically not mixing with water and they are therefore called non-aqueous phase liquids (NAPLs). The presence of NAPLs in the soil system complicates the transport equations since an additional phase is introduced. Furthermore, some NAPLs are volatile and can exist both in liquid and gas phase. Thus, modeling of NAPL transport in soils is a complicated task. Still, however, there is a lack of knowledge regarding basic transport processes occurring in the soil system contaminated by NAPLs (Ewing and Berkowitz, 1998). Most of the existing knowledge about NAPL transport in soils is based on numerical experiments and experimental studies are scarce. An important reason for this is the lack of efficient observation techniques of NAPL concentration. By introducing new observation techniques allowing for more

detailed spatial and temporal experimental data, this basic knowledge would improve and better predictive models could be developed.

The NAPLs are characterized by low dielectric constant and electrical conductivity compared to soil water. Thus, several geoelectrical measuring techniques have been used to measure NAPL concentration. Examples of this are ground penetrating radar, DC resistivity, and time domain reflectometry (TDR) (e.g., Redman *et al*., 1991). The use of TDR to measure the apparent dielectric constant K_a was introduced to geophysics by Topp *et al*., 1980. The K_a for wet soil is highly dependent on the volumetric water content (θ_w). Later, Dalton *et al*. (1984) showed how the attenuation of the TDR signal could be related to bulk electrical conductivity (σ_a).

Redman *et al*. (1991), Brewster *et al*. (1995), and Kueper *et al*. (1993) used K_a measured by TDR to estimate θ_{NAPL} in saturated soil. They took K_a readings before and after a controlled NAPL (tetrachloroethylene) spill. It was assumed that since K_a of water is about 80 and for NAPL 2.3, the decrease in bulk K_a could be used to determine θ_{NAPL}. In later studies, instead a dielectric mixing model was utilized for the calculation of θ_{NAPL} in saturated soil (Redman and DeRyck, 1994). The contaminated saturated soil is a three-phase system (soil matrix-water-NAPL). The contaminated unsaturated zone is, however, a four-phase system (soil matrix-air-water-NAPL), which makes θ_{NAPL} measurements impossible using only K_a if θ_w is unknown. DeRyck *et al*. (1993) used both TDR and neutron probe and could thus estimate both θ_w and θ_{NAPL}. They concluded that the sum of θ_w and θ_{NAPL} was fairly constant in the unsaturated zone for steady state conditions. Using this assumption, the decrease in K_a can be directly related to θ_{NAPL} also in unsaturated soil (Redman and DeRyck, 1994). In the above studies, TDR estimated θ_{NAPL} has shown similarities to θ_{NAPL} determined from soil cores. However, it appears that no controlled calibration experiments of the relation between θ_{NAPL} and K_a have been conducted. Thus, there is a great need for detailed studies of how the presence of NAPLs in the soil affects K_a and σ_a.

In the present paper I extend the above research on TDR to observe NAPLs in both saturated and unsaturated sand. The objective is to evaluate effects of different types of NAPLs on the TDR measurements and examine possibilities of using TDR for measurements of θ_{NAPL} for both saturated and unsaturated conditions. In contrast to earlier studies of TDR and NAPLs, however, I utilize the TDR´s capability of taking both K_a and σ_a measurements. I provide a hypothesis to explain the observed results and close with a discussion on how the results can be practically used in monitoring schemes of NAPL migration.

THEORY

Concepts of Dielectrics

The dielectric properties of a material can be described by the dielectric constant K^*. The dielectric constant consists of a real part K', and an imaginary part K'', or the electric loss. The dielectric constant can be expressed as

$$K^* = K' + j[K'' + (\sigma dc/\omega\varepsilon 0)] \quad [1]$$

where σ_{dc} is the zero-frequency conductivity, ω is the angular frequency, ε_0 is the free-space permittivity, and j is the imaginary number.

The TDR instrument sends a high frequency (20 kHz-1.5 GHz) electromagnetic step pulse through a transmission line of known length L, and the pulse is reflected back at the end of the line. By measuring the apparent length of the transmission line L_a calculated from the TDR trace, the dielectric constant can be estimated as

$$K^* = (L_a/L)^2 \qquad [2]$$

assuming $K'' << K'$, which is true for water at frequencies between 100 MHz and 3-4 GHz. The electrical loss in soils is normally small but it does affect the estimate of K^*. Therefore, the measured dielectric constant is called the apparent dielectric constant, K_a (Topp *et al*., 1980).

Dielectric Mixing Models

Several dielectric mixing models have been developed to estimate the dielectric properties of wet soils. The models calculate the bulk dielectric constant for the soil from the dielectric properties and the volume fractions of the soil components, e.g., water, air, and soil particles. The dielectric constant is about 80 for water, 2-5 for dry soil, and 1 for air. Thus, K_a is highly dependent on θ_w. In the theoretical de Loor model (de Loor, 1964), water is considered to consist of disk-shaped foreign inclusions embedded in a homogeneous isotropic dielectric medium, the mineral phase. The de Loor model contains no calibration parameter and has been successfully applied to determine K_a of soils in several studies (Jacobsen and Schjønning, 1995). Redman and DeRyck (1994) used the law of Bruggeman, Hanai, Shen, and Sen (BHSS) (e.g., Sen *et al*., 1981) for calculating K_a of NAPL contaminated soil. This is a geometrical model in which the shape of the inclusion is accounted for using a depolarisation factor. Normally, spherical inclusion is assumed.

The most commonly used mixing model in TDR applications is the model presented by Birchak *et al*. (1974). Birchak *et al*. (1974) suggested a semi-empirical α-model

$$K_a^{\ a} = \sum_i q_i K_i^a \qquad [3]$$

where θ_i and K_i are the volume fraction and the dielectric constant of component i, respectively, and α is an empirical parameter accounting for soil geometry. The value of α is in the range of -1 to 1. These extreme values represent a perfectly layered medium where the electric field is parallel (α=1) or perpendicular (α=-1) to the layering. Birchak *et al*. (1974) found that α=0.5 for an isotropic medium. Thus, the α value summarizes the geometry of the medium in relation to the applied electric field. For a three-phase system including air, water, and soil particles, it has been shown that the average value of α is about 0.5 with a range from 0.46 to 0.67 (Jacobsen and Schjønning, 1995). For a four-phase system, which also includes bound water, the α value ranged from 0.39 to 0.81 (Jacobsen and Schjønning, 1995).

In the present study, a four-phase dielectric mixing model was used to calculate K_a of the soil according to

$$K_a^{\ a} = q_s K_s^a + q_w K_w^a + q_{NAPL} K_{NAPL}^a + q_{air} K_{air}^a \quad [4]$$

where subscript *s* stands for the mineral phase (soil particles).

Electrical Conductivity Measurements using TDR

Attenuation of the TDR signal can be used to determine σ_a. Following the thin sample approach by Gise and Tiemann (1975), σ_a can be described by

$$\sigma_a = K_p f_T / Z_L \quad [5]$$

where Z_L is the impedance load of the transmission line (in Ω) measured after a long time, f_T is a temperature correction coefficient, K_p is the cell constant of the TDR probe, a calibration constant that can be determined by immersing the probe in solutions with known conductivity.

In general, the σ_a of the soil depends mainly on three variables, (*i*) the effective volumetric water content $\theta_w - \theta_0$, where θ_0 is a correction factor accounting for water close to the solid particles which can be considered immobile (θ_0 can be neglected in coarse textured soils like the sand used in this study), (*ii*) the electrical conductivity of the soil solution (σ_w), and (*iii*) a geometry factor, accounting for the complex geometry of the soil matrix. The σ_a is also affected by the surface conductivity of the soil matrix σ_s. For unsaturated soils Rhoades *et al*. (1976) described σ_a as

$$\sigma_a = \sigma_w \theta_w T(\theta_w) + \sigma_s \quad [6]$$

where $T(\theta_w)$ is the transmission coefficient accounting for the tortuosity of the current flow. Rhoades *et al*. (1976) proposed a linear relationship between $T(\theta_w)$ and θ_w, i.e., $T(\theta_w) = a\theta_w + b$, where *a* and *b* are soil specific parameters. Other models for the σ_a-σ_w-θ_w relationship have also been developed (see e.g., Persson, 1997), however, in this study only (6) was used since it accurately modeled the σ_a-σ_w-θ_w relationship for the sand used.

MATERIALS AND METHODS

TDR System

TDR measurements were carried out using a Tektronix 1502C cable tester with an RS232 interface connected to a laptop computer. Estimates of K_a and σ_a were calculated from the TDR trace using the WinTDR program (developed by the Soil Physics Group at Utah State University). A three-rod probe was used, 0.1 m in length, a wire diameter of 0.003 m, and a wire spacing of 0.05 m (Soilmoisture Equipment Corp., Santa Barbara, CA). The TDR probe was calibrated using the calibration utility of the WinTDR program and was found to accurately measure K_a in air, ethanol, methanol, and water, and σ_a in salt solutions containing KBr with σ_w ranging from 0.01-4.0 dS m^{-1}.

TDR Measurements in Soil Containing Water and NAPL

The influence of NAPLs on the TDR measurements was investigated in homogeneous silica sand with a uniform particle size of 0.001 m. Properties of this sand are presented in Table 1. Three types of NAPLs were used in the experiments, sunflower seed oil, SFSO, (K_a=3.06), a synthetic motor oil, MO, (K_a=2.66), and n-paraffin, NP, (K_a=2.32). However, most measurements were made using SFSO since it is non-volatile and non-toxic. To have a stable background σ_w, distilled water containing 2 g KBr L^{-1} (σ_w=2.42 dS m^{-1}) was used in all experiments. Known amounts of water, sand, and NAPL were mixed and packed into Plexiglas boxes (0.12 by 0.07 by 0.05 m) to a bulk density of 1.56 Mg m^{-3}. These boxes contain the entire measurement volume of the 0.1 m TDR probe (Persson and Berndtsson, 1998b). Immediately after packing, the probe was inserted vertically into the sand.

For the calibration data series, θ_{NAPL} varied from 0 to 0.35 m^3 m^{-3} with an increment of 0.05 m^3 m^{-3} and θ_w from 0 to close to saturation θ_{sat} resulting in totally 43 combinations. The increment in θ_w was 0.02-0.08 m^3 m^{-3}. Another 25 combinations of θ_w and θ_{NAPL} were also prepared to get an independent data set for validation. In each mixture of soil, water, and NAPL, at least 10 measurements were taken and averaged within one hour after packing. Some samples were kept for several days to examine effects of redistribution of water within the sample. The temperature was fairly constant throughout the measurements, however, to achieve high accuracy, temperature corrections of σ_a were made.

Property	Value	Unit
Particle diameter	0.001	m
Particle density	2.62	Mg m^{-3}
Bulk density	1.56	Mg m^{-3}
Porosity	0.405	m^3 m^{-3}
Dielectric constant (K_s)	4.27	-

Table 1. *Properties of the sand used.*

To examine the effects of the distribution of NAPLs within the TDR sampling volume, two sand-water-NAPL samples in the validation data series were prepared in a different way. In these, the lower half of the Plexiglas box contained a sand and water mix, while the upper half contained a sand and SFSO mix. These samples are referred to as the layered samples. TDR measurements were taken, then the volume content was mixed like in the other samples and measurements were taken again. The θ_{SFSO} and θ_w used in these samples were θ_{SFSO}=θ_w=0.05 and θ_{SFSO}=θ_w=0.10 m^3 m^{-3}.

RESULTS AND DISCUSSION

Influence of NAPLs on TDR Measurements

The presence of NAPLs in the soil clearly affected the TDR measured K_a and σ_a. In general σ_a decreased as θ_{NAPL} increased at constant θ_w. The effect of θ_{NAPL} on K_a at constant θ_w was not as expected from the dielectric mixing model (4). When NAPLs were present, (4) always overestimated the K_a if α was kept constant.

Since most measurements were made with SFSO, these data were analyzed first. When θ_{NAPL} was kept constant and θ_w varied from 0 to (θ_{sat}-θ_{NAPL}) the variation in σ_a and K_a could be described by (4) and (6) with a modified parameter set. Thus, each set of data with constant θ_{NAPL} was analyzed separately. The

θ_w-K_a relationship was determined using the four-phase Birchak *et al*. (1974) dielectric mixing model (4) with α as calibration parameter. The K_w was calculated using the measured temperature to minimize temperature errors (Persson and Berndtsson, 1998a). The α value decreased significantly when θ_{NAPL} increased (Table 2).

θ_{NAPL}	(4)		(6)			
[m^3 m^{-3}]	α	r^2	A	B	σ_s	r^2
0	0.4773	0.9955	2.31	0.55	-0.013	0.9860
0.05	0.4168	0.9925	2.60	0.29	-0.001	0.9948
0.10	0.3647	0.9801	1.97	0.34	-0.004	0.9852
0.15	0.3424	0.9957	2.59	0.00	0.007	0.9972
0.20	0.3106	0.9753	2.37	-0.03	0.008	0.9741
0.25	0.2962	0.9783	0.63	0.16	0.006	0.9649
0.30	0.2598	0.9890	0.10	0.21	0.009	0.9969

Table 2. *Parameters for (4) and (6) and their dependency on q_{NAPL}.*

In Figure 1, the K_a determined using (4) with α values presented in Table 2 at θ_w of 0.1 m^3 m^{-3} is plotted against θ_{NAPL} together with observed values. In this figure the K_a calculated using a constant α value (0.4773) is also presented. The de Loor model will always give an increasing K_a when air is replaced by NAPL. Thus, this model was not further analyzed. The BHSS model was also applied to the data, but this model consistently overestimated K_a if spherical inclusion was assumed. If the depolarization factor instead is used as a fitting parameter, the BHSS model can probably be used in a similar way as the Birchak model. However, because of the simplicity of (4) and the wide use of this model in TDR applications, only (4) was evaluated in detail.

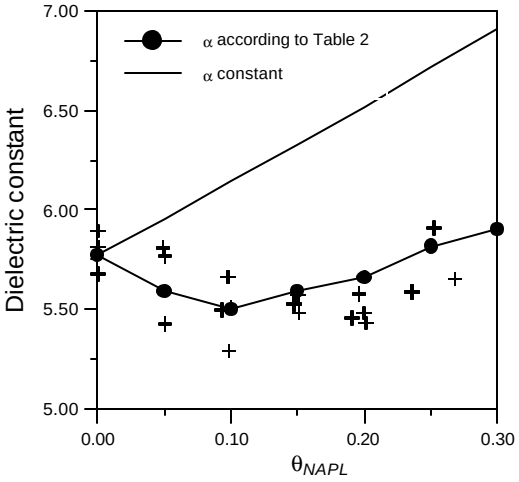

Fig. 1. *The measured K_a vs. known q_{NAPL} at q_w=0.1 m^3 m^{-3}. The lines represent (4) with a constant a and with the a values from Table 2, respectively. Note that each measured value is the average of at least 10 measurements in the same sample.*

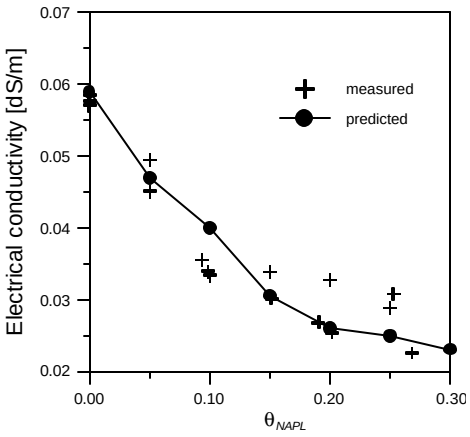

Fig. 2. *The measured s_a vs. known q_{NAPL} at q_w=0.1 m^3 m^{-3}. The dotted line represents (6) with fitted parameter values from Table 2. Note that each measured value is the average of at least 10 measurements in the same sample.*

From Figure 1 it can be seen that the scatter in K_a is rather large compared to the changes in K_a induced by the presence of NAPL. This can be explained by the relatively short probe used in this study, since the sensitivity of the probe towards changes in K_a is proportional to the length of the probe. In future studies I recommend that longer probes should be used to avoid this problem.

The σ_a-θ_w relationship was determined for each θ_{NAPL} using (6). The resulting parameters are shown in Table 2. In Figure 2, measured and predicted values by (6) using the parameters in Table 2 for θ_w=0.1 m^3 m^{-3} are presented.

From the results presented above, it is obvious that both σ_a and K_a are needed for determining θ_w and θ_{NAPL} in unsaturated soils. If a relationship between σ_a and K_a is established, the TDR measured σ_a and K_a can be used for θ_w and θ_{NAPL} estimations in any sand-air-water-NAPL mixture. Using both (4) and (6) with the parameters for each θ_{NAPL}, the relationship between σ_a and K_a can be determined. The result is presented in Figure 3. For clarity, only the σ_a-K_a relationships for θ_{NAPL}=0 and θ_{NAPL}=0.1 m^3 m^{-3} are presented together with the observed data for θ_{NAPL}=0.1 m^3 m^{-3}. In the figure, the σ_a-K_a relationship for saturated conditions is also presented. This curve was obtained by extrapolation of (4) and (6) for each θ_{NAPL} so that $\theta_w+\theta_{NAPL}=\theta_{sat}$, and then fitting a third-order polynomial to the data (r^2=0.99).

The three different NAPLs examined had similar effects on the TDR measurements. The calibrated α for NP was slightly larger than for SFSO for the same θ_{NAPL} but lower for MO. The relationship between σ_a and K_a for NP was not significantly different from SFSO. However, using MO the σ_a was considerably smaller than for SFSO at low θ_w. At higher θ_w, the relationship between σ_a and K_a was close to the one for SFSO.

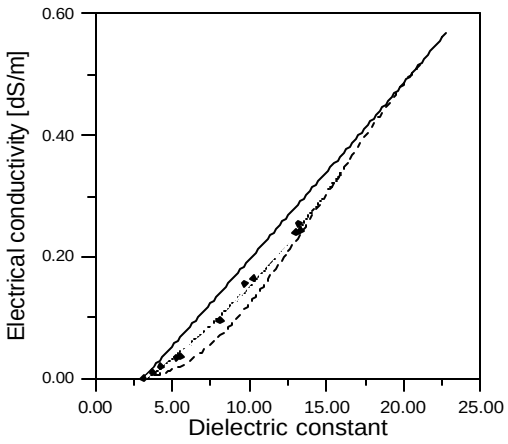

Fig. 3. *K_a vs. s_a. The solid and dotted lines represent the relationship between K_a and s_a when q_{NAPL}=0 and q_{NAPL}=0.1 m^3 m^{-3} respectively. The dashed line represents saturated conditions, i.e., $q_{NAPL}+q_w=q_{sat}$. The points are the measured values at q_{NAPL}=0.1 m^3 m^{-3}. Note that each measured value is the average of at least 10 measurements in the same sample.*

For each sample both the average and standard deviation of the TDR measurements were calculated. The average standard deviation for all samples was 0.03 and 0.003 for K_a and σ_a (in dS m^{-1}), respectively. When samples was left to redistribute for several days, only minor changes in K_a and σ_a were noted.

Explanation of the trend in s_a and q_w with q_{NAPL}

In this section I present a hypothesis that could explain how NAPLs affect TDR measurements. The presented data support the below hypothesis but further experiments are needed. The decreasing α in (4) with increasing θ_{NAPL} can be physically interpreted. The distribution of the four dielectrics (soil particles, air, water, and NAPL) is changing from totally random towards a more layered pattern where layer boundaries are crossed by electrical field lines of the electrostatic field arising between the probe rods. There is probably no change in the distribution of soil particles, and the air will still be located in the largest non-wetted pores. This means that the change in α is likely to be associated with the interaction between water and NAPL. Another observation is that the α value is independent of

θ_w for a given θ_{NAPL}. This indicates that the examined NAPLs tend to concentrate in macro inclusions as soon as the water is present in the soil and the shape and size of these inclusions seem to be independent of θ_w. The average size of the inclusions increases with θ_{NAPL}. As a consequence of the non-homogeneous NAPL distribution and the repulsion between the two liquids, water will also be increasingly non-homogeneously distributed as θ_{NAPL} increases.

The decreasing σ_a with increasing θ_{NAPL} at constant θ_w corroborates the NAPL-water inclusion theory. It is evident that a redistribution of the water takes place when NAPLs are present. If the NAPLs only entered the air filled pores, the major conductivity arising from ions present in the soil water would remain unchanged. Instead, however, the presence of NAPL inclusions increases the tortuosity of the electrical current flow path through the soil and in some cases disrupt flow paths existing prior to the application of NAPLs.

Estimation of NAPL Concentration in Saturated Soil

In Figure 3 it can be seen that both K_a and σ_a are unique functions of θ_w and θ_{NAPL} at saturated conditions. In Figure 4, K_a at saturated conditions is plotted against θ_{NAPL}. Note that in this figure, the K_a is calculated from θ_{NAPL} using the α value corresponding to that θ_{NAPL}. In the previous approach suggested by Redman and DeRyck (1994), this was not accounted for. This is done by keeping the α-value constant and equal to the value when θ_{NAPL}=0. This approach is also presented in Figure 4. The error in θ_{NAPL} using the previous approach can be up to 0.05 m^3 m^{-3}. The σ_a measurement can also be related to θ_{NAPL}. The σ_a-θ_{NAPL} relation for saturated conditions is presented in Figure 5. The decreasing σ_a is attributed to both the decreasing θ_w and the increasing tortuosity when θ_{NAPL} increases. Thus, relating σ_a to θ_{NAPL} in groundwater using TDR or any other geoelectrical method seems to be an efficient approach.

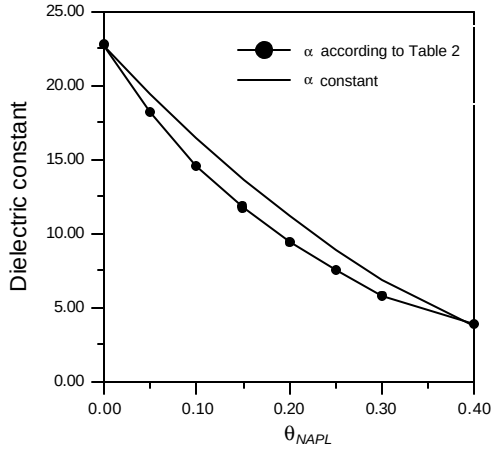

Fig. 4. *The dielectric constant vs. q_{NAPL} using the a values from Table 2, and for a constant a for saturated conditions, i.e., $q_{NAPL}+q_w=q_{sat}$.*

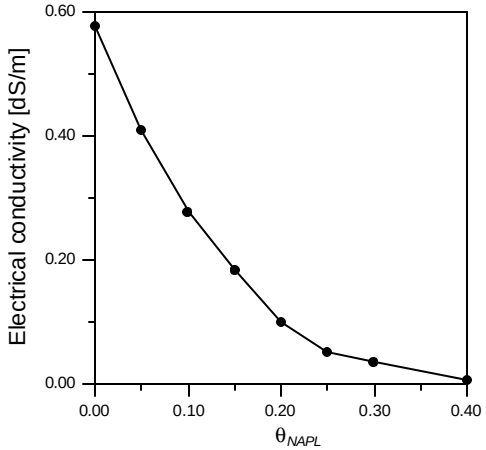

Fig. 5. *Electrical conductivity vs. q_{NAPL} at saturated conditions, i.e., $q_{NAPL}+q_w=q_{sat}$.*

Estimating NAPL Concentration in Unsaturated Soil

Looking at Figure 1, it is interesting to note that K_a is not a unique function of θ_{NAPL} even if θ_w is known. Thus, it is not possible to measure θ_{NAPL} in unsaturated soils using the TDR determined K_a only. If we instead look at Figure 3, each pair of measured K_a and σ_a are related to a pair of θ_w and θ_{NAPL}. A three-dimensional second-order surface was thus fitted to the σ_a-K_a-θ_w relationship. Using this surface, any combination of K_a and σ_a yields a θ_w. In Figure 6, the known θ_w is plotted against the θ_w calculated using this surface (r^2=0.995).

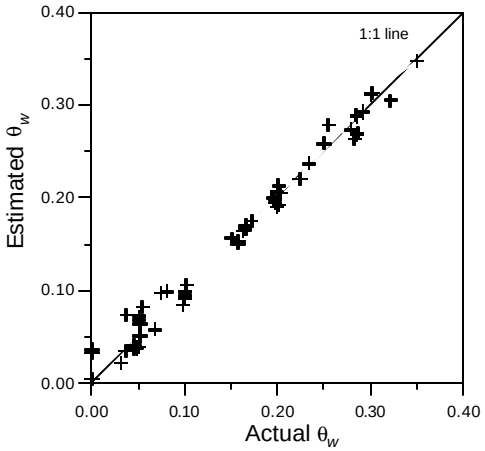

Fig. 6. *Measured vs. known water content. The measured q_w was calculated using $q_w=0.0338*K_a+0.0002*K_a^2+0.1523*s_a+1.2888*s_a^2-0.0701*K_a*s_a-0.093$.*

A similar function was calculated for the σ_a-K_a-θ_{NAPL} data. The fit was good, but this approach was very sensitive to small changes in σ_a. Instead an alternative two-step approach was utilized. First, I used (4) and solved it for θ_w. The resulting expression was inserted into (6). The measured K_a was then used in the combined equation using the different parameters for values of θ_{NAPL} in Table 2. Now, for every given K_a, σ_a can be calculated for θ_{NAPL} from Table 2. Next, the measured σ_a was used to calculate the θ_{NAPL} by interpolating between the two closest σ_a. The result is presented in Figure 7, where actual vs. calculated θ_{NAPL} are plotted. The calculated θ_{NAPL} is normally within a few m^3 m^{-3} of the actual θ_{NAPL} (r^2=0.922, root mean square error=0.031 m^3 m^{-3}). There was a slightly decreasing trend in the residual of the θ_{NAPL} estimation when plotted against θ_{NAPL}. That is, the relative error in the θ_{NAPL} estimation was larger when θ_{NAPL} was low.

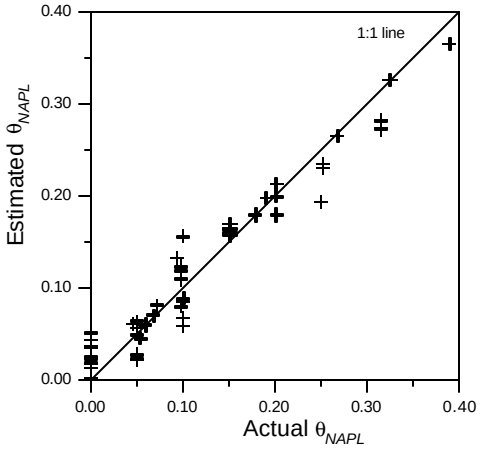

Fig. 7. *Measured vs. known q_{NAPL}. The measured q_w was calculated from the K_a and s_a measurements using the two-step approach described in the text.*

Effects of the Distribution of NAPLs within the Sampling Volume

Another important issue is how NAPLs distribute in the soil within the sample area (*A*) perpendicular to the long axis of the probe rods. The calibration experiments conducted in mixed samples of soil, air, water, and NAPL indicated that both water and NAPL condensed in some macro inclusions depending on the NAPL concentration. A change in the distribution of dielectrics within *A* results in a change of the weighting function determining the weight a given dielectric is contributing to the total, or effective, K_a. Baker and Lascano (1989), e.g., showed that the TDR sampling volume is concentrated between the probe rods with the greatest sensitivity close to the rods. That is, although the area occupied by various dielectrics within *A* is unchanged, their position has a great influence on K_a. This is the reason why α

decreased with increasing θ_{NAPL} and why K_a decreased although air was substituted by NAPL. The mixed samples represent the NAPL distribution in residual phase. These samples are macroscopically homogeneous, i.e., water and air are distributed evenly within the pore space, but the NAPL exists in larger inclusions. As long as the NAPL inclusions are distributed homogeneously within *A* the method presented above will give accurate θ_{NAPL} and θ_w estimations. During NAPL transport in soils the NAPL can also exist in a continuous non-wetting phase occupying a fraction of the wetted pore space. When a part of the TDR sample volume contains a continuous NAPL phase, the location of this with respect to the orientation of the TDR probe becomes important. The two layered samples represent the case when the upper half of the TDR sampling volume contains a continuous NAPL phase and the lower half a continuous water phase. In these both samples, θ_w was slightly over-estimated and θ_{NAPL} slightly under-estimated when they were calculated using the methods described above. However, these errors were less than about 0.02 m^3 m^{-3}. The K_a and σ_a can be calculated theoretically, however, for a specific case. This is when the center of the TDR rods are located at the boundary between the water and NAPL phases. For this case, the K_a and σ_a were calculated as the geometrical average of K_a and σ_a of the respective phase (see Persson and Berndtsson, 1998b). When the resulting K_a and σ_a were used for calculating θ_w and θ_{NAPL}, the θ_w was slightly overestimated but the θ_{NAPL} was significantly underestimated. These results indicate that the approach presented is best suited for θ_{NAPL} determination when the NAPL exists mainly in residual phase. In migration experiments the method could also work if the NAPL front is passing the probe perpendicular to the long axis of the probe rods.

SUMMARY

The use of TDR to simultaneously measure θ_{NAPL} and θ_w in both saturated and unsaturated soil was examined. Earlier studies have only used the TDR measured K_a when calculating θ_{NAPL}. Unlike these studies, the TDR´s capability of taking both K_a and σ_a measurements was utilized in the present paper. In a previous approach (Redman and DeRyck, 1994), a dielectric mixing model was used for estimating θ_{NAPL}. The previous approach suggested a constant α value in the model by Birchak *et al*. (1974). Contrary to this, our results show that the α value is depending on θ_{NAPL}. It was shown that for the sand studied, the previous approach leads to errors up to 0.05 m^3 m^{-3}. In the saturated zone, both K_a and σ_a can be related to θ_{NAPL}. In the unsaturated zone, the TDR measured K_a can not be used for calculations of θ_{NAPL} even if θ_w is known. However, by using observed σ_a and K_a as described in this study, both θ_w and θ_{NAPL} can be estimated. The fit between measured and calculated data was good with r^2 values of 0.987 and 0.922 for θ_w and θ_{NAPL}, respectively. However, since the approach requires detailed calibration data for the K_a-θ_w and σ_a-θ_w relationships for a wide range in θ_{NAPL}, and a constant background σ_w, it might currently be restricted to controlled laboratory experiments in homogeneous materials.

Another problem inherent in the method presented is that θ_{NAPL} is strongly dependent on σ_a. Whereas a redistribution of a certain amount of NAPL and water within the sampling volume has some effect on K_a, the effect on σ_a can be much larger. For example, a concentration of NAPL around one of the rods will make it increasingly difficult for the current to pass through the soil. In conclusion, a NAPL distribution significantly different from the one experienced during the calibration will to some extent influence θ_w, but the influence on θ_{NAPL} is expected to be far greater.

Further studies are needed to examine the relationship between θ_{NAPL} and TDR measurements in different soil types using different NAPLs. The developed approach for measuring θ_w and θ_{NAPL} in unsaturated soil could be used in laboratory experiments of NAPL transport.

ACKNOWLEDGEMENTS

This study was funded by the Swedish Research Council for Engineering Sciences and the Swedish Natural Science Research Council. Equipment was purchased through grants from the Crafoord and Lundberg Foundations.

REFERENCES

Baker, J. M., and Lascano, R. J., 1989, The spatial sensitivity of time domain reflectometry: Soil Sci., **147**, 378-384.

Birchak, J. R., Gardner, C. G., Hipp, J. E., and Victor, J. M., 1974, High dielectric constant microwave probes for sensing soil moisture: IEEE **62**, 93-98.

Brewster, M. L, Annan, A. P., Greenhouse, J. P., Kueper, B. H., Olhoeft, G. R., Redman, J. D., and Sander, K. A., 1995, Observed migration of a controlled DNAPL release by geophysical methods: Ground Water, **33**, 997-987.

Dalton, F. N., Herkelrath, W. N., Rawlins, D. S., and Rhoades, J. D., 1984, Time-domain reflectometry: Simultaneous measurements of soil water content and electrical conductivity with a single probe: Science, **224**, 989-990.

De Loor, G. P., 1964, Dielectric properties of heterogeneous mixtures: Appl. Sci. Res., **B3**, 479-482.

DeRyck, S. M., Redman, J. D., and Annan, A. P., 1993, Geophysical monitoring of a controlled kerosene spill: in Proceedings of the Symposium on the Application of Geophysics to Engineering and Environmental Problems, San Diego, California, 21-38.

Ewing, R.P., and Berkowitz, B., 1998, A generalized growth model for simulating initial migration of dense non-aqueous phase liquids: Water Resour. Res., **34**, 611-622.

Gise, K., and Tiemann, R., 1975, Determination of the complex permittivity from thin-sample time domain reflectometry, improved analysis of the step response waveform: Adv. Mol. Relax. Processes, **7**, 45-49.

Jacobsen, O. H., Schjønning, P., 1995, Comparison of TDR calibration functions for soil water determination: In L.W. Petersen and O.H. Jacobsen (ed.) Proceedings of the symposium: Time-domain reflectometry applications in soil science, Research Centre Foulum, Denmark, Sep. 16. 1994, SP report no. 11 vol. 3, pp. 25-33, Danish Institute of Plant and Soil Sci., Lyngby, Denmark.

Kueper, B. H., Redman, D., Starr, R. C., Reitsma, S., and Mah, M., 1993, A field experiment to study the behavior of tetrachlorethylene below the water table: spatial distribution of residual and pooled DNAPL: Ground Water, **31**, 756-766.

Persson, M., 1997, Soil solution electrical conductivity measurements under transient conditions using time domain reflectometry: Soil Sci. Soc. Am. J., **61**, 997-1003.

Persson, M., and Berndtsson, R., 1998a, Texture and electrical conductivity effects on temperature dependency in time domain reflectometry: Soil Sci. Soc. Am. J., **62**, 887-893.

----------, 1998b, Noninvasive water content and electrical conductivity laboratory measurements using time domain reflectometry: Soil Sci. Soc. Am. J., **62**, 1471-1476.

Redman, J. D., Kueper, B. H., and Annan, A. P., 1991, Dielectric stratigraphy of a DNAPL spill and implications for detection with ground penetrating radar: Aquifer restoration, ground water monitoring and geophysical methods, 5th national outdoor action conf, 1017-1030.

Redman, J. D., and DeRyck, S. M., 1994, Monitoring Non-Aqueous Phase Liquids in the Subsurface with Multilevel Time Domain Reflectometry Probes, Proceedings of the Symposium on Time Domain Reflectometry in Environmental, Infrastructure, and Mining Applications, Evanston, Illinois, Sept 7-9, U.S. Bureau of Mines, Special Publication SP 19-94, NTIS PB95-105789, 207-215.

Rhoades, J. D., Raats, P. A., and Prather, R. J., 1976, Effects of liquid-phase electrical conductivity, water content, and surface conductivity on bulk soil electrical conductivity: Soil Sci. Soc. Am. J., **40**, 651-655.

Sen, P. N., Scala, C., and Cohen, M. H., 1981, A self-similar model for sedimentary rocks with application to the dielectric constant of fused glass beads: Geophysics, **50**, 692-704.

Topp, G. C., Davis, J. L., and Annan, A. P., 1980, Electromagnetic determination of soil water content: Measurements in coaxial transmission lines: Water Resour. Res. **16**, 574-582.

A TDR SYSTEM FOR SUBSURFACE POLLUTANTS DETECTION (I): DESIGN & MODELING

R. A. Said[1], N. K. AlShawawreh[2], A. M. O. Mohamed[3]

[1]Electrical Engineering Department, United Arab Emirates University,
P.O. Box: 17555, Al Ain, United Arab Emirates, rasaid@uaeu.ac.ae
[2]Electrical Engineering Department, United Arab Emirates University,
P.O. Box: 17555, Al Ain, United Arab Emirates
[3]Civil Engineering Department United Arab Emirates University,
P.O. Box: 17555, Al Ain, United Arab Emirates, Mohamed@uaeu.ac.ae

ABSTRACT

This work presents the development of a TDR system for in-situ detection of subsurface pollutants. The developed system is simple to implement using a typical pulse generator, with a repetition rate of 8 MHz and a pulse width of 10ns, and a conducting probe connected via a transmission line (coaxial cable). The system probe is designed to match its input impedance to that of the used transmission line connecting the pulse generator and the probe. This improved the system performance since reflected pulses in this case are due to detected materials and not from mismatches at the probing end. On operation, the pollutant concentration in the soil is detected by measuring and analyzing the variation of soil-pollutant dielectric properties as a function of concentration of the pollutant in the soil. The developed TDR detection system is modeled by electrical parameters using transmission line theory. The modeled system is simulated by an electrical circuit simulator and the electrical parameters were optimized via the determined experimental data and the developed model. Based on the optimized parameters (resistance and capacitance), a criterion is developed in order to quantify pollutant concentration in subsurface soil.

INTRODUCTION

Recently, several researchers have discussed the large potentials of the use of electrical detection techniques for measuring tracer movements in laboratory as well as in field conditions (Kachanoski *et al*., 1992; Wraith *et al*., 1993; Vanclooster *et al*., 1993; Mallants *et al*., 1994; Ward *et al*., 1994). These electrical detection methods operate by analyzing the characteristics of a fast rising electric potential signal as it reflects at the probing end of a transmission line (coaxial cable for example) immersed in a sample under investigation. The characteristics of the reflecting signal are highly influenced by the electrical properties of the specimen, which are dependent on the concentration of the constituents.

A common application of the electrical detection principle is the time-domain-reflectometry (TDR) that is widely used as a concentration detection technique. TDR enables the measurement of total resident concentration from both mobile and immobile water regions for a sample volume with a well-defined geometry. TDR allows data collection of both moisture content and salt concentration at a high spatial and temporal resolution. Automation of TDR has made it even more powerful for use in the laboratory and even more so in field application at remote sites (Heimovaara & Bouten, 1990).

Application of TDR in the area of contaminant hydrology has been reported (Vanclooster *et al*., 1995; Mallants *et al*., 1994; Ward *et al*., 1994; Vanclooster *et al*., 1993; Kachanoski *et al*., 1992; Elrick *et al*., 1992). Most of these studies were carried out on sandy or loamy favorable conditions allowed the researchers to adopt simple hypotheses for water flow and solute transport. The success or failure of TDR technique to accurately predict solute concentration is heavily depends on the appropriateness of the calibration procedure used (Mohamed *et al*., 2000). Application of TDR in the area of pollutant detection in subsurface has yet to be developed due to the nature of the flow and the characteristics (signature) of each pollutant.

This paper discusses the design aspects of a developed TDR system for detecting and monitoring subsurface pollutants concentration. The system operation is demonstrated by experimental measurement of concentration of NaCl solution. A circuit model of the system operation is developed based on transmission line theory. The developed model is verified by simulating different measurement cases that are compared against experimental results. The simulation results are used to extract pollutant signature characterization.

TDR PRINCIPLE OF OPERATION

The schematic diagram shown in Fig. 1 illustrates a typical TDR arrangement for subsurface detection. A monitoring probe is connected to a pulse generator and to an oscilloscope via a transmission line (co-axial cables). The oscilloscope is used to acquire the system response through a measurement point on the transmission line. During measurement, an electrical pulse with a fast rising edge is generated periodically by the pulse generator and launched toward the probe. The pulse signal propagating toward the probe appears on the oscilloscope as it passes a measurement point located at distance L_G from the generator on the transmission line. As the pulse reaches the probe end it reflects back on the transmission line with pulse characteristics dependent on the properties of the media surrounding the probe. The reflected pulse signal propagates back toward the generator and thus appears on the oscilloscope after a delay time, t_r, with respect to the time of appearance of the original pulse. The delay time, t_r, is representative to the distance traveled by the pulse from the measurement point to the probe end, L_P, and back to the measurement point. Also contributing to the time delay, t_r, is the electrical characteristics of the media surrounding the probe.

In general, a signal traveling through a transmission line propagates with a velocity v that can be expressed as:

$$v = \frac{1}{\sqrt{LC}} \qquad [1]$$

where L is the transmission line inductance per unit length and C is its capacitance per unit length.

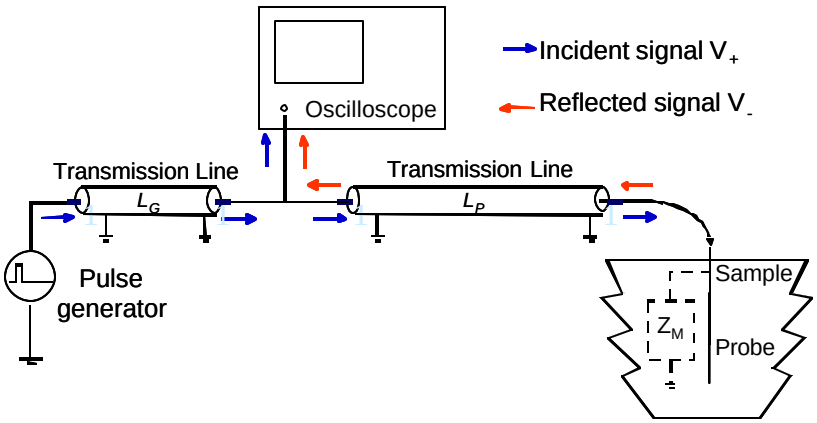

Fig. 1. *A schematic diagram of a typical TDR arrangement for subsurface detection.*

The capacitance and inductance of a transmission line are generally expressed in terms of its characteristic impedance Z_0 as:

$$Z_0 = \sqrt{\frac{L}{C}} \qquad [2]$$

Using eqs. (1) and (2), the velocity of a propagating signal can be written as:

$$v = \frac{1}{Z_0 C} \qquad [3]$$

Thus, the propagation velocity of a traveling signal is a function of the media electrical characteristics, Z_0 and C.

On operation, an incident pulse signal launched by the pulse generator will travel the distance L_G before appearing on the oscilloscope at the test point as indicated in Fig.1. As the incident pulse reaches the test node the pulse splits into two pulses that continue to propagate on the two branches represented by the oscilloscope as one branch and the transmission line with the probe as the other branch. The split pulse voltage distributes on the two branches according to their impedances ratio at the test point. Thus, the incident pulse propagating toward the oscilloscope will appear after a travel time t_i that can be expressed as:

$$t_i = \frac{L_G}{v_i} \qquad [4]$$

where v_i is the propagation velocity of the incident pulse through the transmission line. Using the expression for the propagation velocity in eq. (3), the travel time t_i can be written as:

$$t_i = L_G Z_L C_L \qquad [5]$$

where Z_L is the characteristic impedance of the used transmission line and C_L is its capacitance per unit length.

The other part of the incident pulse propagates toward the probe end and reflects back on the transmission line as it reaches the probe end. On its way back, the reflected signal is detected on the oscilloscope at the measurement point after a delay time t_r measured from the instant of incident pulse appearance on the oscilloscope and the reflected pulse appearance. This time delay t_r is contributed by the traveled distance $2L_P$, as well as the characteristics of the media surrounding the probe at the end of the transmission line. The later can be represented by a terminating impedance Z_M. Thus the delay time, t_r, can be expressed as:

$$t_r = 2L_P Z_{LM} C_{LM} \qquad [6]$$

where Z_{LM} and C_{LM} are the total per unit length impedance and capacitance of the transmission line with a terminating impedance Z_M at the end of the line. The terminating impedance Z_M at the line end represents the combined impedance of the probe and the surrounding media.

Since materials, in general, have different electrical characteristics, the presence of different species in the media surrounding the probe will result in different values of Z_M and Z_{LM}, and consequently will result in different responses of the system for each material. Even the different concentrations of each material will result in corresponding responses of the system, thus enabling to distinguish different concentrations of different materials. For example, changing the material properties (like adding an electrolyte solution) will tend to change the response profile significantly. If the medium around the probe is highly conductive, then most of the pulse will be absorbed and nothing will be reflected back. On the other hand, when the medium has low conductivity then, most of the pulse will be reflected toward the scope meter. Electrically, as conductivity increases, medium resistance decreases. Knowing the resistance of the medium enables one to quantify its ionic concentration in the area around the testing probe.

SYSTEM DESIGN

For proper operation of a TDR system and accurate measurements, it is necessary that pulse reflection occur only at the probe end to extract the parameters of material surrounding the probe. Pulse reflection can occur at system nodes located at interfaces between different parts such as adaptors, connectors, and input/output terminals of the devices used in the system. This is caused by mismatched impedances of parts at both sides of a node. Thus, in the design of a TDR system, the terminal impedances of the different parts should be matched to eliminate multiple reflections. Using devices with standard input/output impedances, such as 50 Ω or 75 Ω, reduces impedance matching requirements. The monitoring probe, however, is usually a custom design and in many instances is not designed with terminal impedance in consideration. The following discusses the design of monitoring probe with terminal impedance matching that of the entire system.

In the constructed TDR system, a pulse generator capable of generating pulses with 125 MHz repetition rate and rise and fall times around 2 ns was used. In the actual operation of the TDR system, the parameters of generated pulses were set such that the repetition rate is 8.3 MHz, rise/fall time is 3 ns, and a pulse width of 10 ns. Figure 2 shows a plot of the used pulse as captured by an oscilloscope with an illustration of the different pulse parameters. The pulse generator had an output terminal impedance of 50 Ω. Co-axial cables with a characteristic impedance of 50 Ω and line capacitance of 101 pF/m were used as the transmission lines.

The probe will terminate the coaxial cable end at the sample side. Thus, its structure should be a continuation to that of the cable and would consist of a signal line and a ground conductor. A simple probe structure that would satisfy this description is that of a monopole antenna that consists of a central straight conductor of length L_p and a ground plane. The input impedance of a monopole antenna will be a function of its length compared to the signal wavelength ? or alternatively its frequency. To achieve an input resistance around 50 O, the monopole's length must be much smaller than the used wavelength (Balanis, 1997)?

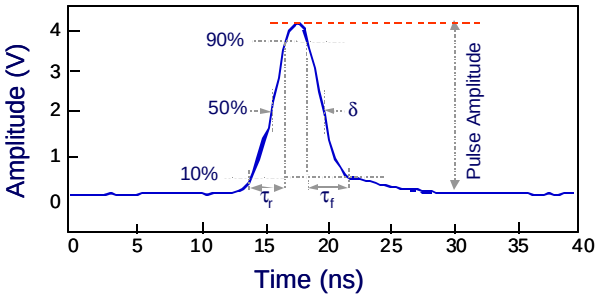

Fig. 2. *A plot of the generated pulse used in the TDR system as captured on the oscilloscope.*

Generally, the monopole input impedance is composed of a resistive and a reactive part. For monopoles with L_p << ? the input impedance Z_P can be written as:

$$Z_P = 40p^2\left(\frac{L_P}{l}\right)^2 - jZ_0\cot\left(\frac{pL_P}{l}\right) \qquad [7]$$

The first term in the right-hand-side of eq. (7) is the monopole resistive input impedance and is almost negligible for cases where L_p << ?. The second term in the right-hand-side of eq. (7) is a reactive impedance and will be purely capacitive if it is negative. Since a monopole with L_p << ? is under consideration, the designed probe input impedance will be capacitive as determined by eq. (7). At the used frequency of operation in this work, 8.3 MHz, the signal wavelength is around 36 m in free space. Using 50 O for Z_P and Z_0 in eq. (7), the probe length is calculated to be around 9cm. It should be pointed out that the used pulse signal has several frequency harmonics of multiples of the fundamental frequency 8.3 MHz. These harmonics are the Fourier components of the pulse signal. The probe design considered earlier was based on matching the probe at the fundamental component.

Based on the results above a probe was fabricated using a 9 cm long Aluminum rod with a diameter of 1cm and a ground disc. Two other rods with diameters smaller than the probe were attached to the ground disc to enhance the coupling between the probe and the ground disc as well as assure contact between the sample and the ground path. Figure 3 shows a photograph of the constructed TDR system with an enlargement of the designed probe. To verify the matching of the different parts of the constructed system, the response of the TDR system was measured with the probe held in air to resemble an open ended system. The measured system response is shown in Fig. 4 and demonstrates a well-matched system.

EXPERIMENTAL DEMONSTRATION

To demonstrate the capability of the system to detect presence of material at the probing end, the measurement of a soil sample mixed with NaCl solution was attempted. The NaCl solution was prepared with a concentration of 1000 ppm. Computer software was used to acquire the waveform displayed by the oscilloscope, thus providing the voltage profile at the measurement point. Figure 5 shows the captured waveform for a soil sample with 18% by weight of moisture content. Focusing on the reflected part of the signal, the measured voltage profile in Fig. 5 shows different characteristics from that in Fig. 4 that corresponds to an open-end system response. Thus, the system is capable of detecting material concentration at the probe end.

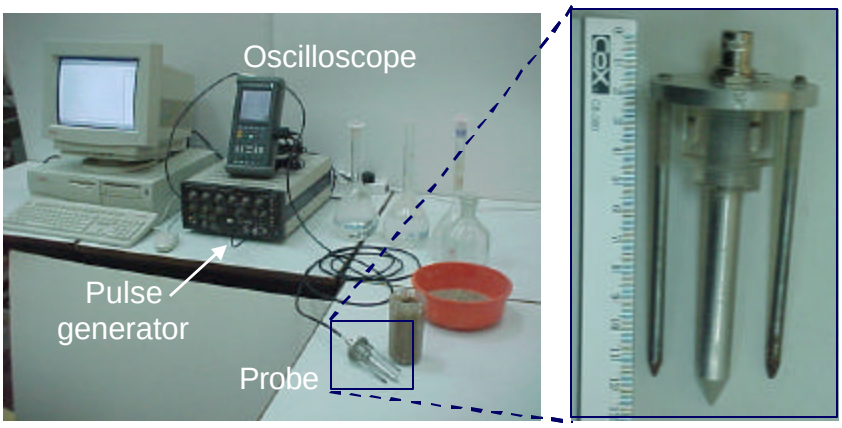

Fig. 3. *Photograph of the constructed TDR Set-up and a close-up of the designed probe*

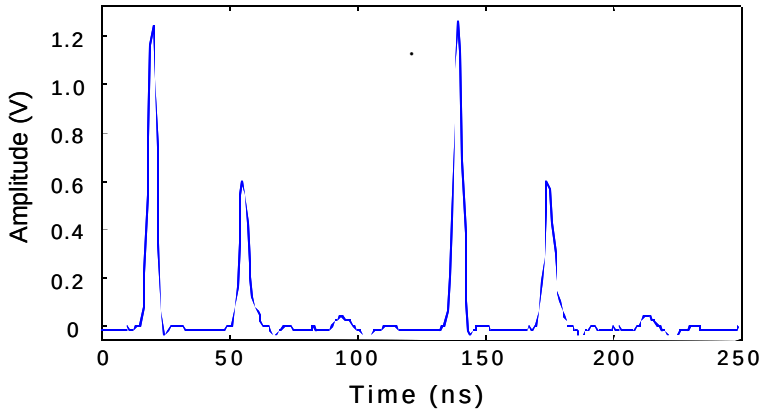

Fig. 4. *Measured response of the designed TDR system with the probe held in air. The system response was captured at the oscilloscope point and demonstrates a reasonably matched system.*

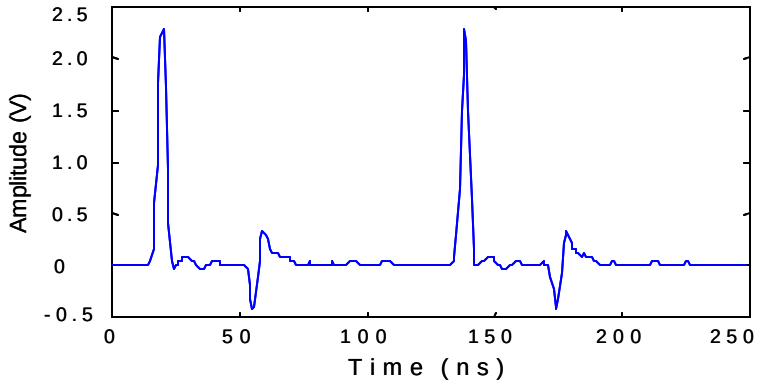

Fig. 5. *Measured response of the designed TDR system with the probe immersed in a soil sample with 18% by weight of moisture content of NaCl solution that has a concentration of 1000 ppm.*

SYSTEM MODELING

In order to quantify the system response and extract the characteristic properties of a sample, a model for the TDR system must be developed. Since the system response is dependent on the electrical characteristics of a sample, it is convenient to represent the system and the sample by electrical circuit model. A proposed model for the developed TDR system is shown in Fig. 6. Here, the pulse generator is represented by an ideal pulse voltage source and a series resistor R_g to represent the internal resistance of the actual source. The coaxial cables connecting the different parts in the system can be represented by loss less transmission lines with time delay equivalent to the length of each used cable. The assumption of loss less lines is valid since the lengths of used cables are less than 2 meters. The oscilloscope is represented by its Thevenin's equivalent at the input port, which is specified as an input resistance of 1 MO and a capacitance of 10 pF.

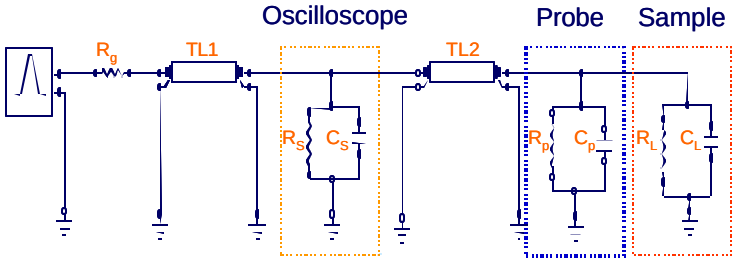

Fig. 6. *Schematic diagram of the proposed circuit model of the developed TDR system.*

The probe and the sample can both be modeled as a parallel combination of a resistance (representing leakage current) and capacitance (representing coupling in the probe structure and the dielectric constant of the media in the sample). The leakage resistance of the probe is very high and can be even omitted in the model since the probe centerline is isolated from the ground disk. The probe capacitance however is unknown and is necessary for a proper simulation of the system operation. The probe capacitance can be determined using numerical calculation methods as well as experimental techniques. A method adopted to evaluate the probe capacitance was to assume a value and simulate the system response with an open end (without presence of sample model) and compare the result with that in Fig. 4. The assumed value of the probe capacitance was then iteratively modified such that the simulated system response best matches that in Fig. 4. The estimated probe capacitance was determined to be 1 pF. Electrical circuit simulation software (Circuit Maker) was used to simulate the system model. During simulation the actual pulse parameters (pulse frequency, rise time, fall time, pulse width and pulse amplitude) were used in the simulation.

The same strategy used in determining the probe capacitance was used to extract the leakage resistance and capacitance representing the sample model. For example, to determine the sample resistance R_L and capacitance C_L of the soil sample tested in Fig. 5, the system model in Fig. 6 was simulated using assumed values of R_L and C_L. The simulation results are compared against measurement results and the values of R_L and C_L are modified accordingly till simulation results best match experimental data.

To verify the validity of the developed system model, simulation of the system response to soil samples with different weight percent (3% - 18%) moisture content of 1000 ppm NaCl solution were attempted. Figure 7 shows the reflected pulse profile for the different moisture contents that were obtained by measurement and simulation. A comparison between the results in Fig. 7 demonstrate the validity of the developed system model as well as the ability of the system to distinguish the different moisture contents at the probe end.

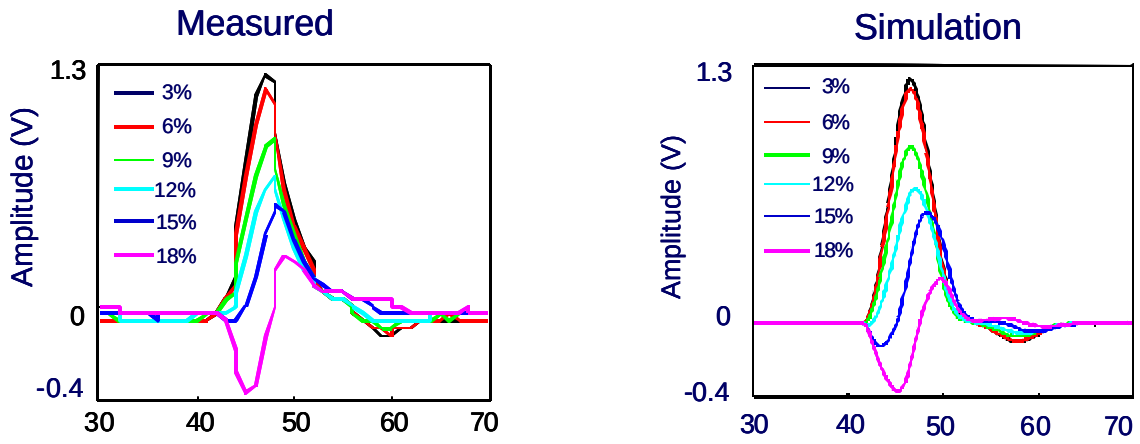

Fig. 7. *The TDR system response to different moist soil samples obtained by experimental measurement (left) and simulation (right) using the developed circuit model of the TDR system. The tested soil samples had different by weight moisture content of NaCl solution that has a concentration of 1000 ppm*

To quantify the obtained measurements, the estimated sample resistance and capacitance in the simulation are plotted for the different sample moisture weight % content as shown by Fig. 8. It can be seen from Fig. 8 that for the same NaCl concentration, as the moisture content increases, the resistance decreases. The capacitance curve in Fig. 8 shows that for the same NaCl concentration, as the moisture content increases, the capacitance increases.

SUMMARY

The development of a TDR-based system for subsurface detection was presented, and the system constructed from off-the-shelf equipment. The probe used in the developed system was designed in the light of antenna theory to match all the parts in the system and improve its performance. The system operation was demonstrated by the detection of NaCl solution in soil samples. A circuit model was proposed based on transmission line theory to simulate the operation of the system. Simulation result were compared against experimentally obtained system response and demonstrate satisfactory agreement between both. Also, a methodology was developed to evaluate material concentration via the use of two important electrical properties for the medium, which are resistance and capacitance. The demonstration presented in this work used NaCl soil solutions as the desired moisture content to be detected, however, the same strategy can be applied for all other pollutants, as discussed by Mohamed *et al*. (2001). This in turn will establish set of databases for different materials that enable one to determine the type of pollutant in the soil and it is approximate concentration.

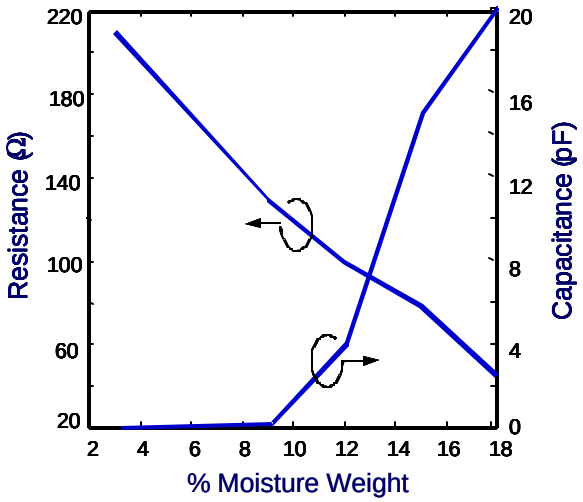

Fig. 8. *NaCl 1000 ppm moist soil sample characterization presented as sample resistance and capacitance as measured by the developed TDR system.*

Knowing that the frequency used in this developed method is about 8.3 MHz, the load response depends on the pulse frequency used. It is convenient to study the frequency spectrum of the soil medium response to create another database that can indicate what is the

moisture content for a specific response based on spectrum analysis. Sweeping the frequency is another successful method to link the soil medium response with its actual moisture content in the soil sample, which is currently under investigation by the authors.

ACKNOWLEDGEMENT

The authors would like to express their great appreciation for the financial support of The Scientific Research Council at The United Arab Emirates University.

REFERENCES

Balanis, C.A., "Antenna Theory," 2nd edition, John Wiley & Sons, Inc., New York, 1997.

Elrick, E.E., Kachanoski, R.G., Pringle, E.A., and Ward, A., 1992, Parameter estimation of field scale transport models based on time domain reflectometry measurements. Soil Sci. Soc. Am. J., **56**, 1663-1666.

Heimovaara, T.J., and Bouten, W., 1990, A computer-controlled 36-channel time-domain reflectometry system for monitoring soil water contents. Water Resour. Res., **26**, 2311-2316.

Kachanoski, R.G., Pringle, E., and Ward, A., 1992, Field measurement of solute travel times using time domain reflectometry, Soil Sci. Soc. Am. J., **56**, 47-52.

Mallants, D., Vanclooster, M., Meddahi, M., and Feyen, J. 1994. Estimating solute transport parameters on undisturbed soil columns using time domain reflectometry. J. Cont. Hydrol., **17**, 91-109.

Mohamed, A.M.O., Said, R.A., AlShawawreh, N., A TDR system for subsurface pollutants detection: I. design and modeling. Proceedings of the Symposium TDR2001: Innovative Applications of TDR Technology, Infrastructure Technology Institute, Northwestern University, Evanston, Illinois, September 5-7, 2001.

----------, 2000, Development of an electrical polarization technique for subsurface pollutants detection. In: Geoengineering in Arid Lands, Mohamed & AlHosani (eds.), Balkema, Rotterdam, pp. 633-639.

Mohamed, A.M.O., and Antia, H.E., 1998, Geoenvironmental Engineering. Elsevier, Science Publishers, Amsterdam, 707p.

Vanclooster, M., Mallants, D., Vanderborght, I., Diels, I., Van Orshoven, J., and Feyen, J., 1995, Monitoring solute transport in a multi-layered sandy lysimeter using time domain reflectometry, Soil Sci. Soc. Am. J., **57**.

Vanclooster, M., Mallants, D., Diels, J., and Feyen, J., 1993, Determining local-scale solute transport parameters using time domain reflectometry, J. Hydrolo., **148**, 93-107.

Ward, A.L., Kachanoski, R.G., and Elrick, D.E., 1994, Laboratory measurements of solute transport using time domain relectometry, Soil Sci. Soc. Am. J. **56**, 1-10.

Wraith, J.M., Comfort, S.D., Woodbury, B.L., and Inskeep, W.P. 1993. A simplified waveform analysis approach for monitoring solute transport using time-domain reflectometry, Soil Sci. Soc. Am. J., 57, pp. 637-64.

A TDR SYSTEM FOR SUBSURFACE POLLUTANTS DETECTION (II): APPLICATION AND ANALYSIS

R. A. Said[1], N. K. AlShawawreh[2], A. M. O. Mohamed[3]

[1]Electrical Engineering Department, United Arab Emirates University,
P.O. Box: 17555, Al Ain, United Arab Emirates, rasaid@uaeu.ac.ae
[2]Electrical Engineering Department, United Arab Emirates University,
P.O. Box: 17555, Al Ain, United Arab Emirates
[3]Civil Engineering Department United Arab Emirates University,
P.O. Box: 17555, Al Ain, United Arab Emirates, Mohamed@uaeu.ac.ae

ABSTRACT

The proposed work utilizes a TDR based system for the in-situ detection of subsurface pollutants. Natural soil samples from Al Ain, UAE and calcium solutions were used in this investigation. Three conjugate anions of chloride, sulfate and carbonates were used for the preparation of the calcium solutions. All calcium solutions were maintained at a fixed concentration of 1000 ppm. Specimens with various moisture contents were prepared and used in the testing program. The TDR system was modeled using transmission line theory and the associated electrical parameters were optimized. Based on the optimized parameters (resistance and capacitance), calibration curves for different conjugate anions and soil moistures were obtained.

INTRODUCTION

Monitoring techniques rely mainly upon driven wells, lysimeters, and leachate under-drains. Wells are the most common means of monitoring the groundwater contamination. This technique tends to be expensive and time consuming to implement. Timely detection of contaminant plume is obviously dependent on the initial layout and the number of monitoring wells. Unfortunately, wells can sample only a small volume of the aquifer. If samples collected from wells are not representative of the area or conditions for which they are intended, misleading and erroneous conclusions may result. It should be noted that by the time a pollutant becomes detected in a monitoring well, a substantial volume of the surrounding soil and groundwater has already been polluted. In addition, the risk of drilling wells and exploratory holes in unknown hazardous waste sites can be substantial. As the number of holes needed to define a problem area increases, the possibility of puncturing buried containers is increased hence, toxic fumes and liquids may be released. Also, explosions and fire may occur in extreme cases.

The limitations associated with present monitoring techniques underscore the need for an alternate approach. Early detection and characterization of subsurface pollutants can minimize its negative impact. Therefore, there is an urgent need for the development of a field diagnostic technique, which allows a rapid determination of the extent of pollutants present in subsurface soils. The developed method should assist in locating a leak in the impounding boundary so that a corrective action can be taken to alleviate the problem. It should also be adaptable to a wide range of chemicals, as opposed to being ion specific. Currently there are about 60,000 substances classified as hazardous by the various environmental agencies.

Recently, several researchers have discussed the large potentials of the use of electrical detection techniques for measuring tracer movements in laboratory as well as in field conditions (Mohamed *et al*., 2000; Mallants *et al*., 1994; Ward *et al*., 1994; Wraith *et al*., 1993; Vanclooster *et al*., 1993; Kachanoski *et al*., 1992). These electrical detection methods operate by analyzing the characteristics of a fast rising electric potential signal as it reflects at the probing end of a transmission line (coaxial cable) immersed in a sample under investigation. The characteristics of the reflecting signal are highly influenced by the electrical properties of the specimen, which are dependent on the concentration of the constituents.

A common application of the electrical detection principle is the time-domain-reflectometry (TDR) that is widely used as a concentration detection technique. TDR enables the measurement of total resident concentration from both mobile and immobile water regions for a sample volume with a well-defined geometry and allows data collection of both moisture content and salt concentration at a high spatial and temporal resolution. Automation of TDR has made it more powerful for use in the laboratory as well as in field application at remote sites (Heimovaara & Bouten, 1990). Application of TDR in the area of contaminant hydrology has been reported (Vanclooster *et al*., 1995; Mallants *et al*., 1994; Ward *et al*., 1994; Vanclooster *et al*., 1993; Kachanoski *et al*., 1992; Elrick *et al*., 1992). The success or failure of TDR technique to accurately predict pollutant concentration depends on the appropriateness of the calibration procedure used. Application of electrical polarization in the area of pollutant detection in subsurface has yet to be developed due to the nature of the flow and the characteristics (signature) of each pollutant.

This paper discusses the application of the developed TDR system and analysis of the experimental results. The design and modeling aspects of the developed TDR system are reported previously by Mohamed *et al*. (2000) and Said *et al*. (2001).

MATERIALS AND METHODS

Experimental Setup

Figure 1 shows the components of the proposed measuring system that consist of pulse generator, oscilloscope, co-axial cables, monitoring probe, and a computer. The scope meter is used to acquire the system response through a measurement point on the transmission line. The measuring probe is connected to a pulse generator and to a scope meter via transmission lines (co-axial cables). The selected co-axial cable had line capacitance of 101 pF/m. The probe was connected to the scope meter using 3.6-meter long co-axial cable. The generated pulse has the following characteristics 8.3 MHz, 4V, and rise and fall times around 3 nano seconds.

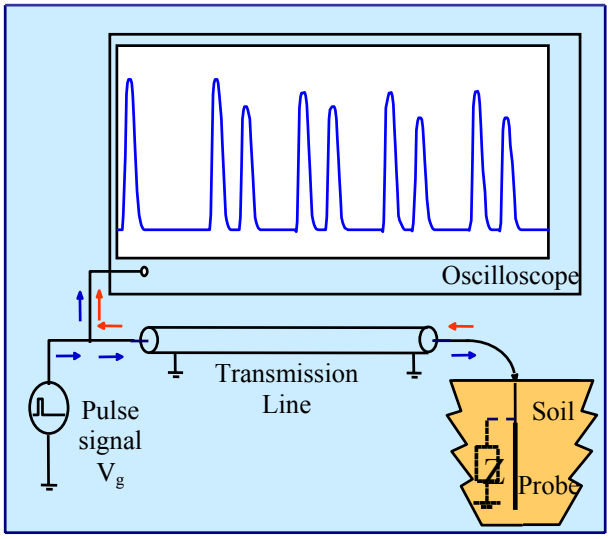

Fig. 1. *A schematic model of the system*

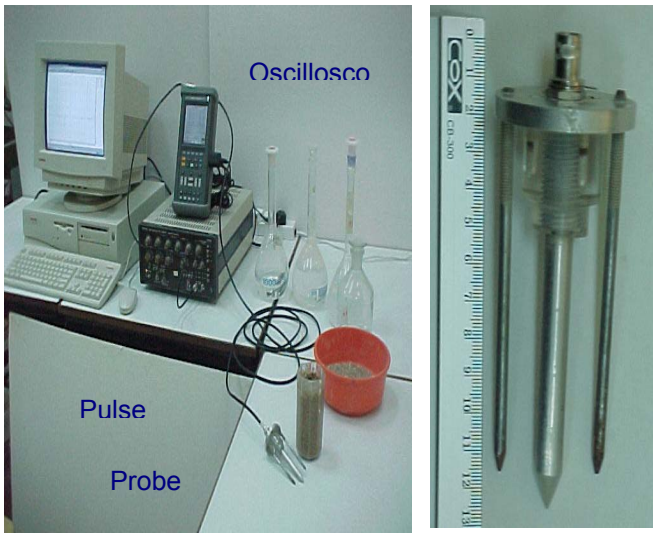

Fig. 2. *The Measurement system (with the probe appears enlarged)*

During measurement, an electrical pulse is generated periodically by the pulse generator and launched toward the probe. The pulse signal propagating toward the probe appears on the scope meter as it passes a measuring point located at a known distance from the generator on the transmission line. As the pulse reaches the probe end it reflects back on the transmission line with pulse characteristics dependent on the properties of the media surrounding the probe. The reflected pulse signal propagates back toward the generator and thus appears on the scope meter after a delay time with respect to the time of appearance of the original pulse. To characterize the system, a test was conducted by leaving the probe in an open air. In this case a major reflected wave appeared.

Soil Material

Soil samples obtained from Al-Jimi district in Al-Ain municipality of UAE were used in this investigation. The selected testing procedures were carried out following procedures described by ASTM standards. Measurements of specific gravity and consistency limits were performed according to ASTM D854, test method for specific gravity of soils, and ASTM D422, method for particle-size analysis of soils. Determination of compaction parameters and permeability coefficients (at maximum dry density) were carried out following ASTM D698, test methods for moisture-density relations of soils and soil-aggregate mixtures, and ASTM D2434, test method for permeability of granular soils, respectively. pH and conductivity measurements of 1:10 soil-water extract were conducted according to ASTM D1293, test method for pH of water, and ASTM D1125, test methods for electrical conductivity and resistivity of water, respectively. A summary of these results is shown in Table 1.

Soil Properties	Pore Fluid Analysis
Geotechnical Specific gravity = 2.68 Consistency limits Liquid limit & Plastic limit = NP Soil Gradation 35% Gravel; 43 %Sand ; 18 % Silt; 4 % Clay Soil Texture Silty Sand Compaction Max. dry density = 1.79 Mg/m^3 & Opt. water content = 12% Hydraulic conductivity = 7.185E-06 m/sec *Mineralogical composition* Major: Quartz, Calcite, Plagioclase Minor: Dolomite, Feldspar, Kaolinite	pH = 8.1 Conductivity (S) = 1.18E-03 Ion Concentrations (ppm) Na^+ 140 K^+ 8.5 Mg^{++} 34 Ca^{++} 48 $CaCO_3^{--}$ 520 HCO_3^- 140 Cl^- 460

Table 1. *Selected properties and composition of tested soil.*

Sample Preparation

Solutions of CaCl, $CaCO_3^{2-}$, and $CaSO_4^{2-}$ were prepared with specified concentration of 1000 ppm. Soil samples were mixed with different amounts of moisture containing the above calcium solutions. The moisture content in the tested specimens varies as 3, 6, 9, 12, 15 and 18% by weight. To ensure homogeneity of the moistures, samples were prepared in advance of testing for about 8-10 hours. Soil specimens were then placed in the testing column at a specified density that allows one to push the testing probe into the soil material without any major disturbance. Then, the probe was connected to the scope meter as shown in Fig. 1.

Experimental measurements

The setup shown in Fig. 2 was adjusted, so that the scope meter can take 32 reading at a time and count for the average. Special computer software (FlukeView) was used to acquire the data measured for each sample.

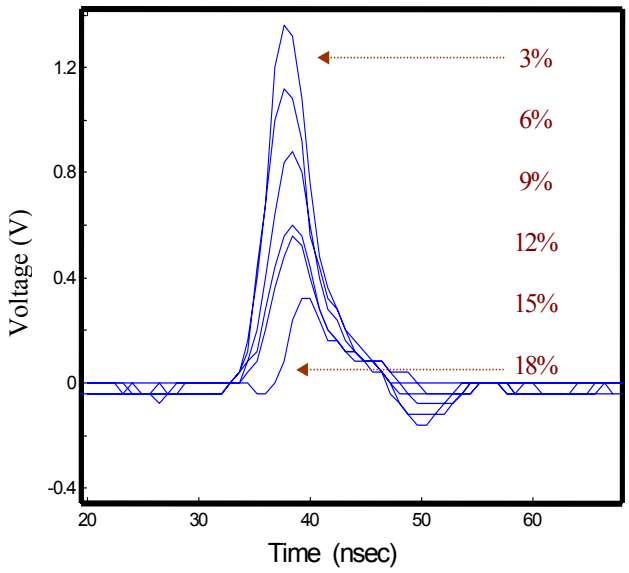

Fig. 3. *Reflected signal for $CaCl_2$ with 1000 ppm concentration and various moisture contents.*

The voltage profile at the measuring point, shown in Fig. 1, was captured and recorded. Six profiles corresponding to moisture contents of 3, 6, 9, 12, 15, and 18% by weight were captured. Focusing on the reflected part of the signal, the measured voltage profiles were compared for CaCl, $CaCO_3^{2-}$, and $CaSO_4^{2-}$ concentration of 1000 ppm as shown in Figs. 3, 4, and 5.

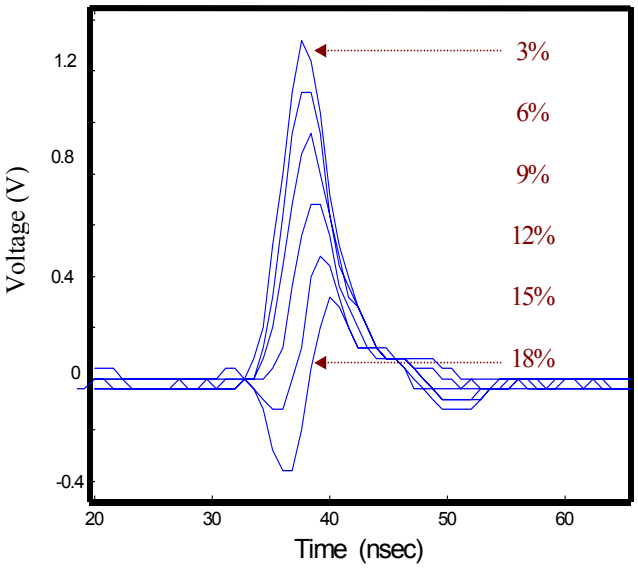

Fig. 4. *Reflected signal for $CACO_3^{2-}$ with 1000 ppm concentration and various moisture contents.*

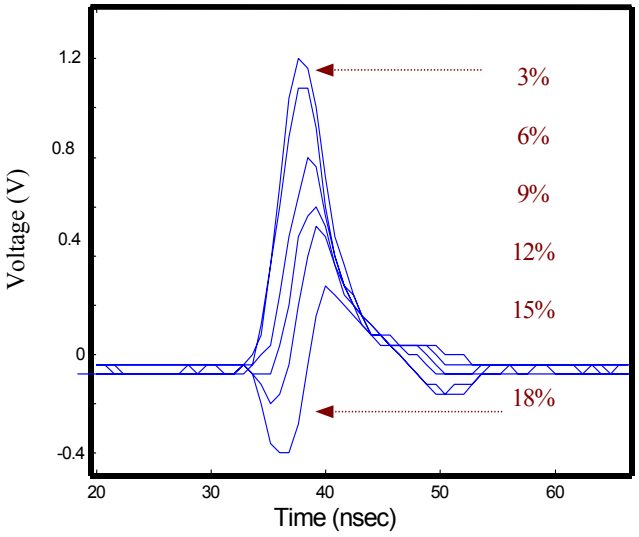

Fig. 5. *Reflected signal for with Ca SO_4^{2-} with 1000 ppm concentration and various moisture contents.*

SIMULATION ANALYSIS

In order to characterize the properties of the soil medium, it is convenient to represent the system by electrical circuit model for simulation purposes as discussed by Said *et al* (2001). A simulation was performed to match the real case profiles and extract the electrical parameters representing the type and concentration of the soil medium around the probe. The simulation results will provide a proper mechanism for distinguishing between different salt species and/or concentrations.

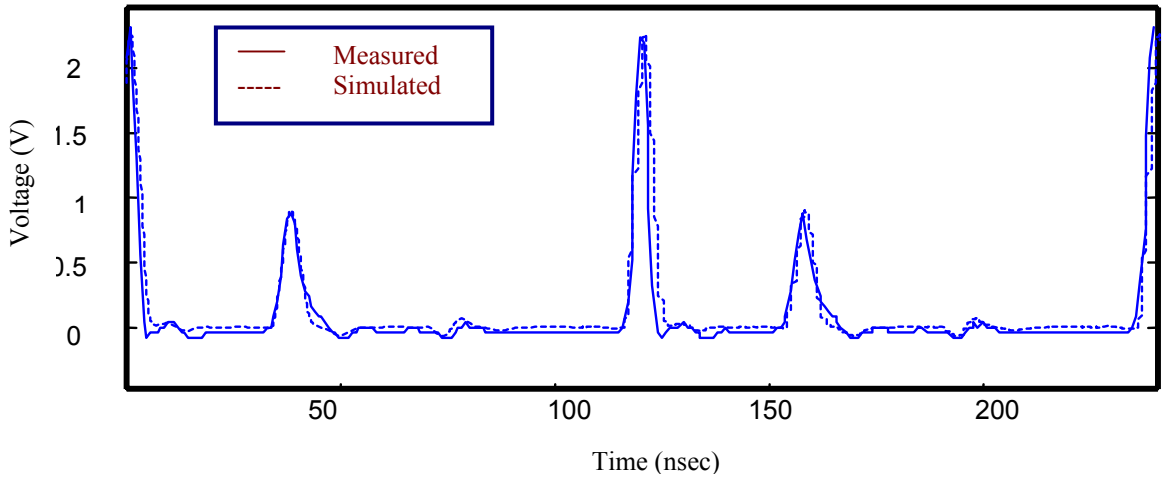

Fig. 6a. *$CaCl_2$ Case*

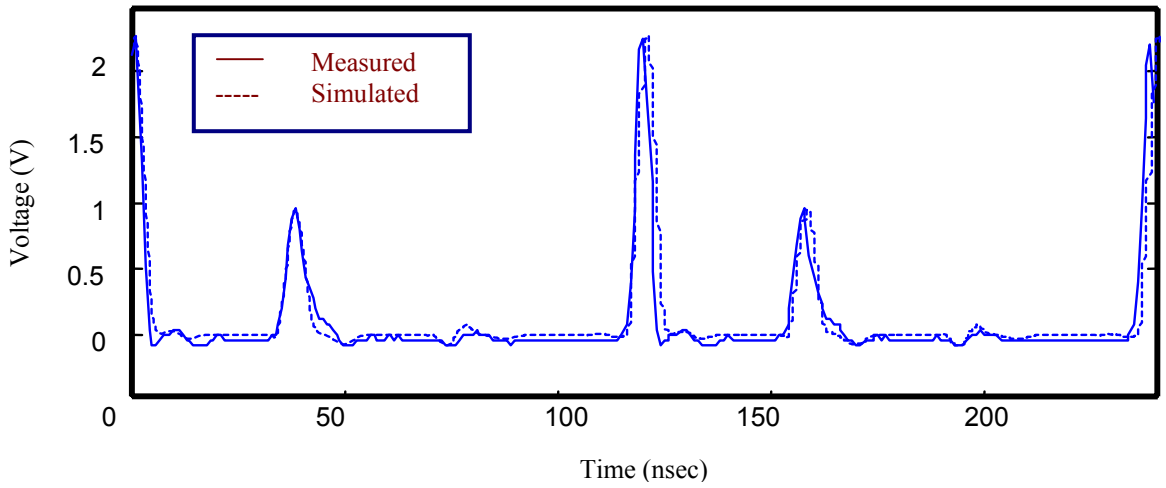

Fig. 6b. *$CaCO_3$ Case*

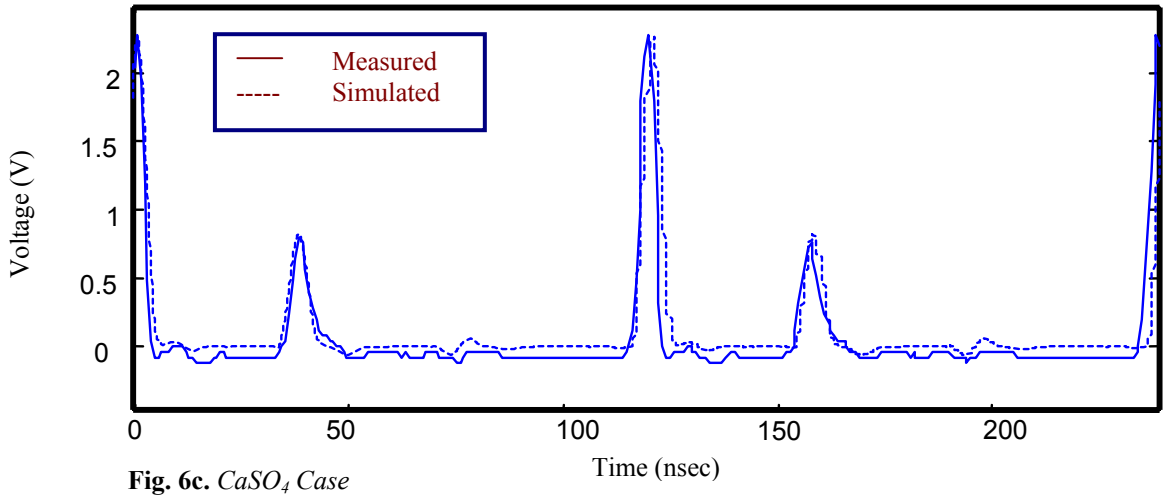

Fig. 6c. *$CaSO_4$ Case*

Fig. 6: *Measured and simulated voltage profiles for $CaCl_2$, $CaCO_3$ and $CaSO_4$ for 9% soil moisture.*

Electrical circuit simulation software (Circuit-Maker) was used to simulate the system model. The co-axial transmission lines in the simulation diagram were considered as lossless transmission lines. This approximation is valid since the length of the coaxial cable is not too long. The probe combined with the soil medium can be expressed electrically by RC circuit (Resistance and a Capacitance). Experiments have shown that the metal probe by it self has no significant effect on the response. In this case, the RC circuit model can best represent the medium properties (Mohamed *et al*, 2000).

The system parameters (pulse frequency, rise time, fall time, pulse width and pulse amplitude) are used in the simulation to match the real pulse and calibrate the system. Another RC circuit is used to simulate the model of the scope meter. The coaxial cable is modeled as a lossless transmission line with $Z_L = 50\Omega$, $C_L = 101\,\text{pF/m}$, and L_G= 1m.

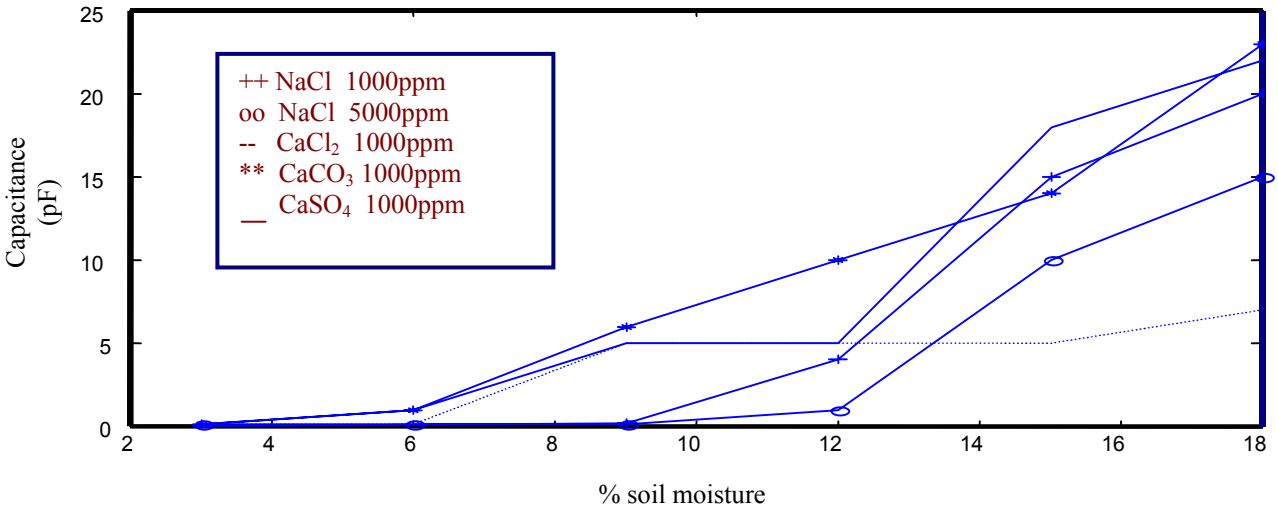

Fig. 7. *The capacitance variations with moisture content and calcium chloride, calcium carbonate, and calcium sulfate concentrations.*

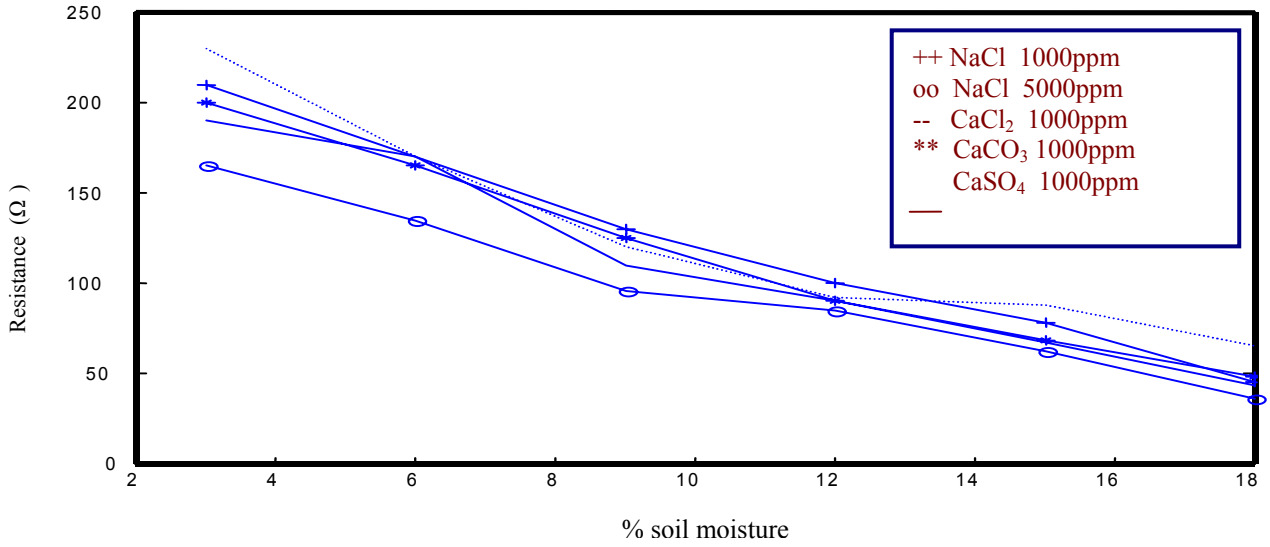

Fig. 8. *The resistance variations with moisture content and calcium chloride, calcium carbonate, and calcium sulfate concentrations.*

To simulate the system with calcium moisture profiles of 1000 ppm concentrations, another transmission line model is used with $Z_0 = 50\Omega$, C= 101 pF/m, and $L_P = 3.6m$. The simulation strategy was based on varying resistance and capacitance parameters until both the real and simulated cases were matched. The simulation was performed for calcium concentrations of 1000 ppm with various conjugate anions of chloride, carbonates, and sulfates. Each tested sample was simulated and compared with the real one. Some of these results are shown in Fig. 6. The figure indicates a very good matching between measured and simulated results.

The variations of the optimized parameters (resistance and capacitance) with moisture content and calcium chloride, calcium carbonate, and calcium sulfate concentrations are shown in Figs. 7 and 8,

respectively. In addition, for comparing the results with previously published data, sodium chloride concentrations of 1000 and 5000 ppm (Mohamed *et al*., 2000), are shown in the same figures. From these figures, one can highlight the effect of soil solution concentration, moisture content, and conjugate anions on the variations of resistance and capacitance.

Concentration Effect

As shown in Fig. 7, for the same moisture content, as NaCl concentration increases, the soil medium capacitance decreases. Also, it is known from the diffuse ion layer theory that as pore fluid concentration increases, soil water potential decreases (Mohamed and Antia, 1998). On the other hand, as soil concentration increases, soil structure tends to be flocculated leading to a decrease in soil water potential. This in turn leads one to conclude that as concentration increases, both capacitance and soil water potential are decreased.

With respect to soil medium resistance, the calculated results shown in Fig. 8 indicate that as NaCl concentration increases, the resistance decreases. This is attributed to the fact that as soil pore fluid concentration increases, electrical conductivity increases hence, decreasing soil medium resistance. Therefore, for the same moisture content, as concentration increases, both capacitance and resistance are decreased.

Moisture Content Effect

The results shown in Fig. 7 indicate that for the same concentration, as moisture content increases, the capacitance increases. This phenomenon could be attributed to the fact that as moisture content increases, the diffuse ion layer will be fully developed and the soil water potential will increase hence, increasing the capacitance on the soil medium.

Furthermore, the results shown in Fig. 8 indicate that for the same concentration, as moisture content increases, soil medium resistance decreases. Once again this could be explained via the fully expanded diffused ion layer as demonstrated previously. Therefore, as moisture content increases, soil medium capacitance increases while, soil medium resistance decreases.

Conjugate Anion Effect

In order to highlight the effect of conjugate anions one has to keep in mind the following phenomena:

(1) As concentration increases, both soil water potential and capacitance are decreased;
(2) As concentration increases, soil tends to have a flocculated structure hence, the resulting soil water potential and capacitance are decreased; and
(3) If the negative charge on a soil colloid surface remains constant, anions of higher charge are repelled than anions of lower charge (i.e., $CO_3^{2-} > SO_4^{2-} > Cl^-$). Therefore, inter-particle repulsion energies would be less for Cl^- than CO_3^{2-} ion association resulting in the formation of flocculated structures in the case of Cl^- and dispersed structure in the case of CO_3^{2-} ions (Mohamed and Antia, 1998).

Therefore, from items 1, 2, and 3, it can be concluded that soil medium capacitance is higher for dispersed structure than for flocculated structures. And with respect to conjugate anions, the order of increasing capacitance could be expressed as $SO_4^{2-} > CO_3^{2-} > Cl^-$ as shown in Fig. 9.

In view of soil medium resistance changes with conjugate anions, the results shown in Fig. 8 indicate that the order of decreasing resistance is $SO_4^{2-} < CO_3^{2-} < Cl^-$. This once again could be attributed to the formation of flocculated structures in the case of SO_4^{2-} and CO_3^2 anions while dispersed structure in the case of Cl^- anion. Noting that at mid-plane, pore fluid concentration in dispersed structure is larger that that of flocculated structure hence, both soil water potential and soil medium resistance are less for dispersed structure than that for flocculated structure. Therefore, soil medium resistance for both SO_4^{2-} and CO_3^2 anions is less than that of Cl^- anion.

CONCLUSION

In this study, the soil system performance due to an externally applied electrical pulse is quantified via two electrical parameters that are capacitance and resistance. These parameters can easily be obtained for various ionic species and set of databases can be developed. This in turn will enable one to detect various pollutants in subsurface soils and determine their approximate concentrations.

Knowing that the frequency used in this developed method is about 8.3 MHz and the load response depends on the pulse frequency used, it is convenient to study the frequency spectrum of the soil medium response to create another data base that can indicate what is the moisture content for a specific response based on spectrum analysis. Sweeping the frequency is another successful method to link the soil medium response with its actual moisture content in the soil sample, which is currently under investigation by the authors.

ACKNOWLEDGEMENT

The authors greatly appreciate the financial support provided by the Scientific Research Council of the United Arab Emirates University.

REFERENCES

Elrick, E.E., Kachanoski, R.G., Pringle, E.A., and Ward, A., 1992, Parameter estimation of field scale transport models based on time domain reflectometry measurements. *Soil Sci. Soc. Am. J.*, **56**, 1663-1666.

Heimovaara, T.J., and Bouten, W., 1990, A computer-controlled 36-channel time-domain reflectometry system for monitoring soil water contents. *Water Resour. Res.*, **26**, 2311-2316.

Kachanoski, R.G., Pringle, E., and Ward, A., 1992, Field measurement of solute travel times using time domain reflectometry, *Soil Sci. Soc. Am. J.*, **56**, 47-52.

Mallants, D., Vanclooster, M., Meddahi, M., and Feyen, J., 1994, Estimating solute transport parameters on undisturbed soil columns using time domain reflectometry. *J. Cont. Hydrol.*, **17**, 91-109.

Mohamed, A.M.O., Said, R.A., and AlShawawreh, N., 2000, Development of an electrical polarization technique for subsurface pollutants detection. In: Geoengineering in Arid Lands, Mohamed & AlHosani (eds.), Balkema, Rotterdam, 633-639.

Mohamed, A.M.O., and Antia, H.E., 1998, *Geoenvironmental Engineering*. Elsevier, Science Publishers, Amsterdam, 707p.

Said, R.A., AlShawawreh, N, and Mohamed, A.M.O., A TDR system for subsurface pollutants detection: I. design and modeling. Proceedings of the Symposium TDR2001: Innovative Applications of TDR Technology, Infrastructure Technology Institute, Northwestern University, Evanston, Illinois, September 5-7, 2001.

Vanclooster, M., Mallants, D., Vanderborght, I., Diels, I., Van Orshoven, J., and Feyen, J., 1995, Monitoring solute transport in a multi-layered sandy lysimeter using time domain reflectometry, *Soil Sci. Soc. Am. J.*, **57**.

Vanclooster, M., Mallants, D., Diels, J., and Feyen, J., 1993, Determining local-scale solute transport parameters using time domain reflectometry, *J. Hydrolo.*, **148**, 93-107.

Ward, A.L., Kachanoski, R.G., and Elrick, D.E., 1994, Laboratory measurements of solute transport using time domain relectometry, *Soil Sci. Soc. Am. J.* **56**, 1-10.

Wraith, J.M., Comfort, S.D., Woodbury, B.L., and Inskeep, W.P., 1993, A simplified waveform analysis approach for monitoring solute transport using time-domain reflectometry, *Soil Sci. Soc. Am. J.*, **57**, 637-64.

TIME DOMAIN REFLECTOMETRY FOR THE CHARACTERISATION OF DIESEL CONTAMINATED SOILS

Djaouida Chenaf and Nabil Amara

Geo-Engineering Centre at Queen's-RMC, Royal Military College of Canada,
Civil Engineering Department, P.O. Box 17000 Stn. Forces, Kingston, Ontario,
K7K 7B4, Canada; Chenaf-d@rmc.ca

ABSTRACT

Hydrocarbon contamination of soils represents a serious geo-environmental problem. In order to achieve rehabilitation of these soils, a rigorous characterisation of the contaminated site is required. The Time Domain Reflectometry (TDR), a geophysical method, is a promising tool for soil characterisation because it is non-destructive, accurate, and simple to use. Moreover, it can be applied both at full (field) and at the laboratory scales. The TDR method is based on the exploitation of the dielectric properties of the soil. The main objective of the present work is to develop an interpretation method based on the changes in the reflected TDR signal caused by the presence of diesel and its concentration in an unsaturated soil.

Multiple soil samples at constant water content and predetermined diesel concentrations are tested. Each test consisted in emitting a TDR signal to the soil sample and receipting the reflected signal. The precision offered by the experimental set-up allowed the characterisation of the temporal delay between the TDR signals reflected by the contaminated soil sample and the reference signal reflected by the clean soil samples. Both the temporal delay and the reflection coefficient have been found to increase when the diesel concentration increases. These findings are in disagreement with what has been found in previous studies when dealing with diesel contaminated soils that are fluid [water and diesel] saturated. Furthermore, this study allowed the identification of some error sources related to the experimental set-up and to samples preparation conditions, likely to deteriorate the TDR signals.

INTRODUCTION

The hydrocarbon soil contamination constitutes a serious geo-environmental problem, given the toxicity level and the high mobility of these organic compounds. The detrimental effects are not limited only to the deterioration of the chemical, physical and mechanical properties of the contaminated soils, but also constitute a real risk to human and live species health. The rehabilitation of these soils requires

identification and a rigorous characterisation of the contaminated site. Thus several geophysical methods have been developed which utilizes the contrast caused by the contaminant on physical properties of the soil, *e.g.* magnetic, electric or elastic properties (Olhoeft, 1986; Pitchford *et al.*, 1989).

The TDR (Time Domain Reflectometry) technique, a geophysical method, is based on the exploitation of soil dielectric properties changes in the presence of contaminants. It is distinguished from other techniques by its accuracy, its non-destructive character and the simplicity of its execution (DeRyck *et al.*, 1993). Since its first applications in soil sciences, the TDR has known several developments (Topp *et al.*, 1994; O'Connor and Dowding, 1999) mainly consisting in the improvement of the excitation electronics and the development of new TDR probe designs to enhance their sensitivity (Feng *et al.*, 1999; Ferré *et al.*, 2000). Soil microstructure, interaction of soil constituents (solids, water, and air) with each other (Tabbagh *et al.*, 2000), soil anisotropy and changes in solid grain geometry (Jones and Friedman, 2000; Robinson and Friedman, 2001) were addressed. Developments are pursued in the sense of a better exploitation of signals to extract relevant information and deduce some characteristics of contaminated soils (Weerts *et al.*, 2001).

TDR is a powerful method for the determination of water content of saturated and unsaturated clean soils (Topp *et al.*, 1980). It has also shown a good efficiency in determining migration pathways of DNAPL and LNAPL contaminants in controlled laboratory and in situ LNAPL's and DNAPL's injection tests (Redman and DeRyck, 1994) using a multilevel TDR probe which measures the dielectric permittivity at regular depth intervals. On field investigations, the multilevel probe is combined with other geophysical methods, generally to Ground Penetrating Radar (GPR), for a more complete characterisation (Redman, 1992; Kueper *et al.*, 1993; Brewster *et al.*, 1995). However, the application of TDR method to hydrocarbon contaminated soils is restricted to saturated soils (Benson and Bosscher, 1999).

This paper presents preliminary results of an ongoing study aimed at the identification of the effect of diesel presence and its concentration in an unsaturated soil, on the reflected TDR signal. This is a direct approach to the problem of the detection of contaminant presence and the estimation of its concentration in an unsaturated soil, based on the numerical treatment of TDR signals.

Four sets of several samples have been prepared at constant water content of 15 %. One of the sets is kept clean while the three others are contaminated with diesel at a diesel content in total fluid (water and diesel) of 11.25 %, 22.30 % and 32.76 % corresponding to diesel concentration in soil of 18 076 ppm, 41 414 ppm and 70 256 ppm, respectively.

A comparison of the collected TDR signals from contaminated and clean reference samples allows the determination of the diesel effect on the TDR signal.

TDR TECHNIQUE AND MIXING MODEL

The TDR signal velocity propagation v is related to the relative dielectric permittivity e of the soil, which is assumed to be lossless, by the following equation (Topp *et al.*, 1980)

$$v = \frac{c}{\sqrt{e}} \qquad [1]$$

where c is the light propagation velocity in vacuum, $c = 3x10^8$ m/s.

The travel time Δt which represents the time consumed by the TDR signal to travel forth and back in the waveguide of length L, can be written:

$$\Delta t = \frac{2L}{c}\sqrt{e} \qquad [2]$$

The last equation yields the direct dependence between the TDR signal travel time and the soil dielectric properties, *i.e.* the permittivity e.

A clean soil is constituted by solid grains, water and air, which relative dielectric permittivities are: $e_s = 4$, $e_w = 80$, $e_{air} = 1$ respectively. The large contrast between the dielectric permittivity of water and the other soil components is noticeable and therefore the soil water content will have a strong influence on the soil dielectric permittivity value.

The mixing model, relating the water content to the dielectric permittivity, is a semi-empirical approach based on physical and geometrical considerations (Roth *et al*., 1990). This model takes into account the contribution of the content and the permittivity of each component and the global dielectric permittivity of the soil. In case of a clean unsaturated soil that is constituted by only three phases: solid grains, water, air, the relative dielectric permittivity is given by the mixing law:

$$e = \left[q\, e_w^b + (1-f)\, e_s^b + (f-q)\, e_{air}^b \right]^{\frac{1}{b}} \qquad [3]$$

with q and f designate respectively, the bulk water content and the soil porosity.

b is a factor related to the grains geometry and their spatial distribution. For a soil assumed to be homogeneous and isotropic (Alharthi and Lange, 1987) $b \approx 0.5$.

In case of soil contaminated by a non-miscible liquid such as diesel, a fourth phase is added to the soil composition. Equation 3 giving the dielectric permittivity is reformulated to take into account the contaminant phase. Noting by y, the diesel bulk concentration and by e_{diesel} its relative dielectric permittivity ($e_{diesel} = 2.88$), the soil dielectric permittivity e is given by the modified mixing model proposed by Chenaf (2000),

$$e = \left[q\, e_w^b + y\, e_{diesel}^b + (1-f)\, e_s^b + (f-q-y)\, e_{air}^b \right]^{\frac{1}{b}} \qquad [4]$$

EXPERIMENTAL SET UP

The experimental set-up consists of an excitation-unit and an acquisition and processing unit. The device synoptic diagram is shown in Figure 1(a).

The excitation bloc is essentially constituted by a TDR signal generator Tektronix 1502C; a TDR probe with two cylindrical waveguides having plane extremities, as illustrated in Figure 1(b); and a one meter length coaxial cable connecting the probe to the signal generator.

The reflected TDR signals are collected by a PC based data acquisition and processing system. The microcomputer controls also the excitation bloc by mean of an interface command. The experimental set-up design offers the advantage of being entirely automated.

The excitation TDR signal is a step electromagnetic impulse of few tenth Volts amplitude, characterised by a very short rise time, less than 150 ps (Tektronix, 1993). The signal is transmitted by a coaxial cable to the TDR probe inserted in the soil sample. The propagating signal along the rods encounters an impedance break, at the extremities of the waveguides, causing the TDR signal to be reflected. The reflected signal carries the *signature* of the sample under study. The exploitation and processing of the signal allows the characterisation of some physical properties of the medium where the probe is inserted, such as the dielectric permittivity and the electrical conductivity.

SOIL SAMPLE PREPARATION

To reduce errors caused by inhomogeneities which can appear during soil preparation and to insure repeatability, 10 soil samples of 400g each have been prepared at constant water content and at three different diesel concentrations: 4 clean and 6 diesel contaminated. Thus, four soil sample sets are otained and identified by the diesel concentration level. Each sample was mixed with 60g of water in order to obtain a constant gravimetric water content of 15 %. Small soil quantities are taken from each sample to determine, by gravimetry, the water content ω_1 at preparation. The water content ω_1 varied

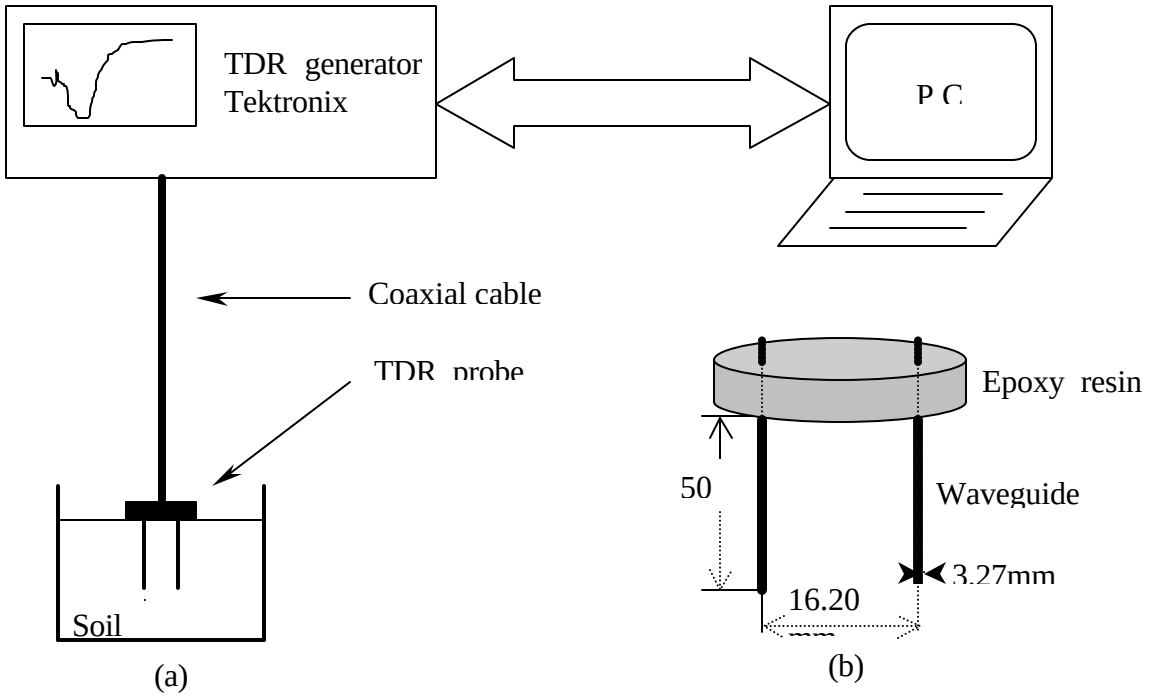

Fig. 1. *Synoptic diagram of the experimental device (a), and geometrical characteristics of the TDR probe (b)*

between 14.69 and 14.92%, which represents a loss of 0.31% to 0.08 % compared to the 15 % target value.

The soil samples are kept for twenty-four hours in sealed plastic bags to avoid any evaporation. The aim of this operation is to insure a uniform moisture distribution within the soil sample and a well water adsorption by the soil grains.

Twenty-four hours later, a second control of the soil water content ω_2 is conducted by gravimetry. The water content ω_2 values after 24 hours varied between 14.26 and 14.43% which represent a loss in water content of 0.74 to 0.57% to the 15% target value. These water content values, are considered as the actual values and are used in total fluid content FC (water and diesel) calculations.

One of the four moist soil samples was kept clean while the three others were mixed with 6.67 g, 15 g and 25.71 g of diesel in order to achieve diesel concentration in soil of 18 076 ppm, 41 414 ppm and 70 256 ppm, respectively. These concentrations are calculated using the actual soil mass sample of 400g minus the soil mass used for gravimetric measurement of water contents ω_1 of about 26.7g, 38g and 34g for sample 2, 3 and 4 respectively.

Therefore, knowing the values of ω_2 , the expected values of the fluid content (water and diesel) FC_1 are calculated and compared to the fluid content FC_2 values, determined by gravimetry at the end of the diesel-soil mixing step. The loss in fluid content increases with increasing diesel concentration, reaching approximately 1% for samples 2 and 3. This reasonable gap shows that the samples preparation was conducted with care. Table 1 summarises the water and fluid content values at the different steps of each soil sample preparation, meaned relatively to the different samples prepared at each diesel concentration.

The soil is then placed in a sample handles of a cylindrical geometry and having sufficiently large dimensions to avoid edge effects. For all tests, the soil is placed in three layers and lightly compacted. At each step, the compacted surface has been scraped to avoid the apparition of plane boundaries which give the sample a stratified behaviour responsible for parasitical reflections on the TDR signal.

	SOIL SAMPLE #			
	1	2	3	4
water content as planned (%)	15	15	15	15
Diesel concentration in soil (ppm)	0	18 076	41 414	70 256
AT PREPARATION				
Gravimetric water content, ω_1 (%)	14.72	14.92	14.69	14.71
AFTER 24 HOURS				
Gravimetric water content, ω_2 (%)	14.27	14.26	14.43	14.42
diesel content in fluid (%)	0	11.25	22.30	32.76
Fluid content, FC_1 (%)	14.27	16.11	18.56	21.44
Fluid content, FC_2 (%)	14.27	15.65	17.63	20.38
Difference (FC_1 - FC_2) (%)	0	0.46	0.93	1.06
Degree of saturation (%), porosity = 0.4)	60.75	69.43	80.29	94.24

Table 1. *Description of water and fluid contents in soil samples*

RESULTS AND DISCUSSION

The TDR measurements, while having a relative simplicity in execution, their accuracy however, depends mainly on the reliability of the experimental device and the adopted measurement technique. The results validity is strongly influenced by the observed rigorous conditions during the preparation of the samples. Any inhomogeneity or anisotropy that appears in the soils is often the source of artefacts. To circumvent this difficulty, besides preparing several samples for each contamination rate, two tests are conducted for each sample. These tests consist in the acquisition of reflected TDR signals corresponding to two perpendicular insertion positions of the rods in the sample. These tests were carried out at a temperature around 22°C.

For all the signals that will follow, it will be meant by signal, the reflection coefficient evolution versus time. The reflection coefficient is defined by the following expression (Cole, 1977):

$$R = \frac{u(t) - u_0}{u_0} \qquad [5]$$

with,

$u(t)$: Read tension at the instant t .

u_0 : Excitation tension.

The first collected signals (Figure 2) are those reflected by clean (non contaminated) samples. Most of these signals show a behaviour trend. If a signal does not follow the released trend, it isn't retained and is probably affected by errors.

The reflected TDR signals by the contaminated samples have been also subject to the same treatment. Figure 3 shows the signals corresponding to the diesel contaminated soil at the concentration of 18 076 ppm. For the others two diesel contaminated soils at concentrations of 41 414 ppm and 70 256 ppm, the reflected TDR signals behave similarly to the first one.

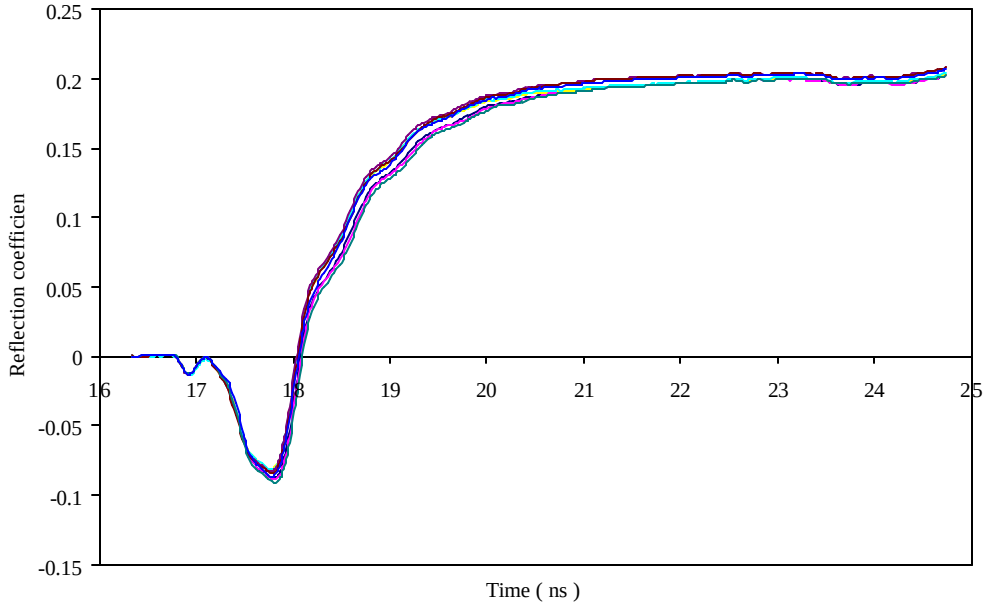

Fig. 2. *TDR reflected signals by the clean sample (Water 15%, Diesel 0 ppm).*

It can be noticed that the clean sample (Figure 2) shows a light disparity in its signals relatively to the contaminated soils. This disparity must be due to the important existing air volume, which may not be distributed in the same manner for all the clean samples. Also, the insertion of the TDR probe rods in the soil sample may have compacted and

disturbed the surrounding soil. Moreover, often air-gaps are trapped between the rods and the soil. The effect of the air-gaps presence on the accuracy of the TDR measurements has been mentioned by Annan (1977), and has confirmed them as being a serious error source in the dielectric permittivity estimation.

The aforementioned disparity for the collected signals from the clean sample is less perceptible for the signals corresponding to the contaminated soils (Figure 3). This is probably due to the existing air volume, which is less important, and probably to a lubrication effect of diesel on the rods, making their insertion easier without large disturbance of the contacting soil.

A plot of the arithmetic mean, at each instant, of the reflection coefficient relatively to each soil is yielded on Figure 4. This global plot shows the diesel contamination effects on the reflected TDR signals. As a first note, it can be mentioned that these effects are observed by separating the signals from one another, especially on their ascending fronts. Then, the reflected signals by the clean and contaminated soils narrow and trend asymptotically to a horizontal level. The tail end of the TDR signal characterises the electrical conductivity of the medium surrounding the probe rods (Dalton *et al*., 1984). The variations of the electrical conductivity are expressed by an excursion in the vertical sense of the signal plane part. The exploitation of this effect allows the determination of the soil electrical conductivity (Topp *et al*., 1988).

Based on our study, the diesel presence has had no effect on this signal characteristic part. It can be concluded that the diesel has no contribution to the soil electrical conductivity, which confirms the non-conductive character of diesel.

Figure 5 presents the sections of the collected signals shown on Figure 4 corresponding to time t = 16.3 ns till time t = 19.7 ns. The portion of the reflected signal before t = 16.8 ns corresponds to the propagation in the coaxial cable Then the propagation takes place in the resin layer, between t = 16.8 ns and t = 17.1 ns. Beyond this instant, the TDR signal propagates in the waveguides inserted in the soil sample. The signals corresponding to the different samples untie clearly from one ~~to~~ another and evolve in a similar manner without crossings at anytime. The propagation velocity is not the same depending on the soil in which the probe is inserted, a delay arises in travel times observed for one sample to another, thus inducing the noticed interval between the TDR signals. It should be noticed

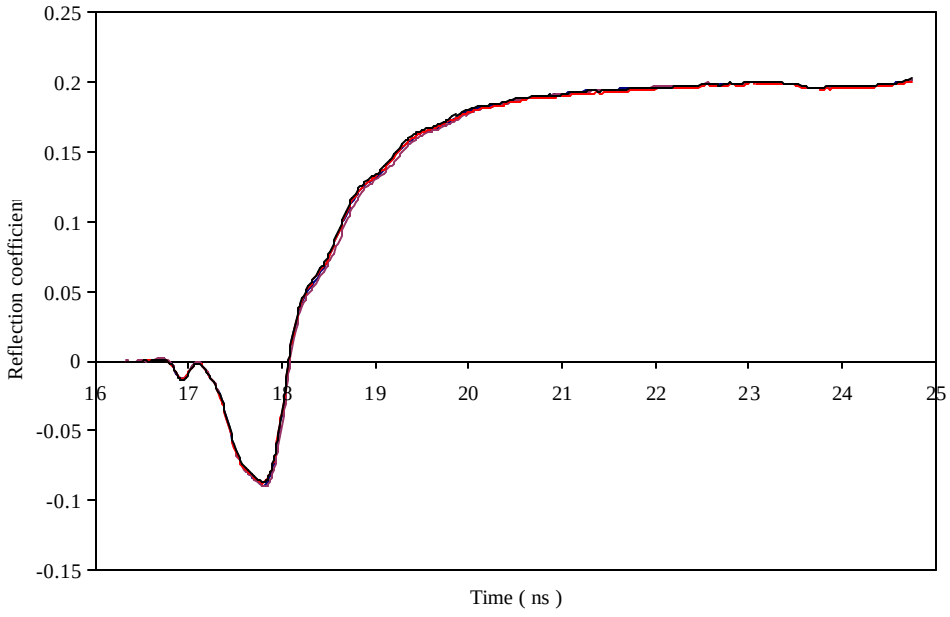

Fig. 3. *TDR reflected signals by the contaminated sample (Water 15%, Diesel 18076 ppm).*

that these delays arise in increasing diesel concentration order. The delay observed relatively to the clean sample increases as the diesel concentration increases in soil.

Moreover, it is possible to notice that the reflection coefficient modulus, at the rods' extremities, increases with the diesel concentration in the soil. The observed behaviours are the direct consequence of the diesel concentration influence on the apparent dielectric permittivity of the composite constituted of solid grains, water and air.

Having in mind that the diesel permittivity is more important than air's permittivity, it is easy to see, by comparing Equations (3) and (4), that the diesel presence in an unsaturated soil has the effect to increase the composite's dielectric permittivity.

In the aim to better traduce the experimental realities, the mixing law (equation 4) has been rewritten as a function of massic concentrations of water q_m and of diesel y_m. This law becomes,

$$e = \left[\frac{r_s}{r_w} q_m e_w^b + \frac{r_s}{r_{diesel}} \frac{q_m y_m}{1-y_m} e_{diesel}^b + (1-f) e_s^b + \left(f - \frac{r_s}{r_w} q_m - \frac{r_s}{r_{diesel}} \frac{q_m y_m}{1-y_m}\right) e_{air}^b \right]^{\frac{1}{b}} \quad [6]$$

ρ_w , ρ_s and ρ_{diesel} designate the bulk densities of water, solid grains and diesel, respectively.

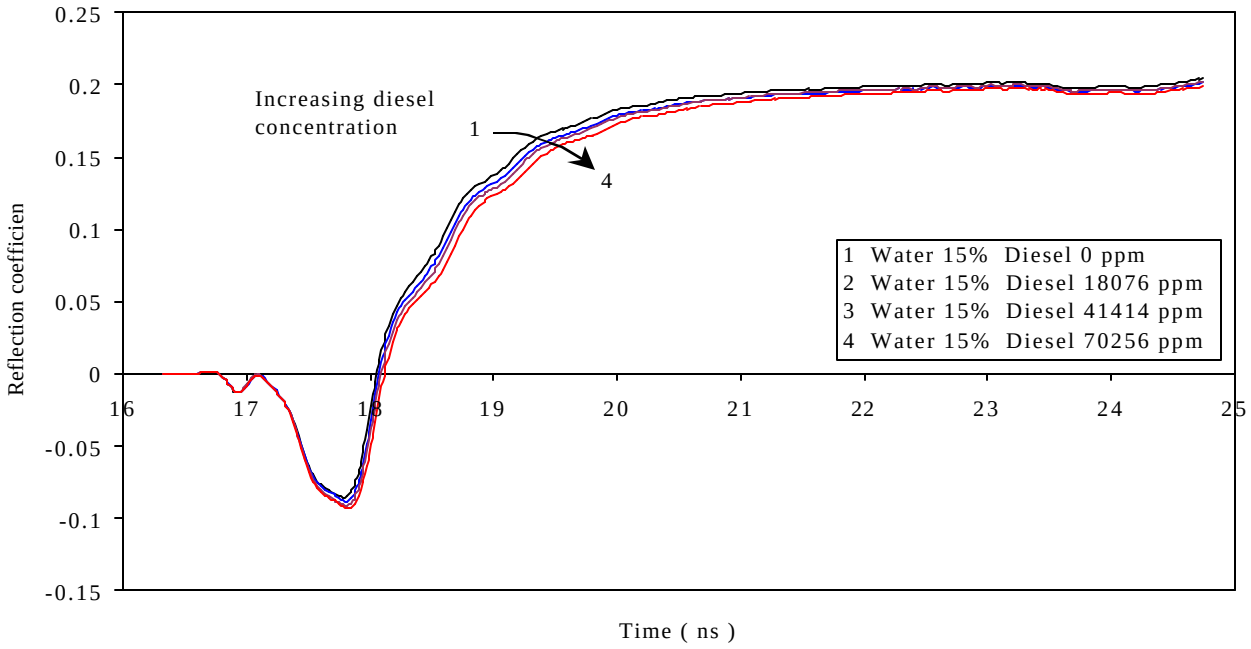

Fig. 4. *TDR reflected signals by the clean and diesel contaminated soils.*

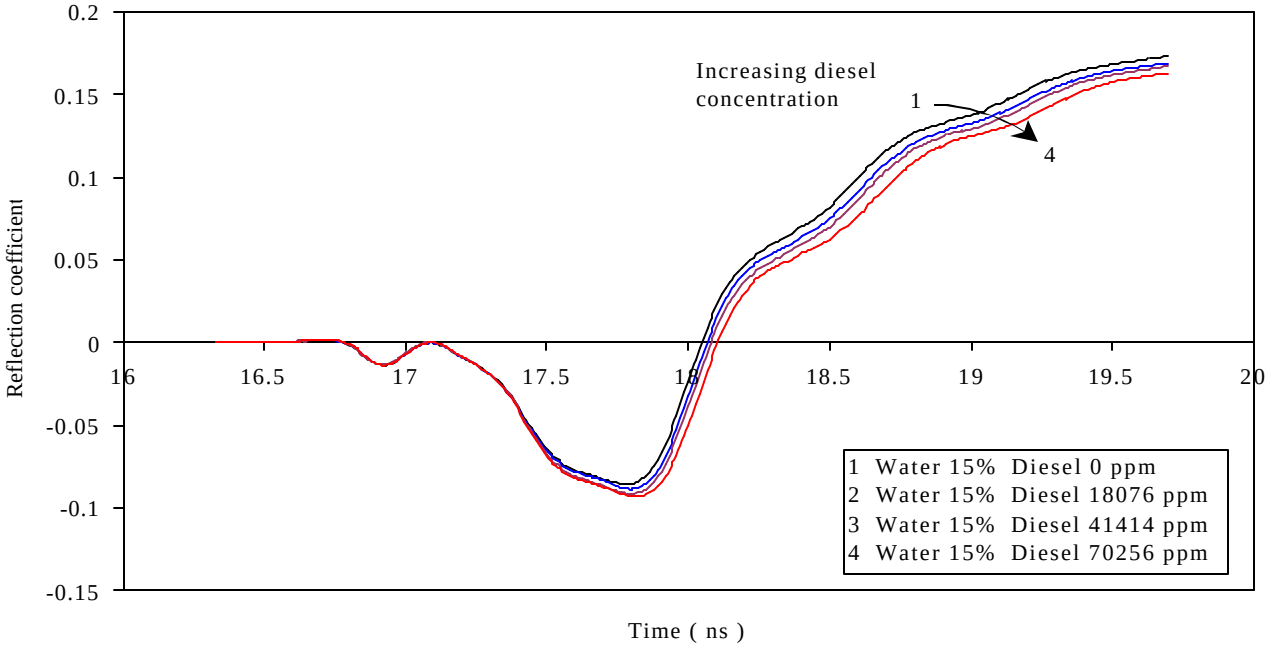

Fig. 5. *Initial part of the TDR reflected signals by the clean and diesel contaminated soils.*

A graphical representation of the relative dielectric permittivity of the clean and diesel contaminated soil as function of the soil water content, predicted by Eq.6 is presented in Figure 6. The numerical values used for the bulk densities are: $\rho_w = 10^3$ kg/m^3, $\rho_s = 2.7 \times 10^3$ kg/m^3 and $\rho_{diesel} = 0.77 \times 10^3$ kg/m^3 . It appears from this last plot that the dielectric permittivity of the soil doesn't considerably increase when the diesel concentration increases. This behaviour can be explained by the fact that the permittivity of diesel is close to that of the air and that of solid grains and relatively small in comparison with the permittivity of water.

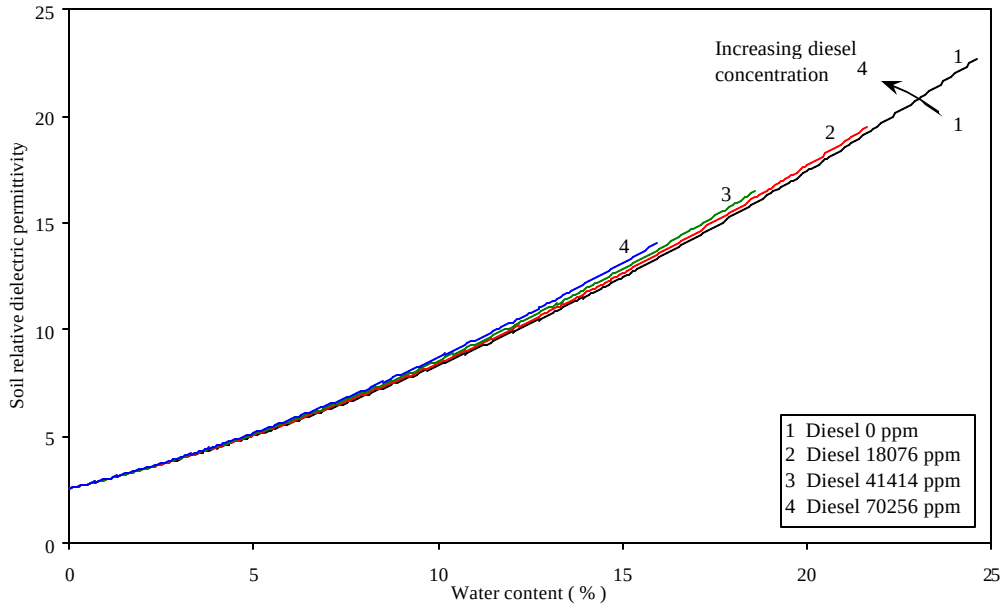

Fig. 6. *Soil relative permittivity, as predicted by the mixing model, versus water content for different diesel concentrations.*

Figure 7 represents the theoretical evolution of the travel time as a function of water content, at constant diesel concentration, obtained by the combination of equations (2) and (6). It appears from this plot that the travel time follows an increasing linear evolution. The delay induced by the soil diesel contamination increases when diesel concentration increases. This confirms what is observed on the experimental TDR signals reported in Figures 4 and 5.

This behaviour is noticeable only for unsaturated soils. In case of initially saturated soils in water, the hydrocarbon presence induces a decrease of the dielectric constant, and of the travel time in the waveguides consequently. So, TDR signals corresponding to contaminated soils will arise on the left of the "clean signal", i.e. earlier on the time scale. These dielectric permittivity and travel time behaviours for the saturated soils were observed by Redman *et al*. (1991), and Redman and Annan (1992). Because of the important gap existing between the permittivities of the hydrocarbon contaminant and the water, the effect of the contaminant presence on the soil's apparent permittivity and on the travel time is noticeable for saturated soils. For unsaturated soils, this remark is not valid, for the dielectric constant and the travel time as much as for the reflected electromagnetic signal's amplitude.

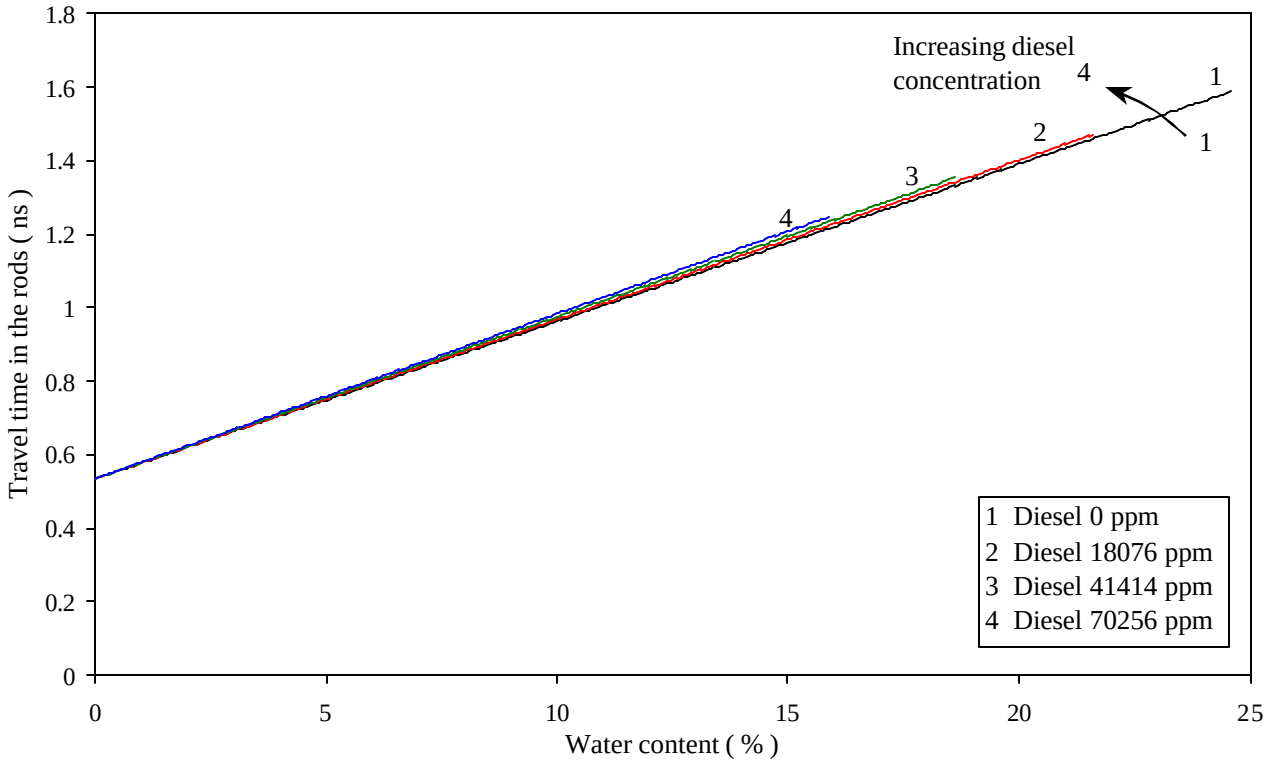

Fig. 7. *Travel time evolution of the TDR signal versus soil water content for different diesel concentrations.*

Although, the reflected signals for clean and diesel contaminated are not superimposed, the difference in the amplitudes is small. In order to qualify and quantify the changes in the difference in signal amplitude with regard to changes in diesel concentration, difference curves at each instant between the signals corresponding to contaminated soils and the signal corresponding to the clean soil, taken as reference signal, are plotted in Figure 8.

The plot was carried out for each contamination rate. The obtained curves yield similar shapes. They arise in a succession of peaks, with a decreasing amplitude and regularly spaced. These curves are untied between them following the diesel concentration. A comparison of the obtained plots shows that the amplitudes' peaks increase with an increase in the diesel concentration in the soil. It can be noticed also that these curves are rowed by increasing diesel concentration.

The peaks' amplitudes are different relatively to a considered sample i.e. following the diesel content. However this is not valid for times when they arise. The peaks appear at the same time for the three contaminated samples. The diesel concentration is more likely not affecting peaks positions. However, peaks positions seem rather to be imposed by the rods dimensions. Further investigations will shed more light on this hypothesis.

Figure 9 presents the plot of the envelope of the peaks appearing in Figure 8. The separation between the curves following the diesel concentration in the sample is noticeable. The obtained curves are decreasing and rowed by increasing diesel concentration. The decrease rate is more important when the diesel concentration increases. The envelope curves narrow one to another and seem to trend to an asymptotic value.

So following these remarks, it can be concluded that the amplitudes peaks of the TDR signal difference curves, are correlated to the diesel content.

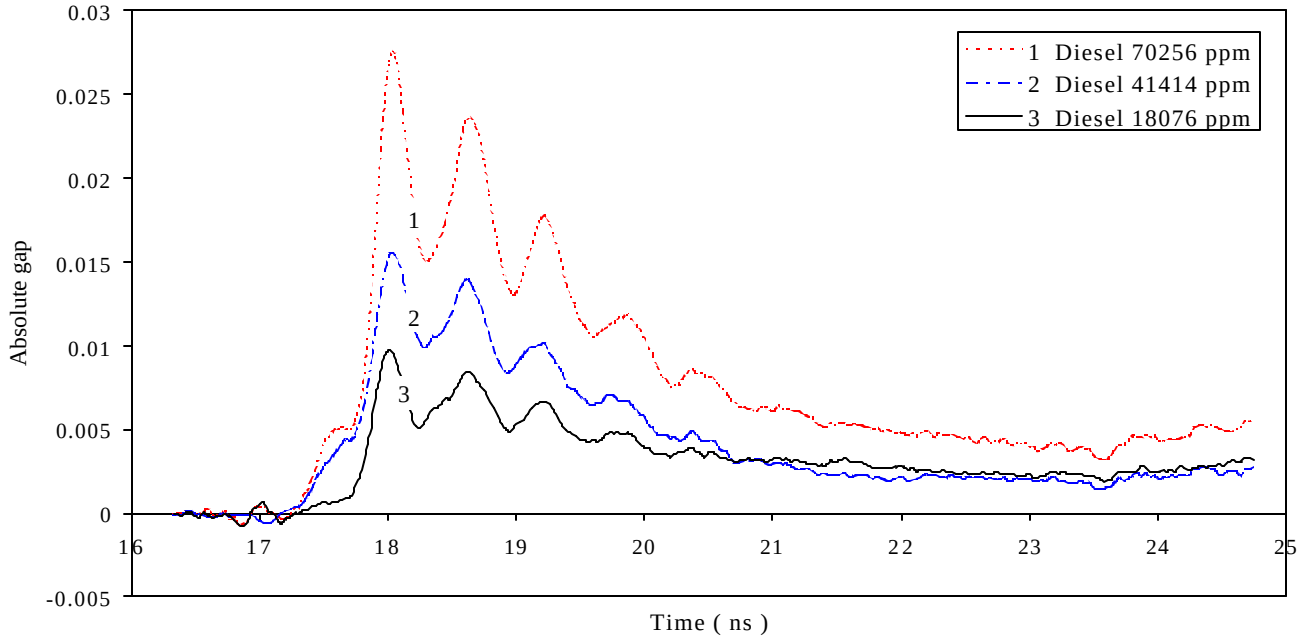

Fig. 8. *TDR signals gap reported to the clean soil signal considered as reference versus time.*

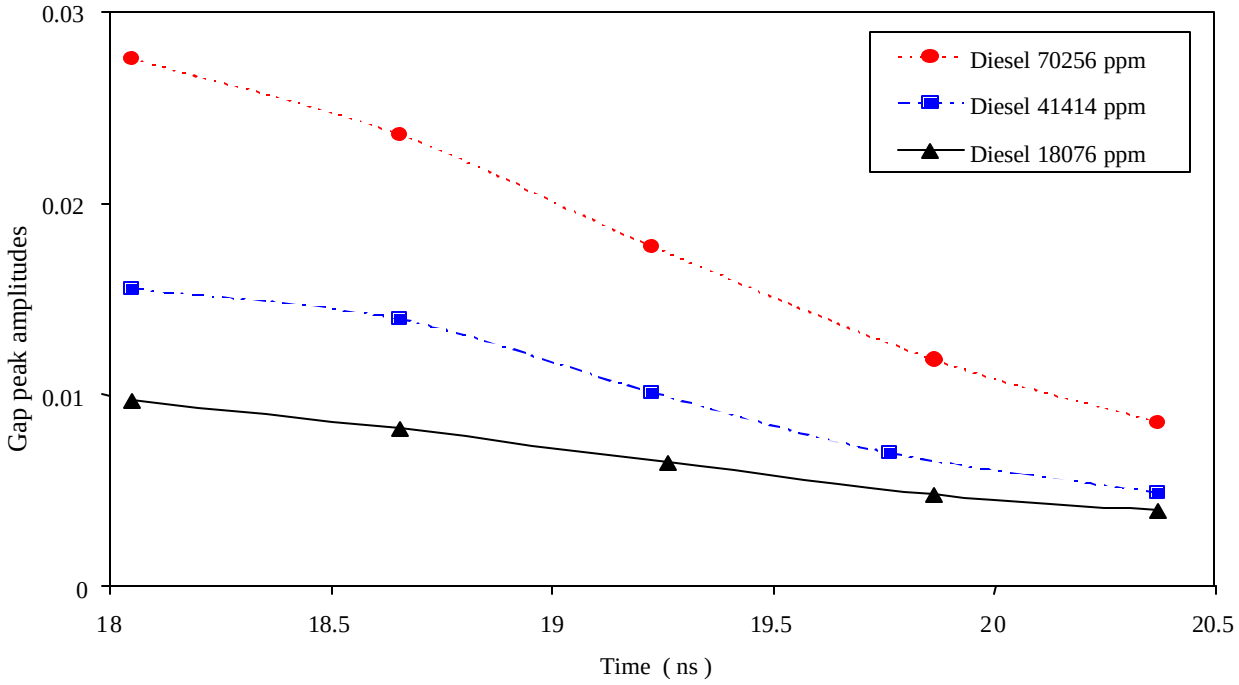

Fig. 9. *Envelope curves of maximum values of the reflection gap curves versus time.*

SUMMARY AND CONCLUSION

In the performed study, the effects induced by a diesel presence in an unsaturated soil, on the reflected TDR signal behaviour were sought. It has been shown experimentally that the diesel presence in an unsaturated soil is traduced by an increase (with an increase of the diesel concentration) of both the TDR signal's delay and the reflection coefficient modulus. A comparison with the existing results in the literature for saturated soils shows an opposite effect on the reflected TDR signal. The importance of the influence induced by the diesel on the TDR signal reflected by an unsaturated soil was noticed and compared to a saturated soil. On the basis of the mixing model, a justification to these opposite behaviours and their relative importance in the two cases is presented.

Also, to underscore the diesel presence effect, the curves showing the difference between the reference signal constituted by the "clean signal" and the "contaminated signals" have been plotted. They show, for all concentrations, an increase of a regular series of peaks, which dynamics is as much important as the diesel content. Despite the weak influence of diesel on the reflected TDR signal by an unsaturated soil, the performed study showed a behaviour of the signal relatively to the diesel and its concentration. It will be useful to improve the exploitation of the TDR signal in order to bypass this sensibility weakness and to be able to quantify the existing diesel concentration. Furthermore, the non-conductive character of diesel may be exploited. The non-contribution of diesel to the soil's electrical conductivity, allied to its dielectric permittivity is a promising tool to solving this difficult problem.

ACKNOWLEDGEMENTS

The research is supported by the Director General of Environment (DGE), The Department of National Defence of Canada (DND). This financial support is gratefully acknowledged. The authors also thank Mr.

Joe Depietriantonio, geotechnical technologist in civil engineering department, Royal Military College of Canada, for his technical support in the laboratory.

REFERENCES

Alharthi, A., and Lange, J., 1987, Soil water saturation: Dielectric determination, Water Resour. Res., **23**, No. 4), 591-595.

Annan, A. P., 1977, Time-domain reflectometry -- air-gap problem for parallel wire transmission lines, in Report of Activities, Part B, Rep. 77-1B, pp. 59-62, Geol. Surv. Of Canada, Ottawa.

Benson, C. H., and Bosscher, P. J., 1999, Time-domain reflectometry (TDR) in geotechnics: a review, Nondestructive and Automated Testing for Soil and Rock Properties, ASTM STP 1350, Marr, W. A., and Fairhurst, C. E., Eds., American Society for Testing and Materials, West Conshohocken, 113-136.

Brewster, M. L., Annan, A. P., Greenhouse, J. P., Kueper, B. H., Olhoeft, G. R., Redman, J. D., and Sander, K. A., 1995, Observed migration of a controlled DNAPL release by geophysical methods, Ground Water, **33**, No. 6, 977-987.

Chenaf, D., 2000, Petroleum oil lubricant mobility in permafrost, Internal Technical Report for DGE, 100p.

Cole, R.H., 1977, Time domain reflectometry, Ann. Rev. Phys. Chem., **28**, 283-300.

Dalton, F. N., Herkelrath, W. N., Rawlins, D. S., and Rhoades, J. D., 1984, Time-domain reflectometry: Simultaneous measurement of soil water content and electrical conductivity with a single probe, Science, **224**, 989-990.

DeRyck, S. M., Redman, J. D., and Annan, A. P., 1993, Geophysical monitoring of a controlled kerosene spill, Proceedings of the Symposium on the Application of Geophysics to Engineering and Environnmental Problems, San Diego, California, April 18-22, 5-20.

Feng, W., Lin, P., Deschamps, R., J., and Drnevich, V.P., 1999, Theoretical model of a multisection time domain reflectometry measurement system, Water Resour. Res., **35**, No. 8, 2321-2331.

Ferré, P. A., Knight, J. H., Rudolph, D. L., and Kachanoski, R. G., 2000, A numerically based analysis of the sensitivity of conventional and alternative time domain reflectometry probes, Water Resour. Res., **36**, No. 9, 2461-2468.

Jones, S. B., and Friedman, S. P., 2000, Particle shape effects on the effective permittivity of anisotropic or isotropic media consisting of aligned or randomly oriented ellipsoidal particles, Water Resour. Res., **36**, No. 10, 2821-2833.

Kueper, B. H., Redman, D., Starr, R. C., Reitsma, S., and Mah, M., 1993, A field experiment to study the behavior of tetrachloroethylene below the water table: Spatial distribution of residual and pooled DNAPL, Ground Water, **31**, No. 5, 756-766.

O'Connor, K. M., Dowding, C. H., 1999, GeoMeasurements by Pulsing TDR Cables and Probes, CRC Press, New York.

Olhoeft, G. R., 1986, Direct detection of hydrocarbon and organic chemicals with ground penetrating radar and complex resistivity, Proceedings of the NWWA/API Conference on Petroleum Hydrocarbons and Organic Chemicals in Ground Water - Prevention, Detection, and Restoration - , Houston, November 12-14, 284-305.

Pitchford, A. M., Mazzella, A. T., and Scarbrough, K. R., Soil-gas and geophysical techniques for detection of subsurface organic contamination, Final Report, January 1989, Air Force Engineering & Services Center, Florida.

Redman, J. D., Kueper, B. H., and Annan, A. P., 1991, Dielectric stratigraphy of a DNAPL spill and implications for detection with ground penetrating radar, Fifth National Outdoor Action Conference on Aquifer Restoration, Ground Water Monitoring, and Geophysical Methods, Las Vegas, Nevada, May 13-16, 1017-1030.

Redman, J. D., 1992, Geophysics and the solvents-in-groundwater program, Proceedings of the Symposium on the Application of Geophysics to Engineering and Environmental Problems, Oakbrook, Illinois, April 26-29, 375-382.

Redman, J. D., and Annan, A. P., 1992, Dielectric permittivity monitoring in a sandy aquifer following the controlled release of a DNAPL, Fourth International Conference on Ground Penetrating Radar, Rovaniemi, Finland, June 8-13, 191-195.

Redman, J. D., and DeRyck, S. M., 1994, Monitoring non-aqueous phase liquids in the subsurface with multilevel time domain reflectometry probes, Symposium and Workshop on the Time Domain Reflectometry in Environmental, Infrastructure, and Mining Applications, Evanston, Illinois, September 7-9, 207-215.

Robinson, D. A., and Friedman, S. P., 2001, Effect of particle size distribution on the effective dielectric permittivity of saturated granular media, Water Resour. Res., **37**, No.1, 33-40.

Roth, K., Schulin, R., Flühler, H., and Attinger, W., 1990, Calibration of time domain reflectometry for water content measurement using a composite dielectric approach, Water Resour. Res., **26**, No. 10, 2267-2273.

Tabbagh, A., Camerlynk, C., and Cosenza, P., 2000, Numerical modeling for investigating the physical meaning of the relationship between relative dielectric permittivity and water content of soils, Water Resour. Res., **36**, No. 9, 2771-2776.

Tektronix, 1993, 1502C Metallic Time Domain Reflectometer, Operator Manual, 070-7169-00, Tektronix Inc., USA.

Topp, G. C., Davis, J. L., and Annan, A. P., 1980, Electromagnetic determination of soil water content: Measurements in coaxial transmission lines, Water Resour. Res., **16**, No. 3, 574-582.

Topp, G. C., Yanuka, M., Zebchuk, W. D., and Zegelin, S., 1988, Determination of electrical conductivity using time domain reflectometry: soil and water experiments in coaxial lines, Water Resour. Res., **24**, No. 7, 945-952.

Topp, G.C., Zegelin, S.J., and White, I., 1994, Monitoring soil water content using TDR: An overview of progress, Symposium and Workshop on the Time Domain Reflectometry in Environmental, Infrastructure, and Mining Applications, Evanston, Illinois, September 7-9, 67-80.

Weerts, A. H., Huisman, J. A., and Bouten, W., 2001, Information content of time domain reflectometry waveforms, Water Resour. Res., **37**, No. 5, 1291-1299.

USE OF TDR TO MONITOR CHANGES IN GROUND WATER LEVEL AND CRUDE OIL THICKNESS

Kevin M. O'Connor

GeoTDR, Inc., 7290 Greencrest Drive, Westerville,
Ohio 43082, kevin@geotdr.com

ABSTRACT

Time domain reflectometry (TDR) measurements were made in a well that was screened in a residual pool of crude oil near Bemidji, Minnesota to evaluate the use of TDR to monitor variations in oil thickness and groundwater levels. The pool is the result of a crude oil pipeline break in 1979 and rests on the water table. The U.S. Geological Survey maintains the site as a research facility and over 250 monitoring wells have been installed to characterize subsurface conditions. Data were acquired automatically using TDR by interrogating an air-dielectric coaxial cable installed in one well. Independent measurements were made manually with an oil-interface probe in several adjacent wells. Both types of measurements indicate a seasonal variation in apparent oil thickness within the wells. This research demonstrates that it is now possible to continuously measure changes in the apparent thickness of light non-aqueous phase liquids (LNAPLs) using TDR, which may prove to be a useful tool in evaluating the long-term effects of on-site remediation of contaminated aquifers.

SITE DESCRIPTION

On August 20, 1979, approximately 16 km northwest of Bemidji, Minnesota, the land surface and shallow subsurface were contaminated when a crude-oil pipeline burst, spraying about 1,700,000 L (about 10,700 barrels) of crude oil onto a glacial outwash deposit (Delin *et al*, 1998). Crude oil also sprayed to the southwest covering an approximately 7,500 m^2 area of land. After cleanup efforts were completed about 400,000 L (about 2,500 barrels) of crude oil remained at the site. Some crude oil percolated through the unsaturated zone to the water table near the rupture site. Some of the sprayed oil flowed over the land surface toward a small wetland forming a second area of oil infiltration (south oil pool).

The land surface is a glacial outwash plain underlain by stratified glacial outwash deposits. Sediments at the test site consist of poorly sorted glacial outwash sand of fine to very coarse grain size, with some fine gravel and cobbles. Iron-cemented laminations, 1- to 10-mm thick, occur between depths of 0.3 and 1.0 m. At a depth of about 25 m, a regionally persistent and uniform layer of low permeability sediment (till) restricts vertical ground water movement. Crude oil floats on the water table, which is about 2.7 m below land surface at the south oil pool.

In order to ensure compliance with Minnesota law, State authorities have mandated oil-recovery remediation of the site. The aim of the remediation is to remove the separate-phase oil that is presently floating on the water table. In the area of the south oil pool, a trench was excavated in October 1999 and oil is being separated from the extracted water-oil mixture.

MEASUREMENT OF LNAPLs IN MONITORING WELLS

The relationship between oil thickness in the well and the water-table level is very complex. Apparent thickness depends not only on the capillary fringe but also on the actual hydrocarbon thickness in the soil or rock formation (Testa and Paczkowski, 1989). For fine-grained formations apparent thickness will be greater than actual thickness whereas for coarse grained formations apparent thickness is apt to be less, although here apparent thickness may be more representative of the real thickness. Water fluctuations created by recovery operations or seasonal variations that result in decreased water table elevations can produce an apparent hydrocarbon layer thickening. Consequently, during ground water recharge, which compresses the capillary zone and therefore lessens elevation difference between the free water table and hydrocarbons, a thinner hydrocarbon layer is apparent.

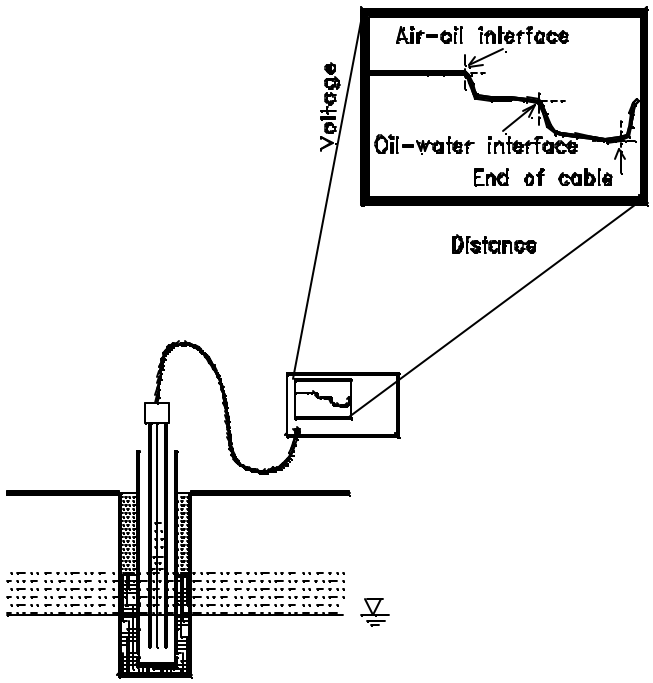

Fig. 1. *Schematic of air-dielectric coaxial cable in well and TDR waveform. The "oil-saturated pancake" is not representative of actual subsurface conditions.*

The distribution of LNAPL in the subsurface will be a function of LNAPL, water and air pressures, and the pore-size distribution of the porous medium (Lenhard and Parker, 1990). At equilibrium, abrupt changes in fluid contents with elevation do not generally occur except in porous media with uniform pore-size distributions or in layered porous media with contrasting pore-size distributions. Thus, oil-saturated "pancakes" as suggested in Figure 1 do not develop in the vast majority of soils and aquifers.

To estimate hydrocarbon specific volume, water and hydrocarbon saturation distributions in the soil must be known (Lenhard and Parker, 1990). For an air-hydrocarbon-water fluid system in water-wet porous media, water saturation depends on the capillary pressure between water and hydrocarbon phases, and total liquid saturation depends on the capillary pressure

between hydrocarbon and gas phases. Fluid saturation distributions, therefore, will be controlled by saturation-capillary pressure relations of the soil which in turn depend on the pore-size distribution.

Kelly *et al* (1995) derived a numerical modeling method for calculating NAPL volume and distribution. They constructed models to calculate vertical NAPL saturation profiles under equilibrium conditions (i.e., non-fluctuating water table) at monitor wells where measurements of NAPL thickness are available. They estimated the total NAPL volume in the stratified aquifers by spatially integrating the vertical saturation profiles at each well over the area of contamination within each aquifer.

There are lots of arguments, and little agreement among people about these matters. One thing is clear. In general, as the water table rises, the thickness of oil in the well decreases, and visa versa. However, the total amount of oil present in the aquifer is not significantly changed when the water table rises. The amount of oil in the well appears to be a rough indicator of how much oil is present in the aquifer above the elevation of the oil-water interface in the well (Herkelrath, 1999).

TDR FOR GROUNDWATER AND CRUDE OIL THICKNESS MONITORING

An air-dielectric coaxial cable can be placed in a well to monitor changes in water level as shown in Figures 1 and 2. When a voltage pulse is transmitted along the cable or wire, a large magnitude negative reflection occurs at the air-water interface (Dowding *et al*, 1996; Nicholson *et al*, 1997), and a large magnitude positive reflection occurs at the end of the cable or wire. In a situation where there is oil resting on the water, there is a reflection at the oil-water interface within the cable.

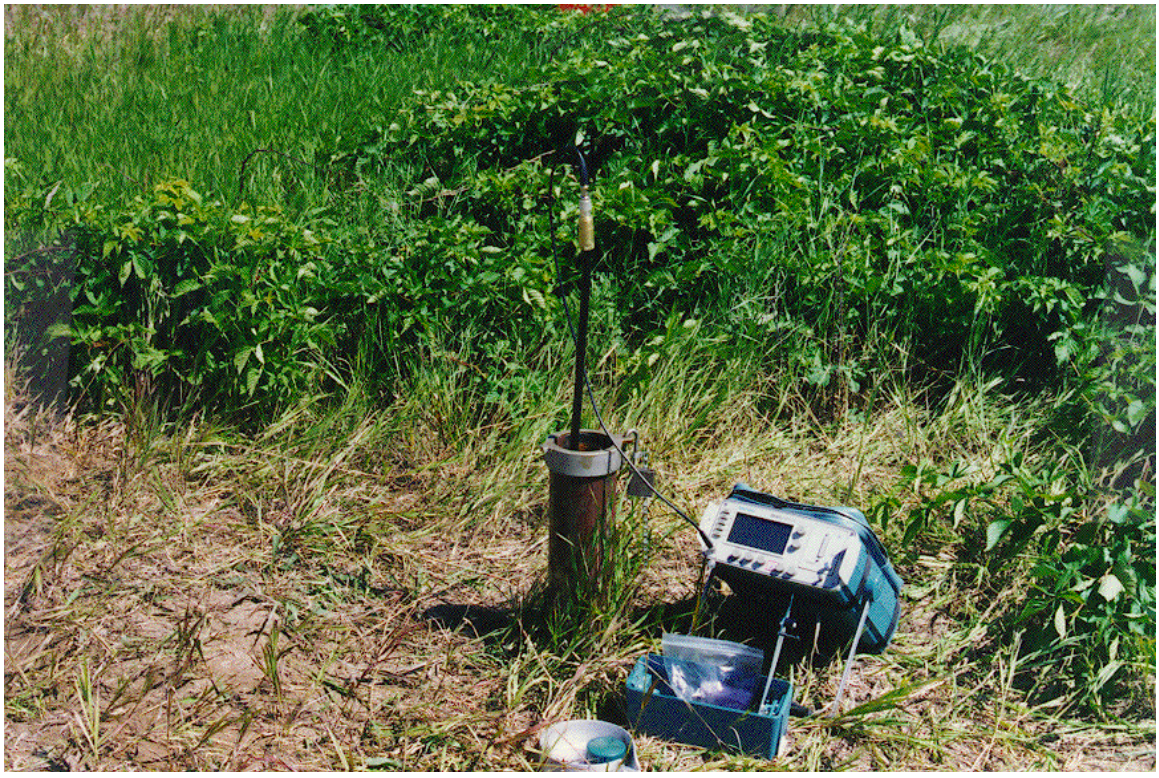

Fig. 2. *Air-dielectric coaxial cable in well*

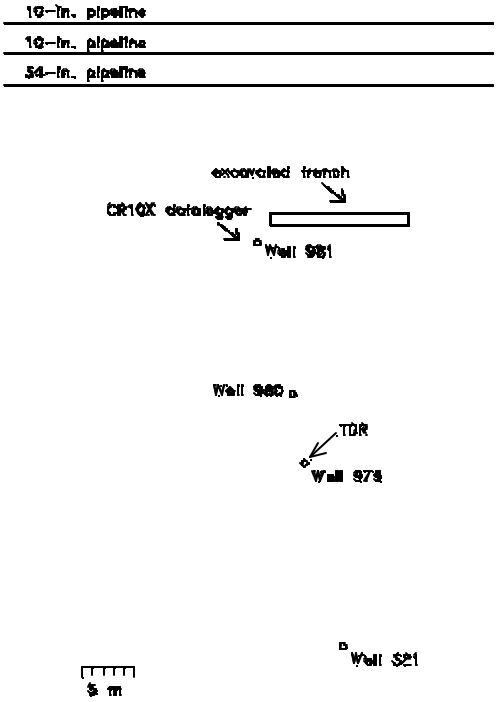

Fig. 3. *Locations of wells relative to trench excavated to pump oil-water mixture.*

An automated data logging system was installed near Well 981 (south oil pool) in late 1996 primarily to compare the performance of several different soil-moisture probes manufactured by Campbell Scientific, Inc. An air-dielectric coaxial cable was installed in well 979, and a lead cable was extended to a coaxial multiplexer which in turn was connected to a Tektronix 1502B TDR cable tester and a CSI CR10X data logger (Figures 3 and 4). The system was initially powered by batteries that were trickle charged with a solar panel. However, the batteries were replaced in the fall of 1997 with a 110 VAC power supply.

Fig. 4. *Junction box installed at top of well 979 in foreground. Low-loss coaxial lead cable is buried and extends to the automated data logger system at well 981 in background.*

RESULTS

Representative TDR waveforms are shown in Figure 5. There are four significant reflections: (1) crimp made in the cable prior to installation, (2) air-oil interface within the cable, (3) oil-water interface within the cable, and (4) end of the cable. The crimp provides a distance benchmark that calibrates each waveform.

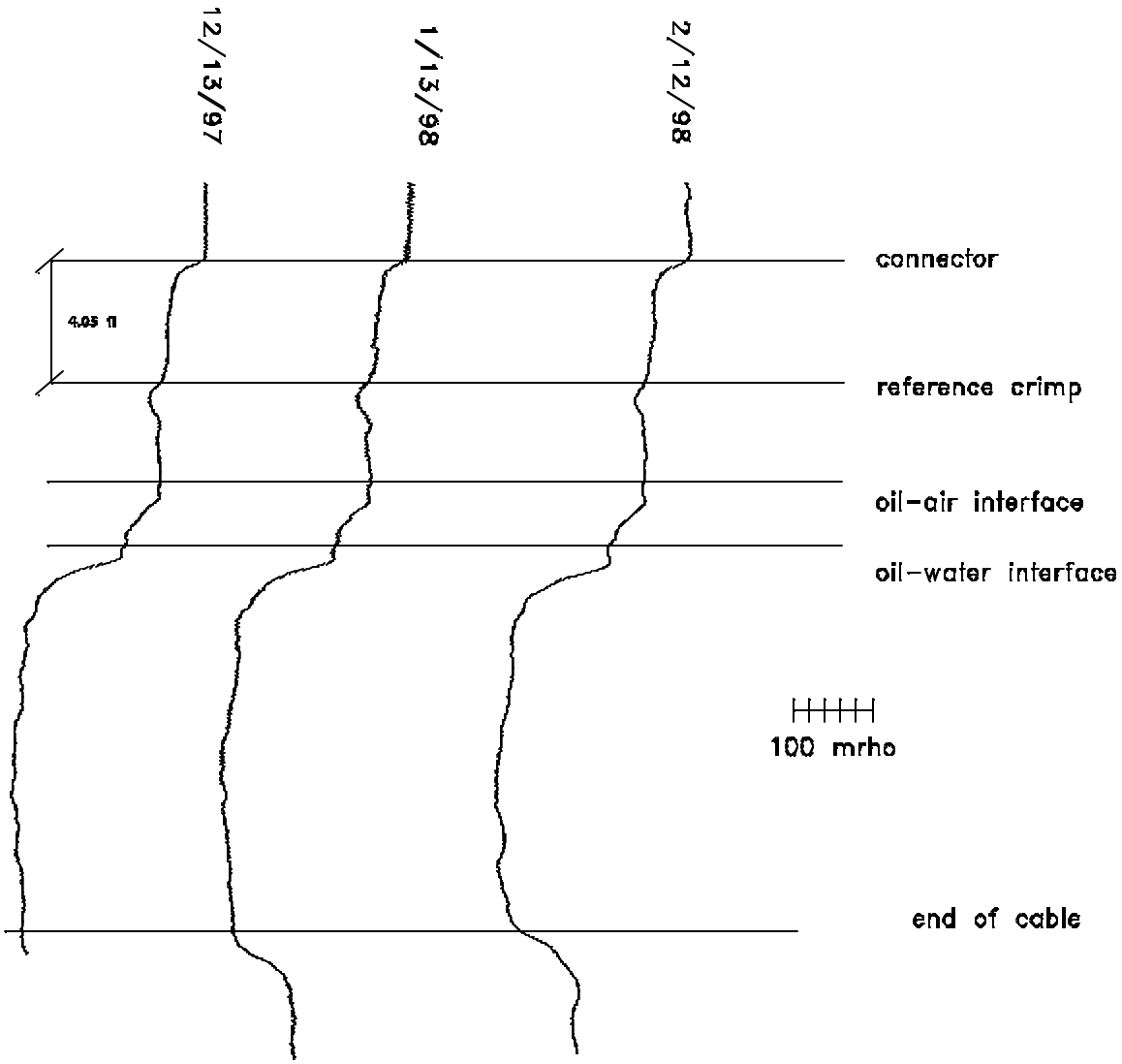

Fig. 5. *Waveforms acquired from air dielectric cable installed in monitoring well. Note that there is a reflection at the oil-air and oil-water interfaces. The crimp made in the cable prior to installation provides a distance calibration for each reading.*

The time history of depth to oil and water surfaces are shown in Figure 6. For comparison, manual measurements of oil pool thickness made in adjacent wells with a conductance probe are plotted in Figure 7. Remediation began in October 1998 and the top of hole connection was damaged during construction activities. This damage was repaired in May 1999 and automated monitoring resumed.

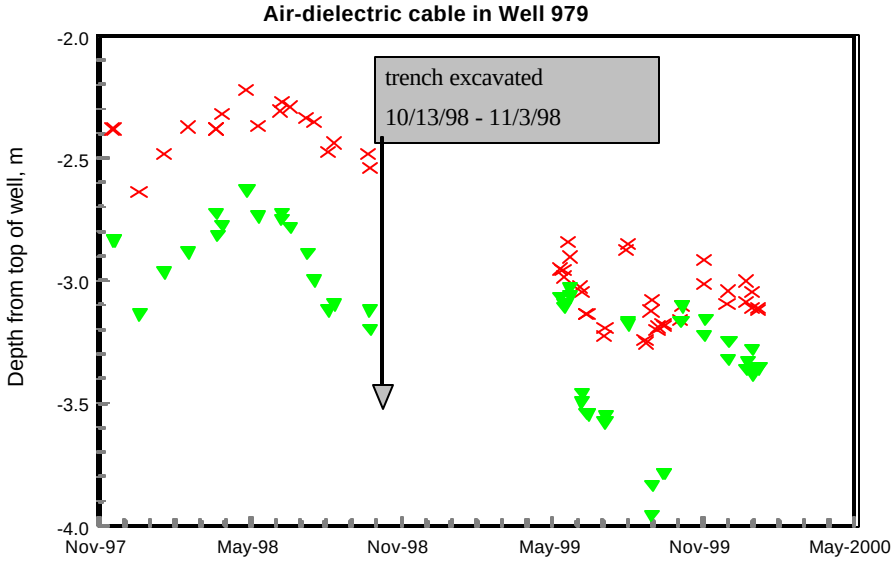

Fig. 6. *Time history of TDR measurement of depth to top-of-oil and depth to oil-water interface.*

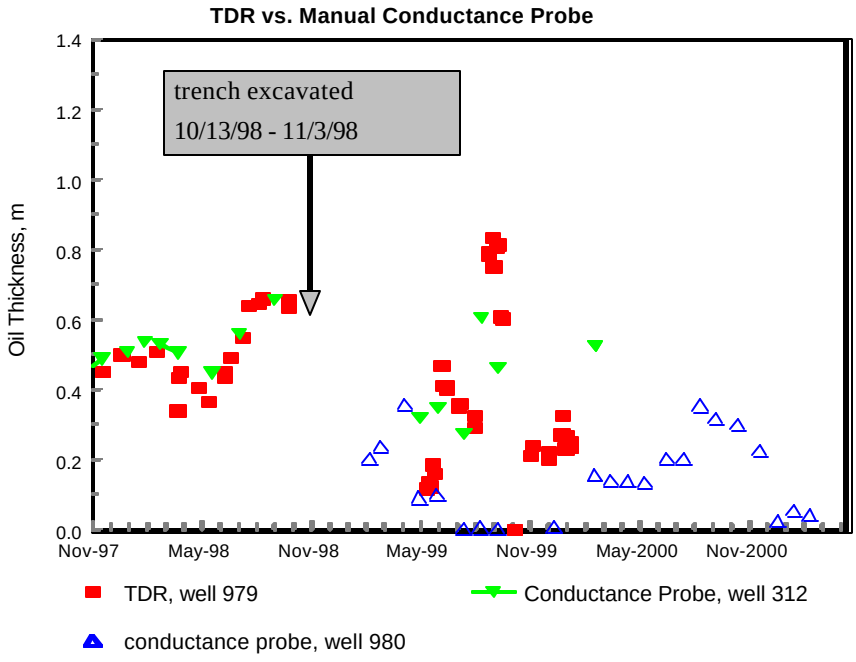

Fig. 7. *Time history of oil pool thickness. Automated TDR measurement is compared with manual measurement made in an adjacent well using a conductance probe.*

Note the consistency between TDR measurements made in well 979 and manual probe measurements made in well 312 prior to remediation (Figure 6). They both show the seasonal variation in oil pool thickness and correlate well. Over the period from April to June 1998, there was a decease in the measured oil thickness as ground water was recharged. The measured oil thickness varied from a minimum of 365 mm in June 1998 to a maximum of 655 mm in October 1998. These variations likely result from oil getting spread out vertically as the water level fluctuates in response to aquifer recharge and discharge. It is hypothesized that oil becomes entrapped in the unsaturated and saturated zones of the aquifer (Herkelrath, 1999). This alternating entrapment and release of oil results in an apparent decrease or increase in oil thickness in the well. The relationship between thickness of oil in a well and the amount of oil in the adjacent aquifer is tenuous under these conditions.

After remediation began, measurements indicate greater fluctuation in the oil pool thickness. The influence of oil recovery is evident by the reduced oil thickness in well 980 (Figure 7) which is 30 m from

the trench (Figure 3). The reduction in oil thickness measured in well 979 (36 m from the trench) is intermediate between the measured thicknesses in well 312 (54 m from the trench) and well 980. In November of 1999, the oil thickness in well 312 had not been impacted, but by that time the thickness in well 979 was reduced and more consistent with the oil thickness in well 980.

DISCUSSION

Technicians can field-estimate hydrocarbon volume recoverable, using the true product thickness and bail-down testing. Field workers can use an oil-water interface gauging probe to measure initial apparent thickness. The depth to product and depth to water table are measured over time and the test is complete when levels have stabilized for three consecutive readings. bail-down testing is a simple field procedure; however, data interpretation is not always straightforward. In addition, data accuracy can be influenced by (Testa and Paczkowski, 1989): inaccurate measuring devices, operator error, rapidly rising fluid levels that prevent the operator from collecting timely data, bailing from low-yield formations, imperfect bailing practices, lengthy water recovery time periods, borehole effects that cause variable product accumulation rates, and imprecise curve evaluation.

These limitations to measurements of NAPL thickness within monitoring wells are inherent in the use of TDR, but there are several advantages which can be realized by automated monitoring with TDR. Data acquisition frequency can be adjusted from one reading per second during bail-out tests to one reading per week for long term monitoring. Several wells can be monitored simultaneously with a since TDR and data acquisition system which would make it possible to assess gradient changes over time.

TDR can also provide additional information about ground water conditions as the reflection at the end of the cable can be attenuated depending on the fluid conductivity (Dalton *et al*, 1984). This technology has also been used to monitor transport of sodium chloride, calcium chloride, kerosene, and tetrachloroethylene (Kachanoski and Ward, 1994; Redman and DeRyck, 1994). It has also been used to monitor heavy metal concentrations in mine tailings (Norland, 1994).

SUMMARY

TDR technology can be used for automated monitoring of changes in crude oil levels in wells. While it may be possible to obtain changes in oil thickness using manual measurements during active pumping, there is still the need to determine long term changes. By virtue of continuous remote monitoring it is possible to observe seasonal variations as well as observe what the actual impact of pumping has on the thickness of oil. Results of this study indicate that it is now possible to economically monitor changes in LNAPLS in several wells. Thus it is possible to observe spatial variations over time.

ACKNOWLEDGMENTS

The author wishes to acknowledge the valuable comments and input provided by Goeff Delin and William N. Herkelrath of the U.S. Geological Survey. Their support for this cooperative research is greatly appreciated.

REFERENCES

Dalton, F. N., Herkelrath, W. N., Rawlins, D. S., and Rhoades, J. D., 1984, Time Domain Reflectometry: Simultaneous Measurement of Soil Water Content and Electrical Conductivity with a Single Probe. Science, **224**, June, 989-990.

Delin, G.N., Essaid, H.I., Cozzarelli, I.M., Lahvis, M.H., and Bekins, B.A., 1998, Ground water contamination by crude oil near Bemidji, Minnesota: U.S. Geological Survey Fact Sheet FS-084-98, 4 p.; http://wwwmn.cr.usgs.gov/bemidji/; http://toxics.usgs.gov/bib/bib-factsheets.html

Dowding, C.H., Huang, F.C., and McComb, P.S., 1996, Groundwater pressure measurement with time domain reflectometry. Geotechnical Testing Journal, GTJODJ, **19**, March, 58-64.

Herkelrath,W.N. 1999. Personal Communication

Kachanoski, R.G. and Ward, A.L., Measurement of subsurface chemical transport using time domain reflectometry. Proc. Sym. on Time Domain Reflectometry in Envir., Infrastr., and Min. Appl., Evanston, IL, September, 1994, 171-182; NTIS PB95-105789.

Kelly, M.E., Yu, G.G., White, M.D., Rosansky, S.H., and Perry, C.J., 1995, A Numerical Method for Determining the Distribution of Nonaqueous Phase Liquid Contamination in a Confined/Unconfined Aquifer Setting. Paper presented at the 10th Annual Soil Contamination Conference.

Lenhard, R.J. and Parker, J.C., 1990, Estimation of Free Hydrocarbon Volume from Fluid Levels in Monitoring Wells. Ground Water, **28**, No. 1, 57-67.

Nicholson, G.A., Powell, J.F., and O'Connor, K.M., 1997, Monitoring groundwater levels using a time domain reflectometry (TDR) pulser. Final Report, CPAR-GL-97-2, U.S. Army Corps of Engineers WES, Vicksburg.

Norland,M.R, TDR waveform analysis of Cd, Pb, and Zn in coaxial cells. Proc. Sym. on Time Domain Reflectometry in Envir., Infrastr., and Min. Appl., Evanston, IL, September 1994, p. 235; NTIS PB95-105789.

O'Connor,K.M. and Dowding, C.H., 1999. GeoMeasurements by Pulsing TDR Cables and Probes. CRC Press, Boca Raton, ISBN 0849305861.

Redman,J.D., and DeRyck, S.M., Monitoring non-aqueous phase liquids in the subsurface with multilevel time domain reflectometry probes. Proc. Sym. on Time Domain Reflectometry in Envir., Infrastr., and Min. Appl., Evanston, IL, September 1994, pp. 207-214; NTIS PB95-105789.

Testa, S.M. and Paczkowski, M.T., 1989, Volume Determination and Recoverability of Free Hydrocarbon. Ground Water Monitoring Review, **9**, No. 1, 120-128

MEASURING WATER TABLE ELEVATIONS WITHIN PAVEMENT SYSTEMS USING TIME DOMAIN REFLECTOMETRY

Ruth Roberson[1] and John Siekmeier[2]

[1]Minnesota Department of Transportation, Office of Materials and Road Research
Maplewood, Mn 55109-2044; ruth.roberson@dot.state.mn.us
[2]Minnesota Department of Transportation, Office of Materials and Road Research
Maplewood, Mn 55109-2044; john.siekmeier@dot.state.mn.us

ABSTRACT

Measuring changes in the water table elevation below pavement systems is important for understanding pavement performance and improving design methods. Typically ground water monitoring wells are installed at some distance from the actual pavement structure, with measurements usually made manually or with electronic pressure transducers. Time Domain Reflectometry (TDR) methods, using air dielectric coaxial cable to locate the air-water interface in monitoring wells, are currently used in a variety of geotechnical applications. This method for measuring the water table elevation may require less maintenance and be more rugged than using pressure transducers, and provide a means for collecting real-time data from directly below the pavement structure. Laboratory and field experiments comparing TDR, pressure transducer, and manual water table elevations were conducted. An algorithm for locating the air-water interface was developed from laboratory results and applied to field data. Water table elevations measured using the air dielectric coaxial cable compared well to both manual and pressure transducer measurements. The automated system now acquires data, applies the algorithm, and loads the calculated values into a database on a daily basis.

INTRODUCTION

Measuring and monitoring the depth of the ground water table is important in a variety of geotechnical applications, and is routinely practiced in such areas as embankment stability and dam seepage applications. Locating the depth to the water table is also important in the field of pavement engineering, both for structural and drainage design purposes. Ongoing improvements in the pavement design process involve new methods for measuring variables such as water table depth. The Minnesota Department of Transportation's implementation of a mechanistic-empirical (ME) design procedure for flexible pavement brings to the forefront the need for improved methods for monitoring and characterizing environmental and subsurface parameters in and around the pavement structure. ME

design procedures incorporate environmental effects and subsurface conditions, i.e. climate and water table depth into pavement layer design. Therefore, there is a need to locate the water table (stiff layer) for improved calculation of layer moduli, thus improving the overall pavement design. The primary objective of this study was to compare the use of traditional methods of measuring water levels with that of Time Domain Reflectometry (TDR) methods, within the pavement structure. A second objective was to develop an algorithm for automating TDR waveform interpretation and apply it to data collected from field installations.

BACKGROUND

Traditionally ground water level measurements, used for pavement design and construction purposes, are taken manually from monitoring wells installed a significant distance from the pavement structure. Measurements are made using a water level indicator. This consists of inserting an electrode connected to a graduated line into a monitoring well. When the electrode contacts water, causing a short, a buzzer sounds and the depth is determined by the location on the line. Manual measurements are time consuming and the frequency of measurement limited. Also there is the chance of missed or lost data.

Pressure transducers use electronic means (change in bridge resistance) to detect a change in pressure head. In cases where automated measurements are needed electronic pressure transducers are typically used. The pressure transducer is installed "down hole" and data is collected using a datalogging device. Two types of transducers can be used, either an absolute or gauge transducer. With the electronics housed in the "down hole" portion of the transducer it is usually desirable to use the type that provides a measure of the absolute pressure head since these are hermetically sealed to prevent corrosion. However this requires that the data be corrected for barometric pressure, thus requiring additional instrumentation. Additionally, pressure transducers are expensive and require calibration particularly when the supply voltage deviates from that used during manufacturer calibration.

Time Domain Reflectometry

TDR technology was originally used in telecommunications for detecting breaks in cables, such as phone lines. However, the technology has been adapted for a number of uses including measuring water table depth (Dowding *et al.*, 1996a; O'Conner and Dowding, 1999). Electromagnetic pulses containing a spectrum of frequencies are sent down a transmission line. As the pulse travels through the transmission line, changes in electrical impedance encountered result in a portion of the signal being reflected back to the source. In the case of water table depth measurement an impedance change at the air-water interface results in a sharp decrease in the propagation velocity. The change in impedance is attributed to the difference in the dielectric constants of air and water, 1 and 81 respectively.

The use of TDR methods for locating the air-water interface dates back to the early 1970's (O'Conner and Dowding, 1999). Field adaptations of the method where accomplished by Dowding (1999). Later work by Dowding (1996b) investigated the use of twisted pair versus air dielectric cable. Results indicated that an air dielectric cable has less signal loss than a simple twisted pair, thus improving the ability to locate an impedance mismatch in the reflected waveform. Work conducted by the Army Corps of Engineers Waterways Experiment Station considered TDR methods for locating the air-water interface in remote ground water monitoring wells (Nickolson *et al.*, 1997). The literature indicates that TDR methods used for measuring water table depth below the pavement structure may provide an

inexpensive and rugged measurement system. The development of an automated remote system is attractive for use in pavement engineering research.

MATERIALS AND METHODS

Laboratory

Fig. 1 *Air dielectric cable, pressure transducer, Tektronix, and CR10 datalogger*

A laboratory experiment was conducted for developing an algorithm that would automate waveform interpretation resulting in water level measurements that can be directly loaded to a database. This was accomplished by comparing manual, pressure transducer, and TDR methods of measuring water levels.

A 0.5 inch diameter air dielectric cable 5.0 feet long, (Vp = 0.89 spiral spacer between center and outer copper conductors) fitted to a 5.0 foot RG8 lead cable, (Vp = 0.79) was used for developing the algorithm. An electronic pressure transducer with a supply voltage of 2.5 volts gave a full range output of 0 - 25 mV over 0-10 psi (Figure 1). A Campbell Scientific CR10X datalogger and a Tektronix 1502B cable tester were used to capture and store the raw TDR waveforms. The waveform resolution was set to 0.30 inch/division, Vp of 0.89. The datalogger also provided the supply voltage to the pressure transducer and collected transducer output. An acrylic pipe (1.6 inch ID and 4.0 feet long) was used to simulate a monitoring well. The pressure transducer and air dielectric cable were fastened together and inserted into the pipe, leaving a 6 inch space between the bottom of the pipe and the sensors.

Tick marks on the outside of the pipe allowed both visual monitoring and manual measurement of water level changes.

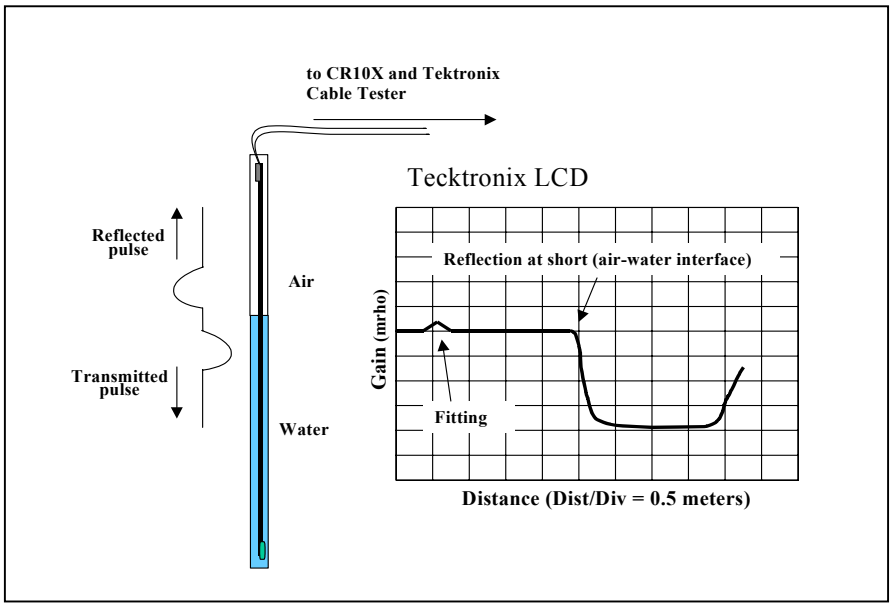

Fig. 2. *Cable tester displaying typical waveform as signal travels the length of the air dielectric coaxial cable.*

An initial water level of 6 inches was measured with additions in 3 inch increments there after, yielding water levels of 6, 9, 12, 18, and 21 inches. At each increment, pressure transducer, TDR, and manual measurements were made.

Automating Waveform Interpretation

As an electromagnetic signal travels along the air dielectric cable an impedance mismatch is encountered at the air-water interface, Figure 3a shows waveforms for various water levels measured in the laboratory.

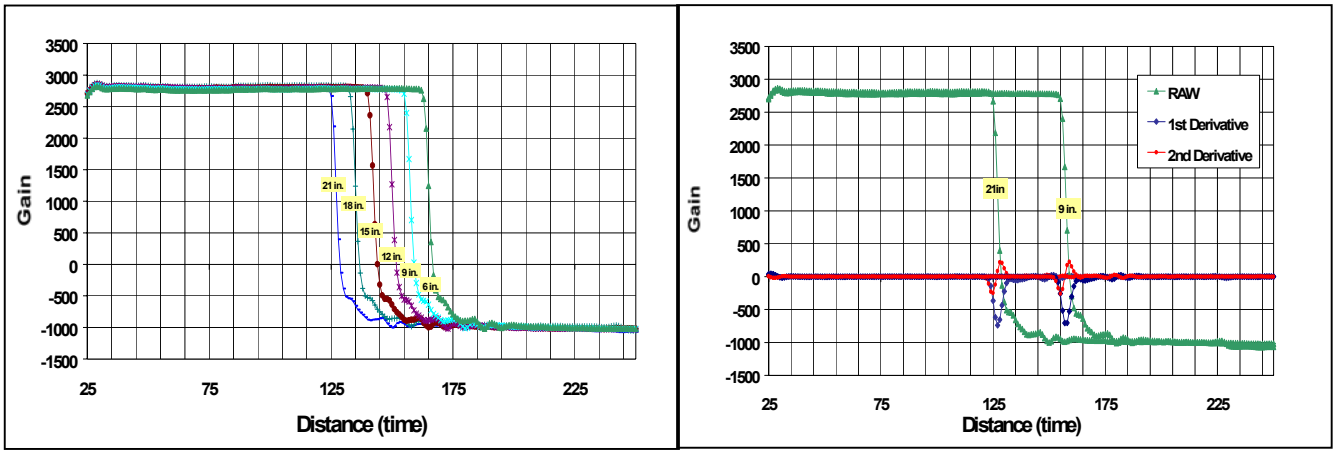

Fig. 3a and b. *(a) Waveforms from laboratory experiment. (b) Waveforms for water levels of 9 and 21 inches with 1st and 2nd derivatives indicating changes in Vp at the air-water interface.*

Developing an algorithm that automates the process of locating the change in impedance, i.e. the instant the signal leaves the air and enters the water, is important for real-time monitoring of short term and seasonal changes in water levels below the pavement. A variety of methods have been developed for automating TDR waveform analysis. Such methods primarily involve locating the initial and final inflection points for determining apparent length (Klemunes, 1998). TDR waveforms produced from water level measurements display one distinct inflection at the air-water interface (Figure 3a and 3b); therefore waveform analysis need only focus on the "initial" inflection.

In the laboratory two methods of waveform analysis were investigated, 1) locating the local minimum of the first derivative (maximum in air) and 2) locating local minimum of the second derivative. These two methods are similar to the Method of Tangents (5) used for determining apparent length.
The Campbell Scientific datalogger was programmed to collect both the raw waveform and the first derivative. The second derivative was calculated using a spreadsheet. The minima of the first and second derivatives were also calculated in a spreadsheet; a macro was used to associate those minimum values with the corresponding point on the raw waveform. Since each of the 250 points in the raw waveform represents a predefined distance (defined in the datalogger programming instructions), the number of the associated point was multiplied by distance to yield a water level value.

Field Installation

In the early 1990's the Minnesota Department of Transportation (Mn/DOT) constructed the Minnesota Road Research Project (Mn/ROAD) in Albertville, Mn. Mn/ROAD consists of 40 pavement test sections each 500 feet in length, with varying structural designs. Each test section includes a ground water monitoring well. The Mn/ROAD site provided the opportunity to test the use of TDR methods for measuring water table elevations within the pavement structure.

During a 1999 pavement reconstruction project, three flexible pavement test sections were reconstructed with ground water monitoring wells located at the centerline of the pavement structure. The wells consist of two pipes, a 10 foot x 2 inch slotted PVC pipe welded to a 5 foot x 2 inch solid PVC pipe. The bottom 10 feet of the well was back-filled with pea gravel, and the upper 5 feet was filled with bentonite. The wells extended 15 feet into the subgrade.

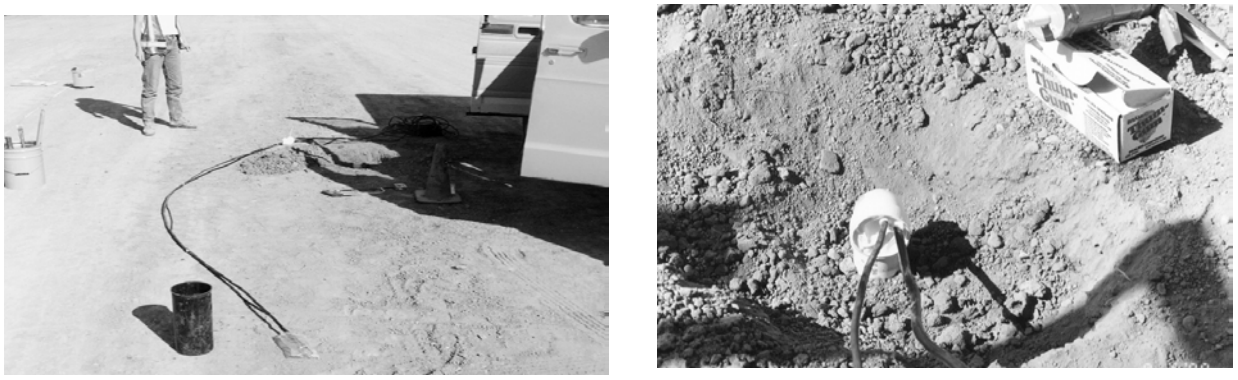

Fig. 4a and b. *Installation of air dielectric cable and pressure transducer below the pavement*.

An electronic pressure transducer and a 14 foot long air dielectric coaxial cable (Figure 4a) were installed in each well. Transducer and coaxial cables were run through a 90 ° PVC elbow used direct the wires horizontally beneath the pavement to the shoulder. Monitoring wells were capped at the top of the subgrade prior to placing the base course. Duct putty and caulk provided a seal around the wires to prevent debris from entering the well (Figure 4b). Manual data was collected from existing wells located on the shoulder of each test section.

A Campbell Scientific datalogger provided 2.5 V supply voltage to the pressure transducer, giving a full range output of 0 - 25 mV for 0-10 psi. An absolute transducer was used for the field installation. The transducer output was corrected for the affects of barometric pressure using the barometric pressure readings taken by an on-site weather station.

RESULTS AND DISCUSSION

The results from the laboratory experiment are shown in Table 1. The first method, using the minimum of the first derivative, resulted in an overestimation of the water level. The overestimation is most likely because this point represents the time when the signal is travelling in both air and water. A more accurate indication of the water depth would be the point or instant in time, when the signal leaves the air and enters the water. This is better represented by the minimum of the second derivative, and therefore this algorithm applied was to field data.

				Error	Error	Error
		1st Der. (min)	2nd Der. (min)		1st Der. (min)	2nd Der. (min)
Tape Measure	Transducer	Coaxial Cable	Coaxial Cable	Transducer	Coaxial Cable	Coaxial Cable
inches	inches	inches	inches	inches	inches	inches
0.0	0.0	-0.4	0.4	0.0	-0.4	0.4
6.0	6.4	5.1	5.9	0.4	-0.9	-0.1
9.0	9.3	8.3	9.0	0.3	-0.7	0.0
12.0	12.3	11.0	11.8	0.3	-1.0	-0.2
15.0	15.6	14.1	14.9	0.6	-0.9	-0.1
18.0	18.2	16.9	17.7	0.2	-1.1	-0.3
21.0	21.6	20.0	20.8	0.6	-1.0	-0.2

Table 1. *Summary of laboratory results*

Field Application of Algorithm

Typical waveforms collected from the field installations can be seen in Figure 5. When the algorithm was applied to TDR waveforms collected in the field the water table depth was underestimated. Noise in the waveform collected from test section 34 suggests that the cable may have been kinked during installation. The waveform from test section 35 indicates the presence of condensation in the cable.

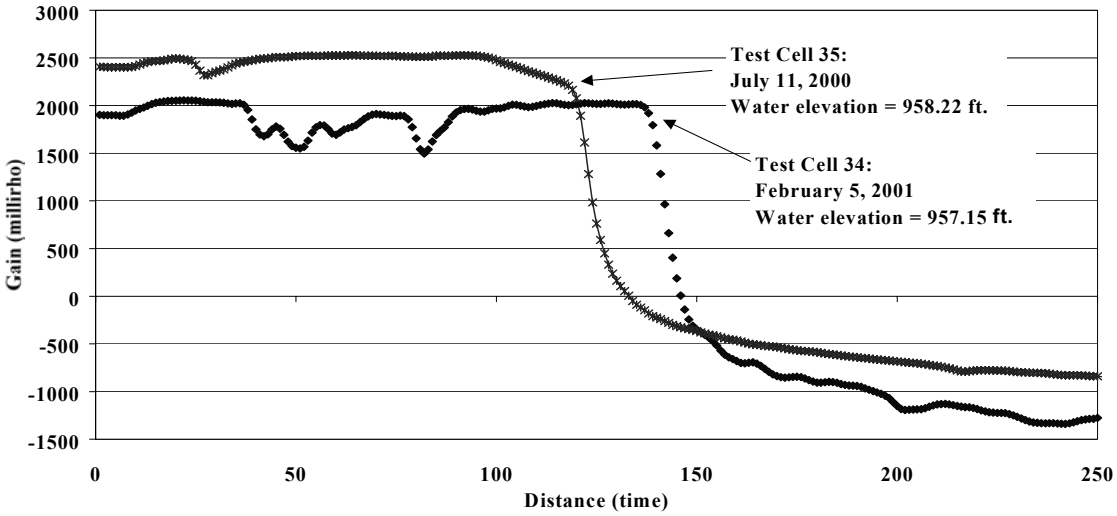

Fig. 5. *Typical waveforms collected from air dielectric cable installed below the pavement in test sections 34 and 35.*

The gradual decrease in the propagation velocity (Vp) as the signal approaches the air-water interface, indicates water droplets or high relative humidity in the cable. There was no indication of this condition during laboratory testing and did not affect water level estimations from field data.

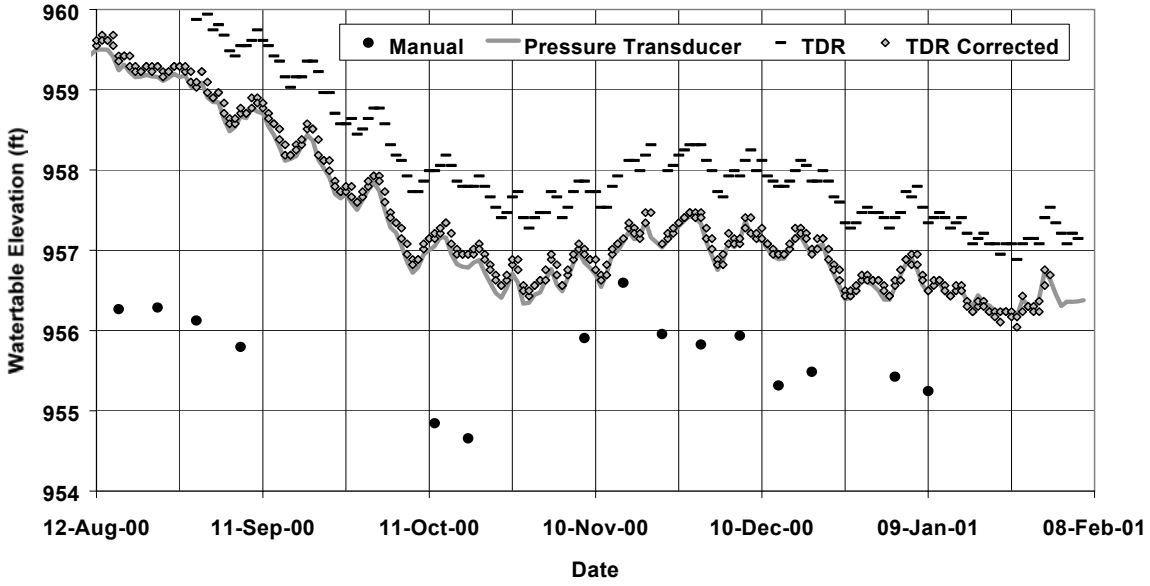

Fig. 6. *Comparison of manual, pressure transducer, and air dielectric water table elevations for test section 34*

Applying the algorithm to waveforms from test section 34 produced water table elevations that were consistently higher than those measured by the pressure transducer, although TDR readings track pressure transducer readings quite well. Seasonal and/or short-term changes in the water table elevation can be easily detected using TDR and air-dielectric methodologies. After careful inspection of the data, it was discovered that the setting for the apparent length of RG8 cable was incorrect. The fitting between the RG8 and the air-dielectric cable was used as the reference distance. An incorrect apparent length value entered into the datalogger program introduced error into the water level measurements. The result of such an error is a consistent over estimation of the water table elevation. The data was corrected and the algorithm was re-applied. The values produced by the algorithm compare well to those measured by the pressure transducer, +/- 4 inches. Similar discrepancies were discovered in the test section 35 data. In both cases, the discrepancies between the transducer and TDR readings were due to inadvertent changes to the datalogger programming instructions, not discovered until later in the project.

In general, there was good agreement between the manual, transducer, and TDR measurements. Differences between the manual data compare to the transducer and TDR data can be explained by the proximity of the monitoring wells. The distance between the original wells located in the shoulder and the wells located beneath the pavement are, 252 feet and 63 feet for test sections 34 and 35, respectively.

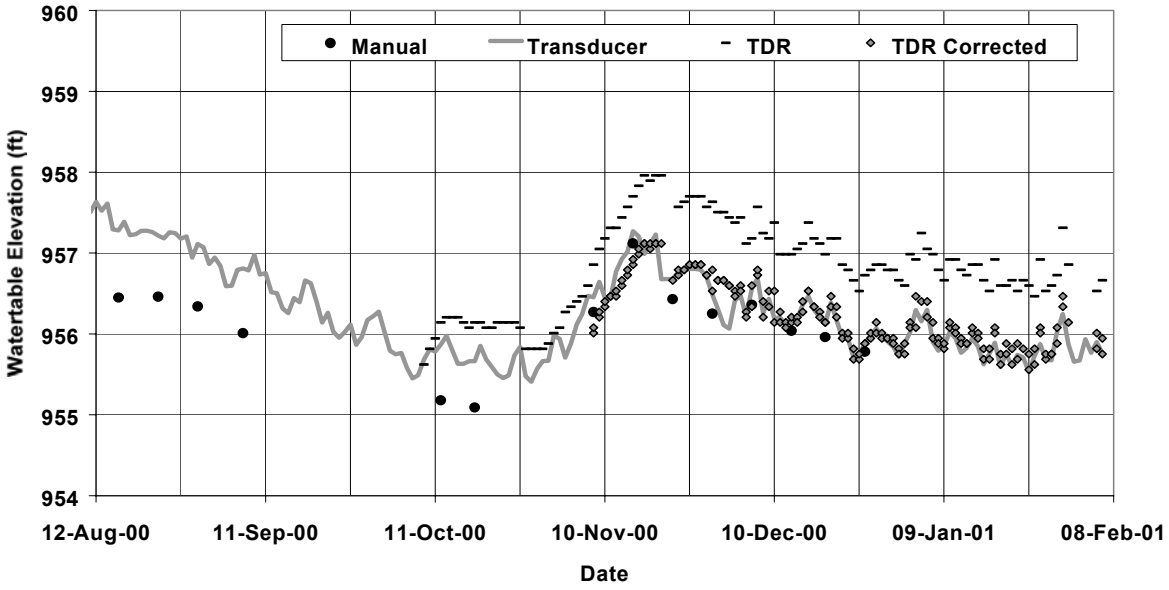

Fig. 7. *Comparison of manual, pressure transducer, and air dielectric water table elevations for cell 35.*

SUMMARY AND CONCLUSIONS

TDR technology in conjunction with air dielectric cable works well when used to locate the air-water interface in monitoring wells located beneath the pavement structure. Additionally, the system requires less maintenance, is less susceptible to power surges, and eliminates the need for labor intensive manual measurements.

The algorithm used to automate waveform interpretation worked well in the laboratory. When the algorithm was applied to field data the results consistently under estimated the distance to the air-water interface, thus over estimating the elevation of the water table below the pavement. This was attributed primarily to problems with datalogger programming instructions, indicating the need for careful data review whenever software or hardware changes are made. The use of TDR methods for tracking seasonal and short-term changes in water table elevations below the pavement structure improve the ability to estimate critical design parameters. TDR methods used in conjunction with automated waveform analysis provides a less expensive and more durable alternative to pressure transducers or manual readings.

REFERENCES

Dowding, C. H., Huang, F. C., and McComb, P. S., 1996a, Water Pressure Measurements with Time Domain Reflectometry Cables, Geotechnical Testing Journal, GTJODJ, **19**, No.1, 58-64.

Dowding, C. H., *et al.*, 1996b, Recent Advancements in TDR Monitoring of Ground Water Levels and Piezometric Pressures, Symposium on North American Rock Mechanics, Montreal, Quebec.

Klemunes, J. Jr., 1998, Determining Soil Volumetric Moisture Content Using Time Domain Reflectometry, FHWA-RD-97-139.

O'Conner, K. M., and Dowding, C. H., 1999, Air-Liquid Interfaces, in GeoMeasurements by Pulsing TDR Cables and Probes: CRC Press, 235-258.

Nicholson, G. A., Powell, J. F., and O'Conner, K. M., 1997, Monitoring Groundwater Levels Using a Time-Domain Reflectometry (TDR) Pulser, US Army Corps of Engineers Waterways Experiment Station, Technical Report CPAR-GL-97-2.

SALINITY COMPENSATION OF A TDT INSTRUMENT USING SLOPE CORRECTION

Ronald McFarlane

E.S.I. Environmental Sensors Inc.
Victoria Canada V8Z 4B9; admin@esica.com

ABSTRACT

A Time Domain Transmissometer (TDT) instrument has been developed to measure the water content of a stream of fluid, principally crude oil. Crude oil pumped from the ground is usually emulsified with water. The salt content of the water phase can be as high as 200 parts per thousand giving rise to conductivity levels of 375 dS/m or higher. The fluid dynamic behavior of the crude oil emulsion is such that the bulk electrical conductivity of the emulsion can randomly vary from zero to these high values in the space of a few seconds. Because the bulk electrical conductivity of the emulsion has an effect on the calibration of the instrument, the variations in this parameter must be accounted for if an accurate water content measurement is to be obtained. An algorithm is described that uses the rise time of the rising edge of the TDT pulse to estimate the bulk electrical conductivity and this estimate is used to compensate the water content measurement.

INTRODUCTION

The water content of a stream of fluid is an import parameter in many industrial processes. In these applications the presence of water is undesirable and removing it can incur a sizable production cost. The production and handling of crude oil is one such application.

The fluid from a producing oil well is a mixture of crude oil, water and sediments. The proportion of the various constituents varies dramatically depending on the geologic formation from which the fluid is produced and the stage at which the formation is in its production life cycle. Formations that have been newly tapped will normally produce fluids with a very low fractional water content, typically 0.10 or less. The term the petroleum industry uses to describe the water content of the production fluid is water cut, the volume fraction of water in the total fluid volume. As the fluid is extracted from the formation the water cut, will gradually increase. Near the end of the formations' production life cycle the water cut

can be very high indeed. Depending on the price of crude oil, it can still be economical to operate a well producing fluid that has a water cut of 0.98. The sensor to be described determines water cut by measuring electromagnetic wave propagation time in the fluid, which depends on the dielectric constant of the composite fluid.

The water component of the produced fluids normally contains mineral salt. The amount of mineral salt varies with the geologic formation and can be as high as 200 parts per thousand. The salt content can also be influenced by the technique used to recover the oil from the formation. In primary recovery, the fluid can either flow from the ground driven by the formation pressure or be mechanically pumped from the ground using the familiar pump jack or a submerged progressive cavity pump. This normally does not affect the naturally occurring salt content. In secondary recovery however, water or steam is injected into the bottom of the formation to force the oil out the top of the formation. Thus, the injection fluid can dilute the naturally occurring formation water. If the injection fluid is fresh water this can cause the salt content of the produced fluids to vary from the naturally occurring level down to very low levels.

Once the fluid is produced from a well it is piped into local storage tanks or into a pipeline that takes the fluid to a large tank farm. Sensors that measure water cut are normally inserted into this piping system. Therefore it is important to understand the flow conditions inside the pipe and how they affect the sensors performance. Produced fluids having a low water cut consist of a stream of oil with water droplets suspended in it. This is called an oil continuous flow. Produced fluids having a high water cut consist of a stream of water with oil droplets suspended in it. This is called a water continuous flow. For water cuts between ~0.25 and ~0.75, whether the flow is oil continuous or water continuous depends on the exact details of the flow conditions. Whether the flow is water continuous or oil continuous matters when the effect of salt is considered. The presence of salt in the fluid causes the water phase of the fluid to become conductive. This conductivity affects measurements of the dielectric constant of the fluid. If the flow is oil continuous the conductive water droplets are generally isolated from one another. If the flow is water continuous the conductive droplets are all touching each other. This increases the overall bulk conductivity of the fluid at lower frequencies. In the water cut range of 0.25 to 0.75 it is possible for the water cut and salinity to remain unchanged but have the flow flip from oil continuous to water continuous or visa versa. This will cause the bulk conductivity of the fluid to change even though there has been no change in the salinity.

Another complicating factor is that it is quite possible to have a well producing fluid that has an erratic water cut. The overall bulk conductivity of the fluid increases as the proportion of conductive water in the fluid increases. This, coupled with the fluid changing back and forth from oil continuous to water continuous, as well as the underlying salinity of the water phase of the fluid changing, gives rise to a very challenging measurement environment in which the water cut and bulk conductivity of the fluid can change dramatically and unpredictably.

Most water cut sensors currently on the market are not able to deal with both the water cut and the bulk conductivity of the fluid changing at the same time. The sensor described in this paper can measure water cut accurately in the face of changing bulk conductivity.

Apparatus

The device described is based on time domain transmissometry (TDT) and is intended for use with two-phase systems. A TDT device has a number of advantages over a time domain reflectometry (TDR) device. Firstly, the signal traverses the sensing portion of a TDR device twice and only once for a TDT device. Therefore, when the medium interacting with the sensing portion of the device is conductive, the loses incurred by a TDR device will be at least twice as great as those incurred by a TDT device. This means that the upper limit of conductivity at which the device will still produce a usable signal will be higher for a TDT device than for a TDR device. Secondly, the signal of interest in the TDT device is the first signal to be received by the electronics. All other signals are extraneous reflections that occur after the signal of interest has been received. In a TDR device there are several extraneous reflection signals received prior to the reception of the signal of interest. The receiving electronics have a much harder time distinguishing the desired signal from the undesired noise.

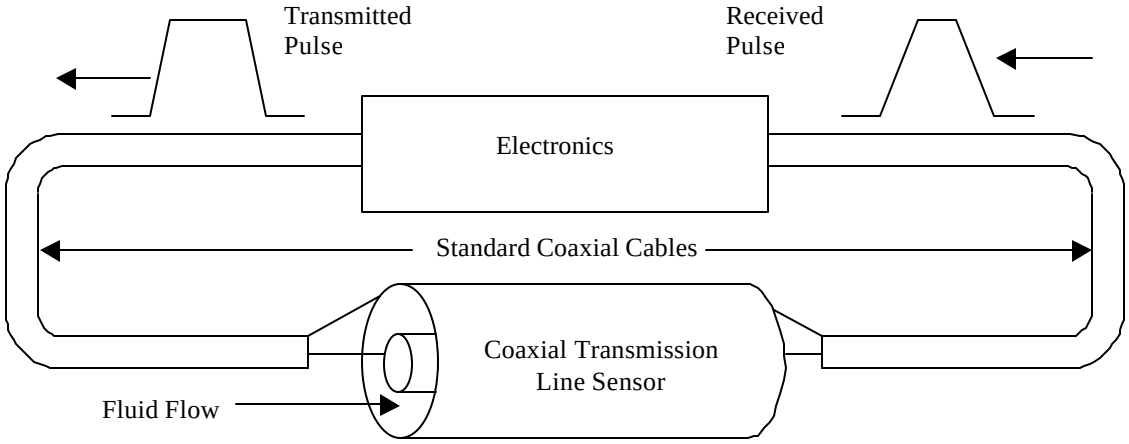

Fig. 1. *Block diagram of TDT sensor*

As shown by the block diagram in figure 1 the device consists of an electronics package connected to a series of transmission lines. The electronics package generates a short pulse with fast rise and fall times. The pulse duration is about 4.5 nanoseconds and the rise and fall times are approximately 900 picoseconds.

The pulse is launched into a standard coaxial transmission line where it propagates toward the sensing portion of the transmission line. The pulse is coupled into the coaxial sensor and after propagating along this portion of the transmission line it is coupled into another standard transmission line to propagate back to the electronics package. The coaxial transmission line sensor is mechanically arranged to allow the fluid under test to flow between the inner and outer conductors, thus forming the dielectric of the transmission line. Figure 1 shows the fluid flowing in the same direction as the pulse. This is an arbitrary choice. The electronics package measures the total transit time of the pulse around the circuit as well as the rise time of the received pulse. The total transit time of the pulse when air fills the coaxial sensor is subtracted from the total transit time of the pulse when the fluid under test fills the sensor. This removes the contribution to the transit time of the standard coaxial lines as well as the delay time through various sections of the electronics package.

It is important to note that when water containing even moderate amounts of salinity fills the coaxial sensor the signal losses caused by the bulk electrical conductivity of the fluid diminish the pulse amplitude severely. To reduce the loss of pulse amplitude to acceptable levels, it is necessary to apply a non-conducting dielectric coating of substantial thickness to the conductors of the coaxial sensor to somewhat isolate the sensor from the effects of the bulk electrical conductivity. A number of people have studied the effect this coating has on the response and sensitivity of TDR sensors (Annan, 1977; Ferré, *et al*, 1996). The presence of these coatings reduces the sensitivity of the coaxial sensor to changes in the dielectric constant of the fluid under test. This is a necessary engineering tradeoff to allow the sensor to operate at very high bulk electrical conductivities.

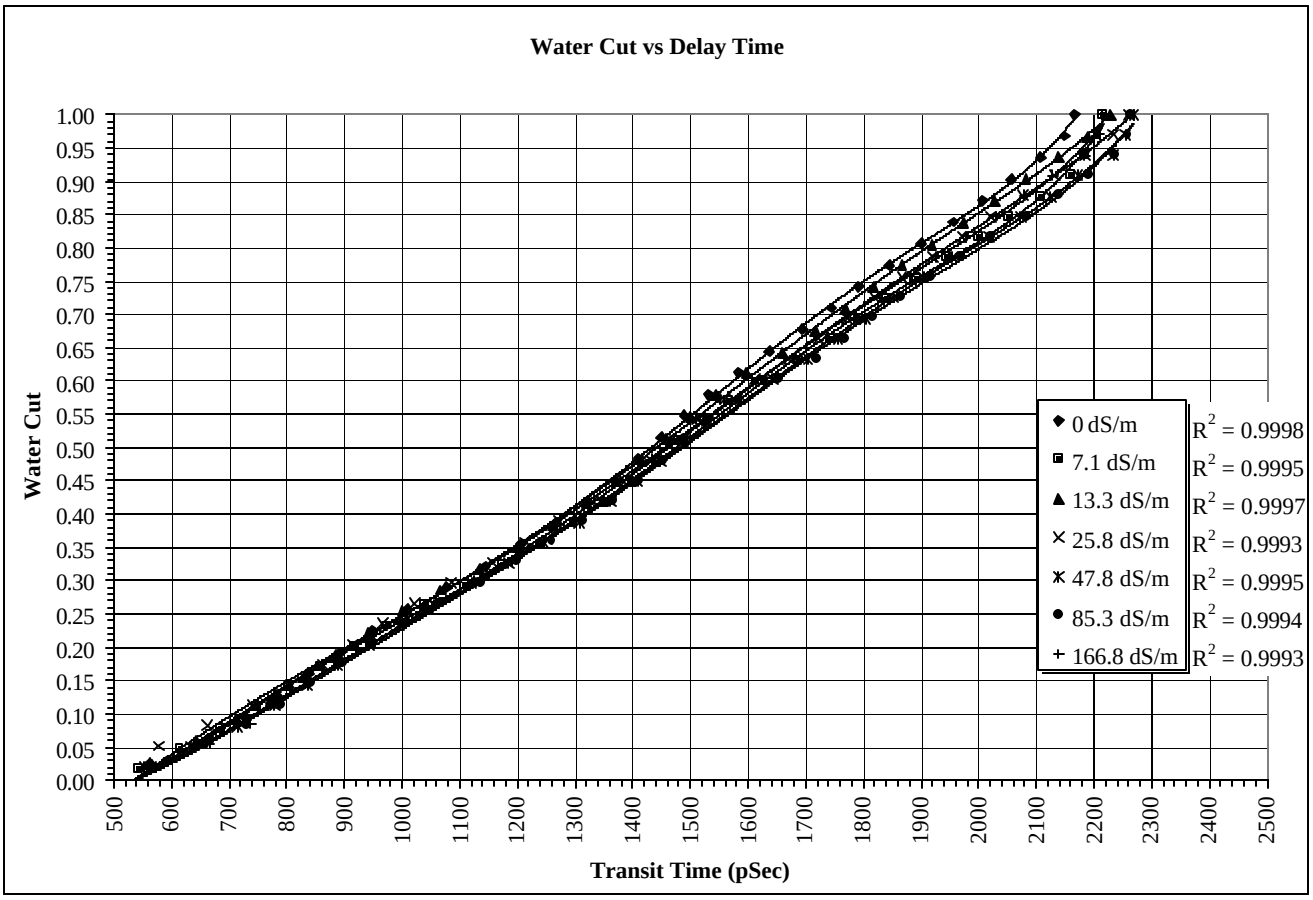

Fig. 2. *Empirical relationship between transit time and water cut.*

Results

Figure 2 shows the empirical relationship between the measured pulse transit time and the water cut of the fluid for various conductivities of the water phase of the fluid. To obtain the data the sensor is first plugged at one end. The sensor is then turned on its end, open end up and filled with clean dry oil. Water of a given salinity is added to the top of the sensor in increments, displacing the oil from the top of the sensor. After each addition the transit time and rise time are measured. The process is repeated for each of the other salinities. This procedure gives results very similar to those obtained using a flow loop. The advantage of the static experiment is that it is much easier to produce water cuts in small increments.

The curves drawn through the data points are 6th order polynomials fit to each data series. The correlation coefficient for each fit is shown next to the legend.

It can be seen from figure 2 that varying the conductivity of the water phase of the fluid can affect the transit time measurement, particularly at high water cuts. If the effects of salinity are not taken into account the difference between the water cut inferred from assuming one particular salinity and the actual water cut could be as high as 0.1 at high water cuts.

This difference can be resolved if the rise time of the received pulse is measured in conjunction with the transit time measurement. Figure 3 shows the rising edge of the received TDT pulse for the cases where the coaxial sensor is completely filled with air, clean dry oil, and water of various salinities. The zero of the time base is arbitrarily set to the beginning of the rising edge of the pulse for the case of air.

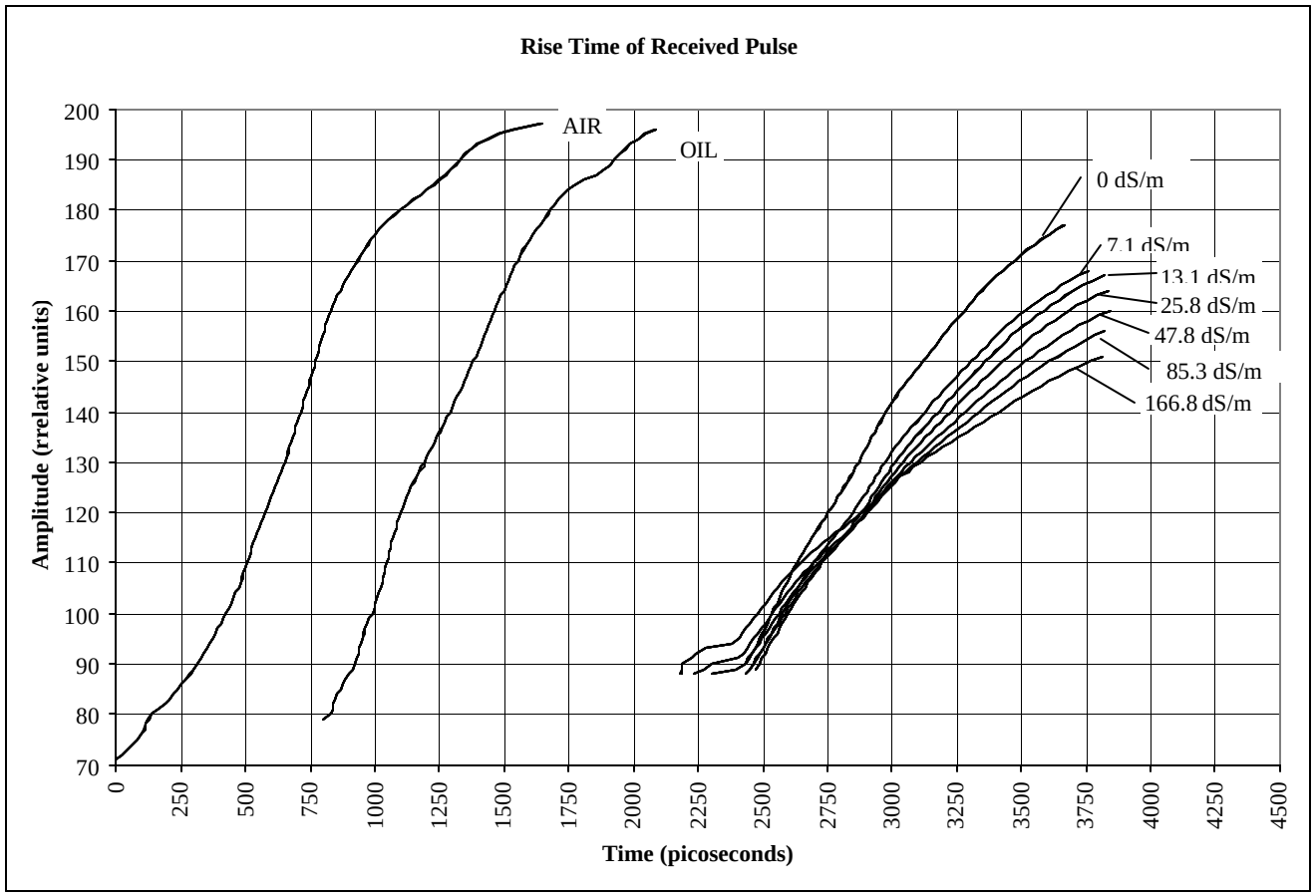

Fig. 3. *Rising edge of received pulse for air, 100% oil, and 100% water of various salinities.*

It is clear that the conductivity of the water has an effect on the rising edge of the received pulse. The rise time is normally defined as the time it takes the amplitude of the pulse to rise from 10% of its final value to 90% of its final value. The choice of 10%/90% as the lower and upper limits is somewhat arbitrary. Furthermore, this definition is predicated on a percentage of the final amplitude of the pulse. Because the amplitude of the pulse varies depending on a number of factors, upper and lower limits are

chosen on an absolute basis rather than relative to the final amplitude of the pulse. The lower limit in this case corresponds to a value of 116 and the upper limit corresponds to a value of 144 on the relative amplitude scale.

Once the definition of rise time has been settled by selecting upper and lower limits, it is possible to characterize the sensor's response to various water cut and salinity conditions. Figure 4 shows a plot of the rise time vs. the transit time. There are seven data series. Each series consists of the measured transit times and rise times for various water cut values where the water phase has a particular conductivity. The conductivities vary from 0 dS/m to 166 dS/m. The water cuts for each of these conductivities vary from 0.0 to 1.0.

All the series begin at the left of the plot with 100% oil, and are coincident as would be expected. As the water cut increases it can be seen that the rise time changes differently with transit time depending on the conductivity of the water phase of the mixture. The exact nature of the variation of rise time with transit time depends on the selection of the upper and lower limits defining the rise time as well as the detailed construction of the coaxial transmission line sensor.

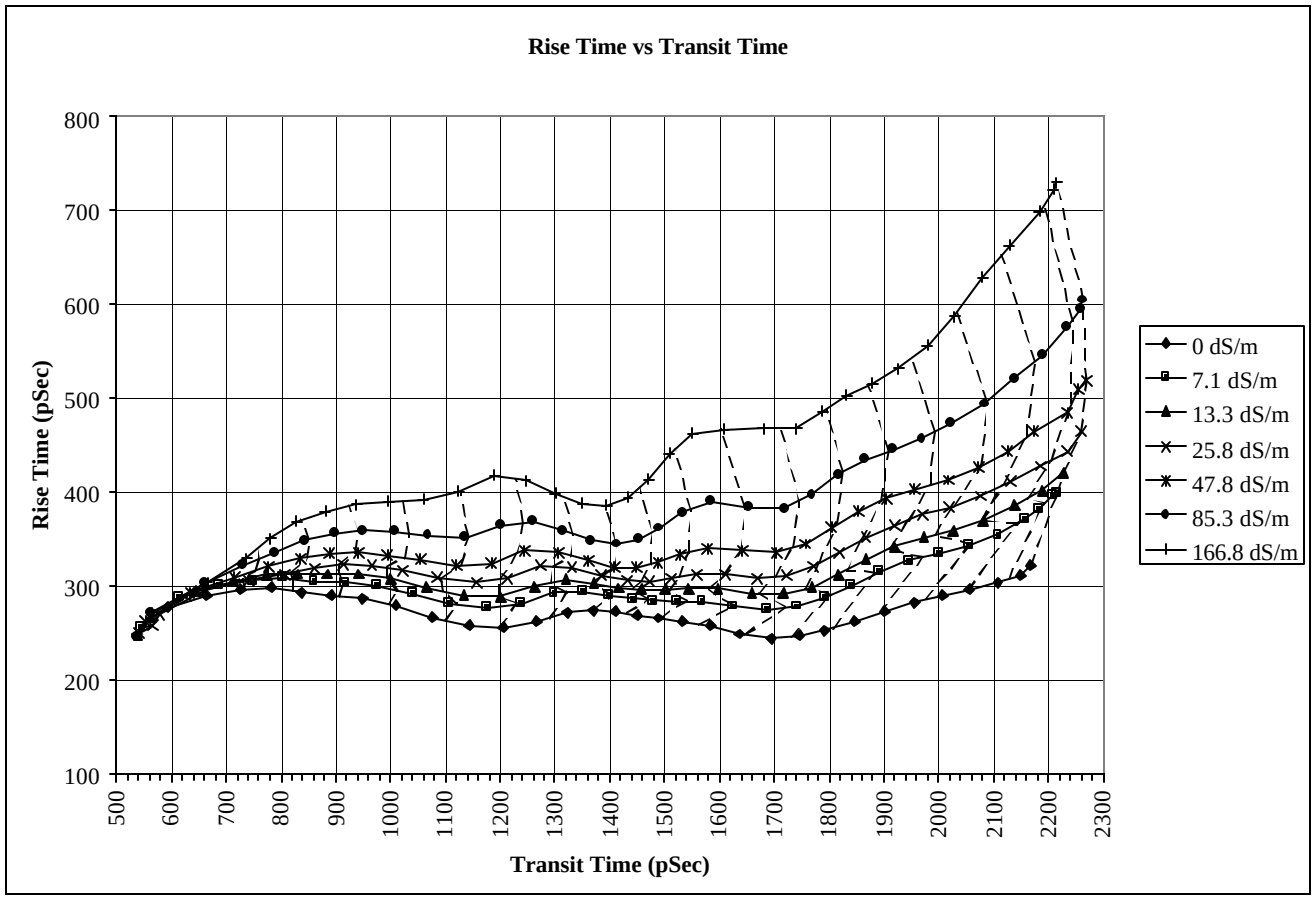

Fig. 4. *Rise time vs. transit time for various conductivities and water cuts.*

Figure 4 can be thought of as a projection of a 3 dimensional surface onto the rise time/transit time plane. The dimension perpendicular to the page represents the water cut. Zero water cut corresponds to

the plane of the page and increasing water cut corresponds to increase height above the page. The dashed lines show areas of equal water cut and represent water cut increments of 0.05.

For practical purposes this surface can be represented either as a lookup table or by an analytical function fit to the experimental data. This device uses the lookup table because of limitations in on board computing power. Once a second it will measure the transit time and rise time. These values are used as coordinates in figure 4 to lookup the water cut.

In the special case of the fluid changing from oil continuous to water continuous, or vice versa, the water cut remains unchanged but the bulk conductivity of the fluid changes abruptly. In this case the rise time/transit time coordinates will jump from one point of the surface to another point on the surface. In the more ordinary case where the water cut remains constant but the bulk conductivity changes slowly, the motion of the point along the surface will be parallel to the dashed lines. In the completely general case where the water cut and the bulk conductivity are changing randomly, the coordinate point will move along the surface in all directions.

SUMMARY

The measurement of water cut in crude oil presents a very challenging application. Oil wells produce a fluid that is an emulsion of crude oil and water. The water phase of the emulsion typically contains dissolved mineral salts. The salinity of the water phase can vary from fresh water to approximately 200 parts per thousand giving rise to very high bulk conductivities. Further, the emulsion can switch from being oil continuous to being water continuous depending on the details of the flow conditions. The switching of the continuous phase can affect the bulk conductivity as well.

A time domain transmissometry device has been fabricated to measure the water cut in produced fluids. TDT is used because it has a number of advantages over TDR. Because the TDT signal traverses the lossy medium only once it incurs less that half the losses normally incurred by a TDR signal. Further, the TDT signal is easy to distinguish from extraneous reflections.

The sensing portion of the TDT device is a coaxial transmission line. The fluid under test flows axially through the coaxial transmission line and occupies the space between the inner and outer conductors. The conductors are coated with a thick dielectric coating to partially isolate the transmission line from the effects of highly conductive fluid flowing through the sensor. While the dielectric coatings allow the sensor to operate with fluids of higher bulk conductivity, this comes at the price of sensor sensitivity.

The electronics of the sensor measure the transit time of a pulse propagating through the coaxial transmission line sensor as well as the rise time of the pulse after it has propagated through the sensor. If transit time alone were used to infer fractional water cut, varying the salinity of the water phase of the emulsion could introduce errors in the water cut as high as 0.1. By taking account of the rise time, the error in estimating the water cut can be reduced significantly. The device is calibrated by characterizing its rise time and transit time responses to various combinations of water cut and salinity. These responses are assembled into a 2-dimensional lookup table with rise time and transit time as the independent variables and water cut as the dependent variable. In normal operation the sensor measures the rise time and transit time and uses these times as coordinates in the lookup table to arrive at water

cut. Measured rise time/transit time coordinates that do not precisely match coordinate values stored in the lookup table are interpolated to produce approximate water cut values.

This device and slope correction scheme are designed to work with two-phase media. Oil/water, water/particulate, water/gas, and water/steam are some of the systems in which water content could be measured. The system could also be applied to three-phase media such as soil/water/air with some modifications to the calibration procedure. Also, the geometry of the sensing portion of the transmission line would need to be modified to be useful for soil applications.

REFERENCES

Annan, A.P., 1977, Time-Domain Reflectometry – Air – Gap Problem in a Coaxial Line: Report of Activities, Part B; Geol. Surv. Can., Paper 77-1B, 55-58.

Ferré, P.A., Rudolph, D.L., and Kachanoski, R.G., February 1996, Spatial Averaging of Water Content by Time Domain Reflectometry: Implications for Twin Rod Probes With and Without Dielectric Coatings: Water Resources Research, **32**, No. 2, 271-279.

Subgrade Monitoring

Determining Frost Depth in Pavement Systems Using a Multi-Segment Time Domain Reflectometry Probe
R. Roberson and J. Siekmeier, *Minnesota Dept. Of Transportation*

Continuous Measurements of Liquid Water Content and Density in Snow Using TDR
P. Waldner and M. Schneebeli, *Swiss Federal Instiute for Snow and Avalanche Research, Switzerland*; C. Huebner and A. Brandelik, *Forschungszentrum Karlsruhe, Germany*; F. Rau, *University of Freiburg, Germany*

Water Content and Density of Soil Insitu by the Purdue TDR Method
V. Drnevich, J. Lovell, and Q. Yi, *Purdue University*; S. Siddiqui, *Earth Exploration Corp*.

Effects of Testing Large Particle-Sized Materials
V. Drnevich, J. Lovell, and Q. Yi, *Purdue University*

Temperature Effects on Dielectric Constant Determined by Time Domain Reflectometry
V. Drnevich, J. Lovell, Q. Yi, X. Yu and J. Tishmack, *Purdue University*

Back to Table of Contents

DETERMINING FROST DEPTH IN PAVEMENT SYSTEMS USING A MULTI-SEGMENT TIME DOMAIN REFLECTOMETRY PROBE

Ruth Roberson[1] and John Siekmeier[2]

[1]Minnesota Department of Transportation, Office of Materials and Road Research
Maplewood, Mn 55109-2044;ruth.roberson@dot.state.mn.us
[2]Minnesota Department of Transportation, Office of Materials and Road Research
Maplewood, Mn 55109-2044;john.siekmeier@dot.state.mn.us

ABSTRACT

Determining frost depth below the pavement is important for timely implementation of winter and spring load limits. Unfortunately, existing instruments such as resistivity probes, frost tubes and moisture blocks are limited both in terms of data acquisition (automated and continuous measurements) and data interpretation. Consequently a delay between data collection, interpretation, and dissemination of information occurs. A laboratory study was conducted by the Minnesota Department of Transportation investigating the use of the Moisture Point probe as an instrument for locating the depth to the freezing front. The Moisture Point probe combines Time Domain Reflectometry with remote diode switching to provide a profile of the aggregate base and subgrade dielectric properties. From this the frost depth can be estimated. The Moisture Point probe works well in locating the frost depth and improves the ability to successfully implement spring and winter load limits. This method also provides the opportunity to validate air temperature-based models currently used to determine when to begin spring and winter load limits. Integrating the Moisture Point probe into the R/WIS communication architecture could significantly improve pavement life in Minnesota by providing additional critical data in a timely and convenient format.

INTRODUCTION

In cold regions freeze-thaw cycling, and spring-thaw weakening contribute to loss of load bearing capacity and subsequent pavement failure. Determining frost depth below the pavement becomes important for timely implementation of winter and spring load limits. Unfortunately, instruments currently being used to measure frost depth (resistivity probes, frost tubes, and moisture blocks) are limited in terms of ease of data collection and analysis methods. As a result a delay in the collection and dissemination of information, critical for determining pavement conditions, occurs. The Minnesota

Department of Transportation (Mn/DOT) is conducting research on the use of Time Domain Reflectometry (TDR) for determining frost depth in aggregate base and subgrade materials.

The use of TDR for measuring soil volumetric moisture content, is well documented (Baker, 1990; Topp *et al.*, 1980). TDR has also been used in a wide variety of geotechnical applications (O'Conner and Dowding, 1999). Recent pavement research indicates that TDR methodologies are successful when used for determining base and subgrade moisture conditions (Baran, 1994; Katdawala *et al.*, 1993; Wright and Rainwater, 1998; Roberson and Birgisson, 1998). TDR methods allow detection of liquid water content in soils because the dielectric constant of liquid water is much higher than that of other bulk soil constituents.

TDR technology has also been examined for use in frozen soils (Davis *et al.*, 1982; Spaans and Baker, 1995) for determining the frozen-unfrozen interface and the liquid water content of the frozen soil. Davis *et al*, (1982) determined that the dielectric constant could be used to distinguish between frozen and unfrozen soil water. The dielectric constant of ice is less than that of liquid water, 3 and 80 respectively. Therefore, the change in dielectric constant due to ice formation results in an electrical discontinuity that can be easily detected in the TDR waveform. This provides the means for distinguishing between frozen and unfrozen soil (Spaans and Baker, 1995; Spaans and Baker, 1996; Roberson and Siekmeier, 2000). According to Hayhoe *et al* (1983) the liquid water content based methods, under thawing conditions, are less limited in their range of application than temperature-based methods for determining frost depth.

The objectives of this study are to 1) evaluate a multi-segment TDR probe for improved frost depth measurements below the pavement and 2) implement field testing at designated Road and Weather Information System (R/WIS) sites around Minnesota. This paper presents the results from a laboratory study in which frost depth is measured using a multi-segment TDR probe and describes the field implementation.

BACKGROUND

Methods currently used to estimate frost penetration are limited in a variety of ways. Table 1 provides a summary of current methods for measuring frost depth within the pavement structure. Frost tubes (plastic fluorescein dye tubes) undergo a color change as a result of freezing. Frost tubes readings are taken manually, can be subjective, and often result in slow dissemination of critical information. Resistivity probes utilize the resistance change between frozen and unfrozen soil to determine the depth of frost penetration. Data analysis can be subjective and may require the use of thermocouple data in conjunction with probe data to determine frost depth. Data is usually collected manually, but in some cases has been automated. Recently moisture blocks, another type of electrical resistance sensor, have been used to estimate frost depth below pavements. Data from the moisture block sensors is analyzed by monitoring the measured resistance in the soil as it increases above normal summer values when the water freezes. This is typically an order of magnitude larger. Since this analysis is somewhat subjective, thermocouples are usually installed next to the moisture block so that temperature data can be used to verify frozen conditions. To date the results are inconclusive, with additional concern as to the long-term stability of the gypsum core (Mn/DOT Frost Resistivity Probe User Guide, 1996).

	Frost Tube	**Resistivity Probe**	**Moisture Block**	**Thermocouple**	**TDR Probe**
Data Collection	Manual	Primarily Manual	Automated	Automated	Automated
Data Interpretation	Subjective	Subjective, requiring temperature data.	Subjective, requiring temperature data.	No accounting for freezing point depression	Potential for developing algorithm for automated analysis.
Installation	Labor intensive. Soil disturbance is extensive.	Labor intensive. Soil disturbance is extensive.	Labor intensive. Soil disturbance is extensive.	Labor intensive. Soil disturbance is extensive.	**Not** labor intensive. Minimal disturbance to soil.

Table 1. *Comparison of methods currently used for measuring frost depth within pavement system.*

Time Domain Reflectometry (TDR) Method

Environmental Sensors Inc. (ESI) manufactures the TDR Moisture Point (MP) probe. The MP probe is a multi-segment TDR probe with switching diodes between TDR segments. When installed vertically, the MP probe provides a segmented profile of the soil dielectric properties and therefore, the frost depth. The electronic switching diodes allow separation of vertically oriented waveguides by causing a short at the segment boundaries. As an electromagnetic pulse is fed into the center of the probe, remote diode shorting causes an amplification of the reflections at the start and end of each segment. The MP system measures the propagation time, or rather the time it takes the electromagnetic pulse to travel twice the length (round trip) of the segment. T_1 is the time at which the measurement system sends the pulse, T_2 is the time the reflected signal returns to the measurement system. The propagation time of the signal as it travels the length of each probe segment is then, $T_2 - T_1$ or Δt. Using the Δt, the dielectric (Ka) of the soil medium can be calculated from the following equation.

$$Ka = \left(\frac{\Delta t * c}{2L} \right)^2 \qquad [1]$$

Where c is the speed of light, 30 (cm/nsec), and L is the length (cm) of the segment.

The MP probe construction and use of remote shorting diodes makes this instrument attractive for measuring the downward movement of frost as it penetrates the aggregate base and subgrade below the pavement.

Road and Weather Information System (R/WIS)

R/WIS is an extension of the 1987 Strategic Highway Research Program (SHRP). It is one of many products resulting from that research. Mn/DOT, among other states, is a participant in the Aurora Program (Federal Highway Administration, 2000). The Aurora Consortium initiatives emphasize technological advancement and improved Road and Weather Information Systems in order to more effectively deal with winter road conditions. While the primary focus of the initiatives have been on winter maintenance operations, Mn/DOT is attempting to evaluate and extend the use of R/WIS technology to spring and winter load studies. The focus of R/WIS is the efficient and effective

integration and dissemination of road and weather information across the state of Minnesota. The R/WIS system is comprised of a network of weather stations that monitor road and weather conditions and subsequently feed data back to a central database for dissemination to the maintenance personnel at the state and local level. A primary goal of R/WIS implementation in Minnesota is the development of a system that is able to accommodate various types of instruments. In particular, a portion of the project is dedicated to testing the system's communication architecture. Studies conducted by Mn/DOT's Road Research Section investigating new methods for determining frost depth, as well as looking for improved data transfer protocols, were well suited for testing the R/WIS communication protocol. Mn/DOT pavement research in combination with the R/WIS initiatives allows for initial testing of the R/WIS communication system in addition to field testing of various instruments for measuring frost depth within pavement structures.

LABORATORY CALIBRATION

Base Material

The aggregate base selected for this study was a Class 5 Special (Cl. 5 Sp.) (Table 1). This aggregate is the most commonly used base material on low volume and load restricted roads in Minnesota. Target moisture content and dry density for this material were 8.5% and 21.0 kN/m^3, respectively.

Sieve #	Opening Size (mm)	Actual Percent Passing	Class 5 Special Specification
1	25.4	100	100
3/4	18.85	96.1	90-100
3/8	9.50	75.6	70-85
4	4.70	59.6	55-70
10	2.00	43.1	35-55
20	0.850	26.1	------
40	0.425	13.6	15-30
60	0.250	6.66	------
140	0.107	2.60	------
200	0.075	1.92	5-10

Table 2. *Class 5 Special Gradation.*

MP Probe

The multi-segment MP probe used in this study was a four-segment *Type K* probe (Fig. 1). Each segment is 15 cm in length. The probe is constructed of two stainless steel rails separated by an epoxy and high-density plastic material. The boundaries of the segments are defined by switching diodes, at the start and end of each segment. A personal computer was used to automatically collect probe scans every 3 hours. The output collected during the probe scan included the raw waveforms and the travel time for each of the four segments. The travel time was used to calculate the Ka during the freezing and thawing cycle.

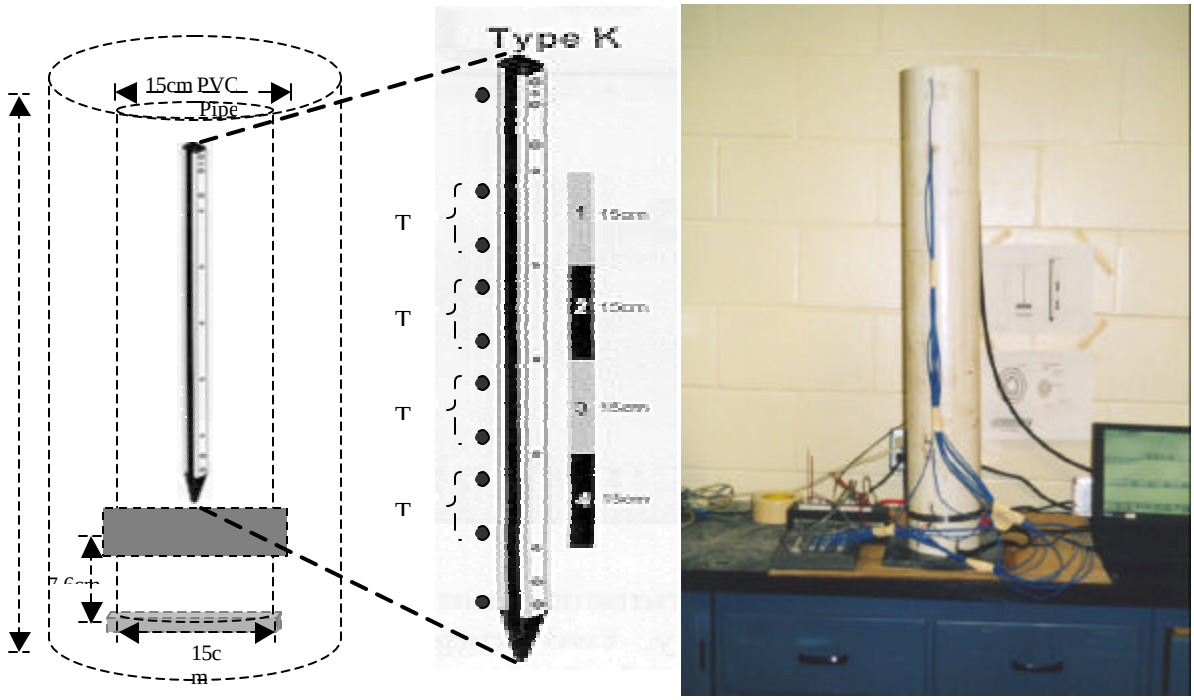

Fig. 1. *Pictured is the Type K Moisture Point probe. The Moisture Point probe is a multi-segment TDR probe with four segments each 15 cm in length. TC = Thermocouple locations in reference to the TDR segments.*

Test Setup

A polyvinyl chloride (PVC) pipe, 15 cm diameter x 91 cm long, was used to construct a soil column in which the MP probe was installed. A heater core was constructed of a 15 cm diameter x 7.6 cm long PVC pipe. Inside the 15 cm diameter outer ring were concentric inner rings of smaller diameter PVC pipe. A heating tape, more commonly used to keep water pipes from

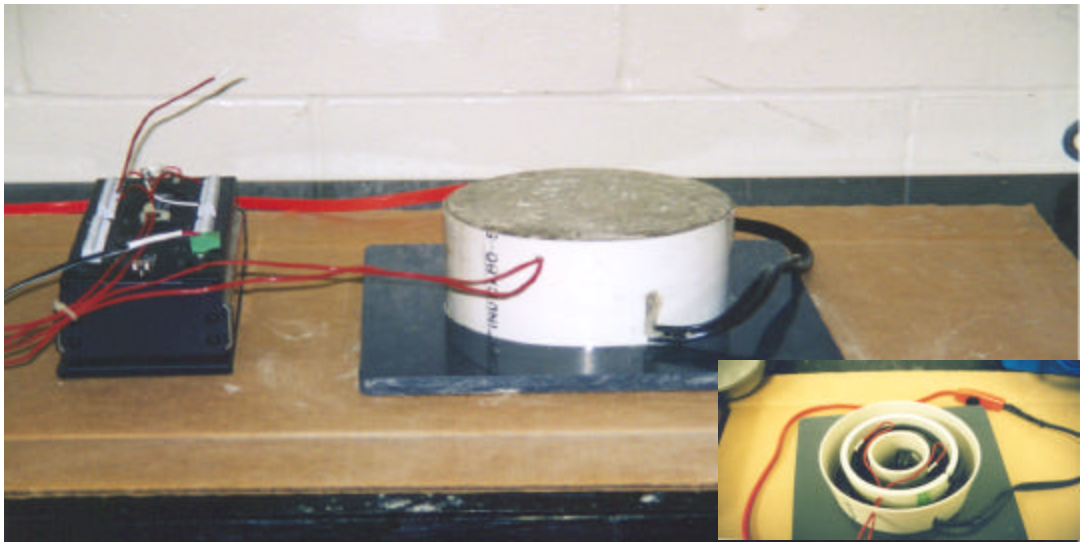

Fig. 2. *PVC heater core with heating tape and thermocouples. Temperature measurements were taken with a Campbell Scientific Inc. CR10 datalogger*

freezing, was wound in between the PVC rings. Two copper-constantan thermocouples were inserted into the core (Fig 2), and the core was filled with *Quickcrete.* The heater core provided a base for the soil column as well as a means for maintaining a temperature gradient through the soil column. A metal pipe clamp attached the soil column to the heater core and silicon caulk prevented moisture from escaping through the joint. Soil was packed in 5 cm lifts, first packing 5 cm of Cl. 5 Sp. at the bottom of the column before installing the MP probe and thermocouples. Thermocouples were installed at 5 cm from the top of the heater core, and then at intervals such

Fig. 3. *R13 fiberglass insulation was packed between the soil column and the cardboard form. The insulation was used to confine the freezing to the surface of the soil column.*

that two thermocouples were associated with each of the four segments. One of the thermocouple positioned at the beginning of the segment, and the other at the end of the segment. After the sensors were installed and the soil was packed into the column, a cardboard sleeve 30 cm diameter x 107 cm long was placed around the outside of the soil column and heater core. Unfaced fiberglass R13 insulation was cut into 18 cm lengths, folded in half and packed between the cardboard sleeve and PVC column (Fig. 3). Moist paper towels and plastic covered the top of the column to eliminate evaporation from the surface. The set-up was left undisturbed for three days to achieve moisture equilibrium, after which the column was placed in a walk-in freezer. During the freezing cycle insulation was removed one layer at a time to both induce frost penetration from the upper surface and to induce step-wise freezing.

RESULTS AND DISCUSSION

Laboratory

When water freezes a significant decrease in the dielectric of the bulk soil occurs. This results in an abrupt decrease in the propagation time, and a dramatic decrease in the Ka at or below 0 °C (assuming little or no freezing temperature depression). Figures 4 and 5 show the change in the Ka for TDR segments 1 (0-15 cm) and 3 (30-45 cm), during a freeze-thaw cycle. In this study there was a measured decrease in the Ka near 0 °C, although the decrease in the Ka of segment 1 was less dramatic than that of segment 3. This is attributable to the rate at which the soil freezes. Segment 1 went through step-wise

freezing, whereas segment 3 went through rapid freezing. This suggests that the rate at which the soil freezes will affect how easily the change in the Ka can be detected. Likewise, the step-wise freezing reduced the maximum change in the Ka around 0 °C. This needs to be considered if an algorithm for automated frost depth measurements is developed.

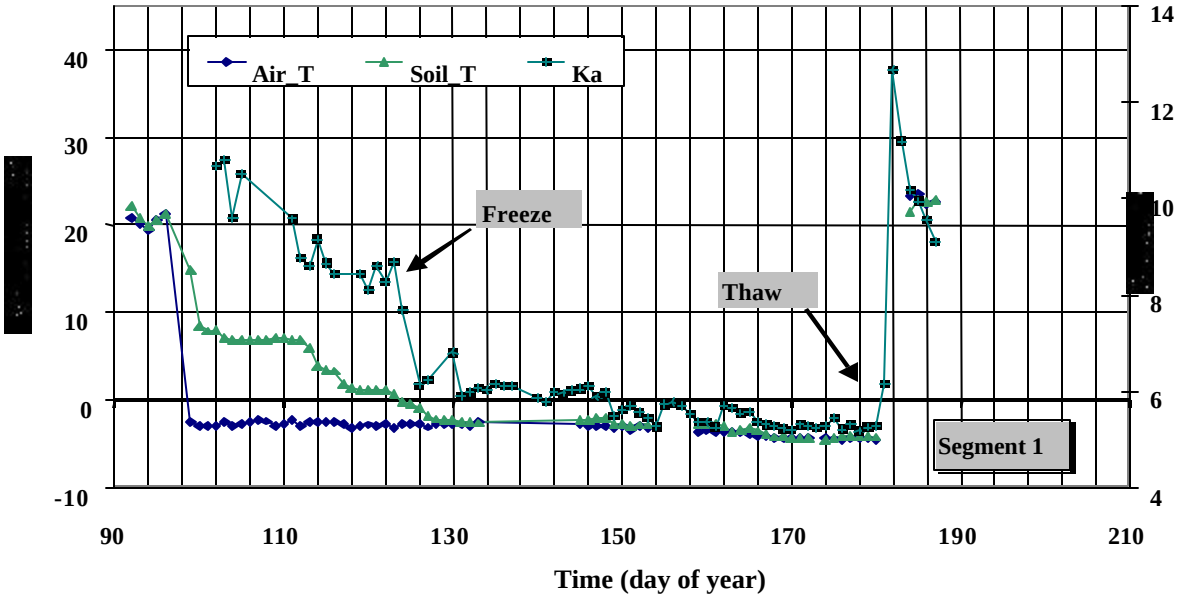

Fig. 4. *Temperature and Ka vs Time for TDR segment 1 (0-15cm). The Soil_T is the average temperature of the two thermocouples located at the top and bottom of the segment. Segment 1 went through a step-wise freezing cycle. Periodically a layer of insulation was removed and the temperature was allowed to stablize. This can be seen between day 98 and 114. A rapid thaw gives a more distinct change in the Ka.*

An additional factor to consider is the initial Ka at which the soil begins to freeze. The Ka is a function of the water content and therefore the maximum change in Ka during the phase change depends on the initial water content. If the water content is high, there will be a relatively large decrease in the Ka as the phase change occurs. This is due simply to the initial volume of water available to go through the phase change. If the initial water content is low then the Ka will also be low. As the soil freezes the change in Ka in a low water content soil will be much less than in a soil near saturation. Therefore, initial water contents in the soil will affect the ability to detect the phase change from liquid to ice. The resolution of the Type K MP probe is limited to the length of each probe segment, in this case 15 cm, because the MP measurement is an integrated value over the length of the segment. This was verified by positioning thermocouples near the top and bottom of each segment (Figure 1). The abrupt decrease in the Ka is only apparent when the temperature of the bottom thermocouple indicates frozen conditions, i.e. the soil along the entire segment is frozen (Fig. 6). For example, on day 117 the thermocouple at the top of the TDR segment drops below 0 °C. The Ka gradually decreases for the next several days, indicating that the freezing front is moving

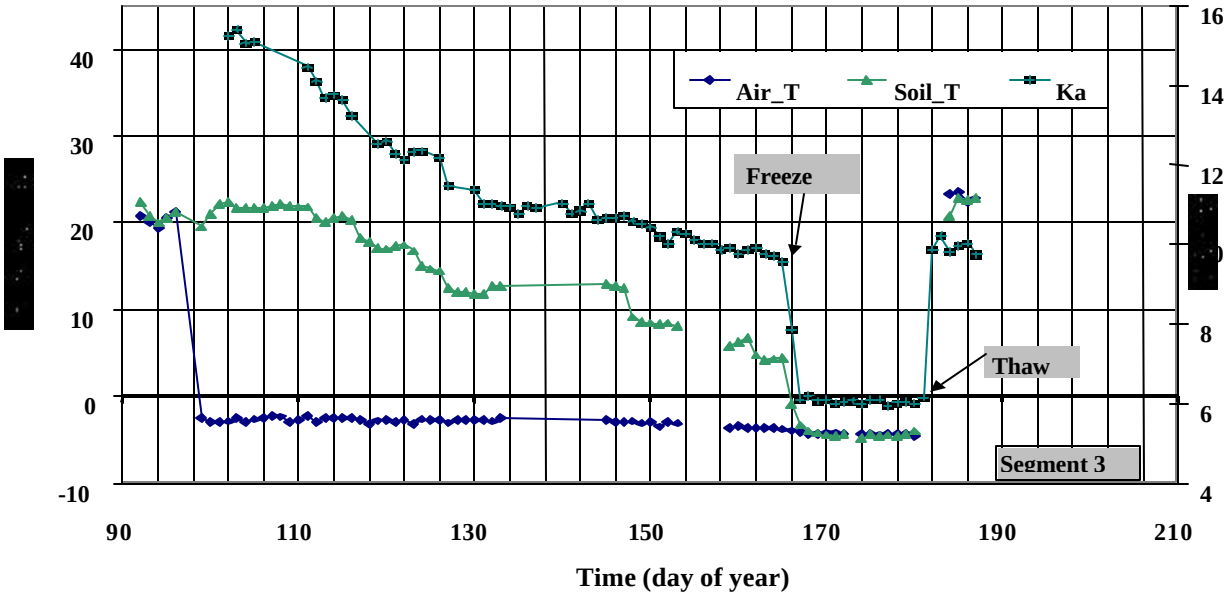

Fig. 5. *Temperature and Ka vs Time for TDR segment 3 (30-45cm). The Soil_T is the average temperature of the two thermocouples located at the top and bottom of the segment. Segment 3 went through a rapid freeze-thaw cycle on day 165 and day 181 respectively.*

down the first segment. On day 126 there is a dramatic decrease in Ka coinciding with the bottom thermocouple dropping below 0 °C. In addition to the TDR and thermocouple measurements the soil was mechanically probed, by drilling into the column with an electric drill, to determine the frost depth. This verified the estimated depth based on the TDR and thermocouple measurements.

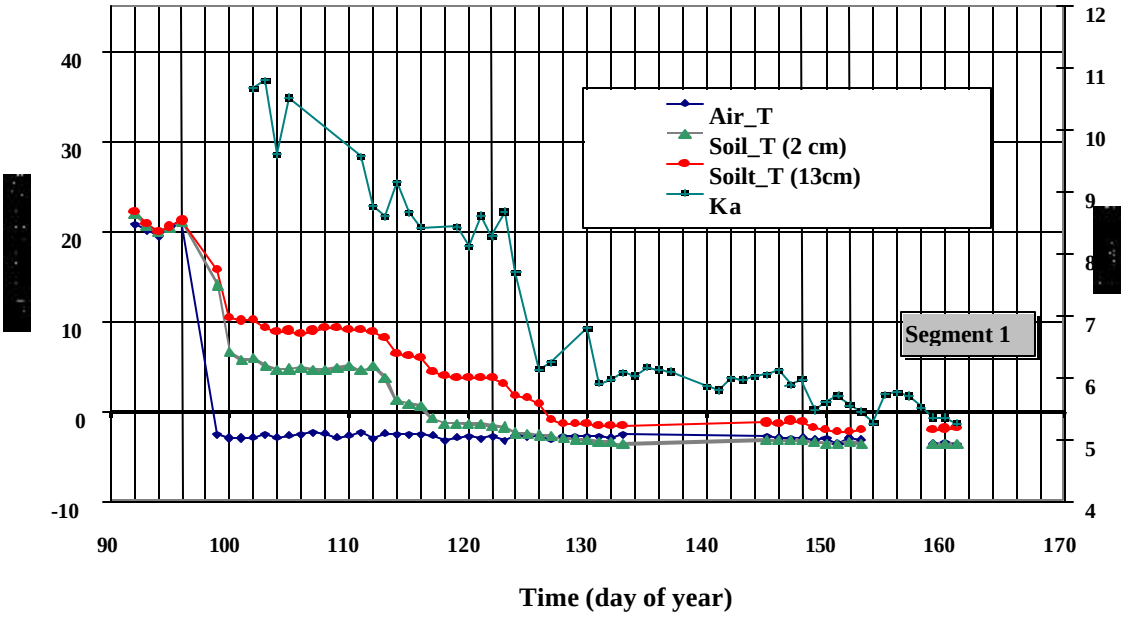

Fig. 6. *A change in the Ka is evident only after Soil_T (13cm) has dropped below 0 °C. Freezing may be occuring in the upper part of the segment , although it is difficult to detect.*

Studies conducted by Davis *et al.* (1982) suggest that analysis of the raw waveform may be a better way of detecting the freezing front; rather than using the Ka calculated from propagation time. However, analysis of the raw waveform would require feeding the signal into the top of the probe. A top fed signal would travel the entire length of the probe and the remote switching diodes would provide inflections at known points along that length. This method would provide a way to monitor the freezing front as it migrates along the length of each segment. This approach is relatively straight forward if manual observation and interpretation of the waveform is used. However, for real-time and continuous monitoring automated interpretation of the waveform is desirable.

Field Testing at Remote Sites

Five remote sites (Figure 7) were selected for testing field measurements of the frost depth below the pavement. Two of the sites were R/WIS sites (Effe and Jacobson). Two of the remote sites were "stand alone" solar powered sites (Marshall and Rochester) (Millner and Roberson, 2000). And one site was located at Mn/Road.

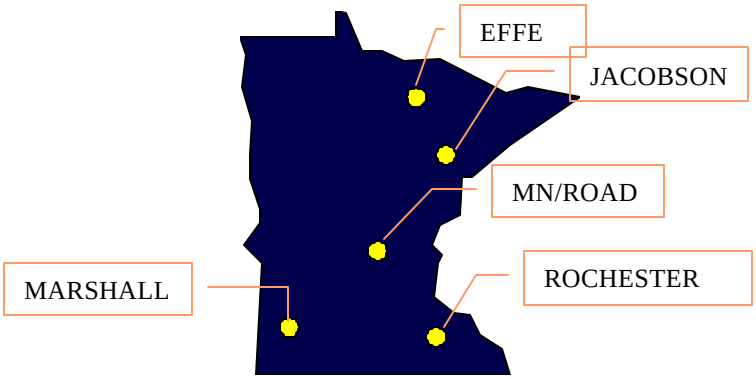

Fig. 7. *Remote site locations*

Road and Weather Information System (R/WIS) sites

Field installations consisted of coring the pavement (Figure 8a) approximately 18 inches from the shoulder. Cable connections at the probe were waterproofed with epoxy filled shrink tubing. A slide hammer and pilot rod were used to drive a pilot hole through the base and subgrade layers. The slide hammer was then used to drive the MP probe into the same pilot hole, stopping when the top of the probe was level with the bottom of the pavement layer (Figure 8b). Cables were directed through saw cuts in the surface of the pavement to a PVC conduit located at the shoulder. Backer rod was placed in the saw cut to prevent abrasions and/or breaks in cables. Epoxy was used to fill the saw cuts, cold patch was used to replace pavement core. MP communication cables were run through the conduit to the R/WIS remote processing unit (RPU) installed adjacent to the roadway. Housed in the RPU is the MP-017, intended for integration into environmental monitoring systems. Data is collected from the MP probe every 10 minutes, and loaded to an internet ftp site on a daily basis. Mn/DOT automatically downloads the data from the ftp site and into an existing database.

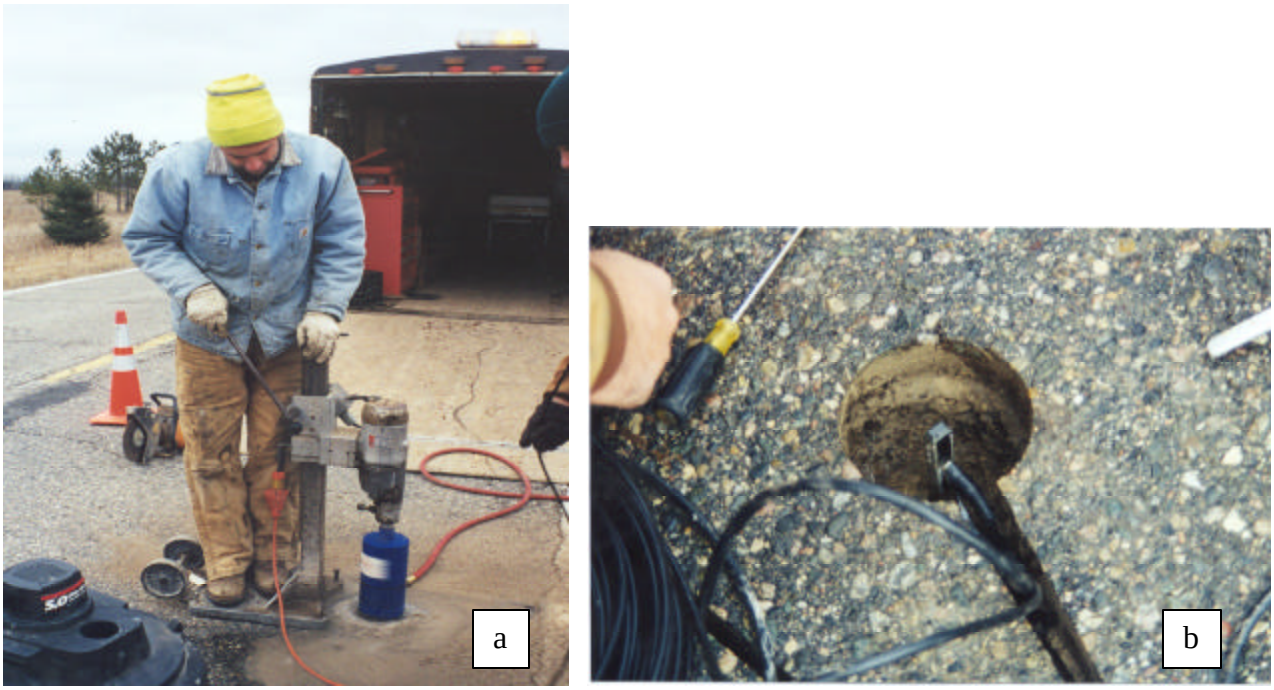

Fig. 8a and b. *A drill press was used to core the pavement. The MP probe installation with wires directed towards PVC conduit via kerf cut.*

CONCLUSIONS

The multi-segment TDR probe shows promise as an instrument for measuring the frost depth within pavement systems. Measured changes in the dielectric of the aggregate material, during a freeze-thaw cycle gave a good indication of the frost depth. Rapid freezing and thawing, as well as high initial moisture content, produce a distinct and measurable change in the dielectric. Whereas, slow rates of freezing and low initial water contents can make data interpretation difficult. These factors should be considered as automated interpretation techniques are developed. The benefits of integrating the MP probe into the R/WIS system architecture, in conjunction with successful field implementation hold promise that could be realized statewide. By accurately determining the frost depth and effectively disseminating the information to maintenance personnel and decision makers we can reduce the damage to the pavement structure due to increased winter loads and spring-thaw weakening. By reducing the damage during these critical periods we stand to significantly reduce maintenance costs.

REFERENCES

Baker, J. M., 1990. Measurement of Soil Water Content. Remote Sensing Reviews, **5**, No. 1, 263-279.

Baran, E. Use of Time Domain Reflectometry for Monitoring Moisture Changes in Crushed Rock Pavements. Proceeding of the Symposium: Time-Domain Reflectomerty in Environmental, Infrastructure, and Mining Applications Sept. 1994, Special Publication SP19-94, 349-356.

Davis, J. L., *et al*, 1982. Locating the Frozen-unfrozen Interface in Soils Using Ttime-Domain Reflectometry. Can. Geotech. J., **19**, 511-517.

Federal Highway Administration, 2000, Let it Snow: Winter Road Maintenance Products and Technologies. FHWA-OP-00-012.

Hayhoe, H. N., Topp G. C., and Edey S. N., 1983, Analysis of Measurement and Numerical Schemes to Estimate Frost and Thaw Penetration of a Soil. Can. J. Soil Sci. **63**, 67-77.

Kotdawala, S. J., Hossain M., and Gisi A J., 1993, Monitoring of Moisture Changes in Pavement Subgrades using Time-Domain Reflectometry (TDR), KDOT, Manhattan.

Millner, C. and Roberson, R., 2000, Solar Powered Systems for Pavement Instrumentation, Minnesota Department of Transportation, Internal Report.

Minnesota Department of Transportation, 1996, Frost Resistivity Probe. User Guide Klute *et al*, 1986. Methods of Soil Analysis: Physical and Mineralogical Methods. No. 9, Part 1. 2nd Edition.

O'Conner, K. M., and Dowding C. H., 1999, GeoMeasurements by Pulsing TDR Cables and Probes. CRC Press LLC.

Roberson, R. and Birgisson B., 1998, Evaluation of water flow through pavement systems. Proceedings: International Symposium on Subdrainage in Roadway Pavements and Subgrades November 1998, 295-302

Roberson, R. L. and Siekmeier, J., 2000, Using a Multisegment Time Domain Reflectometry Probe to Measure Frost Depth in Pavement Systems.

Spanns, E.J.A. and Baker J.M., 1996, Examining the use of Time domain Reflectometry in Frozen Soils.

---------- 1995, Examining the use of Time Domain Reflectometry for Measuring Liquid Water Content in Frozen Soil. Water Resour. Res. **31**, 2917-2925

---------- 1996, The Soil Freezing Characteristic: Its Measurement and Similarity to the Soil Moisture Characteristic. Soil Sci. Soc. Am. J. **60**,13-19

Topp, G. C., Davis J. L., and Annan A. P., 1980, Electromagnetic Determination of Soil Water Content: Measurement in Coaxial Transmission Lines. Water Resources Research, **16**, No. 3, 574-582.

Wright, W. C. and Rainwater N. R., 1998, Calibration of Multiple Segment Time Domain Reflectometry Probes in High Density Materials. Interim Report, State of Tennessee Department of Transportation Research Development and Technology Transfer, Project number (TSNPR) RES1080.

CONTINUOUS MEASUREMENTS OF LIQUID WATER CONTENT AND DENSITY IN SNOW USING TDR

Peter Waldner[1], Christof Huebner[2], Martin Schneebeli[3], Alexander Brandelik[4] and Frank Rau[5]

[1]WSL-Swiss Federal Institute for Snow and Avalanche Research, Switzerland; waldner@slf.ch
[2] Forschungszentrum Karlsruhe, Germany;Christof.Huebner@imk.fzk.de
[3]WSL-Swiss Federal Institute for Snow and Avalanche Research, Switzerland; schneebeli@slf.ch
[4]Forschungszentrum Karlsruhe, Germany; alexander.brandelik@imk.fzk.de
[5]Institute of Physical Geography, University of Freiburg, Germany; frank.rau@ipg.uni-freiburg.de

ABSTRACT

Measuring snow wetness and snow density is essential for many applications in snow hydrology like avalanche warning, flood prediction, optimization of hydro power generation and investigations of glacier melting due to global warming and climate change. So far the snow parameter sensors were not suited for long time continuous measurements when disturbing melting processes around the sensor occur. In many respect the performance moreover suffered from their small measurement volume which is not adequate to achieve representative values for natural snow covers with large spatial variability. Therefore two new sensor have been developed. A light-weight sensor has been designed to position on a snow layer with minimal influence on the snow. This sensor with length 0.3 m is constructed from an aluminum tube of 3 mm diameter. It is convenient for continuous time domain measurement with regard to spatial and temporal variability of snow wetness or density. The other new sensor has a large measurement volume and the capability of monitoring the whole snow cover cycle. It consists of a flat band cable as TDR transmission line up to about 100 m long which is enclosed by snow fall. Time domain measurements or time domain measurements in a combination with low frequency measurements are suited for the determination of both snow wetness and snow density. Besides integral measurements along the flat band cable the possibility of reconstructing vertical snow parameter profiles with sloping transmission lines has also been investigated. Several measurement campaigns demonstrate, on the basis of the measured results, the successful practical application of the methods and sensors developed in this work.

INTRODUCTION

Seasonal snow covers are highly variable both in space and time. Their deposition and depletion represent sporadic rather than continuous processes, the occurrence of which vary with meteorological conditions. After initial deposition of a snow layer, the snow changes by time display a wide range of physical characteristics, from the metamorphism of snow crystals and grains to melting processes and

liquid water transport. The vertical arrangement of different snow layers and their properties is essential for avalanche prediction. In addition understanding of water transport phenomena in snow is important to assess the influences of natural and artificial snow on an ecosystem. To study these processes continuous measurements of liquid water content in snow with an adequate spatial resolution are necessary.

Further the total snow water equivalent represents the available supply for filling the reservoirs of hydro power stations. Monitoring temporal snow wetness variations is the key for determining water percolation through the snow pack and the assessment of flood dangers. Therefore several measurement stations at representative sites within a hydrological basin are required. The sensors themselves have to provide mean snow properties of a sufficiently large area at these sites.

During the last decade there have been many efforts to determine snow parameters with radar remote sensing from satellites. This way the mapping of snow parameters on large areas promises with excellent possibilities for investigations of the snow cover in respect to climatological, meteorological, hydrological or glaciological applications. The signal measured by the radar system is composed partly from surface scattering and from volume scattering from the snow pack. It is influenced by liquid water content, snow grain size, snow density, ice lenses and surface roughness. Therefore ground measurements of the snow properties are required to provide information on the key parameters for the radar image interpretation and calibration. These ground measurements have to provide mean snow properties of areas comparable in size with the pixel size of the radar system which is in the order of 20 x 20 m.

With this background in mind we have investigated conventional snow parameter sensors for determining wetness and density and have developed and tested two new sensor systems.

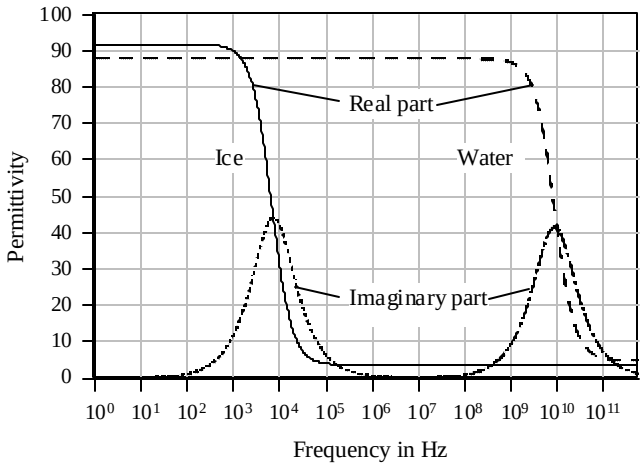

Fig. 1. *Relaxation spectra of water and ice.*

DIELECTRIC PROPERTIES OF SNOW

Wet snow is a mixture of ice crystals, liquid water and air. The permittivity of ice ε_i and water ε_w are frequency dependent as shown in Fig. 1 whereas the permittivity of air ε_a is constant=1. A travel time measurement with time domain reflectometry approximates a frequency domain measurement at about 1 GHz in the case of a typical system configuration (Textronik cable tester 1502B, 20 m coaxial and 40 m flat band cable). Permittivity of ice ε_i is about 3 and of water ε_w about 89 in this frequency range.

The real part of the dielectric permittivity of the mixture is related to the volumetric contents of ice θ_i, water θ_w and air θ_a, according to relations like Looyenga's (1965) formula for spherical intrusions (α=3):

$$\varepsilon_d = (\theta_i \varepsilon_i^{1/\alpha} + \theta_w \varepsilon_a^{1/\alpha} + \theta_a \varepsilon_a^{1/\alpha})^{\alpha} \qquad [1]$$

Hence, in case of dry snow, ε_d is mainly related to snow density as given e.g. by Tiuri *et al*. (1984):

$$\varepsilon_d = 1 + 1.7\,\rho + 0.7\,\rho^2 \qquad [2]$$

They also recommend an equation for the increase of the permittivity $\Delta\varepsilon$ under wet snow conditions with water content θ_w as compared to dry snow:

$$\Delta\varepsilon = 0.089\,\theta_w + 0.0072\,\theta_w{}^2 \qquad [3]$$

Further formulae, most of them similar to (2) and (3), were reviewed by Frolov & Macharet (1999). Although the general validity of these expressions is still under discussion, they will be used as a working model.

A time domain or high frequency measurement of the permittivity of dry snow provides the snow density. In case of wet snow the two unknowns density and water content cannot be determined from only one measurement. One approach is to extrapolate the density development from the latest dry snow measurements which can be distinguished from contaminations of the snow which unpredictably influence the imaginary part of the permittivity. A better solution is to combine high frequency or time domain measurements with a low frequency capitance determination in the kHz domain. Due to the different relaxation spectra two independent measurements allow the derivation of water content and density at the same time.

CONVENTIONAL SENSORS: SPATIAL VARIABILITY

So far the sensors used for time domain reflectometry measurements in snow usually consisted of coaxial lines, two wire lines, microstrip lines or capacitor plates and measure the permittivity of the snow in the surrounding of the sensor (Fig. 2). From the permittivity water content and/or density of the snow can be derived.

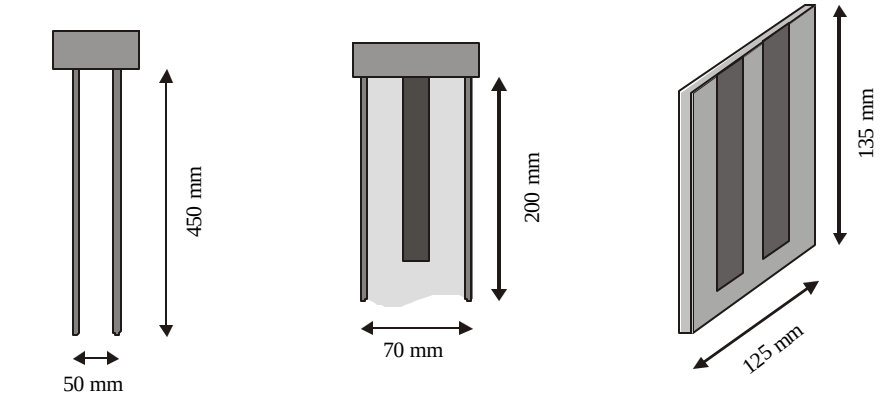

Fig. 2. *Conventional Sensors for measuring dielectric properties of snow from which water content and density may be derived*

We have used one of these sensors during a measurement campaign to determine spatial variability in a natural snow cover. A 16 m long and about 0.5 m deep trench in the snow was excavated. The water content along the trench was measured with the sensor from Denoth (1994) at two consecutive days in a depth of about 0.5 m below snow surface and with 1 m spacing.

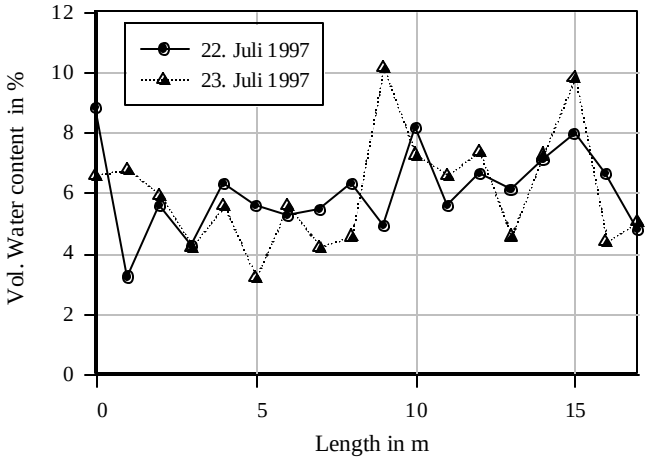

Fig. 3. *Water content along a transect in the snow cover measured with the sensor from Denoth (1994).*

The measurement results in Fig. 3 show strong fluctuations of the water content which are typical for this time of the year with daily melt phases. When water flow starts rapid changes of the snow pack structure occur and preferential percolation paths emerge (Marsh & Woo, 1984; Schneebeli, 1995; Williams *et al.*, 1999). A high temporal and spatial variability of the snow wetness results. Hence, on one hand, destructive methods are not practical to study temporal evolutions. On the other hand representative mean values of snow wetness require a large number of measurements and consequently an enormous expenditure of work.

LIGHT WEIGHT SNOW TDR SENSORS FOR PROCESS STUDIES

In order to investigate the temporal evolution of the snow wetness continuous measurements with a sufficient resolution in time and space are necessary. In a snow cover a permanently placed sensor faces snow creeping, warming up through solar radiation and hence will influence the snow cover itself. Therefore an adapted TDR sensor with minimal influence of the snow cover was designed and tested. The sensors are light-weight such that they can be posed on top of a new snow layer to be covered during the next snow fall period (detailed description: Schneebeli *et al.*, 1998).

They are constructed from a thin-walled aluminum tube (3 mm diameter, thickness of wall 0.3 mm (Fig. 4). White color reduces the adsorption of solar. In the snow the height of the sensors above ground declines according to snow pack settling.

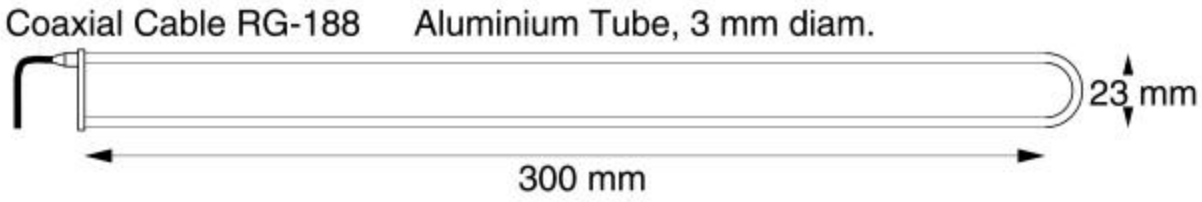

Fig. 4. *Sketch of the construction of the light weight snow TDR sensor. The probe is connected by a thin coaxial cable to a cable tester.*

In order to investigate the temporal and spatial variation of the water content 40 sensors were posed on top of the snow cover on a slightly sloped open field at 1200 m a.s.l. in the valley Alptal (Switzerland) early in the Winter 1998/1999 (Fig. 5).

The TDR signal was measured and digitized with a Tektronix 1502B cable tester and a coaxial multiplexer. To locate the reflection within the digitized waves the algorithm of (Schneebeli *et al*., 1998) had to be adapted to wet snow condition. Further it was simplified such that it could be programmed on a standard data logger. Measurement values are smoothed and the first derivative is calculated hereafter. High values of the first derivative define an impedance mismatch. The algorithm defines the different wave section by looking for the first and the last values of the derivative with a certain percentage range of its maximum or minimum.

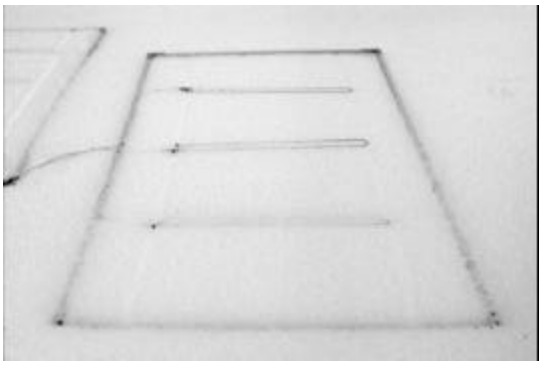

Fig. 5: *The light weight snow TDR sensors were mounted on a frame to pose them on the snow cover before the next snow fall period.*

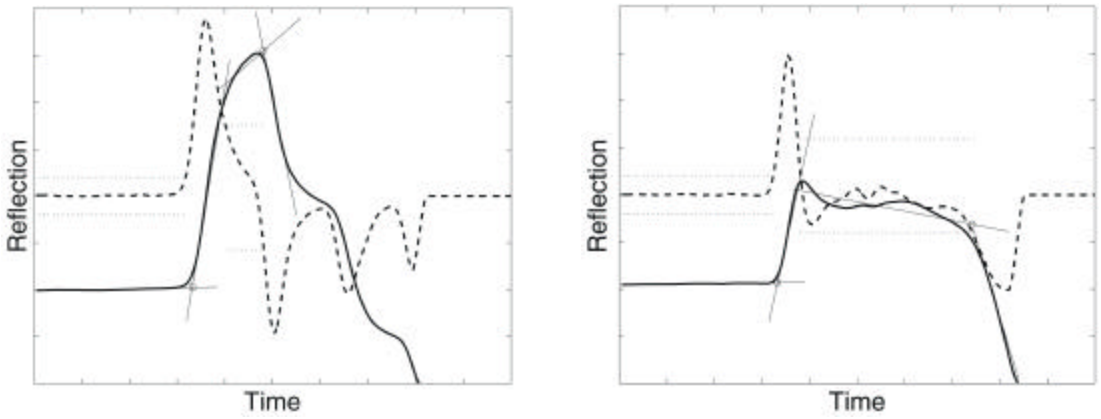

Fig. 6. *Digitized Wave form (solid line) from measurements in dry snow (left part) and wet snow (right part). First derivative (dashed) with check lines (dotted) and straight lines adapted to the wave with the intersection defining the start of an impedance mismatch.*

At these positions straight lines are drawn through the smoothed signal wave. Intersections of these lines define the start of an impedance mismatch as shown in Fig. 6. During the campaign density measurements were carried with nearby snow pit examinations. The measured dielectric permittivity showed good agreement with permittivity calculated with equation (2) from densities for periods with snow temperatures up to -1°C at sensor height. By individually interpolating density values for each sensor, we were able to estimate snow wetness with equation (1).

Fig. 7 shows resulting liquid water content for 4 sensors that have a typical temporal evolution and variability. The high water contents are explained by a highly saturated base flow of melt water at the bottom of the snow pack that subsequently reached the sensor positions.

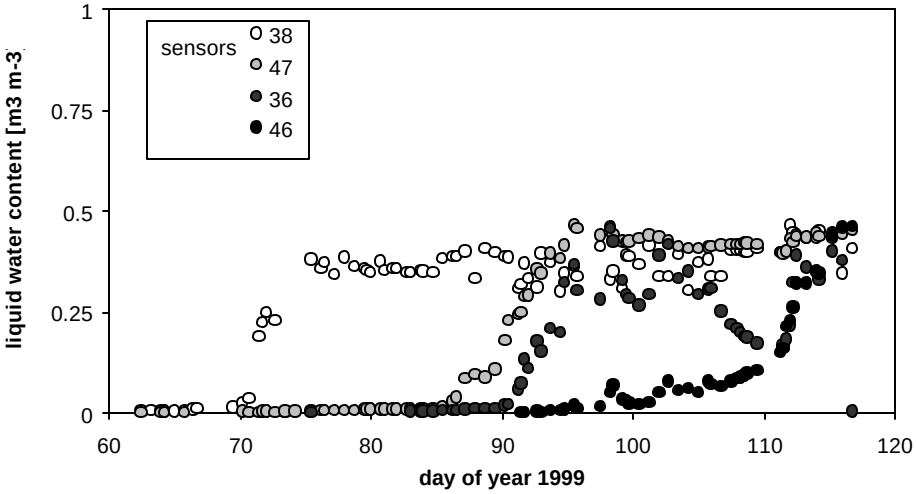

Fig. 7. *Typical temporal evolution of the liquid water content for sensors placed 20 cm above ground in the snow cover with 25 cm spacing. Subsequently the sensors register liquid water contents near saturation.*

Fig. 8. *Installation of the snow parameter measurement system on the glacier Plaine Morte. The site is located near Crans-Montana, Switzerland, at a height of about 2800 m above sea level and has favorable snow conditions even until June or July.*

LONG FLAT BAND CABLE SENSORS

The second sensor system which has been developed is especially suited for continuous measurements over long periods (Huebner and Brandelik, 2000). It consists of flat band cables as TDR transmission lines with lengths up to 100 m. They are permanently installed at the measurement site in different heights and enclosed by snow fall. Fig. 8 shows an exemplary installation on a glacier in Switzerland at the beginning of the snow cover cycle when the cables are still in the air.

The flat band cables can be measured with time domain and additionally with frequency domain signals in order to determine snow wetness and density at the same time. The physical background of the measurement, respectively the dielectric properties of snow are reviewed, followed by a detailed discussion of the cable design, system development and experimental results.

FLAT BAND CABLE SENSOR DESIGN AND MEASUREMENT PRINCIPLE

The typical sensing device for time-domain reflectometry is a metallic fork which is inserted in the material under test. Instead of this rigid construction a flexible flat band cable is proposed which can follow the settlement of the snow cover. A picture of the cable together with a sketch of the cross section is shown in Fig. 9.

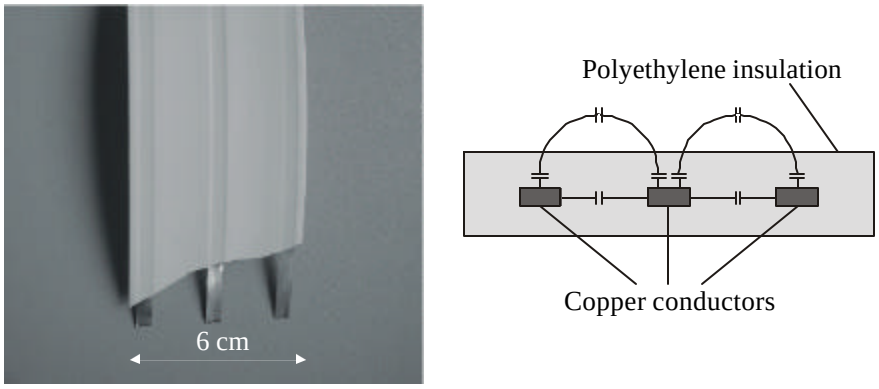

Fig. 9. *Flat band cable and its cross section.*

The white polyethylene insulation reduces the warming up of the cable due to solar radiation and the thin copper conductors have an advantageous low thermal capacity. Nevertheless airgaps will develop around the flat band cable especially after several months of measurements with multiple freezing and thawing cycles.

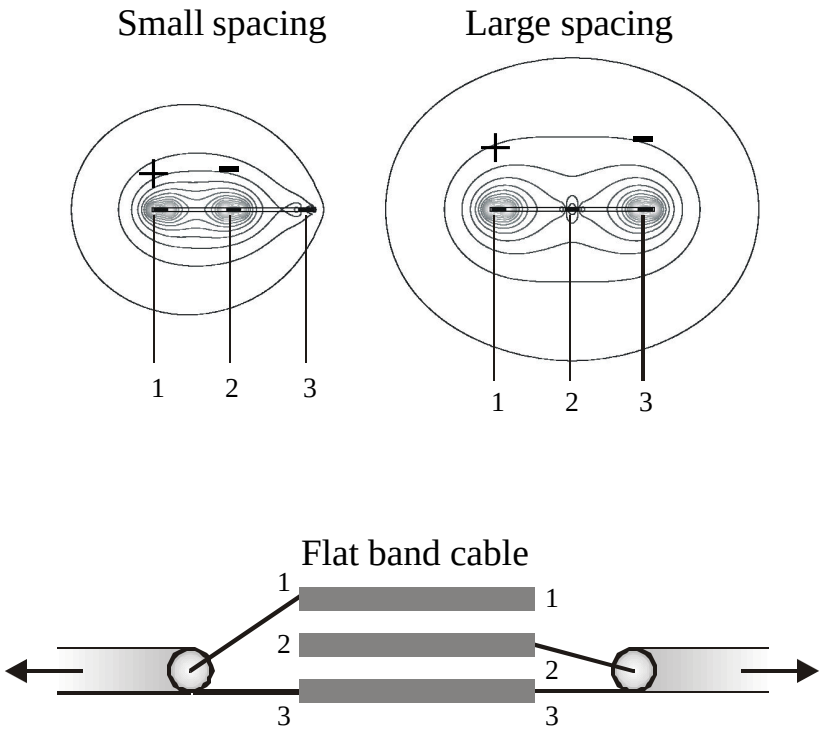

Fig. 10. *Three wire flat band cable: Extension of the electromagnetic field for two different connection possibilities. The cable is connected to time domain reflectometer once from the left and once from the right side.*

These airgaps cause underpredictions of the permittivity of the surrounding snow. To avoid this and compensate for airgap effects the three wire cable is measured twice, with small and with large spacing as shown in Fig. 10. A correction equation has been derived for calculating air gap size and true permittivity of the snow.

EXPERIMENTAL RESULTS

A complete measurement system was installed on the glacier Plaine Morte (Fig. 8) consisting of horizontal snow wetness measurement cables connected to a time-domain reflectometer via a multiplexer, a weather station, snow height and temperature sensors and a computer for control and data acquisition. The horizontal cables were arranged at different heights over a length of about 40 m to obtain representative data from the snow cover. A typical measurement result for a horizontal cable is shown in Fig. 11.

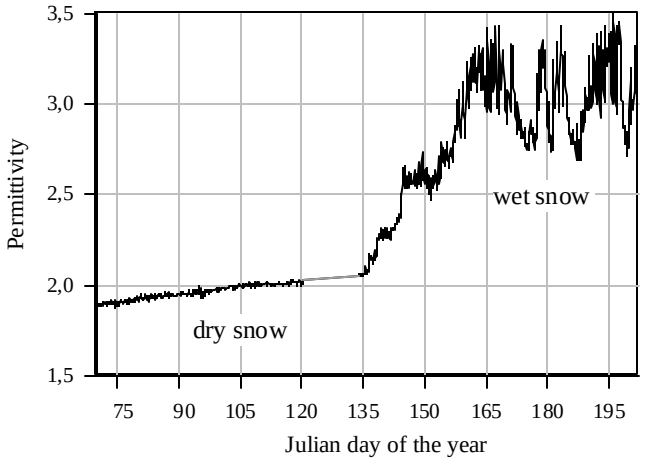

Fig. 11. *Permittivity of a snow cover versus time.*

One can distinguish between the dry snow and the wet snow phase. In the dry snow phase there is a constant increase in the permittivity which is due to compaction of the snow for higher density. The permittivity can be related to the dry density with equation (1) and increases to about 0,55 g/cm³ at the transition from the dry to the wet snow phase which is around the 135th day of the year. At this time a sharp rise in the permittivity due to melting processes can be observed. In the wet snow phase there are strong daily variations of water content which could be seen at finer time resolution and related to actual weather conditions.

Fig. 12 shows the daily variation of water content at the cables in different heights in comparison with air temperature and radiation balance observations. The increase of the air temperature above 0°C forces melting and an increase in the water content in the upper layers of the snow cover. It takes some time for the melt water to percolate through the snow pack and to reach the lower cable which also exhibits lower water contents and less variations.

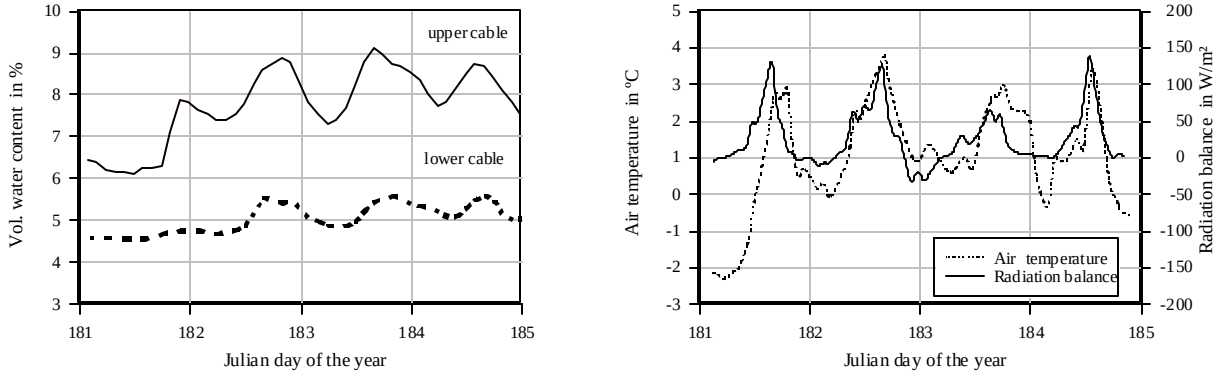

Fig. 12. *Daily variations of snow wetness in comparison with air temperature and radiation balance.*

Besides the vertical structure of the snow pack strong horizontal variations can also be observed. These horizontal structures are visible in the TDR signal as well as in an aerial photograph of the measurement site (Fig. 13).

Fig. 13 shows the part of the TDR signal which corresponds to the flat band cable. The bumps in the signal are areas of higher water content and have been identified with percolation zones in the snow cover. Percolation zones are paths of preferred water transport and show up as dark areas with accumulated contaminations. The possibility of the TDR to resolve spatial structures can be exploited for a determination of vertical snow pack structures. Therefore a field campaign in the Black Forest has been carried out (Fig. 14).

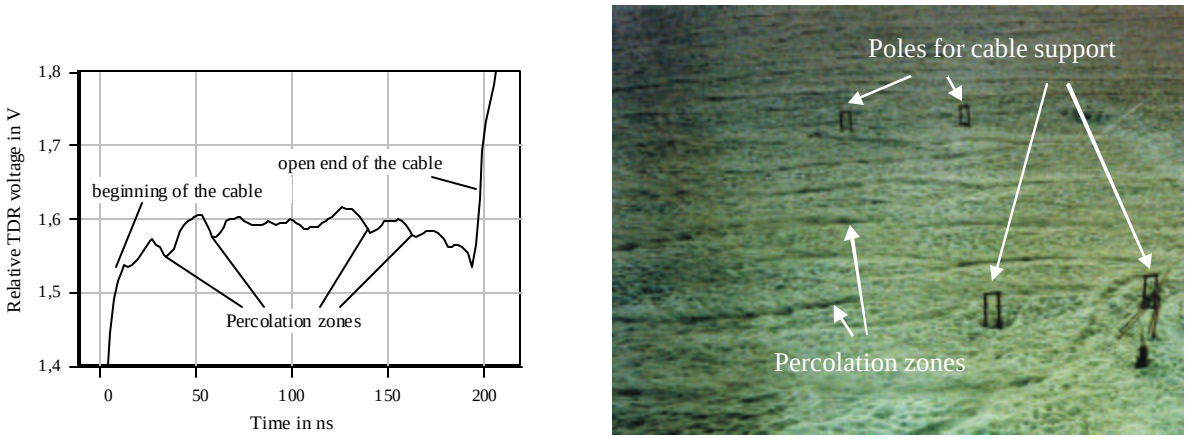

Fig. 13. *Horizontal structure of the snow cover as seen in the TDR signal and in an aerial photograph of the site*

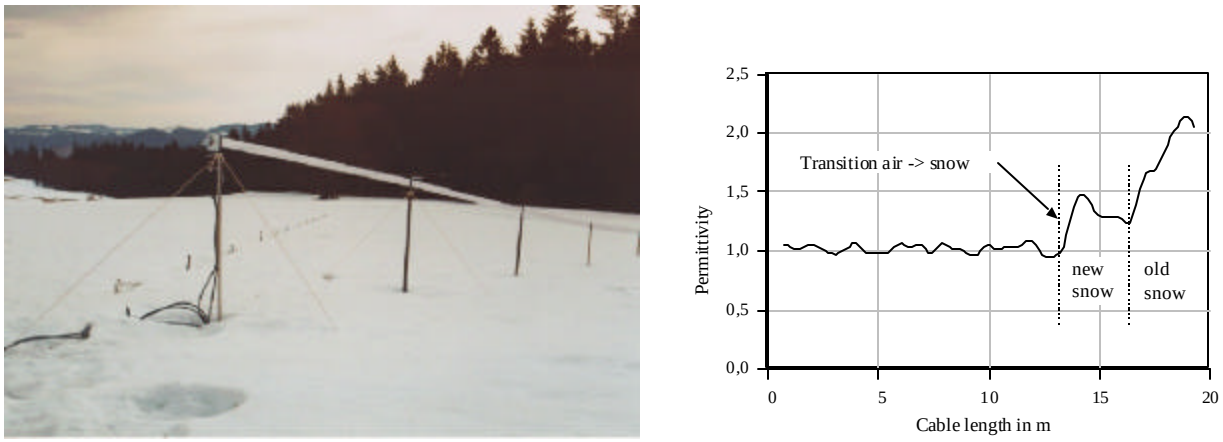

Fig. 14. *Sloping cable for vertical profile measurements: installation and measurement results*

A 20 m long sloping cable was connected to a computer-controlled time-domain reflectometer. The data was processed with a reconstruction software developed by Scheuermann *et al*. (2001) in order to determine the permittivity profile along the flat band cable. Though the total snow height during the campaign was less than expected owing to the warm winter weather, the vertical structure of the snow cover with new and old snow layers could be resolved. At the time of writing another field campaign is

conducted in Switzerland with emphasis on vertical profile measurements together with simultaneous measurements at low frequencies for density determination.

SUMMARY

Two new sensor system for measuring snow wetness and density have been presented. The first sensor is light weight and especially suited for process studies. It consists of a thin aluminium structure which can be posed on the top of a new snow layer to be covered during the next snow fall period. The results of a field campaign show the high temporal evolution and variability of the wetness in a natural snow cover. The second sensor consists of flat band cables as TDR transmission lines with lengths up to 100 m. The cables are enclosed by snow fall and remain in the snow pack until the end of the season. The main advantages of this sensor are the large measurement volume and the possibility of a continuous monitoring of the snow cover development. This is achieved by a three wire cable design, two measurements at different electromagnetic field penetration depths and an airgap correction algorithm. The performance of the sensor is demonstrated in field campaigns. Monitoring of the snow cover development on representative large areas has been achieved for the first time and allows detailed investigations of the water transport processes through a snow pack. By using sloping cable arrangements the possibility of retrieving vertical profiles of snow properties has been demonstrated. A field campaign in this winter will focus on this task and the simultaneous determination of water content and density with additional low frequency measurements.

ACKNOWLEDGEMENT

This work was partly supported by the Swiss National Science Foundation.

REFERENCES

Denoth, 1994, Snow dielectric measurements. Advances in Space Research, **9**, 233-243.

Frolov, A. D. and Macharet, Y. Y., 1999, On the dielectric properties of dry and wet snow: Hydrological processes, **13**, No. 12-13, 1721-1732.

Huebner, C. and Brandelik, A., 2000, Distinguished Problems in Soil and Snow Aquametry: in Sensors Update (Eds. H. Baltes, W. Goepel und J. Hesse), **7**, 317-340, Weinheim: Wiley-VCH.

Looyenga, H., 1965, Dielectric constant of heterogeneous mixtures: Physica, **31**, 401-406.

Mätzler, C., 1996, Microwave Permittivity of Dry Snow: IEEE Transactions on Geoscience and Remote Sensing, **34**, 573-581.

Marsh, P. and Woo, M.-K., 1984, Wetting front advance and freezing of meltwater within a snow cover: 1. Observations in the Canadian Arctic: Water Resources Research, **20**, No. 12, 1853-1864.

Scheuermann, A, Schlaeger, S., Huebner, C., Brandelik, A., and Brauns, J., 2001, Monitoring of the spatial soil water distribution on a full-scale dike model: in Kupfer *et al*. (eds.), Proceedings of the 4th

International Conference on Electromagnetic Wave Interaction with Water and Moist Substances, 347-354.

Schneebeli, M., 1995, Development and stability of preferential flow paths in a layered snowpack: in: K. A. Tonnessen, M. W. Williams & M. Tranter: Biogeochemistry of seasonally snow-covered catchments, Boulder: in IAHS Publication, **228**, 89-95.

Schneebeli, M., Coléou, C., Touvier, F. & Lesaffre, B., 1998, Measurement of density and wetness in snow using time-domain-reflectometry: Ann. Glaciol., **26**, 69-72.

Stein, J., Gaetan, L. and D. Lévesque, 1997, Monitoring the Dry Density and the Liquid Water Content of Snow Using Time Domain Reflectometry (TDR): Cold Regions Science and Technology, **25**, 123-136.

Tiuri, M. T., Sihvola, A. H., Nyfors, E. G. & Hallikainen, M. T., 1984, The complex dielectric constant of snow at microwave frequencies: IEEE J. Oceanic Eng., **OE-9**, No. 5, 377-382.

Williams, M. W., Sommerfeld, R., Massman, S. & Rikkers, R., 1999, Correlation lengths of meltwater flow through ripe snowpacks, Colorado Front Range, USA: Hydrological processes, **13,** No. 12-13, 1721-1732.

WATER CONTENT AND DENSITY OF SOIL IN SITU BY THE PURDUE TDR METHOD

Vincent P. Drnevich[1], Shafiqul I. Siddiqui[2], Janet Lovell[3], and Quanghee Yi[4]

[1]School of Civil Engineering, Purdue University, West Lafayette, IN 47907-1284, drnevich@purdue.edu
[2]Earth Exploration, Inc., Indianapolis, IN 46214-2988, ssiddiqui@email.msn.com
[3]School of Civil Engineering, Purdue University, West Lafayette, IN 47907-1284, lovell@purdue.edu
[4]School of Civil Engineering, Purdue University, West Lafayette, IN 47907-1284, yiq@purdue.edu

ABSTRACT

The Purdue TDR Method is a new technology for determining both water content and density of soil by measuring the apparent dielectric constant on two soil "cables," one in situ and the other on the same soil in a compaction mold. This method generally gives quite accurate water content values compared to oven dry values. Soil density determination is relatively calibration free because it depends on the ratio of two apparent dielectric constant measurements.

Apparent dielectric constants are somewhat dependent on soil temperature. Corrections for temperature are given but are not necessary for tests where soil temperatures are between 15° C and 25° C. Density determinations are much less affected by temperature if the soil temperature is approximately the same for both the in situ and compaction mold.

The Purdue TDR Method applies for a wide variety of soils, including particle sizes passing the 19 mm (3/4-in.) sieve. With ongoing improvements, widespread evaluation, and standardization, it has the potential to become a useful and reliable tool for the geotechnical community.

INTRODUCTION

The Purdue TDR Method for water content and density is a story of two "coaxial cables" where the "insulating" material between the "coaxial lead" and the "shield" is soil. Driving four metal "spikes" into the soil surface in a pattern that simulates a cable creates one of the "coaxial cables." The length of the spikes determines the length of the cable, typically 20 cm (8-inches). The principle of Time Domain Reflectometry (TDR) is used to measure the travel time of an electromagnetic wave in this cable. The travel time allows for determining the "apparent dielectric constant" of the soil contained between the

spikes. The word "apparent" is used because the dielectric permittivity of soil is a complex, frequency dependent function (Siddiqui and Drnevich, 1995).

The second "coaxial cable" consists of a metal compaction mold filled with soil and a metal rod driven into the center of the soil-filled mold for the center lead. The metal mold forms the "shield." The compaction mold is placed on a non-metallic base to complete the simulation. Again, TDR is used to measure the travel time from which the "apparent dielectric constant" is determined. With the total density of the soil known in the compaction mold, the water content can be calculated for the soil using a simple equation. Water contents determined by this method compare exceptionally well with those obtained by oven drying.

If the soil in the compaction mold is the same soil and has the same water content as tested in the first "cable" (in situ), then the density of the soil in situ is determined by a simple equation based on the average dielectric constants measured in situ and in the compaction mold.

In practice, a cable is formed in situ and the dielectric constant of the soil is determined by TDR. The spikes are removed and the soil between the spikes is excavated and quickly hand compacted into a compaction mold. The total density of the soil in the compaction mold is determined by weighing, a center lead is installed, and the dielectric constant of the soil in the compaction mold is determined. The latter dielectric constant and soil density allows for determination of the water content of the soil. The in situ dielectric constant combined with the compaction mold dielectric constant and the soil density allow for calculating the in situ density.

This process was conceived by the author and Dr. Shafiqul Siddiqui as part of his dissertation work at Purdue University and was enhanced and improved by faculty colleagues, Dr. Richard Deschamps and Robert Nowack, by former graduate students: Dr. Wei Feng, Dr. Chihping Lin, and Mr. Jie Zhang, by current graduate students Quanghee Yi and Xiong Yu, and by our laboratory manager, Ms. Janet Lovell. This paper will describe in detail the above procedure and some work in progress, especially the effects of particle size and temperature on the process.

BACKGROUND INFORMATION

Relationship Between Volumetric Water Content and Gravimetric Water Content
Siddiqui and Drnevich (1995), Feng et. al. (1998), Lin et. al. (2000) provide a reasonably complete history of the use of the TDR method for water content determination. For more than 30 years, agronomists have been making extensive use of dielectric properties for measuring the **volumetric** water content of soil (volume of water as a percentage of the total volume of the soil). The volumetric water content is usually represented by the Greek letter theta, θ. Geotechnical engineers work with the **gravimetric** water content of soil (mass of the water/mass of dry soil solids) and it is usually represented by the letter, *w*. Both θ and *w* are expressed as percentages. Volumetric and gravimetric water contents are related by

$$w = q\,\frac{r_w}{r_d} \qquad [1]$$

where r_d is the dry density of the soil and r_w is the density of water.

Research into the dielectric properties of soil in soil science and in civil engineering led to the introduction of many calibration equations. Lin *et al*. (2000) provides an in-depth evaluation of these calibration equations. The theoretical and experimental study by Lin *et al*. (2000) suggested that the density-compensating calibration equation proposed by Siddiqui and Drnevich (1995) provides the best relationship between soil water content and dielectric constant. The "Siddiqui-Drnevich" calibration equation accounts for soil density and soil type:

$$w = \frac{1}{b}\left[\frac{r_w}{r_d}\sqrt{K_a} - a\right] \qquad [2]$$

where r_d is the dry density of soil, r_w is the density of water, a and b are soil-dependent calibration constants. From tests on a variety of soils the value of a is consistently near unity and the value of b is consistently near eight.

Determining the Apparent Dielectric Constant, K_a

Time Domain Reflectometry test devices were originally developed to find distances to breaks or discontinuities in metallic cables. An electromagnetic wave travels down a cable with a velocity, v, given by

$$v = \frac{c}{\sqrt{K_a}} \qquad [3]$$

where c is the velocity of an electromagnetic wave in free space (2.998×10^8 m/s). The travel time of the wave traveling down and back in a cable of length, L, is given by

$$t = \frac{2L}{v} \qquad [4]$$

where t is the measured travel time (down and back). Combining Eqs. 3 and 4 yields

$$K_a = \left(\frac{ct}{2L}\right)^2 \qquad [5]$$

The horizontal axis of the Tektronix 1502B is calibrated in values of $\frac{ct}{2}$ which has units of length and the value of $\frac{ct}{2}$ is defined as apparent length, l_a. The horizontal axis was calibrated in length so that the distance to the break or discontinuity could be quickly determined. Hence the apparent dielectric constant is calculated by

$$K_a = \left(\frac{l_a}{L} \right)^2 \qquad [6]$$

Figure 1 gives a typical curve for a Purdue TDR Method test. Algorithms have been developed and included in the data reduction program TDR++ to automatically determine the apparent length, l_a .

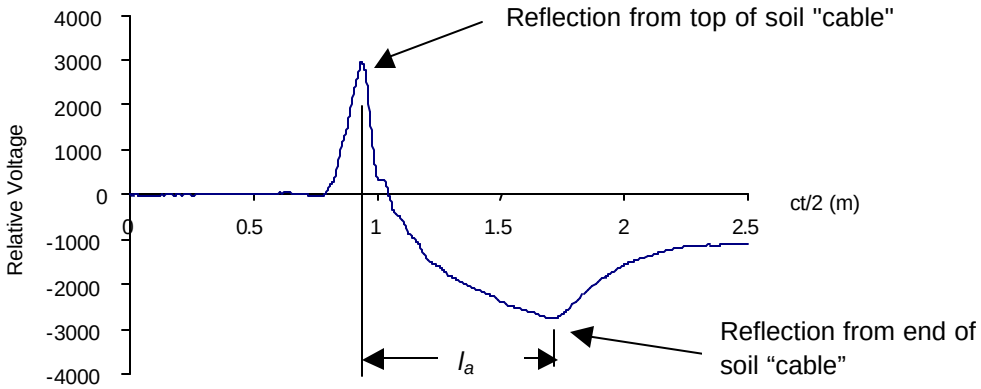

Fig. 1. *Typical TDR curve for soil and measurement of apparent length, l_a.*

Effects of Temperature on Apparent Dielectric Constant

Weast (1986) showed that the apparent dielectric constant of water, $K_{a,\,water}$, decreases linearly from a high of about 88 near freezing to about 70 for 50° C. Wraith and Or (1999) and others have noted that temperature effects for sandy soils behaves similarly (but with reduced sensitivity) to temperature changes, but that clay soils exhibit the opposite behavior, i.e. K_a increases with temperature. The apparent dielectric constant of dry soil minerals is not very temperature sensitive. Experiments at Purdue determined the apparent dielectric constant of a variety of soils, each having a range of water contents and density. A companion paper to this conference by Drnevich *et al.* (2001) provides the details.

Based on this testing, we propose to adjust the values of apparent dielectric constant from the TDR test at a given temperature to a standard temperature of 20°C. These values may be calculated from Eq. (7).

$$K_{a,20°C} = K_{a,T°C} \times TCF \qquad [7]$$

where

TCF = Temperature Correction Function

= 0.97 + 0.0015 $T_{test,\,T?\,C}$ for cohesionless soils, 4°C ≤ $T_{test,\,T?\,C}$ ≤ 40°C

= 1.10 - 0.005 $T_{test,\ T?\ C}$ for cohesive soils, 4°C ≤ $T_{test,\ T?\ C}$ ≤ 40°C.

From Eq. (7) it can be seen that values of $K_{a,\ 20°C}$ will not exceed about ten percent for extremes in temperature covered by this equation. Considering Eq. (2), we see that water content is related to the square root of K_a and hence temperature effects on water content are relatively small. The authors suggest that temperature corrections are not needed for 15°C ≤ $T_{test,\ T?\ C}$ ≤ 25°C. Since the dielectric constant of ice has dramatically different properties from unfrozen water, the TDR method described herein does not apply to frozen soil.

THE PURDUE TDR METHOD

In situ Testing

A "field cable" is first tested to measure the dielectric constant of soil in place ($K_{a,field}$). Four spikes are driven through a template into a smooth and level soil surface as shown in Fig. 2 to form the "field cable." The spikes used have a nominal diameter of 9.5 mm (3/8 inch) and have a nominal length of 229 mm (9 inches). The template has a thickness of 25.4 mm (1 inch) so that about 200 mm (8 inches) of the spikes are in the soil. The template is removed from around the spikes as shown in Fig. 3.

Fig. 2. *Driving spikes through a template for field test*

Fig. 3. *Removal of the template*

This leaves an air gap of approximately 25 mm (1 inch) between the top of the spikes and the soil surface. The length of the spikes in the soil is the length of the "field cable" as shown in Fig. 4. Other length spikes could be used with the practical range of lengths ranging from 150 mm (6 inches) to 300 mm (12 inches), however, for lossy soils, the practical length may be limited to the lower end of this range.

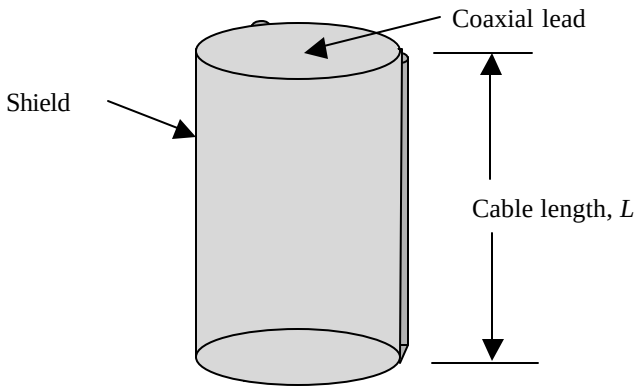

Fig. 4. *"Cable of Soil" created by driving spikes into soil surface*

Fig. 5. *Placement of multiple rod probe head on spikes*

A specially designed multiple rod probe head is placed on the four spikes as shown in Fig. 5. This head forms a transition unit between the spikes and the cable that connects to the TDR test device. All tests to date made use of a Tektronix, model 1502B TDR Cable Tester equipped with a serial port that connects to the serial port on a notebook computer. A computer program, TDR++©, developed by Wei Feng *et al.* (1998) as part of this research, controls the Tektronix 1502B, acquires the data, operates on it, and stores it along with other salient information about the apparatus, test, date, and location. The important information from the field test is the apparent dielectric constant, $K_{a,\,field}$. Use of this will be discussed later.

Once the information is stored in the computer, the probe head is removed and the spikes are removed. The soil is then excavated from the space defined by the outer three spikes. A battery-operated power drill with a 26 mm (1-in) diameter wood auger bit works well for loosening the soil for removal with a small hand scoop (See Fig. 6.). Unlike the sand cone test, disturbance of the soil adjacent to the excavated soil is not a problem.

Compaction Mold Testing

A special compaction mold is used for these tests. It resembles the conventional compaction mold specified by ASTM D698 except that it has twice the length and the bottom plate is made of a non-metallic material. The longer length allows for getting most of the soil from the in situ test into the mold and it allows for more accurate measurements of the travel time.

Soil is compacted into this mold using any desired compaction energy that produces a relatively uniform specimen in the mold. (An aluminum rod 38 mm (1.5 in) in diameter by 400 mm (16 in) in length works well as a hand tamper for routine field tests.) The mass of the soil and mold is determined. Subtracting the mass of the empty mold gives the mass of the soil and with the volume of the mold, the total density of the soil in the mold, $r_{t\,,mold}$ is determined.

Fig. 6. *Loosening soil with a power drill*

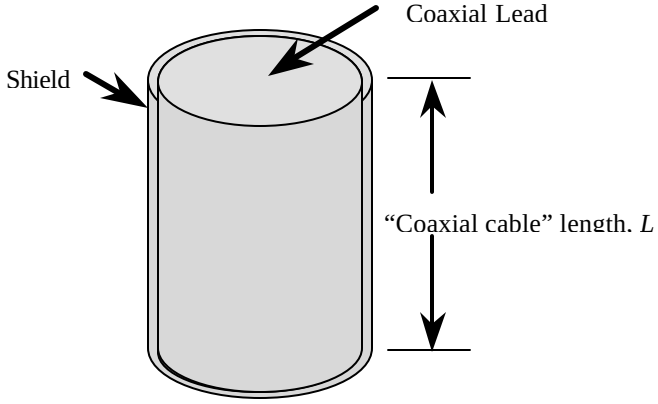

Fig. 7. *Compaction cylinder "Soil Cable"*

The mold containing soil is placed on a firm surface and a guide template is placed on the mold. A center rod is then driven into the mold and the guide template is removed. The mold with the center rod simulates a "cable of soil" as shown in Fig. 7.

A special adapter ring is placed on the mold and the same probe head used for testing in situ is placed on the adapter ring as shown in Fig. 8. A TDR measurement gives the average apparent dielectric constant for the soil in the mold, $K_{a,mold}$.

Fig. 8. *Compaction mold with adapter ring and probe head*

Calculation of Water Content and Density

Equation 2 allows for the calculation of water content with the use of apparent dielectric constant and the soil dry density. The dry density of the soil in the mold, $\rho_{d,mold}$, is related to the total density, $\rho_{t,mold}$, through

$$\rho_{d,mold} = \frac{\rho_{t,mold}}{1+w} \qquad [8]$$

Substituting Eq. 8 into Eq. 2 and solving for w yields

$$w_{mold} = \frac{\sqrt{K_{a,mold}} - a\frac{r_{t,mold}}{r_w}}{b\frac{r_{t,mold}}{r_w} - \sqrt{K_{amold}}} \quad [9]$$

If the process of removal of the soil from the hole in the field and placement into the compaction mold is done quickly, it is valid to assume that the water contents in the mold and in the field test are identical

$$w_{field} = w_{mold} \quad [10]$$

If Eq. 2 is written twice, once for the field test and once for the compaction test and with consideration of Eq. 8, the dry density of the soil in the field, $r_{d,field}$, may be calculated from

$$r_{d,field} = \frac{\sqrt{K_{a,field}}}{\sqrt{K_{a,mold}}} \frac{r_{t,mold}}{1+w_{field}} \quad [11]$$

Note that Eq. 11 does not contain any calibration factors or soil constants. Hence, the accuracy of $r_{d,field}$ is dependent on the accuracy of the total density measurement in the compaction mold, the accuracy of the water content determination, and the accuracy in measuring the apparent dielectric constant in the field and in the compaction mold. With the use of the same probe head and procedures for data acquisition and reduction, there is potential for accurate measurement of these parameters.

Determination of Soil Dependent Parameters *a* and *b*

Equation 2 determines water content in the Purdue TDR method. This equation requires values of *a* and *b*. The easiest way to determine values of *a* and *b* for a given soil is to run a series of tests in the compaction mold with different water contents. Measure the total density and apparent dielectric constant and the water contents for each test by oven drying. Then plot $\sqrt{K_a}\,\frac{r_w}{r_d}$ versus *w* from the test results as shown in Fig. 9. Fit a straight line to the data. The value of *a* is the zero-intercept of the straight line and *b* is the slope. Experience from conducting hundreds of tests on different soils indicates that the value of *a* is typically near unity and the value of *b* is typically near eight. The amount of compaction energy used in these tests, while important for obtaining the compaction curve, does not appear important for determining values of *a* and *b* for a given soil.

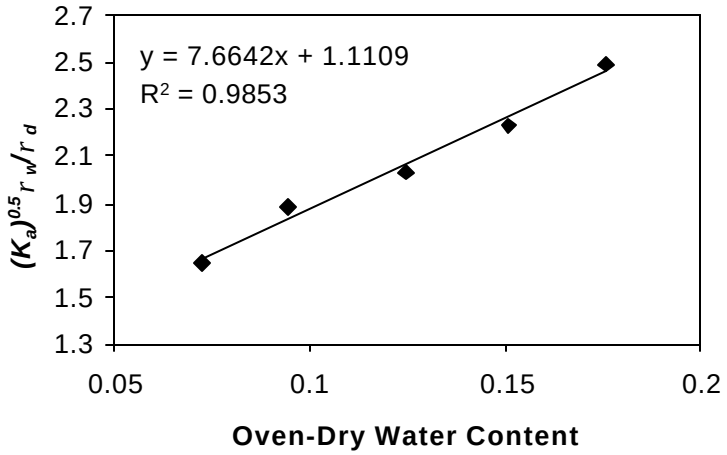

Fig. 9. *Plot for determining values of a and b.*

TYPICAL RESULTS

Water Content

Tests on a variety of soils with the Purdue TDR Method and a nuclear moisture-density meter, as reported by Lin *et al*. (1999) in Fig. 10 show that the Purdue TDR Method appears to be more accurate based on oven-dry water contents. The Purdue TDR Method measures average moisture over the entire length of the soil "cable" which is typically the entire lift thickness. See Lin *et al*. (2000) for additional discussion on water content determination.

Field Density

A number of field density tests have been performed around the state of Indiana where side by side comparisons were made with nuclear density measurements and some also with the sand cone method (ASTM D1556). The results are shown in Fig. 11 where the TDR-measured density is plotted on the abscissa and the nuclear and sand cone densities are plotted on the ordinate.
Some variation of data in Fig. 11 is to be expected because of the spatial variation in density that is likely to occur in the field. The comparison of methods is further complicated by the fact that none of the methods currently available directly measure the field density. Lin *et al*. (1999) report on TDR tests performed in simulated field tests where soil was compacted to controlled density in a large mold. Agreement between the actual and TDR-measured densities was very good.

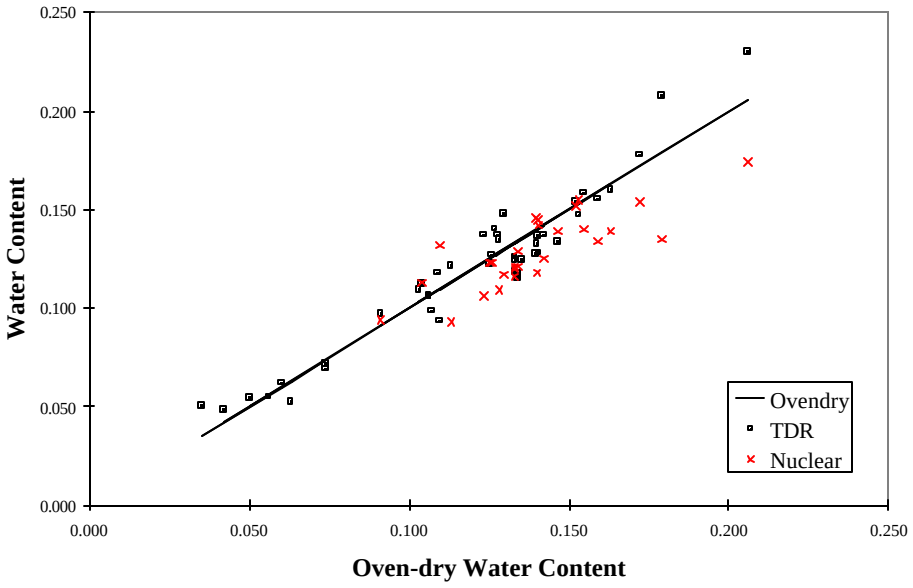

Fig. 10. *Field water content by Purdue TDR and Nuclear Methods (after Lin* et al*., 1999)*

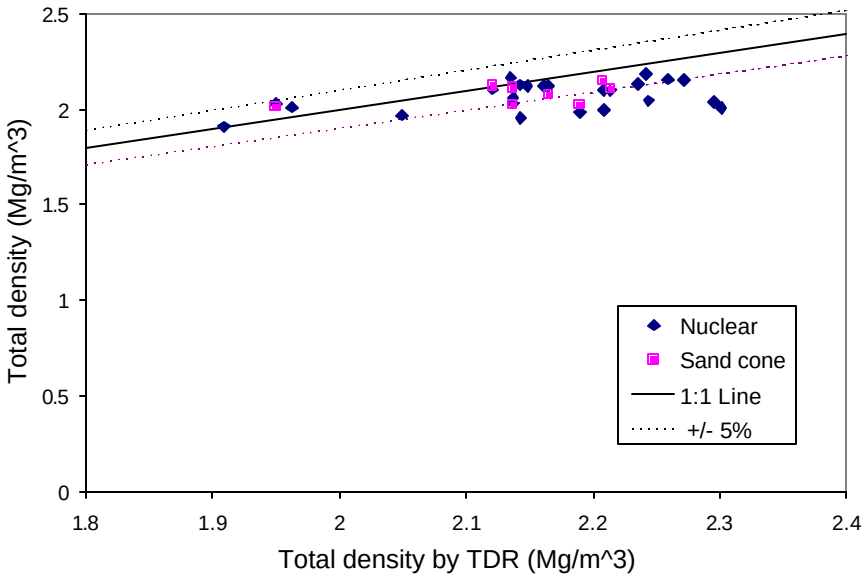

Fig. 11. *Comparison of field densities by Nuclear and Sand Cone with TDR-measured densities (After Lin* et al*., 1999)*

WORK IN PROGRESS

Particle Size Limitations

Coarse-textured soils, particularly those containing gravel or rock, occur at many sites. Work is being performed by Quanghee Yi to study the effects of testing large particle-sized materials on the Purdue TDR Method. Based on preliminary tests and the work of Siddiqui and Drnevich, 1995, the authors are recommending that this method can be used for soils where less than 30 percent of the sample by weight has particle sizes exceeding the 4.75-mm (No. 4) sieve. The basis for this recommendation is given in a companion paper (Yi, *et al.,* 2001).

Standardization

A draft ASTM Standard was created and the process of getting a Standard for this method approved is in the early stages. In ASTM, this work is under the jurisdiction of Committee D18, Subcommittee D18.08. Also, a "Beta Testing Program" is just getting started that will involve twelve agencies/firms/universities from around the country. The purpose of the program is to improve the equipment and procedures and to obtain data for use in precision and bias determination. Standardization and results from a wide spectrum of users will identify shortcomings and establish levels of confidence in the method.

SUMMARY AND CONCLUSIONS

The Purdue TDR Method determines the water content and density of soil by measuring the apparent dielectric constant on two soil "cables," one in situ and the other in a compaction mold. The process is based on the "Siddiqui-Drnevich" equation (Eq. 2) that allows for calculating water content of soil in terms of apparent dielectric constant, soil density, and two soil-dependent parameters, *a* and *b*. Several compaction tests at significantly different water contents with water contents determined by oven drying determine values of *a* and *b*. The value of *a* is typically near unity and the value of *b* is approximately eight.

This method generally gives quite accurate water content values compared to oven dry values. Soil density determination is relatively calibration free because it depends on the ratio of two apparent dielectric constant measurements, one on the soil in situ and the other of the same soil in a compaction mold. The same equipment is used to make both measurements.

Apparent dielectric constants are somewhat dependent on soil temperature. For determining water contents, it appears that corrections for temperature are not necessary for tests where soil temperatures are between 15^{o} C and 25^{o} C. Density determinations are much less affected by temperature if the soil temperature is approximately the same for both the in situ and compaction mold tests because density determination is based on a ratio of the two apparent dielectric constants.

The Purdue TDR Method applies for a wide variety of soils. It may be used for large particle sizes, consistent with particle size specifications of ASTM D-698 where the maximum particle size passes the 19 mm (3/4-in.) sieve.

The Purdue TDR Method is a totally new and different technology for determining both water content and density of soil. With ongoing improvements, widespread evaluation, and standardization, it has the potential to become a useful and reliable tool for the geotechnical community.

ACKNOWLEDGEMENTS

The authors gratefully acknowledge the Indiana Department of Transportation and Federal Highway Administration for the financial support through projects **Indiana HPR-2094, C-36-5S, and Indiana SPR-2201** and assistance with the field experiments. Development of the procedures and theories supporting them has truly been a team effort and the author acknowledges the efforts of all who contributed, especially: Dr. Shafiqul Siddiqui, Dr. Richard Deschamps, Dr. Wei Feng, Dr. Chih Ping Lin, Dr. Robert Nowack, Dr. Jody Tishmack, Mr. Jie Zhang, Mr. Xiong Yu, and Mr. Charlie Crowe (machinist). The authors also wish to acknowledge the enthusiastic support and creative ideas of the Study Advisory Committee for these projects. The members are: Mr. Peter Capon (Rieth Riley Construction), Mr. Donald Johnson (FHWA), Mr. Thomas Kuhn (Kuhn Construction), Dr. Sam Mansukhani (FHWA), Dr. Tommy Nantung (INDoT), Mr. Wes Shaw (INDoT), and Mr. Nayyar Zia (INDoT).

REFERENCES

ASTM, D698, 1998, "Standard Test Method for Laboratory Compaction Characteristics of Soil Using Standard Effort (12,400 ft-lbf/ft^3 (600 kN-m/m^3))," *Annual Book of ASTM Standards*, **4**, No.8, 77-84.

ASTM, D1556, 1998, "Standard Test Method for Density and Unit Weight of Soil in Place by the Sand-Cone Method," *Annual Book of ASTM Standards*, **4**, No. 8, 120-125.

Drnevich, V.P., Lovell, J., Tishmack, J., Yu, X., and Zhang, J., "Temperature Effects on Dielectric Constant Determined by Time Domain Reflectometry," *TDR 2001: Innovative Applications of TDR Technology*, Infrastructure Technology Institute, Northwestern University, Evanston, IL, September, 2001.

Feng, W., Lin, C.P., Drnevich, V.P., and Deschamps, R.J., "Automation and Standardization of Measuring Moisture Content and Density Using Time Domain Reflectometry," Report No.: FHWA/IN/JTRP-98/4, Joint Transportation Research Program, Indiana Department of Transportation - Purdue University, September, 1998. 122 p.

Feng, W., Lin, C.P., Deschamps, R.J., and Drnevich, V.P., 1999, "Theoretical Model of a Multi-Section TDR Measurement System," *Water Resource Research*, **35**, No. 8, Aug., 2321-2331.

Lin, C.P., Drnevich, V.P., Feng, W., and Deschamps, R.J., "Time Domain Reflectometry For Compaction Quality Control," Presented at and publication in *Proc. GeoDenver2000, Use of geophysical methods in construction*, Soheil Nazarian and John Diehl, Editors, Geotechnical Special Publication No. 108, ASCE GeoInstitute Conference, Denver Colorado, August 5-8, 2000, 15-34.

Lin, C-P., Siddiqui, S. I., Feng, W., Drnevich, V. P., and Deschamps, R. J., 2000, "Quality Control of Earth Fills Using Electromagnetic Waves," *Constructing and Controlling Compaction of Earth Fills, ASTM STP 1384*, D. W. Shanklin, K. R. Rademacher, and J. R. Talbot, Eds., American Society for Testing and Materials, West Conshohocken, PA, 290-310.

Siddiqui, S.I., and Drnevich, V.P., 1995, "A New Method of Measuring Density and Moisture Content of Soil Using the Technique of Time Domain Reflectometry," Report No.: FHWA/IN/JTRP-95/9, Joint Transportation Research Program, Indiana Department of Transportation - Purdue University, February, 271 p.

Siddiqui, S.I., Drnevich, V.P., and Deschamps, R.J., "Time Domain Reflectometry Development for Use in Geotechnical Engineering," *Geotechnical Testing Journal*, GTJODJ, **23**, No. 1, March, 2000, 9-20.

Topp, G. C., Davis, J. L., and Annan, A. P., 1980, "Electromagnetic Determination of Soil Water Content and Electrical Conductivity Measurement Using Time Domain Reflectometry," *Water Resources Research*, **16**, 574-582.

Weast, R.C., 1986, "CRC Handbook of Chemistry and Physics," 67th ed., CRC Press.

Yi, Q., Drnevich, V.P., and Lovell, J., "Limitations of the Purdue TDR Method for Soils with Large Particles," *TDR 2001: Innovative Applications of TDR Technology*, Infrastructure Technology Institute, Northwestern University, Evanston, IL, September, 2001.

EFFECTS OF TESTING LARGE PARTICLE-SIZED MATERIALS

Quanghee Yi[1], Vincent P. Drnevich[2], and Janet Lovell[3]

[1]School of Civil Engineering, Purdue University, West Lafayette, IN 47907-1284, yiq@ecn.purdue.edu
[2]School of Civil Engineering, Purdue University, West Lafayette, IN 47907-1284, drnevich@purdue.edu
[3]School of Civil Engineering, Purdue University, West Lafayette, IN 47907-1284, lovell@purdue.edu

ABSTRACT

This paper reports the effects of large particle sizes on the insertion of a TDR probe and the resulting measurements of apparent dielectric constant. The maximum particle size in these tests was 19 mm (3/4-in.). These soils were compacted in a mold using Standard Compaction Energy and tested according to the procedures proposed for the Purdue TDR Method. The tests indicate that the TDR Method gives reasonably accurate information for maximum dry density and optimum water content, but that there is a systematic small error in water contents for water contents in the range of 50 - 80 percent of the optimum water content. At water contents above the optimum water content, the accuracy was quite good for all tests. A special series of tests on dry soil specimens of concrete sand were performed to evaluate the effects of rod insertion. They indicated that results are relatively independent of whether the rod was inserted into the soil or whether the soil was placed about the rod. Preliminary conclusions are that the Purdue TDR Method could be used to obtain reasonably accurate results for soil with large particles where the percentage of large particles is less than half the total sample and where the largest particles are less than 19 mm (3/4-in.).

INTRODUCTION

The apparent dielectric constant of soils as measured by time domain reflectometry (TDR) is affected by many parameters including: water content, temperature, soil particle size and particle size distribution, and by measurement probe configuration and installation. This paper is predominantly about the effects of particle size on the insertion of a TDR probe and the resulting measured apparent dielectric constant, especially for soils that contain large particle sizes, a very common occurrence in both manmade fills and naturally occurring soils. This work is part of an ongoing study that is developing and evaluating the Purdue TDR Method (Drnevich *et al.*, 2001) for determination of soil water content and density for use in engineering practice.

Nearly all existing laboratory and field tests for measuring water content and density of soils have limitations on maximum particle size. In many tests such as the *Standard Test Method for Laboratory Compaction Characteristics of Soil Using Standard Effort (12,400 ft-lbf/ft^3 (600 kN-m/m^3))*, ASTM D698, (1998), for *Method B* where a 101.6 mm (4.0-in.) diameter mold is used, the soil to be tested must pass the 9.5-mm (3/8-in.) sieve and no more than 20 percent by weight of the original soil can be retained on the 9.5 mm (3/8-in.) sieve. In this case, the soil retained on the 9.5-mm (3.8-in.) sieve is considered *oversize particles* and is not used in the test. The *Standard Practice for Correction of Unit Weight and Water Content for Soils Containing Oversize Particles,* ASTM D4718 (1998) provides procedures for correcting water content and density test results to account for the untested oversized particles. Corrections of results from both the lab and the field tests must be made when oversize particles are encountered. The procedures in ASTM D4718 require measurement of the mass and the water content of both the finer and oversize portions of the sample and they are generally valid when the percentage of oversized particles is typically less than 40 percent. It is expected that there would be similar limitations to the TDR method of measuring water content and density and that procedures of ASTM D4718 (1998) also would apply to results of TDR tests. This paper focuses on how the TDR results are affected when large particle sizes are present.

The Purdue TDR Method uses two types of probes, one that is used in situ and one that makes use of a cylindrical mold for the soil. The one for in situ is a multiple rod probe that is formed by driving four steel spikes through a template into the soil surface (See Fig. 1), removing the template, and then placing a Multiple Rod Probe Head on these steel spikes. The test in the cylindrical mold uses a metal mold, similar to a compaction mold for the "shield" and a central rod that is driven into the soil through a guide placed on top of the mold (See Fig. 2). By use of an adapter ring placed on the mold, the same Multiple Rod Probe Head is used to complete the probe arrangement. The testing is done mostly for construction control and the test is frequently performed at multiple locations at a given site.

Fig. 1. *Steel spikes forming multiple rod probe*

Fig. 2. *Driving central rod through a guide placed on the mold*

Steel rods that are separate from the probe head allows for inserting the rods into nearly any soil irrespective of how dense it is or for particle sizes into the gravel range. The rods are reusable, but are sufficiently inexpensive that they could be considered disposable. While this is a very robust system, the question remains on how the rod insertion affects the soil and how representative the measured apparent dielectric constant is of the soil prior to the insertion.

Work done by Siddiqui and Drnevich (1995) and Siddiqui *et al.* (2000) showed that the Purdue TDR Method was generally applicable for soils with sand sizes and below. They examined various models for densification (or loosening) of the soil by rod insertion and for void creation adjacent to the rods by the rod insertion process. They developed a *Spatial Weighting Function* (Eq. 1) that was a function of *b/a*, the ratio of the radius from the center to the shield (mold or outer rods) to the radius of the inner

conductor. The larger the value of this ratio, larger is the influence of the soil immediately adjacent to the inner conductor on the measured apparent dielectric constant.

$$F(r) = \frac{\ln(r/a)}{\ln(b/a)} \qquad [1]$$

where

r = the radius to the point of interest from the axis of the inner conductor

a = the radius of the inner conductor

b = the distance from the axis of the inner conductor to the outer conductor

If the *Central Area* is defined as the area inside the radius r, i.e. $\pi r^2/4$, and the *Total Area* as $\pi b^2/4$ then the *Central Area/Total Area* is measure of the fraction of the soil adjacent to the inner conductor that contributes to the measured dielectric constant. Figure 3 is a plot of the *Spatial Weighting Function* versus *Central Area/Total Area* for various values of *b/a*. From Fig. 3, when *b/a* = 10, the ten percent of soil area adjacent to the inner conductor contributes to half of the apparent dielectric constant. Based on Fig. 3, a small value of *b/a* ratio is desired to obtain a good representation of the material between the inner and outer conductors. However, small values of *b/a* are obtained by making the inner conductor quite large relative to the radius to the outer conductor. This has the effect of disturbing a larger volume of soil, especially the soil adjacent to the inner conductor that is critical to the measurement of the apparent dielectric constant. The disturbance is in the form of densification of soils that are relatively loose and loosening of soils (due to dilation) that are relatively dense prior to insertion of the rod. Siddiqui *et al.* (2000) also developed models for soil densification adjacent to the inner conductor caused by rod insertion and its effect on the apparent dielectric constant. They showed that rod insertion also depends on *b/a* and causes an increase of the apparent dielectric constant over that before rod insertion. Finally, rod insertion generally will cause some air gaps to form adjacent to the inner conductor due to lateral movement or drift of the rod as it is being driven.

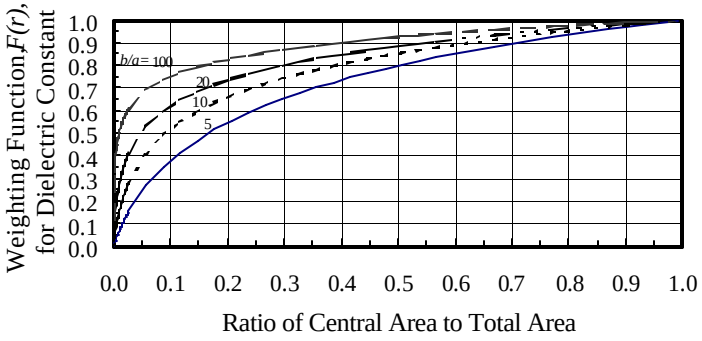

Fig. 3. *Characteristics of the spatial weighting function for a coaxial transmission line (After Siddiqui* et al*., 2000)*

These air gaps cause the measured values of apparent dielectric constant to be lower than those when no air gaps exist. Based on their models and on tests of clays, silts, and sands, Siddiqui *et al.* (2000) suggested that a "*b/a* ratio of 15 is a good value to use." This is consistent with the findings of Annan (1977), Topp *et al.* (1980), and Zegelin *et al.* (1989).

Knight (1992) suggested that for a multiple rod probe, the ratio of the radius of the inner rod to the center-to-center distance between the inner rod and outer rods should be greater than 0.1 [this corresponds to a *b/a* ratio less than 10] and that the radius should be as large as possible compared to the

average pore size of the material. In the Purdue TDR Method, we are using a value of *b/a* of 13.8 for the multiple-rod probe and a value of *b/a* of 12.8 for the mold probe. Both of these numbers result from using readily available standard-sized materials and are approximately consistent with the recommendations of Knight (1992) and Siddiqui *et al.* (2000).

Engineers frequently have to deal with soils where particles range in size from boulders to clays with most sizes in between. Table 1 adapted from ASTM D2487-00 Standard Classification of Soils for Engineering Purposes (Unified Soil Classification System) and Lambe and Whitman (1979) gives the names used by geotechnical engineers for different sizes of particles and their size ranges.

For fine-grained soils containing appreciable amounts of clay, the specific surface (surface area per mass typically in units of m^2/g, (Lambe and Whitman, 1979) of the clay particles is quite large and hence electrical effects have to be considered along with gravitational effects. In clay particles, net negative charges of the particles give rise to adsorbed water and cations on the clay particle surfaces that is described by the Gouy Double Layer theory. A number of researchers (see Or and Wraith, 1999), Ponizovsky, *et al.*, 1999) have documented that apparent dielectric constant of materials within the adsorbed water layer (typically with values 20 to 40) is much different from that of free water in the pore space (typically around 80). These effects on the apparent dielectric constant as measured by the Purdue TDR Method is currently under study and is beyond the scope of this paper.

Name	U.S. Standard Sieve Sizes	
	Upper Limit Size, mm (in. or sieve No.)	Lower Limit Size, mm (in. or sieve No.)
boulders		300 mm (12 in.)
cobbles	300 mm (12 in.)	75 mm (3 in.)
gravels	75 mm (3 in.)	4.75 mm (No. 4)
sands	4.75 mm (No. 4)	0.075 mm (No. 200)
silts*	0.075 mm (No. 200)	0.002 mm (8.0×10^{-5} in.)
clays**	0.002 mm (8.0×10^{-5} in.)	

* By ASTM D2487, passing No. 200 Sieve (4.75 mm) but possessing no plastic behavior.
** By ASTM D2487, passing No. 200 Sieve (4.75 mm) but possessing plastic behavior.

Table 1. *Definitions for particle sizes*

For coarse-textured soils, the shape of the particles also can have an effect on measured dielectric properties. Particle shapes typically are described as angular, subangular, subrounded, rounded, and well-rounded (Lambe and Whitman, 1979). Coarse-textured soils, particularly those containing gravel or rock, occur at many sites. The roundness of large particles would allow for probe rods to slide off these particles and move them aside while for angular particles, there would be an increased tendency of the pointed probe rods to drag the particle along, creating a void along the sides of the rod and disrupting the soil near the rod.

MATERIALS TESTED

Eight different materials were tested. They are described in Table 2 and the particle size distributions are shown in Fig. 4. (Code key: CT= Crosby Till, MG = Medium Gravel, SG = Small Gravel, CS = Concrete Sand.) The Crosby Till is a local silty-clay soil with a Unified Soil Classification of CL. The

rock was a sub-rounded glacial outwash gravel material. Fractions of it by size were mixed with the Crosby Till and the concrete sand to obtain the remaining six of the eight soils for testing.

Soil Code	Medium Gravel 9.5 mm (3/8-in.) to19 mm (3/4-in.) (%)	Small Gravel 4.75 mm (No. 4) to 9.5 mm (3/8-in.) (%)	Sand (%)	Silt (%)	Clay (%)
Crosby Till	0	0	12	59	29
MG-SG-CT50%	20	30	6	30	14
SG-CT50%	0	50	6	30	14
MG-SG-CT70%	20	10	9	41	20
SG-CT70%	0	30	9	41	20
Concrete Sand	0	0	100	0	0

Table 2. *Compositions in Percent by Weight*

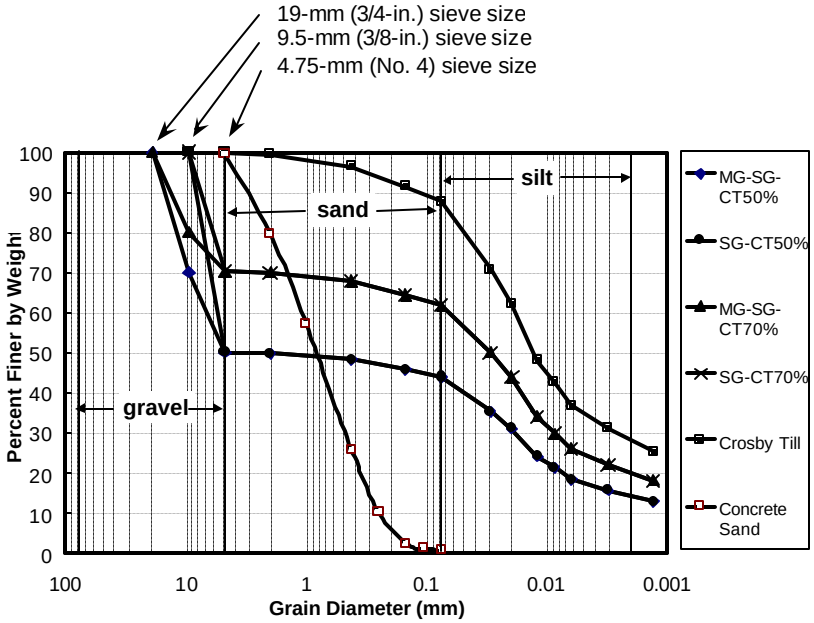

Fig. 4. *Particle size distribution curves for the soils tested*

METHOD OF TESTING

For these tests, a 233.8 mm (9.168-in.) height mold (twice the height of the mold specified in ASTM D698) was used. The longer length allows for increased resolution of the signal travel time of the electromagnetic wave and allows for testing a volume of soil roughly equal to the volume tested by the in situ probe (Fig. 1). The mold diameter was 101.2 mm (4.0-in), which is the size that has been used for nearly all Purdue TDR Method tests to date. The procedures in ASTM D698 limit the use of the 101.2 mm (4.0-in) diameter mold to particles passing the 9.5-mm (3/8-in.) sieve (*MethodB*) and require

the use of a mold with a 152.4 mm (6.0-in.) diameter for the larger-sized particles. Use of a larger diameter mold for TDR tests was thought to be impractical because two sets of molds would have to be carried to locations in the field to conduct tests. Hence, an attempt was made to see if the smaller diameter, but taller mold would provide reasonably accurate results for the field tests where larger sized particles are frequently encountered.

For Crosby Till and the four other specimens containing Crosby Till, five specimens of each of the soils were prepared, one each at a variety of water contents from below optimum to above optimum and allowed to stabilize before compacting into the molds. Compaction was done with a manual rammer according to the procedures in ASTM D698 except that six lifts were used rather than three because the mold height was twice that specified by ASTM D698. This provided the same compaction energy per unit volume as with ASTM D698. Upon completion of the compaction, the mass of the soil-filled mold was determined. This was used along with the mass of the empty mold and the volume of the mold to determine the total density of the soil in the mold. The specimen was prepared for TDR measurement by placing the guide on the mold, driving the central rod into the mold, removing the guide, installing the adapter ring on the mold, and placing the MRP head onto the adapter ring.

For the concrete sand and for the mixtures of gravels with the concrete sand, typically only two specimens were prepared, one at low water content and one at a high water content.

Measurements were made to obtain the TDR curve and from it determine the locations of the first and second reflections as discussed by Drnevich *et al.* (2001). These were used along with the length of the central rod that penetrated the soil specimen to determine the apparent dielectric constant for the specimen.

For oven drying with large particle sizes, the entire mold filled with soil was put into the oven to meet the *ASTM D2216-98 Standard Test Method for Laboratory Determination of Water (Moisture) Content of Soil and Rock by Mass* (ASTM D2216, 1998) criteria of minimum mass of moist test specimen for water content, 2.5 kg (5.5 lb).

TEST RESULTS

For each of the materials tested, procedures described by Drnevich *et al.* (2001) were used to determine the soil dependent parameters *a* and *b* for use in the equation proposed by Siddiqui and Drnevich (1995) to calculate water content.

$$w = \frac{1}{b}\left[\sqrt{K_a}\,\frac{r_w}{r_d} - a\right] \qquad [2]$$

where K_a is the apparent dielectric constant measured by the TDR method, $?_w$ is the density of water, and $?_d$ is the bulk dry density of the compacted soil or soil mixture. To obtain *a* and *b* for a given soil or soil mixture, values of $\sqrt{K_a}\,r_w / r_d$ are plotted versus oven-dry water contents for the tests at different water contents and fitted with a straight line. The zero-water content intercept of the line is the value of *a* and the slope of the line is the value of *b*. Values of *a* and *b* are given for each soil in Table 3 along

with the R^2 values for the fit. The values of *a* and *b* may be used in Eq. 2 to calculate values of water content by the TDR method.

Soil Code	*a*	*b*	R^2
Crosby Till	1.34	6.93	0.996
MG-SG-CT50%	1.07	8.28	0.972
SG-CT50%	1.11	7.66	0.985
MG-SG-CT70%	1.03	8.41	0.999
SG-CT70%	1.14	7.29	0.958
Concrete Sand	1.05	8.19	0.999

Table 3. *Values of a, b, and R^2 for Crosby Till and Gravel-Crosby Till mixtures*

Figure 5 shows a comparison of water contents determined by TDR compared to those for oven drying for all of the materials tested in Table 3. The comparison is quite good except for possibly for water contents between 10 percent and 13 percent in Fig. 5. The deviation from straight-line behavior appears to be systematic rather than random. For example, in the procedure to determine values of *a* and *b*, a plot is made of $\sqrt{K_a}\, r_w / r_d$ versus water content as shown in Fig. 6. Data points at very low water contents always appear on the line or below it. As water contents increase, the data points then move to above the line and then seem to settle on the line as water contents continue to increase. Data in Fig. 6 are fairly consistent with many observations where large particle sizes are tested. There appeared to be a relationship between this behavior and the optimum water content of the soil being tested. To check this out, a normalized plot of data was generated as shown in Fig. 7, which includes all of the data

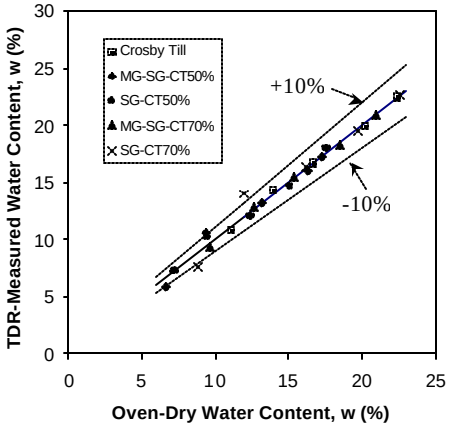

Fig. 5. *Comparison of TDR-Measured water contents with oven-dry-measured water contents*

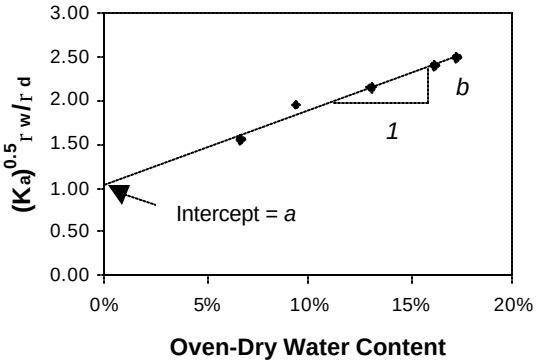

Fig. 6. *Plot of $\sqrt{K_a}\, r_w / r_d$ versus oven-Dry water contents to obtain a and b*

for the Crosby Till – gravel mixtures. The abscissa values are normalized by the optimum water content and the ordinate values are the same as in Fig. 6, but normalized by Y_{norm} that is defined as the value of $a + b\, w_{opt}$ for each of the soil mixtures tested. The value of Y_{norm} is the calculated ordinate value at the optimum water content for a given soil. Examination of Fig. 7 reveals that the data points consistently fall below the line at 50 to 60 percent of the optimum water content and then consistently fall above the line at 70 to 80 percent of the optimum water content. At and above the optimum water content, the data follow the straight line within experimental error. It is hypothesized that at water contents below the

optimum, the soil is quite dense and there is not much water available to lubricate the soil and rock particles as the central rod is driven into the specimen. The driving of the rod tends to punch into and loosen the soil in the vicinity of the rod. At very low water content, the specimen is not as dense and hence there is a tendency for the rod to densify the soil as it is driven into the specimen. Continued study is warranted on this topic.

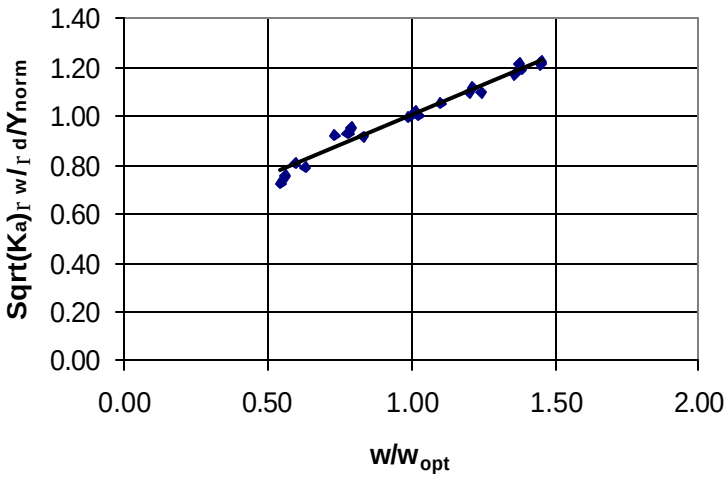

Fig. 7. *Plot of normalized apparent dielectric constant versus water content normalized by the optimum water content to show behavior of soil relative to standard compaction conditions.*

For Crosby Till and mixtures of gravels with Crosby Till, the compaction curves are plotted in Fig. 8. Values of maximum dry density and optimum water content for each of the curves are given in Table 4.

Note the presence of 70 percent Crosby Till almost totally masks the effects of the gravel on both the maximum dry density and optimum water content. However, decreasing the percentage of Crosby Till to 50 percent markedly increases maximum dry density and decreases the optimum water content. The gravel size, whether a medium gravel - small gravel mixture or just all small gravel, appears to have only a minor effect on both the maximum dry density and the optimum water content.

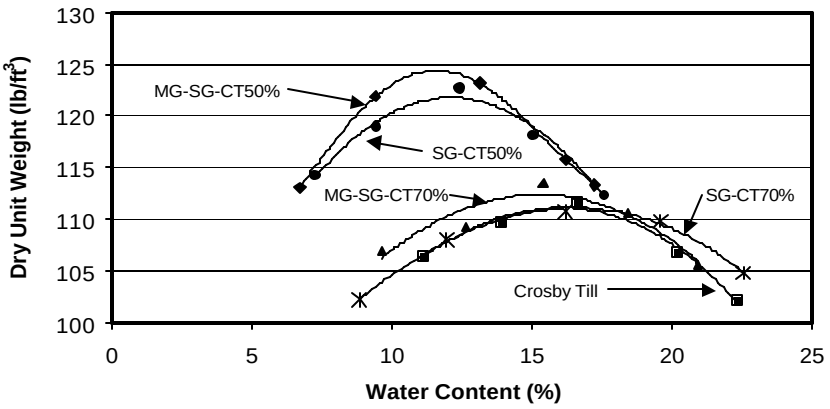

Fig. 8. *Compaction curves for Crosby Till and mixtures of Crosby Till with gravels for specimens compacted into the special compaction mold associated with the Purdue TDR Method and for the application of standard compaction energy per unit volume.*

Soil Code	$w_{opt,\ oven\ dry}$ (%)	$w_{opt,TDR}$ (%)	$\gamma_{dmax,\ oven\ dry}$ (Mg/m^3)	$\gamma_{dmax,oven\ dry}$ (lbf/ft^3)	$\gamma_{dmax,\ TDR}$ (Mg/m^3)	$\gamma_{dmax,TDR}$ (lbf/ft^3)
Crosby Till	15.8	15.5	1.781	111.1	1.772	110.6
MG-SG-CT50%	11.9	11.3	1.983	123.7	1.952	121.8
SG-CT50%	12.1	12.5	1.951	121.7	1.939	121.0
MG-SG-CT70%	15.2	15.1	1.812	113.0	1.805	112.6
SG-CT70%	16.3	16.0	1.780	111.1	1.746	108.9

Table 4. *Optimum water contents and maximum dry densities (Unit Weights) for Crosby Till and mixtures of gravels with Crosby Till*

The optimum water contents and maximum dry densities (unit weights) in Table 4 were obtained by fitting the compaction curves with parabolas and then solving for the values at the peak. In all tests, the total density of the specimen in the mold was known. Oven-dry water contents were used along with dry densities calculated with oven-dry water contents to obtain the data for the oven-dry items reported in Table 4. Similarly, TDR-determined apparent dielectric constants along with soil-specific values of *a* and *b* were used to calculate the TDR-determined water contents and these were used along with the total density to calculate the TDR-determined dry densities.

The effects of TDR-determined water contents versus water contents determined by oven drying are shown in Fig. 9 for Crosby Till and for a mixture of 50 percent Crosby Till with 30 percent small gravel, and 20 percent medium gravel. The latter is the worst case for large particle size tests in this program.

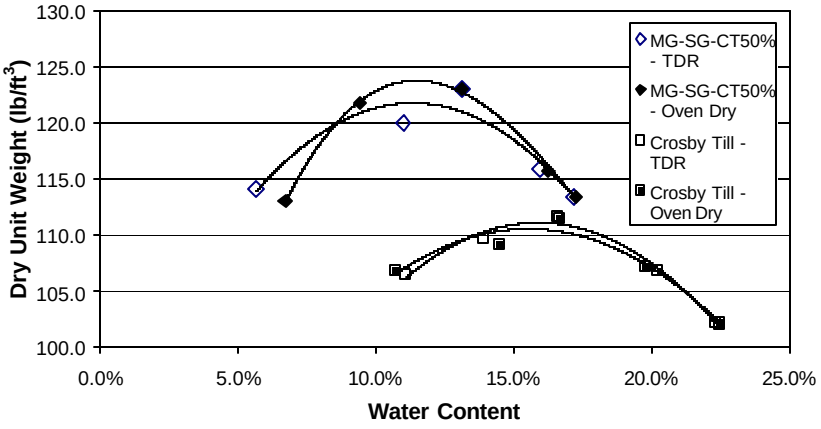

Fig. 9. *Comparison of compaction curves obtained with water contents determined by oven-drying to those obtained with water contents determined by TDR measurements*

The data for Crosby Till alone is quite consistent between the two methods. However, the data for the

gravel mixture with Crosby Till shows some differences. The TDR water contents are too small at the lowest water contents and hence the dry densities are too large. As water contents get closer to the optimum water contents, the TDR water contents are too large and hence the dry densities are too small. Combined, these have the effect of underestimating both the optimum water content and the maximum dry density. For values of water content above the optimum water content, the values are reasonably consistent between the two methods.

Evaluation of *a* from Test of Dry Soils

For dry soils, $w = 0$ and Eq. 2 for this situation may be rearranged to provide values of the soil parameter a as shown in Eq. 3.

$$a = \sqrt{K_a}\,\frac{\rho_w}{\rho_d} \qquad [3]$$

Hence, making a measurement of apparent dielectric constant, K_a, on a dry soil where the bulk dry density, ρ_d, is known allows for calculating the value of a directly. To check the accuracy of this, some special tests were performed on concrete sand in the dry state. Two tests were performed on the dry concrete sand in a very loose state. The first test was performed in the usual way by placing the guide on top of the mold containing the sand and driving the central rod into the specimen. A determination of the apparent dielectric constant, K_a, was made and the value of a was calculated by Eq. 3. The second test was performed by placing the central rod into an empty mold, holding it aligned with a temporary template and then placing the soil into the annular region between the central rod and the mold wall. Again, a determination of K_a was made and the value of a was calculated by Eq. 3. The results of these two tests are compared in the first two rows of Table 5 and it can be seen that while the densities of the loose materials were slightly different, the values of a are the same.

State	**Center Rod**	γ_d (lbf/ft^3)	***a***
Loose	Driven	103.8	1.07
Loose	Installed before soil placement	102.0	1.07
Very Dense	Driven	118.1	0.99
Very Dense	Installed before soil placement	118.1	0.98

Table 5. *Results of Tests on Dry Concrete Sand to Determine Values of a*

Two additional tests were performed in a similar fashion on this concrete sand except that the sand was in a very dense state that was achieved by placing the mold on a vibrating table. The resulting dry densities for these two tests are the same and the values of a are about the same for both tests as shown in the third and fourth rows of Table 5. However, the values of a are about eight percent smaller than the values for the soil in the loosest state.

The values of *a* in Table 5 may be compared with the value of 1.05 from Table 3 that was obtained from tests at different water contents with standard compaction energy per unit volume where the density varied depending on the water content.

Some preliminary conclusions may be drawn from these tests. One is that for very loose granular materials, some densification takes place by insertion of the central rod. A second is that inserting the rod in a very dense, dry granular material does not appreciably affect its density. The third is that the value of *a* is relatively independent of whether the rod is driven into the soil or whether the soil is placed into the mold where the rod is already in place. Finally, it appears that Eq. 3 does not fully account for density effects on the values of *a*. One possibility of accounting for this would be to look at a slightly modified form of Eq. 3 such as:

$$a^* = \sqrt{K_a}\left(\frac{r_w}{r_d}\right)^n \qquad [4]$$

For the data on dry concrete sand, the value of *n* would have to be approximately 0.4 to accommodate the different densities. Study on this issue continues.

SUMMARY, CONCLUSIONS, AND RECOMMENDATIONS

The TDR testing of soils will frequently encounter soils containing particle sizes that are large relative to the dimensions of the probe rods. In an effort to assess the effects of these, tests were performed on a naturally occurring soil to which gravel-sized particles were mixed. The maximum particle size in these tests was 19 mm (3/4-in.). These soils were compacted in a mold with a diameter of 101.6-mm (4.0-in.) and a height of 233.8-mm (9.168-in.) using Standard Compaction Energy. They were tested according to the procedures proposed for the Purdue TDR Method that includes effects of density and soil type in determining water contents through the use of the Siddiqui-Drnevich Equation that involves two soil-dependent constants, *a* and *b*. For the soil tested, the dry density and optimum water contents are significantly affected by large particle sizes when the large particle sizes constitute more than about 30 percent of the total sample. The tests indicate that the TDR Method gives reasonably accurate information on the maximum dry density and optimum water content, but that there is a systematic small error in water content values for water contents in the range of 50 - 80 percent of the optimum water content. At water contents above the optimum water content, the accuracy was quite good for all tests. A special series of tests on dry soil specimens of concrete sand were performed to evaluate the effects of rod insertion on the *a* parameter in the Siddiqui-Drnevich Equation used in the Purdue Method. Values of *a* were relatively independent of whether the rod was inserted into the soil or whether the soil was placed about the rod. However, there was a small, but consistent difference in the determined value of *a* depending on the density of the specimen and this indicates that the accommodation of density in the Siddiqui-Drnevich equation may need to be refined. Preliminary conclusions from this work indicate that the Purdue TDR Method could be used to obtain reasonably accurate results for soil with large particles where less than 30 percent of the total sample is retained on the 4.75 mm (No. 4) sieve. Additional work is underway to establish whether this preliminary conclusion is applicable to a wide variety of soils and over a wide variety of densities.

ACKNOWLEDGEMENTS

The authors gratefully acknowledge the Indiana Department of Transportation and Federal Highway Administration for the financial support through projects **Indiana HPR-2094, C-36-5S, and Indiana SPR-2201** and assistance with the field experiments. Development of the procedures and theories supporting them has truly been a team effort and the author acknowledges the efforts of all who contributed, especially: Dr. Shafiqul Siddiqui, Dr. Richard Deschamps, Dr. Wei Feng, Dr. Chih Ping Lin, Dr. Robert Nowack, Dr. Jody Tishmack, Mr. Xiong Yu, and Mr. Charlie Crowe (machinist). The authors also wish to acknowledge the enthusiastic support and creative ideas of the Study Advisory Committee for these projects. The members are: Mr. Peter Capon (Rieth Riley Construction), Mr. Donald Johnson (FHWA), Mr. Thomas Kuhn (Kuhn Construction), Dr. Sam Mansukhani (FHWA), Dr. Tommy Nantung (INDoT), Mr. Wes Shaw (INDoT), and Mr. Nayyar Zia (INDoT).

REFERENCES

Annan, A.P., 1977, "Time Domain Reflectometry - Air-Gap Problem in a Coaxial Line," Report of Activities, Part B, Paper 77-1B, Geol. Survey Canada, Ottawa, 55-58.

ASTM, D698, 1998, "Standard Test Method for Laboratory Compaction Characteristics of Soil Using Standard Effort (12,400 ft-lbf/ft^3 (600 kN-m/m^3))," *Annual Book of ASTM Standards,* **4**, No. 8, 77-84.

ASTM D2216, 1998, "Standard Test Method for Laboratory Determination of Water (Moisture) Content of Soil and Rock by Mass," *Annual Book of ASTM Standards,* **4**, No. 8, 188-191.

ASTM, D2487, 1998, "Standard Classification of Soils for Engineering Purposes (Unified Soil Classification System)," *Annual Book of ASTM Standards,* **4**, No. 8, 217-227.

ASTM, D4718, 1998, "Standard Practice for Correction of Unit Weight and Water Content for Soils Containing Oversize Particles" *Annual Book of ASTM Standards,* **4**, No. 8, 822-824.

Drnevich, V.P., Siddiqui, S.I., Lovell, J., Yi, Q., "Water Content And Density of Soil In Situ by The Purdue TDR Method," *TDR 2001: Innovative Applications of TDR Technology,* Infrastructure Technology Institute, Northwestern University, Evanston, IL, September, 2001.

Drnevich, V.P., Lovell, J., Tishmack, J., Yu, X., and Zhang, J., "Temperature Effects on Dielectric Constant Determined by Time Domain Reflectometry," *TDR 2001: Innovative Applications of TDR Technology*, Infrastructure Technology Institute, Northwestern University, Evanston, IL, September, 2001.

Feng, W., Lin, C.P., Drnevich, V.P., and Deschamps, R.J., 1998, "Automation and Standardization of Measuring Moisture Content and Density Using Time Domain Reflectometry," Report No.: FHWA/IN/JTRP-98/4, Joint Transportation Research Program, Indiana Department of Transportation - Purdue University, September, 122 p.

Feng, W., Lin, C.P., Deschamps, R.J., and Drnevich, V.P., 1999, "Theoretical Model of a Multi-Section TDR Measurement System," *Water Resource Research*, **35**, No. 8, Aug., 2321-2331.

Knight, J. H., 1992, "The Sensitivity of Time Domain Reflectometry to Lateral Variations in Soil Water Content," *Water Resources Research*, **28**, 2345-2352.

Lambe and Whitman, 1979, *Soil Mechanics, SI Version,* John Wiley and Sons, New York, 553p.

Lin, C.P., Drnevich, V.P., Feng, W., and Deschamps, R.J., "Time Domain Reflectometry For Compaction Quality Control," Presented at and publication in *Proc. GeoDenver2000, Use of geophysical methods in construction,* Soheil Nazarian and John Diehl, Editors, Geotechnical Special Publication No. 108, ASCE GeoInstitute Conference, Denver Colorado, August 5-8, 2000, 15-34.

Lin, C-P., Siddiqui, S. I., Feng, W., Drnevich, V. P., and Deschamps, R. J., 2000, "Quality Control of Earth Fills Using Electromagnetic Waves," *Constructing and Controlling Compaction of Earth Fills, ASTM STP 1384*, D. W. Shanklin, K. R. Rademacher, and J. R. Talbot, Eds., American Society for Testing and Materials, West Conshohocken, PA, 290-310.

Or, D., and Wraith, J.M., 1999, "Temperature Effects on Soil Bulk Dielectric Permittivity Measured by Time Domain Reflectometry: A Physical Model," *Water Resources Research*, **35**, No. 2, February, 371-383.

Ponizovsky, A.A., Chudinova, S.M., and Pachepsky, Y.A., 1999, "Performance of TDR Calibration Models as Affected by Soil Texture," J. of Hydrology, **218**, 35-43.

Siddiqui, S.I., and Drnevich, V.P., 1995, "A New Method of Measuring Density and Moisture Content of Soil Using the Technique of Time Domain Reflectometry," Report No.: FHWA/IN/JTRP-95/9, Joint Transportation Research Program, Indiana Department of Transportation - Purdue University, February, 271 p.

Siddiqui, S.I., Drnevich, V.P., and Deschamps, R.J., 2000, "Time Domain Reflectometry Development for Use in Geotechnical Engineering," *Geotechnical Testing Journal,* GTJODJ, **23**, No. 1, March, 9-20.

Topp, G.C., Davis, J.L., and Annan, A.P., 1980, "Electromagnetic Determination of Soil Water Content: Measurement in Coaxial Transmission Lines," *Water Resources Research*, **16**, No. 3, June, 574-582.

Zegelin, S.J., White, I., and Jenkins, D.R., 1989, "Improved Field Probes for Soil Water Content and Electrical Conductivity Measurement Using Time Domain Reflectometry," *Water Resources Research*, **25**, No.11, Nov., 2367-2376.

TEMPERATURE EFFECTS ON DIELECTRIC CONSTANT DETERMINED BY TIME DOMAIN REFLECTOMETRY

Vincent P. Drnevich[1], Xiong Yu[2], Janet Lovell[3], and Jody Tishmack[4]

[1]School of Civil Engineering, Purdue University, West Lafayette, IN 47907-1284; drnevich@purdue.edu
[2]School of Civil Engineering, Purdue University, West Lafayette, IN 47907-1284; xyu@purdue.edu
[3]School of Civil Engineering, Purdue University, West Lafayette, IN 47907-1284; lovell@purdue.edu
[4]Physical Facilities, Purdue University, West Lafayette, IN 47907; jktishma@purdue.edu

ABSTRACT

This paper addresses the effects of temperature on the apparent dielectric constant of compacted soils. Data are presented from tests on cohesive and noncohesive soils at various water contents and densities, tested at temperatures ranging from 4°C to 40°C. Tests were performed on the soils placed with Standard Compaction Effort into a cylindrical mold that is used in compaction testing. Apparent dielectric constants were determined by inserting a steel rod along the axis of the specimen and using a Multiple Rod Probe Head, developed by the authors, in conjunction with a Tektronix® 1502B Cable Tester. The entire system was placed in a temperature controlled environmental chamber and measurements were made until readings stabilized, typically less than twenty-four hours. Test results reported here found that the apparent dielectric constant of compacted non-cohesive soils follow a similar, but less pronounced behavior as water, i.e. it decreases with increasing temperature. The opposite behavior was observed for compacted cohesive soils, whose apparent dielectric constants increase with increasing temperature. Recommendations are made to correct measured values of apparent dielectric constant to values at 20°C using simple linear corrections. It is shown that effects of temperature on water content determination are likely to be small and can be neglected for temperatures within 5°C of 20°C.

INTRODUCTION

Temperature affects the dielectric properties of materials in different ways depending on the material. While this has been known for over 50 years (Frohlich,1949), details of temperature effects on soils are still not well understood (Wraith and Or,1999). If the apparent dielectric constant is used as a measure of dielectric properties, the apparent dielectric constant for water decreases with increasing temperature. The apparent dielectric constant for most soil solids is relatively independent of temperature in the range of 4°C to 40°C. It is reasonable to expect that the apparent dielectric constant for mixtures of soil solids

and water also would exhibit a decrease in apparent dielectric constant with temperature, but to a lesser extent than for water alone. This holds true for cohesionless soils, but does not hold true for cohesive soils that have significant amounts of clay-sized particles. For these materials, the apparent dielectric constant increases with temperature. Some theories for this behavior were put forth by Wraith and Or (1999) and discussion of the theoretical behavior is beyond the scope of this paper.

This paper presents the results of an extensive series of tests to measure the apparent dielectric constant on a naturally occurring low plastic clay soil, pure kaolinite clay, pure illite clay, concrete sand, and fine sand. Each of the materials was compacted into a Standard Compact Test mold (ASTM D698) with standard compaction energy and with different water contents. With use of a guide template, a center conductor was driven into the specimens to form a soil "cable" with length equal to the height of the mold. A ring adapter and a Multiple Rod Probe Head (MRPH) were used to form a connection between the soil cable and a Tektronix® 1502B cable tester. Specimens were placed in an environmental chamber allowed to equilibrate to temperatures ranging from 4°C to 40°C. Measurements of apparent dielectric constant were made with time until readings stabilized.

The results of the tests are reported and are analyzed. Recommendations are put forth for correcting measured apparent dielectric constant to values at 20°C for cohesionless soils and for cohesive soils. The corrections are typically small and have a minor effect on calculation of water content. Results from this work are important for improving the accuracy of the TDR method for measuring the water content and density of soils as described by Feng *et al.* (1998), Lin *et al.* (1998), Lin *et al.* (2000), Siddiqui and Drnevich (1995), Siddiqui *et al.* (2000), and Drnevich *et al.* (2001).

TEST PROCEDURES AND TEST RESULTS

Soils Tested

Tests were conducted on three cohesive and two noncohesive soils, the properties of which are given in Table 1. The samples were classified according to ASTM D2487, the Unified Soil Classification, their Atterberg Limits (plastic and liquid limits) tested according to ASTM D4318, and their compositions determined by ASTM D422. The authors are grateful to Mr. Jie Zhang who performed most of the tests. The Crosby Till soil is an inorganic silty-clay having low to medium plasticity. It is a naturally occurring soil found in the vicinity of the Purdue University campus. The Kaolinite and Illite samples were pure clay minerals. The kaolinite had slight plasticity and the illite had moderate to high plasticity. The noncohesive soils included a concrete sand that is naturally occurring but has been washed to remove fines. Tests were also conducted on a fine Ottawa sand, which was commonly used in cement and concrete research.

Soil	*Unified Soil Classification*	*Atterberg Limits*		*Composition*		
		Liquid Limit	*Plastic Limit*	*% sand*	*% silt*	*% clay*
Crosby Till	CL	41	18	16	50	34
Kaolinite	CL-ML	30	24	0	0	100
Illite	CL-CH	50	22	0	0	100
Concrete Sand	SW	NA	NA	100	0	0
Fine Sand	SP	NA	NA	100	0	0

Table 1. *Characteristics of Soils Tested*

Test Specimens

Tests were performed on specimens placed in a Standard Compaction Mold (ASTM D698) that had a diameter of 101.6 mm (4.0 in.) and a height of 116.4 mm (4.584 in.) giving a volume of $9.19 * 10^5$ mm^3 (1/30 ft^3). For all soil specimens, the soil specimens were compacted with standard compaction effort 600 kN-m/m^3 (12,400 ft-lb/ft^3) at a variety of different water contents (gravimetric) ranging from below optimum to above optimum. Once a specimen was compacted and the mass of the specimen and mold were determined, the metal bottom plate was replaced with a non-metallic plate. Then a guide template was temporarily placed on top of the mold and a stainless steel center rod with diameter of 7.94 mm (5/16-in.) was driven into the specimen over its full height (See Fig. 1.). When the guide was removed, the rod protruded from the soil surface by approximately 30 mm (1.2 in.). An adapter ring was then placed on the top of the compaction mold as shown in Fig. 2. The ring presented a surface for the outer three legs of the Multiple Rod Probe Head (MRPH) to be supported. The center rod of the MRPH then came in contact with the center rod as shown in Fig. 3.

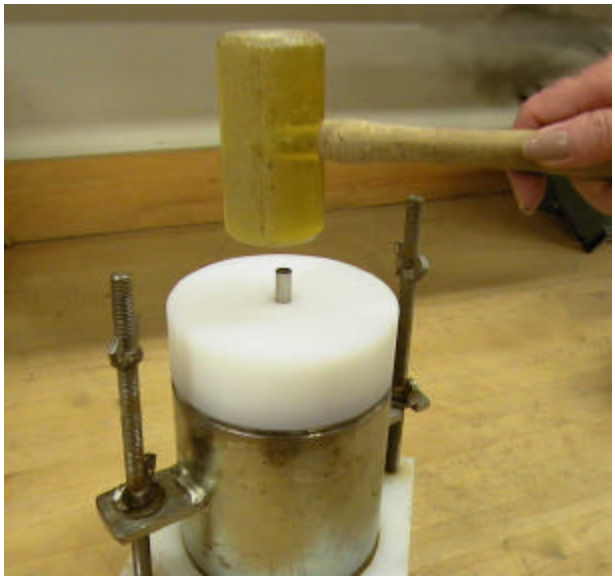

Fig. 1. *Center rod being driven into specimen through guide template*

TDR measurements were made with this arrangement by connecting MRPH with a Tektronix 1502B Cable Tester with a 1 m (3-ft.) coaxial cable with BNC connectors on each end. Additional information about the use of this equipment for determining the apparent dielectric constant, K_a, is available in a companion paper to this conference by Drnevich *et al.* (2001).

One set of tests was done with the mold filled with water to validate that test results were consistent with tests reported in the literature.

Fig. 2. *Mold with center rod and adapter ring ready for multiple rod probe head (MRPH)*

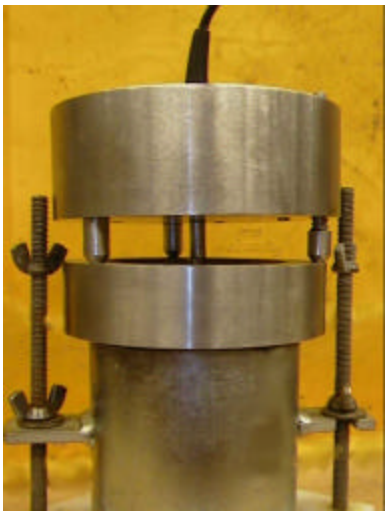

Fig. 3. *Multiple rod probe head ready for making TDR measurements*

Test Environment

Three separate walk-in environmental test chambers were used for tests at 4°C, 10°C, and 20°C where temperatures were reasonably close to the set temperatures for the test duration. For temperatures of 30°C and 40°C, the specimens were placed in a large drying oven where temperatures were maintained within ±1°C of the preset temperature.

Between times when readings were made, the specimens were covered with a plastic film to minimize the amount of moisture lost between readings. Determinations of total mass of the soil, mold, and center rod at the time of each TDR reading allowed for checking any changes in specimen water content.

Testing Sequence

All specimens were constructed at room temperature, 20°C and then placed into the environmental chamber for testing. TDR readings were taken as a function of time to obtain the time required for equilibration. Most of the tests at a given temperature were on specimens tested only at that temperature. An example of this is shown in Fig. 4 for tests on Crosby Till at a target water content of 21 percent. Note that it typically took up to 1000 minutes for the readings to stabilize for the size specimens tested in these experiments.

A given specimen could be tested at different temperatures without significantly affecting the results and some of the measurements were made at multiple temperatures ranging from 4°C to 40°C. Figure 5 gives an example of measurements made at three temperatures on a specimen of Crosby Till with a water content of 41 percent.

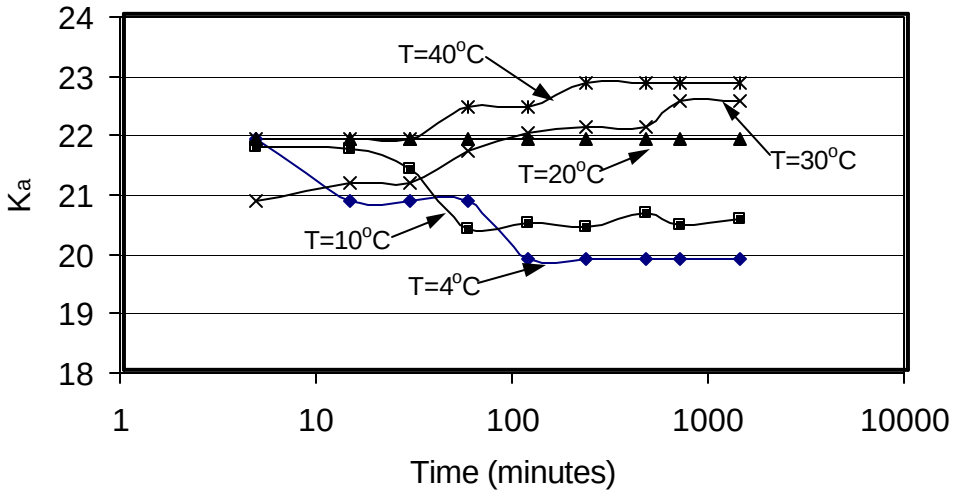

Fig. 4. *Apparent dielectric constant of Crosby Till at a target water content of 21% with tests at all temperatures done with separate soil specimens for each temperature.*

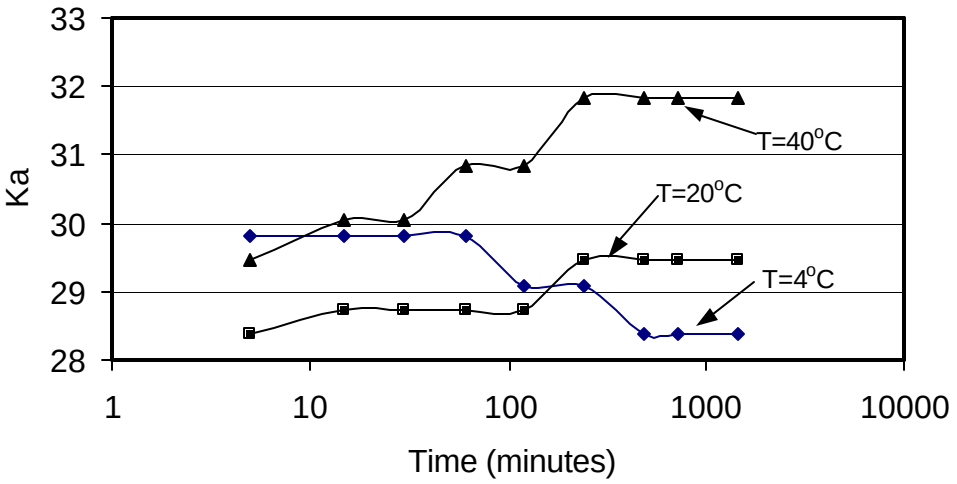

Fig. 5. *Apparent dielectric constant of Crosby Till at a target water content of 41% with measurement at different temperatures made on the same soil specimen.*

The typical testing process involved measurements at 4°C, 10°C, 20°C, 30°C, and 40°C. On some of the soils, testing at some of the temperatures was omitted to save time since equilibration at each temperature took approximately 24 hours. On several of the clay soils at high water content and at high temperatures, accurate apparent length measurements could not be made because the soil was too lossy, i.e. dissipated the signal so that no reflected signal could be detected.

The mass of soil and compaction mold was measured each time a TDR measurement was made. At the end of the test, oven drying was used to determine water content (ASTM D2216). The mass measurements made along with the TDR measurements were used to calculate the water contents at the time of measurement. Table 2 gives the information on water contents, dry densities, and apparent

dielectric constant for the soils tested. The water contents in Table 2 are **gravimetric** water contents. Agronomists make extensive use of TDR for measuring the **volumetric** water content of soil (volume of water as a percentage of the total volume of the soil). The volumetric water content is usually represented by the Greek letter theta, *q*. Geotechnical engineers work with the **gravimetric** water content of soil (mass of the water/mass of dry solids) and it is usually represented by the letter, *w*. Both *q* and *w* are expressed as percentages. Volumetric and gravimetric water contents are related by

$$w = q \frac{r_w}{r_d} \qquad [1]$$

where r_d is the dry density of the soil and r_w is the density of water.

Tests on Water

Figure 6 presents the results for tests on water. Data from Weast (1986) and Mitchell (1993) also are plotted in this figure. The test results compare fairly well with the greatest discrepancy occurring at a temperature of 40°C where the difference is about three percent.

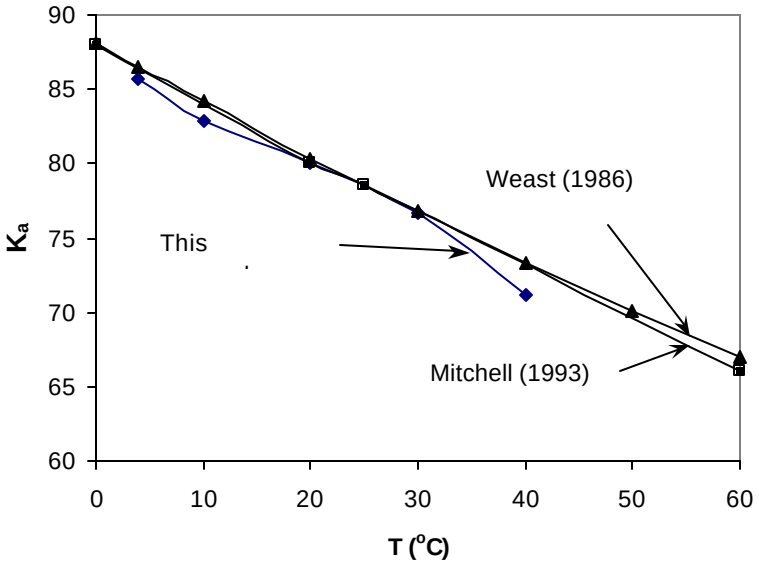

Fig. 6. *Apparent dielectric constant variation with temperature for water*

Soil	Target Water Content (%)	Actual Water Content (%) / Dry Density (Mg/m^3) / K_a	Temperature of Testing (°C)				
			4	10	20	30	40
Crosby Till	3	Water Content	3.1		2.0		3.0
		Dry Density	1.543		1.543		1.543
		K_a	4.121		4.335		4.481
	12	Water Content	11.6	12.0	11.1	11.8	11.9
		Dry Density	1.713	1.713	1.713	1.722	1.706
		K_a	11.940	12.348	12.740	13.660	13.976
	15	Water Content	14.4	14.8	13.9	13.8	14.8
		Dry Density	1.769	1.748	1.759	1.701	1.759
		K_a	15.240	16.124	16.578	17.960	18.920
	18	Water Content	16.8	17.2	16.6	17.1	17.9
		Dry Density	1.789	1.782	1.788	1.782	1.788
		K_a	17.965	19.415	19.906	21.634	21.946
	21	Water Content	20.4	20.8	20.0	20.9	20.5
		Dry Density	1.713	1.694	1.715	1.660	1.715
		K_a	19.906	21.430	21.946	22.367	22.875
	24	Water Content	22.7	23.0	22.3	22.8	23.7
		Dry Density	1.623	1.618	1.638	1.625	1.638
		K_a	20.914	21.946	23.004	25.19	26.32
	41	Water Content	39.0		39.0		38.35
		Dry Density	1.280		1.280		1.280
		K_a	28.558		29.458		31.829
Kaolinite	20	Water Content	20.6		20.5	20.2	
		Dry Density	1.505		1.505	1.505	
		K_a	20.039		20.982	21.301	
	30	Water Content	28.2		28.1		
		Dry Density	1.455		1.455		
		K_a	22.601		23.602		
	40	Water Content	43.4		43.2	42.6	
		Dry Density	1.221		1.221	1.221	
		K_a	31.214		31.994	33.182	
Illite	20	Water Content	19.2		19.1	18.9	
		Dry Density	1.626		1.626	1.626	
		K_a	25.998		28.803	31.571	
	45	Water Content	45.4				
		Dry Density	1.17				
		K_a	36.114				
	50	Water Content	50.1		50.1	49.7	
		Dry Density	1.15		1.15	1.15	
		K_a	47.911		49.037	51.096	
Concrete Sand	0.2	Water Content	0.20		0.20		0.20
		Dry Density	1.785		1.785		1.785
		K_a	3.643		3.643		3.511
	14.6	Water Content	14.5		14.5		13.7
		Dry Density	1.883		1.883		1.883
		K_a	18.515		17.923		16.875
Fine Sand	0.08	Water Content	.08		.08		.03
		Dry Density	1.682		1.682		1.682
		K_a	2.66		2.66		2.66
	19.4	Water Content	19.4		19.4		18.8
		Dry Density	1.742		1.742		1.742
		K_a	21.622		20.982		19.729

Table 2. *Testing Program and Results of Tests on Soils*

ANALYSIS OF THE RESULTS AND RECOMMENDATIONS

Normalized Apparent Dielectric Constant

The apparent dielectric constant data in Table 2 were normalized by dividing each of the values for a soil at a target water content by its corresponding value at 20°C. The results are plotted in Fig. 7. Also plotted in this figure are the normalized data for water. Note that the curve for water exhibits the most dramatic decrease with increase in temperature. The sand soils also exhibit a decrease in apparent dielectric constant with increase in temperature but the decrease is less dramatic. For sands with near zero water content, there is no appreciable change in apparent dielectric constant with temperature.

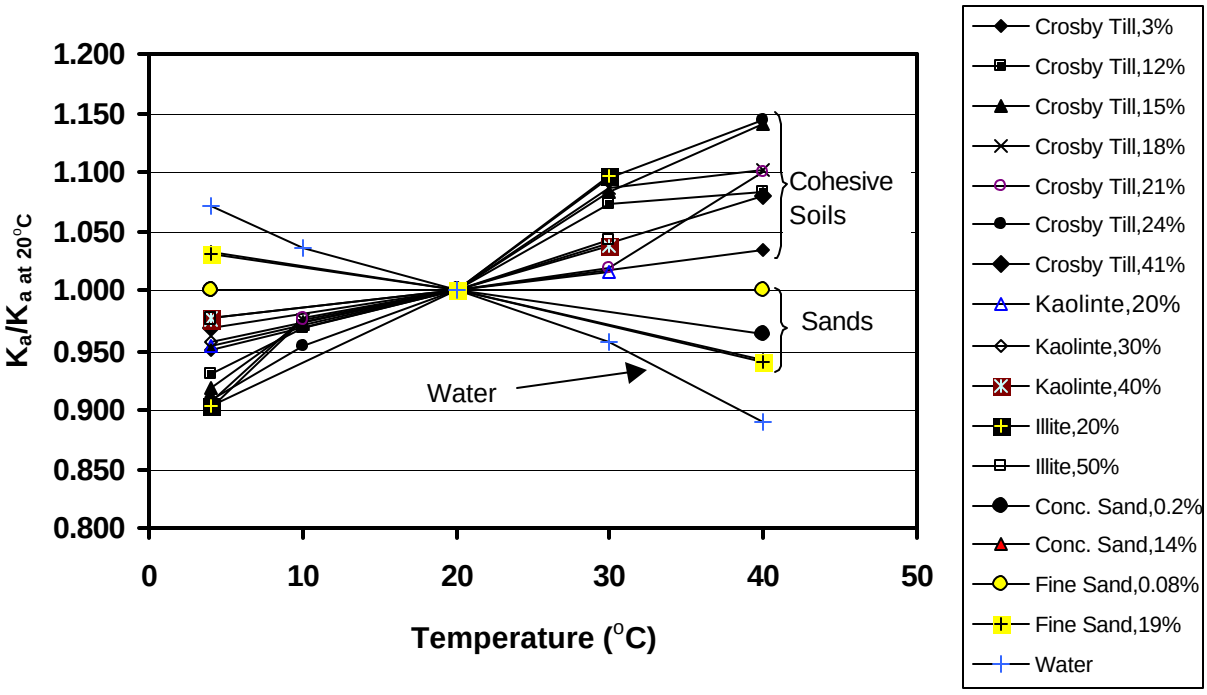

Fig. 7. *Normalized apparent dielectric constants for water and all soils tested.*

The behavior of cohesive soils plotted in Fig. 7 shows the opposite trend from that of water and sands; the dielectric constant increases with increasing temperature. Wraith and Or (1999) and others suggest that this behavior is due to the bound water typically associated with fine-grained soils. A detailed discussion of these phenomena is beyond the scope of this paper.

Effects of Water Content on Behavior of Cohesive Soils

For the soils tested, an attempt was made to discern effects of different water contents on values of apparent dielectric constant. This was done by fitting a straight line by least squares fitting through each of the data sets for the cohesive soils in Fig. 7. Then the slopes of each of these lines were plotted versus water content. Figure 8 presents the results for Crosby Till. The data in Fig. 8 are fitted with a second order polynomial to help accentuate the trend. The slope of these lines increases with increasing

water content to peak and then the slope starts to decrease at higher water contents. It was argued that at very low water contents, the soil solids and the bound water control the behavior. With increasing water content, free water becomes an increasingly large component of the total volume and the effects of temperature on free water begin to dominate.

Note that the curve in Fig. 8 peaks near the Plastic Limit (ASTM D4318) for this soil, which was 18 percent. It was conjectured that below the Plastic Limit, not much unbound water is available to promote plastic behavior of soil and that this might be related to the amount of water available to affect the dielectric properties with temperature. Hence, the Plastic Limit became a candidate for normalizing the water content for the purposes of studying the behavior of all cohesive soils. In Fig. 9 are plotted all of the slope data versus water content normalized by the Plastic Limit for these tests on cohesive soils. While the data set available contains too few types of cohesive soils from which to draw any strong conclusion, plotting of future data in the same manner may provide some useful insight into the phenomena. For example, it appears that the peak in the slopes occurs at water contents approximately 1.3 times the **Plastic Limit**.

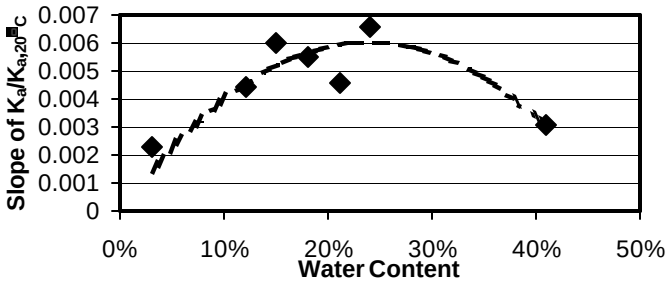

Fig. 8. *Change of slope of normalized temperature effects lines with water content for Crosby Till.*

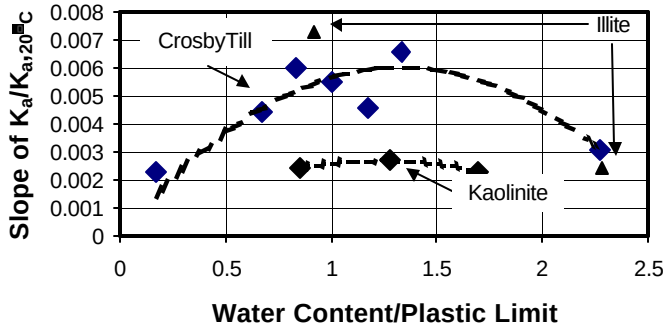

Fig. 9. *Slope of normalized apparent dielectric constant with water content normalized by the plasticity limit.*

Considering that temperature effects on dry soil solids are near zero, the corresponding slope of $K_a/K_{a,20°C}$ would go through origin in Figs 8 and 9. Likewise, as water content gets very large, the slopes would become negative and eventually be asymptotic to the slope for water (-0.354 after Weast,1986).

Temperature Adjustments to Measured Values of Apparent Dielectric Constant

The values of normalized apparent dielectric constant for the cohesive soils in Fig. 7 were averaged at each temperature. These averaged values were then plotted versus temperature to obtain a mean curve that might apply to all of the cohesive soils tested. The same process was applied to all of the sand data in Fig. 7 as well. The data for both the cohesive soils and the sand soils turned was exceptionally linear. For practical purpose, we are recommending that effects of temperature on apparent dielectric constant can be accommodated by simple linear correction as given in Eq. (2).

$$K_{a,20°C} = K_{a,T°C} \times TCF \qquad [2]$$

where

TCF = Temperature Correction Function

= $0.97 + 0.0015\ T_{test,\ T°C}$ for cohesionless soils, $4°C \le T_{test,\ T°C} \le 40°C$

= $1.10 - 0.005\ T_{test,\ T°C}$ for cohesive soils, $4°C \le T_{test,\ T°C} \le 40°C$.

From Eq. (2) it can be seen that values of $K_{a,\ 20°C}$ will not exceed about three percent for cohesionless soils and ten percent cohesive soils for extremes in temperature covered by this equation.

The theoretical and experimental study by Lin *et al*. (2000) suggested that the density-compensating calibration equation proposed by Siddiqui and Drnevich (1995) provides the best relationship between soil water content and apparent dielectric constant. The "Siddiqui-Drnevich" calibration equation accounts for soil density and soil type:

$$w = \frac{1}{b}\left[\frac{r_w}{r_d}\sqrt{K_a} - a\right] \qquad [3]$$

where r_d is the dry density of soil, r_w is the density of water, a and b are soil-dependent calibration constants. From tests on a variety of soils the value of a is consistently near unity and the value of b is consistently near eight. Considering Eq. (3), we see that water content is related to the square root of K_a and hence temperature effects on water content are relatively small. The authors suggest that temperature corrections are not needed for $15°C \le T_{test,\ T?\ C} \le 25°C$. This recommendation and the correction recommended in Eq. (2) are consistent with the findings of Kuraz (1981) who stated, "Temperature effects may be neglected for fluctuations of 5^oC. For wider changes in temperature, a simple linear correction is required."

SUMMARY AND CONCLUSIONS

Apparent dielectric constants in soils are somewhat dependent on soil temperature. Data are presented from tests on cohesive and noncohesive soils at various water contents and densities, measured at temperatures ranging from 4°C to 40°C. Test results show that apparent dielectric constant for sands decrease with increasing temperature similar to the behavior observed in water, but less dramatically. For clays, the opposite behavior was observed, i.e. the apparent dielectric constant increased with increasing temperature. The amount of correction for clays depends on the water content and there exists a water content just higher than the Plastic Limit where temperature effects are the largest. Recommendations are made to correct measured values of apparent dielectric constant to values at 20°C using simple linear corrections. It is shown that effects of temperature on water content determination are likely to be small and can be neglected for temperatures within 5°C of 20°C.

ACKNOWLEDGEMENTS

The authors gratefully acknowledge the Indiana Department of Transportation and Federal Highway Administration for the financial support through projects **Indiana HPR-2094, C-36-5S, and Indiana SPR-2201** and assistance with the field experiments. The authors are indebted to Mr. Jie Zhang who

performed most of the tests reported herein. Development of the procedures and theories supporting them has truly been a team effort and the author acknowledges the efforts of all who contributed, especially: Dr. Shafiqul Siddiqui, Dr. Richard Deschamps, Dr. Wei Feng, Dr. Chih Ping Lin, Dr. Robert Nowack, Mr. Quanghee Yi, Mr. Jie Zhang, and Mr. Charlie Crowe (machinist). The authors also wish to acknowledge the enthusiastic support and creative ideas of the Study Advisory Committee for these projects. The members are: Mr. Peter Capon (Rieth Riley Construction), Mr. Donald Johnson (FHWA), Mr. Thomas Kuhn (Kuhn Construction), Dr. Sam Mansukhani (FHWA), Dr. Tommy Nantung (INDoT), Mr. Wes Shaw (INDoT), and Mr. Nayyar Zia (INDoT).

REFERENCES

ASTM D422, 1998, "Standard Test Method for Particle-Size Analysis of Soils," *Annual Book of ASTM Standards*, **4**, No. 8, 10-16.

ASTM D698, 1998, "Standard Test Method for Laboratory Compaction Characteristics of Soil Using Standard Effort (12,400 ft-lbf/ft^3 (600 kN-m/m^3))," *Annual Book of ASTM Standards*, **4**, No. 8, 77-84.

ASTM D2216, 1998, "Standard Test Method for Laboratory Determination of Water (Moisture) Content of Soil and Rock," *Annual Book of ASTM Standards*, **4**, No. 8, 188-191.

ASTM D2487, 1998, "Standard Classification of Soils for Engineering Purposes (Unified Soil Classification System)," *Annual Book of ASTM Standards*, **4**, No. 8, 217-238.

ASTM D4318, 1998, "Standard Test Method for Liquid Limit, Plastic Limit, and Plasticity Index of Soils," *Annual Book of ASTM Standards*, **4**, No. 8, 519-529.

Drnevich, V.P., Siddiqui, S.I., Lovell, J., and Yi, Q., "Water Content And Density Of Soil In situ by the Purdue TDR Method," *TDR 2001: Innovative Applications of TDR Technology*, Infrastructure Technology Institute, Northwestern University, Evanston, IL, September, 2001.

Feng, W., Lin, C.P., Drnevich, V.P., and Deschamps, R.J., "Automation and Standardization of Measuring Moisture Content and Density Using Time Domain Reflectometry," Report No.: FHWA/IN/JTRP-98/4, Joint Transportation Research Program, Indiana Department of Transportation - Purdue University, September, 1998, 122 p.

Frohich, H., 1949, "Theory of Dielectrics," 2nd Ed. The Clarendon Press, Oxford, 180p.

Kuraz, V., 1981, "Testing of a field soil moisture meter." *Geotechnical Testing Journal*, **4**, No.3, September, 111-116.

Lin, C.P., Drnevich, V.P., Feng, W., and Deschamps, R.J., "Time Domain Reflectometry For Compaction Quality Control," Presented at and publication in *Proc. GeoDenver2000, Use of geophysical methods in construction*, Soheil Nazarian and John Diehl, Editors, Geotechnical Special Publication No. 108, ASCE GeoInstitute Conference, Denver Colorado, August 5-8, 2000, pp. 15-34.

Lin, C-P., Siddiqui, S. I., Feng, W., Drnevich, V. P., and Deschamps, R. J., 2000, "Quality Control of Earth Fills Using Electromagnetic Waves," *Constructing and Controlling Compaction of Earth Fills, ASTM STP 1384*, D. W. Shanklin, K. R. Rademacher, and J. R. Talbot, Eds., American Society for Testing and Materials, West Conshohocken, PA, 290-310.

Mitchell, J.K., 1993, "Fundamentals of Soil Behavior," 2nd Ed., Wiley, New York, 437 p.

Siddiqui, S.I., and Drnevich, V.P., "A New Method of Measuring Density and Moisture Content of Soil Using the Technique of Time Domain Reflectometry," Report No.: FHWA/IN/JTRP-95/9, Joint Transportation Research Program, Indiana Department of Transportation - Purdue University, February, 1995, 271 p.

Siddiqui, S.I., Drnevich, V.P., and Deschamps, R.J., (2000). "Time Domain Reflectometry Development for Use in Geotechnical Engineering," *Geotechnical Testing Journal,* GTJODJ, **23**, No. 1, March, 9-20.

Wraith, J.M., and Or, D., 1999, "Temperature Effects on Soil Bulk Dielectric Permittivity Measured by Time Domain Reflectometry: Experimental Evidence and Hypothesis Development," *Water Resources Research*, **35**, No. 2, February, 361-369.

Weast, R.C., 1986, *CRC Handbook of Chemistry and Physics*, 67th ed., CRC Press.

Yi, Q., Drnevich, V.P., and Lovell, J., "Effects of Particle Size Distribution on the Purdue TDR Method with Rock and Silty Clay Soil," *TDR 2001: Innovative Applications of TDR Technology*, Infrastructure Technology Institute, Northwestern University, Evanston, IL, September, 2001.

Optical TDR and Structural Monitoring

OTDR Distributed Sensing of Liquid Hydrocarbons Using Polymer-Clad Optical Fibers
J. Buerck, S. Roth, K. Kraemer and H. Mathieu, *Research Center Karlsruhe, Germany*

Quasi Distributed OTDR Crack Sensor for Reinforced Concrete Structures
F.Ansari, Z. Chen and X. Gu, *University of Illinois at Chicago*

An Overview of Corrosion Damage Detection in Steel Bridge Strands Using TDR
W. Liu, R. Hunsperger and M. Chajes, *University of Delaware*; E. Kunz, *VETEK Systems Corp*.

Distributed Fibre Optic Sensors for the Detection of Liquid Spills
B. Culshaw, A. MacLean, C. Moran and W. Johnstone, *University of Strathclyde, UK*; D. Marsh and G. Andrews, *PINACL Communications, UK*

Back to Table of Contents

OTDR DISTRIBUTED SENSING OF LIQUID HYDROCARBONS USING POLYMER-CLAD OPTICAL FIBERS

Jochen Buerck[1], Siegmar Roth[2], Karl Kraemer[3], and Heide Mathieu[4]

[1]Research Center Karlsruhe, Institute for Instrumental Analysis, P.O. Box 3640, D-76021 Karlsruhe, Germany; jochen.buerck@ifia.fzk.de
[2]Research Center Karlsruhe, Institute for Instrumental Analysis, P.O. Box 3640, D-76021 Karlsruhe, Germany; siegmar. roth@ifia.fzk.de
[3]Research Center Karlsruhe, Institute for Instrumental Analysis, P.O. Box 3640, D-76021 Karlsruhe, Germany; karl.kraemer@ifia.fzk.de
[4]Research Center Karlsruhe, Institute for Instrumental Analysis, P.O. Box 3640, D-76021 Karlsruhe, Germany; heide.Mathieu@ifia.fzk.de

ABSTRACT

A distributed sensing system for apolar hydrocarbons is presented which is built from a chemically sensitive polymer-clad silica fiber adapted to an optical time domain reflectometer (OTDR) setup. OTDR measurements allow locating and detecting chemicals by measuring the time delay between short light pulses entering the fiber and discrete changes in the backscatter signals that are caused by local extraction of hydrocarbons into the fiber cladding. The light guiding properties of the fiber are affected by interaction of the extracted chemicals with the evanescent wave light field extending into the fiber cladding.

Distributed sensing of pure liquid hydrocarbons (HC) and aqueous HC solutions with a commercially available mini-OTDR adapted to sensing fibers of up to one-kilometer length could be demonstrated. A pulsed laser diode emitting at the 850-nm telecommunication wavelength was applied in the mini-OTDR to locate the HCs by analyzing the step drop (light loss) in the backscatter signal, which is induced by local refractive index changes in the silicone cladding. These refractive index changes are caused by HC extraction into the polymer cladding. The prototype instrument can be applied for monitoring hydrocarbon leakage in large technical installations such as tanks, chemical pipelines or chemical waste disposal containments.

INTRODUCTION

Leakage in pipelines and tanks or the emission of toxic substances from chemical production plants are hazards associated with storing, processing and transporting hydrocarbon (HC) products. Fast detection and location of leakage in technical installations is important to minimize the emission of toxic chemicals to the environment. The spatial extension of these installations makes a distributed sensing technique necessary. In this context optical time domain reflectometry could be an interesting alternative to conventional leakage control systems. OTDR is a well established technique for characterization of fiber optic networks or for the

distributed sensing of physical parameters (strain, temperature, displacement) that detects information from every point along the sensing fiber by measuring from one end of the fiber (Barnoski and Jensen, 1976; Rogers, 1988). Short light pulses are coupled into a quartz glass waveguide. While the light is transported through the fiber by total reflection, a part of it is scattered and guided back to the front end. The backscattered light signals are focused onto a fast photodetector, and the whole process is recorded in the time domain, e.g., by a digitizing oscilloscope. The localization of defects in the fiber (break or sharp bend) is achieved by determining the time delay between the excitation light pulse and a specific change in the OTDR backscatter signal related to this defect. From the time delay and the light velocity in the fiber, the position of the defect can be determined. Due to the evanescent wave tail of the light conducted in the fiber it is also possible to detect changes in the backscatter signal caused by defects in the fiber cladding. If fibers are used that have a cladding, which is permeable for chemical substances, e.g., a polymer coating, the light guiding properties of the fiber and the backscatter signal can be affected by optical effects induced in this cladding due to a penetrating chemical. Thus, it is possible to detect the presence and spatial distribution of analyte molecules along the active length of the fiber. Such a distributed chemical sensor, i.e., an optical fiber that is chemically sensitive over its entire length, will improve the performance of existing fiber-optic single-point sensors in many areas of application, because it can be spread over a larger area to be monitored and it allows getting information from multiple points in this area (Lieberman, 1991). Especially, the visible and near-infrared (NIR) spectral range are predestined for distributed sensing because polymer-coated quartz glass fibers with relatively high light transmission can be used and systems extending over a domain from some ten meters to kilometers can be built up.

Up to now a number of papers on distributed chemical sensing with optical fibers have been published. Sensors for the distributed measurement of the pH value described in the literature utilize the absorption or fluorescence of dyes immobilized in discrete fiber sections in a cellulose acetate or a sol-gel cladding. They react upon changes in the absorption / fluorescence backscatter signal caused by changes in the pH value of the surrounding medium (Kvasnik and McGrath, 1989; Browne *et al.*, 1996). Connected to an OTDR setup these fibers provide quasi-distributed measurements but in principle they can be extended to totally distributed sensors by using completely sol-gel clad fibers. Distributed evanescent wave sensing has also been proposed for measuring oxygen concentrations along a silicone-clad fiber with an immobilized fluorescent dye (Potyrailo and Hieftje, 1998). A multi-point distributed humidity sensing system has been reported which is based on changes in absorption of cobalt chloride in the presence of water (Kharaz and Jones, 1995). To build up a distributed sensor system the indicator was immobilized in a gelatin film that formed the cladding of a multimode optical fiber which was coupled to a two-wavelength OTDR setup to provide intensity referencing. Michie *et al.* (1995) have demonstrated a distributed sensor system for the detection of water. The sensing fiber consists of a core, which is clad with a hydrogel and afterwards wound with a nylon string. The hydrogel swells in the presence of water, which causes microbendings in the fiber core due to the spiral nylon winding. This will lead to a partial loss of the guided light at the fiber section affected by humidity, which can be detected and located by an OTDR system.

The approach made at our institute to develop totally distributed sensor systems for hydrocarbon (HC) species is to adapt a commercially available polymer-clad silica (PCS) fiber, that is coated with a silicone polymer cladding over its entire length to suitable OTDR setups. Such a silicone polymer cladding is intrinsically sensitive to apolar hydrocarbons and recently we have presented an evanescent field absorbance (EFA) sensor for single-point measurements, where such a fiber is used for the determination of hydrocarbons in water (Bürck *et*

al., 1998). The chemicals diffuse into the polymer cladding and are detected by NIR absorption spectroscopy. Basic investigations into OTDR evanescent wave sensing with this PCS fiber revealed that different optical effects caused by HC molecules penetrating into the cladding can be used to design a distributed sensing system. Changes in the backscatter signal can either be induced by a local change of the refractive index (RI) or the absorption and fluorescence properties in the fiber cladding induced by the extracted HC. The different effects lead to distinct patterns in the OTDR response function, which clearly can be separated, from each other and from signals originating from mechanical defects in the fiber (Bürck and Sensfelder, 1998; Sensfelder *et al*., 1998). In this way hydrocarbons can be detected and located directly by OTDR measurements and additional information can be deduced because signal intensities are quantitatively correlated with the hydrocarbon concentration and the interaction length of the sensing fiber with the analyte.

In this paper we present a prototype sensor system based on a commercially available mini-OTDR which can be used for distributed sensing of HCs and aqueous HC solutions. The instrument has been adapted to PCS sensing fibers of up to nearly one kilometer length. Here, laser emission at the 850-nm telecommunication wavelength was applied to locate the HCs by analyzing step drop signals (light loss) in the OTDR backscatter trace which are caused by local increase in RI induced by analyte enrichment in the silicone cladding.

OTDR-EVANESCENT WAVE SENSING

Distributed sensing: Spatial resolution by time resolved detection

The technique of optical time domain reflectometry was first demonstrated by Barnoski and Jensen (1976). OTDR typically involves launching light pulses with 10-1000 ns pulse widths into the input end of an optical fiber and measuring the return signal produced by these test pulses at the same end of the fiber. As a test pulse travels down the fiber, Rayleigh scattering and the intrinsic absorption of the fiber leads to an exponentially decreasing amplitude of the pulse. As illustrated in Figure 1, some of this scattered light reaches the input end of the fiber to produce the measured return signal. Distinct structures in the pulse return function, which represents the magnitude of the energy incident on the detector as a function of time, allow the position of anomalous sections of an optical fiber (′defect′) to be determined. Such defects due to local imperfections in the fiber core / cladding manifest themselves as step drop, changes in slope or discrete reflections in the return function. The power received at the input end of the fiber from a position along the fiber P(x) is given by (Rogers, 1988)

$$P(x) = \frac{1}{2} \cdot v \cdot s \cdot f \cdot c \cdot ?t \cdot P(0) \cdot e^{-2 \cdot d \cdot x} \qquad [1]$$

where v = velocity of the light pulse within a quartz glass fiber: $2.06 \cdot 10^8$ m/s, s = light-scattering coefficient, $f = \frac{3}{8} \cdot \frac{n_1^2 - n_2^2}{n_1^2}$ = fraction of scattered light which is recaptured by the fiber and travels back towards the input end (Neumann, 1978), n_1 = refractive index of fiber core, n_2 = refractive index of fiber cladding, c = coupling efficiency of optics, P(0) = optical output power of the laser, Δt = pulse width of laser, δ = total fiber attenuation caused by scattering and absorption effects in the fiber, x = position along the fiber.

Time-resolved detection following pulsed excitation can be used to probe a distributed fiber-optic sensor and locate the position of interaction with an analyte along the fiber. By evaluating the time delay τ_d between the light pulse entering the fiber and the response signal of a discrete fiber region contacted with the analyte the spatial position of the analyte can be determined. The distance x from the fiber front to the analyte position is given by (Browne *et al*., 1996)

$$x = \left(\frac{v}{2 \cdot n_1} \right) \cdot t_d \qquad [2]$$

For a fiber that is uniformly clad over its entire length with a silicone polymer coating that enriches HC compounds, this provides a simple manner for distinguishing between response signals from different fiber zones that contact the HC analyte.

Modes in a step-index fiber are characterized by discrete values of the ray angles θ (θ is the angle of the ray with respect to the fiber axis). Each fiber mode has two modal parameters U and W given by (Gloge, 1971)

$$U = r \cdot (n_1^2 \cdot k^2 - ß^2)^{1/2} \qquad [3]$$

$$W = r \cdot (ß^2 - n_2^2 \cdot k^2)^{1/2} \qquad [4]$$

where $k = 2\pi/\lambda$ is the free space wavenumber (λ = wavelength of light), β is the propagation constant of the mode ($= n_1 \cdot k \cdot \cos\theta$), and r is the fiber core radius. U and W are related to the normalized frequency V of the fiber by

$$V^2 = U^2 + W^2 \qquad [5]$$

The V number is a measure for the number of modes supported by the fiber and is given by

$$V = \frac{2 \cdot p \cdot r \cdot \sqrt{n_1^2 - n_2^2}}{?} \qquad [6]$$

Light guided by the core of an optical fiber will have an evanescent wave associated with it. The evanescent wave penetrates into the medium surrounding the fiber core (usually the cladding) and can interact with the material of this medium. Therefore, it is possible to obtain spectroscopic information about the cladding by observing the light guided in the core. The 1/e penetration depth d of the evanescent wave in the cladding is approximated by

$$d = \frac{r}{W} \qquad [7]$$

and the transmittance T of the mode is given by (Snyder and Love, 1983)

$$T = \exp(-? \cdot z) \qquad [8]$$

where z is the length of the fiber that contacts the absorber and the evanescent wave attenuation coefficient γ is

$$? = \frac{a \cdot n_2 \cdot U^2}{r \cdot n_1 \cdot V \cdot W} \qquad [9]$$

α is the bulk attenuation coefficient of the compound causing the evanescent wave attenuation. From equation 9 it can be seen that γ is inversely proportional to the V number, so that evanescent attenuation is stronger for few mode fibers. From equation 4 it can be deducted that $W \rightarrow 0$ for highest order modes and thus $\gamma \rightarrow \infty$.

These theoretical equations show that the light guiding characteristics of a fiber can be affected by chemicals in the cladding in different ways. First, if a chemical extracted into the cladding increases the cladding refractive index n_2, then higher order modes will be stripped, leading to a light loss at the position of enrichment. Second, there may be a change in the bulk attenuation coefficient of the influenced fiber section arising, e.g., from light absorbing evanescent wave interactions with the extracted chemical.

EXPERIMENTAL CONSIDERATIONS

Sensing fiber

A commercially available low-hydroxyl silica core fiber with a poly(dimethylsiloxane) cladding and a nylon buffer was used as the basic element of the distributed sensors. The RI of the silica core and the cladding material is 1.456 and 1.436 (@ 633 nm), respectively, resulting in a numerical aperture of NA=0.24. The fiber has a 100-µm o.d. core and a 200-µm o.d. cladding. To turn this PCS fiber into a truly distributed sensing fiber for apolar HCs, the outer nylon buffer with a thickness of 20 - 35 µm was removed chemically over the full length of the fiber. It was dissolved by boiling the fiber in a propylene glycol bath heated to 165°C for about one hour (Sensfelder *et al.*, 1998). The fiber is protected against mechanical stress and breakage, by threading it through a spiral-shaped stainless steel metal hose with a stripwound outer hose, before the dissolution process (see Figure 1). Both protection hoses are easily permeable for liquids. After the coating dissolution process, the input end of the fiber was fixed in an ST connector and polished with abrasive paper to minimize coupling losses.

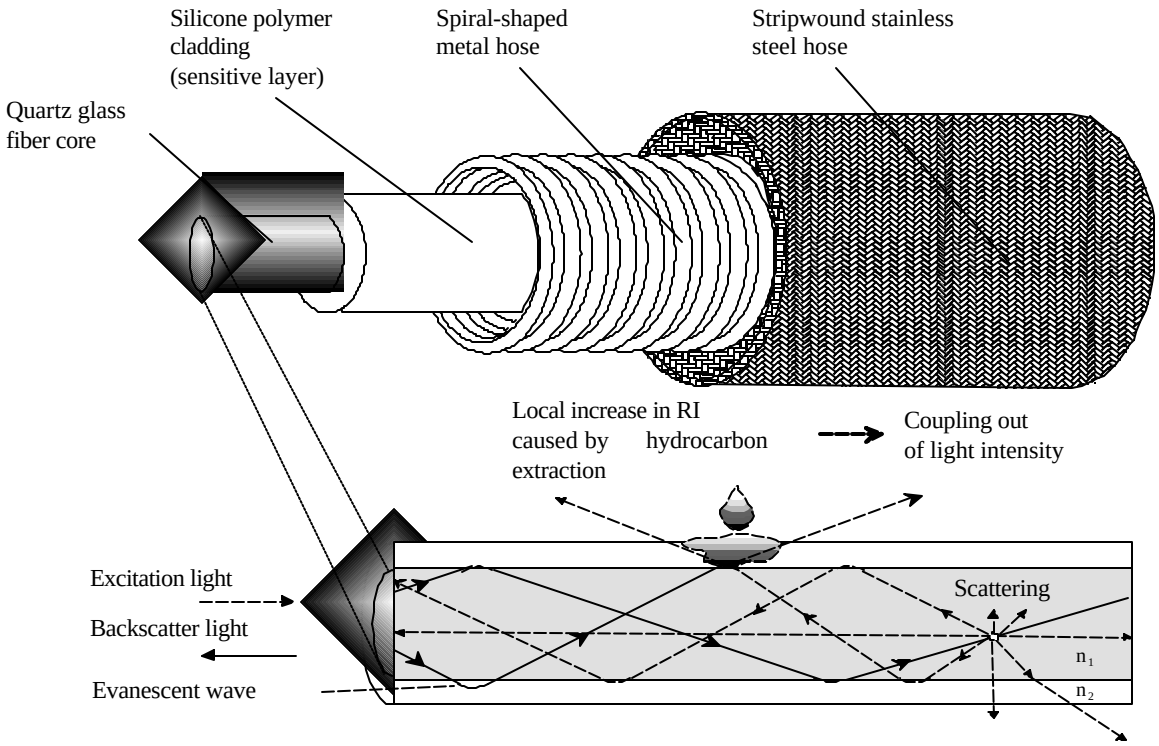

Fig. 1. *Structural elements of the distributed sensing cable and illustration of measuring principle.*

Mini-OTDR

To demonstrate the feasibility of distributed sensing of HC compounds with long PCS fibers and with an instrument that is applied in real world applications, we have adapted sensing fibers to a portable mini-OTDR (TFS 3031, Tektronix), which is normally used for testing of optical fibers, e.g., in telecom-munication networks. The TFS 3031 is a dual-wavelength OTDR capable of performing measurements at wavelengths of 850 and 1300 nm, that can be applied for testing of single- and multimode fibers. The pulse width of the laser diodes can be varied between 10 - 1000 ns. The instrument was combined with different 100-µm-core PCS sensing fibers of up to 934 m length, whose fiber ends were fixed in standard ST connectors. The multimode output port of the instrument is designed for 62.5-µm core fibers typically used in telecommunications. Therefore, laser light launched from the instrument into the 100 µm-core PCS fiber will initially excite only low-order modes in an ′underfilled fiber′ (launch beam diameter < fiber core diameter). To achieve a stable modal distribution a FM-1 mode scrambler (Newport) was placed at a distance of 30 cm from the input end of the fiber. A photograph of the prototype distributed fiber-optical sensor system for localization of HC leakage (OASE) is shown in Figure 2. It consists of the protected sensing fiber that is adapted to the mini-OTDR and a laptop computer for automatic evaluation and documentation of the measurements.

Fig. 2. *Photograph of fiber-optical OTDR sensor system (OASE) for continuous, spatially resolved HC leakage control.*

Sample preparation and measurements

The container for measuring the OTDR response to the analyte solutions was a double-walled, thermostated glass jar with an inner diameter of 20 cm and a 2500-ml volume. It was similar to the one described in detail earlier (Bürck *et al.*, 1997). The fiber section to be contacted with the chemical was led through the lid of the jar and was fixed inside wound up in loops of about 18-20 cm diameter. In most cases a 2-m length of the fiber section has been chosen, but in some experiments the length of the fiber section was varied between 0.75 and 5 m.

After recording the OTDR waveform with the fiber in air or in pure water the analyte solution was poured into the jar and the sample measurement was started. The extraction of an analyte in the fiber cladding was pursued by storing averaged OTDR waveforms at fixed intervals (typically 1 - 2 min). After the measurement, the liquid HC solution was removed from the sample container and the sensor fiber was regenerated either by evaporating volatile HCs in air or by washing with acetone. The response of the sensing fiber in combination with the mini-OTDR to chemical induced RI changes in the cladding was tested either with pure liquid HCs of different RI and polarity (all of analytical grade quality) or with aqueous HC solutions.

RESULTS AND DISCUSSION

OTDR response to cladding RI changes induced by HCs

The penetration of an apolar HC compound into the cladding of a distributed sensing fiber leads to a change in the RI of the matrix surrounding the fiber core. On the one hand, a decrease in the RI of the cladding will occur due to a density reduction associated with swelling of the polymer, and on the other hand, the RI of the extracted HC will contribute to the 'mixed' RI of the swollen cladding. Polymer swelling in the presence of analytes will be influenced by the structure of the polymer, e.g., the degree of cross-linkage and the polymer / analyte interaction. An increase in the RI of the cladding for a mode filled fiber strips off higher order modes and decreases the fiber transmittance (cf. equation 9).

In Figure 3 typical OTDR traces are depicted, which were recorded with the distributed sensor system described above. A series of experiments was performed with pure chlorinated HC solvents that were always contacted with 2-m sections of a fiber of 934-m total length. The OTDR reference trace, which was taken with the fiber in air, shows the excitation pulse and the Fresnel reflection from the far end of the fiber, as well as the decrease in the backscatter light level with increasing distance. This decrease depends on the fiber attenuation properties, and from the slope of the trace the loss of the sensing fiber at the 850-nm laser diode wavelength

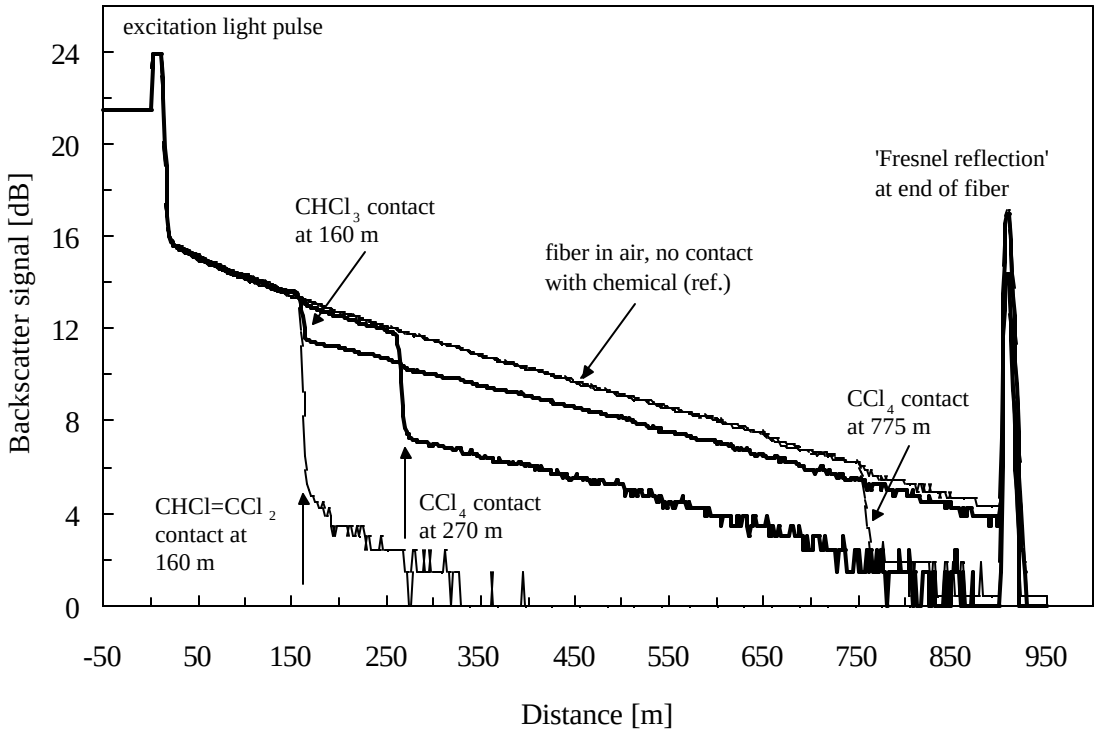

Fig. 3. *OTDR traces recorded by distributed fiber-optical sensor system for contact of chlorinated HCs at different positions along the sensing fiber (length of contact zone: 2m); step drop in backscatter signal intensity indicates position of contact.*

was determined to be 10.6 dB km^{-1}. Using this value and the dynamic range of the backscattered light level the maximum length of this fiber for distributed HC sensing was calculated to be in the range of ~ 1.0 - 1.5 km. If the fiber is immersed in liquid $CHCl_3$, CCl_4 or $CHCl=CCl_2$ at different positions along the fiber, discrete 'step drop' signals occur at the corresponding section in the OTDR trace, which are an indicator for the position of HC / fiber contact. The step drop in backscatter signal intensity is due to the RI increase in the fiber cladding, which leads to stripping of higher order modes and a corresponding reduced backscatter light level in the fiber beyond this section. The step drop signal height in Figure 3 increases in the series trichloromethane (n_D^{20}=1.4459) < tetrachloromethane (n_D^{20}=1.4601) < trichloroethene (n_D^{20}= 1.4773). The step drop signal caused by trichloromethane extraction is distinct enough for good location of the contact and will also allow identifying further points of contact beyond the first contact zone with the chemical. For trichloroethene on the other hand, the corresponding 'mixed' RI in the fiber cladding at the contact zone reaches a value where no light is guided in the fiber beyond the extraction spot and the Fresnel reflection at the fiber end can not be observed. In this case, it would not be possible to see further contact points beyond this section.

Hydrocarbon	**Refractive index n_D^{20}**	**E_T^N Reichardt polarity**	**Step drop signal height dB**
Dichloromethane	1.4242	0.309	0.02
1,2-Propanediole	1.4324	0.722	0.01
1,1,1-Trichloroethane	1.4379	0.170	0.94
1,2-Dichloroethane	1.4448	0.327	0.33
Trichloromethane	1.4459	0.259	1.46
Acetylacetone	1.4494	0.571	0.15
Cyclohexanone	1.4507	0.281	0.39
Tetrachloromethane	1.4601	0.052	4.21
1-Methyl-2-Pyrrolidone	1.4684	0.355	0.03
1,1,2-Trichloroethane	1.4714	0.296	1.36
cis, trans-Decalin	1.4742	0.015	4.11
Dimethyl sulphoxide	1.477	0.444	0.02
Trichloroethene	1.4773	0.160	8.30
Toluene	1.4961	0.099	8.33
1,3,5-Trimethylbenzene	1.4994	0.068	8.44
Benzene	1.5011	0.111	8.44
Tetrachloroethene	1.5053	0.043	8.52
Pyridine	1.5095	0.302	0.81
Dimethylphtalate	1.5138	0.309	0.01
1,2-Dibromopropane	1.5201	0.259	3.00
Chlorbenzene	1.5241	0.188	8.44
Benzonitrile	1.5289	0.333	0.16
Acetophenone	1.5325	0.306	0.16
Benzyl alcohol	1.5396	0.608	0.02
1,2-Dichlorobenzene	1.5515	0.225	8.43
Aniline	1.5863	0.420	0.10

Table 1. *Comparison of step drop signal height obtained from HCs of varying RI and polarity; step drop signal height = difference signal of analyte OTDR trace and air reference OTDR trace (for contact with 2-m fiber section); signals are only obatined for RI >1.436.*

Figure 3 also depicts two tetrachloromethane traces, where the HC was contacted with fiber sections located at distance of 270 and 775 m from the fiber input end. These traces show that the height of the step drop signal for a modefilled fiber and a given analyte and fiber/analyte interaction length is independent on position along the sensing fiber. The spatial resolution, i.e., the possibility to differentiate between two contact zones is dominated by the laser diode pulse width and ranged in our experiments from 1 to 5 m.

From equations 6-9 discussed above it can be stated that a step drop signal in the OTDR trace can only be obtained for HCs whose RI exceeds the RI of the cladding (n_D^{20}=1.436). In further experiments with different liquid HC compounds it turned out that besides the RI of the compound also its polarity has an influence on the analyte signal intensity. Due to the hydrophobicity of the silicone cladding only HCs of low polarity will be extracted into the polymer while a polar liquid like water will not penetrate. Table 1 shows RI and polarity data of different liquid HCs and the corresponding step drop signal heights obtained with the OASE fiber-optical sensor system. The E_T^N values given in Table 1 describe the polarity of a compound on an empirical, spectroscopy based scale given by Reichardt *et al*. (1994). They are obtained by measuring the shift of the absorbance maximum of solvatochromic dyes dissolved in the corresponding HC solvent. The normalized E_T^N scale ranges from 0 to 1. The E_T^N -value for tetramethylsilane = 0 marks the boundary of the scale at the low polarity side, while the E_T^N -value for water = 1 stands for the highest polarity. From the data it in Table 1 it is obvious, that the height of the step drop signal increases for HC compounds with high RI and low polarity, i.e., with an E_T^N value close to zero. We have found that there is a correlation between step drop signal height and the quotient of the RI and E_T^N data of a HC compound, which is given by a sigmoidal function (Bürck *et al.*, 2000). This sigmoidal function allows predicting the signal height for pure liquid HC compounds if their RI and E_T^N data are known.

Influence of interaction length and HC concentration on OTDR response

A distributed chemical sensing system should allow measuring the spatial extension of a fiber segment contacting the chemical. Therefore, it is an important aspect whether the step drop pattern in the OTDR response function allows to extract additional information on the length of the fiber section that contacts the chemical. Therefore, OTDR measurements with pure trichloromethane were performed, where the length of sensing fiber coming into contact with the hydrocarbon has been increased in discrete steps from 0.75 m up to 5.0 m.

The inset in Figure 4 shows two zoomed in OTDR step drop signals obtained during these experiments. From a qualitative comparison of the two signals one can clearly see that both the vertical height and the horizontal width of the step drop increase if the interaction length is extended from 0.75 m to 5 m. In Figure 4 the width and height of the step drop signals caused by trichloromethane extraction have been plotted as a function of the interaction length between sensor fiber and chemical. Here, the width of the step drop signal is defined as the distance between two points directly in front and behind the step drop signal, where the slope of the OTDR trace (attenuation) has the value of the unloaded fiber. Both signals are linearly correlated to the interaction length sensor fiber / chemical. Thus, for a given HC compound or HC mixture in principal one could use both parameters to predict the interaction length. However, due to the fact that the height of the step drop signal additionally is dependent on the RI and polarity of the

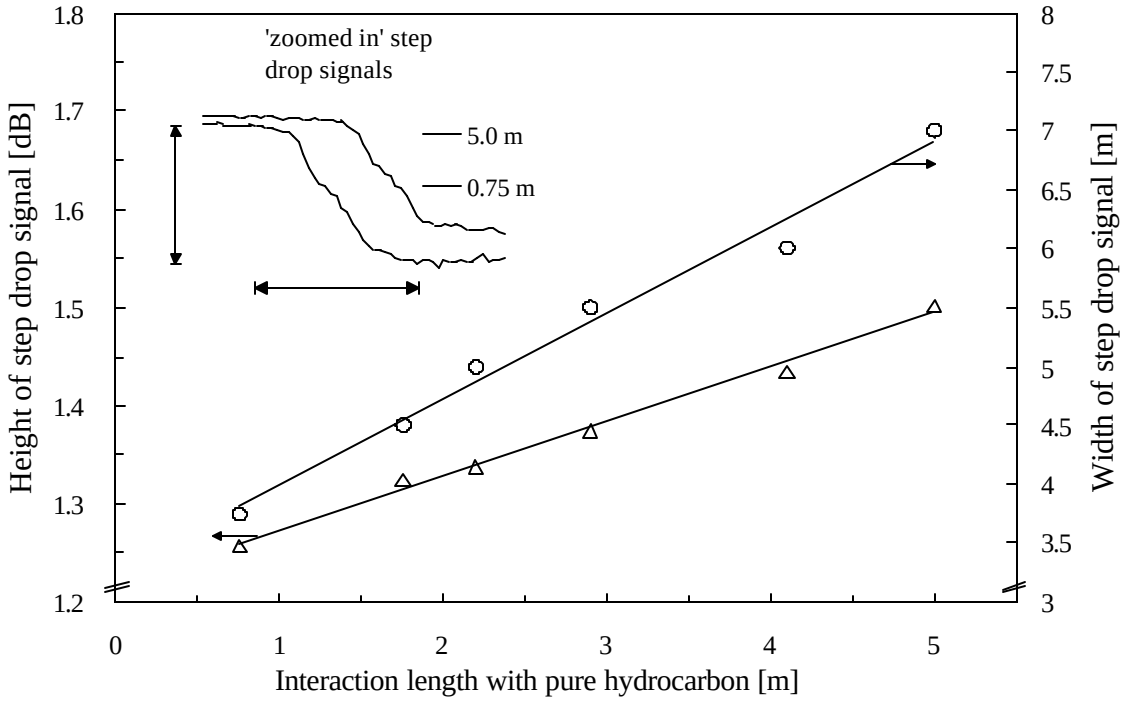

Fig. 4. *Dependence of step drop height and width on the interaction length between hydrocarbon and sensing fiber; extraction of pure* $CHCl_3$.

HC compound, it is preferable to use the width of the step drop in the OTDR response function to calculate the spatial extension of a contact zone.

The hydrophobic silicone cladding of the distributed sensing fiber of OASE prevents any interference from water. Thus, it can be applied for the detection of HCs dissolved in water as well. The (smaller) step drop signals obtained for aqueous solutions of trichloroethene and p-xylene resemble those obtained with the pure compounds. Fig. 5. shows the step drop signal height as a function of HC concentration for both HC compounds. For a given HC compound or HC mixture the vertical height of the step drop signal can be used as a quantitative measure of HC concentration. For both compounds the signal height is linearly correlated with the concentration up to values close to the saturation solubility. The detection limits calculated on the base of a 0.2 db noise level are 223 $mg \cdot l^{-1}$ for trichloroethene and 17 $mg \cdot l^{-1}$ for p-xylene. The ability of the system to detect apolar HCs in water at these concentrations opens up the possibility for leakage monitoring at liners of waste disposal sites that contain leachable HC compounds.

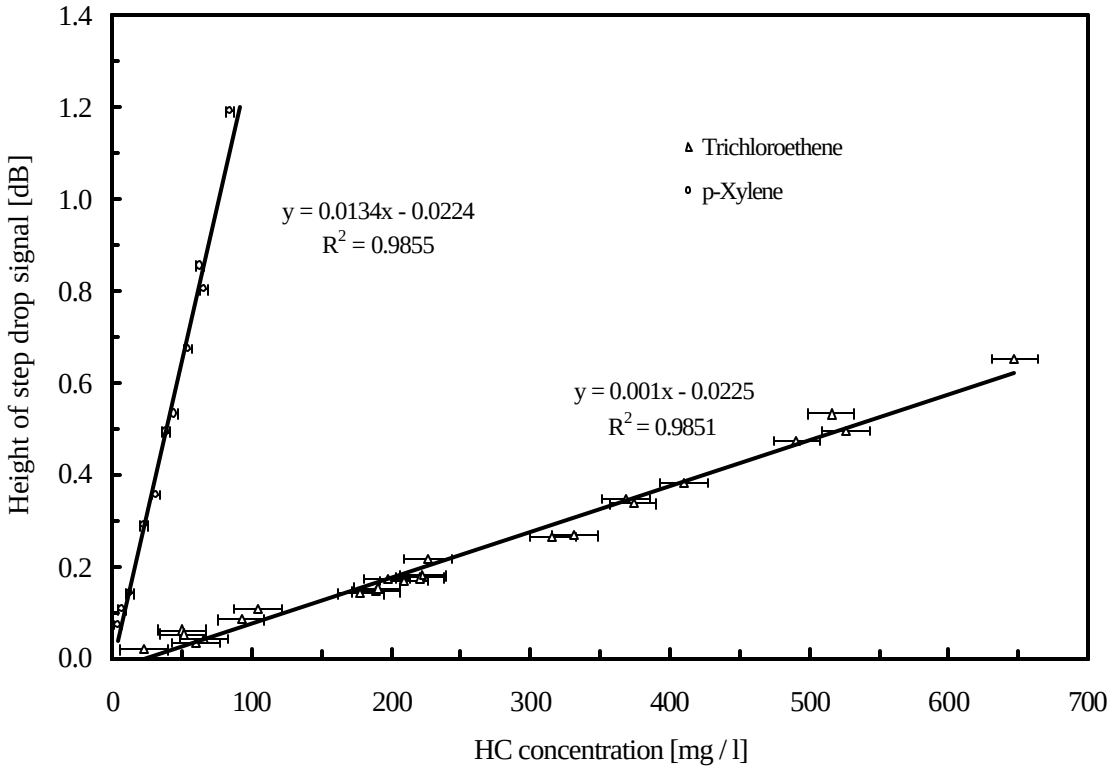

Fig. 5. *Step drop signal height vs. HC concentration for aqueous solutions of p-xylene and trichloroethene; length of contact zone: 2 m; difference signal of sample solution and water reference.*

SUMMARY

The investigations presented in this paper prove the feasibility of distributed chemical sensing of liquid apolar HCs and of aqueous HC solutions by using optical time-domain reflectometry in a polymer-clad optical fiber. In these experiments the backscatter light from the sensing fiber was affected via the evanescent wave by the RI increase induced by HCs penetrating into the cladding. The local RI increase in the cladding leads to a step drop signal in the backscatter trace, which can be used to localize the HC contact point. The height of the obtained step drop signal (sensitivity) is strongly dependent on the RI and polarity of the HC compound. Due to the fact that the signal width of this step drop signal is correlated with the interaction length between sensing fiber and the HC it is possible to extract additional information on the spatial extension of a HC contamination. The sensor fiber can have a length of up to 1 km and location of HC leakage is possible with a typical spatial resolution of 1-5 m depending on the laser diode pulse width used for the measurement. Typical response times of the system for contact with liquid HCs (which have not been discussed in this paper) are in the range of 30 s - 3 min.

These features open up possibilities for applications of the distributed fiber-optical sensor system in HC leakage control, e.g., in tank farms or chemical pipelines. Due to the absence of any water interference, the hydrophobic sensor cable can also be deployed in aqueous environments and is able to detect even apolar HCs that are homogeneously dissolved in water. Thus, it could also be applied for leakage monitoring at liners of waste

disposal sites. This could be an advantage compared with commercially available MTDR systems with HC sensitive coaxial cables.

Further work is in progress to optimize the control software of the sensor system and the evaluation algorithms for automatic localization of the position of an HC contact and the spatial extension of the contact zone.

REFERENCES

Barnoski, M. K., and Jensen, S. M., 1976, Fiber waveguides: a novel technique for investigating attenuation characteristics: Appl. Optics, **15**, 2112-2115.

Browne, C. A., Tarrant, D. H., Olteanu, M. S., Mullens, J. W., and Chronister, E. L., 1996, Intrinsic sol-gel clad fiber-optic sensors with time-resolved detection: Anal. Chem., **68**, 2289-2295.

Bürck, J., Krämer, K., and Roth, S., 2000, Faseroptisches Sensorsystem zur Erkennung und Ortung von Kohlenwasserstoff-Leckagen: Technische Überwachung, **41** (11/12), 18-22.

Bürck, J., Mensch, M., and Krämer, K., 1998, Field experiments with a portable fiber-optic sensor system for monitoring hydrocarbons in water: Field Anal. Chem. & Technol., **2**, 205-219.

Bürck, J., and Sensfelder, E., 1998, Optical fiber sensors for the distributed measurement of hydrocarbons; Symposium on Chemical, Biochemical, and Environmental Fiber Sensors X, SPIE 3540, Bellingham, 98-109.

Bürck, J., Sensfelder, E., and Ache, H. J., 1997, Distributed sensing of hydrocarbons using evanescent wave interactions in a silicone-clad optical fiber; Symposium on Chemical, Biochemical, and Environmental Fiber Sensors IX, SPIE 3105, Bellingham, 21-30.

Gloge, D., 1971, Weakly guiding fibers: Appl. Optics, **10**, 2252-2258.

Kharaz, A., and Jones, B. E., 1995, A distributed optical-fiber sensing system for multi-point humidity measurements: Sensors & Actuators A, 46-47, 491-493.

Kvasnik, F., and McGrath, A. D., 1989, Distributed chemical sensing utilizing evanescent wave interactions; Symposium on chemical, biochemical, and environmental fiber sensors I, SPIE 1172, Bellingham, 75-82.

Lieberman, R. A., 1991, Distributed and multiplexed chemical fiber optic sensors; Symposium on distributed and multiplexed fiber optic sensors, SPIE 1586, Bellingham, 80-91.

Michie, W. C., Culshaw, B., McKenzie, I., Konstantaki, M., Graham, N. B., Moran, C., Santos, F., Bergqvist, E., and Carlstrom, B., 1995, Distributed sensor for water and pH measurements using fiber-optics and swellable polymeric systems: Optics Letters, **20**, 103-105.

Michie, W. C., Culshaw, B., Konstantaki, M., McKenzie, I., Kelly, S., Graham, N. B., and Moran, C., 1995, Distributed pH and water detection using fiber-optic sensors and hydrogels: J. Lightwave Technol., **13**, 1415-1420.

Neumann, E.G., 1978, Optical time domain reflectometer: comment: Appl. Optics, **17**, 1675.

Potyrailo, R. A., and Hieftje, G. M., 1998, Optical time-of-flight chemical detection: Spatially resolved analyte mapping with extended-length continuous chemically modified optical fibers: Anal. Chem., **70**, 1453-1461.

Reichardt, Ch., 1994, Solvatochromic dyes as solvent polarity indicators: Chem. Rev., **94**, 2319-2358.

Rogers, A. J., 1988, Distributed optical-fiber sensors for the measurement of pressure, strain and temperature: Physics Reports, **169**, 99-143.

Sensfelder, E., Bürck, J., and Ache, H. J., 1998, Characterization of a fiber-optic system for the distributed measurement of leakages in tanks and pipelines: Appl. Spectrosc., **52**, 1283-1298.

Snyder, A. W., and Love, J. D., 1983, Optical Waveguide Theory: Chapman and Hall, London, 127-130.

QUASI DISTRIBUTED OTDR CRACK SENSOR FOR REINFORCED CONCRETE STRUCTURES

Zhongyu Chen[1], Xianglin Gu[2], and Farhad Ansari[3]

[1]University of Illinois at Chicago, Dept. of Civil & Materials Engineering,
842 W. Taylor St., Chicago, Illinois 60607-7023.
[2]University of Illinois at Chicago, Dept. of Civil & Materials Engineering,
842 W. Taylor St., Chicago, Illinois 60607-7023; gxiangl@online.sh.cn
[3]University of Illinois at Chicago, Dept. of Civil & Materials Engineering,
842 W. Taylor St., Chicago, Illinois 60607-7023.
(312) 996-2437, fansari@uic.edu

ABSTRACT

A quasi-distributed fiber optic sensor is developed for embedment in concrete structures. The sensor principles are simple, and therefore, practical for crack detection and deformation measurement in civil structural applications. The distributed sensor developed herein operates based on the intensity measurements of optical power. The sensor consists of a number of individual segments on one line, with gauge lengths designed according to the structural and materials requirements. An optical time domain reflectometers (OTDR) was employed for interrogation of the sensor signal. The study reported herein is aimed at demonstrating the applicability of this sensor in monitoring performance of concrete structures. Crack detection methodologies were established through experiments with plain concrete beams. Structural monitoring capability of the sensor was evaluated through experiments with reinforced concrete beams.

INTRODUCTION

Full-scale monitoring of structures requires sensing at multiple points and within large volumes. Therefore, many sensors are normally required. For this reason, various multiplexing technologies have been considered in civil structural applications (Sirkis, 1998). The Bragg grating has been the dominant sensor of choice in most cases (Morey, et. al., 1989, Kersey, 1993). Bragg grating sensor architectures have been successfully employed in concrete elements in order to monitor strains in reinforcing bars and prestressing tendons (Nawy, 1992). Distributed sensors are most suited for large structural applications, since all the segments of the optical fiber act as sensor, and therefore, the perturbations within various segments of the structure can be sensed. However, distributed sensors have not found widespread usage in civil structural applications. There is a need for development of optimum distributed sensing technologies for civil structures.

Two of the most widely employed distributed sensor methodologies correspond to optical time domain reflectometry (Ansari, 1997) and Brillouin scattering (Brown, et. al.,1998). In optical time domain reflectometry, Rayleigh or Fresnel scattering is used for transduction of structural perturbations. On the other hand, in Brillouin scattering the Doppler shift in the frequency of light is related to the measurands. It is also possible to develop sensors that provide average values of measurands over specific gauge lengths. A multi-gauge-distributed sensor is comprised of the assemblage of individual sensors in series, each measuring an average value of measurand over distinct segments. One such sensor is developed here for application in concrete structures. The basic principle of operation for the crack sensor is based on intensity variation of the optical power within the fiber due to the initiation and opening of cracks. This article reports on the functional characteristics of the sensor in terms of resolution, hysteresis, and sensitivity. Moreover, it demonstrates the applicability of the sensor in condition monitoring of reinforced concrete elements under monotonic and fatigue loading conditions.

METHODOLOGY

Optical Time Domain Reflectometers (OTDR) have been developed for characterization of anomalies in the telecommunication links. It is an important tool for detection of transmission irregularities due to splice losses, and local damage along the fiber length. OTDR also provides capability for one-port operation at the fiber input with no need to access the fiber output. In a basic OTDR measurement, a laser transmitter launches an optical pulse into the fiber under test. The optical signal travels through the optical fiber and then it is reflected back through the fiber into the OTDR. Signal reflection occurs due to Rayleigh and Fresnel back scattering events. Microscopic density fluctuations within the core of the fiber material give rise to refractive index impurities which in turn are responsible for Rayleigh back scattering. Fresnel reflections originate from many points along the fiber where abrupt and discrete discontinuities occur in the index of refraction. One example is poorly spliced and or connectorized regions along the length of the fiber. Straining of the fiber within a segment bounded by the spliced regions result in intensity fluctuations of the reflected signal, which is due to the loss of optical power at the air-to-fiber interface in the spliced point.

Single Gauge Sensor

The multi-gauge sensor developed here requires optical segmentation of the fiber at several points along its length in order to create Fresnel reflection points. In this way, an optical fiber is divided into several gauge lengths through which monitoring of cracking and deformations are accomplished. The back-reflected Fresnel signal is employed to pin point, L, the location of the disturbance along the total length of the fiber. Moreover, the deformation is sensed through the intensity variations of the Fresnel-peaks in the back-scattered signal. Fresnel points can be created by using a special precision optical fiber cleaver in order to slice the fiber into a number of smaller segments, each representing a gauge length. The cleaved fibers are spliced along one line in order to create the distributed sensor. In the formulations to follow, both transmission and reflection losses are used in the transduction of the measurand.

A typical segment of a sensor between two Fresnel points is shown in Fig.1. The Fresnel signals are also given in the schematics representing the OTDR screen. It is assumed that the optical fiber consists only of one gauge length between the two Fresnel points representing the reference and reflector planes R0 and R1, respectively. The pulse of laser enters the fiber from the reference plane at R0 with intensity I0. It is partially transmitted and reflected at the reflector plane R_1. The reflected signals re-enter the OTDR

and create the Fresnel peaks. The incident, transmitted and reflected signals are represented by I_0, I_T and I_R, respectively. Accordingly only a portion of the incident signal is transmitted, whereas, the rest is reflected. The insertion loss, I_{lo}, that represents the ratio of incident and the actual transmitted signal is given in logarithmic scale in decibels (db) as:

$$I_{lo} = 10 \log \frac{I_0}{I_T} \quad [1]$$

In a similar manner the return loss of the incident light is:

$$R_{lo} = 10 \log \frac{I_0}{I_R} \quad [2]$$

In the absence of strain, I_{lo} and R_{lo} remain constant. However, upon straining, I_{lo} and R_{lo} vary with strain. Variations in I_{lo} and R_{lo} are manifested in the amplitude of the Fresnel reflection peaks. Accordingly, the insertion and return losses can be employed for the determination of strain or deformation through the following relationships:

$$\Delta I_{lo} = \left| I_{lol} - I_{lo} \right| \quad [3]$$

$$\Delta R_{lo} = \left| R_{lol} - R_{lo} \right| \quad [4]$$

$$d \text{ or } e = a \Delta I_{lo} \left(or \quad e = b \Delta R_{lo} \right) \quad [5]$$

Where,

ΔI_{l0} = insertion loss after strain
ΔR_{lo} = return loss after strain
e = average strain within the gauge length, d, of the optical fiber
d = deformation of the optical fiber along the gauge length, d
a, b = proportionality constant relating deformations and strains to the optical loss factors.

As noted in Eq.(6), both of the loss parameters, ΔI_{l0}, and ΔR_{l0} can be employed for the determination of strain. However, at the same strain level, more sensitivity can be achieved with the reflection loss, since upon reflection the optical signal travels through twice as many Fresnel points.

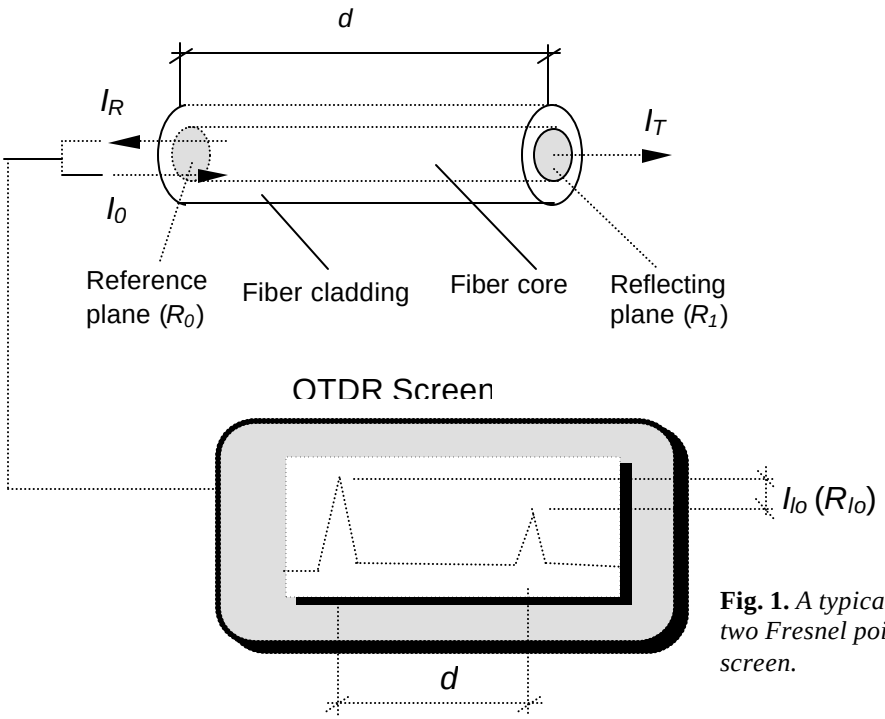

Fig. 1. *A typical segment of the sensor between two Fresnel points and their peaks in the OTDR screen.*

Multi-Gauge Distributed Sensor

A distributed sensor consisting of *n*-segments in series is schematically depicted in Fig. 2. The insertion and return losses for the i-th reflector plane (R_i) with respect to the reference plane (R_0) is expressed as:

$$I_{lo}^{\ i} = 10\log\frac{I_0}{I_{Ti}} \qquad (i = 1,2.\cdots,n) \qquad [6]$$

$$R_{lo}^{\ i} = 10\log\frac{I_0}{I_{Ri}} \qquad (i = 1,2,\cdots,n) \qquad [7]$$

where, $I_{lo}^{\ i}$ and $R_{lo}^{\ i}$ pertain to the insertion and return losses of the i-th segment at the reference plane. The reference plane, R_0, corresponds to the point of laser pulse entry into the first segment (i=1). I_{Ti} and I_{Ri} are the transmitted and the return light intensities of the *i*-th fiber optic segment, respectively. I_{Ti} and I_{Ri} represent accumulated insertion and reflection losses from sensor 1 all the way to sensor *i*. To monitor and measure strain and deformation in the i-th sensor alone, it is necessary to obtain the insertion and return loss of the *i*-th fiber optic segment according to the following relationships:

$$I_{lo}^{\ (i)} = 10\log\frac{I_{Ti-1}}{I_{Ti}} \qquad (i = 1,2,\cdots,n) \qquad [8]$$

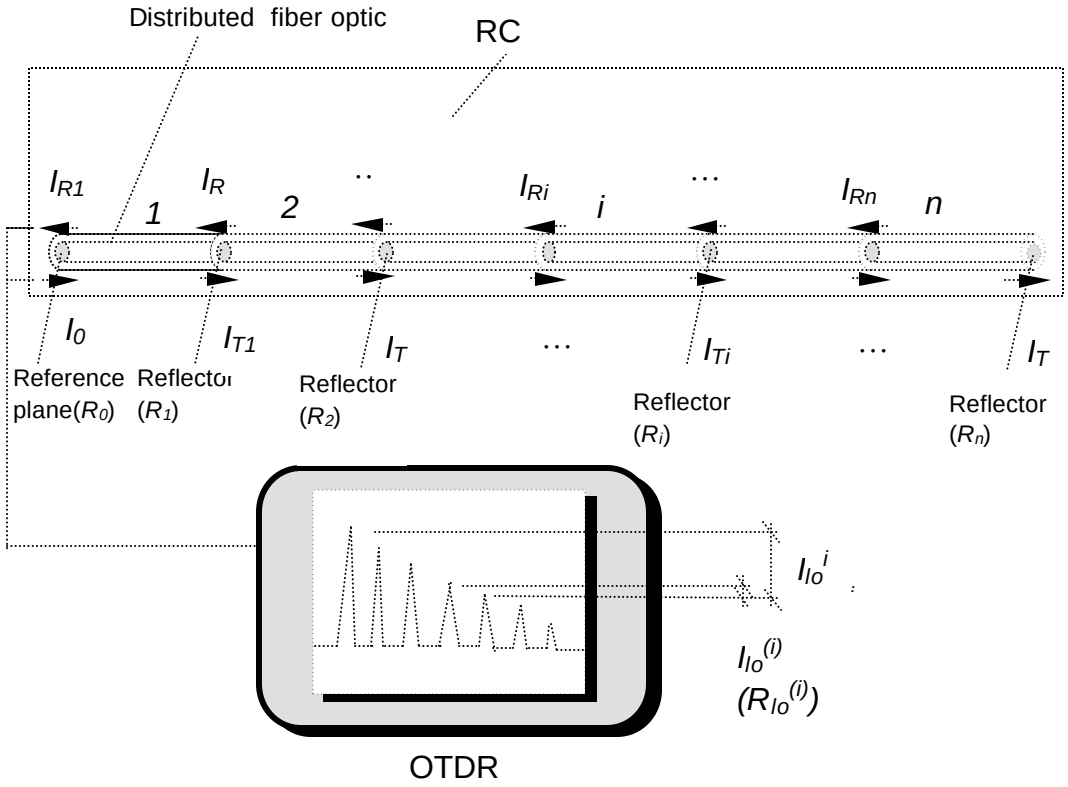

Fig.2. *Multi-gauge fiber optic sensor*

$$R_{lo}^{(i)} = 10\log\frac{I_{Ti-1}}{I_{Ri}} \qquad (i = 1,2,\cdots,n) \tag{9}$$

By combining Eqs. 6 and 8, the following expressions may be derived:

$$\begin{cases} I_{lo}^{(1)} = I_{lo}^{1} \\ I_{lo}^{(i)} = 10\log\dfrac{I_{Ti-1}}{I_{Ti}} = 10\log\dfrac{I_0/I_{Ti}}{I_0/I_{Ti-1}} = I_{lo}^{i} - I_{lo}^{i-1} \qquad (i = 2,3,\cdots,n) \end{cases} \tag{10}$$

Where, $I_{lo}^{(i)}$ corresponds to the transmission loss of the the *i*-th fiber optic segment alone. To develop an expression for the return loss of the i-th segment alone, Eq. (7) is used in the following manner:

$$R_{lo}^{i} - R_{lo}^{i-1} = 10\log\frac{I_0/I_{Ri}}{I_0/I_{Ri-1}} = 10\log I_{Ri-1} - 10\log I_{Ri} \qquad (i = 2,3,\cdots,n) \tag{11}$$

Combining Eqs.(8) and (9) results in the following expression :

$$R_{lo}^{(i-1)} - I_{lo}^{(i-1)} = 10\log\frac{I_{Ti-2}}{I_{Ri-1}} - 10\log\frac{I_{Ti-2}}{I_{Ti-1}} = 10\log\frac{I_{Ti-1}}{I_{Ri-1}}$$
$$= 10\log I_{Ti-1} - 10\log I_{Ri-1} \qquad (i = 2,3,\cdots,n) \qquad [12]$$

Return loss in the i-th segment, $R_{lo}^{(i)}$, is obtained by combining Eqs. (11) and (12):

$$\begin{cases} R_{lo}^{(1)} = R_{lo}^{1} \\ R_{lo}^{(i)} = R_{lo}^{i} - R_{lo}^{i-1} + R_{lo}^{(i-1)} - I_{lo}^{(i-1)} \qquad (i = 2,3,\cdots,n) \end{cases} \qquad [13]$$

It is important to note that the R_{l0}^{i-1} and $R_{lo}^{(i-1)}$ do not cancel out as they different per definition. It is then possible to evaluate strain in the individual segments *i=1…n* through Eqs. (3), (4), and (5). The optical fiber sensor will be able to sense the cracking and the deformations within its various segments. Either one of the expressions for the insertion loss or the reflection loss would yield similar results. These expressions are directly programmed in the OTDR for real-time sensing and monitoring activities. The transform coefficients, a and b in Eq. (5) which relate the intensity losses to strain, are determined through experimentation. This will be discussed next.

EXPERIMENTAL PROGRAM

Capability of the distributed sensor in sensing and measurement of crack widths were evaluated through a series of tests with reinforced concrete beams. It was however necessary to determine the crack detection capability of the sensor prior to the experimentation with the reinforced concrete elements. For this reason, the crack monitoring capability of the sensor was evaluated through experimentation with plain concrete specimens. Experimentation with plain concrete specimens involved embeddment of a single sensor in concrete beams. Beam dimensions were 508mm × 76.2mm × 76.2mm (20in. × 3in. × 3in.), with a span of 457.2mm (18in.). Beams were tested under three-point-bending in tabletop closed-loop materials testing system. Beams were notched at center span (notch length 1.5 inch), and a Linear Variable Differential Transformer (LVDT) was employed for monitoring of crack opening at the notch tip. The optical fiber sensor was embedded along the span length of the fiber. The sensor was embedded along the line traversing the notch tip. The LVDT attachment was designed to monitor the opening of the crack tip at the level of the optical fiber sensor. The specimen loading was accomplished in displacement control in order to obtain the post-peak (post-cracking) response of the concrete beam. Fig.3 corresponds to typical return loss measurements (in dB), versus the displacement of the crack tip by the LVDT. Examination of results indicated that the optical fiber did not respond to deformation levels below 0.006 inches (0.15mm). This result was expected, since in contrast to other categories of fiber optic sensors, the intensity type sensor exhibits lower sensitivity. However, comparison of the optical fiber signal with the load displacement relationship reveals that the sensor effectively responds to the initiation and progression of cracks (Fig.4). This is indicated by increase in the return loss of the optical fiber in the post peak load region (post-cracking region) after a period of dormancy in the pre-peak region. Moreover, it can be observed that the relationship between the return loss and the crack opening after the peak is for all practical purposes linear. These findings indicate that the particular type of intensity sensor developed here responds only to the crack openings, and this relationship can be employed for measurement of the crack width. Evaluations of the distributed sensor in reinforced concrete beams are discussed next.

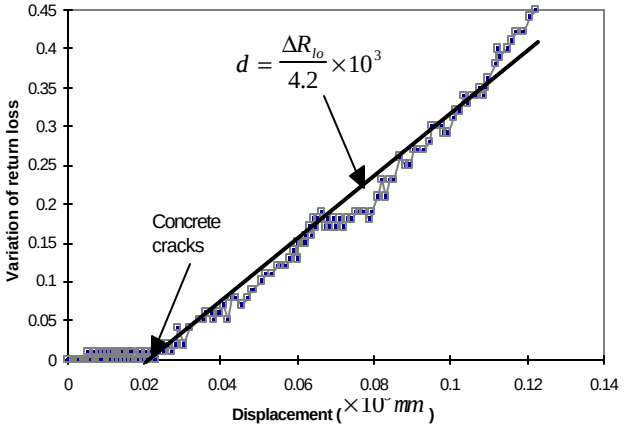

Fig. 3. *Typical return loss versus displacement response of the optic fiber.*

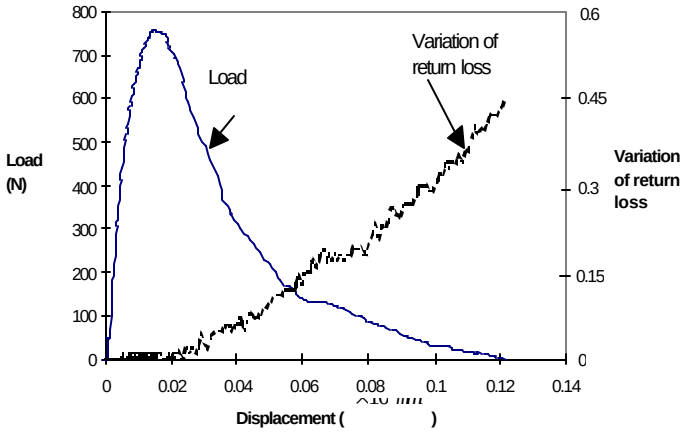

Fig. 4. *Comparison of the load-displacement relationship with the optical fiber sensor response to cracking*

Experimentation with reinforced concrete (RC) beams included both fatigue as well as monotonic loadings. Beam dimensions and the reinforcement pattern for the three RC beams are shown in Fig.5a. The RC beams were given alphabetic designations A, B, and C. Beam C was constructed with reduced rebars in order to produce larger crack widths. This allowed for assessment of the sensor's capability in

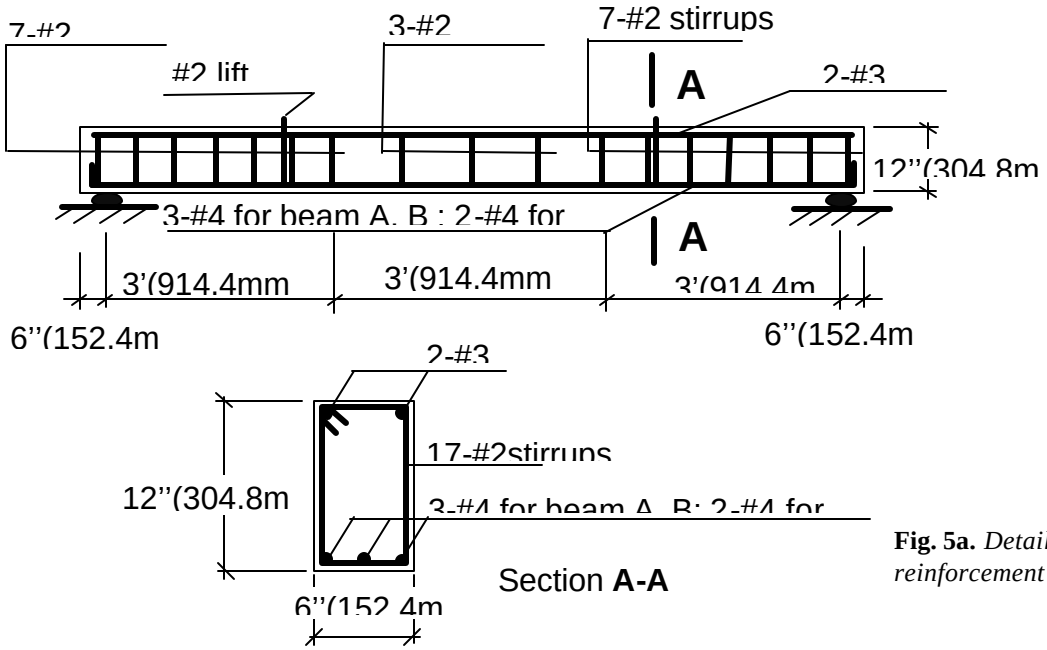

Fig. 5a. *Details of the reinforcement pattern in beams*

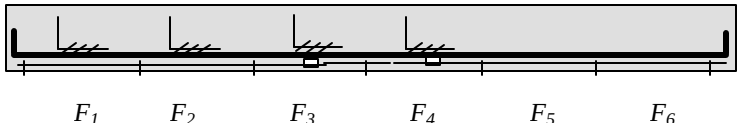

Fig. 5b. *Fiber optic sensor location and the gauge length designations in the beam*

Fig. 5. *Beam dimensions, reinforcement, and fiber optic sensor gauge designations in RC-beams*

measuring a range of crack widths. The distributed sensor was strategically placed below the tensile steel in the concrete cover, near the bottom surface of the beam. At this location, it was easy to compare the crack detection and measurement capability of the sensor against visual observations and measurements. The single line distributed sensor consisted of six gauge lengths (457-mm) along the span (F_1 through F_6 in Fig.5b).

Beams were tested in a closed-loop servo-hydraulic testing system under four-point bending with loads applied at the middle third of the span. Beam A was subjected to fatigue loading for 1–million cycles at 5-Hz. Fatigue load amplitude was varied between 17.8 and 53.4 KN (4 to 12 Kips). Data acquisition posed a problem, since a tremendous amount of data was being accumulated for the duration of 1-million cycles. Accordingly, it was decided to program the system so that data could be collected after every 36000 and/or 72000 load cycles. At the end of the millionth cycle, the beam was loaded monotonically until failure. Cracking of the beam was monitored by the optical fiber sensor and visual inspections. Visual inspections involved marking the crack locations; their progression and measurement of crack widths by a micrometer scale graduated caliper (crack comparator). Beams B and C were instrumented in a manner similar to beam A and they were loaded monotonically until failure.

Experimental Results

The focus of the experimental observations was the pertinence of the sensor in structural monitoring applications. Survivability of the sensor under large deformation cyclic loads, crack detection and measurement capabilities, signal referencing after periods of data acquisition dormancy, and strain monitoring capabilities were among important observations made during this study. Accordingly, the sensor was embedded within the concrete in a location that was obviously prone to severe cracking and large deformations. This allowed for the evaluation of the crack sensor in terms of its practicality for structural monitoring applications

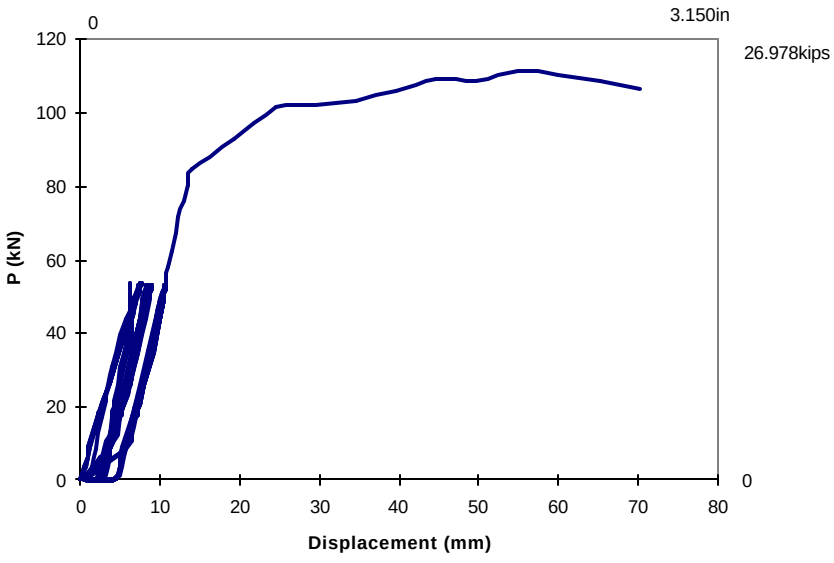

Fig. 6. *Load-displacement relationship for beam A*

A typical load versus center-span deflection curve for the reinforced concrete beam is shown in Fig.6. This figure corresponds to beam A, which was fatigue loaded to million cycles and then the load was monotonically increased until failure. Several cracks formed along each individual gauge length of the optical fiber sensor (F_1 through F_6). The sensor detected the initiation of all the cracks along the span, and it measured crack widths along individual gauge lengths. Crack widths were acquired in a cumulative manner within the individual gauge lengths.

Crack patterns at failure, and crack width measurements as acquired by the optical fiber sensors in beams A, B and C are shown in Figs. 7 through 9. Fig.5 pertains to beam A, which was loaded in fatigue. Crack widths after the first and 1-millionth loading cycles are compared in this figure. Figs 8 and 9 pertain to crack widths for beams B and C tested under monotonic loading conditions. It is possible to discern the effect of cyclic loading on crack widths by comparison of results for beams A and B since they had similar designs. As shown in Figs. 7 and 8, at the same load level of 12 kips, the maximum crack width in beam A after the millionth cycle was approximately 4-times larger than the maximum crack width in beam B. Deterioration of the beam due to cyclic loading is also apparent in Fig.7 by observing that the cracks readily remained open during the unloading cycles.

CONCLUSIONS

A multi-gauge-distributed sensor is developed for applications in concrete structures. The sensor operates based on the intensity measurements of optical power. An experimental program was undertaken in order to study the feasibility of the embedded sensor in detection of cracks and measurement of deformations in concrete structures. Experiments with plain concrete provided the basis for crack detection capabilities of the sensor. Subsequently the distributed sensor was embedded in the tension zone of reinforced concrete beams, where it would be easy to keep a good accounting of the cracks formed. This arrangement facilitated evaluation of the sensor in monitoring of cracks. Experimental program involved monotonic as well as fatigue loading of reinforced concrete beams. The multi-gauge sensor was capable of measuring the cracks widths within the individual segments of the sensor. These sensors do not exhibit hysteresis, and for this reason they can be used in applications pertaining to bridge structures where the mode of loading is that of fatigue. Future research should include sensors of various gauge lengths in order to match the sensor gauge to the size of the structural element.

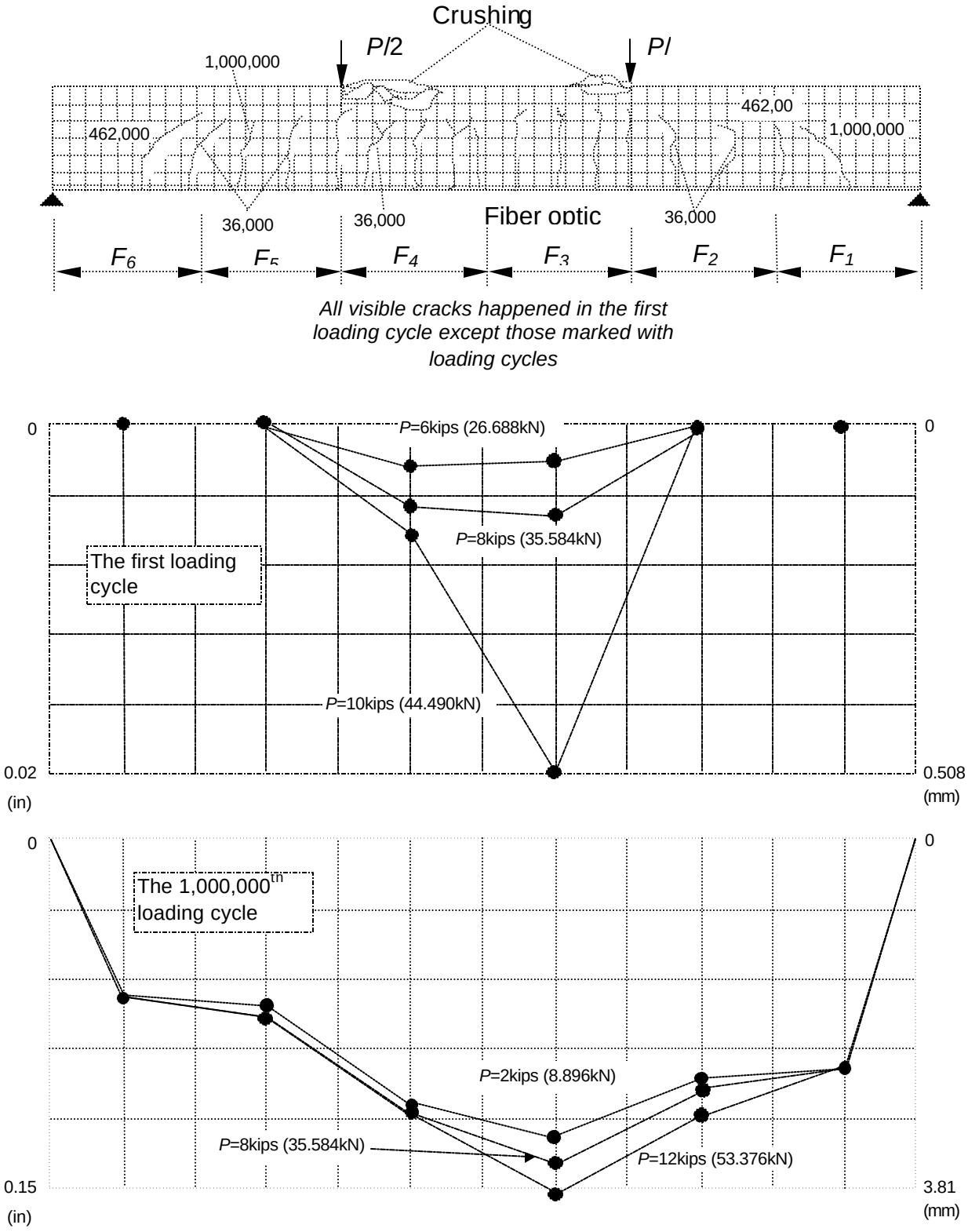

Fig. 7. *Distribution of cracks and crack openings for beam A*

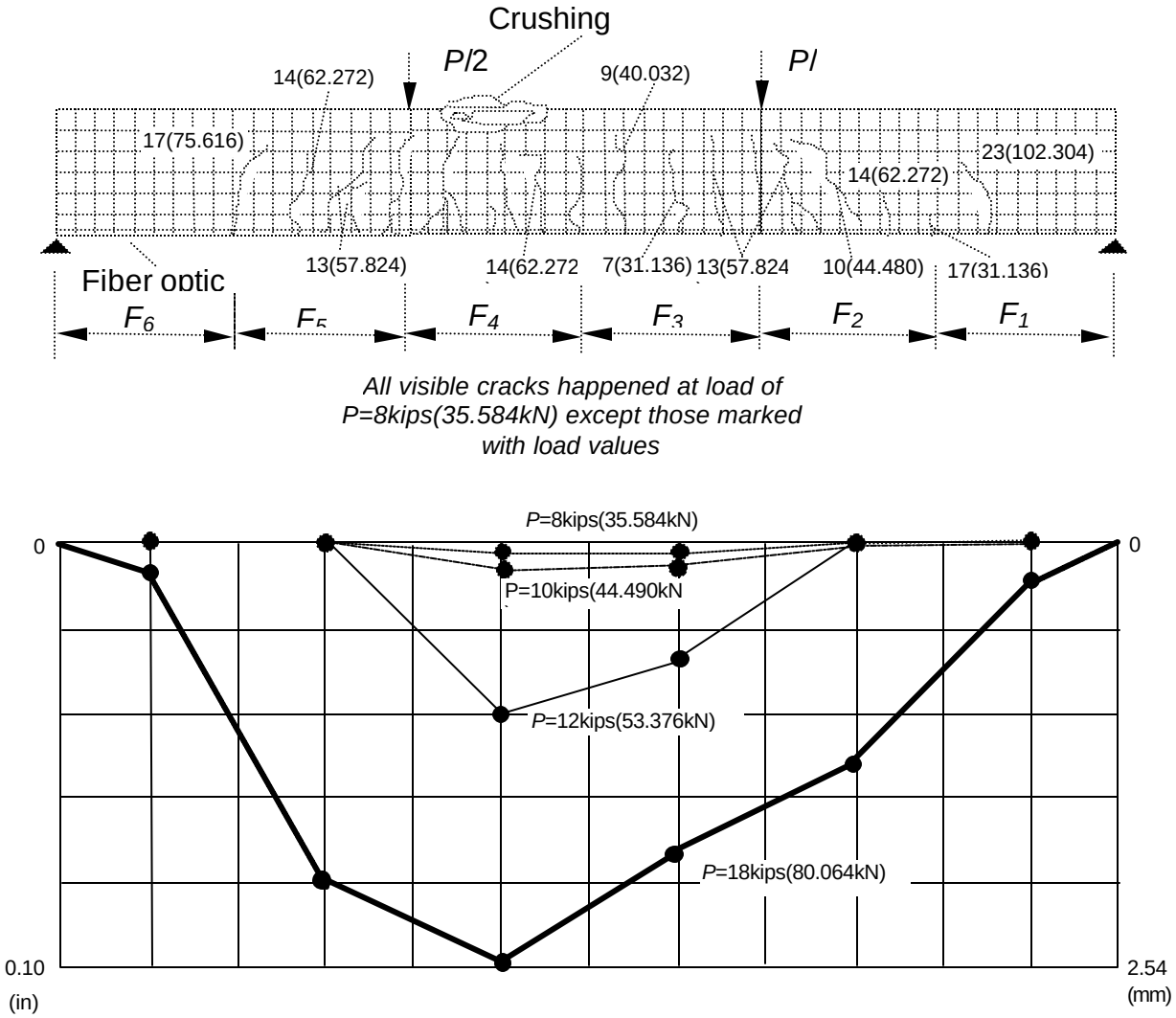

Fig.8. *Distribution of cracks and crack openings for beam B*

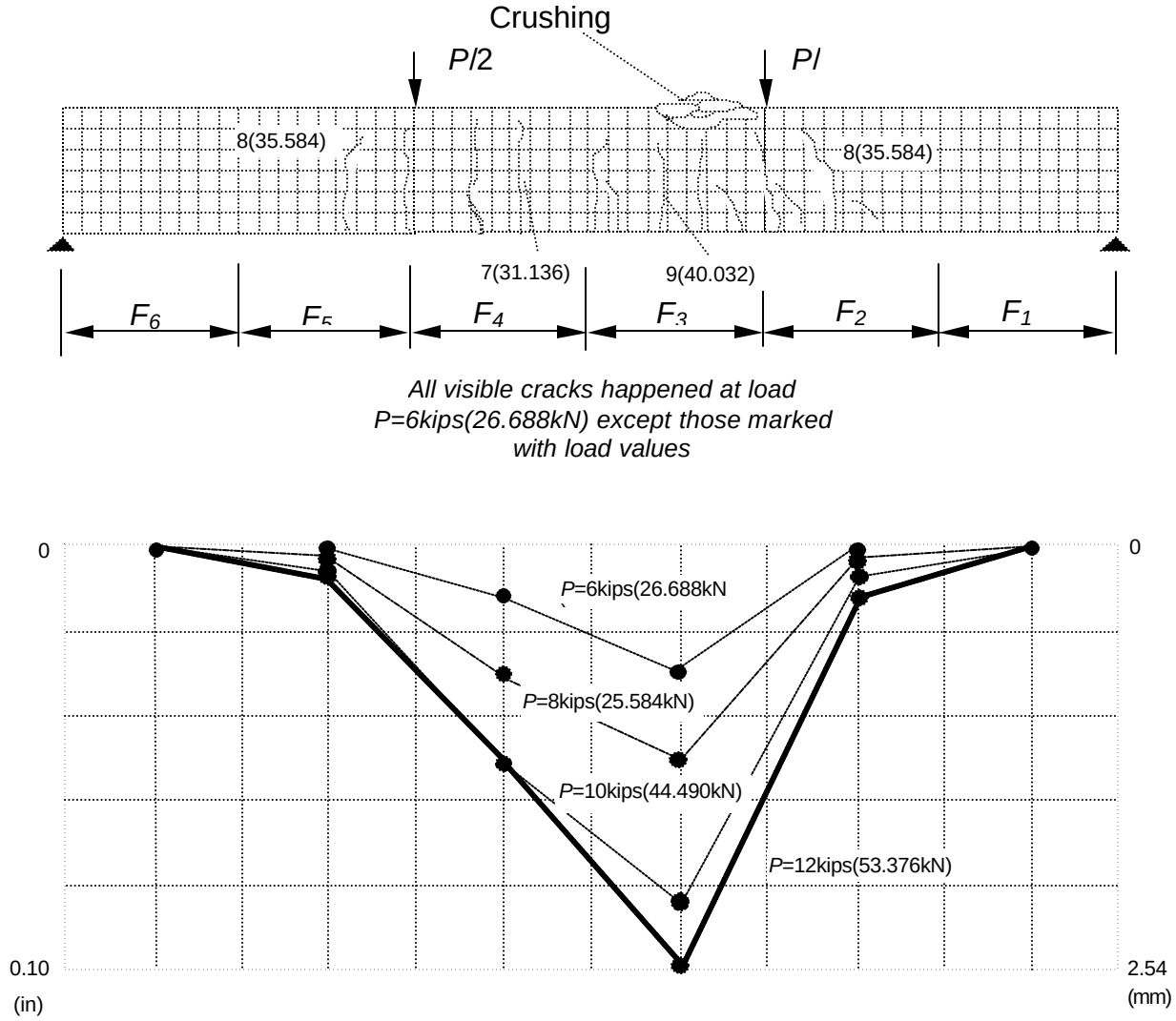

Fig. 9. *Distribution of crack and crack openings for beam C*

REFERENCES

Ansari, F., 1997, State-of-the-art in the Applications of Fiber Optic Sensors to Cementitious Composites, Cement & Concrete Composites, **19**, No. 1, 3-19.

Brown, A., De Merchant, M., Bao, X., Bremner, T., 1998, Advances in Distributed Sensing Using Brillouin Scattering Proc. SPIE, 3330: 294-300.

Kersey, A.D., Morey, W.W., 1993, Multiplexed Bragg Grating Fiber – Laser Strain Sensor System with Mode-Locked Interrogation Electronics Lett. **29**, 112

Morey, W., Meltz, G., and Glenn, D. H., 1989, Fiber Optic Bragg Grating Sensors, Proc. SPIE, 1169, Fiber Optic and Laser Sensors: 98-108.

Nawy, E., Prohaska, J., 1992, Fiber Optic Bragg Grating Sensor in Large Scale Concrete Structures,Proc. SPIE, 1798:1-22.

Sirkis, J.S., 1998, Using Bragg Grating Sensor Systems in Construction Materials and Bridges: Perspectives and Challenges, in Fiber Optic Sensors for Construction Materials & Bridges, Ansari, F. Ed., Technomic Press, Lancaster, PA: 44-61.

AN OVERVIEW OF CORROSION DAMAGE DETECTION IN STEEL BRIDGE STRANDS USING TDR

Wei Liu[1], Robert Hunsperger[2], Michael Chajes[3], and Eric Kunz[4]

[1] Dept. of Electrical & Computer Engineering, Univ. of Delaware, Newark, DE 19716; wliu@ee.udel.edu
[2]Dept. of Electrical & Computer Engineering, Univ. of Delaware, Newark, DE 19716; hunsperg@ee.udel.edu
[3] Dept. of Civil & Environmental Engineering, Univ. of Delaware, Newark, DE 19716; chajes@ce.udel.edu
[4] VETEK Systems Corp. 6 Oak Road, Elkton, MD 21921; VETEKsys@aol.com

ABSTRACT

The corrosion of metallic reinforcement is a major threat to aging infrastructure. Prestressed structures such as the bridges built in the early 1950's and 1960's are showing signs of deterioration. The current corrosion detection methods for embedded or encased steel reinforcement suffer from several significant drawbacks. A nondestructive evaluation technique has been developed that is capable of determining the location and severity of corrosion of embedded or encased steel rebar and strands. This technique utilizes time domain reflectometry (TDR). By applying a sensor wire alongside of steel reinforcement (such as a prestressing strand), a transmission line is created. Physical defects of the reinforcement will change the electromagnetic properties of the line. Both analytical models and small-scale laboratory tests have shown that TDR can be effectively utilized to detect, locate and identify the extent of damage in steel reinforcement in this manner. Currently, the TDR method is being used as a permanent corrosion monitoring method for Bridge 8F, a prestressed high-performance concrete adjacent box beam bridge in Fredrica, Delaware. Differential TDR measurements are used to monitor serious damage due to corrosion of the steel. Experimental results from both small-scale laboratory tests and field implementation will be reported.

INTRODUCTION

The corrosion of metallic reinforcement represents one of the leading causes of durability problems affecting aging civil infrastructure. The high-strength steel used for the cables of suspension and cable-stayed bridges is very sensitive to corrosion, and failure of cables is a serious problem due to the limited degree of redundancy in the structure. A reliable, accurate, and economical method for detecting the existence, location, and severity of corrosion-induced damage will lead to increased levels of safety for civil infrastructure, and may enable significant savings to the public by reducing maintenance costs through early corrosion detection.

Historically, visual inspection has been the most effective method of corrosion detection. However, it cannot be used for embedded or encased steel strands. Several indirect nondestructive corrosion detection methods have been developed. They can be grouped into two main categories: mechanical methods and electromagnetic methods. Mechanical methods use force measurement. The tension force in a bridge cable is measured either directly by pulling on the cable or indirectly by observing its free damped vibrations. The vibration frequency reveals the tension in the cable. Electromagnetic methods are based on the fact that the high-strength steel cables are very good electrical conductors. Damage to the cable will change its electrical properties. One can use resistance measurement, potential measurement (utilizing electrochemical reaction due to active corrosion) (Wietek and Kunz, 1995), or magnetic inductance scanning to detect corrosion (Zahn and Bitterli, 1995). To date, these methods have had varying degrees of success in detecting the presence of corrosion, but all have disadvantages, and many are uneconomical. One common drawback to these methods is that the location and nature of the corrosion is very difficult to determine.

In this paper, a nondestructive evaluation technique for detecting damage in steel strands and rebars using time domain reflectometry (TDR) is described. The method being developed has the advantage over existing methods in that it can detect, locate, and identify the extent of corrosion.

TDR is a well-established technique in the field of electrical engineering that has been used for many years to detect faults in transmission lines (Hewlett-Packard, 1988). There are obvious similarities between bridge cables and transmission lines. The bridge cable can be modeled as an asymmetric, twin-conductor transmission line by applying a sensor wire along with the cable (Bhatia *et al*., 1998). Physical defects of the steel strand, such as abrupt pitting corrosion, general surface corrosion, and voids in the grout, will change the electromagnetic properties of the line. These defects, which can be modeled as different kinds of discontinuities, can be detected by TDR.

ANALYTICAL MODELS

Modeling Bridge Cables

Time domain reflectometry is traditionally used in the field of electrical engineering to detect discontinuities in a transmission line. A bridge cable is a good conductor embedded in a dielectric (concrete). By applying a sensor wire along side of the steel cable, the twin-conductor transmission line geometry is obtained (see Figure 1). However, there are still some important differences between this system and the classic transmission line. First, the two conductors have different diameters. Next, they are embedded in grout and encased in a tube; this imposes a complicated boundary condition. However, if the dimension of the grout is much larger than the dimension of the steel cable and the sensor wire, one can assume these two conductors are in a uniform concrete medium, i.e., the influence of the tube is neglected. This simplification will not appreciably affect the analysis since the electromagnetic field is concentrated between the two conductors and does not significantly extend through the grout to the tube.

For a thorough analysis of the wave propagation in this transmission line, one needs to solve Maxwell's equations with boundary conditions imposed by the physical nature of the bridge cable and surrounding grout. It is also possible to represent the line by distributed parameter equivalent circuit and discuss wave propagation in terms of voltage and current. The distributed parameter equivalent circuit is shown in Figure 2. It possesses a uniformly distributed series resistance R, series inductance L, shunt

capacitance C, and shunt conductance G. (R, L, C, and G are defined per unit length.) By studying this equivalent circuit, several characteristics of the transmission line can be determined.

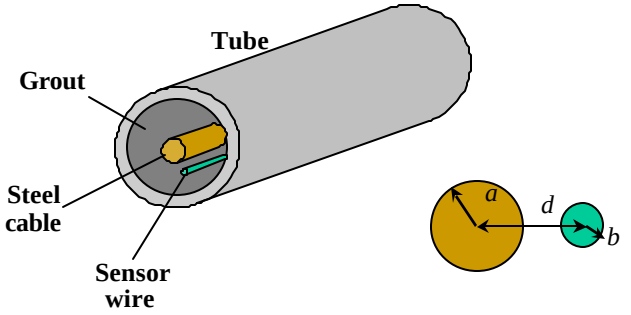

Fig. 1. *Twin-conductor transmission line geometry of a bridge cable with sensor wire, where a is the radius of the steel cable, b is the radius of the sensor wire, and d is the center-to-center distance between the cable and wire.*

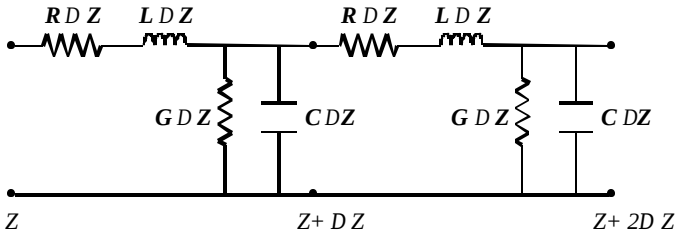

Fig. 2. *Distributed parameter equivalent circuit of a transmission line.*

The propagation constant, γ, defines the phase shift β and attenuation α per unit length. It is given by

$$g = a + jb = \sqrt{(R + jwL)(G + jwC)}$$

The velocity at which the voltage travels down the line can be defined in terms of β:

$$v_p = w/b$$

The characteristic impedance, Z_0 , defines the relationship between voltage and current in the line. It is given by

$$Z_0 = \sqrt{\frac{R + jwL}{G + jwC}}$$

Distributed Parameters

To study the electrical properties of the cable, it is desirable to obtain the distributed parameters associated with the cable. The capacitance per unit length is calculated by considering the electric field of two parallel infinitely long straight line charges of equal and opposite uniform charge densities. The equipotential surfaces are cylinders with axes parallel to the line charges. If a perfectly conducting cylinder is placed in any equipotential surface, the electric field will not be disturbed. By placing the two conductors in two equipotential surfaces, and calculating the potential difference, the capacitance per unit length of the line is obtained to be (Liu, 1998)

$$C = \frac{2p\,e}{\cosh^{-1}\left(\frac{d^2 - a^2 - b^2}{2ab}\right)}$$

Since L and C are related by $LC=\mu\varepsilon$ (the product of permeability and permittivity), one can get inductance per unit length from the expression

$$L = \frac{m}{2p}\cosh^{-1}\left(\frac{d^2 - a^2 - b^2}{2ab}\right)$$

The resistance per unit length R has two parts, R_a and R_b, which are the resistance of the bridge cable and sensor wire respectively. To calculate the resistance at high frequency, skin effects must be taken into account. When the operating frequency is f, the resistance of the transmission line is

$$R = R_a + R_b = \sqrt{\frac{fm}{4p}}\left(\frac{1}{a\sqrt{s_a}} + \frac{1}{b\sqrt{s_b}}\right)$$

where, σ is the conductivity of the conductor.

Characteristic Impedance

Since at very high frequencies R increases as the square root of f, whereas ωL increases directly as f, the ratio $R/\omega L$ decreases as the square root of f. Let us consider the case of a single 7-wire prestressing strand (a=0.635cm), the sensor wire being used (b=0.05cm), and a typical distance between them (d=3.175cm). At f=50MHz, the ratio $R/\omega L$ is 1.08×10^{-2}, which is negligible compared with unity; it will clearly become still more negligible at higher frequencies. For concrete with low water content, the conductance is quite small. Additionally, there is an isolating layer of plastic insulation around the sensor wire. Therefore, the conductance G can be considered to be zero. $G/\omega C$ will therefore be approximately zero. Under these circumstances the characteristic impedance is given to a high degree of accuracy by the simplified expression

$$Z_0 = \sqrt{\frac{R + jwL}{G + jwC}} \approx \sqrt{\frac{L}{C}}$$

Upon substituting for C and L the following expression for Z_0 results

$$Z_0 = \frac{1}{2p}\sqrt{\frac{m}{e}}\cosh^{-1}\left(\frac{d^2 - a^2 - b^2}{2ab}\right)$$

The characteristic impedance of the line is a function of a, b, and d. Note that b is much smaller than a and d (see Figure 1), and it remains the same value along the line. However, the radius of the steel cable, a, may be changed if corrosion occurs.

When $b << d$,

$$\frac{dZ_0}{da} \approx -\frac{1}{2p}\sqrt{\frac{m}{e}}\frac{1}{a}\frac{d^2+a^2}{d^2-a^2}$$

This expression has a negative value. This means that the characteristic impedance will increase for a small decrease of a. Since radius a always decreases at a corrosion site, corrosion will cause higher characteristic impedance. This change of impedance can be detected by time domain reflectometry.

It is also noticed that dZ_0/da depends on the value of d^2-a^2. When the sensor wire is close to the steel cable, d^2-a^2 is small, and dZ_0/da is large. In this case, the characteristic impedance will have a greater change for the same decrease of a, and hence the TDR method will be more sensitive.

Modeling different types of corrosion

In order to utilize TDR to detect corrosion, the damage sites of a bridge cable need to be modeled as electrical discontinuities in a transmission line. Several physical defects are of great interest when considering the durability of bridge cables. Among them are abrupt pitting corrosion, general surface corrosion, and voids in the grout.

Pitting Corrosion

Abrupt pitting corrosion is a severe localized damage. It greatly reduces the cross-sectional area of the steel cable. Its length is small compared to the wavelength of the excitation signal. Therefore, it is modeled as an inductor in series with the line. The localized impedance should increase abruptly if pitting corrosion occurs. In TDR measurement, a positive reflection from the site of pitting corrosion is expected. The location of the corrosion site is obtained from the transit time. The reflection amplitude indicates the magnitude of the damage.

Surface Corrosion

Surface corrosion tends to reduce the radius of the cable on the order of a few percent over a part of length of the line. Its length is longer than the wavelength of the excitation signal. Therefore, it can be modeled as a section of transmission line with different characteristic impedance. The extent and length of the corrosion can be determined from the magnitude and duration of the reflection, respectively.

Voids in Grout

Although a void in the grout will not change the strength of the reinforcing cable, it leaves a section of the cable vulnerable to corrosion. The characteristic impedance also depends on ε, which is the dielectric constant of the system. A void in the grout will change this dielectric constant since the contents of the void, usually air and some water, have different electrical properties. Voids tend to reduce the dielectric constant and therefore increase the characteristic impedance. Also, voids will also change the velocity of propagation in the transmission line.

Validation of Transmission Line Model

The bridge cable/wire system is different from traditional transmission lines in many aspects, such as material, geometry, and dimension. The system is not embedded in a uniform medium. For this reason it cannot support pure TEM wave, since the phase velocities in different media would be different. Inside, the propagation mode is quasi-TEM mode. In other words, the fields are essentially the same as those of the static case with only minor differences. Thus, expressions for propagation constant and characteristic impedance (obtained from static solutions) are good approximations.

To test if losses were occurring due to radiative modes of the samples, a 1-meter control sample was checked for electromagnetic radiation using a vector network analyzer. The intensity of the radiative electric and magnetic fields was measured along the length of the sample when an input waveform was applied. It was found that over a range of frequencies from 500 MHz to 20 GHz, the electric field radiated power was more than 60 dB down from the input power. Also, the magnetic field radiated power was 40 dB down from the input power over the range from 50 MHz to 20 GHz (Bhatia *et al.*, 1998). Thus, very little of the energy being sent down the cable is being radiated away as electric or magnetic fields. Therefore, the bridge cable/wire system can be treated as a transmission line.

Existing Structures

While it is true that the model being described here will be applicable only to new structures fabricated with the monitoring wire, the methodology is extendible to various kinds of existing structures.

For detecting corrosion in existing structures, a monitoring wire can be placed outside the grout as long as the wire is parallel to the steel cable and the distance d is not too large. This method is very easy to use. However, the biggest disadvantage of the external sensor wire is that the TDR measurement is less sensitive. The characteristic impedance is less sensitive to the change of the radius a when the sensor wire is far away from the steel cable (i.e. d^2-a^2 is large), since dZ_0/da is inversely proportional to the product of a and d^2-a^2, as mentioned above. However, the corrosion detection will become sensitive when a is small, as in the cases of serious damages. It means that the external sensor wire can be used to detect serious corrosion as well as the internal wire. This fact is of great significance because it allows the evaluation of existing structures.

Theoretically, it is possible to use the metal shielding of a bridge cable as a monitoring wire for defect detection. For existing structures having a metal duct, the metal duct and the embedded steel strand form a coaxial transmission line. The wave propagation, attenuation, and discontinuities in coaxial transmission lines are well studied. If the diameter of the metal shielding is too big compared to the diameter of the strand, undesirable wave propagation modes may exist in the transmission line. A mode is a wave propagation pattern with unique spatial distribution of electromagnetic energy. The TEM mode is the only desirable and allowed mode in most transmission lines. However, a coaxial cable may support TE and TM modes at very high frequencies. In practice, it is important to be aware of the cutoff frequency of the lowest order non-TEM modes to avoid some deleterious effects, such as superposition of two or more propagating modes with different velocity. The presence of TE or TM modes will make TDR measurement difficult since it is equivalent to sending several different signals down the line simultaneously.

EXPERIMENTAL PROGRAM

Small-scale Laboratory TDR Tests

Small-scale laboratory tests have been conducted to verify the effectiveness of TDR in locating and characterizing simulated corrosion sites. Several 1-meter and 3-meter specimens, made from standard rebar and seven-wire strand, with built-in defects were used to study the ability of TDR to detect damage sites. TDR tests were performed on both grouted and ungrouted specimens. Preliminary testing indicated that damage detection for the ungrouted specimens was very similar to that of grouted specimens. According to the analytical model, both propagation constant and characteristic impedance depend on ε_r, the dielectric constant of the surrounding material. Since $\varepsilon_{r\_concrete} > \varepsilon_{r\_air}$, grouted sample will have smaller impedance and smaller propagation velocity. The grout should not introduce significant energy loss over a short length since the monitoring wire is fully insulated. Different grout mixes may have slightly different dielectric constants. However, it will not affect TDR measurements. Because the researchers have access to the damage site when measuring specimens that are not embedded in concrete, such specimens are more convenient to use to study the electromagnetic properties of the simulated corrosion. As a result, bare specimens were mainly used in small-scale TDR tests.

The specimens were connected to the time domain reflectometer through standard 50Ω coaxial cables. The far end of the specimen was connected to a terminating resistive load. A pulse was then sent down the sample and the reflections shown on the oscilloscope. The terminating load was changed from an open to a short to determine where the end of the sample was. The propagation velocity was then calculated.

Figure 3 shows the TDR reflection from a 3-meter steel rebar sample. This sample has 50% pitting corrosion in the middle (1.55m from the front end). Pitting corrosion was simulated by locally grooving the rebar specimens. The TDR measurement was made on a bare specimen. The first step in the waveform corresponds to the generation of the step wave (point A). The wave is launched into a coaxial cable, which is used to connect the sample to the measuring system. The characteristic impedance of this coaxial cable is 50Ω. However, the sample has higher impedance. As a result, there is a positive reflection at the beginning of the sample (point B). The wave travels down the line at v_p, the velocity of propagation. At every point that the excitation signal crosses, the transmission line equations must be obeyed. However, there is a simulated corrosion site at point C. The physical damage changes its electromagnetic properties. Therefore, the transmission line equations are not satisfied and a reflection is generated at this point. The reflected wave is separated from the incident wave in time. This time, $T = T_C - T_B$, is the transit time from point B to the mismatch and back again. At the end of the sample, the wave goes up because the line is terminated by an open circuit (point D). The time interval between points B and D is 23.0ns, which gives a propagation velocity of 2.61×10^8 m/s, i.e.

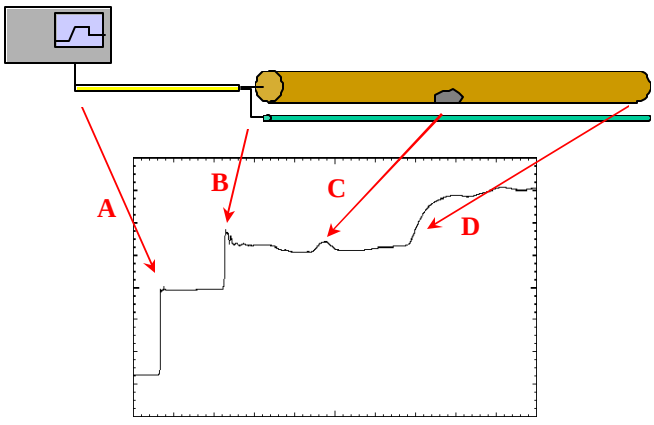

Fig. 3. *TDR return of a 3-meter rebar specimen. The sample has 50% pitting corrosion in the middle.*

about 87% of the speed of light. The location of the damage site is determined as 1.58m from point B since T_C - T_B =12.1ns, which is the correct location.

TDR can not only locate the corrosion, but also reveal the severity of corrosion. Figure 4 shows TDR returns from two seven-wire steel strand samples. The strands are 0.95m long and each strand is 1.27cm (1/2 inch) in diameter. Corrosion was simulated by severing several wires of the strand specimen. The damage was produced over a 7.5cm length, 44cm from the end of the sample. The first marker indicates the initial reflection from the front of sample, and the third marker indicates the reflection from the end of sample 9.94ns later. The propagation velocity is 1.91×10^8 m/s. The initial reflection is positive, which shows that the characteristic impedance of the sample is larger than 50Ω. The impedance is measured as 56Ω. It is close to 52Ω, which is predicated by the analytical model. Because the sample was terminated by a short circuit, the reflection from the end of the sample is negative. The second marker indicates the reflection from the simulated corrosion site. Note that an accurate location is identified. Experimental results indicate that the magnitude of the reflection depends on the severity of the damage. The sample on the right has severe damage in which six strands are severed, while the other sample has two severed strands.

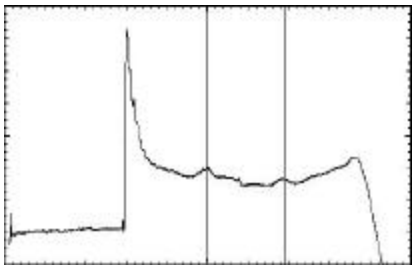

Fig. 4. *TDR returns from 3-meter reinforcing steel rebar sample.*

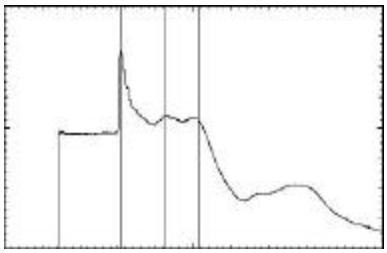

Two Severed Strands

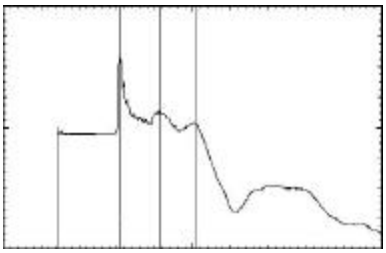

Six Severed Strands

Fig. 5. *TDR returns from 95cm seven-wire strand cable samples. The first and third markers indicate the beginning and the end of the sample, respectively, while the second marker indicates the simulated corrosion site.*

TDR is able to detect multiple damage sites. Figure 5 shows the TDR reflection from a 3-meter steel rebar sample. The two markers in Figure 5 indicate the pulse reflections from two simulated damage sites. Both of them are detected through a single measurement. The reflections are small (because the damage extends over only a short length) but are clearly identifiable.

The sensitivity and accuracy of TDR measurement depends on several other factors. They need to be considered before TDR installation and measurement. Among them are

- diameter of the sensor wire,
- distance between sensor wire and steel element,
- relative position of the sensor wire and damage site,
- system rise time of the measuring system, which describes how fast the signal is,
- water content of the surrounding concrete.

As predicted by the analytical model, TDR measurement is more sensitive when two conductors are close together. However, if two conductors are too close, axial current distribution will be modified by

the proximity effect. The density of axial current is increased in adjacent parts of parallel conductors with oppositely directed currents and is decreased at more remote parts. Therefore, corrosion occurring on remote parts is hard to detect. Laboratory experiments also indicate that the TDR measuring system must have a small system rise time to produce acceptable results.

Differential TDR Measurements

In field applications involving complex structures like an actual bridge, noise will be present in the TDR measurements. Other than random noise, undesirable wave reflections can be created by

- electric field disturbance caused by steel components near the cable being tested,
- variations in *d*, the distance between the steel cable and the sensing wire, since the characteristic impedance depends on *d*.

However, once a concrete girder is instrumented, the location of the steel components causing noise, and the distance *d* between the steel strand and sensing wire will remain constant. While reflections created due to these reasons can be relatively large, they are repeatable. Differential TDR measurement can be used to effectively distinguish corrosion sites from repeatable noise. If several TDR measurements are made for the same strand over a long time period, the later TDR results should be identical to the former ones except for the corrosion sites. A differential comparison of stored signals with newly measured ones can reveal corrosion that occurred between the two measurements. The differential TDR method has been tested experimentally. Figure 6 shows TDR results obtained from a 1-meter seven-wire strand bare sample. This sample has two severed strands over a 4.0cm length, 48cm from the front end of the sample. From waveform 1, it is hard to tell whether or not the sample is damaged and where the damage is. However, if this waveform is differentially compared with waveform 2, which is the TDR return obtained from the same sample when it did not have any electrical discontinuities, the damage site can be easily identified.

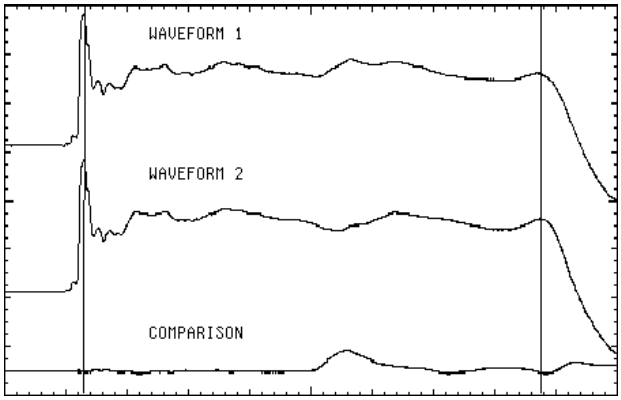

Fig. 6. *TDR results obtained from a 95cm seven-wire strand sample before (waveform 2) and after (waveform 1) a simulated damage is made to the sample. The differential comparison in the bottom reveals the damage site.*

Field Demonstration – Bridge 8F Experimental Program

The effectiveness of the TDR corrosion detection method has been proven through laboratory tests. In order to ready this technology for field implementation, full-scale experiments and field demonstrations are necessary. Bridge 8F is the first field demonstration of the TDR corrosion monitoring technology.

In 1999, the Delaware Department of Transportation (DelDOT) received funds to design and construct Bridge 8F in Fredrica, Delaware. It is a two-span, prestressed concrete, adjacent box beam bridge utilizing high-performance concrete (HPC) in both the beams and deck. HPC is concrete that is optimized for a specific application and often possesses qualities such as high strength, low

permeability, good workability, and excellent long-term durability. Bridge 8F, which replaced a deteriorated four-span structure, was completed in October 2000.

Bridge 8F consists of 22 adjacent prestressed concrete box beams. Each of the 22 adjacent prestressed concrete box beams is 19.0 m (62 ft. 4 in) long and 0.686 m (27 in) deep. Each beam was prestressed using 12.7 mm (0.5 in) diameter, Grade 270 (1863 MPa), seven-wire low relaxation strands. The test program focuses on three beams. Prior to casting, long-term monitoring instrumentation was installed in each beam. TDR monitoring wires have been installed alongside a total of five strands in these three beams. The wire is fully insulated, silver-coated copper wire, which is commercially available. A section of coaxial cable was connected to the strand/wire to provide electrical access.

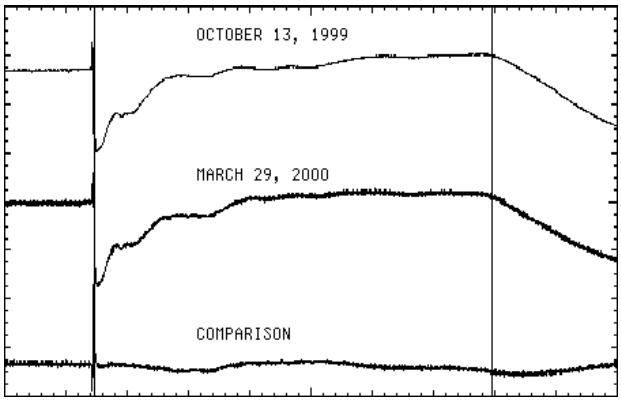

Fig. 7. TDR return from strand #2 of Beam B7(4) in Bridge 8F.

Corrosion monitoring with TDR began at the time of fabrication, and is continuing now that the bridge is in service. The TDR signal is noisy due to the presence of other electrically connected conductors. Therefore, differential TDR is used in the monitoring. Figure 7 shows TDR readings taken on October 13, 1999 and March 29, 2000, which are 9 days and 177 days after fabrication of the beam, respectively. The end of the sample can be easily identified indicating that energy loss for the embedded transmission line is not a major problem. The electrical length of the sample is significantly longer than the one without concrete (prior to the concrete pour). Also shown in Figure 7 is the differential comparison of the two waveforms. It shows the total changes that occurred in the 168-day time period. TDR returns from this strand are repeatable with minor changes likely due to the small changes in the concrete's water content. Furthermore, the beams have been moved around in the fabricator's yard during the monitoring process. This change in the environment also can cause minor changes in the waveform. The repeatability of the TDR returns demonstrates the effectiveness of differential comparison.

SUMMARY

A novel nondestructive evaluation technique for detecting damage in embedded or encased steel reinforcement or bridge cables using time domain reflectometry has been developed and demonstrated. Asymmetric transmission line models apply to steel elements with sensor wires and give an accurate prediction of the system characteristics. TDR can reveal the existence, location, and severity of corrosion on steel elements. Its effectiveness has been demonstrated through both small-scale laboratory tests and field implementation. Differential TDR method is being used as a permanent corrosion monitoring method for steel prestressing strands in an HPC bridge. The nature and repeatability of initial measurements have demonstrated that the method is viable for actual field use. The TDR nondestructive evaluation technique need not be limited to the application of new bridges. It can also be applied to other steel reinforced structures.

ACKNOWLEDGMENTS

This work was supported in part by the National Science Foundation under grant CMS-9700164 and the Delaware Transportation Institute under grant No.929.

REFERENCES

Bhatia, S. K., Hunsperger, R. G., and Chajes, M. J., 1998, Modeling Electromagnetic Properties of Bridge Cables for Non-destructive Evaluation; International Conference on Corrosion and Rehabilitation of Reinforced Concrete Structures: Federal Highway Administration, Orlando, Florida.

---------- 1998, Time Domain Reflectometry Theory; Hewlett-Packard Application Note 1304-2, Hewlett-Packard Company, Palo Alto, Calif.

Liu, W. 1998, Nondestructive Evaluation of Bridge Cables Using Time Domain Reflectometry; Master's thesis, Department of Electrical and Computer Engineering, University of Delaware.

Wietek, B. and Kunz, E., 1995, Permanent Corrosion Monitoring for Reinforced and Prestressed Concrete Structures; Symposium on Extending the Lifespan of Structures: International Association for Bridge and Structural Engineering, San Francisco, Calif.

Zahn, F. A. and Bitterli, B., 1995, Developments in Non-Destructive Stay Cable Inspection Methods; Symposium on Extending the Lifespan of Structures: International Association for Bridge and Structural Engineering, San Francisco, Calif.

DISTRIBUTED FIBER OPTIC SENSORS FOR THE DETECTION OF LIQUID SPILLS

Alistair MacLean[1], Chris Moran[2], Walter Johnstone[3], Brian Culshaw[4], Dan Marsh[5], Geoff Andrews[6]

[1] Optoelectronics Division, University of Strathclyde, Royal College Building,
204 George St., Glasgow, G1 1 XW, UK.
[2] Dept. of Pure & Applied Chemistry, University of Strathclyde, Royal College Building, 204 George St., Glasgow, G1 1 XW, UK. Tel: +44 141 548 4277, Fax: +44 141 553 1955; a.maclean@eee.strath.ac.uk
[3] Optoelectronics Division, University of Strathclyde, Royal College Building,
204 George St., Glasgow, G1 1 XW, UK.
[4] Optoelectronics Division, University of Strathclyde, Royal College Building,
204 George St., Glasgow, G1 1 XW, UK.
[5] PINACL Communications, Kinmel Park, Bodelwyddan, Denbighshire,
LL18 5TZ, UK. Tel: +44 1745 584 545, Fax: +44 1745 584 780; dan.marsh@pinacl.co.uk
[6] PINACL Communications, Kinmel Park, Bodelwyddan, Denbighshire, LL18 5TZ, UK.

PINACL
Communication Systems

ABSRACT

A range of distributed fibre optic sensors for the detection and location of aqueous, chemical and hydrocarbon fluid spills is presented. The sensors incorporate polymers that convert the swelling into a localised loss on an optical fibre when fluid exposure occurs. Optical Time Domain Reflectometry (OTDR) techniques are employed to rapidly detect and locate target liquids and chemicals at multiple positions along the sensor length. Sensor exposure to fluid can typically be located within 30 seconds to an accuracy of ± 2 m over a total length of 10 km. Once the polymer has dried out, the sensor returns to a non-activated state where further spill events may be detected.

A brief description of the basic sensor construction and of the underlying technology utilised in its operation is given. Results from experimental tests of prototype sensors manufactured to detect water, humidity, hydrocarbon fuels and organic solvents are then discussed. The response characteristics of the sensors in a range of varying environmental conditions and their performance during practical field trials are outlined. We conclude with a summary of the important advantages of the sensor design and the range of applications where it can be effectively implemented.

INTRODUCTION

The ability to rapidly detect and locate liquid spills is an important capability in industrial sectors where large volumes of liquids are regularly stored or transported. In the water and petrochemical industries this capability is critical to ensure that supplies are safely and efficiently controlled. Early warning of water or hydrocarbon fuel leaks can reduce downtime costs and more importantly minimise the potentially damaging impact on the surrounding environment. Distributed fibre optic sensors are well suited to such applications since they are passive, do not require an electrical supply at the sensing location and provide multiple spill detection capability over the entire sensor length. Optical Time Domain Reflectometry (OTDR) techniques are employed to detect the occurrence of such events and

locate the positions anywhere along the length of the sensor. The distributed nature of the OTDR measurement method offers distinct installation and cost advantages over conventional point sensor solutions to monitoring many separate locations.

In this paper we describe a range of distributed optical fibre microbend sensors designed for the detection of water, solvents or hydrocarbon fuels. The sensors incorporate polymers that transduce their swelling into a localised microbending on the fibre when activated by the target liquid. The localised bending is detected on the OTDR trace as a change in the attenuation for that position. Experimental results showing the polymer response to the target liquids are described, followed by experimental evaluation of the sensor response to a range of fluids in field trials.

PRINCIPLES OF SENSOR OPERATION

The basic sensor design consists of a glass reinforced plastic (GRP) central strength member coated in a thin layer of the liquid sensitive material, typically 100 to 200µm thick. Two distinct polymer types are used; a water swelling hydrogel polymer for water detection and a silicone based material for organic solvents and hydrocarbon fluid detection. A 62.5/125 graded index multimode optical fibre with an outer diameter of 250 µm is held against the coated GRP core by a helical Kevlar thread that is wrapped along the entire sensor length. A section of the sensor detailing its constituent components is shown in Figure 1. The polymer coating swells when exposed to the target fluid, the extent being dependent on the activating liquid, the particular type and thickness of the polymer coating. Swelling of the polymer causes the optical fibre to be squeezed against the Kevlar thread, thus inducing a periodic lateral deformation in the fibre at the exposed location.

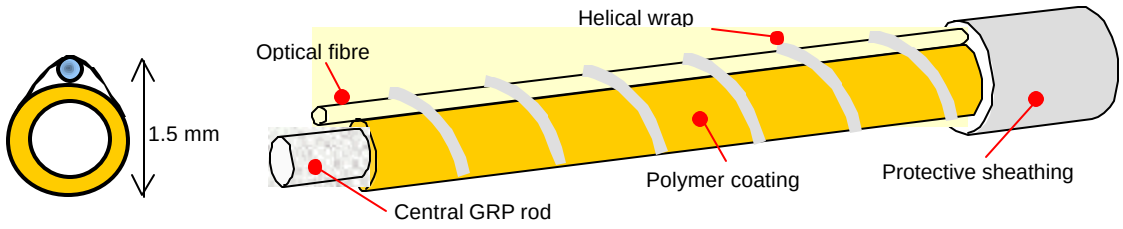

Fig. 1.*Section of fibre optic sensor element*

Light passing through the optical fibre at the activated location will suffer a microbend loss caused by mode coupling between the guided and radiative modes. Energy is lost as it is coupled from the highest guided mode to the first radiation mode and subsequently attenuated in the cladding. The period of the deformation has a critical effect on the degree of attenuation that occurs. It was found by Fields [1] that maximum mode coupling occurs in a parabolic index multimode fibre for the specific periodic spacing Λ, given by Equation 1,

$$\Lambda = \frac{2pa}{\sqrt{(2\Delta)}} \qquad [1]$$

where a is the core radius and Δ is the maximum relative difference between the refractive indices of the core and the cladding of the fibre. Both Fields [1] and Deimeer [2] determined that a multiple of this spacing could also be used to induce high loss. For the multimode fibre used in the sensor, Λ is equivalent to a

value of ~1 mm, thus periodic spacings of 2, 3, & 4mm may be used. The Kevlar wrap may therefore be applied at these values, thus reducing the sensitivity of the sensor to small variations in the pitch. Sensor lengths can range from tens of metres to several kilometres, the maximum length that can be detected being limited by the dry loss of the sensor and dynamic range of the OTDR instrument. The current limit is 2.5 km although it is anticipated that this can be extended to 10km with the use of longer interrogation wavelengths.

The OTDR operates by sending short pulses of light into the optical fibre and monitors the Rayleigh back-scattered light that is returned as a function of distance along the fibre. When a localised section of the sensor is exposed to the activating fluid, the increase in attenuation causes a reduction in intensity of the back-scattered light for that fibre section. The OTDR trace shows the loss event as an increase in the gradient of the trace that can be readily identified if compared with a dry reference trace. A schematic of a typical set-up and OTDR trace for two separate events on the same sensor is shown in Figure 2.

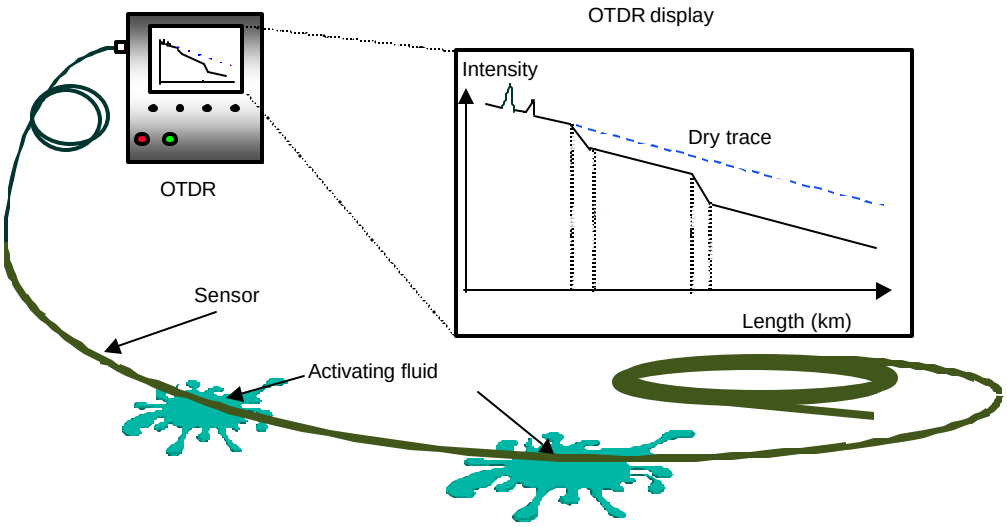

Fig. 2. *Schematic of OTDR trace showing two wet sections*

SENSOR MATERIAL SWELLING RESPONSE

The sensors described in this paper may incorporate a range of materials that are chosen to swell on contact with the fluid they are designed to detect. Two different material types were used in the sensors designed to detect water and hydrocarbons, but clearly other suitable polymers that experience sufficient volumetric change when in contact with the target chemical species may be used. The materials must display certain characteristics that are critical for effective sensor operation. They must retain their physical strength when swollen and preferably return to their original dry state when the liquid is removed.

WATER SENSITIVE POLYMER

A hydrogel polymer material is coated onto the GRP core of the sensors that are designed for water and humidity detection. The hydrogel material will swell but not dissolve in aqueous media. It is one of a range of poly (ethylene oxide)-co-poly(propylene oxide) block copolymer polyurethane-urea hydrogels [3]. The hydrogel consists of hydrophilic poly(ethylene oxide) (PEO) and hydrophobic poly(propylene oxide) (PPO) polymeric segments, joined by urethane and urea linkages. The urethane / urea linkages, being hydrophobic, act as physical cross-links that hold the swollen structure together. The presence of water causes volumetric expansion, the extent being dependent on the percentage swelling and the ratio of PEO to PPO in the hydrogel structure. The ratio of PEO to PPO in the hydrogel is chosen to provide maximum mechanical strength when fully swollen in water and is equivalent to a 40% volumetric expansion. For the current polymer design, swelling begins above a relative humidity (RH) of 70 %. The effect of the humidity on the swelling of 200µm thick film samples of hydrogel is shown in Figure 3. There is clearly a distinct increase in the swelling when the hydrogel is in direct contact with liquid water (shown in Figure 3 as 100% RH).

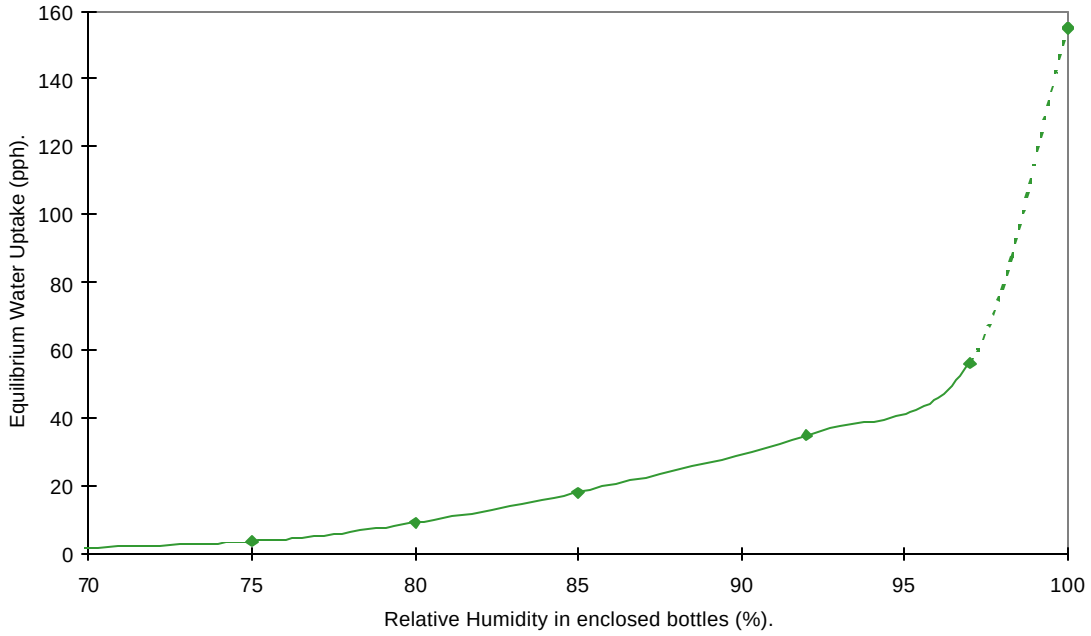

Fig. 3. *Effect of relative humidity on hydrogel swelling*

HYDROCARBON SENSITIVE POLYMER

For the hydrocarbon sensors, silicone or rubber-based polymers are employed as the activating materials to detect a wide range of fuels and solvents. A range of different polymer materials was tested to determine the most suitable for fuel and solvent detection. Several 200µ thick samples of Silicone, Ethy-propyl-diene-monomer (EPDM) and Butyl rubber were placed into each of the hydrocarbon fuels to determine their swelling response. The materials typically attained their maximum swelling within 1 minute of immersion in the highly volatile fuels and within several minutes for the heavier fuels. The results of these swelling tests are shown for three different polymer materials in Figure 4. It is clear that the silicone material is the best suited to detecting volatile liquids since they induce the most rapid and highest swelling whereas EPDM is more suited to the detection of heavier fuels and oils. Following

these observations, additional tests were conducted to determine the effect of common solvents on the silicone polymer. Two separate tests were conducted, initially with silicone samples immersed in the solvents and then suspended above them in a sealed environment. The maximum swelling of the silicone material in each of these solvents in liquid and vapour form is shown in Figure 5. It is clear that high swelling occurs rapidly and that the solvents affect the silicone significantly even in their vapour form. By simply considering the degree of activation, all the solvents with the exception of methyl ethyl ketone and acetone should be detectable using the current sensor design. Tests were conducted to estimate the force exerted by the swollen polymer films and they confirmed that the degree of swelling was sufficient to induce a detectable loss on the sensor.

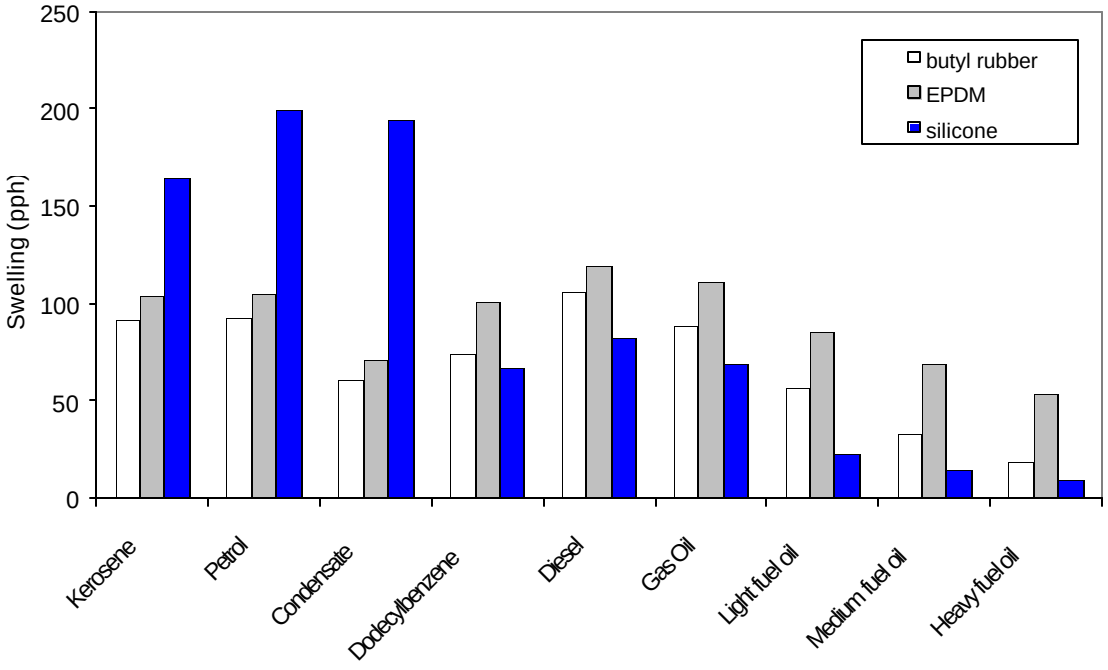

Fig. 4. *Swelling of three different polymers in hydrocarbon fuels*

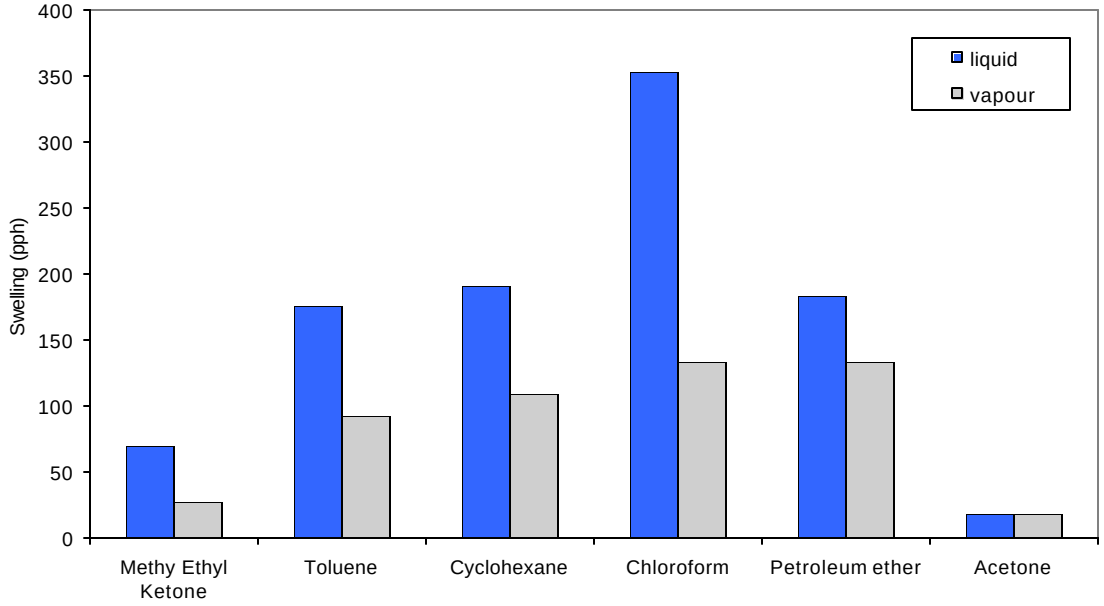

Fig. 5. *Swelling of silicone in solvents (liquid and vapour)*

EXPERIMENTAL SENSOR RESPONSE

Water and Humidity Sensor

Following the experimental evaluation of suitable polymer materials, several prototype sensors were produced and tested in a range of differing environments. Water sensors were manufactured using thin coatings of hydrogel and wrapping the Kevlar thread onto the multimode optical fibre at a pitch of 2mm. Laboratory tests were then conducted to determine the event resolution on a 100m long prototype sensor. Two separate 1m sections were immersed in water, after 2 minutes the dry and wet OTDR traces were compared. The resulting OTDR trace shown in Figure 6 clearly indicates that water intrusion has occurred at positions of 332m and 378m on the trace. Analysis of the trace confirmed that the degree of attenuation for many of the sensors was high enough to have been detected if only 50cm of the sensor had been affected by water exposure.

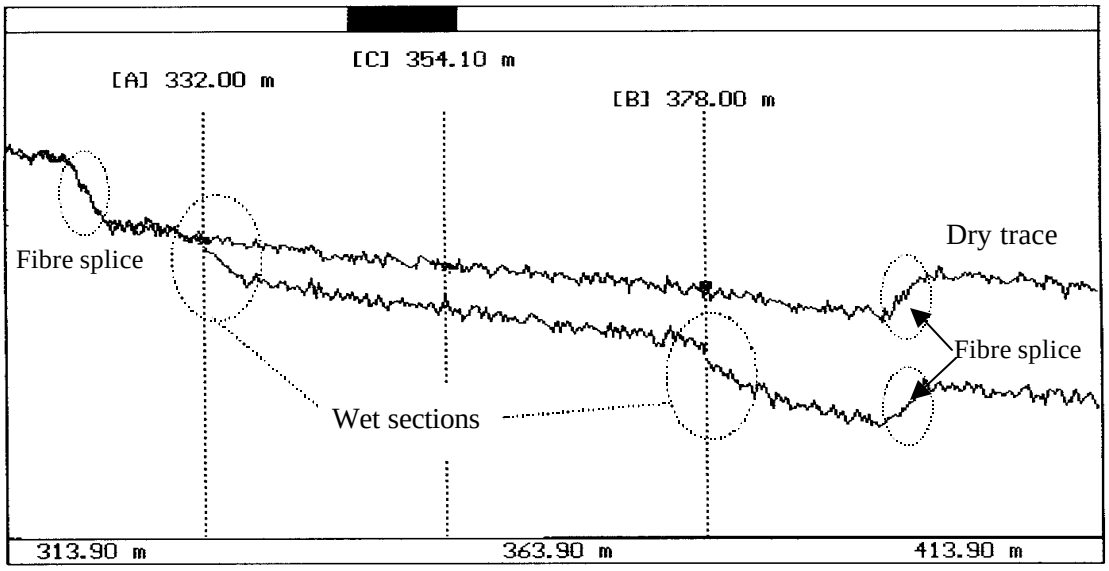

Fig. 6. *OTDR trace showing two separate 1 metre long water exposures*

An estimate of sensor response in a variety of environments is important to evaluate if external parameters will affect its ability to detect water. The sensor is designed to activate when immersed in liquid water but as shown in Figure 3, the hydrogel swelling is also affected by the amount of humidity in the environment. It is possible that high relative humidity (RH) will activate the sensor causing a false reading that indicates that water ingress has occurred. It is also possible that if the sensor can be accurately calibrated it may be used as a humidity sensor. To investigate this further a super-saturated salt solution providing 97% RH in the surrounding environment at equilibrium was placed with 25m of coiled sensor inside a sealed chamber. The sensor attenuation and RH were monitored as the enclosed environment came to equilibrium over several days. The resulting attenuation response of the sensor is shown in Figure 7. It gives a clear indication that high humidity has a considerable effect on the attenuation that is induced, with a 15dB/km loss at a RH of 97% in comparison with the 45 dB/km loss for liquid immersion. It can therefore be concluded from the experiment that the sensor is affected by very high humidity, but in such an environment it is also likely that free water would be present.

The sensor may have advantages over conventional technology when used for civil engineering applications such as grout quality monitoring in ducts of pre-stressed bridges or concrete beams. A common method of bridge construction uses steel tendons to exert a compressive load on the concrete to ensure that it does not experience tensile loads that cause cracks. The tendons are covered in grout to protect them from water or salt ingress, thus preventing corrosion. If the tendon is exposed due to ineffective grouting, the corrosion introduces a risk of structure failure. There are three possible uses for the sensor in this application, firstly to monitor the grouting process as it takes place, to monitor the curing or drying-out period and finally to detect water ingress in cracks post- setting. At present, there is no conventional method available to provide these measurements although a previous paper using this water sensor has reported its use as a grout flow monitor.

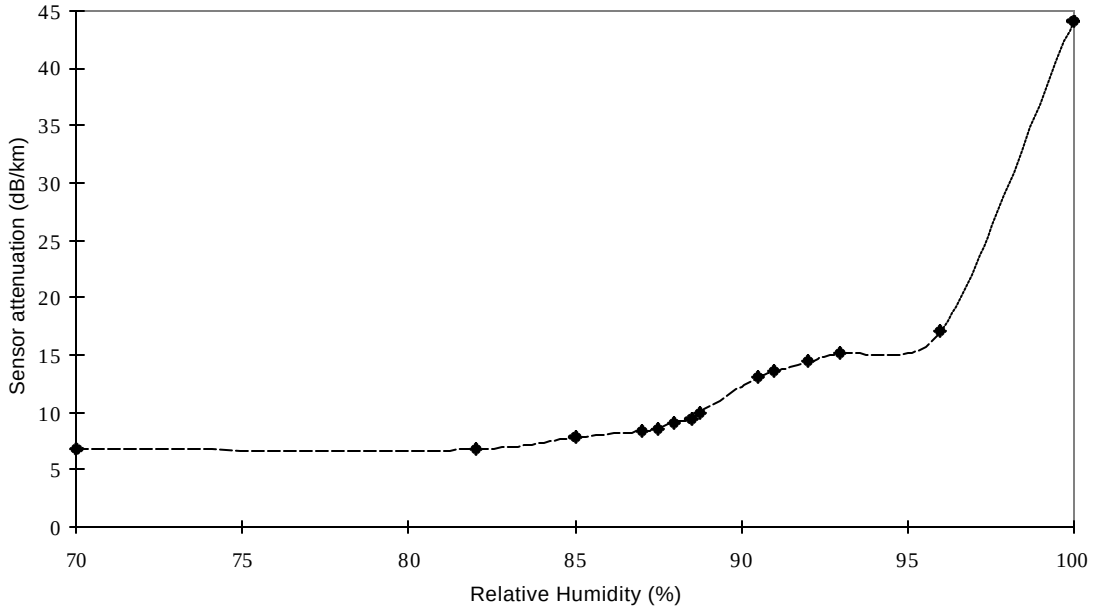

Fig. 7. *Water sensor attenuation as a function of relative humidity*

To monitor the grouting procedure, three different types of water sensor were placed into a 4 m long open duct, before the grout was poured. One of the sensors was manufactured with no hydrogel coating on the GRP rod to estimate the physical effects of curing on the optical fibre. The other two sensors had optimised response and were physically protected in either a PVC braiding or a porous Vyon™ tubing. The attenuation levels for all three sensors were monitored during the grout pouring and then at periodic intervals over several weeks. The active sensors exhibited maximum attenuation during the grout pouring procedure due to the amount of free water available. It is clear from the results shown in Figure 8 that significant moisture is present within the first 48 hours, indicating that the grout is still drying out. After this time it appears that the grout has dried out significantly and is no longer inducing loss in the sensors. The PVC braiding having a large pore size appears to have allowed more rapid water penetration than the Vyon with the smaller pore size.

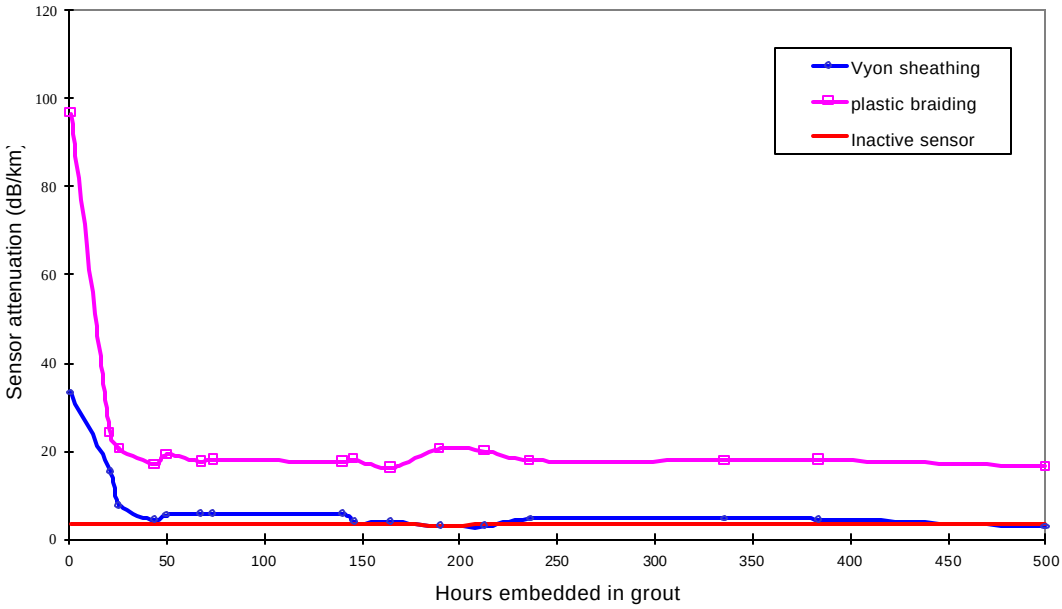

Fig. 8. *Attenuation response of sensors in open grouted duct*

HYDROCARBON LIQUID SENSOR

The sensors designed for hydrocarbon fluids were manufactured in a similar manner to the water sensor, with the GRP core coated with a silicone-based polymer in place of the hydrogel and using an optical fibre with a protective coating. Laboratory tests were conducted to determine the response of a 100-metre long prototype hydrocarbon sensor. Before sensor evaluation commenced, a dry reference trace was taken for comparative purposes. To determine if multiple short events could be located on this sensor, three separate 50cm-long sections on the sensor were identified. The three sections of the sensor were then exposed to petrol and the wet trace taken after sensor exposure. As can be seen from the corresponding OTDR trace in Figure 9, the wetted sections located at 35, 61 and 80 metres can be clearly seen. A loss of 0.2 dB was induced by the sensor activation at each of these locations and was visible within 30 seconds of petrol exposure. After the petrol had evaporated from the silicone polymer, the sensor returned to its original dry attenuation reading.

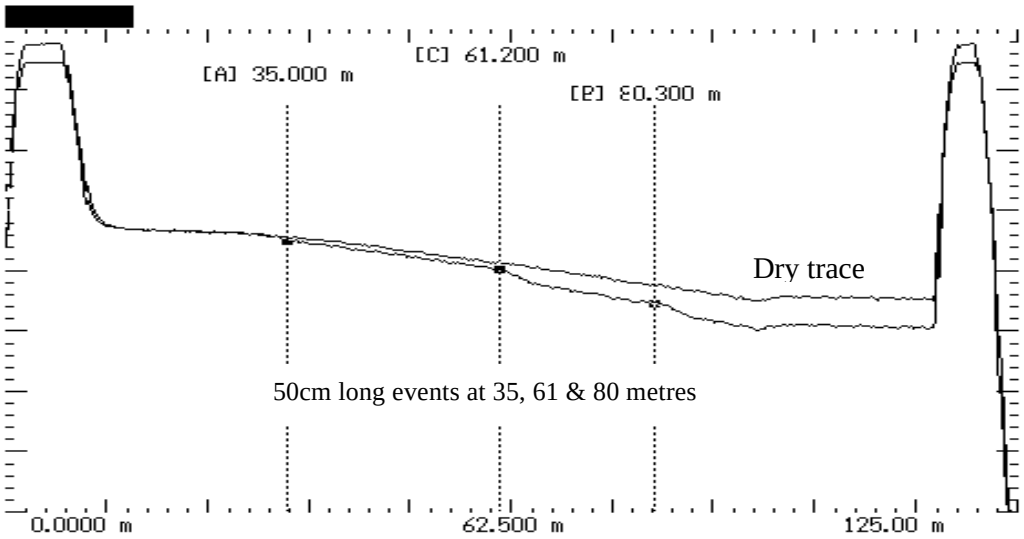

Fig. 9. *OTDR trace showing three 50cm-long sections exposed to petrol*

The experiment displays the ability of distributed sensors to make multiple simultaneous measurement, which is clearly advantageous where extensive industrial plant areas need to be monitored. If the sensor is also capable of repeat measurements, it eliminates the requirement to replace sensor sections that have been activated by fuel exposure. Several tests were thus conducted using petrol to determine the ability to make repeat measurements on the same sensor section. The results of these tests indicated that if the fuel evaporates completely after exposure, the polymer retains its ability to swell and induce the same degree of force on the fibre for repeated swelling. The sensor may not however have repeat measurement capability for example when exposed to heavier fuels that do not rapidly evaporate. Estimation of the drying-off times for a wide range of typical fuels is still ongoing.

To determine the sensor response to other hydrocarbons, a variety of sensors were manufactured with different parameters and then tested using the same fuels used in the material evaluation. The sensors were shown to respond to kerosene, diesel and dodecylbenzene (a power cable coolant), inducing varying attenuation dependent on the activating fuel and sensor type. These tests were then repeated using several commonly available solvents and the sensors responded rapidly to chloroform, toluene and petroleum ether. As predicted by the swelling analysis on the silicone polymer, the chloroform induced a high loss in the fibre that was rapidly detectable at a position of 61m on the trace shown in Figure 10. Of all the fuels and solvents tested to date, chloroform produced the highest and most rapid response. It is envisaged that it should be possible to detect other common solvents such as xylene and dichloromethane although experimental verification has yet to commence.

The most recent tests conducted on these sensors required their installation in an environment out of the laboratory where all previous experimentation had been conducted. Two 400m lengths of ruggedised sensor were laid out and installed in a location where they were exposed to atmospheric conditions and temperature variations over several weeks. The sensors were tested after this period and despite being covered in moisture during testing, responded well when petrol exposure took place. Repeat measurements confirmed that the sensors were as responsive as they had been during laboratory trials. These outdoor field trials also saw the first successful interrogation of the sensors using a low cost OTDR instrument that was custom-built for this application. The instrument provides a simple OTDR function that is used to provide an automatic alarm that detects and locates the position of an exposure event when it occurs.

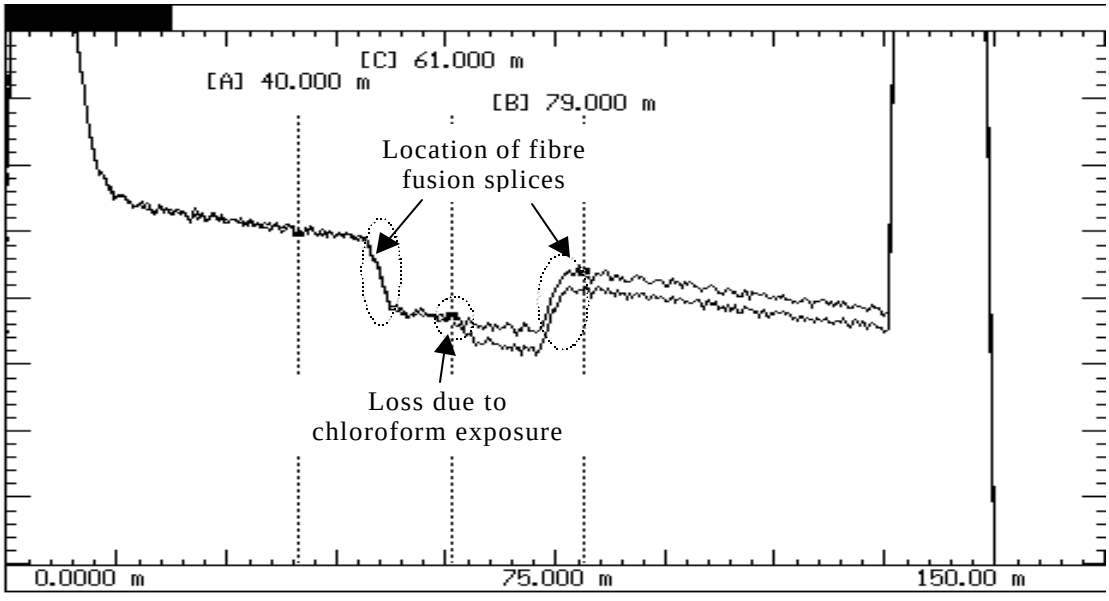

Fig. 10. *OTDR trace showing 1 metre long section exposed to chloroform*

It is thus apparent that environmental variations and the presence of water will not have an adverse effect on the hydrocarbon sensor operational capability. Further environmental testing of these sensors is ongoing and will include sensor activation at sub-zero temperatures.

CONCLUSIONS

A distributed fibre optic sensor that has the potential to monitor many different target species using a generic sensor design has been demonstrated. The sensor is sensitive to the target fluid over its entire length and will activate when exposed to metre-long liquid spills. Detection of water and humidity has been demonstrated using a sensor that incorporates a hydrogel polymer that swells when it comes into contact with moisture. This type of sensor was employed for the monitoring of grouted ducts and successfully demonstrated concrete drying out during the curing stage.

In the second type of sensor discussed, the hydrogel was replaced with a silicone-based polymer that was sensitive to hydrocarbon fuels and solvents. The silicone materials were shown to swell on contact with a wide range of common fuels and solvents. Rapid detection of 1-metre sensor sections exposed to petrol, kerosene, chloroform and toluene among others was demonstrated using a ruggedised sensor design. Field trials in which the sensor was subjected to prolonged environmental exposure over several weeks demonstrated that it was still capable of repeated petrol detection on the same sensor section.

Several important applications exist for a sensor that has the potential to monitor for intrusion of aqueous and hydrocarbon fluids along the same extended sensor length. Rapid water intrusion detection is important in sensitive computer and telecommunications installations, semiconductor plants and large civilian buildings. The detection of moisture ingress in pre-stressed concrete is one potential application within civil engineering where these sensors have a unique role. They may be employed to give early warning of moisture ingress and prevent structure failure due to corrosion of the reinforcing bars.

Detection of hazardous fuel and chemical spills in the petrochemical industry is an application where a fibre optic sensor has significant advantages over conventional electrical alternatives. Established methods are limited to detecting whether a leak has occurred or locating spills at point locations. The presence of electrical current poses an additional risk of explosions where spills occur. The fibre optic sensor is ideally suited to such applications since it does not require an electrical supply at the sensing location and may be remotely monitored some distance away. In addition, the sensor is easy to install due to its cable-like form, may extend to several kilometres in length and is capable of monitoring an extensive plant area.

This type of fibre optic sensor is aimed at a market where conventional electrical sensors have been predominantly used for many years and are the industry standard. A combination of comparatively low cost sensors in conjunction with a custom built OTDR detection instrument provides a cost-effective and viable alternative solution to monitoring many locations where fluid spills may occur.

ACKNOWLEDGEMENTS

The Department of Trade & Industry (DTI) and Engineering & Physical Sciences Research Council (EPSRC) are thanked for their financial support of the most recent work presented in this paper through the Distributed Industrial Sensors for Hydrocarbons ('DISH') LINK scheme. The contributions of the industrial partners Pinacl Communications, SDA Protec and OptoSci throughout the project are gratefully acknowledged.

REFERENCES

Diemeer M.B.J. and Trommel E.S., 1994, Fibre optic sensors: Sensitivity as a function of distortion wavelength, Opt. Lett, **9**, No.6.

Fields J.N., 1979, Attenuation of a parabolic index fibre with periodic bends, App. Phys. Lett., **36**, p779-801.

Peppas N.A., 1987, Hydrogels in medicine and pharmacy Vol. 2, Polymers, C R C Press, Boca Raton, FL.

Michie W.C. *et al*, 1994, Optical fibre grout flow monitor for post tensioned reinforced tendon ducts, SPIE Vol. 2361, Proc. 2nd European Conference on Smart Structures, pp186-189.

Author Index

Adak, P. 352
AlShawawreh, N. K. 374, 384
Amara, Nabil 394
Anderson, Tom 95, 346
Andrews, Geoff 534
Ansari, Farhad 510
Beauchamp, Yves 334
Beck, Timothy J. 305
Belansky, Richard 22
Blume, Peter 53
Bolvin, Herve 171
Brandelik, Alexander 446
Bréda, Nathalie 82
Buerck, Jochen 496
Chajes, Michael 523
Chambarel, André 160, 171
Chanzy, André 82, 160
Charette, Francois 334
Chen, Zhongyu 510
Chenaf, Djaouida 394
Chevallier, Claude 82
Cole, R. G. 38
Culshaw, Brian 534
Delage, Laurent 82
Delin, Geoffrey N. 262
Dowding, Charles H., 4, 38
Drnevich, Vincent P. 457, 470, 483
Drumm, Eric C. 281
Duncan, Maurice J. 95
Edwards, M. 62
Ferrari, Philippe 160
Ferré, Paul A. 210, 196
Ferry, Evelyne 160, 171
Gjerapic, Gordan 325
Gorski, B. P. 346
Gottlieb, Johannes 236
Grayson, Rodger B. 95
Gu, Xianglin 510
Heimovaara, Timo J. 9
Herkelrath, William N. 262
Huang, Y. 183
Huebner, Christof 236, 446
Hughes, Jeremy J. 305
Hunsperger, Robert 523
Johnstone, Walter 534
Jones, Scott B. 140, 149
Judge, K. 346
Kane, William F. 305
Knight, John H. 196, 210
Koehler, Kurt 53
Kraemer, Karl 496
Kunz, Eric 523
Lapen, D. R. 62
Laurent, Jean-Paul 82, 160
Lin, Chih-Ping 117
Liu, Wei 523
Lovell, Janet 457, 470, 483
MacLean, Alistair 534
Marsh, Dan 534
Mathieu, Heide 496
Matsura, Edson E. 72, 273
McAlister, Cary M. 315, 352
McFarlane, Ronald 426
Mohamed, A. M. O. 374, 384
Moldrup, Per 196, 210
Moran, Chris 534
Nadler, Arie 291
Nakhkash, M. 183
Nissen, Henrik H. 196, 210
O'Connor, Kevin 325, 409
Olszak, Chris 95
Or, Dani 140, 149
Persson, Magnus 128, 362
Pierce, Charles E. 38, 315, 352
Pongetti, Thomas 22
Poulter, Don A. 325
Rainwater, N. Randy 281
Rau, Frank 446
Roberson, Ruth 417, 435
Roth, Siegmar 496
Ruelle, Pierre 82
Ruf, Ruediger 53
Said, R. A. 374, 384
Scheuermann, Alexander 236
Schlaeger, Stefan 236
Schneebeli, Martin 446
Schofield, Tracy G. 250

Author Index

Seikmeier, John	417, 435
Siddiqui, Shafiqul I.	457
Souza, C. F.	72, 273
Stacheder, Markus	53
Sun, Zongjia	109, 225
Tarr, K..	346
Testezlaf, R.	72, 273
Thompson, Julian	95
Tisch, B.	346
Tishmack, Jody	483
Todoroff, Pierre	160
Topp, G. Clarke	62
Truss, Steven W.	183
Waldner, Peter	446
Wanser, Keith	22
Ward, A. L.	291
West, L. J.	183
Western, Andrew W.	95
Wilson, David	95
Winship, P.	183
Wraith, Jon M.	149
Wright, Wesley C.	281
Yi, Quanghee	457, 470, 483
Yoder, Ronald	281
Young, G. D.	62, 109, 225
Young, Rodger	95
Yu, Xiong	483
Znidarcic, Dobroslav	325
Zuo, Gang	281

Back to Table of Contents